ADVANCES IN BIOLOGICAL UNDERSTANDING OF TUMOR RADIATION RESISTANCE

EDITED BY: Ira Ida Skvortsova and Paul N. Span
PUBLISHED IN: Frontiers in Oncology

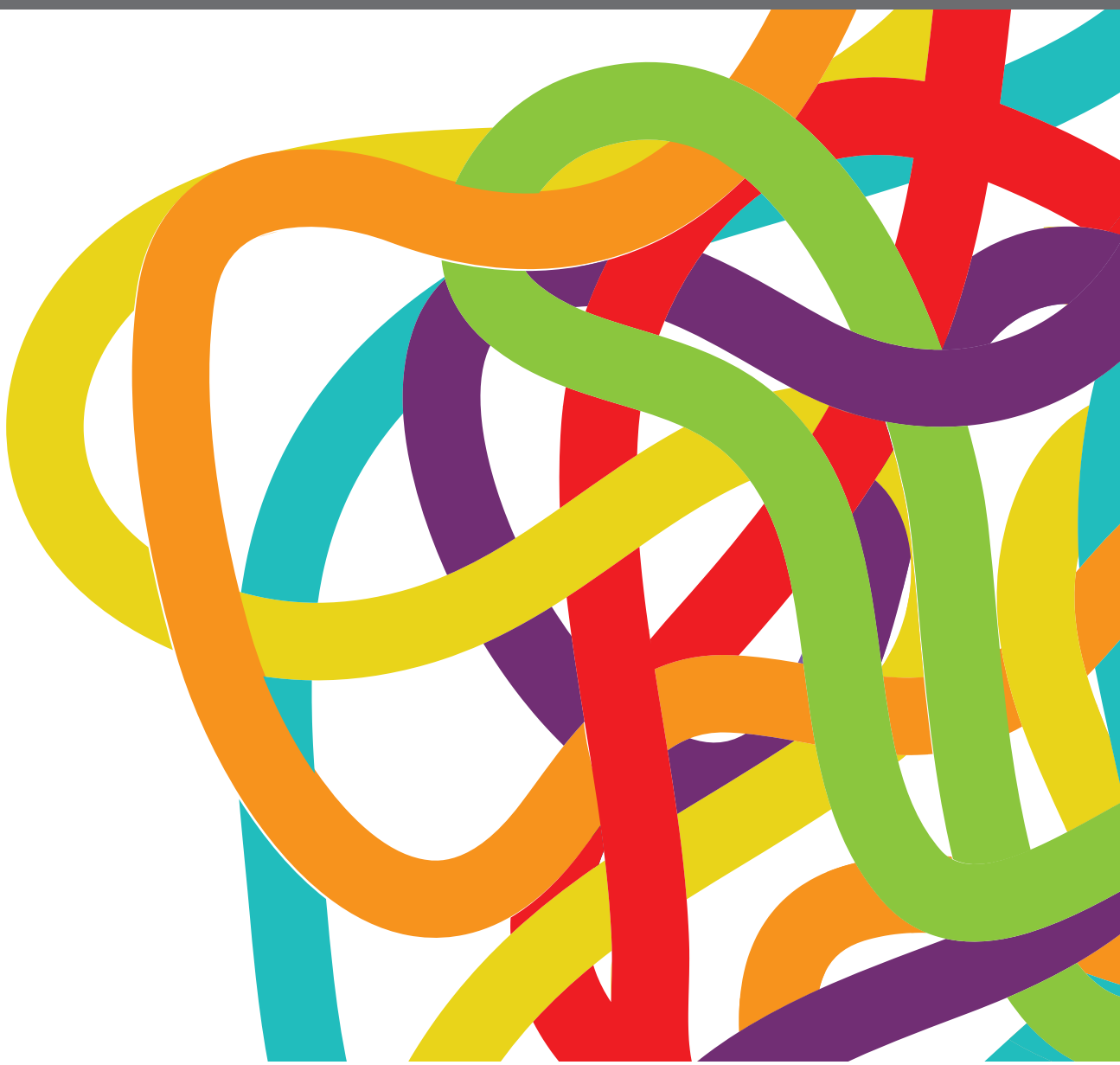

frontiers Research Topics

Frontiers eBook Copyright Statement

The copyright in the text of individual articles in this eBook is the property of their respective authors or their respective institutions or funders. The copyright in graphics and images within each article may be subject to copyright of other parties. In both cases this is subject to a license granted to Frontiers.

The compilation of articles constituting this eBook is the property of Frontiers.

Each article within this eBook, and the eBook itself, are published under the most recent version of the Creative Commons CC-BY licence. The version current at the date of publication of this eBook is CC-BY 4.0. If the CC-BY licence is updated, the licence granted by Frontiers is automatically updated to the new version.

When exercising any right under the CC-BY licence, Frontiers must be attributed as the original publisher of the article or eBook, as applicable.

Authors have the responsibility of ensuring that any graphics or other materials which are the property of others may be included in the CC-BY licence, but this should be checked before relying on the CC-BY licence to reproduce those materials. Any copyright notices relating to those materials must be complied with.

Copyright and source acknowledgement notices may not be removed and must be displayed in any copy, derivative work or partial copy which includes the elements in question.

All copyright, and all rights therein, are protected by national and international copyright laws. The above represents a summary only. For further information please read Frontiers' Conditions for Website Use and Copyright Statement, and the applicable CC-BY licence.

ISSN 1664-8714
ISBN 978-2-88966-053-7
DOI 10.3389/978-2-88966-053-7

About Frontiers

Frontiers is more than just an open-access publisher of scholarly articles: it is a pioneering approach to the world of academia, radically improving the way scholarly research is managed. The grand vision of Frontiers is a world where all people have an equal opportunity to seek, share and generate knowledge. Frontiers provides immediate and permanent online open access to all its publications, but this alone is not enough to realize our grand goals.

Frontiers Journal Series

The Frontiers Journal Series is a multi-tier and interdisciplinary set of open-access, online journals, promising a paradigm shift from the current review, selection and dissemination processes in academic publishing. All Frontiers journals are driven by researchers for researchers; therefore, they constitute a service to the scholarly community. At the same time, the Frontiers Journal Series operates on a revolutionary invention, the tiered publishing system, initially addressing specific communities of scholars, and gradually climbing up to broader public understanding, thus serving the interests of the lay society, too.

Dedication to Quality

Each Frontiers article is a landmark of the highest quality, thanks to genuinely collaborative interactions between authors and review editors, who include some of the world's best academicians. Research must be certified by peers before entering a stream of knowledge that may eventually reach the public - and shape society; therefore, Frontiers only applies the most rigorous and unbiased reviews.
Frontiers revolutionizes research publishing by freely delivering the most outstanding research, evaluated with no bias from both the academic and social point of view. By applying the most advanced information technologies, Frontiers is catapulting scholarly publishing into a new generation.

What are Frontiers Research Topics?

Frontiers Research Topics are very popular trademarks of the Frontiers Journals Series: they are collections of at least ten articles, all centered on a particular subject. With their unique mix of varied contributions from Original Research to Review Articles, Frontiers Research Topics unify the most influential researchers, the latest key findings and historical advances in a hot research area! Find out more on how to host your own Frontiers Research Topic or contribute to one as an author by contacting the Frontiers Editorial Office: researchtopics@frontiersin.org

ADVANCES IN BIOLOGICAL UNDERSTANDING OF TUMOR RADIATION RESISTANCE

Topic Editors:
Ira Ida Skvortsova, Innsbruck Medical University, Austria
Paul N. Span, Radboud University Nijmegen Medical Centre, Netherlands

Citation: Skvortsova, I. I., Span, P. N., eds. (2020). Advances in Biological Understanding of Tumor Radiation Resistance. Lausanne: Frontiers Media SA. doi: 10.3389/978-2-88966-053-7

Table of Contents

05 ***Editorial: Advances in Biological Understanding of Tumor Radiation Resistance***
Ira Ida Skvortsova and Paul N. Span

07 ***Combining the DNA Repair Inhibitor Dbait With Radiotherapy for the Treatment of High Grade Glioma: Efficacy and Protein Biomarkers of Resistance in Preclinical Models***
Julian Biau, Emmanuel Chautard, Nathalie Berthault, Leanne de Koning, Frank Court, Bruno Pereira, Pierre Verrelle and Marie Dutreix

17 ***Flavonoid Derivative of* Cannabis *Demonstrates Therapeutic Potential in Preclinical Models of Metastatic Pancreatic Cancer***
Michele Moreau, Udoka Ibeh, Kaylie Decosmo, Noella Bih, Sayeda Yasmin-Karim, Ngeh Toyang, Henry Lowe and Wilfred Ngwa

26 ***Corrigendum: Flavonoid Derivative of* Cannabis *Demonstrates Therapeutic Potential in Preclinical Models of Metastatic Pancreatic Cancer***
Michele Moreau, Udoka Ibeh, Kaylie Decosmo, Noella Bih, Sayeda Yasmin-Karim, Ngeh Toyang, Henry Lowe and Wilfred Ngwa

29 ***Exploring Radiation Response in Two Head and Neck Squamous Carcinoma Cell Lines Through Metabolic Profiling***
Eva Lindell Jonsson, Ida Erngren, Mikael Engskog, Jakob Haglöf, Torbjörn Arvidsson, Mikael Hedeland, Curt Petterson, Göran Laurell and Marika Nestor

45 ***Exosomes in Cancer Radioresistance***
Jie Ni, Joseph Bucci, David Malouf, Matthew Knox, Peter Graham and Yong Li

54 ***The Effects of Neoadjuvant Chemoradiation in Locally Advanced Rectal Cancer—The Impact in Intratumoral Heterogeneity***
Fabiana Bettoni, Cibele Masotti, Bruna R. Corrêa, Elisa Donnard, Filipe F. dos Santos, Guilherme P. São Julião, Bruna B. Vailati, Angelita Habr-Gama, Pedro A. F. Galante, Rodrigo O. Perez and Anamaria A. Camargo

64 ***Identification of Schlafen-11 as a Target of CD47 Signaling That Regulates Sensitivity to Ionizing Radiation and Topoisomerase Inhibitors***
Sukhbir Kaur, Anthony L. Schwartz, David G. Jordan, David R. Soto-Pantoja, Bethany Kuo, Abdel G. Elkahloun, Lesley Mathews Griner, Craig J. Thomas, Marc Ferrer, Anish Thomas, Sai-Wen Tang, Vinodh N. Rajapakse, Yves Pommier and David D. Roberts

82 ***Altering DNA Repair to Improve Radiation Therapy: Specific and Multiple Pathway Targeting***
Julian Biau, Emmanuel Chautard, Pierre Verrelle and Marie Dutreix

92 ***Optical Imaging Approaches to Investigating Radiation Resistance***
Sina Dadgar and Narasimhan Rajaram

103 ***Difference in Acquired Radioresistance Induction Between Repeated Photon and Particle Irradiation***
Katsutoshi Sato, Takashi Shimokawa and Takashi Imai

115 ***Targeting the Innate Immune Kinase IRAK1 in Radioresistant Cancer: Double-Edged Sword or One-Two Punch?***
Peter H. Liu and Samuel Sidi

122 ***Radiation-Induced Changes in Tumor Vessels and Microenvironment Contribute to Therapeutic Resistance in Glioblastoma***
Yun-Soo Seo, In Ok Ko, Hyejin Park, Ye Ji Jeong, Ji-Ae Park, Kwang Seok Kim, Myung-Jin Park and Hae-June Lee

132 ***The Dual Cell Cycle Kinase Inhibitor JNJ-7706621 Reverses Resistance to CD37-Targeted Radioimmunotherapy in Activated B Cell Like Diffuse Large B Cell Lymphoma Cell Lines***
Gro Elise Rødland, Katrine Melhus, Roman Generalov, Sania Gilani, Francesco Bertoni, Jostein Dahle, Randi G. Syljuåsen and Sebastian Patzke

149 ***The Extracellular, Cellular, and Nuclear Stiffness, a Trinity in the Cancer Resistome—A Review***
Sara Sofia Deville and Nils Cordes

163 ***Biological Determinants of Chemo-Radiotherapy Response in HPV-Negative Head and Neck Cancer: A Multicentric External Validation***
Martijn van der Heijden, Paul B. M. Essers, Monique C. de Jong, Reinout H. de Roest, Sebastian Sanduleanu, Caroline V. M. Verhagen, Olga Hamming-Vrieze, Frank Hoebers, Philippe Lambin, Harry Bartelink, C. René Leemans, Marcel Verheij, Ruud H. Brakenhoff, Michiel W. M. van den Brekel and Conchita Vens

180 ***Ultra-High Dose Rate (FLASH) Radiotherapy: Silver Bullet or Fool's Gold?***
Joseph D. Wilson, Ester M. Hammond, Geoff S. Higgins and Kristoffer Petersson

192 ***Linking NRP2 With EMT and Chemoradioresistance in Bladder Cancer***
Alexander Schulz, Ielizaveta Gorodetska, Rayk Behrendt, Susanne Fuessel, Kati Erdmann, Sarah Foerster, Kaustubh Datta, Thomas Mayr, Anna Dubrovska and Michael H. Muders

205 ***The Role of Cancer Stem Cells in Radiation Resistance***
Christoph Reinhold Arnold, Julian Mangesius, Ira-Ida Skvortsova and Ute Ganswindt

217 ***Novel Therapeutic Strategies for Ovarian Cancer Stem Cells***
Nastassja Terraneo, Francis Jacob, Anna Dubrovska and Jürgen Grünberg

frontiers in Oncology

EDITORIAL
published: 12 May 2020
doi: 10.3389/fonc.2020.00754

Editorial: Advances in Biological Understanding of Tumor Radiation Resistance

Ira Ida Skvortsova[1,2] *and Paul N. Span*[3]*

[1] Laboratory for Experimental and Translational Research on Radiation Oncology (EXTRO-Lab), Department of Therapeutic Radiology and Oncology, Innsbruck Medical University, Innsbruck, Austria, [2] Tyrolean Cancer Research Institute, Innsbruck, Austria, [3] Radiotherapy and OncoImmunology Laboratory, Department of Radiation Oncology, Radboud University Medical Center, Nijmegen, Netherlands

Keywords: radiotherapy, treatment resistance, DNA damage repair, hypoxia, cancer stem cells

The Editorial on the Research Topic

Advances in Biological Understanding of Tumor Radiation Resistance

Radiation therapy (RT) is a frequently-applied powerful treatment approach generally leading to enhanced local tumor control. However, clinical outcome may be compromised by ineffective eradication of cancer cells that exhibit intrinsic or acquired radiation resistance. Although with increased doses of irradiation these radioresistant carcinoma cells can successfully be killed, it is usually impossible to reach these doses without pronounced damage to healthy tissue. To enhance the efficacy of RT, it is important to elucidate the molecular mechanisms regulating radiation resistance of tumor cells. The development of novel chemo- or targeting therapeutics targeting these mechanisms may thereby improve RT efficacy.

A number of mechanisms are known to be involved in cancer cell insensitivity to irradiation. Among them are mutations in genes related to DNA damage and repair, activation of intracellular pro-survival signaling pathways, affected cell cycle regulation, compromised cell death machinery, etc. Furthermore, microenvironmental factors are also very much involved in tumor cell radioresistance. For example, hypoxia, tumor-associated fibroblasts, immune cells, etc. could diminish tumor responses to ionizing radiation. Additionally, cancer stem cells (CSC) encapsulate in a single concept many of the above-mentioned explanations of tumor insensitivity to cytotoxic radiotherapy. Therefore, the role of CSCs in tumor formation, development and response to anti-tumor therapies is at present under intense investigation.

In this Special Issue, several reviews and original research papers address these different mechanisms of radioresistance.

For example, targeting of the repair of RT-induced Double Stranded Breaks in DNA may enhance RT efficacy (Biau, Verrelle et al.), for example via the DNA repair inhibitor Dbait (Biau, Berthault et al.).

Considering the association of intracellular signaling pathways and immunity with radioresistance, (Liu and Sidi) discuss how specific Innate Immune Kinase IRAK1 inhibitors might attenuate tumor radioresistance, while enhancing innate anti-tumor immune responses. Furthermore, Rødland et al. found that the dual-specific CDK1/2 and AURA/B kinase inhibitor JNJ-7706621 inhibits resistance to radioimmunotherapy in Diffuse Large B Cell Lymphoma. A role for the gene Schlafen11 (SLFN11) in determining cancer cell sensitivity to DNA-damaging chemotherapeutic agents and patient outcomes for several cancers has been described. Kaur et al. shows that CD47 is involved in this SLFN11-associated radioresistance.

The tissue microenvironment (TME) influences radiosensitivity. In the multicentric validation study of van der Heijden et al., (acute and chronic) hypoxia, stem cell-ness, tumor growth, epithelial-to-mesenchymal transition (EMT) and DNA repair were found to be related to locoregional control in chemoradiotherapy treated HNSCC patients. Radiosensitivity is also

OPEN ACCESS

Edited and reviewed by:
Timothy James Kinsella, Warren Alpert Medical School of Brown University, United States

***Correspondence:**
Paul N. Span
paul.span@radboudumc.nl

Specialty section:
This article was submitted to Radiation Oncology, a section of the journal Frontiers in Oncology

Received: *16 April 2020*
Accepted: *20 April 2020*
Published: *12 May 2020*

Citation:
Skvortsova II and Span PN (2020) Editorial: Advances in Biological Understanding of Tumor Radiation Resistance. Front. Oncol. 10:754. doi: 10.3389/fonc.2020.00754

modified by mechanical cues from the TME as reviewed by Deville and Cordes, and cells communicate radioresistance via exosomes as described in Ni et al.. Reciprocally, RT induces extensive changes in the TME that subsequently contribute to radioresistance, as found in glioblastoma (Seo et al.). This latter effect seems mediated via glioblastoma stem cells. This role of CSCs in radioresistance is discussed by Arnold et al.. Herein, the authors indicate that CSC targeting therapy is relevant for the efficacy of RT, but that correct identification of CSCs and reliable distinction from healthy cells is necessary. Furthermore, Terraneo et al. highlight mechanisms of CSC therapy resistance such as EMT and stemness, and describe novel therapeutic strategies for ovarian CSC. Indeed, Neuropilin-2 (NRP2) is associated with radioresistance in bladder cancer, and in Schulz et al. this is reportedly mediated via effects on EMT.

Lindell Jonsson et al. used liquid chromatography-mass spectrometry (LC-MS) to compare the metabolism between 2 HNSCC cell lines with differing radiosensitivity before and after irradiation, and found important differences that may account for their radiosensivity. Notably, Dadgar and Rajaram review different approaches to assess cellular metabolism, such as two-photon microscopy, diffuse reflectance, and Raman spectroscopy, which yield functional and molecular differences between radiation-resistant and sensitive tumors in response to radiation.

Other reviews consider alternative modes of irradiation as a way of alleviating radioresistance. For example, differences in photon vs. particle irradiation exist, as reviewed by Sato et al.. Furthermore, Ultra-High Dose Rate irradiation (FLASH) appears to have differential effects on normal tissues vs. tumors, making -to a certain extent- higher, more effective doses feasible (Wilson et al.). Moreau et al. finds that FBL-03G, a flavonoid cannabis derivative, radiosensitizes metastatic pancreatic cancer. On the other hand, Bettoni et al. report how in rectal cancer, neoadjuvant chemoradiation can increase intratumoral genetic heterogeneity, thereby leading to an increased risk in more aggressive residual tumors.

Overall, this Special Issue has addressed a multitude of potential mechanisms associated with radioresistance, and report on new targets for sensitizing treatment options. Knowledge on how these different mechanisms are induced and interact, how these occur in different cancers, and how these may be countered, will aid in assessing, preventing and/or targeting radioresistance. As radiotherapy is still one of the most effective and widely applied cancer treatment options, countering radioresistance may have far reaching effects on clinical outcome of many cancer patients.

AUTHOR CONTRIBUTIONS

PS wrote the first draft. IS contributed and finalized the manuscript.

Conflict of Interest: The authors declare that the research was conducted in the absence of any commercial or financial relationships that could be construed as a potential conflict of interest.

Copyright © 2020 Skvortsova and Span. This is an open-access article distributed under the terms of the Creative Commons Attribution License (CC BY). The use, distribution or reproduction in other forums is permitted, provided the original author(s) and the copyright owner(s) are credited and that the original publication in this journal is cited, in accordance with accepted academic practice. No use, distribution or reproduction is permitted which does not comply with these terms.

frontiers in Oncology

ORIGINAL RESEARCH
published: 19 June 2019
doi: 10.3389/fonc.2019.00549

Combining the DNA Repair Inhibitor Dbait With Radiotherapy for the Treatment of High Grade Glioma: Efficacy and Protein Biomarkers of Resistance in Preclinical Models

Julian Biau[1,2,3,4,5,6*], *Emmanuel Chautard*[5,7], *Nathalie Berthault*[1,2,3,4], *Leanne de Koning*[8,9], *Frank Court*[10], *Bruno Pereira*[11], *Pierre Verrelle*[1,6,12,13] *and Marie Dutreix*[1,2,3,4]

[1] Centre de Recherche, Institut Curie, PSL Research University, Paris, France, [2] UMR3347, CNRS, Orsay, France, [3] U1021, INSERM, Orsay, France, [4] Research Department, Université Paris Sud, Orsay, France, [5] INSERM, U1240 IMoST, Université Clermont Auvergne, Clermont Ferrand, France, [6] Radiotherapy Department, Centre Jean Perrin, Université Clermont Auvergne, Clermont-Ferrand, France, [7] Pathology Department, Centre Jean Perrin, Université Clermont Auvergne, Clermont-Ferrand, France, [8] Laboratory of Proteomic Mass Spectrometry, Centre de Recherche, Institut Curie, Paris, France, [9] Department of Translational Research, Institut Curie, PSL Research University, Paris, France, [10] GReD Laboratory, CNRS UMR 6293, INSERM U1103, Université Clermont Auvergne, Clermont-Ferrand, France, [11] Biostatistics Department, DRCI, Clermont-Ferrand Hospital, Clermont-Ferrand, France, [12] U1196, INSERM, UMR9187, CNRS, Orsay, France, [13] Radiotherapy Department, Institut Curie Hospital, Paris, France

OPEN ACCESS

Edited by:
Paul N. Span,
Radboud University Nijmegen Medical Centre, Netherlands

Reviewed by:
Ranjit Bindra,
Yale Medicine, United States
Dalong Pang,
Georgetown University, United States

***Correspondence:**
Julian Biau
Julian.biau@clermont.unicancer.fr

Specialty section:
This article was submitted to Radiation Oncology, a section of the journal Frontiers in Oncology

Received: *27 March 2019*
Accepted: *05 June 2019*
Published: *19 June 2019*

Citation:
Biau J, Chautard E, Berthault N, de Koning L, Court F, Pereira B, Verrelle P and Dutreix M (2019) Combining the DNA Repair Inhibitor Dbait With Radiotherapy for the Treatment of High Grade Glioma: Efficacy and Protein Biomarkers of Resistance in Preclinical Models. Front. Oncol. 9:549. doi: 10.3389/fonc.2019.00549

High grade glioma relapses occur often within the irradiated volume mostly due to a high resistance to radiation therapy (RT). Dbait (which stands for DNA strand break bait) molecules mimic DSBs and trap DNA repair proteins, thereby inhibiting repair of DNA damage induced by RT. Here we evaluate the potential of Dbait to sensitize high grade glioma to RT. First, we demonstrated the radiosensitizer properties of Dbait in 6/9 tested cell lines. Then, we performed animal studies using six cell derived xenograft and five patient derived xenograft models, to show the clinical potential and applicability of combined Dbait+RT treatment for human high grade glioma. Using a RPPA approach, we showed that Phospho-H2AX/H2AX and Phospho-NBS1/NBS1 were predictive of Dbait efficacy in xenograft models. Our results provide the preclinical proof of concept that combining RT with Dbait inhibition of DNA repair could be of benefit to patients with high grade glioma.

Keywords: radiation therapy, high grade glioma, Dbait, preclinical study, double-strand break, single-strand break, radioresistance

INTRODUCTION

High grade gliomas are the most frequent primary brain tumors in adults (1, 2). They represent an important source of morbidity and mortality and are a public health care challenge (3, 4). Maximal possible surgery is generally the first step of the management of high grade gliomas. Radiotherapy (RT) (+/- chemotherapy), is a major adjuvant therapy that improves survival (5, 6). Despite these treatments, median survival remains very low (1, 4). Early recurrence often occurs in the irradiated volume due to a high radioresistance of glioblastoma cells (7–10). These recurrences emphasize the

need to overcome tumor radioresistance with new molecules that target pathways underlying the mechanisms of such resistance (10–12).

The cytotoxicity of RT is mostly due to DNA damage (13). About 10,000 damaged bases, 1,000 single-strand breaks (SSB) and 40 double-strand breaks (DSB) are produced per gray, and per cell (13, 14). The most severe RT-induced DNA damages are DSB that are lethal to the cell if not repaired (15). The capacity of cancer cells to recognize DNA damages and initiate repair plays a major role in radioresistance (16–18). DNA repair inhibition could make cancer cells particularly sensitive to the DNA damaging treatments like RT (18, 19). Therefore, to inhibit DNA repair, we designed innovative molecules called Dbait (for DNA strand break bait). Dbait are 32 base-pair deoxyribonucleotides forming intramolecular DNA double helix mimicking DNA damages (18, 20–22). They act as a bait for DNA damage signaling enzymes inducing a "false" DNA damage signal that prevents repair enzyme recruitment at damage site and ultimately inhibits DSB and SSB repair pathways (**Figure 1**) (18, 20–22). Dbait was tested in combination with RT in first-in-human phase 1 clinical trial for the treatment of skin metastases of melanoma with encouraging results (23).

To decipher the mechanisms sustaining resistance to anticancer treatments is one of the most current challenges to avoid treatment escape. High-throughput screening strategies are widely used for the identification of predictive and prognostic biomarkers (24, 25). The most currently used analyzed the RNA content (transcriptome) or DNA modification (genome). However, in mammalian, it is widely accepted that regulatory modifications occur at the protein levels (25–27). Therefore, to explore *in vivo* predictive biomarkers of RT efficacy we used reverse-phase protein array (RPPA), a technology using high-throughput antibody-based detection. It requires just a few micrograms of protein lysate and allows measuring protein expression and their main modification in a highly quantitative manner (25, 27, 28). Hundreds of samples can be analyzed simultaneously and thus generate large datasets to identify potential biomarkers (25, 29).

In this preclinical study, we analyzed the potential of Dbait to sensitize high grade glioma to RT. First, we demonstrated the radiosensitizer properties of Dbait *in vitro*. Secondly, animal studies were performed to test the clinical potential of the combination of Dbait and RT for the treatment of high grade glioma. We identified potential protein biomarkers of resistance using RPPA. For that purpose, we assayed a selection of proteins and modifications involved in different RT signaling pathways.

MATERIALS AND METHODS

Cell Culture and Dbait Molecules

Nine human high grade glioma cell lines were used (CB193, MO59J, MO59K, SF763, SF767, SNB19, T98G, U87MG, and U118MG) and were grown using a 10% Fetal Calf Serum DMEM medium in a humidified incubator containing 5% CO2 at 37°C as previously described (25).

As already described (18): Dbait molecules consist in 32 base-pair oligonucleotides (5'-GCTGTGCCCACAACCCAGCAAACAAGCCTAGA-(H)-TCTAGGCTTGTTTGCTGG GTTGTGGGCACAGC-3', Eurogentec, Seraing, Belgium). A short inactive molecule, Dbait-8H (5'-ACGCACGG-(H)-CCGTGCGT-3') was used as control in the *in vitro* experiments. H is a hexaethyleneglycol linker and the letters underlined indicate the phosphorodiamidate nucleosides.

In vitro Dbait and Irradiation Treatments and Cell Survival Assay

Dbait (1.25 mg.L^{-1}) or transfection control, complexed with 11 kDa polyethylenimine (PEI) (Polypus-transfection, Illkirch, France) were used to treat the cells as previously published (18, 21). Cells were incubated during 5 h for transfection in serum-free RPMI medium (in twenty-four-well plates). After transfection, the medium was removed and replaced with complete DMEM (Gibco, Cergy Pontoise, France) (18). Cells were then subjected to 2.5-Gy irradiation, using a ^{137}Cs unit (0.5 Gy/min). Nine days later, cell fixation (paraformaldehyde 4%) and permeabilization (Triton X100 0.5%) were done, and the number of nuclei was estimated following staining with TO-PRO3 for 10 min. Nuclear staining signals were determined by imaging with an infrared scanner (LI-COR Odyssey).

Western Blot

Cells were harvested and boiled 10 min in Laemmli buffer and subjected to SDSPAGE. Proteins were transferred to nitrocellulose membranes, blocked by incubation (1 h) with Odyssey buffer (LI-COR Biosciences, Lincoln, NE, USA). Membranes were incubated overnight at 4°C with primary antibody diluted in Odyssey buffer. Depending on primary antibodies, the membranes were then probed with goat secondary antibodies (anti-mouse or anti-rabbit) conjugated to Alexa Fluor 680 (Invitrogen) or IRdye 800 (Rockland Immunochemicals, Gilbertsville, PA, USA). Anti-γ-H2AX (Upstate, Millipore, Molsheim, France) and anti-β-actin clone AC-15 mouse monoclonal antibodies (Sigma-Aldrich, Saint-Quentin-Fallavier, France) were used. The obtained signals were analyzed with the Odyssey Infrared Imaging System (LI-COR Biosciences) and Odyssey software.

Dbait and Irradiation Treatments in Mice

Xenografts derived from cell lines (CDX) and patient derived xenograft (PDX; ODA-17GIR, GBM-1-HAM, GBM-14-RAV, GBM-14-CHA, ODA-4-GEN) were, respectively obtained by injecting 4×10^6 cells of each cell line into the flank, and by successive grafting into scapular area of adult female nude mice (Swiss nu/nu, 6–8 weeks, Janvier, Le Genest Saint Isle, France) (10). Small fragments of PDX tumors were grafted subcutaneously into the flank of nude mice before experiments. When the tumor volume were around 125 mm^3, mice were divided into uniform groups ($n = 6$ to 12) (18): no treatment (*NT*), RT alone for 2 weeks (RT_{2w}: 6x5Gy), Dbait alone for 2 weeks (*Dbait*: 6x3nmol) and RT + Dbait for 2 weeks (RT_{2w}+*Dbait* 6x5Gy+6x3nmol). We had previously checked

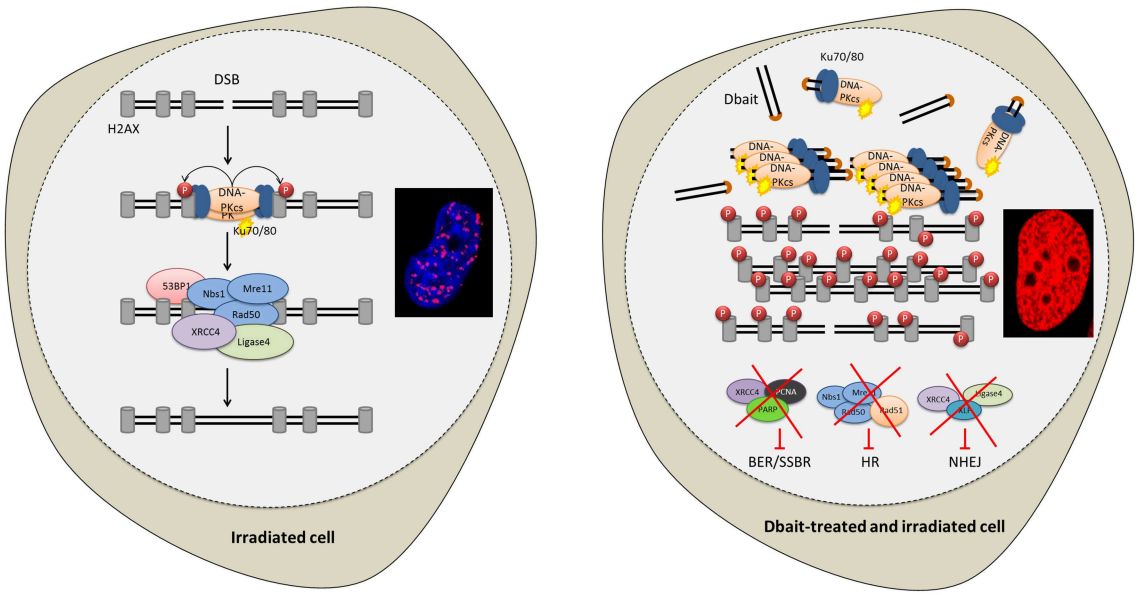

FIGURE 1 | Disrupting DNA repair with Dbait molecules. Radiation and Dbait treatment induce DNA repair signaling disturbance. Dbait recognize and activates DNA-PK complex leading to its activation and its subsequent nuclear targets phosphorylation visualized by pan-nuclear γ-H2AX. When a DSB occurs in the DNA, the DNA damage signaling system activated by Dbait is spread across modified chromatin and prevents the arrival of proteins involved in DSB repair at site of the damage. Consequently, both non-homologous end joining (NHEJ) and homologous recombination (HR) were inhibited. Moreover, Dbait can also recognize PARP (mainly involved in BER and SSBR) causing its autoPARylation and leading to several BER and SSBR proteins recruitment on Dbait molecules. All these factors are thus hijacked far from the DNA damage site causing to BER/SSBR inhibition.

that mock treated animals did not show any change in tumor growth or survival as compared to animals only treated with or without RT (21). In the same way as beforehand (18), Dbait molecules with *in vivo*-jet polyethylenimine (PEI) reagent (Polyplus Transfection) at the N/P ratio 6 were diluted in 100 μL of 5% glucose. Dbait was combined with PEI to facilitate cellular delivery (21). Prior to injection, the Dbait-PEI mixture was incubated for 15 min at room temperature. Dbait intratumoral injections were realized 5 h before each RT session. To deliver RT by a ^{137}Cs unit (0.5 Gy/min), a shield was conceived to spare about two-thirds of the animal's body. Doses were measured by thermoluminescence dosimetry. Tumors were monitored for all experiments with a digital caliper every 2–3 days. The formula (length × width × width/2) was used to calculate the tumor volumes. Mice weight was determined every week and followed up for 200 days. When tumors attained 2000 mm^3, animals were sacrificed according to ethical recommendations. All animals were housed in our animal facility, and all experiments were approved by the Local Committee on Ethics of Animal Experimentation.

Immunofluorescence Staining and Dog MRI

The MRI of a boxer dog having spontaneously developed a brain tumor was performed at the Veterinary School of Maisont-Alfort (94-France) by Dr. P. Devauchelle and tumor samples were obtained with the consent of the dog owner. For immunofluorescence staining, cells were processed as previously described (20, 30). Microscopy was performed at room temperature with the Leica SP5 confocal system, attached to a DMI6000 stand, with a 636/1.4 oil immersion objective. Images were processed with the freely available ImageJ software (http:// rsb.info.nih.gov.gate1.inist.fr/ij/) and the Leica SP5 confocal system.

Antibodies and Validation for RPPA

We explored 39 total proteins, 26 phosphoproteins and then calculated 23 ratios of phosphoproteins on total proteins giving a total of 88 protein biomarkers (**Table S1**) involved in 10 different signaling pathways: tyrosine kinase signaling, SAPK/JNK signaling, stress signaling, DNA repair, PI3K pathway, apoptosis, cell cycle, adhesion/cytoskeleton, MAPK/ERK signaling and NFκB signaling. As reported earlier, before being used in RPPA, the antibodies quality and specificity were confirmed by Western blotting on a large panel of cell lines (25).

Reverse Phase Protein Array (RPPA)

Proteins from 11 subcutaneous xenograft models were analyzed (6 replicates with 2 different locations in three different tumors per model). Tumors were mechanically dissociated (10) and protein concentration was determined using the Reducing Agent Compatible BCA kit (Pierce, Rockford, USA). The samples were then processed using previously reported method (10). Briefly, serial dilutions of samples (from 2 to 0.125 mg/ml) were placed on nitrocellulose-covered slides (2470 Arrayer, Aushon Biosystems, Billerica, MA) before incubation overnight at 4 °C with specific antibodies. Slides were

then probed with horseradish peroxidase-coupled secondary antibodies (Jackson ImmunoResearch, Newmarket, UK) for 1 h at room temperature. After an amplification step, the arrays were probed with Cy5-streptavidin (Jackson ImmunoResearch) for 1 h at room temperature. Finally, the processed slides were scanned with a GenePix 4000B microarray scanner (Molecular Devices, Sunnyvale, CA) and Spot intensity was evaluated with MicroVigene 4.0.0.0 software (VigeneTech Inc., Carlisle, MA). Quantification of the data was done with SuperCurve (31), and the data were normalized against negative control slides and Sypro Ruby slides.

Statistical Analysis

Data analysis was realized with R v2.15.1 (http://www.cran.r-project.org). The tests were two-sided, with a Type I error set at $\alpha = 0.05$. To explore variations between groups, Mann-Whitney tests were done according to sample size, and if assumptions of parametric test are not met (normality and homoscedasticity). The Kaplan–Meier method was used to draw the survival curves. The log-rank test was used to compare the survival fraction of groups (NT: not treated, RT or RT+Dbait). $P \leq 0.05$ was considered to be a significant difference.

RESULTS

Dbait Disorganizes Repair of Radio-Induced DNA Damage in High Grade Glioma Cell Lines and Leads Proliferation Inhibition

In a previous study, we have shown that Dbait lead to activation of the DNA-dependent protein kinase (DNA-PK) (20). This hyperactivation triggers phosphorylation of H2AX and other markers such as RPA32, CHK2 and HSP90 (20, 30), prevents detection of the radio-induced DSBs and further recruitment of DNA repair enzymes at damage site (**Figure 1**). First, we tested the potential of Dbait to induce DNA-PK activation in human glioblastoma cell lines by assaying phosphorylated H2AX proteins by Western blot in the 9 high grade glioma cell lines. Western blot analysis showed that in all the glioma cell lines except in the DNA-PK deficient MO59J cell line, Dbait induced phosphorylation of H2AX (**Figure 2A**). As already published (20) Dbait induced phosphorylation of H2AX is strictly dependent of DNA-PKcs kinase activity. In contrast, irradiation induced γ-H2AX foci that are mainly due to ATM activation, in all cell lines including MO59J. Combining Dbait and irradiation induced equal to superior level of γ-H2AX. The level of H2AX was not significantly affected by the various treatments (**Supplementary Figure 1**). As we had access to samples from a dog that spontaneously developed a glioblastoma (**Figure 2B**), we confirmed that Dbait induced phosphorylation of both H2AX and HSP90 in dissociated cells from the brain tumor (**Figure 2C**). As previously observed, γ-H2AX formed foci after irradiation, at location of radio-induced DNA DSB in irradiated cells whereas it distributed all over the chromatin after Dbait treatment (in at least 65% of the cells), showing DNA-PK activation in absence of chromosome damage (20).

The consequences of DNA-PK hyperactivation for cell survival after irradiation were investigated. Nine high-grade glioma cell lines were treated with Dbait or control (Dbait-8h) 5 h before RT to allow DNA-PK activation before inducing damage (**Figure 3**). As we have previously reported (18), without RT, Dbait treatment itself was able to decrease cell survival. For 6/9 cell lines (MO59K, SF763, SNB19, U118MG, U87MG, and T98G), the combination of Dbait and RT led to a significant radiosensitization ($p < 0.05$). SF763 was sensitized only at the highest dose of Dbait. For 3/9 cell lines (CB193, MO59J and SF767), radiosensitization was not statistically significant. γ-H2AX increase after Dbait treatment was observed in SF767 (**Figure 2**) eliminating the possibility that the lack of sensitization could be due to defect in transfection or incapacity to activate DNA-PKcs as it is the case of MO59J cells.

Radiosensitizing Effect of Intratumoral Injections of Dbait *in vivo*

We have recently shown that protein status are well conserved between cell lines and tumors formed by xenografting of these cell lines (25). However, micro-environment plays an important role in tumor cell response to treatment and could modify therapy response. Therefore, we reproduced our survival analysis *in vivo* using athymic nude mice bearing glioma CDX obtained by grafting the cell lines characterized *in vitro*. Among the 9 cell lines tested *in vitro*, only six models form tumors with enough efficacy and homogeneity to allow *in vivo* treatment efficiency study. Consistent with one of the currently used stereotactic RT protocols for the reirradiation of high grade glioma (32), 6 fractions of 5 Gy were given locally over a 2 weeks period. Dbait was administered locally 5 h prior to RT, every other day (for a total of 6 sessions; **Figure 4A**). The combined treatment (RT_{2w}+Dbait) significantly decreased tumor growth and enhanced survival of 3/6 models (**Figure 4B**). The survival enhancement by addition of Dbait to radiotherapy in U118MG, SF763 and T98G was, respectively of 129, 136 and 234%. SF763 which was sensitized only at the highest dose of Dbait *in vitro* appeared to be sensitive to Dbait addition to radiotherapy *in vivo*. The CB193 and SF767 models were not radiosensitized consistently with *in vitro* results. Dbait effect did not depend upon the tumor growth speed. While U87MG cells were radiosensitized *in vitro* (**Figure 3**), addition of Dbait to radiotherapy had no impact on survival of U87-MG *in vivo* models.

In order to confirm that the Dbait effect is not a specificity of CDX models we performed in parallel a similar analysis on five PDX directly derived from patient samples (**Figure 4C**). Three were radiosensitized by Dbait with increase in survival compared to RT alone of 125% for GBM-14-RAV, 128% for GBM-14-CHA and 188% for ODA-4-GEN. The two other models (ODA-17-GIR and GBM-1-HAM) were not radiosensitized by such a treatment. Interestingly, in all the treated animal models, no significant skin toxicity was observed in irradiated and Dbait-treated healthy tissue. Depending on *in vivo* model, tumor growth after Dbait

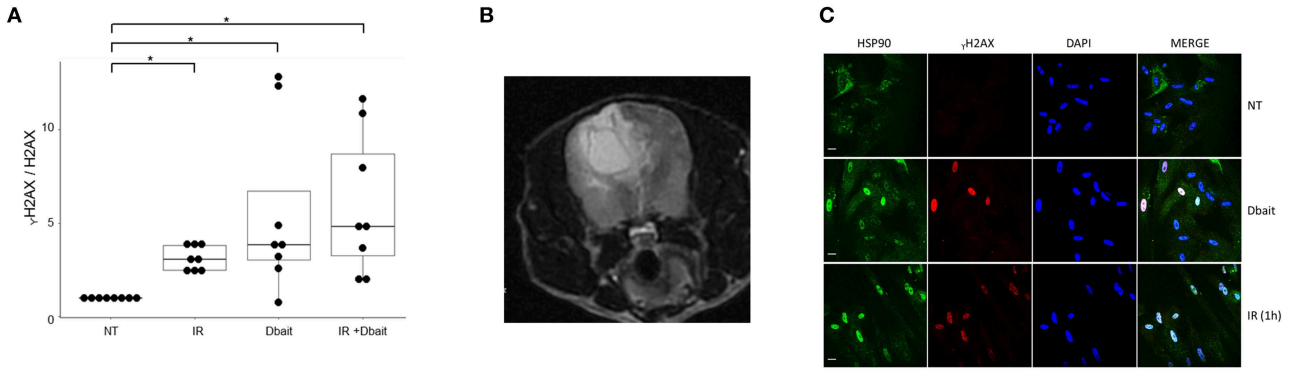

FIGURE 2 | γH2AX induction in gliomas cells after Dbait treatment. **(A)** γH2AX induction in human gliomas cell lines after Dbait treatment. The nine glioma cell lines were untreated (NT), irradiated (IR, 10Gy), treated with Dbait (5h) or treated with Dbait and irradiated. One hour after treatment completion, total proteins were electrophoresed followed by immunobloting. The blots were analyzed using the Odyssey Infrared Imaging System (LI-COR Biosciences) and Odyssey software. The induction of γH2AX (γH2AX on H2AX ratio) is presented. Mann-Whitney test was performed (*$p < 0.05$). **(B)** MRI of a boxer dog with a spontaneously brain tumor. **(C)** Activation of DNA damage response in dog glioblastoma. Dissociated cells of dog glioblastoma were untreated (NT), irradiated or treated with Dbait (5 h). Cells were fixed and permeabilized after treatment before the use of anti- γH2AX, anti-HSP90 antibodies and DAPI.

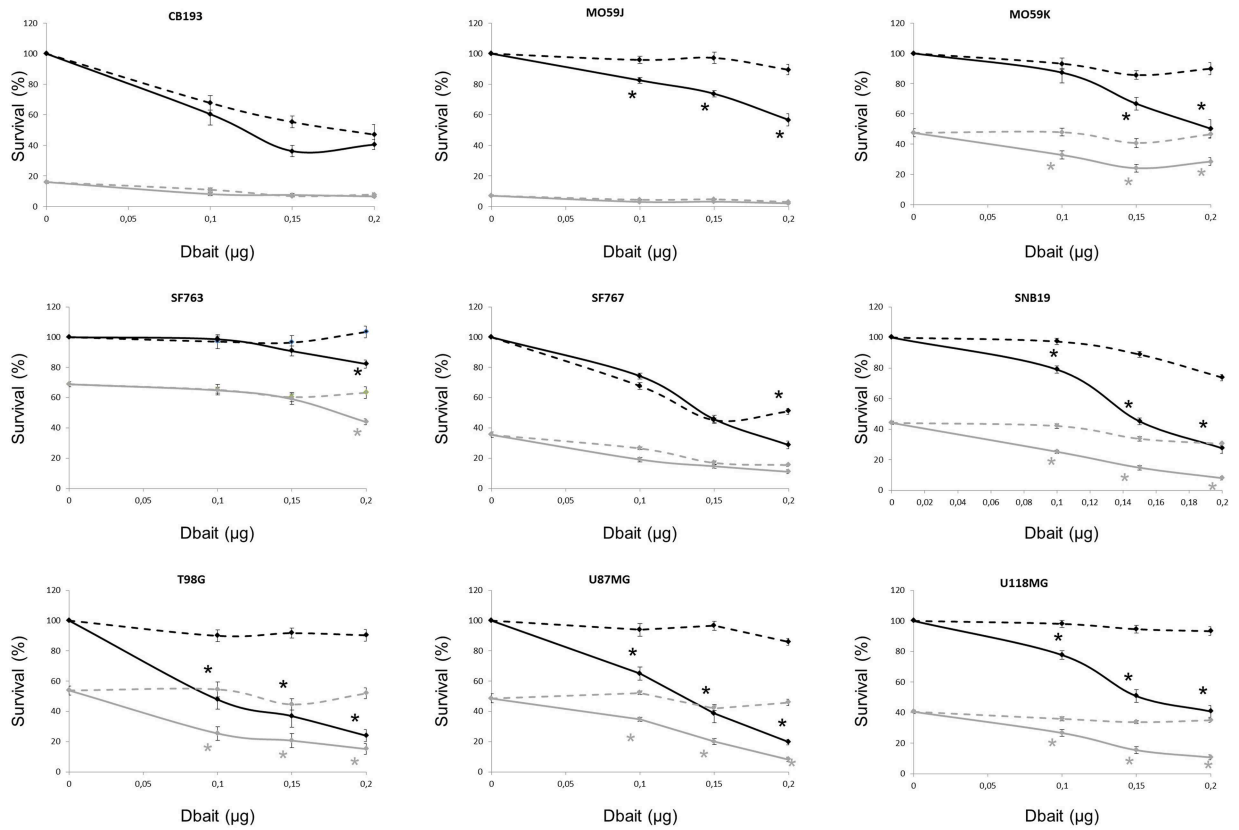

FIGURE 3 | Dbait impact on cell survival. Cell survival assay of high grade glioma cell lines were treated with Dbait (solid line) or control (dotted line). Cells were irradiated at 2.5Gy (gray line) or not (black line) 5 h after Dbait treatment. Data are represented as mean values ± standard error. Mann-Whitney test was performed (*$p < 0.05$).

treatment alone, was at the best very similar to those observed following RT alone, making the combination a better option in most of the cases.

Predictive Biomarkers of Dbait Efficacy

We then used a RPPA approach to identify protein biomarkers predictive of Dbait response of the 6 CDX and 5 PDX to

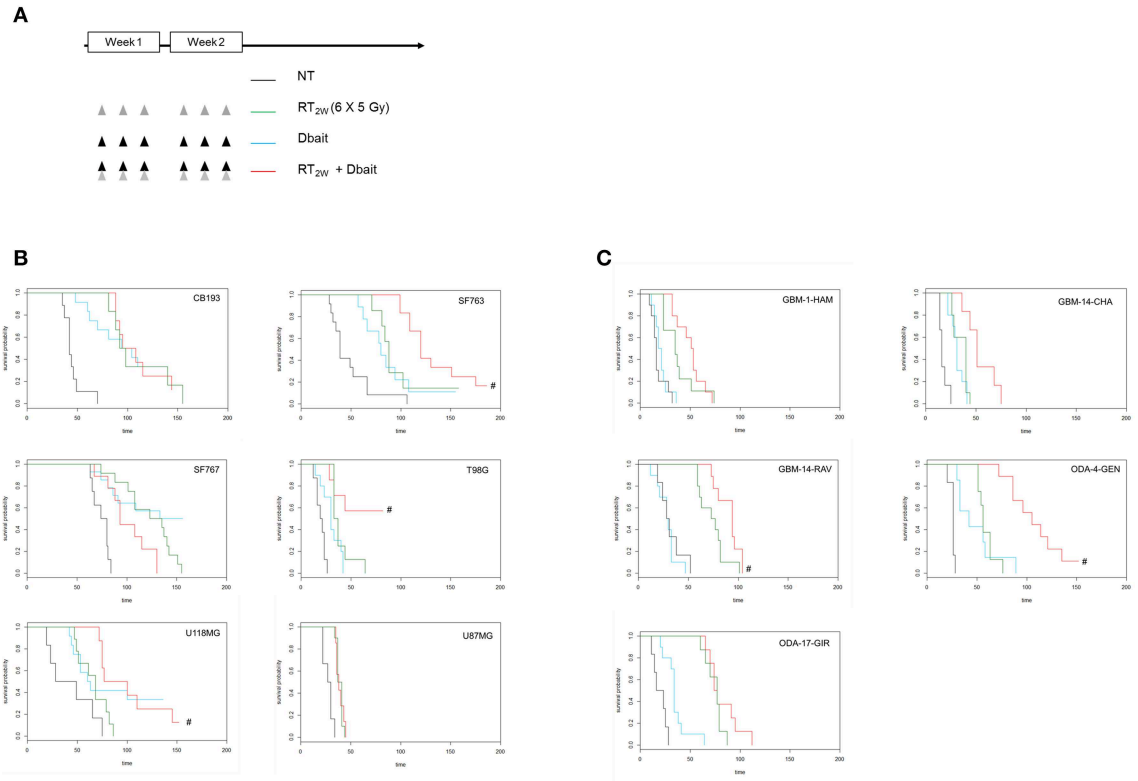

FIGURE 4 | Effect of Dbait combined with radiation *in vivo*. **(A)** Xenograft models were treated with hypofractionated radiotherapy (RT; 6x5Gy in 2 weeks; green), Dbait (6 local administrations in 2 weeks; blue) or a combination of Dbait and RT (red) or untreated (black). For Cell lines Derived Xenografts (CDX, **B**) and for Patient Derived xenograft (PDX, **C**) the survival curves of groups were plotted according to the Kaplan–Meier method. The survival fraction of groups was compared using log-rank test. #$p < 0.05$ between RT_{2W} and RT_{2W}+Dbait.

RT+Dbait. Eighty-eight protein markers were analyzed: 39 total proteins, 26 phosphoproteins and 23 ratios of phosphoproteins/total proteins were analyzed. A Mann-Whitney test was performed between radiosensitized and not radiosensitized xenografts. We identified 2/88 protein biomarkers predictive of Dbait efficacy: the two most significant biomarkers were the ratio of phosphorylated forms on native forms of the two repair proteins NBS1 and H2AX. Actually Phospho-H2AX/H2AX ($p = 0.05$, fold change = 2.2) and Phospho-NBS1/NBS1 ($p < 0.01$, fold change = 1.6) were significantly higher in the xenografts that were not radiosensitized (**Figure 5**). Interestingly, Phospho-H2AX was not sufficient ($p = 0.66$) to predict sensitivity to Dbait radiosensitizing effect. The total amount of H2AX, which has been shown to vary extensively between cell lines (**Figure 1**) and tumors was also not predictive of the Dbait radiosensitization ($p = 0.66$) however their ratio became highly indicative ($p = 0.05$).

DISCUSSION

The resistance of cancer cells to RT is increased by efficient DNA repair activity (18, 33, 34). In the past years, many DNA repair inhibitors have been developed (18, 35–39). These strategies are mainly based on specific target inhibition. They may be overpassed by target mutation or activation of another repair pathway. On the other hand, Dbait is not a specific enzyme inhibitor. It represents a new drug strategy targeting the whole DNA DSB repair system via perturbation of DNA repair signaling (18, 20, 21). On the one side, the DNA DSB signaling system induced by Dbait is dispersed all over the chromatin and inhibits the recruitment of the DSB repair proteins at damage site. On the other side, Dbait molecules can also be recognized by PARP [major protein involved in base excision repair (BER) and single strand break repair (SSBR)]. This leads to its autoPARylation which allows the recruitment of various BER and SSBR proteins on Dbait molecules inducing BER/SSBR inhibition (18, 40).

In the present study, Dbait molecules were used to radiosensitize human high grade glioma. The experimental design was planned to assay the clinical relevance of a current hypofractionated stereotactic RT protocol used for high grade glioma reirradiation (32) and local administration of Dbait. Hypofractionated stereotactic RT is particularly interesting due to its ability to precisely deliver high doses of RT to a specific target volume in a low numbers of fractions and to spare surrounding organs at risk. Hypofractionated stereotactic RT appeared to be associated with acceptable toxicity if certain limits were observed in terms of treated volume and radiation dose

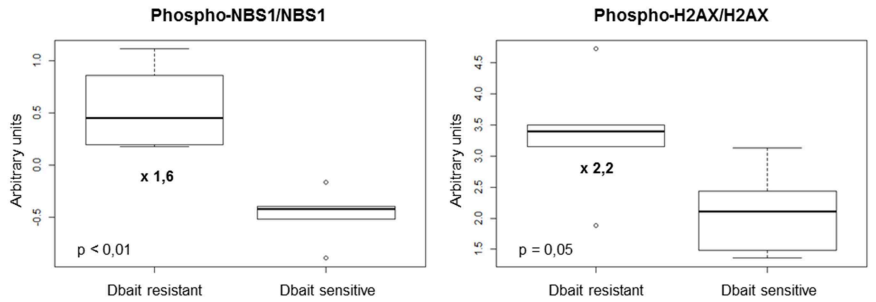

FIGURE 5 | Markers involved in Dbait treatment resistance. We analyzed a total of 88 proteic markers (see **Table S1**) to explore tyrosine kinase signaling, SAPK/JNK signaling, stress signaling, DNA repair, PI3K pathway, apoptosis, cell cycle, adhesion/cytoskeleton, MAPK/ERK signaling and NFκB signaling. Data obtained for 11 models (without any treatment) were analyzed with 6 replicates for each xenograft models to identify makers that can predict resistance to Dbait treatment. A Mann-Whitney test was performed ($p < 0.05$) between the two groups of models (sensitive and resistant to Dbait treatment).

(41–45). In these series, median survival was low (about 7–13 months from time of salvage treatment) suggesting a therapeutic effect in selected patients. Despite modern developments in spatial targeting, long term control of diseases is not achieved, emphasizing the need to overcome tumor radioresistance with innovative agents (10). Combined Dbait and hypofractionated stereotactic RT treatment is addressing this major challenge, and is particularly attractive to treat recurrent high grade glioma as it provides a double targeting through molecular pathway by Dbait and highly focalized ionizing radiation beam by hypofractionated stereotactic RT. This should achieve a better local control which is the main clinical objective for high grade glioma.

In this study, we used local administration of Dbait, which might limit clinical transfer in this specific indication. However, local administration to high grade glioma of different molecules has already been studied. For example, Gliadel wafer containing carmustine (BCNU) as an interstitial chemotherapy treatment is already approved for malignant glioma (46). Other modalities of local delivery such as convection-enhanced delivery have also shown preclinical and clinical promising results (22, 47, 48). Dbait distribution to the brain has already been evaluated in an RG2 rat glioma model and showed promising results (22).

One of the drawbacks of our preclinical study is that we chose to use flank xenografts rather than intracranial orthotopic xenografts (49–51). We preferred flank xenografts in this preclinical study for different reasons: the number of models and conditions tested (over 300 mice); the use of a 137Cs unit (0.5 Gy/min) which did not allow focal cerebral irradiation (necessary for 6x5Gy delivery); the need of repeated Dbait intratumoral injections; and difficulties in rigorous tumor monitoring with orthotopic xenografts by repeated imaging with high number of animals. Despite the above-cited advantages of flank xenograft models, the drawbacks include: a different microenvironment as it would be within the brain; and a lack of blood brain barrier that can alter the pharmaceutical kinetics (49–51). If the lack of blood brain barrier is not a major issue in our setting as we studied direct intratumoral injections of Dbait, the different microenvironment might significantly influence the results (52). In the past years, most documented resistance mechanisms involve secondary pathway mutations or bypass mechanisms within the tumor cells. However, the recent identification of mechanisms of therapeutic resistance that were conferred largely by alterations, not only in the tumor cells, but also in their microenvironment, indicates the importance of taking into account the tumor cell extrinsic compartments. The nature of the vasculature, the presence of cancer associated fibroblasts, the presence/absence of immune cells, the signaling network between tumor cells and stromal cells are the most studied components that could influence treatment response (52).

As previously shown, Dbait administration to mice did not increase the sensitivity of healthy tissue around the tumor to RT (18). In a previous study, we showed that Dbait does not induce cell cycle arrest (18, 20). Hence the specificity of action of Dbait in tumor cells could be due to an impairment in cell cycle checkpoints that is frequently reported in tumors. Tumors cells would be able to divide despite Dbait induced unrepaired breaks and therefore enter mitotic catastrophe. p53 mutations are often associated with this deficient cell cycle controls (18, 53). At the contrary, non-tumor cells with proficient cell cycle control stop dividing until repair is completed, that can take place when Dbait molecules have disappeared (18, 54). Therefore, Dbait, which does not make new lesions on chromosomes but prevents DNA repair of RT induced damage, is toxic for dividing tumor cells but not for healthy tissues. Dbait toxicology studies were realized in wistar rats and cynomolgus monkeys. They showed that the only side effect was a slight to moderate, dose-dependent and reversible inflammatory response at injection sites (18, 55). The tolerance of the clinical form of Dbait (called AsiDNA) in association with RT has been tested in first-in-man phase 1 trial (DRIIM) for patients with in-transit metastases of melanoma (23). No dose-limiting toxicity was observed and the maximum-tolerated dose was not reached.

Oncology has entered an era of personalized medicine in which the selection of treatments for each cancer patient becomes more individualized (56). Identifying predictive biomarkers of treatment sensitivity or resistance is becoming a major challenge.

In this study, we have chosen the RPPA technology to search for potential protein biomarkers of Dbait resistance. This technology presents many advantages: it requires only a few micrograms of protein lysate to study activation of cell signaling pathways and allows the comparison of hundreds of samples in the same experiment (10). Thus, we included replicate samples for the cell lines, and different tumor regions of multiple mice for the xenografts. We were able to obtain robust data and assess heterogeneity within and among tumors (10). Here we showed that basal Phospho-H2AX/H2AX and Phospho-NBS1/NBS1 activations [two major actors of DNA damage signaling and cell cycle control (57, 58)] were significantly correlated with Dbait resistance. Interestingly, whereas the amount of phosphorylated H2AX and NBS1 was moderately indicative of sensitivity to Dbait, the frequency of phosphorylated molecules became highly indicative suggesting that resistance is linked to the intensity of chromatin modification. These constitutive activations may reflect that tumor cells are used to survive despite a basal disturbance of DNA damage signaling and cell cycle control and thus are resistant to Dbait. We have previously reported that Dbait molecules disorganize the downstream DNA damage response notably through H2AX and NBS1 disruption (20). In models with a constitutive high level of NBS1 and H2AX activations, low-dose Dbait failed to enhance these disturbances once more and higher concentrations were required. If we compare the results obtained from Dbait-resistant CDX (CB193, SF767 and U87MG) with the ones of the corresponding cell lines, we can note that CB193 and SF797 were also Dbait-resistant *in vitro* while U87MG was Dbait-sensitive. Interestingly, concerning CB193 and SF767 cell lines, they were also the two cell lines harboring the highest level of Phospho-NBS1/NBS1 activation and among the highest level of Phospho-H2AX/H2AX activation. Concerning U87MG, the difference in Dbait response could, at least partly, be explained by the differences in the proteic profiles that can exist between a cell line and its corresponding xenograft. We have previously showed (25) that U87MG had a relatively important difference between *in vitro* and *in vivo* proteic profiles with 37/89 (42%) proteins differentially expressed with a fold change >1.5.

In this study, we provide the preclinical proof of concept that a combination of RT with Dbait (an inhibitor of DNA repair) could be of interest in the treatment of high grade glioma. A first-in-human phase I trial has evaluated the therapeutic potential of local Dbait injections in combination with RT to treat patients with in-transit metastases of melanoma and provided encouraging results (18, 23). The preclinical data we report suggest that a clinical trial combining HSRT and Dbait could be considered in the treatment of recurrence high grade glioma.

DATA AVAILABILITY

All datasets generated for this study are included in the manuscript and/or the **Supplementary Files**.

ETHICS STATEMENT

The Local Committee of Institut Curie on Ethics of Animal Experimentation approved all experiments.

AUTHOR CONTRIBUTIONS

JB and EC designed the study, collected, and analyzed the data. They also wrote the manuscript. MD designed the study and carefully revised the manuscript. NB, LdK, and FC have contributed to all experiments. They also gave important intellectual input and carefully revised the manuscript. BP have done statistical analysis and carefully revised the manuscript. PV supervised the study and contributed to data interpretation. All authors approved the final manuscript for submission.

FUNDING

This work benefited from the technical support of the Institut Curie animal facility, microscopy, experimental irradiation RADEXp and RPPA platforms. This study was supported by the Institut Curie, the Centre National de la Recherche Scientifique, and the Agence Nationale de la Recherche (ANR -08-BiotecS-009).

ACKNOWLEDGMENTS

The PDX models were provided by Dr. Marie-France Poupon and the laboratory of preclinical investigation (LIP) of Institut Curie. The dog model was provided by Patrick Devauchelle (MICEN, Creteil). We thank Marie-Christine Lienafa and Mano Sayarath (DNA Therapeutics) for technical assistance. The Institut Curie animal facility, microscopy, experimental irradiation RADEXp and RPPA platforms were very convenient to achieve this study. The Institut Curie, the Centre National de la Recherche Scientifique, and the Agence Nationale de la Recherche (ANR—08-BiotecS-009) sustained this work.

SUPPLEMENTARY MATERIAL

The Supplementary Material for this article can be found online at: https://www.frontiersin.org/articles/10.3389/fonc.2019.00549/full#supplementary-material

REFERENCES

1. Ricard D, Idbaih A, Ducray F, Lahutte M, Hoang-Xuan K, Delattre JY. Primary brain tumours in adults. *Lancet*. (2012) 379:1984–96. doi: 10.1016/S0140-6736(11)61346-9
2. Louis DN, Perry A, Reifenberger G, von Deimling A, Figarella-Branger D, Cavenee WK, et al. The 2016 World Health Organization classification of tumors of the central nervous system: a summary. *Acta Neuropathol*. (2016) 131:803–20. doi: 10.1007/s00401-016-1545-1
3. DeAngelis LM. Brain tumors. *N Engl J Med*. (2001) 344:114–23. doi: 10.1056/NEJM200101113440207
4. Stupp R, Brada M, Bent MJ van den, Tonn JC, Pentheroudakis G. High-grade glioma: ESMO Clinical Practice Guidelines for diagnosis, treatment and follow-up. *Ann Oncol*. (2014) 25:iii93–101. doi: 10.1093/annonc/mdu050

5. Stupp R, Hegi ME, Mason WP, van den Bent MJ, Taphoorn MJB, Janzer RC, et al. Effects of radiotherapy with concomitant and adjuvant temozolomide versus radiotherapy alone on survival in glioblastoma in a randomised phase III study: 5-year analysis of the EORTC-NCIC trial. *Lancet Oncol*. (2009) 10:459–66. doi: 10.1016/S1470-2045(09)70025-7
6. Stupp R, Mason WP, van den Bent MJ, Weller M, Fisher B, Taphoorn MJB, et al. Radiotherapy plus concomitant and adjuvant temozolomide for glioblastoma. *N Engl J Med*. (2005) 352:987–96. doi: 10.1056/NEJMoa043330
7. Walker MD, Green SB, Byar DP, Alexander EJ, Batzdorf U, Brooks WH, et al. Randomized comparisons of radiotherapy and nitrosoureas for the treatment of malignant glioma after surgery. *N Engl J Med*. (1980) 303:1323–29. doi: 10.1056/NEJM198012043032303
8. Walker MD, Strike TA, Sheline GE. An analysis of dose-effect relationship in the radiotherapy of malignant gliomas. *Int J Radiat Oncol Biol Phys*. (1979) 5:1725–31.
9. Bleehen NM, Stenning SP. A medical research council trial of two radiotherapy doses in the treatment of grades 3 and 4 astrocytoma. The Medical Research Council Brain Tumour Working Party. *Br J Cancer*. (1991) 64:769–774.
10. Biau J, Chautard E, De Koning L, Court F, Pereira B, Verrelle P, et al. Predictive biomarkers of resistance to hypofractionated radiotherapy in high grade glioma. *Radiat Oncol*. (2017) 12:123. doi: 10.1186/s13014-017-0858-0
11. Khan N, Khan MK, Almasan A, Singh AD, Macklis R. The evolving role of radiation therapy in the management of malignant melanoma. *Int J Radiat Oncol Biol Phys*. (2011) 80:645–54. doi: 10.1016/j.ijrobp.2010.12.071
12. Stevens G, McKay MJ. Dispelling the myths surrounding radiotherapy for treatment of cutaneous melanoma. *Lancet Oncol*. (2006) 7:575–83. doi: 10.1016/S1470-2045(06)70758-6
13. Ward JF. DNA damage and repair. *Basic Life Sci*. (1991) 58:403–15.
14. Burkart W, Jung T, Frasch G. Damage pattern as a function of radiation quality and other factors. *C R Acad Sci III, Sci Vie*. (1999) 322:89–101.
15. Radford IR. The level of induced DNA double-strand breakage correlates with cell killing after X-irradiation. *Int J Radiat Biol Relat Stud Phys Chem Med*. (1985) 48:45–54.
16. Bradbury PA, Middleton MR. DNA repair pathways in drug resistance in melanoma. *Anticancer Drug*. (2004) 15:421–426. doi: 10.1097/01.cad.0000127665.74096.93
17. Wang C, Lees-Miller SP. Detection and repair of ionizing radiation-induced DNA double strand breaks: new developments in nonhomologous end joining. *Int J Radiat Oncol Biol Phys*. (2013) 86:440–449. doi: 10.1016/j.ijrobp.2013.01.011
18. Biau J, Devun F, Jdey W, Kotula E, Quanz M, Chautard E, et al. A preclinical study combining the DNA repair inhibitor Dbait with radiotherapy for the treatment of melanoma. *Neoplasia*. (2014) 16:835–44. doi: 10.1016/j.neo.2014.08.008
19. Helleday T, Petermann E, Lundin C, Hodgson B, Sharma RA. DNA repair pathways as targets for cancer therapy. *Nat Rev Cancer*. (2008) 8:193–204. doi: 10.1038/nrc2342
20. Quanz M, Chassoux D, Berthault N, Agrario C, Sun JS, Dutreix M. Hyperactivation of DNA-PK by double-strand break mimicking molecules disorganizes DNA damage response. *PLoS ONE*. (2009) 4:e6298. doi: 10.1371/journal.pone.0006298
21. Quanz M, Berthault N, Roulin C, Roy M, Herbette A, Agrario C, et al. Small-molecule drugs mimicking DNA damage: a new strategy for sensitizing tumors to radiotherapy. *Clin Cancer Res*. (2009) 15:1308–16. doi: 10.1158/1078-0432.CCR-08-2108
22. Coquery N, Pannetier N, Farion R, Herbette A, Azurmendi L, Clarencon D, et al. Distribution and radiosensitizing effect of cholesterol-coupled dbait molecule in rat model of glioblastoma. *PLoS ONE*. (2012) 7:e40567. doi: 10.1371/journal.pone.0040567
23. Le Tourneau C, Dreno B, Kirova Y, Grob JJ, Jouary T, Dutriaux C, et al. First-in-human phase I study of the DNA-repair inhibitor DT01 in combination with radiotherapy in patients with skin metastases from melanoma. *Br J Cancer*. (2016) 114:1199–205. doi: 10.1038/bjc.2016.120
24. Hayes DF. Biomarker validation and testing. *Mol Oncol*. (2015) 9:960–966. doi: 10.1016/j.molonc.2014.10.004
25. Biau J, Chautard E, Court F, Pereira B, Verrelle P, Devun F, et al. Global conservation of protein status between cell lines and xenografts. *Transl Oncol*. (2016) 9:313–321. doi: 10.1016/j.tranon.2016.05.005
26. Henry NL, Hayes DF. Cancer biomarkers. *Mol Oncol*. (2012) 6:140–146. doi: 10.1016/j.molonc.2012.01.010
27. Gallagher RI, Espina V. Reverse phase protein arrays: mapping the path towards personalized medicine. *Mol Diagn Ther*. (2014) 18:619–630. doi: 10.1007/s40291-014-0122-3
28. Masuda M, Yamada T. Signaling pathway profiling by reverse-phase protein array for personalized cancer medicine. *Biochim Biophys Acta*. (2015) 1854:651–7. doi: 10.1016/j.bbapap.2014.10.014
29. Akbani R, Becker KF, Carragher N, Goldstein T, de Koning L, Korf U, et al. Realizing the promise of reverse phase protein arrays for clinical, translational, and basic research: a workshop report: the RPPA (Reverse Phase Protein Array) society. *Mol Cell Proteom*. (2014) 13:1625–43. doi: 10.1074/mcp.O113.034918
30. Quanz M, Herbette A, Sayarath M, de Koning L, Dubois T, Sun JS, et al. Heat shock protein 90α (Hsp90α) is phosphorylated in response to DNA damage and accumulates in repair foci. *J Biol Chem*. (2012) 287:8803–15. doi: 10.1074/jbc.M111.320887
31. Troncale S, Barbet A, Coulibaly L, Henry E, He B, Barillot E, et al. NormaCurve: a SuperCurve-based method that simultaneously quantifies and normalizes reverse phase protein array data. *PLoS ONE*. (2012) 7:e38686. doi: 10.1371/journal.pone.0038686
32. Vordermark D, Kölbl O, Ruprecht K, Vince GH, Bratengeier K, Flentje M. Hypofractionated stereotactic re-irradiation: treatment option in recurrent malignant glioma. *BMC Cancer*. (2005) 5:55. doi: 10.1186/1471-2407-5-55
33. Zhu Y, Hu J, Hu Y, Liu W. Targeting DNA repair pathways: a novel approach to reduce cancer therapeutic resistance. *Cancer Treat Rev*. (2009) 35:590–6. doi: 10.1016/j.ctrv.2009.06.005
34. Lord CJ, Ashworth A. The DNA damage response and cancer therapy. *Nature*. (2012) 481:287–94. doi: 10.1038/nature10760
35. Chalmers AJ, Lakshman M, Chan N, Bristow RG. Poly(ADP-ribose) polymerase inhibition as a model for synthetic lethality in developing radiation oncology targets. *Semin Radiat Oncol*. (2010) 20:274–81. doi: 10.1016/j.semradonc.2010.06.001
36. Sarkaria JN. Identifying inhibitors of ATM and ATR kinase activities. *Methods Mol Med*. (2003) 85:49–56. doi: 10.1385/1-59259-380-1:49
37. Shinohara ET, Geng L, Tan J, Chen H, Shir Y, Edwards E, et al. DNA-dependent protein kinase is a molecular target for the development of noncytotoxic radiation-sensitizing drugs. *Cancer Res*. (2005) 65:4987–92. doi: 10.1158/0008-5472.CAN-04-4250
38. Kashishian A, Douangpanya H, Clark D, Schlachter ST, Eary CT, Schiro JG, et al. DNA-dependent protein kinase inhibitors as drug candidates for the treatment of cancer. *Mol Cancer Ther*. (2003) 2:1257–64.
39. Raju U, Riesterer O, Wang ZQ, Molkentine DP, Molkentine JM, Johnson FM, et al. Dasatinib, a multi-kinase inhibitor increased radiation sensitivity by interfering with nuclear localization of epidermal growth factor receptor and by blocking DNA repair pathways. *Radiother Oncol*. (2012) 105:241–249. doi: 10.1016/j.radonc.2012.08.010
40. Croset A, Cordelières FP, Berthault N, Buhler C, Sun JS, Quanz M, et al. Inhibition of DNA damage repair by artificial activation of PARP with siDNA. *Nucleic Acids Res*. (2013) 41:7344–55. doi: 10.1093/nar/gkt522
41. McKenzie JT, Guarnaschelli JN, Vagal AS, Warnick RE, Breneman JC. Hypofractionated stereotactic radiotherapy for unifocal and multifocal recurrence of malignant gliomas. *J Neurooncol*. (2013) 113:403–9. doi: 10.1007/s11060-013-1126-2
42. Yazici G, Cengiz M, Ozyigit G, Eren G, Yildiz F, Akyol F, et al. Hypofractionated stereotactic reirradiation for recurrent glioblastoma. *J Neurooncol*. (2014) 120:117–23. doi: 10.1007/s11060-014-1524-0
43. Khalil T, Lemaire JJ, Dedieu V, Donnarieix D. MRI tumor response and clinical outcomes after LINAC radiosurgery on 50 patients with recurrent malignant gliomas. *J Radiosurg SBRT*. (2013) 4:291–305.
44. Noël G, Mazeron JJ. [Reirradiation in primary or secondary brain tumors]. *Cancer Radiother*. (2010) 14:421–37. doi: 10.1016/j.canrad.2010.06.014
45. Noël G, Ben Ammar CN, Feuvret L, Valery CA, Cornu P, Boisserie G, et al. [Results of salvage stereotactic radiosurgery in 14 patients with grade III or IV gliomas]. *Rev Neurol*. (2004) 160:539–545.
46. Brem H, Piantadosi S, Burger PC, Walker M, Selker R, Vick NA, et al. Placebo-controlled trial of safety and efficacy of intraoperative controlled

delivery by biodegradable polymers of chemotherapy for recurrent gliomas. The Polymer-brain Tumor Treatment Group. *Lancet*. (1995) 345:1008–12.
47. Frosina G. Advances in drug delivery to high grade gliomas. *Brain Pathol*. (2016) 26:689–700. doi: 10.1111/bpa.12423
48. Jahangiri A, Chin AT, Flanigan PM, Chen R, Bankiewicz K, Aghi MK. Convection-enhanced delivery in glioblastoma: a review of preclinical and clinical studies. *J Neurosurg*. (2016) 126:1–10. doi: 10.3171/2016.1.JNS151591
49. Miyai M, Tomita H, Soeda A, Yano H, Iwama T, Hara A. Current trends in mouse models of glioblastoma. *J Neurooncol*. (2017) 135:423–32. doi: 10.1007/s11060-017-2626-2
50. Kegelman TP, Hu B, Emdad L, Das SK, Sarkar D, Fisher PB. *In vivo* modeling of malignant glioma: the road to effective therapy. *Adv Cancer Res*. (2014) 121:261–330. doi: 10.1016/B978-0-12-800249-0.00007-X
51. Stylli SS, Luwor RB, Ware TMB, Tan F, Kaye AH. Mouse models of glioma. *J Clin Neurosci*. (2015) 22:619–26. doi: 10.1016/j.jocn.2014.10.013
52. Junttila MR, de Sauvage FJ. Influence of tumour micro-environment heterogeneity on therapeutic response. *Nature*. (2013) 501:346–54. doi: 10.1038/nature12626
53. Roemer K. Mutant p53: gain-of-function oncoproteins and wild-type p53 inactivators. *Biol Chem*. (1999) 380:879–87. doi: 10.1515/BC.1999.108
54. Vermeulen K, Van Bockstaele DR, Berneman ZN. The cell cycle: a review of regulation, deregulation and therapeutic targets in cancer. *Cell Prolif*. (2003) 36:131–149. doi: 10.1046/j.1365-2184.2003.00266.x
55. Schlegel A, Buhler C, Devun F, Agrario C, Urien S, Lokiec F, et al. Pharmacokinetics and toxicity in rats and monkeys of coDbait: a therapeutic double-stranded DNA oligonucleotide conjugated to cholesterol. *Mol Ther Nucleic Acids*. (2012) 1:e33. doi: 10.1038/mtna.2012.27
56. La Thangue NB, Kerr DJ. Predictive biomarkers: a paradigm shift towards personalized cancer medicine. *Nat Rev Clin Oncol*. (2011) 8:587–96. doi: 10.1038/nrclinonc.2011.121
57. Komatsu K. NBS1 and multiple regulations of DNA damage response. *J Radiat Res*. (2016) 57 (Suppl 1):i11–i17. doi: 10.1093/jrr/rrw031
58. Turinetto V, Giachino C. Multiple facets of histone variant H2AX: a DNA double-strand-break marker with several biological functions. *Nucleic Acids Res*. (2015) 43:2489–2498. doi: 10.1093/nar/gkv061

Conflict of Interest Statement: MD is cofounder of DNA Therapeutics, Onxeo.

The remaining authors declare that the research was conducted in the absence of any commercial or financial relationships that could be construed as a potential conflict of interest.

Copyright © 2019 Biau, Chautard, Berthault, de Koning, Court, Pereira, Verrelle and Dutreix. This is an open-access article distributed under the terms of the Creative Commons Attribution License (CC BY). The use, distribution or reproduction in other forums is permitted, provided the original author(s) and the copyright owner(s) are credited and that the original publication in this journal is cited, in accordance with accepted academic practice. No use, distribution or reproduction is permitted which does not comply with these terms.

frontiers in Oncology

ORIGINAL RESEARCH
published: 23 July 2019
doi: 10.3389/fonc.2019.00660

Flavonoid Derivative of *Cannabis* Demonstrates Therapeutic Potential in Preclinical Models of Metastatic Pancreatic Cancer

Michele Moreau[1,2], *Udoka Ibeh*[1,3], *Kaylie Decosmo*[1,4], *Noella Bih*[1], *Sayeda Yasmin-Karim*[1], *Ngeh Toyang*[5], *Henry Lowe*[5] *and Wilfred Ngwa*[1,2]*

[1] Brigham and Women's Hospital, Dana-Farber Cancer Institute, Harvard Medical School, Boston, MA, United States, [2] Department of Physics, University of Massachusetts Lowell, Lowell, MA, United States, [3] Department of Biology, University of Massachusetts Boston, Boston, MA, United States, [4] Department of CaNCURE Program, Northeastern University, Boston, MA, United States, [5] Flavocure Biotech Inc., Baltimore, MD, United States

Pancreatic cancer is particularly refractory to modern therapies, with a 5-year survival rate for patients at a dismal 8%. One of the significant barriers to effective treatment is the immunosuppressive pancreatic tumor microenvironment and development of resistance to treatment. New treatment options to increase both the survival and quality of life of patients are urgently needed. This study reports on a new non-cannabinoid, non-psychoactive derivative of cannabis, termed FBL-03G, with the potential to treat pancreatic cancer. *In vitro* results show major increase in apoptosis and consequential decrease in survival for two pancreatic cancer models- Panc-02 and KPC pancreatic cancer cells treated with varying concentrations of FBL-03G and radiotherapy. Meanwhile, *in vivo* results demonstrate therapeutic efficacy in delaying both local and metastatic tumor progression in animal models with pancreatic cancer when using FBL-03G sustainably delivered from smart radiotherapy biomaterials. Repeated experiments also showed significant ($P < 0.0001$) increase in survival for animals with pancreatic cancer compared to control cohorts. The findings demonstrate the potential for this new cannabis derivative in the treatment of both localized and advanced pancreatic cancer, providing impetus for further studies toward clinical translation.

Keywords: pancreatic cancer, flavonoids, cannabis, metastasis, radiotherapy, smart biomaterials

OPEN ACCESS

Edited by:
Paul N. Span,
Radboud University Nijmegen Medical Centre, Netherlands

Reviewed by:
James William Jacobberger,
Case Western Reserve University, United States
Hyuk-Jin Cha,
Seoul National University, South Korea

***Correspondence:**
Wilfred Ngwa
wngwa@lroc.harvard.edu

Specialty section:
This article was submitted to Radiation Oncology, a section of the journal Frontiers in Oncology

Received: *28 March 2019*
Accepted: *05 July 2019*
Published: *23 July 2019*

Citation:
Moreau M, Ibeh U, Decosmo K, Bih N, Yasmin-Karim S, Toyang N, Lowe H and Ngwa W (2019) Flavonoid Derivative of Cannabis Demonstrates Therapeutic Potential in Preclinical Models of Metastatic Pancreatic Cancer. Front. Oncol. 9:660. doi: 10.3389/fonc.2019.00660

INTRODUCTION

Pancreatic ductal adenocarcinoma is an antagonistic internecine ailment of the exocrine pancreas with < 8% of patients surviving within a 5-year period (1, 2). A major challenge shared by pancreatic cancers is its aggressiveness, which often metastasizes to other organs before the patient is even diagnosed (3, 4).

Current treatment options for pancreatic cancer include: surgery, chemotherapy, targeted therapy, immunotherapy, and radiation therapy. Curative treatment is available only if the tumor is found early and can be removed by surgery before metastasis. If the cancer has metastasized, the standard of care is chemotherapy, or radiotherapy. However, pancreatic cancer is notoriously defiant to current therapies including chemotherapy, radiotherapy and immunotherapy (1, 5).

Cannabinoids, which are the bioactive components of *Cannabis sativa* and their derivatives, have been investigated as both anti-cancer agents and for managing the side effects of conventional cancer treatments like chemotherapy and radiotherapy (6). Previous studies have indicated that medical cannabis derivatives could enhance survival in pancreatic cancer animal models, when used in synergy with radiotherapy (7). Smart materials for drug delivery like the smart radiotherapy biomaterials (SRBs) system have also been investigated for delivering cannabinoids into tumors to enhance radiotherapy treatment for pancreatic cancer (8). A major benefit of the SRB approach is their ability to be employed in place of currently used inert radiotherapy biomaterials (e.g., spacers, or fiducial markers) and hence their use could come at no additional inconvenience to patients.

In this study, we investigate a new non-cannabinoid, non-psychoactive derivative of cannabis, called FBL-03G, to assess its potential for the treatment of pancreatic cancer. We hypothesize that the use of FBL-03G will have therapeutic potential and can enhance radiotherapy during the treatment of pancreatic cancer. To investigate this hypothesis, *in vitro* studies were first carried out with and without radiotherapy (RT). *In vitro* studies, *in vivo* studies were also conducted in small animals employing FBL-03G sustainably delivered from smart radiotherapy biomaterials, allowing continual exposure of the tumor to the cannabis derivative payloads over time.

Apart from the antineoplastic properties of cannabis derivatives, the immune system modulative properties of these extracts have been well documented (8–12). Different volumes and concentrations of FBL-03G payloads were also investigated for their potential to generate systemic tumor responses. In particular, we investigated the abscopal effect, whereby radiotherapy (RT) at one site may lead to regression of metastatic cancer at distant sites that are not irradiated (13). The abscopal effect has been connected to mechanisms involving the immune system (14). However, the abscopal effect is rare because at the time of treatment, established immune-tolerance mechanisms may hamper the development of sufficiently robust abscopal responses. Today, the growing consensus is that combining radiotherapy with immunoadjuvants provides an opportunity to boost abscopal response rates, extending the use of radiotherapy to treatment of both local and metastatic disease (15). With in this context, the cannabis derivative FBL-03G was also investigated as a potential immunoadjuvant to radiotherapy.

MATERIALS AND METHODS

Materials and Antibody

Acetone, Dimethyl sulfoxide (DMSO), Poly (lactic-co-glycolic) acid (PLGA) (M.W.: 50–50 kDa), and Crystal Violet dye were acquired from Sigma-Aldrich. The Harvard apparatus was obtained from Harvard Bioscience (Holliston, MA, USA), and silicone tubing (ID 1/32″) was purchased from Saint-Gobain Performance Plastics Laboratory Division (USA). Brachytherapy needles were purchased from IZI Medical Products (MD, USA). All cell culture products (DMEM, RPMI, Trypsin, Fetal Bovine Serum, MEM non-essential amino acids, sodium pyruvate, β-mercaptoethanol, penicillin/streptomycin, and PBS pH 7.4) were obtained from Gibco, Thermo Fisher, and Life Technologies (Waltham, MA, USA). Flavocure Biotech Inc. (Baltimore, MD, USA) supplied the test molecule, FBL-03G with a purity of 98.7% determined by High Performance Liquid Chromatography (HPLC).

FBL-03G Synthesis

FBL-03G, a flavonoid derived from *Cannabis sativa* L., is the unnatural isomer of Cannflavin B, a metabolite of Cannabis. Through a bioactivity guided isolation approach, 11 flavonoids were isolated using flash chromatography and characterized by nuclear magnetic resonance (NMR) and mass spectrometry (MS) methods (2, 16, 17). Generated spectroscopic data for FBL-03G were similar to those of the following 11 previously isolated and characterized compounds of the Cannabis plant; apigenin (1), Chrysoeriol (2), kaempferol (3), luteolin (4), quercetin (5), vitexin (6), isovitexin (7), orientin (8) and prenylated flavonoids including Cannflavin A (9), Cannflavin B (10) and Cannflavin C (11) (**Figure S1**) (16–21). The molecules were further screened for kinase inhibition, and chrysoeriol (Cresorol) demonstrated significant activity against FLT3, FLT3-ITD, and FLT3-D835Y and moderate activity against CSF1R (2). FBL-03G demonstrated significant activity against CSF1R kinase and moderate activity against FLT3, FLT3-ITD, FLT3-D835Y, CK2a, CK2a2, Aurora A, Aurora B, Aurora C, and Pim2 (2).

Fabrication of Smart Radiotherapy Biomaterials (SRB)

This study used combination treatment of FBL-03G (Mw = 368.38 g/mol) as an immunoadjuvant, delivered from smart radiotherapy biomaterial (SRB), and radiotherapy (RT). SRBs were developed following previously reported procedures for fabricating and loading drugs into SRBs. Briefly, 300 mg of Poly (lactic-co-glycolic) acid (PLGA) polymer added to 3.5 mL of acetone was homogenously mixed into a hydrogel (8, 22). The Harvard apparatus was used to provide a constant flow rate of the mixture into the silicon tubing with inner diameter of 1/32′. The PLGA hydrogel loaded in silicon tubing was allowed to cure under 50°C for 48 h. After curing, the silicon tubing was cut to 5 mm length and the SRBs were extracted. Three different concentrations of FBL-03G, respectively, were used as payloads in the SRBs. A small animal radiation research platform (SARRP, Xtrahl, Inc., Suwanee, GA, USA) was used for radiotherapy using 220 kVp, 13 mA, (10 × 10) mm nozzle, and 0.15 mm copper (Cu) filter to deliver 6 gray (Gy) dose. In addition, computed tomography (CT) images of the mice were taken using at 65-kVp and 0.8-mA. Mice were anesthetized with isoflurane and image-guided radiotherapy was used to specifically irradiate tumors on one site as needed.

Cell Culture

Pancreatic cancer cell line, Panc-02, was obtained from the National Cancer Institute and cultured with Dulbecco's Modified Eagle's Medium (DMEM) with 10% FBS and 1% penicillin/streptomycin. Another pancreatic cancer cell line, Ptf1/p48-Cre (KPC) cells were a gift from Dr. Anirban Maitra

(MD Anderson Cancer center). KPC cell line was derived from an LSL-Kras; p53+/floxed, Pdx-cre mouse. KPC cells were cultured in RPMI media supplemented with 10% FBS, 2 mmol/L L-glutamine, 1% penicillin/streptomycin, 1% MEM non-essential amino acids, 1 mmol/L sodium pyruvate, and 0.1 mmol/L β-mercaptoethanol. All cells were cultured at 37°C in a humidified incubator with 5% CO_2.

Clonogenic Survival Assay

Actively growing monolayers of KPC and Panc-02 cancer cells were trypsinized and 300 cells per well were seeded in 6-well plates. 24 hours later, seeded cells were treated with 0, 1, 2, or 4 μM of FBL-03G concentrations per well. The cells were irradiated at 0, 2, or 4 Gy using 220 kVp energy, 13 mA, 24 h after the FBL-03G treatment. A small animal radiation research platform (SARRP) was used to deliver external beam radiation. The growing colonies (≥ 50 cells/colony) were fixed with 75% ethanol and stained with 1% crystal violet 9–12 days after treatment. Colonies were counted using ImageJ software and a percent survival was calculated following standard protocol.

Mice and Generation of Syngeneic Pancreatic Cancer Models

Wild-type C57BL/6 strain male and female mice were acquired from Taconic Biosciences, Inc. at 8-weeks old. Animal experiments followed the guidelines and regulations set by the Dana-Farber Cancer Institute Institutional Animal Care and Use Committee (IACUC). Mice maintenance in Dana-Farber Cancer Institute animal facility was in accordance with the Institutional Animal Care and Use Committee approved guidelines. All treatments were given directly to one tumor either by direct intra-tumoral injection or by intra-tumoral implantation of loaded SRB for sustain release. For cohorts treated in conjunction with radiotherapy, a Small Animal Radiation Research platform (SARRP) was used for image-guided radiation therapy at 220 kVp and 13 mA. The study design included a randomization process of the mice followed by assortment into the following cohorts of: no treatment, RT dose of 6 Gy, FBL-03G with/without 6Gy, and SRB loaded with FBL- 03G and with/without 6Gy. All mice that received FBL-03G treatment in the first and second trials were treated with 100-μg of FBL-03G immunoadjuvant. The same amount of payload was used in SRBs as with other administration routes. SRBs were administered in the right tumors using a 17-Gauge clinical brachytherapy needle. Dimethyl sulfoxide (DMSO) was used as a solvent to dissolve FBL-03G powder. To investigate the potential of FBL-03G as an immunotherapy, different concentrations for FBL-03G in the amount of 100, 200, and 300 μg were considered. Same procedure of drug loading into SRBs were followed as the first and second trials. Tumor volumes were measured for both tumors on day of treatment and at least 1–2 times/week post-treatment. A survival study was also performed. Mice were euthanized when either tumor exceeded 20 mm in diameter collectively and/or when tumors were ulcerated or ruptured. A control cohort was created with no treatment of FBL-03G but an inoculation of DMSO.

In 3 independent animal studies, the mice were randomized and divided into some the following cohorts of: no treatment, 6 Gy, FBL-03G with/without 6Gy, and SRB loaded with/without FBL-03G and with/without 6Gy. Mice inoculated with FBL-03G

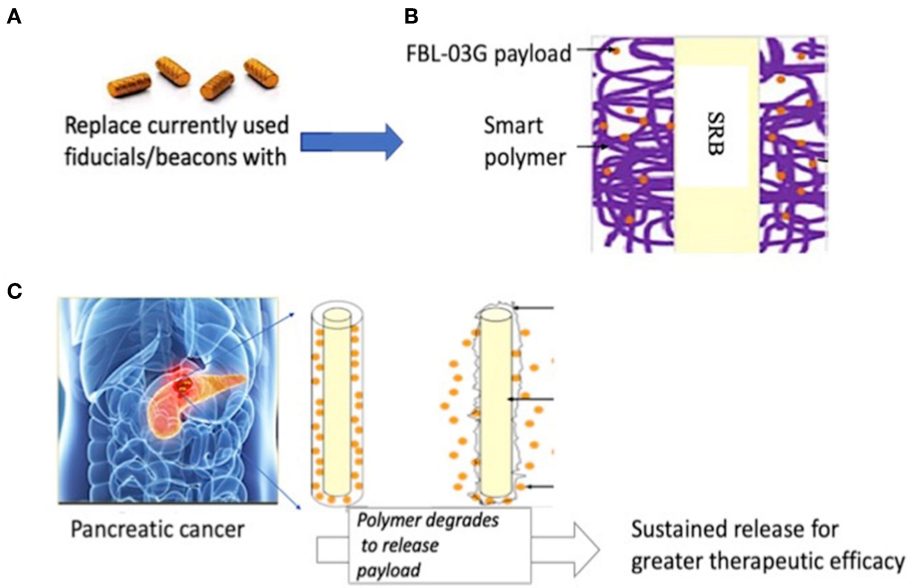

FIGURE 1 | Illustration of pancreatic therapy approach using non-cannabinoid cannabis derivative, FBL-03G. **(A)** Currently used commercially-available inert radiotherapy biomaterials e.g., fiducial (CIVCO Medical)/beacons used during radiotherapy to ensure geometric accuracy **(B)** smart radiotherapy biomaterials (SRB) with FDA approved polymer component loaded with FBL-03G; **(C)** potential clinical translation pathway is envisioned where the SRBs could simply replace the inert biomaterials (in **A**). Such replacement would come at no additional inconvenience to cancer patients. Once in place the SRBs can be activated by tumor microenvironment to sustainably release FLB-03G as the polymer component degrades for greater effective tumor cell kill, potentially with or without radiotherapy.

treatment received either 100, 200, or 300 ug of FBL-03G. Payload of the same amount of FBL-03G was used in SRBs as with other administration routes.

Tumor Volume Assessment

Directly after treatment, a digital Vernier caliper was used to measure the length and width of the dermal tumors. Tumor volume formula used: (length $\times$ width^2)/2. Measurement imaginary longitude to the leg was chosen as length and the vertical was for width. The tumors were restrained between the skin surface layers. The tumor volume was plotted against time. Animal survival was performed for treatments following IACUC-approved protocol, which was predetermined based on published evidence justifying such a study design. Tumor attainment > 1 cm in diameter on both flanks or tumor burst were determined as excessive tumor burden and mouse was euthanized following the protocol.

Statistical Analysis

The *in-vitro* experiments were conducted in triplicate, and data were presented as mean ± standard error or in the form quantified otherwise. Mice tumor volume were scrutinized using

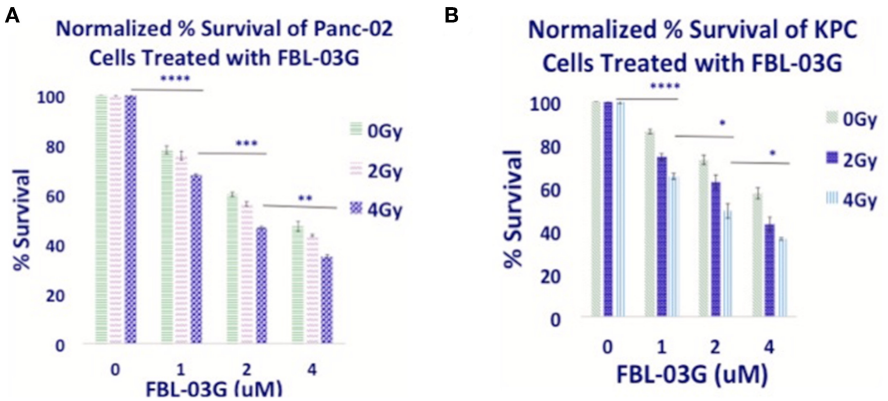

FIGURE 2 | *In-vitro* anti-cancer effect of FBL-03G. FBL-03G drug from flavonoids shows anti-cell proliferation effects in combination with radiotherapy. Average results of normalized clonogenic assays are shown, respectively, for Panc-02 and KPC cells. **(A,B)** Results of synergistic outcomes when combining radiotherapy at 4Gy with different FBL-03G doses. Statistics is shown for cohorts treated at 4Gy at different doses of FBL-03G. Statistical Analyses using Student's *T*-Test for the Cell % survival at different concentrations of FBL-03G graphs ($n = 3$ independent trials), (*$P < 0.05$; **$P < 0.01$; ***$P < 0.001$; ****$P < 0.0001$).

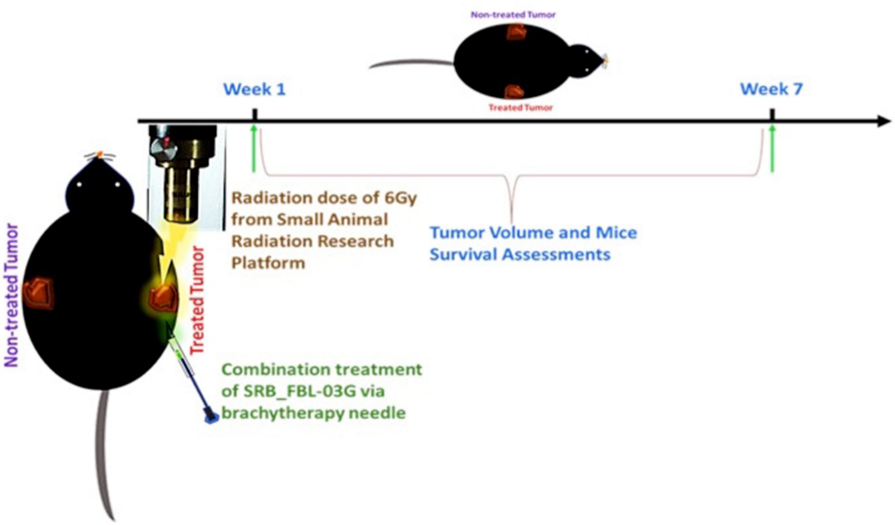

FIGURE 3 | Schematic diagram showing the treatment design with radiotherapy and/or intra-tumor injection of FBL-03G/SRB_FBL-03G for subcutaneously inoculated pancreatic adenocarcinoma tumors. Week 1 represents the treatment week as depicted above after pancreatic cancer (KPC) tumor reached 3.5–4 mm in diameter. The treatment parameters included a single fraction of 6Gy dose of radiotherapy followed by either an inoculation of flavocure drug (FBL-03G) or an implant of smart radiotherapy biomaterials loaded with similar concentration of the drug, FBL-03G. Tumor volume and mice survival were assessed for up to 7-weeks post treatment.

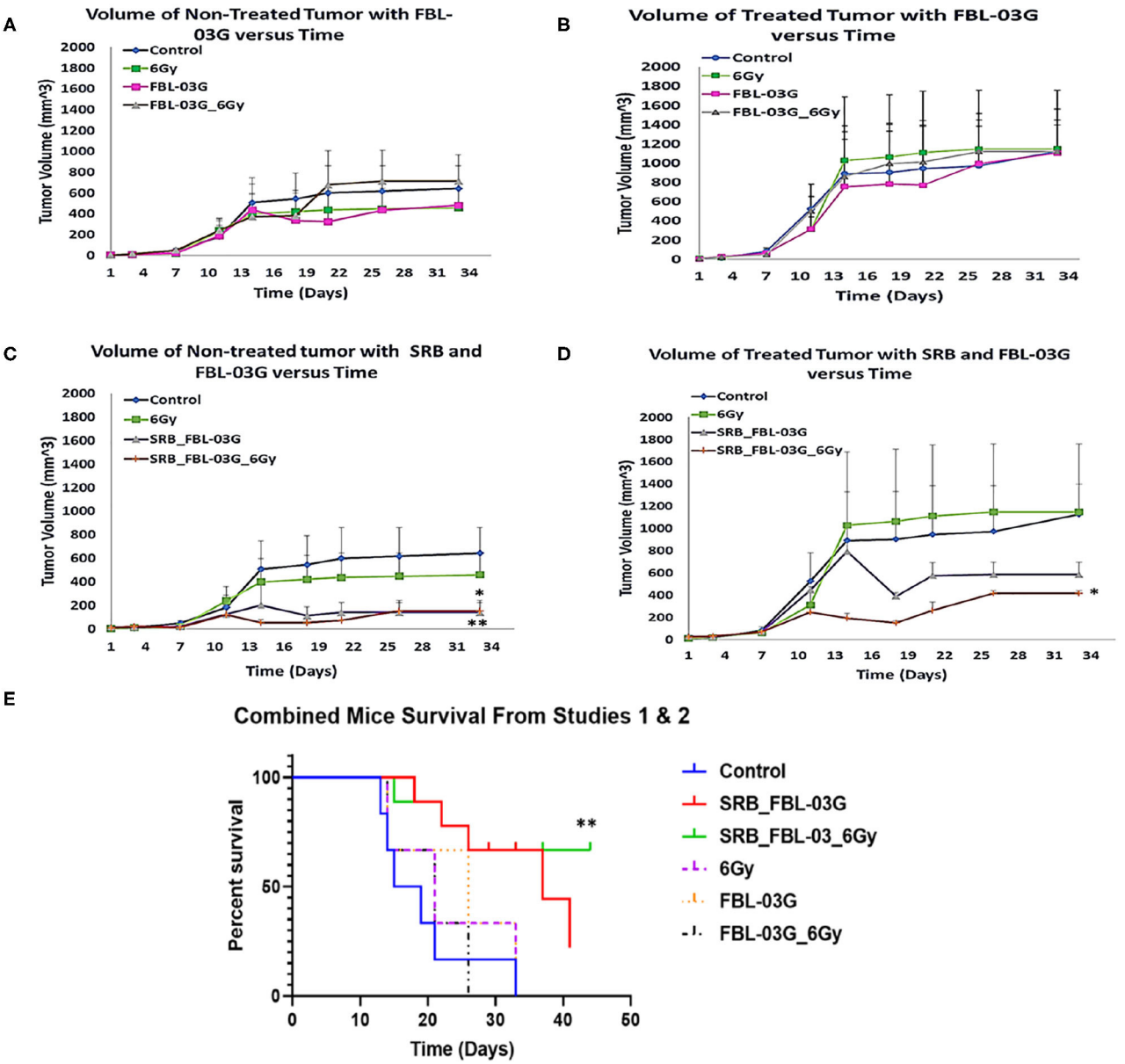

FIGURE 4 | *In-vivo* treatment of C57BL/6 mice. Mice were inoculated with 50 μL of KPC cells in PBS suspension at concentrations of 5×10^4 pancreatic cancer cells, on each left and right flank of mouse using a 22-Gauge syringe. When right side tumors reached palpable size, mice were randomized and treatments were administered. Mice were observed at least twice per week and tumor measurements were performed using precision calipers at least once per week. The abscopal effect was examined by monitoring the non-treated tumor. Smart radiotherapy biomaterials (SRB) loaded with FBL-03G (100 μg) significantly boosts the abscopal effect in pancreatic cancer slowing down tumor growth for both treated and untreated tumors. Two experiments were conducted simultaneously: Study 1 results are shown in graphs **(A–D)** and combined survival results for study 1 and study 2 results are displayed in **(E)**. **(A)** Volumes of non-treated tumors over time without SRB ($n = 3$ for each cohort). **(B)** Volumes of treated tumors over time ($n = 3$ for each cohort). **(C)** Volume of non-treated tumors over time with SRB and FBL-03G ($n = 3$ for control and 6Gy cohorts respectively; $n = 4$ for SRB loaded with FBL-03G with/without radiotherapy cohorts respectively). **(D)** Volume of treated tumors over time for cohorts treated with SRB and FBL-03G ($n = 3$ for control and 6 Gy cohorts respectively; $n = 4$ for SRB loaded with FBL-03G with/without radiotherapy cohorts respectively). **(E)** Survival results show significant increase in survival for cohorts treated with SRB loaded with FBL-03G (each $n = 9$) compared to control ($n = 6$), 6Gy/FBL-03G/FBL-03G_6Gy (each $n = 3$). For Statistical Analyses ($^*P < 0.05$; $^{**}P < 0.01$) Student's *T*-Test was used for comparing the volumes of tumors for each treatment group versus those of the control group with no additional corrections, and Log-rank (Mantel-Cox) was used for the survival graphs.

standard Student's two-tailed *t*-test. Mice survival were analyzed using GraphPad Prism 8.0. A *p*-value of $^*P < 0.05$, $^{**}P < 0.01$, $^{***}P < 0.001$, and $^{****}P < 0.0001$ were deemed as statistically significant difference.

RESULTS

Figure 1 illustrates the therapy approach using FBL-03G loaded in smart radiotherapy biomaterials (SRBs) for sustained delivery

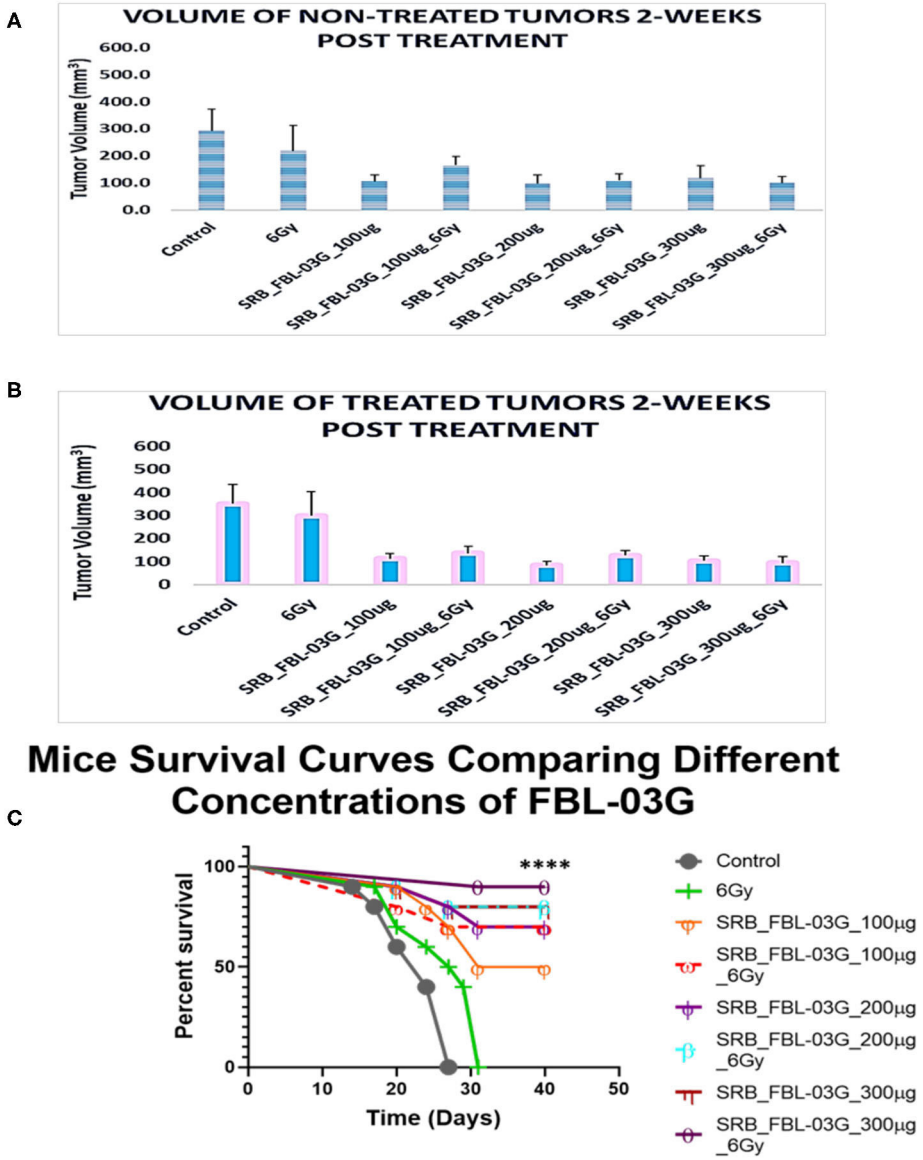

FIGURE 5 | Investigating the optimal concentration of FBL-03G loaded in SRB to enhance the abscopal effect. Smart radiotherapy biomaterial (SRB) loaded, respectively, with FBL-03G (100, 200, or 300 µg). C57BL/6 mice were inoculated with pancreatic cancer cells (KPC) on both flanks. Tumor volume and survival (n = 10 for each cohort) were assessed. **(A)** Volumes of non-treated tumors 2-weeks post treatment (n = 10 for each cohort); **(B)** volumes of treated tumors 2-weeks post treatment (n = 10 for each cohort). This study investigated using different concentrations of FBL-03G with/without 6Gy to determine its potential effect on mice survival over time. **(C)** Represents a Log-rank (Mantel-Cox) survival graph (n = 10) (****$p < 0.0001$). **(C)** Survival results show no difference in survival for cohorts treated with different concentrations of SRB loaded with FBL-03G.

to tumor cells. Before *in-vivo* studies with the FBL-03G, *in-vitro* studies were carried out with sustained exposure of cancer cells with FBL-03G. Clonogenic assay was performed to identify the anti-cancer effect of the FBL-03G drug with and without radiotherapy on 2 pancreatic cancer cell lines, KPC and Panc-02. **Figure 2** highlights enhanced tumor cell death for the combination treatment of FBL-03G and radiation compared to individual treatments alone. The clonogenic survival results show that the use of 1 µM of FBL-03G has synergistic effect on pancreatic cells with exposure to 4 Gy of radiotherapy in terms of decreasing pancreatic cancer cell proliferation. These findings were observed for both Panc-02 and KPC pancreatic cancer cell lines. This demonstrates therapy potential for the FBL-03G. Moreover, the use of 4 µM of FBL-03G was apparently more effective in killing pancreatic cancer cells than 4 Gy of radiotherapy. This suggests that FBL-03G can induce apoptosis and inhibit cancer cell proliferation with optimized drug concentrations. The FBL-03G effect on cancer cells combined with DNA damage from radiotherapy could account for the observed synergistic outcomes.

Using smart radiotherapy biomaterials for prolonged delivery of FBL-03G into tumors can also boost malignant cell death *in-vivo* with FBL-03G. The *in-vivo* study design is illustrated in **Figure 3**. The results are shown in **Figure 4**. **Figures 4A–D** shows a distinction between direct intra-tumor injection of FBL-03G vs. using the same concentration of FBL-03G with the smart radiotherapy biomaterial platform. **Figures 4C,D** shows reduction of tumor growth in animal cohorts treated with FBL-03G loaded in SRB compared to cohorts treated with direct administration of the same dose of FBL-03G shown in **Figures 4A,B** vs. control and irradiated cohorts. Remarkably, the results in **Figure 4D** revealed that nearby non-treated (abscopal) tumors, representing metastasis, were also significantly affected with slowed tumor growth. Repeated experiments showed significant increase in mice survival (**Figures 4E,F**) compared to control cohorts. The findings provide a basis for further studies to optimize different parameters for maximal outcomes via this approach.

In another study we evaluated the effect of FBL-03G using 3 different concentrations (100, 200, and 300 ug) loaded in smart radiotherapy biomaterials with/without radiotherapy. The findings in **Figure 5** show no significant difference in tumor volume between using smart radiotherapy biomaterials with FBL-03G alone vs. using SRBs with FBL-03G payloads in combination with radiotherapy. However, a significant difference between 6Gy and control cohorts vs. combination of FBL-03G in SRB treated groups is observed in **Figures 5A,B**, where tumor growth of both treated and non-treated tumors is inhibited compared to control and 6Gy cohorts. Overall, the data demonstrates significant therapeutic potential for using FBL-03G in the treatment of both local and metastatic disease, significantly increasing survival (**Figure 5C**).

DISCUSSION

From the results of this study, the key findings include, observation that a non-cannabinoid derivative of cannabis can enhance radiotherapy treatment outcomes *in-vitro* and *in-vivo* as highlighted in **Figures 2**, **4**. Secondly, the sustained delivery of the cannabis derivative FBL-03G from smart radiotherapy biomaterials (SRBs) results in tumor growth inhibition of both locally treated and distant untreated tumors, with and without radiotherapy. The use of smart radiotherapy biomaterials (SRBs) (8, 23) was recently proposed as a novel approach to deliver cannabinoids, allowing for prolonged exposure of tumor cells to these cannabis derivatives, which is expected to be more effective (10). The FBL-03G payload used in this study is a flavonoid non-cannabinoid derivative of cannabis, and the potential to inhibit both local and metastatic tumor progression is remarkable, especially for pancreatic cancer, with a dismal 5-year survival rate of 8% (1).

While ongoing studies are in progress to address the specific mechanism for this immunotherapy potential of this cannabis derivative, the possibility of leveraging such a therapy approach to treat metastasis or increase survival is significant, given that most pancreatic cancer patients are diagnosed already with metastatic disease, with limited treatment options. The results highlight the potential of using non-cannabinoid/non-psychoactive derivatives of cannabis for such treatment. Further work to optimize therapeutic efficacy for such cannabis derivatives and evaluate toxicity could set the stage for clinical translation. An advantage of the SRB approach here is also that this could minimize any toxicity due to *in-situ* delivery and use of multifold less immunoadjuvant. Furthermore, the use of a single dose of RT as done in this project would minimize normal tissue toxicity.

Although **Figure 4** shows no significant difference between using SRBs alone vs. SRBs with RT, SRBs could simply be used like fiducial markers (23) (**Figure 1**) offering a viable pathway to clinical translation at no additional inconvenience to patients. Another advantage of using SRBs for sustained *in-situ* delivery of payloads is the relative convenience in delivering the immunoadjuvants, compared to repeated injections. Using only one fraction of RT would also be more convenient for cancer patients who usually must come in repeatedly over many weeks to be treated with several fractions of radiotherapy. This should significantly reduce treatment time and costs. It would be a benefit in resource-poor-settings where access to RT services is limited, reducing cancer health disparities, with major impact in global health.

While the results indicate that sustained exposure of tumor cells to FBL-03G can boost both local and metastatic tumor cell kill, the mechanism of such action needs to be further investigated. One hypothesis is that, FBL-03G can serve as an immunotherapy agent, inhibiting growth of locally treated and untreated tumors, representing metastasis. Metastasis accounts for most of all cancer associated suffering and death, and questionably presents the most daunting challenge in cancer management. Henceforth, the observed significant increase in survival is promising, especially for pancreatic cancer which is often recalcitrant to treatments. Another hypothesis is that sustained delivery allows FBL-03G to reach the untreated tumor over a prolonged period as well. Either way, the FBL-03G results reveal a new potential non-cannabinoid cannabis derivative with major potential for consideration in further investigations in the treatment of pancreatic cancer, where new therapy options are urgently needed.

CONCLUSION

In this study, a flavonoid derivative of cannabis demonstrates significant therapy potential in the treatment of pancreatic cancer, including radio-sensitizing and cancer metastasis treatment potential. The results justify further studies to optimize therapy outcomes toward clinical translation.

DATA AVAILABILITY

All datasets generated for this study are included in the manuscript and/or the **Supplementary Files**.

ETHICS STATEMENT

Animal experiments and protocol followed the guidelines and regulations set by the Dana-Farber Cancer Institute Institutional

Animal Care and Use Committee (IACUC). Mice maintenance in Dana Farber Cancer Institute animal facility was in accordance with the Institutional Animal Care and Use Committee approved guidelines.

AUTHOR CONTRIBUTIONS

MM provided intellectual contributions to the design of the mice study, generated all the results in this study, designed the smart radiotherapy biomaterial (SRB) to implant in mice, and wrote most of the manuscript. SY-K reviewed the manuscript. UI, KD, and NB helped in tumor measurements for mice and reviewed the manuscript. NT and HL provided the FBL-03G drug, contributed to study design, made input in manuscript including reviewing the manuscript. WN is the principal investigator who designed the study and wrote a portion of the manuscript.

FUNDING

Funding support for this work is acknowledged from the USA National Institutes of Health (NIH), grant number R21CA205094 and Flavocure Biotech Inc.

ACKNOWLEDGMENTS

We thank all the members at Ngwa's lab at Dana Farber Cancer Institute and Harvard Medical School, Boston, Massachusetts for their support, and Servicebio Inc., Woburn, Massachusetts for technical support. Bio-Tech R&D Institute, University of the West Indies, Mona, Jamaica is also acknowledged for its technical support.

SUPPLEMENTARY MATERIAL

The Supplementary Material for this article can be found online at: https://www.frontiersin.org/articles/10.3389/fonc.2019.00660/full#supplementary-material

Figure S1 | Structures of Cannabis flavonoids and the unnatural molecule FBL-03G. Through a bioactivity guided isolation approach, Cannflavin B (**10**) was isolated from a flavonoid rich fraction of Cannabis using flash chromatography along with 10 other compounds and characterized by NMR and MS spectroscopic methods. The spectroscopic data were similar to the data of the following 11 compounds previously isolated and characterized from the Cannabis plant; apigenin (**1**), Chrysoeriol (**2**), kaempferol (**3**), luteolin (**4**), quercetin (**5**), vitexin (**6**), isovitexin (**7**), orientin (**8**) and prenylated flavonoids including Cannflavin A (**9**), Cannflavin B (**10**), and Cannflavin C (**11**).

REFERENCES

1. Ryan DP, Hong TS, Bardeesy N. Pancreatic adenocarcinoma. *N Engl J Med.* (2014) 371:1039–49. doi: 10.1056/NEJMra1404198
2. Lowe H, Toyang NJ. *Therapeutic Agents Containing Cannabis Flavonoid Derivatives Targeting Kinases, Sirtuins and Oncogenic Agents for the Treatment of Cancers*. Virginia USA Patent Application 15/778,899, Alexandria (2018).
3. Hidalgo M. Pancreatic cancer. *New Engl J Med.* (2010) 362:1605–17. doi: 10.1056/NEJMra0901557
4. Gnoni A, Licchetta A, Scarpa A, Azzariti A, Brunetti AE, Simone G, et al. Carcinogenesis of pancreatic adenocarcinoma: precursor lesions. *Int J Mol Sci.* (2013) 14:19731–62. doi: 10.3390/ijms141019731
5. Yasmin-Karim S, Bruck PT, Moreau M, Kunjachan S, Chen GZ, Kumar R, et al. Radiation and local anti-CD40 generate an effective *in situ* vaccine in preclinical models of pancreatic cancer. *Front Immunol.* (2018) 9:2030. doi: 10.3389/fimmu.2018.02030
6. Guzman M. Cannabinoids: potential anticancer agents. *Nat Rev Cancer.* (2003) 3:745–55. doi: 10.1038/nrc1188
7. Scott KA, Dalgleish AG, Liu WM. The combination of cannabidiol and Delta9-tetrahydrocannabinol enhances the anticancer effects of radiation in an orthotopic murine glioma model. *Mol Cancer Ther.* (2014) 13:2955–67. doi: 10.1158/1535-7163.MCT-14-0402
8. Yasmin-Karim S, Moreau M, Mueller R, Sinha N, Dabney R, Herman A, et al. Enhancing the therapeutic efficacy of cancer treatment with cannabinoids. *Front Oncol.* (2018) 8:114. doi: 10.3389/fonc.2018.00114
9. Grotenhermen F. Pharmacokinetics and pharmacodynamics of cannabinoids. *Clin Pharmacokinet.* (2003) 42:327–60. doi: 10.2165/00003088-200342040-00003
10. Abrams DI, Guzman M. Cannabis in cancer care. *Clin Pharmacol Ther.* (2015) 97:575–86. doi: 10.1002/cpt.108
11. Whiting PF, Wolff RF, Deshpande S, Di Nisio M, Duffy S, Hernandez AV, et al. Cannabinoids for medical use: a systematic review and meta-analysis. *JAMA.* (2015) 313:2456–73. doi: 10.1001/jama.2015.6358
12. Andre CM, Hausman JF, Guerriero G. *Cannabis sativa*: the plant of the thousand and one molecules. *Front Plant Sci.* (2016) 7:19. doi: 10.3389/fpls.2016.00019
13. Mole RH. Whole body irradiation; radiobiology or medicine? *Br J Radiol.* (1953) 26:234–41. doi: 10.1259/0007-1285-26-305-234
14. Demaria S, Ng B, Devitt ML, Babb JS, Kawashima N, Liebes L, et al. Ionizing radiation inhibition of distant untreated tumors (abscopal effect) is immune mediated. *Int J Radiat Oncol Biol Phys.* (2004) 58:862–70. doi: 10.1016/j.ijrobp.2003.09.012
15. Ngwa W, Irabor OC, Schoenfeld JD, Hesser J, Demaria S, Formenti SC. Using immunotherapy to boost the abscopal effect. *Nat Rev Cancer.* (2018) 18:313–22. doi: 10.1038/nrc.2018.6
16. Radwan MM, Ross SA, Slade D, Ahmed SA, Zulfiqar F, Elsohly MA. Isolation and characterization of new Cannabis constituents from a high potency variety. *Planta Med.* (2008) 74:267–72. doi: 10.1055/s-2008-1034311
17. Radwan MM, Elsohly MA, Slade D, Ahmed SA, Khan IA, Ross SA. Biologically active cannabinoids from high-potency *Cannabis sativa*. *J Nat Prod.* (2009) 72:906–11. doi: 10.1021/np900067k
18. Crombie L, Crombie WML, Jamieson SV. Extractives of Thailand cannabis: synthesis of canniprene and isolation of new geranylated and prenylated chrysoeriols. *Tetrahedron Lett.* (1980) 21:3607-10. doi: 10.1016/0040-4039(80)80248-6
19. Barrett ML, Gordon D, Evans FJ. Isolation from *Cannabis sativa* L. *of* cannflavin–a novel inhibitor of prostaglandin production. *Biochem Pharmacol.* (1985) 34:2019–24. doi: 10.1016/0006-2952(85)90325-9
20. Barrett ML, Scutt AM, Evans FJ. Cannflavin A and B, prenylated flavones from *Cannabis sativa* L. *Experientia.* (1986) 42:452–3. doi: 10.1007/BF02118655
21. Choi YH, Hazekamp A, Peltenburg-Looman AM, Frederich M, Erkelens C, Lefeber AW, et al. NMR assignments of the major cannabinoids and cannabiflavonoids isolated from flowers of *Cannabis sativa*. *Phytochem Anal.* (2004) 15:345–54. doi: 10.1002/pca.787
22. Moreau M, Yasmin-Karim S, Kunjachan S, Sinha N, Gremse F, Kumar R, et al. Priming the abscopal effect using multifunctional smart radiotherapy biomaterials loaded with immunoadjuvants. *Front Oncol.* (2018) 8:56. doi: 10.3389/fonc.2018.00056

23. Ngwa W, Kumar R, Moreau M, Dabney R, Herman A. Nanoparticle drones to target lung cancer with radiosensitizers and cannabinoids. *Front Oncol.* (2017) 7:208. doi: 10.3389/fonc.2017.00208

Conflict of Interest Statement: NT and HL work for Flavocure Biotech Inc., a for-profit company.

The remaining authors declare that the research was conducted in the absence of any commercial or financial relationships that could be construed as a potential conflict of interest.

Copyright © 2019 Moreau, Ibeh, Decosmo, Bih, Yasmin-Karim, Toyang, Lowe and Ngwa. This is an open-access article distributed under the terms of the Creative Commons Attribution License (CC BY). The use, distribution or reproduction in other forums is permitted, provided the original author(s) and the copyright owner(s) are credited and that the original publication in this journal is cited, in accordance with accepted academic practice. No use, distribution or reproduction is permitted which does not comply with these terms.

frontiers in Oncology

CORRECTION
published: 21 August 2020
doi: 10.3389/fonc.2020.01434

Corrigendum: Flavonoid Derivative of *Cannabis* Demonstrates Therapeutic Potential in Preclinical Models of Metastatic Pancreatic Cancer

Michele Moreau[1,2], *Udoka Ibeh*[1,3], *Kaylie Decosmo*[1,4], *Noella Bih*[1], *Sayeda Yasmin-Karim*[1], *Ngeh Toyang*[5], *Henry Lowe*[5] *and Wilfred Ngwa*[1,2]*

[1] Brigham and Women's Hospital, Dana-Farber Cancer Institute, Harvard Medical School, Boston, MA, United States, [2] Department of Physics, University of Massachusetts Lowell, Lowell, MA, United States, [3] Department of Biology, University of Massachusetts Boston, Boston, MA, United States, [4] Department of CaNCURE Program, Northeastern University, Boston, MA, United States, [5] Flavocure Biotech Inc., Baltimore, MD, United States

Keywords: pancreatic cancer, flavonoids, cannabis, metastasis, radiotherapy, smart biomaterials

OPEN ACCESS

Edited by:
Paul N. Span,
Radboud University Nijmegen Medical Centre, Netherlands

Reviewed by:
Otto Kalliokoski,
University of Copenhagen, Denmark

***Correspondence:**
Wilfred Ngwa
wngwa@lroc.harvard.edu

Specialty section:
This article was submitted to Radiation Oncology, a section of the journal Frontiers in Oncology

Received: *30 April 2020*
Accepted: *07 July 2020*
Published: *21 August 2020*

Citation:
Moreau M, Ibeh U, Decosmo K, Bih N, Yasmin-Karim S, Toyang N, Lowe H and Ngwa W (2020) Corrigendum: Flavonoid Derivative of Cannabis Demonstrates Therapeutic Potential in Preclinical Models of Metastatic Pancreatic Cancer. Front. Oncol. 10:1434. doi: 10.3389/fonc.2020.01434

A Corrigendum on

Flavonoid Derivative of *Cannabis* Demonstrates Therapeutic Potential in Preclinical Models of Metastatic Pancreatic Cancer

by Moreau, M., Ibeh, U., Decosmo, K., Bih, N., Yasmin-Karim, S., Toyang, N., et al. (2019). Front. Oncol. 9:660. doi: 10.3389/fonc.2019.00660

In the original article, there was a mistake in **Figures 4E, 4F**, and **5C** as published. This was due to errors during use of analysis software. The survival data in **Figures 4E,F** has been combined into one **Figure 4E**. The figure legend of **Figure 4** has been updated to reflect the correction made in the figure. The corrected **Figures 4** and **5** appear below.

The data for the tumor volume and survival results has also now been published as **Supplementary Material**.

SUPPLEMENTARY MATERIAL

The Supplementary Material for this article can be found online at: https://www.frontiersin.org/articles/10.3389/fonc.2020.01434/full#supplementary-material

The authors apologize for this error and state that these do not change the scientific conclusions of the article in any way. The original article has been updated.

Copyright © 2020 Moreau, Ibeh, Decosmo, Bih, Yasmin-Karim, Toyang, Lowe and Ngwa. This is an open-access article distributed under the terms of the Creative Commons Attribution License (CC BY). The use, distribution or reproduction in other forums is permitted, provided the original author(s) and the copyright owner(s) are credited and that the original publication in this journal is cited, in accordance with accepted academic practice. No use, distribution or reproduction is permitted which does not comply with these terms.

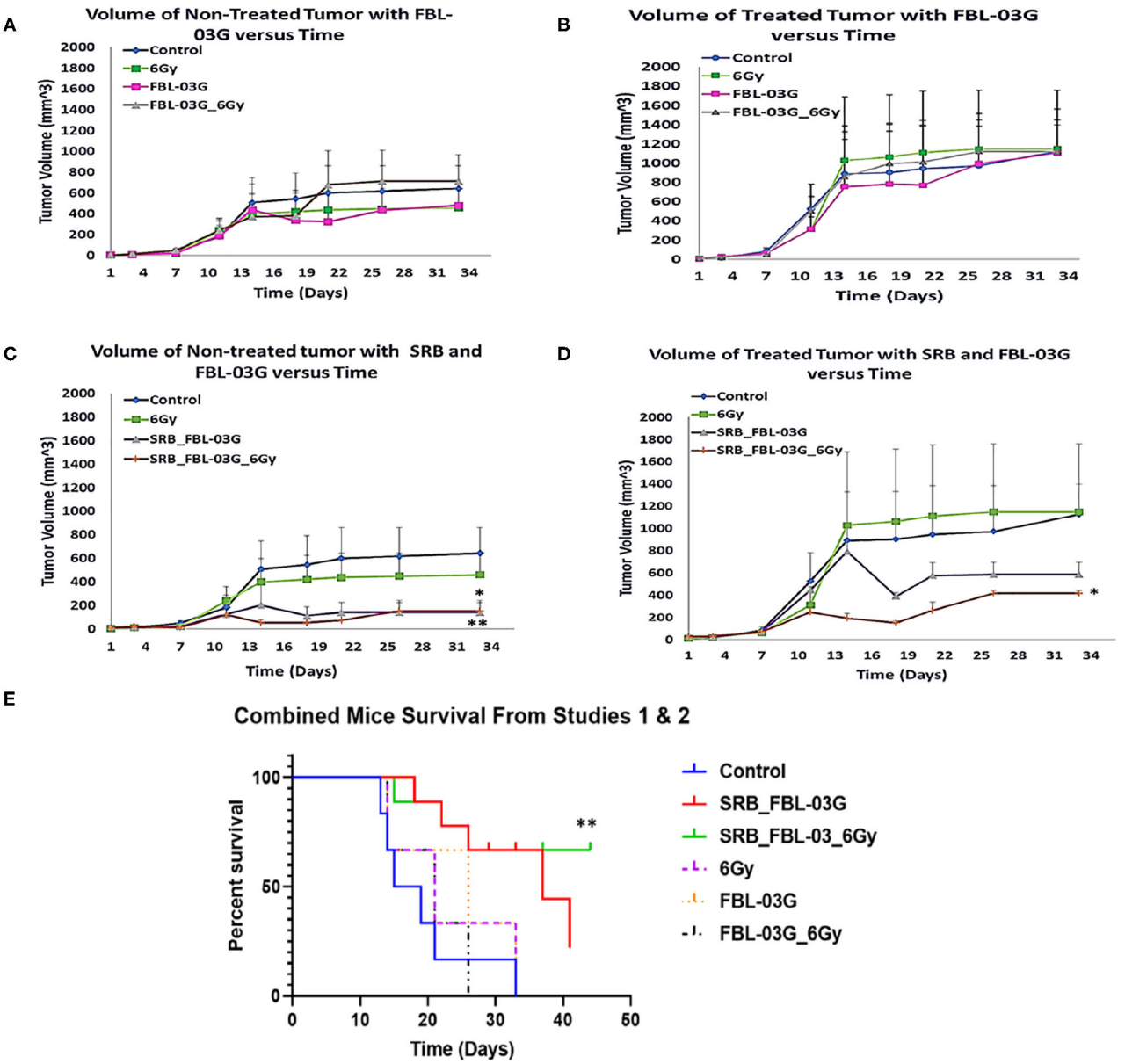

FIGURE 4 | *In-vivo* treatment of C57BL/6 mice. Mice were inoculated with 50 μL of KPC cells in PBS suspension at concentrations of 5×10^4 pancreatic cancer cells, on each left and right flank of mouse using a 22-Gauge syringe. When right side tumors reached palpable size, mice were randomized and treatments were administered. Mice were observed at least twice per week and tumor measurements were performed using precision calipers at least once per week. The abscopal effect was examined by monitoring the non-treated tumor. Smart radiotherapy biomaterials (SRB) loaded with FBL-03G (100 μg) significantly boosts the abscopal effect in pancreatic cancer slowing down tumor growth for both treated and untreated tumors. Two experiments were conducted simultaneously: Study 1 results are shown in graphs **(A–D)** and combined survival results for study 1 and study 2 results are displayed in **(E)**. **(A)** Volumes of non-treated tumors over time without SRB ($n = 3$ for each cohort). **(B)** Volumes of treated tumors over time ($n = 3$ for each cohort). **(C)** Volume of non-treated tumors over time with SRB and FBL-03G ($n = 3$ for control and 6Gy cohorts respectively; $n = 4$ for SRB loaded with FBL-03G with/without radiotherapy cohorts respectively). **(D)** Volume of treated tumors over time for cohorts treated with SRB and FBL-03G ($n = 3$ for control and 6 Gy cohorts respectively; $n = 4$ for SRB loaded with FBL-03G with/without radiotherapy cohorts respectively). **(E)** Survival results show significant increase in survival for cohorts treated with SRB loaded with FBL-03G (each $n = 9$) compared to control ($n = 6$), 6Gy/FBL-03G/FBL-03G_6Gy (each $n = 3$). For Statistical Analyses (*$P < 0.05$; **$P < 0.01$) Student's *T*-Test was used for comparing the volumes of tumors for each treatment group versus those of the control group with no additional corrections, and Log-rank (Mantel-Cox) was used for the survival graphs.

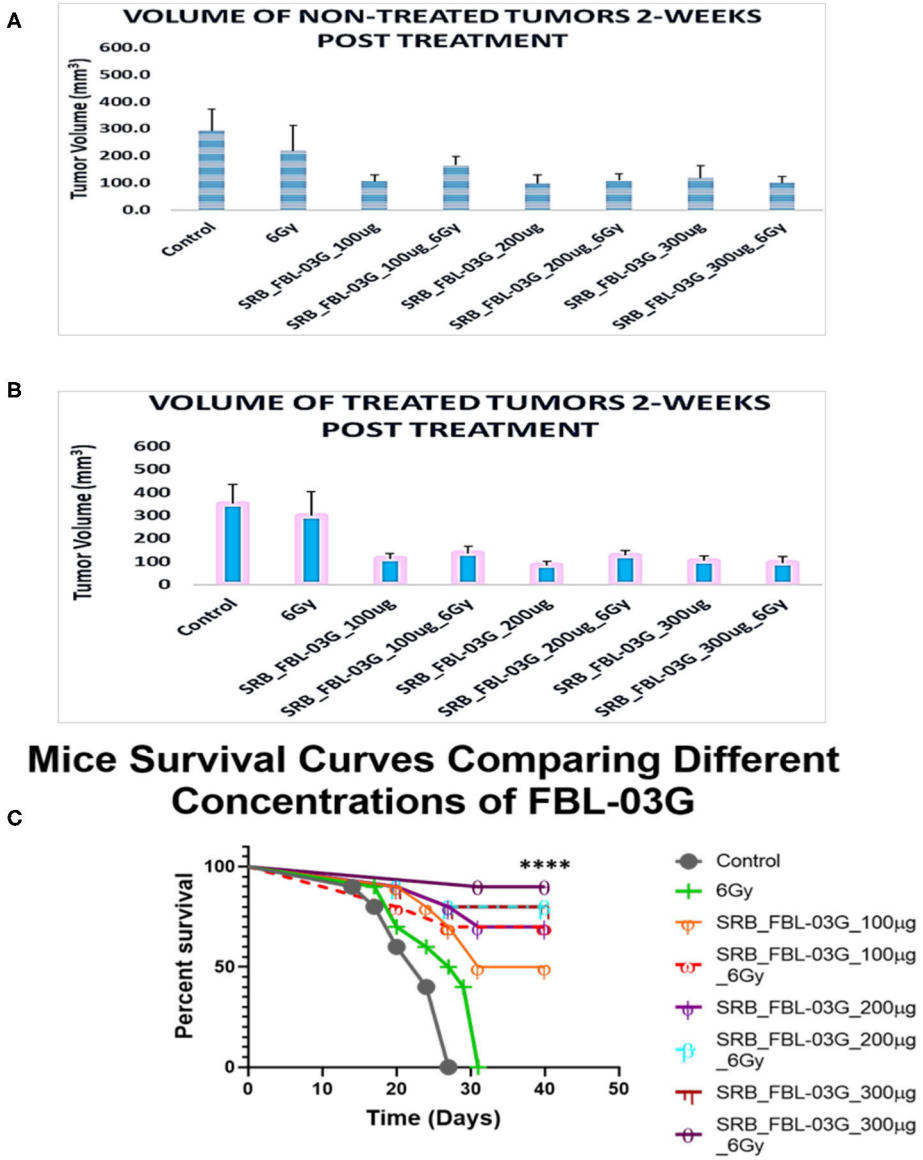

FIGURE 5 | Investigating the optimal concentration of FBL-03G loaded in SRB to enhance the abscopal effect. Smart radiotherapy biomaterial (SRB) loaded, respectively, with FBL-03G (100, 200, or 300 µg). C57BL/6 mice were inoculated with pancreatic cancer cells (KPC) on both flanks. Tumor volume and survival (n = 10 for each cohort) were assessed. **(A)** Volumes of non-treated tumors 2-weeks post treatment (n = 10 for each cohort); **(B)** volumes of treated tumors 2-weeks post treatment (n = 10 for each cohort). This study investigated using different concentrations of FBL-03G with/without 6Gy to determine its potential effect on mice survival over time. **(C)** Represents a Log-rank (Mantel-Cox) survival graph (n = 10) (****$p < 0.0001$). **(C)** Survival results show no difference in survival for cohorts treated with different concentrations of SRB loaded with FBL-03G.

frontiers in Oncology

ORIGINAL RESEARCH
published: 30 August 2019
doi: 10.3389/fonc.2019.00825

Exploring Radiation Response in Two Head and Neck Squamous Carcinoma Cell Lines Through Metabolic Profiling

Eva Lindell Jonsson[1†], Ida Erngren[2†], Mikael Engskog[2], Jakob Haglöf[2], Torbjörn Arvidsson[2,3], Mikael Hedeland[2], Curt Petterson[2], Göran Laurell[1] and Marika Nestor[4]*

[1] Department of Surgical Sciences, Uppsala University, Uppsala, Sweden, [2] Department of Medicinal Chemistry, Uppsala University, Uppsala, Sweden, [3] Medical Product Agency, Uppsala, Sweden, [4] Department of Immunology, Genetics and Pathology, Uppsala University, Uppsala, Sweden

OPEN ACCESS

Edited by:
Paul N. Span, Radboud University Nijmegen Medical Centre, Netherlands

Reviewed by:
Mansi Babbar, National Institute on Aging (NIA), United States
Kerstin Borgmann, University Medical Center Hamburg-Eppendorf, Germany

***Correspondence:**
Marika Nestor
marika.nestor@igp.uu.se

[†] *These authors have contributed equally to this work*

Specialty section:
This article was submitted to Radiation Oncology, a section of the journal Frontiers in Oncology

Received: *17 April 2019*
Accepted: *12 August 2019*
Published: *30 August 2019*

Citation:
Lindell Jonsson E, Erngren I, Engskog M, Haglöf J, Arvidsson T, Hedeland M, Petterson C, Laurell G and Nestor M (2019) Exploring Radiation Response in Two Head and Neck Squamous Carcinoma Cell Lines Through Metabolic Profiling. Front. Oncol. 9:825. doi: 10.3389/fonc.2019.00825

Head and neck squamous cell carcinoma (HNSCC) is the sixth most common form of cancer worldwide. Radiotherapy, with or without surgery, represents the major approach to curative treatment. However, not all tumors are equally sensitive to irradiation. It is therefore of interest to apply newer system biology approaches (e.g., metabolic profiling) in squamous cancer cells with different radiosensitivities in order to provide new insights on the mechanisms of radiation response. In this study, two cultured HNSCC cell lines from the same donor, UM-SCC-74A and UM-SCC-74B, were first genotyped using Short Tandem Repeat (STR), and assessed for radiation response by the means of clonogenic survival and growth inhibition assays. Thereafter, cells were cultured, irradiated and collected for subsequent metabolic profiling analyses using liquid chromatography-mass spectrometry (LC-MS). STR verified the similarity of UM-SCC-74A and UM-SCC-74B cells, and three independent assays proved UM-SCC-74B to be clearly more radioresistant than UM-SCC-74A. The LC-MS metabolic profiling demonstrated significant differences in the intracellular metabolome of the two cell lines before irradiation, as well as significant alterations after irradiation. The most important differences between the two cell lines before irradiation were connected to nicotinic acid and nicotinamide metabolism and purine metabolism. In the more radiosensitive UM-SCC-74A cells, the most significant alterations after irradiation were linked to tryptophan metabolism. In the more radioresistant UM-SCC-74B cells, the major alterations after irradiation were connected to nicotinic acid and nicotinamide metabolism, purine metabolism, the methionine cycle as well as the serine, and glycine metabolism. The data suggest that the more radioresistant cell line UM-SCC-74B altered the metabolism to control redox-status, manage DNA-repair, and change DNA methylation after irradiation. This provides new insights on the mechanisms of radiation response, which may aid future identification of biomarkers associated with radioresistance of cancer cells.

Keywords: radioresistance, radiosensitivity, metabolomics, mass spectrometry, redox status

INTRODUCTION

Every year more than half a million new cases of squamous cell carcinoma of the head and neck (HNSCC) are reported (1), which makes it the 6th most common type of cancer worldwide (2). HNSCC is a heterogeneous disease, including epithelial cancers of the oral cavity, lip, nasal cavity, paranasal sinuses, larynx, pharynx, and salivary glands. Despite the high frequency of HNSCC worldwide, it has one of the lowest survival rates among the more common cancer types (3), and almost 50% of all patients with HNSCC will die from their disease (4). Treatment challenges include complex anatomy, functional preservation of substantial organs, and minimization of side effects (5).

Radiotherapy (RT), the clinical application of ionizing radiation, is one of the most effective tools in therapy of cancer today (6). Even though advances in treatment methods have been made during recent decades, RT with or without surgery remains the major approach to curative treatment of HNSCC (7). The efficacy of RT is however still limited by different technological, biological, and clinical constraints. HNSCC is on average only moderately radiosensitive, which means that radiotherapy often must be given to such an extent that it approaches the maximum tolerated dose for the surrounding normal tissue. This may cause substantial acute and late toxicities, resulting in significant morbidity and altered quality of life (8). Moreover, the individual heterogeneity in terms of HNSCC radiosensitivity is immense, and therapeutic responses to RT have been shown to vary from complete to no response (9, 10). Consequently, there is a great need for individualized radiotherapy treatment approaches in HNSCC, to aid in predicting and monitoring tumor response to radiotherapy before, during, and after treatment. This requires new insights on the mechanisms of radiation response, novel markers to predict tumor response to radiotherapy, as well as potential treatment targets to enhance radiation-sensitivity.

The metabolism of cancer cells differs from normal differentiated cells (11). Tumor progression, the development of increasingly aggressive and resistant tumor cells, has increasingly been understood to be associated with perturbations in cellular metabolism, such as increased glutaminolysis and fatty acid oxidation, the Warburg effect, as well as altered patterns of macromolecule synthesis and storage (11). Cancer cells are able to adapt metabolically to many types of cellular stress, for example, hypoxia, nutrient depletion, and radiation, and studies have shown several mechanistic links between cellular metabolism and growth control (11). No doubt, the plasticity of cancer cell metabolism can be vital for causing many patients to relapse into disseminated and treatment-resistant disease.

Cancer metabolism is altered by ionizing radiation. Radiation exposure induces different types of genome damage, including DNA single- and double-strand breaks and bulky lesions. Thereby multiple signaling pathways are activated, involved in e.g., DNA damage response, signal transduction pathways, and regulation of survival (9, 12, 13). Enzymatic pathways quickly repair many of these lesions, but lesions that are not repaired correctly lead to chromosomal abnormalities and a possible change of cell phenotype, culminating in cell cycle arrest and/or cell death. In addition to rapid proliferation, many cancer cells are also deficient in repair proteins and cell cycle checkpoints, making them more sensitive to radiation (12). Cellular exposure to ionizing radiation also triggers a complex series of molecular responses that can affect metabolism, either directly or indirectly, by altering cell growth (14). Ionizing radiation also impacts multiple cellular compartments even at relatively modest doses, which can also trigger a variety of signaling pathways (15). These molecular events are not only important for the therapeutic response, but may also influence the inflammatory response at a local and systemic host level. Subsequently, ionizing radiation will result in different alterations in the metabolome, depending on what pathways and processes that the specific cell alters in response to radiation.

Several studies have identified different molecular entities associated with radioresistance, nevertheless the underlying mechanisms are still inconclusive (16). Suggested mechanisms include hypoxia, alterations of the DNA damage response, activation of pathways involved in pro-survival or cell cycle regulation, as well as vascular, stromal, and immunological changes (17–26). However, a majority of these studies are based on genome, transcriptome, and proteome data. Consequently, it would be of major interest to conduct studies in this field closer to the phenotype, such as metabolite profiling (27). Metabolomics in radiation biology have previously been used for two main purposes (i) metabolic profiling for utilization in biodosimetry or for biomarker discovery of radiation exposure (14, 28–39) and (ii) metabolic profiling for a more mechanistic understating of the radiation response of the metabolome (14, 34, 40–43) However, to date no study has focused on investigating the different metabolic responses of genetically similar cells with divergent radiation sensitivities.

Metabolic profiling is the comprehensive and quantitative analysis of small endogenous metabolites that are the downstream products in biological systems. It can be a powerful approach to study the phenotype of cancer cells, since it analyses the biochemical outcome of the activities of the proteome (27). The promise of metabolomics as a scientific tool has been fueled largely by the advancement in nuclear magnetic resonance (NMR) and mass spectrometry (MS), and could be a well-suited and cost-effective complement to current genomic and proteomic data in the field (14).

Even though our current understanding of the mechanisms in play during radiation of tumor cells, and how they are related to radiosensitivity, is incomplete (40), it has been shown to at least in part be due to the different metabolic alterations that the tumor can make (44). Ionizing radiation induces complex biological responses that interfere with gene and protein expression, which disrupts normal metabolic processes in cells and organs. As a result, metabolites related to classical pathways of radiation damage, including oxidative stress and subsequent DNA breakdown have been shown to be affected. Additionally, polyunsaturated fatty acids (PUFA) metabolism can be disrupted as an inflammatory effect of radiation exposure (14). Changes in nicotinate and nicotinamide metabolism and cofactor biosynthesis have also been reported in radiation related research, suggested to be linked to DNA repair (14, 45, 46).

Consequently, metabolomics may provide insights into the mechanism behind a reduced sensitivity to radiotherapy by identifying differences in metabolites produced in response of irradiation in cancer cells with different sensitivity to radiotherapy. This may provide significant mechanistic understanding related to cellular response due to perturbations caused by radiation treatment (14), which might be a possible way to find a pharmacologically alterable pathway that is altered in the less sensitive cells, or to predict response or non-response to radiation therapy.

In the present study, we investigate the relationship between radiation response and the metabolome of HNSCC in a unique model system, using two HNSCC cell lines from the same donor but with different radiosensitivity. This enables the study of their metabolic response to radiation in an exceptionally controlled setting, and has to our knowledge not been performed previously. The aim was to assess the metabolic differences between the two cell lines, and how this was affected by radiation. Cells were first genotyped, and assessed for radiosensitivity using clonogenic survival and long-term growth inhibition assays at several radiation doses. Cell-based metabolic profiling using liquid chromatography hyphenated to high resolution mass spectrometry (LC-HRMS) was then performed to investigate the influence of early and intermediate radiation responses on metabolites, and to assess the potential correlation to the different radiosensitivities of the cells. In the long-term, the study may contribute to provide new insights on the mechanisms of radiation response, discover possible biomarkers for radiation-sensitivity, and possibly present potential treatment targets in order to enhance radiation-sensitivity of HNSCC.

MATERIALS AND METHODS

This study has been conducted in accordance with Frontiers guidelines on study ethics. It does not involve any animal or human subjects or identifiable human data, thus does not require ethical permission.

Cell Lines

The squamous cell carcinoma cell lines UM-SCC-74A and UM-SCC-74B were kindly provided by Professor TE Carey (University of Michigan, USA), and have previously been described by Brenner et al. (47). The cell lines were taken from the same male patient with oral squamous cell carcinoma after radiochemotherapy (UM-SCC-74A) and then again at surgery for persistent cancer (UM-SCC-74B) (47). Cells were cultured at 37°C, in 5% CO_2 in DMEM medium containing 2 mM l-glutamine (Biochrom GmbH, Germany), supplemented with 5% fetal bovine serum (Sigma-Aldrich, Germany), MEM non-essential amino acids (Sigma-Aldrich AB, Germany), and antibiotics (100 IU penicillin and 100 µg/ml streptomycin) (Biochrome GmbH, Germany).

Genotyping

UM-SCC-74A and UM-SCC-74B cells were Genotyped using Short Tandem Repeat (STR) Analysis in order to verify the origin and similarity of the cell lines. DNA was extracted from frozen cell cultures and analyzed using the AmpFLSTR® Identifiler® PCR Amplification Kit. The Identifiler kit amplifies 15 loci and Amelogenin in a single tube and provides loci consistent with major worldwide STR databasing standards.

Clonogenic Survival

Clonogenic survival assays were performed as described previously (48), in order to assess the radiosensitivity of UM-SCC-74A and UM-SCC-74B cells. In short, cells were pre-plated into 25 cm^2 culture flasks with 8 ml complete medium. After 48 h, cells were exposed to external beam radiation using ^{137}Cs gamma-ray photons at a dose-rate of ∼1 Gy/min (Best Theratronics Gammacell® 40 Exactor, Springfield, USA), corresponding to a dose of 0, 2, 4, 6, or 8 Gy. Colonies were allowed to form for 10–14 days. Cells were then fixated with 95% ethanol and stained with crystal violet. The colonies were inspected under a microscope, and only cells giving rise to colonies consisting of 50 or more cells were considered clonogenic survivors. Plating efficiency, PE (number of colonies formed/number of cells seeded in the control), and the survival fraction (number of colonies formed after treatment/number of cells seeded × PE) were calculated in Microsoft Office Excel 2016 for Mac version 14.6.1 (Microsoft, Redmond, WA, USA). Statistical analyses were performed using GraphPad Prism 6 (GraphPad Software, San Diego, CA, USA). Differences in normalized survival fractions of 2 Gy irradiated UM-SCC-74A cells vs. UM-SCC-74B cells were assessed using an unpaired *t*-test and were considered statistically significant if $P < 0.05$.

Radiation Induced Long-Term Growth Inhibition

As a complement to the clonogenic- and 3D cell culture assays, the long-term growth inhibitory effects of radiation were evaluated using a growth inhibition assay as described earlier (49). In short, UM-SCC-74A or UM-SCC-74B cells were pre-plated into 25 cm^2 culture flasks with complete medium. After 48 h, cells were exposed to external beam radiation corresponding to a dose of 0, 2, 4, 6, or 8 Gy. Cells were then counted and reseeded about once a week, and the corresponding total cell numbers were calculated. The increase in cell number was followed for 4 weeks. Cell doubling times were calculated using the least square fitting method. In order to determine any statistically significant differences from the untreated group at the last data point, total cell numbers were analyzed using one-way ANOVA followed by Dunnett's multiple comparisons test in GraphPad Prism and were considered statistically significant if $P < 0.05$.

Radiation Response in 3D Cell Culture

For liquid overlay 3D multicellular tumor spheroid formation, 96-well plates were coated with 0.15% agarose dissolved in PBS with 1% penicillin/streptomycin. One thousand UM-SCC-74B cells/well or 1500 UM-SCC-74A cells/well were seeded and incubated at 37°C in supplemented media for 3 days prior to irradiation with 2 Gy or mock radiation (0 Gy) using ^{137}Cs gamma-ray photons as described above. Spheroid images were obtained at start of treatment and 10 days after treatment

using a Canon EOS 700D camera mounted on an inverted Nikon Diaphot-TMD microscope. The images were analyzed using ImageJ version 1.48 (NIH, Bethesda, MD, USA), by measuring the surface area of each spheroid and calculating the volume, assuming each spheroid retained a spherical form. Each spheroid was normalized to its own starting volume at the start of treatment (Day 0, growth ratio = 1). Statistical analyses were performed using GraphPad Prism 6 (GraphPad Software, San Diego, CA, USA). Differences in normalized spheroid growth ratios of UM-SCC-74A cells vs. UM-SCC-74B cells were assessed using an unpaired *t*-test and were considered statistically significant if $P < 0.05$.

Measurement of Cleaved Poly ADP Ribose Polymerase (PARP)

Levels of cleaved PARP1 in cell lines were measured using ELISA. The assay detects the presence of the 89 kDa PARP1 fragment containing the catalytic domain. The proteolysis of PARP1 by activated caspase-3 renders the enzyme inactive, which further facilitates apoptotic cell death. Thus, the presence of the 89 kDa PARP1 fragment is considered to be a reliable biomarker of apoptosis. Cells were incubated for 48 h prior to irradiation (2 Gy) or mock radiation (0 Gy) using ^{137}Cs gamma-ray photons as described above. Whole-cell lysates were prepared 12 h after irradiation according to standard protocols. Cell lysates were diluted 1:1,000. The Cleaved PARP1 Human SimpleStep ELISA® Kit (Abcam, Cambridge, UK) was used according to the manufacturer's protocol. The OD was then measured at 450 nm using a microtiter plate reader (BioRad, USA). Statistical analyses were performed using GraphPad Prism 6.

Differences in cleaved PARP1 levels were assessed using an unpaired *t*-test and were considered statistically significant if $P < 0.05$.

Irradiation of Cells for Metabolic Profiling

Two days before irradiation (18–25) $\times$ 10^6 UM-SCC-74A or (10–25) $\times$ 10^6 UM-SCC-74B cells were cultured in cell culture plates ($n = 46$ and $n = 52$, respectively, Nunclon Surface, 15 cm diameter, Cat No. 168 381, 145 cm^2) at 37°C, in 5% CO_2 in supplemented DMEM medium. At the time of irradiation, cells were exposed to external beam radiation corresponding to a dose of 0 or 2 Gy. Cells were subsequently harvested at ∼75% confluence at 4 h ($n = 20$ and 22 for UM-SCC-74A and UM-SCC-74B, respectively) and 24 h ($n = 26$ and 30 for UM-SCC-74A and UM-SCC-74B, respectively) after irradiation as according to Engskog et al. (50). The time points were chosen in order to detect IR-induced perturbations in the cell metabolome in the most optimal settings possible. These time points have been shown to be relevant for IR-induced early- and intermediate cellular responses in previous cell-based radiation metabolomic assessments (40, 41, 43). Moreover, while the cellular responses have occurred at these time points, they have not yet resulted in apoptosis in the majority of cells. Consequently, in these experimental settings a majority of the irradiated cells can be harvested, reducing any risk of selection-biased analyses. All cell sample harvesting was performed on ice. Cell medium was removed and cells were rapidly washed three times with cold, sterile phosphate buffered saline (PBS, Medicago, Uppsala, Sweden), followed by detachment of cells using a 23 cm long rubber-tipped Nunc cell scraper (Thermo Scientific). The detached cells were collected in 3.5 ml cold MilliQ water, transferred to 15 mL polypropylene brown tubes (Greiner bio-one GmbH, Germany) and snap-frozen in liquid N_2 followed by thawing at 37°C for 10 min. The freeze/thaw cycle was then repeated twice with subsequent sonication on ice for 30 s. Samples were stored at −80°C until metabolite extraction.

Metabolite Extraction

Prior to extraction of the intracellular metabolites, the samples were randomized into five separate sample batches comprised of 20 samples each. Each sample batch was prepared and analyzed separately. The samples were thawed at room temperature and centrifuged at 2000 RCF for 10 min at 4°C. A quality control (QC) sample was created for each batch by pooling an equal volume from all samples within each batch. The QC sample was extracted as described below. The five QC samples were pooled after extraction of all five batches. The aqueous supernatants were transferred to fresh extraction tubes followed by addition of chloroform and methanol for the final proportion 2.85:4:4 water:methanol:chloroform (51–53). The samples were vortexed gently and stored at 8°C for 20 min. to the samples were the centrifuged for 20 min at 2000 RCF and 4°C. The aqueous phases were recovered and evaporated to dryness at 40°C under a gentle stream of N_2(g).The samples were stored at −80°C after evaporation. Prior to analysis the samples were reconstituted in acetonitrile:Milli-Q water 76:24.

Metabolite Profiling With LC-MS

All metabolite profiling analyses were performed on an Acquity UPLC I-class system from Waters (Manchester, UK) hyphenated to a G2S Synapt Q-TOF equipped with an electrospray ionization (ESI) source (Waters). All systems were controlled using Masslynx version 4.1 (Waters). For chromatographic sample separation prior to detection a Acquity BEH amide column (1.7 µm, i.d. 2.1 × 50 mm) from Waters was used. The column temperature was kept at 40°C for all analyses and the injection volume was 5 µl. Mobile phase A consisted of 95:5 acetonitrile/water with 10 mM ammonium formate and 0.1% FA and mobile phase B consisted of 50:50 acetonitrile/water with 10 mM ammonium formate and 0.1% FA. A non-linear elution gradient from 100% A to 100% B was used, the flow rate was set to 0.3 ml/min. In detail: 100% A was kept for 0.5 min then decreased non-linearly (slope-factor 8 in MassLynx) over 12.5 min to 100% B, 100% B was held for 4 min followed by 6 min at 100% A to re-equilibrate the column for a total run-time of 23 min. Detection was performed in both positive and negative ionization mode in resolution MS^E-mode within the scan-range *m/z* 50–800. All samples were analyzed in negative ionization mode first, followed by positive ionization mode. The capillary voltage was 1 and −2 kV and the cone voltage was set to 30 and 25 V in positive and negative ionization mode, respectively.

In both ionization modes the source temperature was 120°C. Nitrogen was used as desolvation gas at the flow-rate 800 l/h and the desolvation temperature was 500°C and 450°C in positive and negative mode, respectively. Nitrogen was used as cone gas as well at a flow-rate of 50 l/h. and. A collision energy ramp from 20 to 45 eV was used for MS^E acquisition with argon as collision gas. Lock-mass correction for accurate *m/z* measurements was applied using a solution of leucine-enkephalin (*m/z* 556.2766). Each sample batch was analyzed separately, i.e., one sample batch per day. Prior to each sample batch analysis the instrument was mass calibrated and the sample cone was cleaned. A reference mix (30 μM of hypoxanthine, cytidine, phenylalanine, tryptophan, and glutamine, respectively) was analyzed before and after each batch to check the system suitability with regard to mass accuracy, instrument sensitivity, and column performance. The QC sample was analyzed repeatedly prior to the study samples for system conditioning, to ensure stable analytical conditions, as well as, between the randomized study samples in regular intervals to monitor the analytical stability throughout the analysis (54).

Chemicals

Formic acid, FA(LC-MS grade), ammonium formate (LC-MS grade), methanol (LC-MS grade), Cytidine (99%), hypoxanthine (≥99%), and tryptophan (≥99.5%) were purchased from Sigma Aldrich (Steinheim, Germany). Phenylalanine (>99%) was purchased from MERCK (Kenilworth, N.J., USA) while glutamine (>99%) was purchased from Fluka (Buchs, Switzerland). Acetonitrile (LC-MS grade) was obtained from Fischer Scientific (Zurich, Switzerland) and chloroform (analytical grade) was purchased from BDH Laboratory Supplies (Poole, England, UK). Leucine-encephalin was prepared and certified by ERA (Golden, CO, USA). The water was purified using a Milli-Q™ water system from MilliPore (Bedford, MA, USA).

Data Processing

Data quality was assessed through in-depth examinations of five representative metabolites spread out in the obtained chromatograms; hypoxanthine, cytidine, phenylalanine, tryptophan, and glutamine. The evaluation was performed by univariate data analysis based on all QC sample injections, in total 25 injections (20% of all sample injections), prior to data pre-processing and multivariate data analysis. Mass accuracy, retention time, and peak area was monitored to check system stability throughout the analysis. DataBridge (Masslynx version 4.1, Waters) was used to convert the raw data files to NetCDF files. The R-based software XCMS was used for peak detection, retention time alignment, and peak grouping (55). The centWave function was used for peak detection with the following function parameters; the maximal deviation in m/z between scans was set to 10 ppm, the boundaries for peak width was set between 5 and 45 s and the signal to noise ratio cut-off was set to 5. The "obiwarp" function was used for retention time alignment. The processed data was subjected to adduct, isotope and fragment annotation using the R-Package, CAMERA (56). The resulting dataset was exported to Microsoft Excel and prior to normalization all features with a retention time <50 s were removed. The data was normalized using LocalMean correction where all features were normalized to the feature mean of the QC:s in the respective batches (57). After normalization, all features with coefficient of variance (CV) >30% in the QC samples were removed (54, 58, 59).

Multivariate and Univariate Data Analysis

The reduced and filtered data sets from the data processing were analyzed by multivariate data analysis using SIMCA-P+ (version 14, Umetrics, Umeå, Sweden). All data was pareto scaled prior to multivariate data analysis. Principal Component Analysis (PCA) was used to find sample clustering, identify possible sample outliers, and systematic trends in the data. Orthogonal Projection to Latent Structures- Discriminant Analysis (OPLS-DA) in combination with S-Plots were used analyse differences between sample groups and to identify differentiating features between sample groups (60, 61).

Comparisons were made between the two cell line controls as well as between irradiated cells and controls of the respective SCC cell lines. The irradiated cells were further divided into subgroups of rapid response and intermediate response depending on the time between cell irradiation and cell sample harvesting. Rapid response subgroups were harvested 4 h after irradiation and intermediate response subgroups were harvested 24 h after irradiation.

Features with *p*-corr values >0.4 were selected and annotated. Molecular weight, isotopic patterns, fragmentation and, when possible, retention time comparison to an in-house database were utilized for feature annotation. The Human Metabolome Database (HMDB), METLIN and in-house databases was utilized to search for the experimental *m/z* values with a molecular weight difference tolerance of 30 ppm. The raw data signal isotopic pattern, fragmentation (when reference spectra was available) as well as related adducts present at the same retention time in the raw data were all matched against the plausible hits from the data base search. All annotated metabolites should be considered putatively annotated (level 2) according to the Metabolomics Standards Initiative nomenclature (62). All annotated metabolites were subjected to pathway analysis using MetaboAnalyst 3.0 and the highest score pathways were subjected to further data analysis. One-Way Analysis of Variance (ANOVA) and *post-hoc* Tukey tests using Origin 2015 (OriginLab corporation, Northampton, MA, USA) was used for univariate significance testing of all annotated features and *p*-values <0.05 was considered significant. The significantly altered metabolite are presented as fold changes with 95% confidence intervals. The confidence intervals of fold changes were calculated using Fieller's theorem.

RESULTS

Genotyping

STR results demonstrated identical results for unirradiated UM-SCC-74A and UM-SCC-74B (**Supplemental Table 1**), verifying the origin and similarity of UM-SCC-74A and UM-SCC-74B cells.

Clonogenic Survival, Cell Growth, and Apoptosis Assays

The effect of radiation on UM-SCC-74A and UM-SCC-74B cell viability was studied using clonogenic survival assays, 3D cell growth assays, and long term growth inhibition assays, and can be seen in **Figures 1**, **2**. In all three assays, UM-SCC-74A cells proved more sensitive to radiation than UM-SCC-74B cells.

In the clonogenic survival assay (**Figures 1A,B**), UM-SCC-74A cells demonstrated a lower survival fraction than UM-SCC74B at all radiation doses assessed (**Figure 1A**). Accordingly, a radiation dose of 2 Gy to UM-SCC-74A resulted in a survival fraction of 24 ± 5 (SEM)% of the unirradiated controls, whereas the survival fraction of irradiated UM-SCC-74B cells was significantly higher, 52 ± 6% (**Figure 1B**).

In the three-dimensional cell growth assay (**Figure 1C**), spheroid growth was followed for 10 days after irradiation, reflecting effects of both cell death and growth inhibition in a more *in vivo*-like environment (63). Also here, UM-SCC-74B cells were significantly less affected by radiation, where a radiation dose of 2 Gy resulted in a normalized spheroid size of 84 ± 5 (SEM)% of unirradiated controls, compared to 44 ± 3% for UM-SCC-74A spheroids.

In the long-term cell growth assay, cell growth was followed for 4 weeks' time, reflecting long-term effects of both cell death and growth inhibition. Doubling times of unirradiated UM-SCC-74A and UM-SCC-74B cells were 1.48 and 1.28 days, respectively. Also in this assay, UM-SCC-74A cells were more affected by radiation than UM-SCC-74B cells (**Figures 2A,B**). At the last assessed time point (27 days), UM-SCC-74A cells exposed to 2 Gy of irradiation were 52 ± 19% (SEM) of unirradiated controls. For 4, 6, and 8 Gy, the corresponding numbers were 5.9 ± 2.0, 1.0 ± 0.1, and 0.01 ± 0.01% (**Figure 2C**). For UM-SCC-74B cells, 2 Gy irradiation resulted in a cell number of 65 ± 12% of unirradiated controls at day 27, and for 4, 6, and 8 Gy the corresponding numbers were 37 ± 16, 4.2 ± 0.9, and 0.11 ± 0.05% (**Figure 2D**).

Moreover, apoptosis was also studied in the cells using a cleaved PARP1 assay (**Supplemental Figure 1**). Levels of cleaved PARP1 were significantly increased in 2 Gy irradiated UM-SCC-74A cells compared to unirradiated cells, whereas levels did not significantly differ for UM-SCC-74B cells.

Consequently, as all these independent assays demonstrated UM-SCC-74A cells to be clearly more affected by radiation in terms of cell viability and growth than UM-SCC-74B cells, UM-SCC-74A are referred to as "radiosensitive" and UM-SCC-74B cells as "radioresistant" in the present study. These are to be viewed as relative terms, where UM-SCC-74A cells are "radiosensitive" in relation to UM-SCC-74B cells and vice versa.

Metabolic Profiling Data Quality Control

Mass accuracy, retention time, and peak area of five metabolites; hypoxanthine, cytidine, phenylalanine, tryptophan, and glutamine were monitored in the QC samples throughout the analysis to verify system stability. The mass error was found to be within 10 and 12 ppm in positive and negative ionization mode, respectively, and the variation in retention time displayed a CV-value below 1.5% throughout the analysis. The peak areas over the five analytical batches evidenced, as expected, some batch variations; this was however corrected for after the normalization by local mean correction as no sample separation due to batch effects were found in the multivariate data analysis. The peak areas of hypoxanthine, cytidine, phenylalanine and tryptophan varied from 26 to 48% (CV) in the raw data while glutamine showed huge variations of up to 128%.

Metabolic Profiling

Multivariate data analysis was performed on the pre-processed and filtered data using PCA and OPLS-DA. All samples were analyzed with the unsupervised model PCA to examine possible sample group separations and sample clustering behavior. The PCA scores plot revealed clear discrimination between the intracellular metabolome of the SCC cell lines in the second component (PC2) (**Figure 3**). There was some separation between irradiated cells and controls along the first component (PC1), the separation was most pronounced for the less radiosensitive UM-SCC-74B cell line. However, for both cell lines the controls cluster at the left hand side of the scores plot with the irradiated cells on the right hand side.

The supervised model OPLS-DA was used to analyse the metabolic changes due to irradiation in the two SCC cell lines as well as the metabolic differences between the SCC cell line controls (unirradiated controls). The metabolic changes after irradiation in each SCC cell line was separated into rapid response (cells were harvested 4 h after irradiation) and intermediate response (cells were harvested 24 h after irradiation), respectively.

The metabolic profiling demonstrated a number of significant ($p < 0.05$) metabolic differences between the two non-irradiated cell line controls (**Table 1**). Several metabolites connected to nicotinate and nicotinamide metabolism such as nicotinic acid, nicotinamide, and nicotinic acid mononucleotide were found altered in the UM-SCC-74B cell line as compared to UM-SCC-74A ($p = 0.005$). Moreover, guanosine, inosine, xanthine, and the purine intermediate 5-phosphoribosylamine were found at significantly different levels in the two cell lines indicating changes in purine metabolism and biosynthesis between UM-SCC-74A and UM-SCC-74B ($p = 0.006$).

In the radiosensitive cell line UM-SCC-74A, very few metabolic alterations were observed after irradiation (**Table 2**). The main metabolic alterations were linked to tryptophan metabolism through tryptophan and 5-hydroxyindoleacetic acid (5-HIAA) ($p = 0.0006$). In contrast, the less radiosensitive cell line UM-SCC-74B showed numerous metabolic alterations after irradiation, where the main metabolic alterations were connected to nicotinate and nicotinamide metabolism ($p = 0.003$), the methionine cycle ($p = 0.05$), and purine metabolism ($p = 0.001$) (**Table 3**). A number of metabolites involved in the nicotinate and nicotinamide metabolism such as 1-methylnicotinamide, niacinamide, beta-nicotinamide D-ribonucleotide, nicotinic acid mononucleotide, and nicotinamide adenine dinucleotide (NAD) were all down-regulated in the UM-SCC-74B 24 h after irradiation. Several metabolites involved in the methionine cycle as well as the glycine and serine biosynthesis and

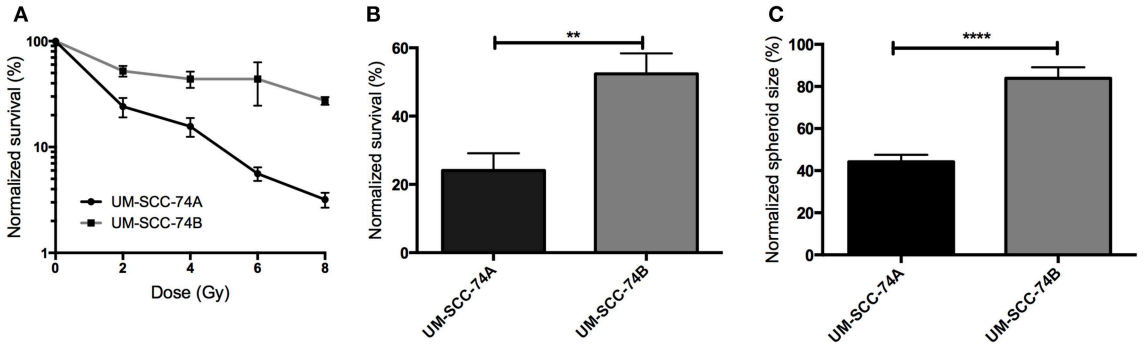

FIGURE 1 | (A) Clonogenic survival assay of UM-SCC-74A and UM-SCC-74B cells treated with a radiation dose of 0, 2, 4, 6, and 8 Gy. $N > 3$. Groups are normalized to the plating efficiency of the non-irradiated controls. Error bars represent the standard error of mean. **(B)** Comparison of clonogenic survival of UM-SCC-74A and UM-SCC-74B cells treated with a radiation dose of 2 Gy. $N > 6$. Difference in survival fraction was assessed using an unpaired *t*-test. $^{**}p < 0.01$. **(C)** Assessment of UM-SCC-74A and UM-SCC-74B spheroid growth 10 days after 2 Gy irradiation. Groups are normalized to the growth ratio of the non-irradiated controls. N > 5. Difference in spheroid growth was assessed using an unpaired *t*-test. $^{****}p < 0.0001$.

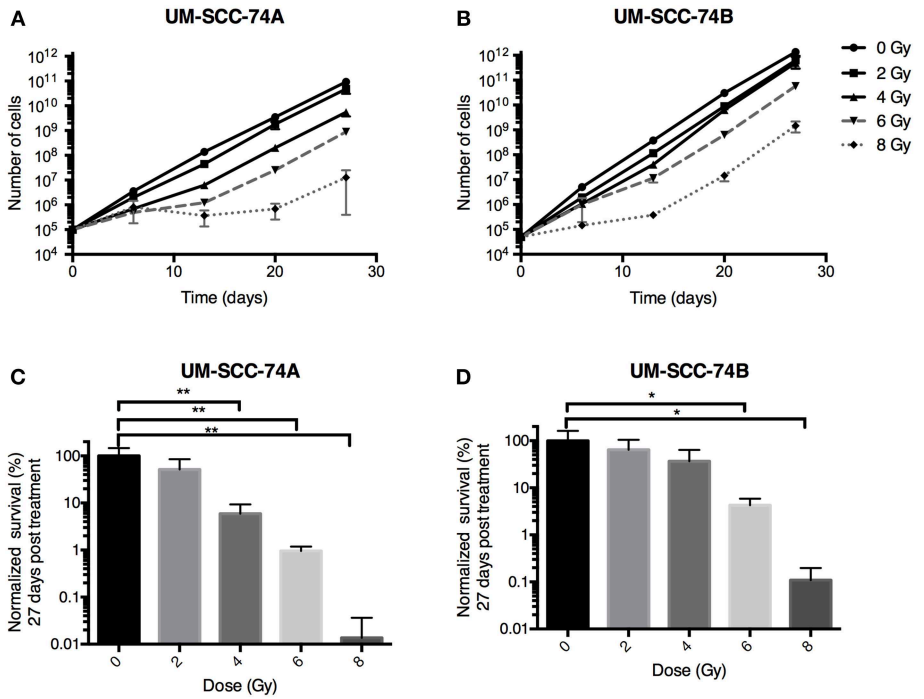

FIGURE 2 | Growth inhibition studies of UM-SCC-74A and UM-SCC-74B cells treated with radiation (0, 2, 4, 6, or 8 Gy). Error bars represent the standard error of mean. $N = 3$. **(A,B)** Cell growth followed over time. **(C,D)** Comparison at day 27. Differences in total cell numbers from control at day 27 were analyzed using one-way ANOVA followed by Dunnett's multiple comparisons test. $^{*}p < 0.05$, $^{**}p < 0.01$.

metabolism were found altered in the irradiated UM-SCC-74B cells. Increased levels of methionine were observed 4 h after irradiation, while the levels of S-adenosylmethionine (SAM) was increased both 4 h and 24 h after irradiation. Metabolites involved in purine metabolism such as adenosine, guanosine, and guanine were upregulated 24 h after irradiation while guanosine mono phosphate (GMP) was found in significantly higher levels 4 h after irradiation as compared to 24 h after irradiation.

DISCUSSION

A current clinical problem in HNSCC is the varying therapeutic response to irradiation, from complete to no response, moreover relapse and resistance is common (64). Individualized dosimetry, e.g., by predicting or monitoring tumor radiation response before, during, or after treatment, could help optimize radiotherapy, improve therapeutic outcome, and reduce normal tissue complication after radiotherapy. The plasticity of cancer

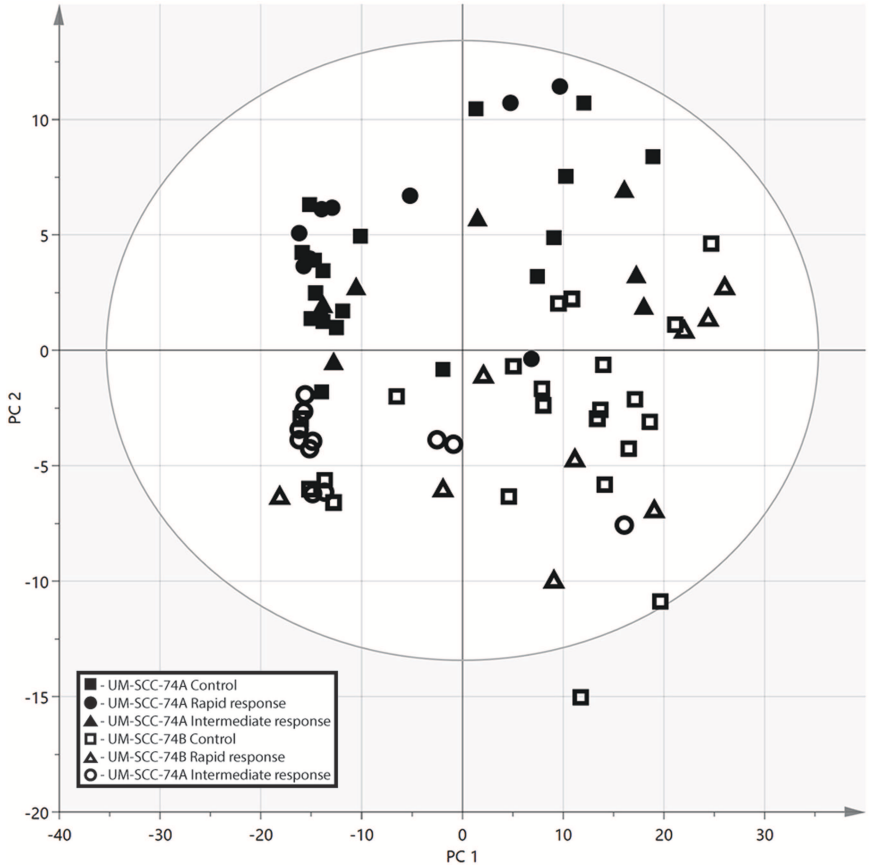

FIGURE 3 | PCA score plot from the metabolic profiling in negative ionization mode, the two SCC cell lines are separated along the second principal component (PC2). Along the first component (PC1) there is some separation between the controls and irradiated cells, however, no clear clustering. UM-SCC-74A Control (■), UM-SCC-74A Rapid response (4 h after 2 Gy irradiation) (▲), UM-SCC-74A Intermediate response (24 h after 2 Gy irradiation) (●), UM-SCC-74B Control (□), UM-SCC-74B Rapid response (△), and UM-SCC-74B Intermediate response (○).

cell metabolism plays a major role in cancer cell survival and treatment-resistant disease. Cancer cells are able to adapt metabolically to many types of cellular stress, such as radiation, and previous studies have demonstrated alterations in cellular metabolites after irradiation of the cells (40, 41, 43, 65–68). Consequently, a feasible way to provide significant understanding on the mechanisms of radiation response may be through metabolic profiling. In the present study, we have assessed metabolic profiling as a mean to investigate the relationship between radiation response and the metabolome. This was done by utilizing a unique *in vitro* model, in which two HNSCC cell lines from the same donor were employed. These cells exhibited the same STR genetic profile (**Supplemental Table 1**) but were shown to display different radiosensitivities, where UM-SCC-74A was shown to be clearly more sensitive to radiation than UM-SCC-74B in four independent assays (**Figures 1**, **2**, **Supplemental Figure 1**). These assays reflect different thresholds, parameters, and time-frames for assessment of cell viability and growth. Consequently, they are to be seen as important complements to each other in order to assess the full spectrum of radiation response.

UM-SCC-74B Cells Were More Radioresistant Than UM-SCC-74A Cells

In the clonogenic survival assay, considered as a gold standard in radiation research (48, 69), UM-SCC-74A displayed a lower survival fraction at all radiation doses assessed, at 2 Gy approximately half of that of UM-SCC-74B (**Figures 1A,B**). The assay combines contribution of all types of cell death, encompassing both early and late events. However, the impact of cell-to-cell communication is disregarded. Moreover, quiescent cells and cells growing at a slower rate may be counted as non-surviving clones in the clonogenic survival assay.

In contrast, the long-term growth inhibition assay, and in particular the 3D cell culture assay, include cell-to-cell communication, and both assays reflect both cell death and cell growth inhibition. The long-term growth inhibition assay is an especially suitable complement to clonogenic survival assays at higher doses, where the plating efficiency for clonogenic survival may be too low to ensure reliable results. The longer time-frame also enables visualization of delayed or reduced growth. This was demonstrated in the present study, e.g., for the 8 Gy irradiated samples, where UM-SCC-74A cells resumed growth after 3 weeks, whereas, UM-SCC-74B growth

TABLE 1 | Significantly different metabolites ($p < 0.05$) between non-irradiated cell lines UM-SCC-74A and UM-SCC-74B are presented as fold changes (95% confidence).

POSITIVE IONIZATION	
Metabolite ID	**A control vs. B control**
5-phosphoribosylamine	−2.10 ± 0.66
DMAPP	2.39 ± 1.20
NEGATIVE IONIZATION	
Metabolite	**A control vs. B control**
Tyrosine	−2.01 ± 0.74
Valine	−3.35 ± 1.72
Alanine, sarcosine, beta-alanine	−3.39 ± 1.95
Homoserine, threonine	−6.80 ± 5.20
Hydantoin-5-propionic acid	−2.14 ± 0.72
Diphosphoinositol pentakisphosphate	−2.35 ± 1.02
Myo-inositol hexakisphosphate	−2.54 ± 1.21
Leukotriene D4	14.54 ± 5.01
Leukotriene E4	−4.21 ± 1.67
Xanthine	39.62 ± 14.12
Guanosine	12.71 ± 9.35
Inosine	3.83 ± 2.20
Cytidine	2.67 ± 1.22
Nicotinic acid mononucleotide	−5.93 ± 2.50
Nicotinic acid	2.30 ± 0.93
Niacinamide	−2.13 ± 0.62
Pantothenic acid	−3.17 ± 1.59
2-Aminomuconic acid semialdehyde	1.96 ± 0.68

The p-values were calculated using ANOVA followed by a Tukey test and the fold changes were calculated using Fieller's theorem for a 95% confidence interval. A positive fold change indicates a higher level in 74A UM-SCC-74A as compared to 74B UM-SCC-74B

TABLE 2 | Significantly altered metabolites ($p < 0.05$) in the cell line UM-SCC-74A between cells irradiated with 2 Gy [assessed 4 h (rapid) or 24 h (intermediate) after irradiation] vs. non-irradiated cells (control) from the analysis in negative ionization mode are presented as fold changes (95% confidence intervals).

Metabolite	**Rapid vs. control**	**Intermediate vs. control**	**Rapid vs. intermediate**
NEGATIVE IONIZATION			
Phenylalanine		1.84 ± 0.62	
Uridine	−2.27 ± 0.88	1.62 ± 0.55	−3.54 ± 1.51
Adenosine			3.94 ± 2.20
2-Aminomuconic acid semialdehyde			−1.54 ± 0.51
5-Hydroxyindoleacetic acid		2.26 ± 1.10	−2.49 ± 1.28
POSITIVE IONIZATION			
Tryptophan	2.23 ± 0.94		2.48 ± 1.15

The p-values were calculated using ANOVA followed by a Tukey test and the fold changes were calculated using Fieller's theorem for a 95% confidence interval. A positive fold change indicates a higher level in the radiated cells as compared to the control.

was resumed already after 2 weeks (**Figures 2A,B**). Results in the long-term growth inhibition assay (**Figure 2**) verified the clear differences in radiosensitivity at higher doses observed in the clonogenic survival assays (**Figure 1A**). Also at 2 Gy, UM-SCC-74A cells demonstrated lower cell growth and viability than UM-SCC-74B cells, although not as pronounced as in the clonogenic survival assay, potentially reflecting the different time-frames, culture conditions, and assessed parameters in the different assays. The long-term growth assay also visualized the different doubling times of the cell lines, where UM-SCC-74B demonstrated a shorter doubling time than UM-SCC-74A. This is consistent with clinical experiences, where the recurrence of a tumor is often faster growing and more aggressive. The differences in growth rates were also in line with the clearly separated PCA scores plot (**Figure 3**), and reflected in some of the metabolic differences between the unirradiated cell lines (**Table 1**), discussed more in detail below. The fact that the STR profiles were the same, whereas factors such as growth rates, radiation resistance, and metabolic profiles were not, also demonstrates the advantage of complementing genetic data with cell assays and metabolomic profiling.

The 3D cell culture assay visualizes radiation effects on viability and cell growth in the same time frame as clonogenic survival. However, in the 3D assay, cells are cultured in a more *in vivo* like situation. In addition to cell-to-cell communication, important factors such as oxygen and nutritient gradients are mimicking the environment of small non-vascularized metastases (63). Results from the 3D cell culture assay were in line with the clonogenic survival assay, where both assays demonstrated approximately twice as many surviving UM-SCC-74B cells than UM-SCC-74A cells 10–14 days after 2 Gy irradiation (**Figures 1B,C**), further validating the difference in radiosensitivity between the cell lines. Consequently, we conclude that in all three independent assays UM-SCC-74A cells were clearly more affected by radiation in terms of cell viability and growth than UM-SCC-74B cells. This was also in line with the apoptosis assay, demonstrating increased levels of cleaved PARP1 in irradiated UM-SCC74A cells, but not in UM-SCC-74B cells (**Supplemental Figure 1**). Thus, we concluded that the cell lines were a suitable model system for subsequent complex metabolic evaluations of radiation response.

Unirradiated Cells Differed in Nicotinamide and Nicotinic Acid Metabolism and Purine Metabolism Pathways

Even though unirradiated UM-SCC-74A and UM-SCC-74B cells were identical according to STR genotyping, metabolic profiles differed clearly between the two unirradiated cell lines, as they were distinctly separated in the PCA scores plot (**Figure 3**). The nicotinamide and nicotinic acid metabolism pathways were indicated as important differences in the pathway analysis between the two cell lines, with metabolites such as nicotinamide, nicotinic acid, and nicotinic acid mononucleotide significantly different between the two control groups (**Figure 4**, **Table 1**). Nicotinamide and nicotinic acid mononucleotide were found at significantly higher levels in unirradiated UM-SCC-74B cells compared to UM-SCC-74A cells, while nicotinic acid was found in higher levels in unirradiated UM-SCC-74A cells compared

TABLE 3 | Significantly altered metabolites ($p < 0.05$) in the cell line UM-SCC-74B between cells irradiated with 2 Gy [assessed 4 h (rapid) or 24 h (intermediate) after irradiation] vs. non-irradiated cells (control) from the analysis in positive ionization mode are presented as fold changes (95% confidence).

Metabolite	Rapid vs. control	Intermediate vs. control	Rapid vs. intermediate
POSITIVE IONIZATION			
Phenylalanine	2.18 ± 1.18		3.51 ± 2.18
Proline	2.64 ± 1.47		3.72 ± 2.12
Tyrosine	3.89 ± 2.63		8.32 ± 6.08
Glutamine			2.62 ± 1.35
Methionine	2.94 ± 1.27		3.68 ± 2.23
Valine	2.70 ± 1.74		5.07 ± 3.53
Taurine	2.93 ± 1.38		5.20 ± 2.87
Alanine, beta-alanine, sarcosine			1.60 ± 0.43
Creatine	4.14 ± 2.81		7.64 ± 5.24
Glucosamine, fructosamine			4.02 ± 2.89
N-Acetyl-glucosamine-1-phosphate	2.27 ± 1.23		3.90 ± 2.50
Glucosamine-1-phosphate	2.06 ± 0.75		4.90 ± 3.28
Dihydroneopterin triphosphate		1.58 ± 0.37	
Glycerophosphocholine	5.73 ± 4.13		10.56 ± 8.03
Hydroxyindole	1.71 ± 0.70		2.20 ± 0.96
Dityrosine			2.43 ± 1.30
Thiamine triphosphate	2.26 ± 1.19		3.81 ± 2.36
1-Methylnicotinamide			2.01 ± 0.88
Pantothenic acid			8.52 ± 7.61
UMP			3.35 ± 1.94
NEGATIVE IONIZATION			
Tyrosine		−9.01 ± 2.63	7.81 ± 3.92
Arginine		−4.37 ± 1.92	
Proline		−17.16 ± 7.94	
Valine		−23.50 ± 8.91	
Taurine		−13.71 ± 6.30	
Alanine, beta-alanine, sarcosine		−28.73 ± 23.88	
Homoserine, threonine		−39.49 ± 34.97	
L-Dopa	−3.78 ± 2.15		
Choline		−5.81 ± 2.33	5.06 ± 3.08
Docosanaoyl-CoA		45.98 ± 21.19	
Linolenoyl-CoA		−13.44 ± 11.25	
Oleoyl-CoA		−7.94 ± 4.77	
S-Adenosylmethionine	5.19 ± 3.36	4.74 ± 2.96	
Hydantoin-5-propionic acid		−6.50 ± 2.61	6.20 ± 3.38
1-Arachidonoylglycerophosphoinositol		3.74 ± 2.01	
Diphosphoinositol pentakisphosphate		−16.08 ± 3.31	
Myo-inositol hexakisphosphate		−7.94 ± 2.88	
Leukotriene E4		−24.29 ± 14.42	5.55 ± 0.38
Guanine		6.21 ± 2.41	−20.50 ± 19.17
Adenosine		3.59 ± 2.52	
Guanosine		19.83 ± 18.36	
Pantothenic acid		−19.21 ± 7.12	
Nicotinic acid mononucleotide		−8.92 ± 3.90	7.56 ± 5.20
1-methylnicotinamide		−6.75 ± 1.87	
Niacinamide		−6.34 ± 1.97	5.96 ± 2.41
beta-nicotinamide D-ribonucleotide		−5.11 ± 1.59	6.86 ± 4.32
NAD		−6.50 ± 2.79	8.18 ± 5.27
CMP			21.64 ± 19.67
GMP			17.49 ± 15.52

The p-values were calculated using ANOVA followed by a Tukey test and the fold changes were calculated using Fieller's theorem for a 95% confidence interval. A positive fold change indicates a higher level in the radiated cells as compared to the control.

to UM-SCC-74B cells (**Figure 4**). This indicates a lower rate of biosynthesis of nicotinic acid mononucleotide and ultimately in nicotinamide adenosine dinucleotide (NAD+) in the UM-SCC-74A cell line. The other main pathway that was found differentiating between the two non-irradiated cell lines was purine metabolism. Xanthine, inosine, and guanosine were all found at significantly higher levels in the UM-SCC-74A cells than in the UM-SCC-74B cells. The higher levels of inosine and xanthine in UM-SCC-74A may indicate a higher purine degradation in the UM-SCC-74A cell line. In UM-SCC-74B, 5-phosphoribosylamine was found in higher concentration, which is an intermediate in *de novo* purine synthesis, and might indicate a higher rate of *de novo* synthesis of purine nucleotides in the UM-SCC-74B cells. Higher rates of purine *de novo* synthesis have previously been linked to increased growth rates (70), and is in line with the results from the growth inhibition assay, where unirradiated UM-SCC-74B cells demonstrated a shorter doubling time than UM-SCC-74A cells (**Figure 2**).

Altered Tryptophan and Serotonin Metabolism in Irradiated UM-SCC-74A Cells

In general, very few metabolic alterations were observed after irradiation in UM-SCC-74A cells compared to UM-SCC-74B

cells. In the UM-SCC-74A cell line the most important radiation induced metabolic perturbation was the alteration in tryptophan metabolism. Tryptophan was found at higher levels as compared to the control 4 h after radiation but was reduced to the same levels as the control 24 h after radiation. Tryptophan has two main metabolic fates, it can be used in the biosynthesis of quinolinic acid, which is a precursor to nicotinic acid mononucleotide, or it can be converted to serotonin via 5-hydroxytryptophan. The increase in tryptophan levels 4 h after irradiation could be an indication of a shift in the metabolism toward an increase in quinolinic acid and nicotinic acid mononucleotide biosynthesis in the UM-SCC-74A cell line. However, this assumption could not be verified, as the nicotinic acid mononucleotide levels were not altered neither 4, nor 24 h after irradiation in UM-SCC-74A, and quinolinic acid was not detected in this analysis. Moreover, the serotonin metabolite 5-hydroxyindoleacetic acid (5-HIIA) was found increased 24 h after irradiation the UM-SCC-74A cell line, which might suggest an increase in serotonin degradation to 5-HIIA. Serotonin has been shown to exhibit growth stimulatory effects on several types of carcinoma and other tumor cells, and to play a role in radiation-induced bystander effect (71). In previous studies, serotonin concentrations in culture media have been shown to be depleted after exposure of cells to radiation, suggesting that serotonin may be bound by membrane receptors after irradiation, thus facilitating calcium entry into cells, production of ROS and activation of apoptosis pathways (71, 72). Serotonin can also act as both vasoconstrictor and promote angiogenesis in solid tumors, and could therefore have important effects on the tumor hypoxia which have been linked to radiation sensitivity previously (73).

Decreased Levels of NAD+ and Increased NAD+ Turnover Suggest Initiated DNA Repair Mechanisms in Irradiated UM-SCC-74B Cells

In the UM-SCC-74A cell line, no investigated metabolites in the nicotinamide and nicotinic acid metabolism demonstrated significantly altered levels after irradiation. This is in contrast to the UM-SCC-74B cell line, where the metabolites nicotinamide, 1-methylnicotinamide, nicotinamide ribotide, nicotinic acid mononucleotide, NADH as well as NAD+ were all almost depleted 24 h after irradiation (**Figure 4**). This demonstrates inherent differences in nicotinamide and nicotinate metabolism in the two cell lines both before and after irradiation. While the decrease in NAD+ could be due to an increase in turnover from NAD+ to NADP/NADPH to maintain the redox status in the cells, regenerate glutathione, and an increased biosynthesis (45), the fact that NADP+ and NADPH were not detected in the analysis contradicts this explanation. Thus, a more likely explanation is that the decreased levels of NAD+ and increased NAD+ turnover in UM-SCC-74B cells after irradiation is due to an increased ADP-ribosylation by poly(ADP-ribose)polymerases (PARPs) to initiate DNA repair mechanisms (74–77). The PARP proteins are the main consumers of NAD+ during genotoxic stress, and the levels of NAD+ can be depleted following ionizing radiation to meet the demands for DNA-repair signaling by ADP-ribosyl (74–76). PARP1 is a member of the PARP family of enzymes. Its primary function is to detect and repair DNA damage, where amplified PARP1 activity results in high NAD+ consumption. This process is blocked by rapid cleavage and inactivation of PARP1 by the action of caspases. In the present study, the cleaved PARP1 assay demonstrated that the levels of inactivated PARP1 were increased in irradiated UM-SCC-74A cells, whereas levels in UM-SCC-74B cells were unchanged after radiation (**Supplemental Figure 1**), which could further support this hypothesis. Moreover, previous studies have demonstrated that inhibition of PARP or PARP silencing increase radiosensitivity (78–85). Van Vuurden et al. (81) observed an overexpression of PARP1 as well as a radiosensitizing effect by the PARP1 inhibitor olaparib in pediatric medulloblastoma, ependymoma, and high grade glioma cell lines. Similarly, Owonikoko et al. (84) investigated the PARP1 inhibitor veliparib in combination with DNA-damaging treatments including radiation in small cell lung cancer cells, and found that veliparib sensitized some cells to DNA damaging treatment. Both Godon et al. (80) and Noël et al. (82) found that the radiosensitizing effect of PARP1 inhibition by 4-amino-1,8-naphthalimide (ANI) was cell cycle dependent, and that rapidly growing cells with high fraction of cells in the S-phase were more sensitive to PARP-inhibition in combination with radiation. Consequently, our data suggest that PARP inhibition may be especially suitable to overcome the radioresistance in the radioresistant UM-SCC-74B cells, and should be evaluated in future studies.

Increased Levels of Guanosine and Adenosine Indicate a Functioning Purine Salvage Pathway and More Efficient ROS Protection in Irradiated UM-SCC-74B Cells

In UM-SCC-74B, the levels of adenosine, guanosine and guanine were increased 24 h after irradiation, while the levels of adenosine monophosphate (AMP) and guanosine monophosphate (GMP) were decreased (not significantly) 24 h after irradiation. This indicates a functioning purine salvage pathway with an increased degradation of the purine nucleotides to the corresponding nucleosides and nucleobases. This is in line with previous studies, where guanosine have been shown to protect DNA *in vitro* from oxidative damage induced by reactive oxygen species (ROS), and to serve as a radioprotector (86). Adenosine has demonstrated the same effect as guanosine however not as strong, while the pyrimidine nucleobases had the opposite effect (86). In contrast, this pattern was not observed in the UM-SCC-74A cell line, where altered (although not significant) levels of inosine, hypoxanthine, and xanthine instead might indicate an increased purine nucleotide catabolism through the transformation of inosine to hypoxanthine to xanthine. This data suggests that the UM-SCC-74B cells may have enabled a more efficient ROS protection through increased levels of guanosine and adenosine after irradiation.

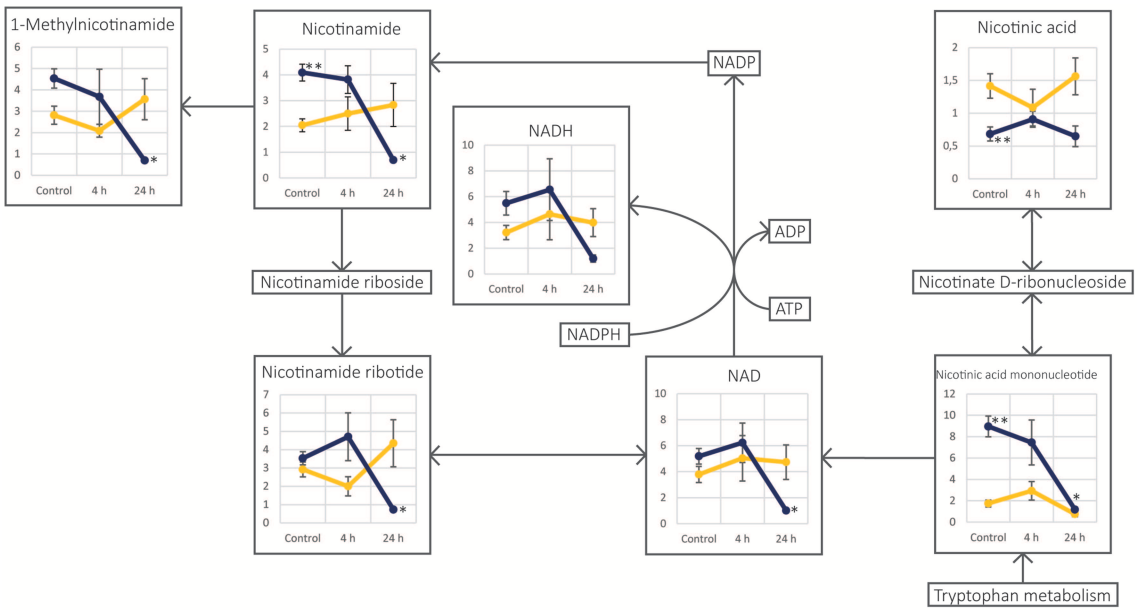

FIGURE 4 | Schematic figure of the nicotinamide and nicotinic acid metabolism pathway in the two cell lines UM-SCC-74A (yellow lines) and UM-SCC-74B (dark blue lines). Each annotated metabolite is represented by a line-plot with normalized peak area on the y-axis and the three different sample groups; Control, 4 and 24 h after irradiation, on the x-axis. Error bars represent standard error of the mean. *Metabolite level was significantly ($p < 0.05$) altered as compared to the respective control group. **Metabolite level was found significantly different ($p < 0.05$) between the two cell line control groups.

Increased Levels of SAM Indicate Alterations in the DNA Methylation in Irradiated UM-SCC-74B Cells

The pathway of cysteine and methionine metabolism was altered in the UM-SCC-74B cell line after irradiation, in contrast to UM-SCC-74A cells (**Figure 5**). S-adenosylmethionine (SAM) is a methyl donor, involved in almost all methylation reactions in the cells, such as DNA and histone methylation but also methyl transfer reactions to proteins, lipids, and secondary metabolites (3, 4). SAM is also an important component in many trans-sulfuration reactions and aminopropylation reactions (87). After irradiation, there was an increase in both methionine and SAM in UM-SCC-74B cells, suggesting an increased turnover from homocysteine to methionine, which can be driven by either the folate cycle or methyl-group transfer by betaine (87). As the levels of glycine and serine were not found altered after irradiation and neither were the levels of 5-methyltetrahydrofolate (data not shown), data suggest that the turnover from homocysteine to methionine was not driven by the folate cycle but rather betaine (88). This was supported by the decreased levels on choline, the main precursor of betaine, 24 h after irradiation. Moreover, the levels of glutathione in UM-SCC-74B cells were lower after irradiation, indicating that homocysteine is not converted to cystathionine, but mainly reconverted to methionine, since cysteine is the rate-limiting precursor for biosynthesis of glutathione (87). Consequently, our data suggest that irradiated UM-SCC-74B cells mobilized the homocysteine-methionine cycle, thereby increasing the synthesis of SAM to avoid radiation induced DNA-hypomethylation (89). This is in line with previous studies, linking global changes in DNA methylation to ionizing radiation (90–93), and to the development of radioresistance in oral squamous cell carcinoma (93) and lung cancer (92). Kim et al. (92) found that several key regulators in radiosensitivity in lung cancer were epigenetically controlled by CpG methylation. Batra et al. (94) demonstrated that methyl donor deficient diets increased the irradiation induced metabolic stress in mice and decreased DNA methyl transferase activity, indicating decreased DNA methylation (94, 95). Moreover, Batra et al. (96) demonstrated that L-methionine supplementation might help to alleviate radiation induced loss of genomic DNA methylation in murine liver tissue. This could open up for new possibilities of sensitizing tumors to radiation treatment and in the future avoid radio-resistance in radiation treatment.

CONCLUSION

Our data strongly implicates that the radioresistant cells changed their metabolism to control the redox status, DNA repair as well as DNA methylation. A lot of preclinical efforts have over time been devoted to the development of strategies to sensitize cancer cells to radiation therapy. This study was a first step in the understanding of which metabolic pathways in SCC that were important for the differences in radiosensitivity between the two cell lines UM-SCC-74A and UM-SCC-74B. The elucidation of the mechanisms behind radioresistance could lead to better prediction of radiation treatment outcome or possibilities to sensitize tumors to radiation. However, all

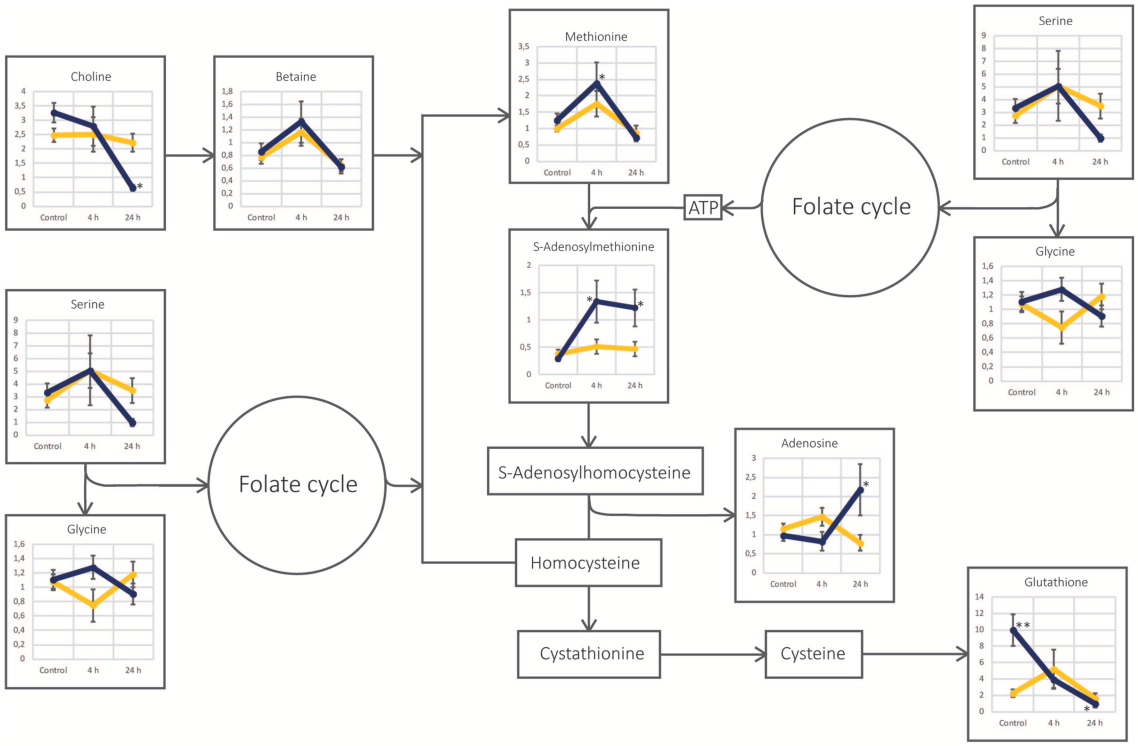

FIGURE 5 | Schematic figure of the cysteine and methionine metabolism pathway in the two cell lines UM-SCC-74A (yellow line) and UM-SCC-74B (dark blue line). Each annotated metabolite is represented by a line-plot with normalized peak area on the y-axis and the three different sample groups; Control, 4 and 24 h after irradiation, on the x-axis. Error bars represent standard error of the mean. *Metabolite level was significantly ($p < 0.05$) altered as compared to the respective control group. **Metabolite level was found significantly different ($p < 0.05$) between the two cell line control groups.

metabolites and metabolic pathways investigated in this study all require further investigation as to whether they will be able to pose as targets for prediction of radiation response or to enhance radiation sensitivity.

DATA AVAILABILITY

The datasets for this study are available on request.

AUTHOR CONTRIBUTIONS

EL, IE, ME, JH, TA, CP, GL, and MN designed the study. EL, IE, ME, JH, TA, MH, CP, GL, and MN contributed to data analysis and interpretation, and revised the manuscript. EL and IE contributed to experimental studies and drafted the manuscript.

FUNDING

This study was supported by grants from the Swedish Cancer Society (CAN 2018/494, CAN 2015/1080, and CAN 2015/385), and the Swedish Research Council (2013-30876-104113-30). Targeted funding for development of metabolomics research was obtained from the disciplinary domain of medicine and pharmacy at Uppsala University, and ALF-grants were obtained from Uppsala University Hospital.

ACKNOWLEDGMENTS

The authors would like to acknowledge Sara Häggblad Sahlberg and Jörgen Carlsson for kind manuscript feedback, and Christina Atterby, Anja Mortensen, and Tabassom Mohajer Shojai for help with cell culturing, cell assays, and harvesting.

SUPPLEMENTARY MATERIAL

The Supplementary Material for this article can be found online at: https://www.frontiersin.org/articles/10.3389/fonc.2019.00825/full#supplementary-material

Supplemental Figure 1 | Levels of cleaved PARP1 in UM-SCC-74A (black bars) and UM-SCC-74B (gray bars) cells 12 h after 0 or 2 Gy irradiation, measured by ELISA. Error bars represent the standard error of mean $N = 3$.

Supplemental Table 1 | STR analysis of non-irradiated UM-SCC-74A and UM-SCC-74B.

REFERENCES

1. Ferlay J, Shin H-R, Bray F, Forman D, Mathers C, Parkin DM. Estimates of worldwide burden of cancer in 2008: GLOBOCAN 2008. *Int J Cancer*. (2010) 127:2893–917. doi: 10.1002/ijc.25516
2. Curado MP, Boyle P. Epidemiology of head and neck squamous cell carcinoma not related to tobacco or alcohol. *Curr Opin Oncol.* (2013) 25:229–34. doi: 10.1097/CCO.0b013e32835ff48c
3. Siegel RL, Miller KD, Jemal A. Cancer statistics, 2015. *CA Cancer J Clin*. (2015) 65:5–29. doi: 10.3322/caac.21254
4. Jemal A, Siegel R, Ward E, Hao Y, Xu J, Murray T, et al. Cancer Statistics, 2008. *CA Cancer J Clin*. (2008) 58:71–96. doi: 10.3322/CA.2007.0010
5. Bhide SA, Newbold KL, Harrington KJ, Nutting CM. Clinical evaluation of intensity-modulated radiotherapy for head and neck cancers. *Br J Radiol.* (2012) 85:487–94. doi: 10.1259/bjr/85942136
6. Siegel R, DeSantis C, Virgo K, Stein K, Mariotto A, Smith T, et al. Cancer treatment and survivorship statistics, 2012. *CA Cancer J Clin.* (2012) 62:220–41. doi: 10.3322/caac.21149
7. Blanchard P, Baujat B, Holostenco V, Bourredjem A, Baey C, Bourhis J, et al. Meta-analysis of chemotherapy in head and neck cancer (MACH-NC): a comprehensive analysis by tumour site. *Radiother Oncol.* (2011) 100:33–40. doi: 10.1016/j.radonc.2011.05.036
8. Kelly C, Paleri V, Downs C, Shah R. Deterioration in quality of life and depressive symptoms during radiation therapy for head and neck cancer. *Otolaryngol Neck Surg.* (2007) 136:108–11. doi: 10.1016/j.otohns.2006.06.1278
9. Orth M, Lauber K, Niyazi M, Friedl AA, Li M, Maihöfer C, et al. Current concepts in clinical radiation oncology. *Radiat Environ Biophys.* (2014) 53:1–29. doi: 10.1007/s00411-013-0497-2
10. Anniko M, Bernal-Sprekelsen M, Bonkowsky V, Bradley PJ, Iurato S. *Otorhinolaryngology, Head and Neck Surgery*. Berlin; Heidelberg: Springer Berlin Heidelberg (2010). doi: 10.1007/978-3-540-68940-9
11. Vander Heiden MG, Cantley LC, Thompson CB. Understanding the Warburg effect: the metabolic requirements of cell proliferation. *Science*. (2009) 324:1029–33. doi: 10.1126/science.1160809
12. Valerie K, Yacoub A, Hagan MP, Curiel DT, Fisher PB, Grant S, et al. Radiation-induced cell signaling: inside-out and outside-in. *Mol Cancer Ther*. (2007) 6:789–801. doi: 10.1158/1535-7163.MCT-06-0596
13. Ward JF. The yield of DNA double-strand breaks produced intracellularly by ionizing radiation: a review. *Int J Radiat Biol.* (1990) 57:1141–50. doi: 10.1080/09553009014551251
14. Menon SS, Uppal M, Randhawa S, Cheema MS, Aghdam N, Usala RL, et al. Radiation metabolomics: current status and future directions. *Front Oncol.* (2016) 6:20. doi: 10.3389/fonc.2016.00020
15. Bernier J, Hall EJ, Giaccia A. Radiation oncology: a century of achievements. *Nat Rev Cancer*. (2004) 4:737–47. doi: 10.1038/nrc1451
16. Chaiswing L, Weiss HL, Jayswal RD, St. Clair DK, Kyprianou N. Profiles of radioresistance mechanisms in prostate cancer. *Crit Rev Oncog.* (2018) 23:39–67. doi: 10.1615/CritRevOncog.2018025946
17. Skvortsova I, Debbage P, Kumar V, Skvortsov S. Radiation resistance: cancer stem cells (CSCs) and their enigmatic pro-survival signaling. *Semin Cancer Biol*. (2015) 35:39–44. doi: 10.1016/j.semcancer.2015.09.009
18. Barker HE, Paget JT, Khan AA, Harrington KJ. The tumour microenvironment after radiotherapy: mechanisms of resistance and recurrence. *Nat Rev Cancer*. (2015) 15:409–25. doi: 10.1038/nrc3958
19. Goldstein M, Kastan MB. The DNA damage response: implications for tumor responses to radiation and chemotherapy. *Annu Rev Med.* (2015) 66:129–43. doi: 10.1146/annurev-med-081313-121208
20. Pastorek J, Pastorekova S. Hypoxia-induced carbonic anhydrase IX as a target for cancer therapy: from biology to clinical use. *Semin Cancer Biol.* (2015) 31:52–64. doi: 10.1016/j.semcancer.2014.08.002
21. Chan N, Milosevic M, Bristow RG. Tumor hypoxia, DNA repair and prostate cancer progression: new targets and new therapies. *Future Oncol.* (2007) 3:329–41. doi: 10.2217/14796694.3.3.329
22. Shibata A, Jeggo PA. DNA double-strand break repair in a cellular context. *Clin Oncol.* (2014) 26:243–9. doi: 10.1016/j.clon.2014.02.004
23. Lavelle C, Foray N. Chromatin structure and radiation-induced DNA damage: from structural biology to radiobiology. *Int J Biochem Cell Biol.* (2014) 49:84–97. doi: 10.1016/j.biocel.2014.01.012
24. Skvortsov S, Jimenez CR, Knol JC, Eichberger P, Schiestl B, Debbage P, et al. Radioresistant head and neck squamous cell carcinoma cells: intracellular signaling, putative biomarkers for tumor recurrences and possible therapeutic targets. *Radiother Oncol.* (2011) 101:177–82. doi: 10.1016/j.radonc.2011.05.067
25. Skvortsov S, Dudás J, Eichberger P, Witsch-Baumgartner M, Loeffler-Ragg J, Pritz C, et al. Rac1 as a potential therapeutic target for chemo-radioresistant head and neck squamous cell carcinomas (HNSCC). *Br J Cancer*. (2014) 110:2677–87. doi: 10.1038/bjc.2014.221
26. Pawlik TM, Keyomarsi K. Role of cell cycle in mediating sensitivity to radiotherapy. *Int J Radiat Oncol.* (2004) 59:928–42. doi: 10.1016/j.ijrobp.2004.03.005
27. Fiehn O. Metabolomics - The link between genotypes and phenotypes. *Plant Mol Biol.* (2002) 48:155–71. doi: 10.1007/978-94-010-0448-0_11
28. Tandle AT, Shankavaram U, Brown MV, Ho J, Graves C, Lita E, et al. Urinary metabolomic profiling of patients with glioblastoma multiforme. *J Proteomics Bioinform*. (2013) S6:003. doi: 10.4172/jpb.S6-003
29. Laiakis EC, Mak TD, Anizan S, Amundson SA, Barker CA, Wolden SL, et al. Development of a metabolomic radiation signature in urine from patients undergoing total body irradiation. *Radiat Res*. (2014) 181:350–61. doi: 10.1667/RR13567.1
30. Broin P, Vaitheesvaran B, Saha S, Hartil K, Chen EI, Goldman D, et al. Intestinal microbiota-derived metabolomic blood plasma markers for prior radiation injury. *Int J Radiat Oncol Biol Phys*. (2015) 91:360–7. doi: 10.1016/j.ijrobp.2014.10.023
31. Jelonek K, Pietrowska M, Widlak P. Systemic effects of ionizing radiation at the proteome and metabolome levels in the blood of cancer patients treated with radiotherapy: the influence of inflammation and radiation toxicity. *Int J Radiat Biol.* (2017) 93:683–96. doi: 10.1080/09553002.2017.1304590
32. Pannkuk EL, Laiakis EC, Authier S, Wong K, Fornace AJ. Global metabolomic identification of long-term dose-dependent urinary biomarkers in nonhuman primates exposed to ionizing radiation. *Radiat Res.* (2015) 184:121–33. doi: 10.1667/RR14091.1
33. Johnson CH, Patterson AD, Krausz KW, Kalinich JF, Tyburski JB, Kang DW, et al. Radiation metabolomics. 5. Identification of urinary biomarkers of ionizing radiation exposure in nonhuman primates by mass spectrometry-based metabolomics. *Radiat Res.* (2012) 178:328–40. doi: 10.1667/RR2950.1
34. Reisz JA, Bansal N, Qian J, Zhao W, Furdui CM. Effects of ionizing radiation on biological molecules—mechanisms of damage and emerging methods of detection. *Antioxid Redox Signal.* (2014) 21:260–92. doi: 10.1089/ars.2013.5489
35. Laiakis EC, Pannkuk EL, Chauthe SK, Wang YW, Lian M, Mak TD, et al. A serum small molecule biosignature of radiation exposure from total body irradiated patients. *J Proteome Res*. (2017) 16:3805–15. doi: 10.1021/acs.jproteome.7b00468
36. Golla S, Golla JP, Krausz KW, Manna SK, Simillion C, Beyoglu D, et al. Metabolomic analysis of mice exposed to gamma radiation reveals a systemic understanding of total-body exposure. *Radiat Res.* (2017) 187:612–29. doi: 10.1667/RR14592.1
37. Xiao X, Hu M, Zhang X, Hu JZ. NMR-based metabolomics analysis of liver from C57BL/6 mouse exposed to ionizing radiation. *Radiat Res*. (2017) 188:44–55. doi: 10.1667/RR14602.1
38. Laiakis EC, Pannkuk EL, Diaz-Rubio ME, Wang YW, Mak TD, Simbulan-Rosenthal CM, et al. Implications of genotypic differences in the generation of a urinary metabolomics radiation signature. *Mutat Res*. (2016) 788:41–9. doi: 10.1016/j.mrfmmm.2016.03.003
39. Goudarzi M, Mak TD, Chen C, Smilenov LB, Brenner DJ, Fornace AJ. The effect of low dose rate on metabolomic response to radiation in mice. *Radiat Environ Biophys.* (2014) 53:645–57. doi: 10.1007/s00411-014-0558-1
40. Patterson AD, Li H, Eichler GS, Krausz KW, Weinstein JN, Fornace AJ, et al. UPLC-ESI-TOFMS-based metabolomics and gene expression dynamics inspector self-organizing metabolomic maps as tools for understanding the cellular response to ionizing radiation. *Anal Chem.* (2008) 80:665–74. doi: 10.1021/ac701807v
41. Wu L, Hu Z, Huang Y, Yu Y, Liang W, Zheng Q, et al. Radiation changes the metabolic profiling of melanoma cell line B16. *PLoS ONE*. (2016) 11:e0162917. doi: 10.1371/journal.pone.0162917

42. Haritwal T, Maan K, Rana P, Parvez S, Singh AK, Khushu S, et al. Trichostatin A, an epigenetic modifier, mitigates radiation-induced androphysiological anomalies and metabolite changes in mice as evident from NMR-based metabolomics. *Int J Radiat Biol.* (2019) 95:443–51. doi: 10.1080/09553002.2018.1524989
43. Kwon YK, Ha IJ, Bae HW, Jang WG, Yun HJ, Kim SR, et al. Dose-dependent metabolic alterations in human cells exposed to gamma irradiation. *PLoS ONE*. (2014) 9:e113573. doi: 10.1371/journal.pone.0113573
44. Jose C, Bellance N, Rossignol R. Choosing between glycolysis and oxidative phosphorylation: a tumor's dilemma? *Biochim Biophys Acta Bioenerg.* (2011) 1807:552–61. doi: 10.1016/j.bbabio.2010.10.012
45. Sauve AA. NAD+ and vitamin B3: from metabolism to therapies. *J Pharmacol Exp Ther*. (2007) 324:883–93. doi: 10.1124/jpet.107.120758
46. Hassa PO, Haenni SS, Elser M, Hottiger MO. Nuclear ADP-ribosylation reactions in mammalian cells: where are we today and where are we going? *Microbiol Mol Biol Rev.* (2006) 70:789–829. doi: 10.1128/MMBR.00040-05
47. Brenner JC, Graham MP, Kumar B, Saunders LM, Kupfer R, Lyons RH, et al. Genotyping of 73 UM-SCC head and neck squamous cell carcinoma cell lines. *Head Neck*. (2010) 32:417–26. doi: 10.1002/hed.21198
48. Franken NA, Rodermond HM, Stap J, Haveman J, van Bree C. Clonogenic assay of cells *in vitro*. *Nat Protoc*. (2006) 1:2315–9. doi: 10.1038/nprot.2006.339
49. Nestor M, Persson M, van Dongen GA, Jensen HJ, Lundqvist H, Anniko M, et al. *In vitro* evaluation of the astatinated chimeric monoclonal antibody U36, a potential candidate for treatment of head and neck squamous cell carcinoma. *Eur J Nucl Med Mol Imaging.* (2005) 32:1296–304. doi: 10.1007/s00259-005-1848-2
50. Engskog M, Björklund M, Haglöf J, Arvidsson T, Shoshan M, Pettersson C. Metabolic profiling of epithelial ovarian cancer cell lines: evaluation of harvesting protocols for profiling using NMR spectroscopy. *Bioanalysis*. (2015) 7:157–66. doi: 10.4155/bio.14.235
51. León Z, García-Cañaveras JC, Donato MT, Lahoz A. Mammalian cell metabolomics: experimental design and sample preparation. *Electrophoresis*. (2013) 34:2762–75. doi: 10.1002/elps.201200605
52. Viant MR. Revealing the metabolome of animal tissues using 1H nuclear magnetic resonance spectroscopy. *Methods Mol Biol.* (2007) 358:229–46. doi: 10.1385/1-59745-244-0:229
53. Teng Q, Huang W, Collette TW, Ekman DR, Tan C. A direct cell quenching method for cell-culture based metabolomics. *Metabolomics*. (2009) 5:199–208. doi: 10.1007/s11306-008-0137-z
54. Engskog MKR, Haglöf J, Arvidsson T, Pettersson C. LC–MS based global metabolite profiling: the necessity of high data quality. *Metabolomics*. (2016) 12:114. doi: 10.1007/s11306-016-1058-x
55. Smith CA, Want EJ, O'Maille G, Abagyan R, Siuzdak G. XCMS: processing mass spectrometry data for metabolite profiling using nonlinear peak alignment, matching, and identification. *Anal Chem*. (2006) 78:779–87. doi: 10.1021/ac051437y
56. Kuhl C, Tautenhahn R, Böttcher C, Larson TR, Neumann S. CAMERA: an integrated strategy for compound spectra extraction and annotation of liquid chromatography/mass spectrometry data sets. *Anal Chem.* (2012) 84:283–9. doi: 10.1021/ac202450g
57. Kamleh MA, Ebbels TM, Spagou K, Masson P, Want EJ. Optimising the use of quality control samples for signal drift correction in long urine metabolic profiling studies. *Anal Chem*. (2012) 84:2670–7. doi: 10.1021/ac202733q
58. Want EJ, Wilson ID, Gika H, Theodoridis G, Plumb RS, Shockcor J, et al. Global metabolic profiling procedures for urine using UPLC-MS. *Nat Protoc.* (2010) 5:1005–18. doi: 10.1038/nprot.2010.50
59. Dunn WB, Broadhurst D, Begley P, Zelena E, Francis-Mcintyre S, Anderson N, et al. Procedures for large-scale metabolic profiling of serum and plasma using gas chromatography and liquid chromatography coupled to mass spectrometry. *Nat Protoc.* (2011) 6:1060–83. doi: 10.1038/nprot.2011.335
60. Bylesjö M, Rantalainen M, Cloarec O, Nicholson JK, Holmes E, Trygg J. OPLS discriminant analysis: combining the strengths of PLS-DA and SIMCA classification. *J Chemom.* (2006) 20:341–51. doi: 10.1002/cem.1006
61. Trygg J, Holmes E, Lundstedt T. Chemometrics in metabonomics. *J Proteome Res*. (2007) 6:469–79. doi: 10.1021/pr060594q
62. Creek DJ, Dunn WB, Fiehn O, Griffin JL, Hall RD, Lei Z, et al. Metabolite identification: are you sure? And how do your peers gauge your confidence? *Metabolomics*. (2014) 10:350–3. doi: 10.1007/s11306-014-0656-8
63. Hirschhaeuser F, Menne H, Dittfeld C, West J, Mueller-Klieser W, Kunz-Schughart LA. Multicellular tumor spheroids: an underestimated tool is catching up again. *J Biotechnol*. (2010) 148:3–15. doi: 10.1016/j.jbiotec.2010.01.012
64. Deeken JF, Newkirk K, Harter KW, Marshall MB, Banovac F, Johnson L, et al. Effect of multimodality treatment on overall survival for patients with metastatic or recurrent HPV-positive head and neck squamous cell carcinoma. *Head Neck*. (2015) 37:630–5. doi: 10.1002/hed.23644
65. Baroni F, Marraccini C, Merolle L, Piccagli V, Lambertini D, Iori M, et al. Red blood cells metabolome changes upon treatment with different X-ray irradiation doses. *Ann Hematol*. (2018) 97:1909–17. doi: 10.1007/s00277-018-3386-6
66. Varghese RS, Cheema A, Cheema P, Bourbeau M, Tuli L, Zhou B, et al. Analysis of LC-MS data for characterizing the metabolic changes in response to radiation. *J Proteome Res*. (2010) 9:2786–93. doi: 10.1021/pr100185b
67. Sappington DR, Siegel ER, Hiatt G, Desai A, Penney RB, Jamshidi-Parsian A, et al. Glutamine drives glutathione synthesis and contributes to radiation sensitivity of A549 and H460 lung cancer cell lines. *Biochim Biophys Acta*. (2016) 1860:836–43. doi: 10.1016/j.bbagen.2016.01.021
68. Wang M, Keogh A, Treves S, Idle JR, Beyoglu D. The metabolomic profile of gamma-irradiated human hepatoma and muscle cells reveals metabolic changes consistent with the Warburg effect. *PeerJ.* (2016) 4:e1624. doi: 10.7717/peerj.1624
69. Brown JM, Attardi LD. The role of apoptosis in cancer development and treatment response. *Nat Rev Cancer*. (2005) 5:231–7. doi: 10.1038/nrc1560
70. Kondo M, Yamaoka T, Honda S, Miwa Y, Katashima R, Moritani M, et al. The rate of cell growth is regulated by purine biosynthesis via ATP production and G1to S phase transition. *J Biochem*. (2000) 128:57–64. doi: 10.1093/oxfordjournals.jbchem.a022730
71. Azzam EI, de Toledo SM, Little JB. Oxidative metabolism, gap junctions and the ionizing radiation-induced bystander effect. *Oncogene*. (2003) 22:7050–7. doi: 10.1038/sj.onc.1206961
72. Lyng FM, Maguire P, McClean B, Seymour C, Mothersill C. The involvement of calcium and MAP kinase signaling pathways in the production of radiation-induced bystander effects. *Radiat Res*. (2006) 165:400–9. doi: 10.1667/RR3527.1
73. Sarrouilhe D, Clarhaut J, Defamie N, Mesnil M. Serotonin and cancer: what is the link? *Curr Mol Med.* (2015) 15:62–77. doi: 10.2174/1566524015666150114113411
74. Fouquerel E, Sobol RW. ARTD1 (PARP1) activation and NAD+ in DNA repair and cell death. *DNA Repair*. (2014) 23:27–32. doi: 10.1016/j.dnarep.2014.09.004
75. Sharif T, Martell E, Dai C, Ghassemi-Rad MS, Kennedy BE, Lee PWK, et al. Regulation of cancer and cancer-related genes via NAD +. *Antioxid Redox Signal*. (2018) 30:906–23. doi: 10.1089/ars.2017.7478
76. Surjana D, Halliday GM, Damian DL. Role of nicotinamide in DNA damage, mutagenesis, and DNA repair. *J Nucleic Acids*. (2010) 2010:157591. doi: 10.4061/2010/157591
77. Virág L, Szabó C. The therapeutic potential of poly (ADP-Ribose). *Pharmacol Rev*. (2002) 54:375–429. doi: 10.1124/pr.54.3.375
78. Chalmers A, Johnston P, Woodcock M, Joiner M, Marples B. PARP-1, PARP-2, and the cellular response to low doses of ionizing radiation. *Int J Radiat Oncol Biol Phys*. (2004) 58:410–9. doi: 10.1016/j.ijrobp.2003.09.053
79. Guillot C, Favaudon V, Herceg Z, Sagne C, Sauvaigo S, Merle P, et al. PARP inhibition and the radiosensitizing effects of the PARP inhibitor ABT-888 in *in vitro* hepatocellular carcinoma models. *BMC Cancer*. (2014) 14:603. doi: 10.1186/1471-2407-14-603
80. Godon C, Cordelières FP, Biard D, Giocanti N, Mégnin-Chanet F, Hall J, et al. PARP inhibition versus PARP-1 silencing: different outcomes in terms of single-strand break repair and radiation susceptibility. *Nucleic Acids Res*. (2008) 36:4454–64. doi: 10.1093/nar/gkn403
81. Van Vuurden DG, Hulleman E, Meijer OLM, Wedekind LE, Kool M, Witt H, et al. PARP inhibition sensitizes childhood high grade medulloblastoma and ependymoma to radiation. *Oncotarget*. (2011) 2:984–96. doi: 10.18632/oncotarget.362

82. Noël G, Godon C, Fernet M, Giocanti N, Mégnin-Chanet F, Favaudon V. Radiosensitization by the poly(ADP-ribose) polymerase inhibitor 4-amino-1,8-naphthalimide is specific of the S phase of the cell cycle and involves arrest of DNA synthesis. *Mol Cancer Ther.* (2006) 5:564–74. doi: 10.1158/1535-7163.MCT-05-0418
83. Wurster S, Hennes F, Parplys AC, Seelbach JI, Mansour WY, Zielinski A, et al. PARP1 inhibition radiosensitizes HNSCC cells deficient in homologous recombination by disabling the DNA replication fork elongation response. *Oncotarget*. (2016) 7:9732–41. doi: 10.18632/oncotarget.6947
84. Owonikoko TK, Zhang G, Deng X, Rossi MR, Switchenko JM, Doho GH, et al. Poly (ADP) ribose polymerase enzyme inhibitor, veliparib, potentiates chemotherapy and radiation *in vitro* and *in vivo* in small cell lung cancer. *Cancer Med*. (2014) 3:1579–94. doi: 10.1002/cam4.317
85. Karam SD, Reddy K, Blatchford PJ, Waxweiler T, DeLouize AM, Oweida A, et al. Final report of a phase I trial of olaparib with cetuximab and radiation for heavy smoker patients with locally advanced head and neck cancer. *Clin Cancer Res.* (2018) 24:4949–59. doi: 10.1158/1078-0432.CCR-18-0467
86. Gudkov SV, Shtarkman IN, Smirnova VS, Chernikov AV, Bruskov VI. Guanosine and inosine display antioxidant activity, protect DNA *in vitro* from oxidative damage induced by reactive oxygen species, and serve as radioprotectors in mice. *Radiat Res*. (2006) 165:538–45. doi: 10.1667/RR3552.1
87. Lu SC. S-Adenosylmethionine. *Int J Biochem Cell Biol.* (2000) 32:391–5. doi: 10.1016/S1357-2725(99)00139-9
88. Maddocks ODK, Labuschagne CF, Adams PD, Vousden KH, Serine metabolism supports the methionine cycle and DNA/RNA methylation through *de novo* ATP synthesis in cancer cells. *Mol Cell.* (2016) 61:210–21. doi: 10.1016/j.molcel.2015.12.014
89. Detich N, Hamm S, Just G, Knox JD, Szyf M. The methyl donor S -Adenosylmethionine inhibits active demethylation of DNA. *J Biol Chem*. (2003) 278:20812–20. doi: 10.1074/jbc.M211813200
90. Miousse IR, Kutanzi KR, Koturbash I. Effects of ionizing radiation on DNA methylation: from experimental biology to clinical applications. *Int J Radiat Biol.* (2017) 93:457–69. doi: 10.1080/09553002.2017.1287454
91. Koturbash I, Miousse IR, Sridharan V, Nzabarushimana E, Skinner CM, Melnyk SB, et al. Radiation-induced changes in DNA methylation of repetitive elements in the mouse heart. *Mutat Res.* (2016) 787:43–53. doi: 10.1016/j.mrfmmm.2016.02.009
92. Kim EH, Park AK, Dong SM, Ahn JH, Park WY. Global analysis of CpG methylation reveals epigenetic control of the radiosensitivity in lung cancer cell lines. *Oncogene*. (2010) 29:4725–31. doi: 10.1038/onc.2010.223
93. Huang KH, Huang SF, Chen IH, Liao CT, Wang HM, Hsieh LL. Methylation of RASSF1A, RASSF2A, and HIN-1 is associated with poor outcome after radiotherapy, but not surgery, in oral squamous cell carcinoma. *Clin Cancer Res.* (2009) 15:4174–80. doi: 10.1158/1078-0432.CCR-08-2929
94. Batra V, Mishra KP. Modulation of DNA methyltransferase profile by methyl donor starvation followed by gamma irradiation. *Mol Cell Biochem*. (2007) 294:181–7. doi: 10.1007/s11010-006-9258-8
95. Batra V, Kesavan V, Mishra KP. Modulation of enzymes involved in folate dependent one-carbon metabolism by gamma-radiation stress in mice. *J Radiat Res*. (2004) 45:527–33. doi: 10.1269/jrr.45.527
96. Batra V, Verma P. Dietary l-methionine supplementation mitigates gamma-radiation induced global DNA hypomethylation: enhanced metabolic flux towards S-adenosyl-l-methionine (SAM) biosynthesis increases genomic methylation potential. *Food Chem Toxicol.* (2014) 69:46–54. doi: 10.1016/j.fct.2014.03.040

Conflict of Interest Statement: The authors declare that the research was conducted in the absence of any commercial or financial relationships that could be construed as a potential conflict of interest.

Copyright © 2019 Lindell Jonsson, Erngren, Engskog, Haglöf, Arvidsson, Hedeland, Petterson, Laurell and Nestor. This is an open-access article distributed under the terms of the Creative Commons Attribution License (CC BY). The use, distribution or reproduction in other forums is permitted, provided the original author(s) and the copyright owner(s) are credited and that the original publication in this journal is cited, in accordance with accepted academic practice. No use, distribution or reproduction is permitted which does not comply with these terms.

frontiers in Oncology

REVIEW
published: 06 September 2019
doi: 10.3389/fonc.2019.00869

Exosomes in Cancer Radioresistance

Jie Ni[1,2], *Joseph Bucci*[1,2], *David Malouf*[1,3], *Matthew Knox*[1,2], *Peter Graham*[1,2] *and Yong Li*[1,2,4*]

[1] Cancer Care Centre, St. George Hospital, Sydney, NSW, Australia, [2] St. George and Sutherland Clinical School, Faculty of Medicine, University of New South Wales (UNSW) Sydney, Kensington, NSW, Australia, [3] Department of Urology, St. George Hospital, Sydney, NSW, Australia, [4] School of Basic Medical Sciences, Zhengzhou University, Zhengzhou, China

Radiation is a mainstay of cancer therapy. Radioresistance is a significant challenge in the treatment of locally advanced, recurrent and metastatic cancers. The mechanisms of radioresistance are complicated and still not completely understood. Exosomes are 40–150 nm vesicles released by cancer cells that contain pathogenic components, such as proteins, mRNAs, DNA fragments, non-coding RNAs, and lipids. Exosomes play a critical role in cancer progression, including cell-cell communication, tumor-stromal interactions, activation of signaling pathways, and immunomodulation. Emerging data indicate that radiation-derived exosomes increase tumor burden, decrease survival, cause radiation-induced bystander effects and promote radioresistance. In addition, radiation can change the contents of exosomes, which allows exosomes to be used as a prognostic and predictive biomarker to monitor radiation response. Therefore, understanding the roles and mechanisms of exosomes in radiation response may shed light on how exosomes play a role in radioresistance and open a new way in radiotherapy and translational medicine. In this review, we discuss recent advances in radiation-induced exosome changes in components, focus on the roles of exosome in radiation-induced bystander effect in cancer and emphasize the importance of exosomes in cancer progression and radioresistance for developing novel therapy.

Keywords: cancer, exosomes, radiotherapy, bystander, radioresistance

OPEN ACCESS

Edited by:
Paul N. Span,
Radboud University Nijmegen Medical Centre, Netherlands

Reviewed by:
James William Jacobberger,
Case Western Reserve University, United States
Evagelia C. Laiakis,
Georgetown University, United States

***Correspondence:**
Yong Li
y.li@unsw.edu.au

Specialty section:
This article was submitted to Radiation Oncology, a section of the journal Frontiers in Oncology

Received: *10 July 2019*
Accepted: *21 August 2019*
Published: *06 September 2019*

Citation:
Ni J, Bucci J, Malouf D, Knox M, Graham P and Li Y (2019) Exosomes in Cancer Radioresistance. Front. Oncol. 9:869. doi: 10.3389/fonc.2019.00869

INTRODUCTION

Cancer is a major health burden. Radiotherapy (RT) is widely used in more than 50% of localized cancer patients (1), and is a critical and inseparable component of comprehensive cancer treatment and care (2). In addition, RT is often combined with surgery, chemotherapy, and more recently, immunotherapy (3). Despite progress made in radiation delivery approaches and precision medicine, tumor therapeutic resistance and recurrence frequently occur in clinical settings.

Radioresistance is a complicated biological process associated with abnormal DNA damage response (DDR), apoptosis, autophagy, gene mutations, cell cycle checkpoint, and deregulated signaling pathways (4). It leads to poor prognosis in cancer patients and represents a major clinical obstacle for RT, which ultimately leads to tumor relapse and metastasis (5). Tumor microenvironment is an important factor affecting tumor progression and therapeutic response (6, 7). It was reported radioresistance is highly associated with tumor microenvironment (8, 9).

Exosomes are important components and regulators of the tumor microenvironment. Exosomes are small extracellular vesicles (40–150 nm) secreted by different cells. Exosomes are representative of the original cells and can reflect a regulated sorting mechanism (10). These vesicles are composed

of proteins (receptors, transcription factors, enzymes), nucleic acids [nuclear DNA, mitochondrial DNA (mtDNA), mRNA, microRNA (miRNA), long non-coding RNA (lncRNA), and circular RNA (circRNA)], and lipids (11–14). Exosome cargos such as nucleic acid and proteins from originating tumor cells communicate with neighbor cells or recipient cells, resulting in cancer progression and recurrence (15, 16).

Stressful conditions affect exosome secretion, composition, abundance, and potential binding on recipient cells. It was reported that different physiological and environmental conditions could alter the composition of exosomes shed from cells (17). Accumulating evidence indicates an increased release of exosomes after exposure to RT and the altered contents from donor cells were more oncogenic (18–21). Several recent studies have confirmed irradiated cells were involved in radiation-related communication between cells (20, 22, 23).

Despite the progress that has been made in exosome-mediated functions in *in vitro* models, there are still many challenges to be faced in exosomes and radiation oncology research. Here, we review recent advances in the radiation-induced exosome changes, discuss the roles of exosome in radiation-induced bystander effect (RIBE) in cancer and emphasize the importance of exosomes in cancer radioresistance and progression for the development of novel therapeutic strategies.

RADIATION-INDUCED EXOSOME CHANGES IN CANCER RADIOTHERAPY

Cellular stress affects the composition and abundance of exosomes, as well as their potential impact on the recipient cells. Exosomes are a major environmental factor for cellular stress, and radiation can enhance the release of exosomes and affect exosome-based intercellular communication, which has been observed in various types of normal and tumor cell lines (18, 19, 24).

An increased level of exosomal CD276 was observed in the irradiated and senescent 22RV1 prostate cancer cell line, suggesting that this marker may provide a non-invasive way to monitor the efficacy of RT for prostate cancer patients (25). It was reported that circulating Hsp72 level was increased after radiation exposure in prostate cancer mouse xenografts and clinical sample; and that the exosomes containing Hsp72 are a possible contributor, leading to pro-inflammatory cytokine production and immune modulation (26). Khan et al. found that the level of exosomal survivin was increased after proton irradiation in HeLa cells and the rate of exosome secretion was not influenced (27). These findings suggest exosomal survivin may be associated with cancer recurrence after RT and could be a potential therapeutic target for preventing cervical cancer progression.

Radiation also alters the molecular composition within the exosomes. In one study, it was found radiation increased levels of exosomal connective tissue growth factor (CTGF) and Insulin Like Growth Factor Binding Protein 2 (IGFBP2) proteins, both of which are important in cell migration. By transferring CTGF mRNA, exosomes from irradiated cells were found to upregulate the migration-related signaling molecules including neurotrophic tyrosine kinase receptor type 1, focal adhesion kinase, Paxillin, and proto-oncogene tyrosine-protein kinase Src in recipient cells (18). In another study, exosomes released from the irradiated head and neck squamous carcinoma cell (HNSCC) FaDu cells demonstrated a distinctive protein expression profile compared to those from non-irradiated cells (20). Interestingly, most of the proteins that are specifically overexpressed in exosomes are those involved in transcription, translocation, and cell division, indicating that exosomal cargo is reflective of radiation-induced changes in cells (20). Similarly, exosomes derived from irradiated HNSCC BHY cells were found to be associated with not only immunity but also cell adhesion and motility, the underlying molecular mechanism being enhanced AKT-signaling triggered by the exosomal proteins (28). Using a shotgun liquid chromatography–tandem mass spectrometry (LC-MS/MS) approach, Abramowicz et al. found 472 exosomal proteins that are significantly affected by ionizing radiation (IR) in HNSCC UM-SCC6 cells and identified their role in mediating the cellular response to IR (29). Zhao et al. recently identified 63 upregulated and 48 downregulated circular RNAs from the exosomes of radioresistant glioma cells compared with those in control cells. Using qRT-PCR, they found circATP8B4 from radioresistant exosomes of glioma cells may be transferred to radiation-naïve cells and promoted cell radioresistance by acting as a microRNA(miR)-766 sponge (30).

The role of exosomes in radiation has garnered increasing attention in recent years. One study screened 752 exosome-derived miRNAs of locally advanced non-small cell lung cancer (NSCLC) patients and demonstrated that increased radiation dosage reduced miR29a-3p and miR150-5p expression (31), indicating that circulating exosomal miRNAs could help predict RT toxicity. In another study evaluating the outcome of HNSCC patients treated with chemoradiation therapy (CRT), exosomes from pooled plasma samples of patients who had complete or incomplete responses to CRT were screened. They identified a distinctive expression pattern of proteins between patients who had a complete response and who did not (32). In a recent Phase I clinical trial, 18 HNSCC patients receiving a combination of cetuximab, ipilimumab and RT were serially monitored for tumor cell-derived exosomes and T cell-derived exosomes. The results suggested tumor cell-derived exosomes and T cell-derived circulating exosomes instead of immune cells were suitable for monitoring of patients' responses to oncological therapy, supporting the potential role of exosomes as a non-invasive tumor and immune cell biomarkers in cancer (33).

The exosomes in RT research is stating to move from bench to bedside. However, the main limitation is the sample numbers tested from patiensts are still low and the preliminary results obtained need to be further validated in a large cohort of patients. Another challenge is the methods used for detecting exosome contents (biomarkers) such as proteomics and next generation sequencing need to be further optimimised to obtain the maximum number of interesting pontential biomarkers for

verification. Although advances in exosome-based biomarkers such as proteins and miRNAs highlight an optimistic outlook for RT, the great progress has not been achieved due to limited reports in clinical research. Future direction in this area should move on the translational research and clinical trials.

In summary, the studies so far on radiation-induced changes in exosome composition have mainly been confined to their proteome contents using *in vitro* cancer cell line models (Summarized in **Table 1**), and there is a big gap in understanding how these changes are regulated, with the hope of translating into their functional importance. Future studies in this area should focus on (1) investigating the mechanisms of how the components of exosomes from donor cells after radiation are transferred to receipt cells; (2) establishing *in vivo* animal models for further studying the changes of exosomal components on the effect of RT; (3) investigating whether the changes of exosomal components could be used as biomarkers to evaluate the efficacy of RT; and (4) investigating whether the changes of exosomal components could be used as useful therapeutic targets to overcome radioresistance and improve the current RT.

THE BYSTANDER EFFECTS BY RADIATION-INDUCED EXOSOMES

Radiation affects not only its direct targeted cells but also non-irradiated neighbors. This is evidenced by RIBE that cells that were not exposed to radiation exhibit effects as a result of intercellular communication. RIBE can also lead to biological changes in bystander cells and tissues, including chromosomal rearrangement, genomic instability, DNA damage, gene expression alteration, and apoptosis (34).

Numerous studies have demonstrated a large and complex interconnected web of mechanisms that contribute to the generation of RIBE, including reactive oxygen species (ROS), cytokines, free radicals, immune system, and epigenetic modulators (35–37). As previously reviewed more than a decade ago, it was believed that RIBE was mediated by both "a soluble secreted factor" and the cell-to-cell gap junction (38). It was not until recently that the important role of exosomes mediating RIBE had been recognized (39). Exosomes shed by irradiated cells are putatively involved in different aspects of the systemic response to IR, including the RIBE (40–42). Jella et al. showed

TABLE 1 | Changes of exosomal components in cancel cell lines *in vitro* after radiation treatment.

Source of exosomes	Study model	Dose of IR	Time from IR to exosome isolation	Changed components	Test approach	Isolation method	Effect	References
22RV1 cell line	Human CaP *in vitro*	4 Gy	4 days	CD276	SDS-PAGE	UC	Exosomes can transfer cargos with both immunoregulatory potential and genetic information	(25)
HeLa cell line	Human cervical carcinoma *in vitro*	3 Gy	24 h	Survivin	Western blotting, LC-MS/MS	UC	Exosomes represent a novel secretory pathway by which proteins can be actively released from cells.	(27)
LN18, U87MG, U251cell lines	GBM *in vitro*	2 to 8 Gy	12 to 48 h	CTGF mRNA and IGFBP2	Immunoblot analysis, qRT-PCR	UC	Radiation influences exosome abundance, specifically alters their molecular composition.	(18)
FaDu cell line	HNSCC *in vitro*	2Gy	18 h	Proteins (n = 236)	LC-MS/MS	Total exosome isolation kit	Exosomal cargo reflected radiation-induced changes in cellular processes like transient suppression of transcription and translation or stress-induced signaling.	(20)
BHY cell line	HNSCC *in vitro*	6 Gy	24 h	Up-regulayed (n = 39) and downregulated n = 36) proteins	LC-MS/MS	UC	Exosomes may act as driver of HNSCC progression during radiotherapy.	(28)
UM-SCC6 cell line	Human HNSCC *in vitro*	A single 2, 4 or 8 Gy	24 h	Proteins (n = 472)	LC-MS/MS	SEC	The protein profiles of exosomes released by radiaton were established.	(29)
RR-U251cell line	Human GBM cell line *in vitro*	60 Gy	N/A	circATP8B4	RNA sequencing	UC	circRNA acts as a miRNA sponge, which may regulate tumor radioresistance.	(30)

CaP, prostate cancer; CTGF, connective tissue growth factor; HNSCC, head and neck squamous cell carcinoma; GBM, glioblastoma; IGFBP2, insulin-like growth factor binding protein 2, LC-MS/MS, liquid chromatography-tandem mass spectrometry; N/A, not applicable; SEC, size-exclusion chromatography; UC, ultracentrifugation.

that exosomes released from gamma-irradiated keratinocyte HaCaT cells induced increased cell death and ROS production in non-irradiated cells (24).

Mechanistically, IR elicits a set of dysregulated proteins and nucleic acids within the cell. These effectors, such as proteins, miRNAs and mtDNAs, are packaged into exosomes during their formation, which are then released to the extracellular environment. These cargos within the radiation-targeted cell-released exosomes subsequently get access to the adjacent cells as a result of exosome migration and internalization, and prompt RIBE in the non-targeted distant cells (21, 43–45).

These components of exosomes have different functions in RIBE, such as regulation of inflammation and modulation of DDR (46).

One report demonstrated that the production and release of exosomes following radiation-induced DNA damage were regulated by the p53 pathway (47). Tian et al. demonstrated that miR-21, a well-established DDR-related miRNA, played a mediating role in bystander DNA damage since it elevated ROS levels and increased the double-strand break (DSB) marker p53-binding protein 1 (53BP1) foci in non-irradiated cells (48). The role of miR-21 in RIBE was also validated by Yin et al. and Xu et al. using different experiment models (21, 49). Exosomal miR-1246 was also found to act as a messenger and contribute to DNA damage by directly repressing the DNA Ligase 4 (LIG4) gene (22). In combination, Yentrapalli et al. found that proteins such as afamin and serpine peptidase F1 along with miRNAs including miR-204-5p, miR-92a-3p, and miR-31-5p, play an important role in inducing and regulating RIBE (50). Another group also demonstrated that exosomal proteins and RNAs could mediate short- and long-term RIBE in human MCF-7 breast cancer cells (19, 51), implying that proteins and miRNAs may work synergistically during this process.

Moreover, exosomal miRNAs are able to travel remotely to influence cellular functions and regulate the niche-host reaction in targeted or non-targeted cells. It is worth mentioning that the role of a miRNA as either a positive or negative regulator in the RIBE varies from cell type to cell type. Interestingly, cells affected by RIBE and their progeny also showed the ability to secrete exosomes, and this cascade could potentially lead to a delayed RIBE-related inflammatory response (19). We have summarized exosome-mediated RIBE studies in cancer RT in **Table 2**. The mechanistic diagram demonstrating effects of radiation-inducible exosomal miRNAs and proteins in mediating RIBE is shown in **Figure 1**.

In the therapeutic arena, on the one hand, RIBE is harmful to normal tissues, but on the other hand may be beneficial to induce non-irradiated cancer cell death during the treatment. RIBEs have critical implications in cancer RT. As direct effects of RT and RIBE are mechanistically distinctive and therefore it is important to develop different types of drugs to specifically target each mechanism, such as novel radiosensitisers to upregulate RIBE to kill more adjacent tumor cells; or adjuvant inhibitors to minimize the RIBE-induced systemic toxicity after RT.

TABLE 2 | Summary of RIBEs caused by exosomes in recipient cells.

Donor cells	Recipient cells	Dose of IR	Time from IR to exosome isolation	Isolation method	RIBEs in receipt cells	Effect	References
Human non–small cell lung cancer cell lines (H460, H1299)	H460, H1299	5 Gy	48 h	UC	p53-dependent response to DNA damage (Western blot) after 24 h of incubation.	The p53 pathway regulates the production of exosomes for cancer communication	(47)
Human breast cancer cell line (MCF-7)	MCF-7	2 Gy	4 h	UC	DNA (comet assay) and chromosomal (metaphases analysis) damage after 24 h of incubation	Exosomes are partially involved in the bystander effect and genomic instability	(51)
Human breast cancer cell line (MCF-7)	MCF-7	2 Gy	4 h	UC	DNA (comet assay) and chromosomal (metaphases analysis damage) after 24 h of incubation up to 20 cell-doublings	Exosomes are associated with signaling of the non-targeted effects (NTE) of IR, initiated by both exosomal RNA and protein molecules.	(19)
Human HNSCC cell lines (BHY, FaDu)	BHY, FaDu	0–9 Gy	24–48 h	UC	Increase uptake of exosomes and survival and affect rates of DNA double-strand break repair after 24–48 h of incubation	Exosomes transmit prosurvival effects by promoting the proliferation and radioresistance	(52)
Human papillomavirus–immortalized human bronchial epithelial (BEP2D),	BEP2D	2 Gy	4–8 h	UC	miR-1246 packaged in exosomes affecting DNA damage by directly repressing the LIG4 gene after 24 h of incubation	Exosomal microRNAs have potentials as a messenger and contribute to DNA damage by directly targeting mRNA.	(22)

h, hours; HNSCC, head and neck squamous cell carcinoma; UC, ultracentrifugation.

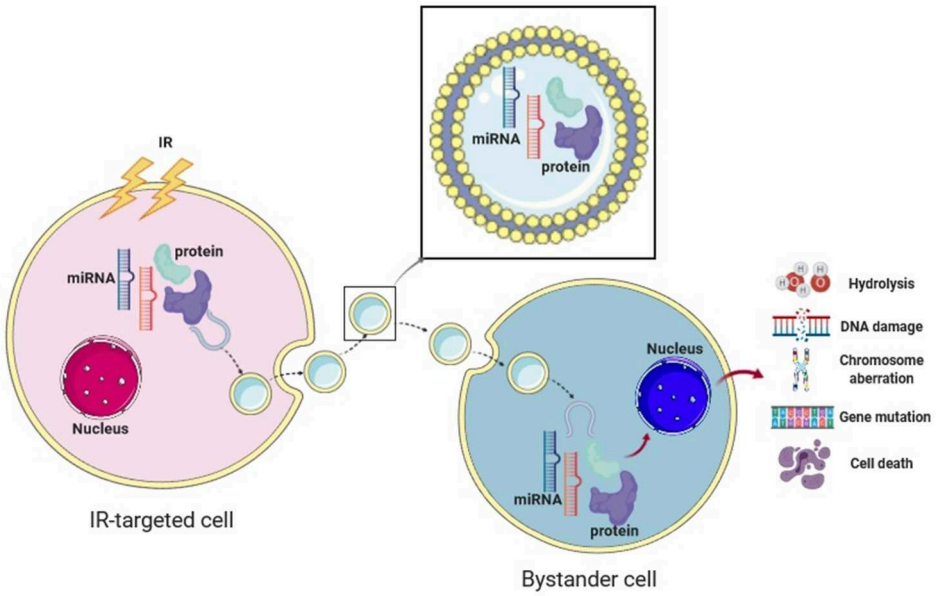

FIGURE 1 | The bystander effect of exosomes in cancer radiotherapy. The mechanistic diagram displaying the effect of radiation-induced exosomal proteins and microRNAs in mediating cellular and molecular changes in RIBE. Created with BioRender.

Moreover, although *in vitro* studies bring promise for using exosomes and their cargo to regulate DDR and RIBE, it remains unclear whether these findings can be translated into the clinical setting. In future studies, the mechanisms of RIBE need to be deeply investigated, and *in vivo* animal models and clinical samples should be applied.

EXOSOMES IN CANCER PROGRESSION AFTER RADIOTHERAPY

RT itself may increase the motility of surviving cancer cells, evidenced in glioblastoma (GBM), lung cancer and HNSCC, thus facilitating the spread of the tumor to local and distant sites (53–55). Radiation-induced exosomes have recently found to be an accomplice in promoting tumor cell motility and assisting in the pre-metastatic niche formation, the effectors again being the exosomal cargo incorporated by the recipient cells. Arscott et al. showed that radiation-derived exosomes enhanced U87MG GBM cell migration in co-culture (18). Using a wound healing assay, Mutschelknaus et al. found a pro-migratory role of exosomes in boosting the migratory capacity of BHY and FaDu HNSCC cells, in a dose-dependent and AKT-dependent manner (28). Apart from cell motility, angiogenesis also plays a crucial role in RT and tumor metastasis. Zheng et al. recently demonstrated that in lung cancer, the exosome-induced pro-angiogenesis effect was enhanced when the A549 and H1299 lung cancer cells were exposed to IR, and the miR23-mediated phosphatase and tensin homolog (PTEN) downregulation played an important role in this process (56). These findings indicate that radiation-induced exosomes function as a driver of cancer progression and metastasis during RT, and may represent a putative target to improve RT strategies.

The recent striking responses to immune-checkpoint inhibitors in the treatment of melanoma and solid tumors are paradigm-shifting and stirring up much research interest in the combination of immune-checkpoint inhibitors with RT. There is a close association between radiation response and immunity (57). RT plays either an immune-suppressive role (due to the sensitivity of leukocytes) or an immune-stimulatory role, evidenced by enhancing several antigen processing and presentation pathways (58, 59). Conventionally, the immune stimulation is believed to be T cell-mediated, but it is not until recently have we found that T cell-derived exosomes also plays a role in promoting esophageal cancer metastasis, via activation of epithelial-mesenchymal transition (EMT), β-catenin, and NF-κB/SNAIL pathways (60). This study provides a rationale for targeting exosomes during the synergy between RT and immunotherapy, but there are still quite a few unsolved riddles in this synergy, such as the sequencing, dose, and fractionation. Clearer mechanistic understandings of RT's immune-stimulatory role and further investigations on exosomes' functions in immune modulation are needed to expand this research field.

EXOSOMES IN RADIORESISTANCE

Despite the recent advances in RT, many cancer patients, especially the locally advanced ones, failed radiation treatment (radioresistance), leading to a local recurrence or even distant metastasis. As previously reviewed (4), radioresistance can arise either from genetic or phenotypic changes within the tumor or as

a result of the tumor stromal and microenvironment protecting the tumor against IR. Exosomes are one of the key components of the tumor microenvironment and increasing evidence suggests that they play a significant role in facilitating the development of radioresistance.

The key players in exosome-mediated radiosensitivity are found to be exosomal non-coding RNAs, proteins, and the crosstalk with survival and apoptotic pathways. Mutschelknaus et al. recently demonstrated that exosomes derived from irradiated HNSCC cells transmitted pro-survival signals to recipient cells via exosome cargos (52). In breast cancer, RNAs within exosomes were found to regulate radioresistance via an antiviral STAT1/NOTCH3 pathway (61). Radiation-induced exosomal miR-208a increased the proliferation and radioresistance via targeting p21 with activation of the AKT/mTOR pathway in lung cancer (62). In GBM, Mrowczynski et al. recently discovered that exosomes could enhance cell survival to radiation exposure by increasing levels of oncogenic miRNAs, mRNAs and pro-survival pathway proteins and at the same time decreasing levels of tumor-suppressive miRNAs and mRNAs (23). Recently, other exosomal non-coding RNAs were also found to be involved in the promotion of radioresistance, such as long non-coding RNA AHIF in glioblastoma (63), and circATP8B4 in glioma (30).

While exosomes were reported to play an important role in the promotion of cancer radioresistance, other reports were controversial. Wang et al. recently reported that autocrine secretions enhance the radioresistance of H460 NSCLC cell line in an exosome-independent manner and that these secretions mainly affect the DNA repair process (64). In another study, it was shown that exosomes derived form mesenchymal stem cells (MSCs), combined with RT, enhance RT-induced cell death in tumor and metastatic tumor foci in a melanoma mouse model. The finding provides a rationale to use MSCs-derived exosomes as an adjuvant to support and complement RT (65). These data indicate the role of exosomes in cancer radioresistance is complicated and could be affected by many factors such as tumor type, tumor microenvironment, experimental methods or different combinations of therapies.

Cancer is highly heterogeneous and includes a small subset of cells that possess the capacity of self-renewal and differentiation, referred to as cancer stem cells (CSCs) (66). CSCs are inherently more resistant to radiation than ordinary cancer cells, and more likely to survive after being exposed to RT. On one hand, these surviving CSCs may release exosomes to transfer resistant or refractory phenotypes to recipient cells, limiting the treatment efficacy. It was found that lncRNA H19 in exosomes derived from CSCs induced angiogenesis in hepatocellular carcinoma (67). Exosomes released from prostate and breast CSCs were also capable to induce autophagy (68), which has been shown to modulate sensitivity of cancer to RT (69). On the other, CSCs can also be eliminated via being reprogrammed into non-tumorigenic cells, using exosomes derived from adipose-derived stem cells (70). It not only re-justifies that the CSCs have to be eradicated during cancer therapy, but also preludes the usage of exosomes with modified surface or cargos to target CSCs.

In summary, all the data indicate that radiation-derived exosomes play important roles in cancer radioresistance through re-programmed cargos and intercellular communication. mRNAs, non-coding RNAs and signaling pathway proteins

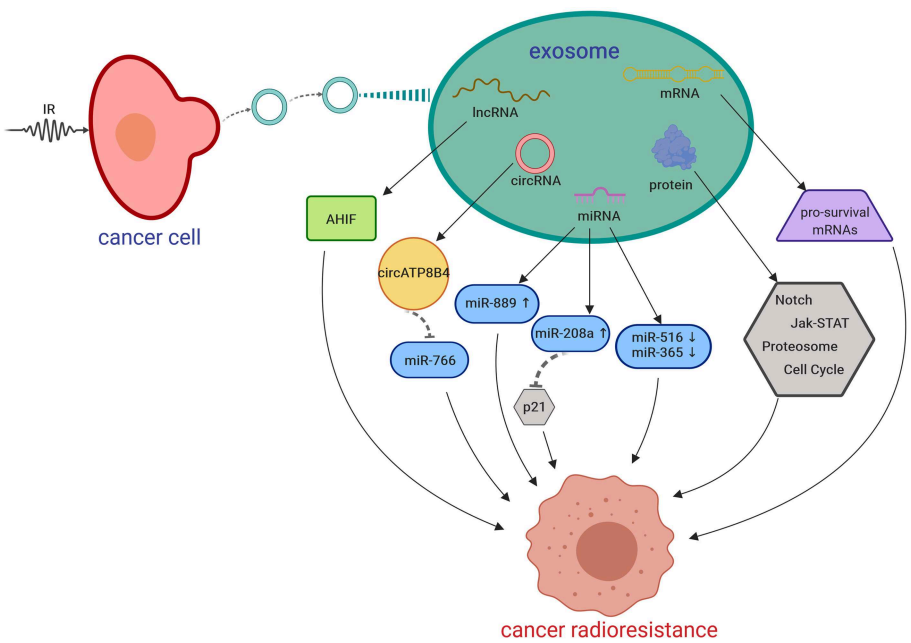

FIGURE 2 | Putative mechanisms of IR-induced exosomes in promoting cancer radioresistance. AHIF, a natural antisense transcript; circRNA, circular RNA; IR, irradiation; lncRNA, long non-coding RNA; miRNA, microRNA; mRNA, messenger RNA. Created with BioRender.

are closely related in exosome-associated radioresistance. CSC-associated exosomes are also a potential player in radioresistance and should be deeply investigated in the future study. The potential mechanisms of exosomes in radioresistance are shown in **Figure 2**.

CONCLUSIONS

Exploiting the biological functions of exosomes is intriguing, as they provide a snapshot of the entire tumor, transfer molecules intercellularly and can be used as a therapeutic target. In order to achieve these goals, isolation of exosomes should be standardized and optimized.

Exosomes in radiation research is a new and developing area. Radiation affects not only the production of exosomes but also the composition within, which makes exosomes an ideal prognostic and/or predictive biomarker to monitor the radiation response.

The radiation-altered exosomal cargos can be taken up by recipient cells, thus exerting various biological functions to impact radiosensitivity, and it is also worthwhile to note that this impact can be the results of synergistic or opposing effects of different exosomes for the sake of their heterogeneity. Due to the unique physical and biological features of exosomes, using functional exosomes to target CSCs and facilitate immunotherapy, is a promising avenue to be explored in RT, since exosomes are more stable, endogenous, and can be easily engineered or labeled.

There are still many challenges existing for exosome study. The future development of methodologies for exosome isolation and purification should be universal, precise, and suitable for clinical settings. Our experience is the combination of two or more approaches is a better choice for exosome isolation. In addition, the optimal sample source should be determined based on the cancer types and the preservation conditions of samples should be standardized. Furthermore, specific biomarkers of tumor exosomes should be screened and exploited for investigating the mechanisms of radioresistance.

Currently, knowledge of exosomes in cancer RT is in its infancy and mostly limited in *in vitro* studies. Further *in vivo* and clinical studies are warranted. Increasing knowledge of the biology of exosome and its cargo, along with standardized methods for exosome isolation and characterization will greatly contribute to a better understanding of mechanisms of exosome-mediated RT response and a good harnessing of exosomes as a therapeutic target, which might ultimately lead to the development of novel treatment strategies.

AUTHOR CONTRIBUTIONS

JN, JB, DM, MK, PG, and YL reviewed the literature, developed the structures, wrote the review, and approved the final manuscript.

FUNDING

This work is mainly supported by the St. George Hospital Cancer Research Trust Fund and Prostate & Breast Cancer Foundation.

REFERENCES

1. Barton MB, Jacob S, Shafiq J, Wong K, Thompson SR, Hanna TP, et al. Estimating the demand for radiotherapy from the evidence: a review of changes from 2003 to 2012. *Radiother Oncol.* (2014) 112:140–4. doi: 10.1016/j.radonc.2014.03.024
2. Atun R, Jaffray DA, Barton MB, Bray F, Baumann M, Vikram B, et al. Expanding global access to radiotherapy. *Lancet Oncol.* (2015) 16:1153–86. doi: 10.1016/S1470-2045(15)00222-3
3. Yaromina A, Krause M, Baumann M. Individualization of cancer treatment from radiotherapy perspective. *Mol Oncol*. (2012) 6:211–21. doi: 10.1016/j.molonc.2012.01.007
4. Ni J, Bucci J, Chang L, Malouf D, Graham P, Li Y. Targeting MicroRNAs in prostate cancer radiotherapy. *Theranostics*. (2017) 7:3243–59. doi: 10.7150/thno.19934
5. Rycaj K, Tang DG. Cancer stem cells and radioresistance. *Int J Radiat Biol.* (2014) 90:615–21. doi: 10.3109/09553002.2014.892227
6. Swartz MA, Iida N, Roberts EW, Sangaletti S, Wong MH, Yull FE, et al. Tumor microenvironment complexity: emerging roles in cancer therapy. *Cancer Res.* (2012) 72:2473–80. doi: 10.1158/0008-5472.CAN-12-0122
7. Son B, Lee S, Youn H, Kim E, Kim W, Youn B. The role of tumor microenvironment in therapeutic resistance. *Oncotarget*. (2016) 8:3933–45. doi: 10.18632/oncotarget.13907
8. Barker HE, Paget JTE, Khan AA, Harrington KJ. The tumour microenvironment after radiotherapy: mechanisms of resistance and recurrence. *Nat Rev Cancer*. (2015) 15:409–25. doi: 10.1038/nrc3958
9. Chan R, Sethi P, Jyoti A, McGarry R, Upreti M. Investigating the radioresistant properties of lung cancer stem cells in the context of the tumor microenvironment. *Radiat Res*. (2016) 185:169–81. doi: 10.1667/RR14285.1
10. Valadi H, Ekström K, Bossios A, Sjöstrand M, Lee JJ, Lötvall JO. Exosome-mediated transfer of mRNAs and microRNAs is a novel mechanism of genetic exchange between cells. *Nat Cell Biol.* (2007) 9:654–9. doi: 10.1038/ncb1596
11. Mathivanan S, Ji H, Simpson RJ. Exosomes: extracellular organelles important in intercellular communication. *J Proteomics*. (2010) 73:1907–20. doi: 10.1016/j.jprot.2010.06.006
12. D'Asti E, Garnier D, Lee TH, Montermini L, Meehan B, Rak J. Oncogenic extracellular vesicles in brain tumor progression. *Front physiol.* (2012) 3:294. doi: 10.3389/fphys.2012.00294
13. Fanale D, Taverna S, Russo A, Bazan V. Circular RNA in Exosomes. *Adv Exp Med Biol.* (2018) 1087:109–17. doi: 10.1007/978-981-13-1426-1_9
14. Sansone P, Savini C, Kurelac I, Chang Q, Amato LB, Strillacci A, et al. Packaging and transfer of mitochondrial DNA via exosomes regulate escape from dormancy in hormonal therapy-resistant breast cancer. *Proc Natl Acad Sci USA*. (2017) 114:E9066–75. doi: 10.1073/pnas.1704862114
15. Malla B, Zaugg K, Vassella E, Aebersold DM, Dal Pra A. Exosomes and exosomal microRNAs in prostate cancer radiation therapy. *Int J Radiat Oncol Biol Phys.* (2017) 98:982–95. doi: 10.1016/j.ijrobp.2017.03.031
16. Mathieu M, Martin-Jaular L, Lavieu G, Théry C. Specificities of secretion and uptake of exosomes and other extracellular vesicles for cell-to-cell communication. *Nat Cell Biol.* (2019) 21:9–17. doi: 10.1038/s41556-018-0250-9
17. Villarroya-Beltri C, Baixauli F, Gutiérrez-Vázquez C, Sánchez-Madrid F, Mittelbrunn M. Sorting it out: regulation of exosome loading. *Semin Cancer Biol.* (2014) 28:3–13. doi: 10.1016/j.semcancer.2014.04.009
18. Arscott WT, Tandle AT, Zhao S, Shabason JE, Gordon IK, Schlaff CD, et al. Ionizing radiation and glioblastoma exosomes: implications in tumor biology and cell migration. *Transl Oncol.* (2013) 6:638–48. doi: 10.1593/tlo.13640

19. Al-Mayah A, Bright S, Chapman K, Irons S, Luo P, Carter D, et al. The non-targeted effects of radiation are perpetuated by exosomes. *Mutat Res.* (2015) 772:38–45. doi: 10.1016/j.mrfmmm.2014.12.007
20. Jelonek K, Wojakowska A, Marczak L, Muer A, Tinhofer-Keilholz I, Lysek-Gladysinska M, et al. Ionizing radiation affects protein composition of exosomes secreted *in vitro* from head and neck squamous cell carcinoma. *Acta Biochim Pol.* (2015) 62:265–72. doi: 10.18388/abp.2015_970
21. Xu S, Wang J, Ding N, Hu W, Zhang X, Wang B, et al. Exosome-mediated microRNA transfer plays a role in radiation-induced bystander effect. *RNA Biol.* (2015) 12:1355–63. doi: 10.1080/15476286.2015.1100795
22. Mo L-J, Song M, Huang Q-H, Guan H, Liu X-D, Xie D-F, et al. Exosome-packaged miR-1246 contributes to bystander DNA damage by targeting LIG4. *Br J Cancer.* (2018) 119:492–502. doi: 10.1038/s41416-018-0192-9
23. Mrowczynski OD, Madhankumar AB, Sundstrom JM, Zhao Y, Kawasawa YI, Slagle-Webb B, et al. Exosomes impact survival to radiation exposure in cell line models of nervous system cancer. *Oncotarget.* (2018) 9:36083–101. doi: 10.18632/oncotarget.26300
24. Jella KK, Rani S, O'Driscoll L, McClean B, Byrne HJ, Lyng FM. Exosomes are involved in mediating radiation induced bystander signaling in human keratinocyte cells. *Radiat Res.* (2014) 181:138–45. doi: 10.1667/RR13337.1
25. Lehmann BD, Paine MS, Brooks AM, McCubrey JA, Renegar RH, Wang R, et al. Senescence-associated exosome release from human prostate cancer cells. *Cancer Res.* (2008) 68:7864–71. doi: 10.1158/0008-5472.CAN-07-6538
26. Hurwitz MD, Kaur P, Nagaraja GM, Bausero MA, Manola J, Asea A. Radiation therapy induces circulating serum Hsp72 in patients with prostate cancer. *Radiother Oncol.* (2010) 95:350–8. doi: 10.1016/j.radonc.2010.03.024
27. Khan S, Jutzy JM, Aspe JR, McGregor DW, Neidigh JW, Wall NR. Survivin is released from cancer cells via exosomes. *Apoptosis.* (2011) 16:1–12. doi: 10.1007/s10495-010-0534-4
28. Mutschelknaus L, Azimzadeh O, Heider T, Winkler K, Vetter M, Kell R, et al. Radiation alters the cargo of exosomes released from squamous head and neck cancer cells to promote migration of recipient cells. *Sci Rep.* (2017) 7:12423. doi: 10.1038/s41598-017-12403-6
29. Abramowicz A, Wojakowska A, Marczak L, Lysek-Gladysinska M, Smolarz M, Story MD, et al. Ionizing radiation affects the composition of the proteome of extracellular vesicles released by head-and-neck cancer cells *in vitro*. *J Radiat Res.* (2019) 60:289–97. doi: 10.1093/jrr/rrz001
30. Zhao M, Xu J, Zhong S, Liu Y, Xiao H, Geng L, et al. Expression profiles and potential functions of circular RNAs in extracellular vesicles isolated from radioresistant glioma cells. *Oncol Rep.* (2019) 41:1893–900. doi: 10.3892/or.2019.6972
31. Dinh T-KT, Fendler W, Chałubinska-Fendler J, Acharya SS, O'Leary C, Deraska PV, et al. Circulating miR-29a and miR-150 correlate with delivered dose during thoracic radiation therapy for non-small cell lung cancer. *Radiat Oncol.* (2016) 11:61. doi: 10.1186/s13014-016-0636-4
32. Rodrigues-Junior DM, Tan SS, de Souza Viana L, Carvalho AL, Lim SK, Iyer NG, et al. A preliminary investigation of circulating extracellular vesicles and biomarker discovery associated with treatment response in head and neck squamous cell carcinoma. *BMC Cancer.* (2019) 19:373. doi: 10.1186/s12885-019-5565-9
33. Theodoraki MN, Yerneni S, Gooding WE, Ohr J, Clump DA, Bauman JE, et al. Circulating exosomes measure responses to therapy in head and neck cancer patients treated with cetuximab, ipilimumab, and IMRT. *Oncoimmunology.* (2019) 8:1593805. doi: 10.1080/2162402X.2019.1593805
34. Morgan WF. Non-targeted and delayed effects of exposure to ionizing radiation: I. Radiation-induced genomic instability and bystander effects *in vitro*. *Radiat Res.* (2003) 159:567–80. doi: 10.1667/0033-7587(2003)159[0567:NADEOE]2.0.CO;2
35. Shao C, Folkard M, Prise KM. Role of TGF-beta1 and nitric oxide in the bystander response of irradiated glioma cells. *Oncogene.* (2008) 27:434–40. doi: 10.1038/sj.onc.1210653
36. He M, Zhao M, Shen B, Prise KM, Shao C. Radiation-induced intercellular signaling mediated by cytochrome-c via a p53-dependent pathway in hepatoma cells. *Oncogene.* (2010) 30:1947–55. doi: 10.1038/onc.2010.567
37. Hei TK, Zhou H, Ivanov VN, Hong M, Lieberman HB, Brenner DJ, et al. Mechanism of radiation-induced bystander effects: a unifying model. *J Pharm Pharmacol.* (2008) 60:943–50. doi: 10.1211/jpp.60.8.0001
38. Morgan WF, Sowa MB. Non-targeted bystander effects induced by ionizing radiation. *Mutat Res.* (2007) 616:159–64. doi: 10.1016/j.mrfmmm.2006.11.009
39. Jelonek K, Widlak P, Pietrowska M. The influence of ionizing radiation on exosome composition, secretion and intercellular communication. *Protein Pept Lett.* (2016) 23:656–63. doi: 10.2174/0929866523666160427105138
40. Albanese J, Dainiak N. Ionizing radiation alters Fas antigen ligand at the cell surface and on exfoliated plasma membrane-derived vesicles: implications for apoptosis and intercellular signaling. *Radiat Res.* (2000) 153:49–61. doi: 10.1667/0033-7587(2000)153[0049:IRAFAL]2.0.CO;2
41. Peinado H, Lavotshkin S, Lyden D. The secreted factors responsible for pre-metastatic niche formation: old sayings and new thoughts. *Semin Cancer Biol.* (2011) 21:139–46. doi: 10.1016/j.semcancer.2011.01.002
42. Record M, Subra C, Silvente-Poirot S, Poirot M. Exosomes as intercellular signalosomes and pharmacological effectors. *Biochem Pharmacol.* (2011) 81:1171–82. doi: 10.1016/j.bcp.2011.02.011
43. Le M, Fernandez-Palomo C, McNeill FE, Seymour CB, Rainbow AJ, Mothersill CE. Exosomes are released by bystander cells exposed to radiation-induced biophoton signals: reconciling the mechanisms mediating the bystander effect. *PLoS ONE.* (2017) 12:e0173685. doi: 10.1371/journal.pone.0173685
44. Ariyoshi K, Miura T, Kasai K, Fujishima Y, Nakata A, Yoshida M. Radiation-Induced bystander effect is mediated by mitochondrial DNA in exosome-like vesicles. *Sci Rep.* (2019) 9:9103. doi: 10.1038/s41598-019-45669-z
45. Szatmári T, Kis D, Bogdándi EN, Benedek A, Bright S, Bowler D, et al. Extracellular vesicles mediate radiation-induced systemic bystander signals in the bone marrow and spleen. *Front Immunol.* (2017) 8:347. doi: 10.3389/fimmu.2017.00347
46. Klammer H, Mladenov E, Li F, Iliakis G. Bystander effects as manifestation of intercellular communication of DNA damage and of the cellular oxidative status. *Cancer Lett.* (2015) 356:58–71. doi: 10.1016/j.canlet.2013.12.017
47. Yu X, Harris SL, Levine AJ. The regulation of exosome secretion: a novel function of the p53 protein. *Cancer Res.* (2006) 66:4795–801. doi: 10.1158/0008-5472.CAN-05-4579
48. Tian W, Yin X, Wang L, Wang J, Zhu W, Cao J, et al. The key role of miR-21-regulated SOD2 in the medium-mediated bystander responses in human fibroblasts induced by α-irradiated keratinocytes. *Mutat Res.* (2015) 780:77–85. doi: 10.1016/j.mrfmmm.2015.08.003
49. Yin X, Tian W, Wang L, Wang J, Zhang S, Cao J, et al. Radiation quality-dependence of bystander effect in unirradiated fibroblasts is associated with TGF-β1-Smad2 pathway and miR-21 in irradiated keratinocytes. *Sci Rep.* (2015) 5:11373. doi: 10.1038/srep11373
50. Yentrapalli R, Merl-Pham J, Azimzadeh O, Mutschelknaus L, Peters C, Hauck SM, et al. Quantitative changes in the protein and miRNA cargo of plasma exosome-like vesicles after exposure to ionizing radiation. *Int J Radiat Biol.* (2017) 93:569–80. doi: 10.1080/09553002.2017.1294772
51. Al-Mayah AH, Irons SL, Pink RC, Carter DR, Kadhim MA. Possible role of exosomes containing RNA in mediating nontargeted effect of ionizing radiation. *Radiat Res.* (2012) 177:539–45. doi: 10.1667/RR2868.1
52. Mutschelknaus L, Peters C, Winkler K, Yentrapalli R, Heider T, Atkinson MJ, et al. Exosomes derived from squamous head and neck cancer promote cell survival after ionizing radiation. *PLoS ONE.* (2016) 11:e0152213. doi: 10.1371/journal.pone.0152213
53. Vilalta M, Rafat M, Graves EE. Effects of radiation on metastasis and tumor cell migration. *Cell Mol Life Sci.* (2016) 73:2999–3007. doi: 10.1007/s00018-016-2210-5
54. Moncharmont C, Levy A, Guy JB, Falk AT, Guilbert M, Trone JC, et al. Radiation-enhanced cell migration/invasion process: a review. *Crit Rev Oncol Hematol.* (2014) 92:133–42. doi: 10.1016/j.critrevonc.2014.05.006
55. Edalat L, Stegen B, Klumpp L, Haehl E, Schilbach K, Lukowski R, et al. BK K+ channel blockade inhibits radiation-induced migration/brain infiltration of glioblastoma cells. *Oncotarget.* (2016) 7:14259–78. doi: 10.18632/oncotarget.7423
56. Zheng Y, Liu L, Chen C, Ming P, Huang Q, Li C, et al. The extracellular vesicles secreted by lung cancer cells in radiation therapy promote endothelial cell angiogenesis by transferring miR-23a. *PeerJ.* (2017) 5:e3627. doi: 10.7717/peerj.3627
57. Lumniczky K, Candéias SM, Gaipl US, Frey B. Editorial: radiation and the immune system: current knowledge and future perspectives. *Front Immunol.* (2017) 8:1933. doi: 10.3389/fimmu.2017.01933

58. Golden EB, Pellicciotta I, Demaria S, Barcellos-Hoff MH, Formenti SC. The convergence of radiation and immunogenic cell death signaling pathways. *Front Oncol.* (2012) 2:88. doi: 10.3389/fonc.2012.00088
59. Buchwald ZS, Efstathiou JA. Immunotherapy and radiation - a new combined treatment approach for bladder cancer? *Bladder Cancer*. (2015) 1:15–27. doi: 10.3233/BLC-150014
60. Min H, Sun X, Yang X, Zhu H, Liu J, Wang Y, et al. Exosomes derived from irradiated esophageal carcinoma-infiltrating T cells promote metastasis by inducing the epithelial-mesenchymal transition in esophageal cancer cells. *Pathol Oncol Res.* (2018) 24:11–8. doi: 10.1007/s12253-016-0185-z
61. Boelens MC, Wu TJ, Nabet BY, Xu B, Qiu Y, Yoon T, et al. Exosome transfer from stromal to breast cancer cells regulates therapy resistance pathways. *Cell.* (2014) 159:499–513. doi: 10.1016/j.cell.2014.09.051
62. Tang Y, Cui Y, Li Z, Jiao Z, Zhang Y, He Y, et al. Radiation-induced miR-208a increases the proliferation and radioresistance by targeting p21 in human lung cancer cells. *J Exp Clin Cancer Res.* (2016) 35:7. doi: 10.1186/s13046-016-0285-3
63. Dai X, Liao K, Zhuang Z, Chen B, Zhou Z, Zhou S, et al. AHIF promotes glioblastoma progression and radioresistance via exosomes. *Int J Oncol.* (2019) 54:261–70. doi: 10.3892/ijo.2018.4621
64. Wang S, Gao P, Li N, Chen P, Wang J, He N, et al. Autocrine secretions enhance radioresistance in an exosome-independent manner in NSCLC cells. *Int J Oncol.* (2019) 54:229–38. doi: 10.3892/ijo.2018.4620
65. de Araujo Farias V, O'Valle F, Serrano-Saenz S, Anderson P, Andrés E, López-Peñalver J, et al. Exosomes derived from mesenchymal stem cells enhance radiotherapy-induced cell death in tumor and metastatic tumor foci. *Mol Cancer.* (2018) 17:122. doi: 10.1186/s12943-018-0867-0
66. Ni J, Cozzi P, Hao J, Duan W, Graham P, Kearsley J, et al. Cancer stem cells in prostate cancer chemoresistance. *Curr Cancer Drug Targets.* (2014) 14:225–40. doi: 10.2174/1568009614666140328152459
67. Conigliaro A, Costa V, Lo Dico A, Saieva L, Buccheri S, Dieli F, et al. CD90+ liver cancer cells modulate endothelial cell phenotype through the release of exosomes containing H19 lncRNA. *Mol Cancer.* (2015) 14:155. doi: 10.1186/s12943-015-0426-x
68. Kumar D, Gupta D, Shankar S, Srivastava RK. Biomolecular characterization of exosomes released from cancer stem cells: possible implications for biomarker and treatment of cancer. *Oncotarget.* (2015) 6:3280–91. doi: 10.18632/oncotarget.2462
69. Li L, Liu WL, Su L, Lu ZC, He XS. The role of autophagy in cancer radiotherapy. *Curr Mol Pharmacol.* (2019). doi: 10.2174/1874467212666190809154518
70. Lee KS, Choi JS, Cho YW. Reprogramming of cancer stem cells into non-tumorigenic cells using stem cell exosomes for cancer therapy. *Biochem Biophys Res Commun.* (2019) 512:511–6. doi: 10.1016/j.bbrc.2019.03.072

Conflict of Interest Statement: The authors declare that the research was conducted in the absence of any commercial or financial relationships that could be construed as a potential conflict of interest.

Copyright © 2019 Ni, Bucci, Malouf, Knox, Graham and Li. This is an open-access article distributed under the terms of the Creative Commons Attribution License (CC BY). The use, distribution or reproduction in other forums is permitted, provided the original author(s) and the copyright owner(s) are credited and that the original publication in this journal is cited, in accordance with accepted academic practice. No use, distribution or reproduction is permitted which does not comply with these terms.

frontiers in Oncology

ORIGINAL RESEARCH
published: 27 September 2019
doi: 10.3389/fonc.2019.00974

The Effects of Neoadjuvant Chemoradiation in Locally Advanced Rectal Cancer—The Impact in Intratumoral Heterogeneity

Fabiana Bettoni[1†], *Cibele Masotti*[1†], *Bruna R. Corrêa*[1], *Elisa Donnard*[1], *Filipe F. dos Santos*[1], *Guilherme P. São Julião*[2], *Bruna B. Vailati*[2], *Angelita Habr-Gama*[2], *Pedro A. F. Galante*[1], *Rodrigo O. Perez*[2] *and Anamaria A. Camargo*[1,3*]

[1] Hospital Sírio Libanês, São Paulo, Brazil, [2] Instituto Angelita and Joaquim Gama, São Paulo, Brazil, [3] Ludwig Institute for Cancer Research, São Paulo, Brazil

OPEN ACCESS

Edited by:
Sunil Krishnan,
University of Texas MD Anderson Cancer Center, United States

Reviewed by:
Edmund Mroz,
The Ohio State University, United States
Ira Ida Skvortsova,
Innsbruck Medical University, Austria

***Correspondence:**
Anamaria A. Camargo
aacamargo@mochsl.org.br

[†]These authors have contributed equally to this work

Specialty section:
This article was submitted to Radiation Oncology, a section of the journal Frontiers in Oncology

Received: 01 March 2019
Accepted: 13 September 2019
Published: 27 September 2019

Citation:
Bettoni F, Masotti C, Corrêa BR, Donnard E, dos Santos FF, São Julião GP, Vailati BB, Habr-Gama A, Galante PAF, Perez RO and Camargo AA (2019) The Effects of Neoadjuvant Chemoradiation in Locally Advanced Rectal Cancer—The Impact in Intratumoral Heterogeneity. Front. Oncol. 9:974. doi: 10.3389/fonc.2019.00974

Purpose: Intratumoral genetic heterogeneity (ITGH) is a common feature of solid tumors. However, little is known about the effect of neoadjuvant chemoradiation (nCRT) in ITGH of rectal tumors that exhibit poor response to nCRT. Here, we examined the impact of nCRT in the mutational profile and ITGH of rectal tumors and its adjacent irradiated normal mucosa in the setting of incomplete response to nCRT.

Methods and Materials: To evaluate ITGH in rectal tumors, we analyzed whole-exome sequencing (WES) data from 79 tumors obtained from The Cancer Genome Atlas (TCGA). We also compared matched peripheral blood cells, irradiated normal rectal mucosa and pre and post-treatment tumor samples (PRE-T and POS-T) from one individual to examine the iatrogenic effects of nCRT. Finally, we performed WES of 7 PRE-T/POST-T matched samples to examine how nCRT affects ITGH. ITGH was assessed by quantifying subclonal mutations within individual tumors using the Mutant-Allele Tumor Heterogeneity score (MATH score).

Results: Rectal tumors exhibit remarkable ITGH that is ultimately associated with disease stage (MATH score stage I/II 35.54 vs. stage III/IV 44.39, $p = 0.047$) and lymph node metastasis (MATH score N0 35.87 vs. $N+$ 45.79, $p = 0.026$). We also showed that nCRT does not seem to introduce detectable somatic mutations in the irradiated mucosa. Comparison of PRE-T and POST-T matched samples revealed a significant increase in ITGH in 5 out 7 patients and MATH scores were significantly higher after nCRT (median 41.7 vs. 28.8, $p = 0.04$). Finally, we were able to identify a subset of "enriched mutations" with significant changes in MAFs between PRE-T and POST-T samples. These "enriched mutations" were significantly more frequent in POST-T compared to PRE-T samples (92.9% vs. 7.1% $p < 0.00001$) and include mutations in genes associated with genetic instability and drug resistance in colorectal cancer, indicating the expansion of tumor cell subpopulations more prone to resist to nCRT.

Conclusions: nCRT increases ITGH and may result in the expansion of resistant tumor cell populations in residual tumors. The risk of introducing relevant somatic mutations

in the adjacent mucosa is minimal but non-responsive tumors may have potentially worse biological behavior when compared to their untreated counterparts. This was an exploratory study, and due to the limited number of samples analyzed, our results need to be validated in larger cohorts.

Keywords: neoadjuvant therapy, rectal cancer, intratumoral heterogeneity, clonal evolution, therapy resistance

INTRODUCTION

Neoadjuvant chemoradiotherapy (nCRT) is one of the preferred treatment strategies for locally advanced rectal cancer (1, 2). In addition to providing improved local disease control (particularly for patients with high-risk features for local recurrence), nCRT may allow the opportunity for organ-preservation among patients with complete clinical response (cCR). However, treatment of patients with low-risk for local recurrence with nCRT, for the sole purpose of organ-preservation, may result in significant detrimental functional and biological consequences among patients who do not achieve a cCR and still need radical surgery.

Intratumoral genetic heterogeneity (ITGH) was first described in the early 1980's (3). However, only recently, the full extent and the functional implications of ITGH have been appreciated (4). ITGH increases phenotypic variation and is currently seen as a critical mechanism underlying disease progression and therapeutic failure (5, 6). We and others have recently characterized the clonal architecture of locally advanced rectal tumors through multi-region whole-exome sequencing (WES). We demonstrated that non-treated rectal tumors exhibit a complex clonal architecture and significant, ITGH with 27–97% of exonic somatic mutations shared among all regions of an individual's tumor and with a mutant allele frequency (MAF) correlation between disparate tumor regions ranging from $R^2 = 0.69–0.96$ (7, 8). However, in these studies ITGH, was determined using a small number of tumors, and the effect of nCRT in shaping the mutational landscape and clonal architecture of rectal cancer was not addressed. Ultimately, tumors that do not respond completely to nCRT may acquire novel mutations and/or harbor selected tumor cells subpopulations compared to their baseline counterparts, leading to increased ITGH. Here, we evaluated ITGH in untreated rectal tumors and examined its association with disease stage and presence of lymph node metastasis. Also, we analyzed the impact of nCRT in the mutational landscape and ITGH of rectal tumors with incomplete response to nCRT and searched for somatic mutations introduced by nCRT in the adjacent normal irradiated mucosa.

MATERIALS AND METHODS

TCGA Data

To evaluate ITGH in rectal tumors and determine its association with disease stage and presence of lymph node metastasis, we analyzed whole-exome sequencing (WES) data from 79 rectal tumors from The Cancer Genome Atlas (TCGA) colorectal cohort (9, 10). Clinical, pathological and mutational data for all 79 rectal tumors are provided in **Supplementary Table 1**.

Rectal Cancer Patients and nCRT

Consecutive patients with rectal cancer (adenocarcinoma biopsy-proven), located no more than 7 cm from the anal verge, and treated at the Angelita & Joaquim Gama Institute between 2007 and 2010, were eligible for the study. Only patients undergoing neoadjuvant chemoradiation were recruited for the study. Inclusion criteria included tumors with cT3/T4 or cN+ disease by radiological staging using magnetic resonance (MR) or endorectal ultrasound. Additionally, patients with cT2N0 otherwise considered for abdominal perineal excision or ultra-low anterior resections were also referred for neoadjuvant chemoradiation and included in the study. Patients with metastatic disease were excluded from the study. Patients with clinical and radiological findings consistent with cCR were also excluded from the present study. Only patients with $\geq$10% residual cancer cells in the final pathological assessment were included in an attempt to avoid contamination of "incomplete responders" with "near-complete responders" that could eventually develop complete response if longer resting intervals had been used (**Table 1**). Macrodissection of tumor regions was performed whenever necessary prior to DNA extraction to increase sample purity. Tumor sections were required to contain at least 80% tumor cell nuclei with <20% necrosis for inclusion in the study. We have randomly selected one of the patients for the analysis of the nCRT effect on the normal rectal mucosa. Baseline staging and assessment of patients included digital rectal examination (DRE), proctoscopy and high-resolution MR. All patients underwent long-course chemoradiation therapy as described previously (11).

Assessment of Tumor Response

All patients were assessed for tumor response after at least 12 weeks from the last day of nCRT completion. Assessment of tumor response was performed with DRE, proctoscopy and MR. Patients with incomplete clinical response (clinical or radiological) were referred to immediate radical surgery.

Tumor and Blood Samples

Tumor samples were collected at diagnosis (PRE-T samples) and during surgical removal of the residual tumor (POST-T samples). Tumor-adjacent normal colonic mucosa exposed to nCRT (Nrx) was also collected from one patient immediately after tumor resection. Peripheral blood cells (BC) were collected from all patients before nCRT. This study was approved by the Ethics Committee of Hospital Alemão Oswaldo Cruz, São Paulo, Brazil (reference number 19/08) and was conducted in

TABLE 1 | Clinical and pathological data of rectal cancer patients submitted to nCRT.

Patient	Tumor size (cm)	Distance from anal verge (cm)	Baseline stage	Type of operation	Pathology	TRG (% tumor)
PT01	5	5	cT3N0M0	LAR	ypT3N0	80
PT02	4	6	cT3N1M0	LAR	ypT2N1	80
PT03	4	7	cT3N1M0	LAR	ypT2N0	90
PT04	3	5	cT2N1M0	LAR	ypT2N2	30
PT05	5	4	cT2N1M0	APR	ypT3N0	70
PT06	5	6	cT2N1M0	LAR	ypT2N0	90
PT07	4	4	cT3N0M0	LAR	ypT3N1	80

LAR, low anterior resection; APR, abdominal perineal resection; TRG, tumor regression grade.

accordance with the Declaration of Helsinki. Patients provided written informed consent for tumor sample collection and study participation. Samples were processed as described in **Supplementary Material**.

Whole Exome Sequencing (WES)

Whole-exome libraries were prepared using SureSelect Human All Exon Target Enrichment kit (Agilent Technologies, Santa Clara, CA) and sequences were generated on a 5500xl SOLiD sequencing platform (Thermo-Fisher Scientific, Waltham, MA). Sequencing and coverage information are provided in **Supplementary Table 2**.

SNV Calling and Somatic Mutation Detection

SNVs were identified using a combination of published and local pipelines (8, 12, 13) as described in **Supplementary Material**. Somatic point mutations were annotated using ANNOVAR (14).

ITGH and MATH Score

Significant changes in allele frequencies were used as a surrogate for changes in clonal structure and were detected using exact binomial tests. False discovery rate (FDR) was calculated using the p.adjust R function to correct for multiple-testing (15). ITGH was measured using the mutant allele tumor heterogeneity (MATH) score (16, 17). The MATH score is a quantitative measure of ITGH based on the Mutant Allele Frequency (MAF) distribution. MATH scores were calculated as the width ratio to the center of MAFs' distribution for somatic point mutations present within individual tumors. Due to the presence of genetically distinct cellular populations, heterogeneous tumors exhibit a broader allele frequency distribution compared to homogeneous tumors and higher scores. The MATH score is the most cost-effective method to compare ITGH among different tumors and to monitor global changes in ITGH (16–21).

Mutational Spectrum and Signatures

Mutational spectrum and signature analyses were performed, according to a previously published pipeline (22) and are detailed in **Supplementary Material**.

Gene Set Enrichment Analysis

Gene set enrichment analysis (GSEA) was performed using the Molecular Signatures Database v5.0 (MSigDB) as detailed in **Supplementary Material** (23).

RESULTS

ITGH in Rectal Tumors Is Associated With Disease Stage and Progression

To expand the characterization of ITGH in rectal tumors, we used WES data from 79 non-treated rectal tumors obtained from TCGA (**Supplementary Figure 1**). Since multi-region WES data was not available for TCGA samples, we used the MATH score to measure ITGH in these samples (16–21). Rectal tumors exhibit remarkable variability in ITGH, with MATH scores ranging from 18.2 to 66.7 (median = 40.1; mean = 41; first quartile = 31.1; third quartile = 49.8; **Figure 1A**). We also observed a significant positive association between MATH values, disease stage (Stage I/II median of 35.54 vs. stage III/IV median of 44.39, $p = 0.047$, Wilcoxon test, **Figure 1B**) and lymph node metastases (N0 median of 35.87 vs. N1+N2 median of 45.79, $p = 0.026$, Wilcoxon paired test, **Figure 1C**).

The MATH score is a simple and cost-effective method to measure ITGH that shows little influence of copy number variations (CNVs) and provides a first-order correction for the presence of contaminating normal tissue in tumor samples (16–21). To determine the influence of CNVs in our analysis we examined the correlation between MATH scores and total number of CNVs in all 79 individual tumors. As shown in **Supplementary Figure 2**, there is no significant correlation between higher MATH scores and aberrant CNV profiles in rectal tumors (cor = −0.03, $p = 0.8$, Pearson correlation). Likewise, we did not observe a significant association between the total number of CNVs, disease stage (Stage I/II median of 13.5 vs. stage III/IV median of 17.0, Wilcoxon test, $p = 0.53$, **Supplementary Figure 2**) or lymph node metastases (N0 median of 13 vs. N1+N2 median of 17, Wilcoxon paired test $p = 0.42$, **Supplementary Figure 2**). We also evaluated the impact of tumor sample purity in our results by analyzing the correlation between MATH scores and sample purity information provided for all 79 TGCA samples. As shown in **Supplementary Figure 3**, there is no significant correlation between MATH scores and tumor sample purity (cor = −0.037,

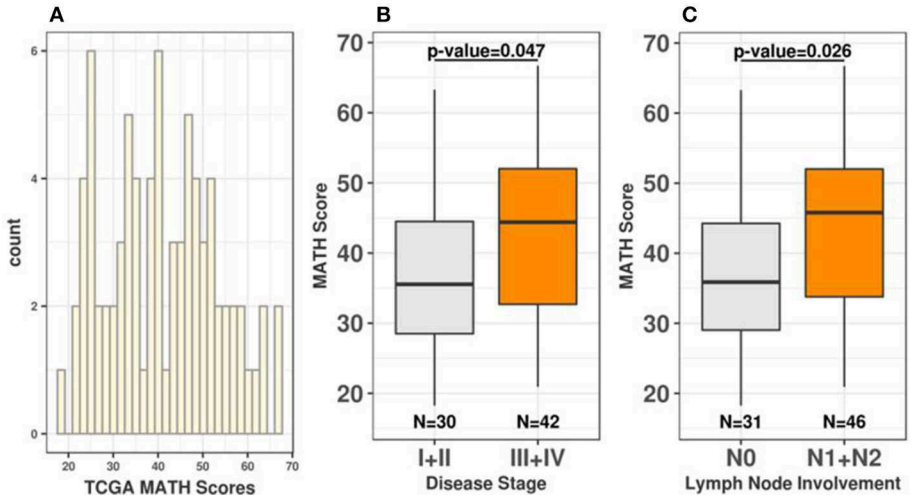

FIGURE 1 | Rectal tumors exhibit continuous variability in ITGH. **(A)** Distribution of MATH scores among 79 rectal cancers from TCGA. **(B)** Distribution of MATH scores according to disease stage (Wilcoxon test p-value=0.047 for I+II vs. III+IV comparisons). **(C)** Distribution of MATH scores according to lymph node involvement (Wilcoxon test $p = 0.026$ for N0 vs. N1+N2).

$p = 0.75$, Pearson correlation). Therefore, non-treated rectal tumors exhibit a remarkable variability in ITGH, which is not significantly influenced by underlying somatic CNVs and tumor sample purity and is significantly associated with disease stage and lymph node metastases.

Effects of nCRT in Normal Adjacent Mucosa

To evaluate the iatrogenic effect of nCRT, we compared the mutational landscape of a matched set of peripheral blood cells collected before nCRT (BC), tumor adjacent colonic mucosa exposed to nCRT (Nrx) and pre (PRE-T) and post-treatment (POST-T) tumor samples derived from a single rectal cancer patient.

We first compared the total set of single nucleotide variants (SNVs) detected in BC and Nrx to determine if nCRT could introduce novel somatic mutations in the irradiated rectal colonic mucosa. As expected, since both samples are derived from the same patient, the majority of the SNVs (99.87%, 9,698/9,711) was shared between both samples and only a very small fraction of SNVs is exclusively detected in BC (0.06%, 6/9,711) or in Nrx sample (0.07%, 7/9,705) (**Figure 2A**). We next searched for significant variations in allele frequencies of SNVs shared between BC and NrX samples. PRE-T and POST-T samples were used as positive controls for allele frequency variations. Significant variations in allele frequencies were observed in the comparison between BC and POST-T (**Figure 2D**) and, to a lesser extent, in the comparison between BC and PRE-T (**Figure 2C**). In contrast, only 10 variants presented significant variations in allele frequencies between BC and Nrx (**Figure 2B**). None of these variants occurred in regions involved in V(D)J recombination but they are dispersed throughout the genome. Also, we observed a significant direct correlation of allele frequencies for SNVs present in both BC and NRX samples ($R^2 = 0.91$; $p < 2 \times 10 -$ 16, Pearson Correlation test, **Figure 2B**). Although these results need to be validated using a larger number of matched samples, they indicate that nCRT *per se* does not seem to introduce detectable novel somatic mutations or copy number variations in the irradiated mucosa.

ITGH Increases After nCRT

To address the effect of nCRT on the clonal structure of rectal tumors, we generated WES data from 7 matched PRE-T and POST-T samples (**Supplementary Table 2**). PRE-T and POST-T samples presented a median of 133 (min. 42, max. 341) and 83 (min. 50, max. 676) somatic point mutations, respectively (**Supplementary Table 3**). No significant difference in the number of mutations between PRE-T and POST-T tumors was observed (Wilcoxon test, $p = 0.9$). We also did not observe significant alterations in the spectrum of DNA base changes between PRE-T and POST-T samples (**Supplementary Figure 4**) and we were unable to detect a DNA damage mutational signature in POST-T samples (**Supplementary Figure 5**). Overall, the most frequent mutations observed in our cohort are also consistent with results reported by TCGA (**Supplementary Table 4**) (24). On average, only 20% (min. 10%—max. 32%) of the somatic mutations were shared between PRE-T and POST-T samples, with MAF correlations between matched samples ranging from $R^2 = 0.025–0.393$ (**Supplementary Table 3**).

To quantify the effect of nCRT on the clonal structure of rectal tumors, we next determined MAF distributions and calculated MATH scores for the 7 matched PRE-T and POST-T samples (**Figures 3A,B**). Median MAF and MATH scores varied from 0.13 to 0.33 and from 23 to 60.1 among all 14 samples, respectively (**Supplementary Table 3**). Overall MATH scores were significantly higher in POST-T samples compared to PRE-T samples (median 41.7 vs. 28.8, $p =$

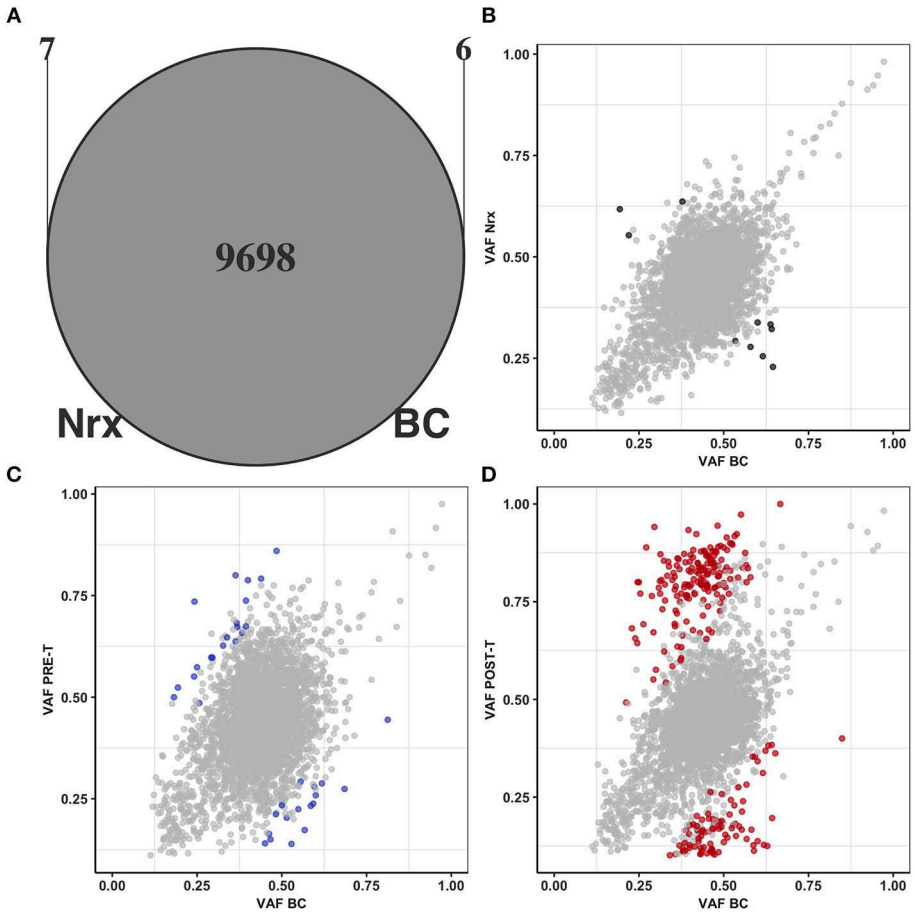

FIGURE 2 | nCRT does not introduce novel somatic mutations nor affects normal tissue genetic heterogeneity. **(A)** Overlap between SNVs present in BC ($n = 9{,}704$) and in Nrx ($n = 9{,}705$). Comparisons of allele frequencies from SNVs shared by BC, Nrx, PRE-T, and POST-T samples: **(B)** BC vs. Nrx, **(C)** BC vs. PRE-T, and **(D)** BC vs. POST-T. Significant variations in allele frequencies are highlighted in black, blue, and red, respectively ($p < 0.05$; Binomial test, Bonferroni adjusted).

0.04, Wilcoxon paired test, **Figure 3C**). Noteworthy, five out of the seven tumors with incomplete response to nCRT presented an increase in MATH values in POST-T sample (**Figure 3B** and **Supplementary Table 3**). This suggests that nCRT can significantly alter clonal structure in residual tumors, increasing ITGH.

nCRT Acts as a Strong Selective Pressure

To examine if nCRT can select pre-existing tumor cell subpopulations more prone to resist to nCRT, we monitored tumor cell subpopulation dynamics before and after nCRT. Since MATH score does not allow direct enumeration of distinct tumor cell subpopulations, we monitored their dynamics by applying binomial tests to identify somatic mutations with significant changes in MAFs between PRE-T and POST-T samples (named as enriched mutations). For this analysis, we focused on 401 coding and splice site somatic mutations shared between PRE-T and POST-T samples, since they are more likely to have a deleterious impact on protein function.

We identified a total of 210 somatic mutations (52.4%) enriched in PRE-T or POST-T samples (**Figure 4**). Mutation enrichment was validated using Sanger Sequencing (**Supplementary Figure 6**). Enriched mutations were significantly more frequent in POST-T compared to PRE-T samples [195/210 (92.9%) vs. 15/210 (7.1%), $p < 0.00001^{7}$, Fisher's exact test, **Supplementary Table 5**]. Noteworthy, we observed an excess of deleterious non-synonymous mutations over neutral synonymous mutations in POST-T [136 non-synonymous (N) and 46 synonymous (S), N/S = 2.96] compared to PRE-T-enriched mutations [8 non-synonymous (N) and 5 synonymous (S), N/S = 1.6]. The observed difference, however, was not statistically significant, probably due to the small number of enriched mutations in the PRE-T samples ($p = 0.23$, Fisher's exact test).

Finally, we used GSEA to verify if nCRT could select tumor cell subpopulations more prone to resist to nCRT. In addition to the 210 enriched mutations, we found a total of 634 somatic mutations that were exclusively detected in POST-T samples. More than 59% of these POST-T specific

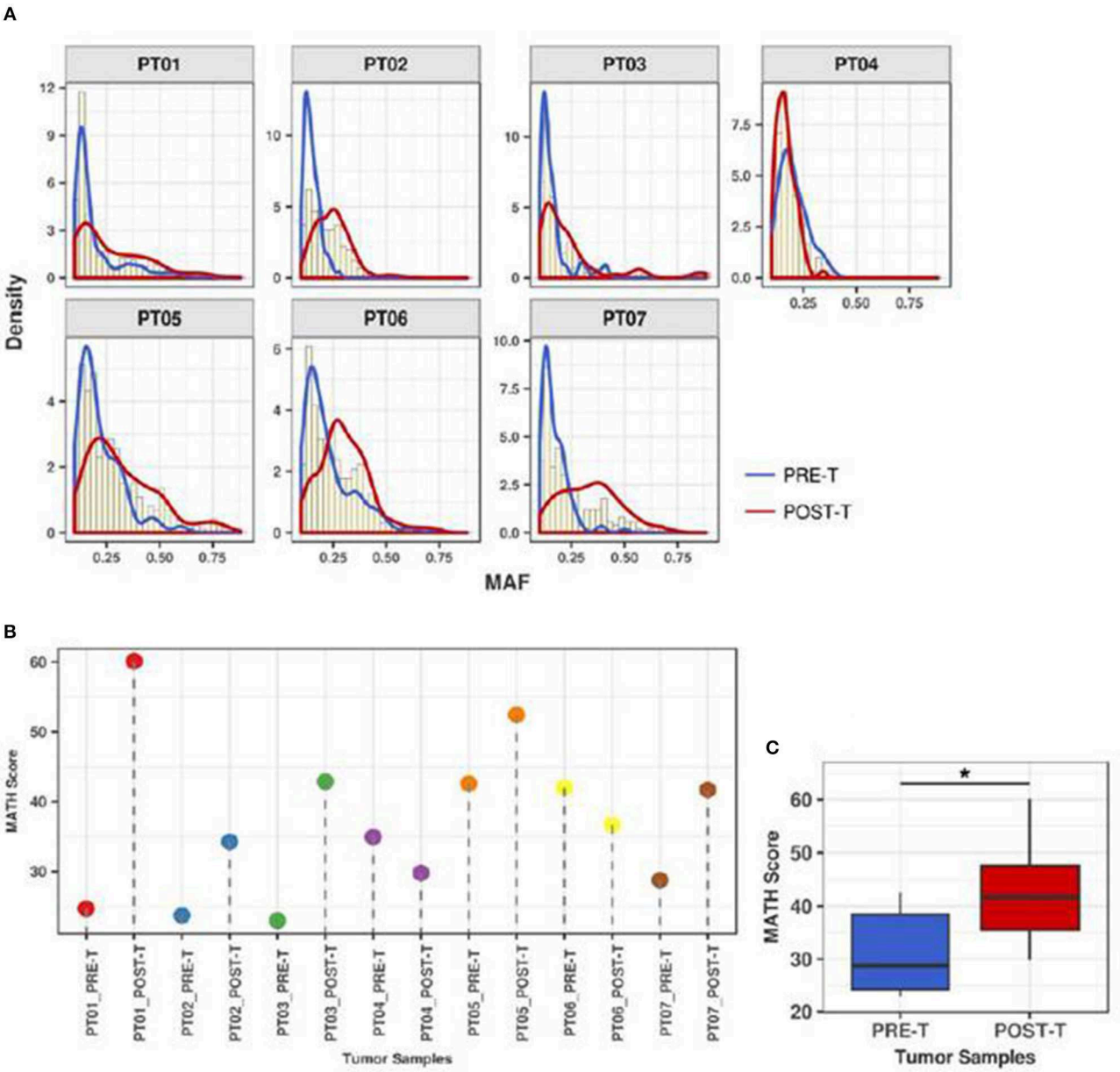

FIGURE 3 | ITGH increases after nCRT. **(A)** MAF distributions for PRE-T (blue), POST-T (red), and total samples (yellow histograms) from 7 patients with rectal cancer presenting incomplete clinical response to nCRT (PT01-PT07). **(B)** MATH scores for PRE-T and POST-T samples. **(C)** Comparison between MATH scores distribution in PRE-T and POST-T samples from 7 patients with rectal cancer (*$p = 0.04$; paired Wilcoxon Signed-Rank Test).

mutations were observed in a single patient (PT02 377/634) with high tumor mutational burden. Although the presence of some of these POST-T specific mutations could be attributed to tumor topographic heterogeneity, not contemplated in the samples used for sequencing, some of these mutations could indeed result from tumor genetic instability and clonal selection during neoadjuvant therapy and were, therefore, used for GSEA. We observed that POST-T specific and POST-T enriched mutations frequently occurred in genes associated with cell cycle regulation and proliferation (mitotic spindle assembly and mitotic checkpoint gene sets) as well as with cell survival and differentiation (*K-Ras*, *TNF-alpha*, and Hedgehog signaling gene sets) (**Supplementary Table 6**). Among POST-T enriched mutations, we found non-synonymous mutations in genes associated with genetic instability and drug resistance in colorectal cancer, including mutations in the *ATM* (25, 26), *DIDO1* (27, 28), and *AKAP9* (29) (**Supplementary Figure 7**). Among POST-T specific mutations, we also found non-synonymous mutations in genes involved in DNA repair and apoptosis, including *ERCC6* previously associated with resistance

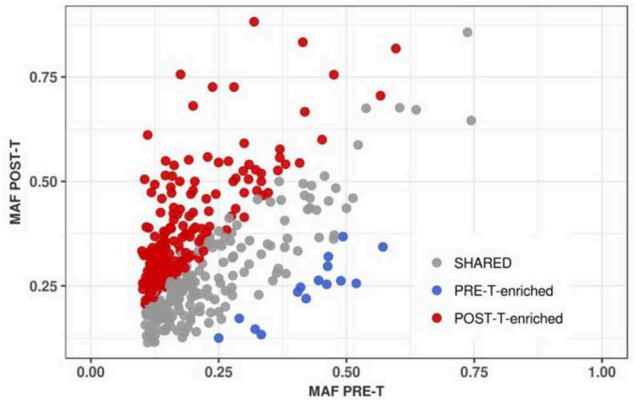

FIGURE 4 | Positive selection of tumor cell subpopulations after nCRT. MAF correlation for 401 somatic point mutations shared between PRE-T and POST-T samples ($R^2 = 0.3$). Enriched mutations in PRE-T ($n = 15$) and POST-T ($N = 195$) samples are highlighted in blue and red, respectively.

to 5-Fluorouracil and poor prognosis (30). This suggests that nCRT may act as a strong selective pressure resulting in the selection of tumor cell subpopulations in the residual tumor that are more prone to resist to nCRT.

DISCUSSION

nCRT may result in significant primary tumor regression. Ultimately, tumors that achieve complete or even near-complete response may allow for organ-preserving strategies (31, 32). In this setting, even patients with early rectal cancer (cT2N0), otherwise considered for abdominal perineal resections or ultra-low anterior resections, have been considered for nCRT in order to avoid a definitive colostomy or poor anorectal function (11). However, even though patients with early stage disease are more likely to achieve a cCR, many patients will still harbor residual disease requiring surgical resection (33). In these patients, nCRT may contribute to significant increases in postoperative complications and worsening of functional anorectal outcomes (34, 35). Here, we demonstrated that nCRT may also have significant biological consequences to the residual cancer in the setting of incomplete tumor response.

In the present study, we showed that non-treated rectal tumors exhibited a remarkable variability in ITGH that is directly associated with disease stage and lymph node metastases. Studies using large tumor collections have shown that ITGH impacts clinical outcome (36, 37) and may contribute to drug resistance in different tumors (38). ITGH has been previously reported in colon (39–43) and rectal cancers (7, 8), however, for most of these studies, ITGH was determined only for a small number of tumors and the prognostic and predictive significance of ITGH for these cancers remains to be determined. Recently, the MATH score was used in two independent studies to quantify ITGH in colorectal tumors. Zhang et al. analyzed WES data from 284 colorectal tumors obtained from TCGA and 187 colorectal tumors obtained from the International Cancer Genome Consortium (ICGC) (43). The mean MATH value was 41.58 and 46.1 for the TCGA and ICGC cohorts, respectively. Similarly to our results, higher MATH scores were associated with disease stage and lymph node metastasis. Although the authors observed a significant difference in MATH scores between rectal and colon tumors (MATH = 45.9 vs. 39.96 $p = 0.004$), a separate analysis for rectal cancer was not performed and samples previously treated with nCRT were not excluded. Hardiman et al. have used the MATH score to analyze ITGH in 7 stage II/III rectal tumors, MATH scores in these tumors varied from 9.08 to 25.24 and were significantly higher in stage III tumors (7). Although further studies will be necessary to determine the prognostic significance of ITGH in rectal cancers, the strong association between ITGH and disease stage and lymph node involvement—both known predictors of survival after surgical treatment among these patients—supports a possible role for ITGH as a prognostic biomarker in rectal cancer.

Another relevant finding was that nCRT, *per se*, does not introduce detectable somatic mutations in the irradiated colonic mucosa. To the best of our knowledge, our study was the first to directly address the potentially iatrogenic effect of nCRT. The use of treatment-exposed normal colonic mucosa was critical to distinguish treatment-induced mutations from those arising from tumor genetic instability and positive clonal selection after treatment exposure. Until present, few studies have indirectly addressed the impact of radiation and chemotherapy by comparing mutational landscapes of matched PRE-T and POST-T samples (44–47). Although post-treatment mutation spectrum shifts have been reported for esophageal adenocarcinoma following platinum-based neoadjuvant chemotherapy (45), WES of matched anal squamous cell carcinomas before and after chemoradiation revealed a similar number of somatic mutations and a similar pattern of DNA substitutions in pre and post-treatment tumors (47).

The most relevant finding of the present study is that MATH scores are significantly higher in POST-T compared to PRE-T samples. This suggests that nCRT can significantly affect ITGH in residual tumors. Significant alterations in ITGH have been reported for esophageal adenocarcinoma after exposure to neoadjuvant chemotherapy. Murugaesu et al. found that mutations in post-chemotherapy samples were rarely clonal (3%), while 50% of the somatic mutations identified prior to chemotherapy were clonal (45). Findlay et al. observed a variety of clonal behaviors in esophageal tumors after chemotherapy, including samples showing little changes in clonal composition and samples with marked differences in the clonal architecture after therapy (44). Most importantly, in both studies, there was a significant association between ITGH and response to neoadjuvant chemotherapy. More recently, marked clonal landscape remodeling has also been described for hormone-positive breast cancer exposed to neoadjuvant aromatase inhibitor treatment, but no associations between ITGH and treatment response were established (48). By comparing PRE-T and POST-T samples, we observed a

significant overall increase in ITGH. Five out 7 patients presented a significant increase in ITGH. Interestingly, tumor regression in these 5 samples was minimal (20–30% tumor regression). In contrast one of the 2 patients showing minimal changes in ITGH presented the most significant tumor response (70% tumor regression). Even though these results could indicate a possible association between ITGH and tumor response to nCRT, the limited size of our cohort, and the fact that we have only analyzed tumors in the setting of incomplete response to nCRT, did not allow us to fully explore this association in the present work.

Finally, we monitored tumor cell subpopulation dynamics during nCRT by identifying enriched somatic mutations with significant changes in allele frequencies between PRE-T and POST-T samples. Enriched mutations were more frequently found in POST-T samples. We also observed higher proportion of potentially deleterious mutations in these samples. Enriched mutations in POST-T samples were frequently present among genes involved in DNA damage repair, genetic instability, cell cycle regulation, proliferation, survival, and differentiation (25–29). All these molecular pathways have been shown to contribute to chemoradiotherapy resistance to colorectal tumor cells, suggesting that nCRT may result in tumors more aggressive than their baseline counterparts in the setting of incomplete response. Clonal evolution in response to neoadjuvant therapy has been previously studied in breast, esophageal, and anal squamous cell carcinomas (44, 45, 47, 48). Together with our study, these studies indicate that neoadjuvant therapy can profoundly affect tumor clonal architecture by promoting significant changes in the frequency of somatic mutations owing to the outgrowth of subclones with selective growth advantages in the residual tumor.

There are some limitations to this study that should be considered for the interpretation of our results and prevent the immediate application of our findings in clinical practice. First, we used a single set of matched samples in the analysis of the iatrogenic effect of nCRT in the normal colonic mucosa. Confirmation of our findings in larger cohorts is definitively necessary. Also, we cannot exclude the possibility that our sequencing strategy was not sensitive enough to detect novel somatic alterations, present in individual cells in the normal adjacent irradiated mucosa, which have not expanded significantly in the sampled population. Second, although we observed a significant variation in ITGH between PRE-T and POS-T samples, these observations were also based on a limited number of matched samples and in a single tumor region. We and others have described significant topographical intratumor heterogeneity in rectal cancer, and therefore, the impact of nCRT in ITGH and clonal selection in rectal tumors needs further evaluation. Most importantly, in the present work, we monitored tumor cell population dynamics by identifying "enriched mutations" with significant changes in MAFs between PRE-T and POST-T samples. Apart from a subclonal distribution and the presence of local somatic CNVs, the observed MAF at a specific locus is also directly influenced by tumor sample purity. Therefore, variations in sample purity, rather than in subclonal composition, could result in significant MAF differences between PRE-T and POST-T samples and consequently influence our analysis of tumor cell subpopulation dynamics before and after nCRT. In the present work, all tumor samples were microdissected by an experienced pathologist to enrich for tumor purity and minimize this possibility. Tumor sections were required to contain at least 80% tumor cell nuclei with <20% necrosis for inclusion in the study.

In conclusion, nCRT *per se* does not seem to introduce novel somatic mutations in the irradiated normal rectal mucosa. Instead, nCRT may drive a marked clonal selection in residual rectal tumors. This results in frequent increases in ITGH in residual cancers when compared to their baseline counterparts, which are driven by significant alterations in the frequency of biologically relevant mutations in genes associated with response to nCRT. The risk of more heterogeneous residual tumors leading to more biologically aggressive cancers may constitute a potential disadvantage of nCRT among incomplete responders. This may be particularly relevant among patients with early stage disease considering nCRT solely for the purpose of achieving cCR and organ-preservation. Future studies should address the oncological impact of significant ITGH increase after nCRT and incomplete response in rectal cancer.

DATA AVAILABILITY STATEMENT

Sequence data has been deposited at the European Genome-phenome Archive (EGA, http://www.ebi.ac.uk/ega/), which is hosted by the EBI, under accession number EGAS00001003250.

ETHICS STATEMENT

This study was approved by the Ethics Committee of Hospital Alemão Oswaldo Cruz, São Paulo, Brazil (reference number 19/08) and was conducted in accordance with the Declaration of Helsinki. Patients provided written informed consent for tumor sample collection and study participation.

AUTHOR CONTRIBUTIONS

AC and RP designed the study. FB performed experiments and acquired data. AC, BC, CM, ED, FS, FB, PG, and RP analyzed and interpreted data. RP, AH-G, GS, and BV recruited patients and acquired samples for analysis. AC, RP, and PG supervised the study. AC, AH-G, PG, and RP acquired funding for the study. AC, CM, FB, and RP prepared the manuscript. AC, AH-G, BC, CM, ED, FB, PG, and RP performed critical revision of the manuscript. All authors read and approved the final manuscript.

FUNDING

This work was supported by The Ludwig Institute for Cancer Research (LICR) and Fundação de Amparo a Pesquisa do Estado

de São Paulo (FAPESP 2015/17208-9 to CM; 2013/07159-5 to BC; 2010/12658-2 to ED, and 2011/51130-6 to RP).

ACKNOWLEDGMENTS

We thank Drs. Romualdo Barroso and Marcelo Negrão for reading the manuscript and Natália Felicio and Bruna Hessel for technical assistance. We are also indebted to with patients enrolled in this study.

SUPPLEMENTARY MATERIAL

The Supplementary Material for this article can be found online at: https://www.frontiersin.org/articles/10.3389/fonc.2019.00974/full#supplementary-material

REFERENCES

1. Sauer R, Becker H, Hohenberger W, Rödel C, Wittekind C, Fietkau R, et al. Preoperative versus postoperative chemoradiotherapy for rectal cancer. *N Engl J Med*. (2004) 351:1731–40. doi: 10.1056/NEJMoa040694
2. Kosinski L. Shifting concepts in rectal cancer management. *CA Cancer J Clin*. (2012) 62:173–202. doi: 10.3322/caac.21138
3. McGranahan N, Swanton C. Clonal heterogeneity and tumor evolution: past, present, and the future. *Cell*. (2017) 168:613–28. doi: 10.1016/j.cell.2017.01.018
4. Ding L, Raphael BJ, Chen F, Wendl MC. Advances for studying clonal evolution in cancer. *Cancer Lett*. (2013) 340:212–9. doi: 10.1016/j.canlet.2012.12.028
5. Gerlinger M, Swanton C. How Darwinian models inform therapeutic failure initiated by clonal heterogeneity in cancer medicine. *Br J Cancer*. (2010) 103:1139–43. doi: 10.1038/sj.bjc.6605912
6. Swanton C. Intratumor heterogeneity: evolution through space and time. *Cancer Res*. (2012) 72:4875–82. doi: 10.1158/0008-5472.CAN-12-2217
7. Hardiman KM, Ulintz PJ, Kuick RD, Hovelson DH, Gates CM, Bhasi A, et al. Intra-tumor genetic heterogeneity in rectal cancer. *Lab Investig*. (2016) 96:4–15. doi: 10.1038/labinvest.2015.131
8. Bettoni F, Masotti C, Habr-Gama A, Correa BR, Gama-Rodrigues J, Vianna MR, et al. Intratumoral genetic heterogeneity in rectal cancer: are single biopsies representative of the entirety of the tumor? *Ann Surg*. (2017) 265:e4–6. doi: 10.1097/SLA.0000000000001937
9. Cerami E, Gao J, Dogrusoz U, Gross BE, Sumer SO, Aksoy BA, et al. The cBio cancer genomics portal: an open platform for exploring multidimensional cancer genomics data. *Cancer Discov*. (2012) 2:401–4. doi: 10.1158/2159-8290.CD-12-0095
10. Gao J, Aksoy BA, Dogrusoz U, Dresdner G, Gross B, Sumer SO, et al. Integrative analysis of complex cancer genomics and clinical profiles using the cBioPortal. *Sci Signal*. (2013) 6:pl1. doi: 10.1126/scisignal.2004088
11. Habr-Gama A, São Julião GP, Vailati BB, Sabbaga J, Aguilar PB, Fernandez LM, et al. Organ preservation in cT2N0 rectal cancer after neoadjuvant chemoradiation therapy: the impact of radiation therapy dose-escalation and consolidation chemotherapy. *Ann Surg*. (2017) 269:102–7. doi: 10.1097/SLA.0000000000002447
12. Donnard E, Asprino PF, Correa BR, Bettoni F, Koyama FC, Navarro FCP, et al. Mutational analysis of genes coding for cell surface proteins in colorectal cancer cell lines reveal novel altered pathways, druggable mutations and mutated epitopes for targeted therapy. *Oncotarget*. (2014) 5:9199–213. doi: 10.18632/oncotarget.2374
13. Torrezan GT, Ferreira EN, Nakahata AM, Barros BDF, Castro MTM, Correa BR, et al. Recurrent somatic mutation in DROSHA induces microRNA profile changes in Wilms tumour. *Nat Commun*. (2014) 5:4039. doi: 10.1038/ncomms5039
14. Wang K, Li M, Hakonarson H. ANNOVAR: functional annotation of genetic variants from high-throughput sequencing data. *Nucleic Acids Res*. (2010) 38:e164. doi: 10.1093/nar/gkq603
15. Benjamini Y, Yekutieli D. The control of the false discovery rate in multiple testing under depencency. *Ann Stat*. (2001) 29:1165–88. doi: 10.1214/aos/1013699998
16. Mroz EA, Tward ADM, Hammon RJ, Ren Y, Tward ADM, Hammon RJ, et al. Intra-tumor genetic heterogeneity and mortality in head and neck cancer: analysis of data from the cancer genome atlas. *PLoS Med*. (2015) 12:e1001786. doi: 10.1371/journal.pmed.1001786
17. Mroz EA, Tward AD, Pickering CR, Myers JN, Ferris RL, Rocco JW. High intratumor genetic heterogeneity is related to worse outcome in patients with head and neck squamous cell carcinoma. *Cancer*. (2013) 119:3034–42. doi: 10.1002/cncr.28150
18. Rocco JW. Mutant Allele Tumor Heterogeneity (MATH) and head and neck squamous cell carcinoma. *Head Neck Pathol*. (2015) 9:1–5. doi: 10.1007/s12105-015-0617-1
19. Ma D, Jiang YZ, Liu XY, Liu YR, Shao ZM. Clinical and molecular relevance of mutant-allele tumor heterogeneity in breast cancer. *Breast Cancer Res Treat*. (2017) 162:39–48. doi: 10.1007/s10549-017-4113-z
20. Rajput A, Bocklage T, Greenbaum A, Lee JH, Ness SA. Mutant-allele tumor heterogeneity scores correlate with risk of metastases in colon cancer. *Clin Colorectal Cancer*. (2016) 16:e165–70. doi: 10.1016/j.clcc.2016.11.004
21. Mroz EA, Rocco JW. MATH, a novel measure of intratumor genetic heterogeneity, is high in poor-outcome classes of head and neck squamous cell carcinoma. *Oral Oncol*. (2013) 49:211–5. doi: 10.1016/j.oraloncology.2012.09.007
22. Gehring JS, Fischer B, Lawrence M, Huber W. SomaticSignatures: inferring mutational signatures from single-nucleotide variants. *Bioinformatics*. (2015) 31:3673–5. doi: 10.1101/010686
23. Subramanian A, Tamayo P, Mootha VK, Mukherjee S, Ebert BL, Gillette MA, et al. Gene set enrichment analysis: a knowledge-based approach for interpreting genome-wide expression profiles. *Proc Natl Acad Sci USA*. (2005) 102:15545–50. doi: 10.1073/pnas.0506580102
24. The Cancer Genome Atlas Network. Comprehensive molecular characterization of human colon and rectal cancer. *Nature*. (2012) 487:330–7. doi: 10.1038/nature11252
25. Zhou Y, Wan G, Spizzo R, Ivan C, Mathur R, Hu X, et al. miR-203 induces oxaliplatin resistance in colorectal cancer cells by negatively regulating ATM kinase. *Mol Oncol*. (2014) 8:83–92. doi: 10.1016/j.molonc.2013.09.004
26. Yao J, Huang A, Zheng X, Liu T, Lin Z, Zhang S, et al. 53BP1 loss induces chemoresistance of colorectal cancer cells to 5-fluorouracil by inhibiting the ATM–CHK2–P53 pathway. *J Cancer Res Clin Oncol*. (2017) 143:419–31. doi: 10.1007/s00432-016-2302-5
27. Rojas AM, Sanchez-Pulido L, Fütterer A, Van Wely KHM, Martinez-A C, Valencia A. Death inducer obliterator protein 1 in the context of DNA regulation: Sequence analyses of distant homologues point to a novel functional role. *FEBS J*. (2005) 272:3505–11. doi: 10.1111/j.1742-4658.2005.04759.x
28. Trachana V, van Wely KHM, Guerrero AA, Fütterer A, Martínez-A C. Dido disruption leads to centrosome amplification and mitotic checkpoint defects compromising chromosome stability. *Proc Natl Acad Sci USA*. (2007) 104:2691–6. doi: 10.1073/pnas.0611132104
29. Jo YS, Kim MS, Yoo NJ, Lee SH. Frameshift mutations of AKAP9 gene in gastric and colorectal cancers with high microsatellite instability. *Pathol Oncol Res*. (2016) 22:587–92. doi: 10.1007/s12253-016-0042-0
30. Zhao Z, Zhang G, Li W. Elevated expression of ERCC6 confers resistance to 5-fluorouracil and is associated with poor patient survival in colorectal cancer. *DNA Cell Biol*. (2017) 36:781–6. doi: 10.1089/dna.2017.3768
31. van der Valk MJM, Hilling DE, Bastiaannet E, Meershoek-Klein KE, Beets GL, Figueiredo NL, et al. Long-term outcomes of clinical complete responders after neoadjuvant treatment for rectal cancer in the International Watch &

Wait Database (IWWD): an international multicentre registry study. *Lancet*. (2018) 391:2537–45. doi: 10.1016/S0140-6736(18)31078-X
32. Rullier E, Rouanet P, Tuech JJ, Valverde A, Lelong B, Rivoire M, et al. Organ preservation for rectal cancer (GRECCAR 2): a prospective, randomised, open-label, multicentre, phase 3 trial. *Lancet*. (2017) 390:469–79. doi: 10.1016/S0140-6736(17)31056-5
33. Chadi SA, Malcomson L, Ensor J, Riley RD, Vaccaro CA, Rossi GL, et al. Factors affecting local regrowth after watch and wait for patients with a clinical complete response following chemoradiotherapy in rectal cancer (InterCoRe consortium): an individual participant data meta-analysis. *Lancet Gastroenterol Hepatol*. (2018) 3:825–36. doi: 10.1016/S2468-1253(18)30301-7
34. Loos M, Quentmeier P, Schuster T, Nitsche U, Gertler R, Keerl A, et al. Effect of preoperative radio(chemo)therapy on long-term functional outcome in rectal cancer patients: a systematic review and meta-analysis. *Ann Surg Oncol*. (2013) 20:1816–28. doi: 10.1245/s10434-012-2827-z
35. Battersby NJ, Juul T, Christensen P, Janjua AZ, Branagan G, Emmertsen KJ, et al. Predicting the risk of bowel-related quality-of-life impairment after restorative resection for rectal cancer: a multicenter cross-sectional study. *Dis Colon Rectum*. (2016) 59:270–80. doi: 10.1097/DCR.0000000000000552
36. Morris LGT, Riaz N, Desrichard A, Senbabaoglu Y, Hakimi AA, Makarov V, et al. Pan-cancer analysis of intratumor heterogeneity as a prognostic determinant of survival. *Oncotarget*. (2016) 7:10051–63. doi: 10.18632/oncotarget.7067
37. Andor N, Graham TA, Jansen M, Xia LC, Aktipis CA, Petritsch C, et al. Pan-cancer analysis of the extent and consequences of intratumor heterogeneity. *Nat Med*. (2015) 22:105–13. doi: 10.1038/nm.3984
38. McGranahan N, Favero F, de Bruin EC, Birkbak NJ, Szallasi Z, Swanton C. Clonal status of actionable driver events and the timing of mutational processes in cancer evolution. *Sci Transl Med*. (2015) 7:283ra54. doi: 10.1126/scitranslmed.aaa1408
39. Sveen A, Løes IM, Alagaratnam S, Nilsen G, Høland M, Lingjærde OC, et al. Intra-patient inter-metastatic genetic heterogeneity in colorectal cancer as a key determinant of survival after curative liver resection. *PLOS Genet*. (2016) 12:e1006225. doi: 10.1371/journal.pgen.1006225
40. Kim TM, Jung SH, An CH, Lee SH, Baek IP, Kim MS, et al. Subclonal genomic architectures of primary and metastatic colorectal cancer based on intratumoral genetic heterogeneity. *Clin Cancer Res*. (2015) 21:4461–72. doi: 10.1158/1078-0432.CCR-14-2413
41. Braxton DR, Zhang R, Morrissette JD, Loaiza-Bonilla A, Furth EE. Clinicopathogenomic analysis of mismatch repair proficient colorectal adenocarcinoma uncovers novel prognostic subgroups with differing patterns of genetic evolution. *Int J Cancer*. (2016) 139:1546–56. doi: 10.1002/ijc.30196
42. Jesinghaus M, Pfarr N, Kloor M, Endris V, Tavernar L, Muckenhuber A, et al. Genetic heterogeneity in synchronous colorectal cancers impacts genotyping approaches and therapeutic strategies. *Genes Chromosom Cancer*. (2016) 55:26877. doi: 10.1002/gcc.22330
43. Zhang J, Yan S, Liu X, Gan L, Wu Z, Gong Y, et al. Gender-related prognostic value and genomic pattern of intra-tumor heterogeneity in colorectal cancer. *Carcinogenesis*. (2017) 38:837–46. doi: 10.1093/carcin/bgx046
44. Findlay JM, Castro-Giner F, Makino S, Rayner E, Kartsonaki C, Cross W, et al. Differential clonal evolution in oesophageal cancers in response to neo-adjuvant chemotherapy. *Nat Commun*. (2016) 7:11111. doi: 10.1038/ncomms11111
45. Murugaesu N, Wilson GA, Birkbak NJ, Watkins TBK, McGranahan N, Kumar S, et al. Tracking the genomic evolution of esophageal adenocarcinoma through neoadjuvant chemotherapy. *Cancer Discov*. (2015) 5:821–32. doi: 10.1158/2159-8290.CD-15-0412
46. Faltas BM, Prandi D, Tagawa ST, Molina AM, Nanus DM, Sternberg C, et al. Clonal evolution of chemotherapy-resistant urothelial carcinoma. *Nat Genet*. (2016) 48:1490–9. doi: 10.1038/ng.3692
47. Mouw KW, Cleary JM, Reardon B, Pike J, Braunstein LZ, Kim J, et al. Genomic evolution after chemoradiotherapy in anal squamous cell carcinoma. *Clin Cancer Res*. (2017) 23:3214–22. doi: 10.1158/1078-0432.CCR-16-2017
48. Miller CA, Gindin Y, Lu C, Griffith OL, Griffith M, Shen D, et al. Aromatase inhibition remodels the clonal architecture of estrogen-receptor-positive breast cancers. *Nat Commun*. (2016) 7:12498. doi: 10.1038/ncomms12498

Conflict of Interest: The authors declare that the research was conducted in the absence of any commercial or financial relationships that could be construed as a potential conflict of interest.

Copyright © 2019 Bettoni, Masotti, Corrêa, Donnard, dos Santos, São Julião, Vailati, Habr-Gama, Galante, Perez and Camargo. This is an open-access article distributed under the terms of the Creative Commons Attribution License (CC BY). The use, distribution or reproduction in other forums is permitted, provided the original author(s) and the copyright owner(s) are credited and that the original publication in this journal is cited, in accordance with accepted academic practice. No use, distribution or reproduction is permitted which does not comply with these terms.

frontiers in Oncology

ORIGINAL RESEARCH
published: 01 October 2019
doi: 10.3389/fonc.2019.00994

Identification of Schlafen-11 as a Target of CD47 Signaling That Regulates Sensitivity to Ionizing Radiation and Topoisomerase Inhibitors

Sukhbir Kaur[1†], Anthony L. Schwartz[1†‡], David G. Jordan[1], David R. Soto-Pantoja[1‡], Bethany Kuo[1], Abdel G. Elkahloun[2], Lesley Mathews Griner[3], Craig J. Thomas[3], Marc Ferrer[3], Anish Thomas[4], Sai-Wen Tang[4], Vinodh N. Rajapakse[4], Yves Pommier[4] and David D. Roberts[1]*

[1] Laboratory of Pathology, Center for Cancer Research, National Cancer Institute, National Institutes of Health, Bethesda, MD, United States, [2] Cancer Genetics Branch, National Human Genome Research Institute, National Institutes of Health, Bethesda, MD, United States, [3] National Center for Advancing Translational Sciences, National Institutes of Health, Bethesda, MD, United States, [4] Developmental Therapeutics Branch and Laboratory of Molecular Pharmacology, Center for Cancer Research, National Cancer Institute, National Institutes of Health, Bethesda, MD, United States

Knockdown or gene disruption of the ubiquitously expressed cell surface receptor CD47 protects non-malignant cells from genotoxic stress caused by ionizing radiation or cytotoxic chemotherapy but sensitizes tumors in an immune competent host to genotoxic stress. The selective radioprotection of non-malignant cells is mediated in part by enhanced autophagy and protection of anabolic metabolism pathways, but differential H2AX activation kinetics suggested that the DNA damage response is also CD47-dependent. A high throughput screen of drug sensitivities indicated that CD47 expression selectively sensitizes Jurkat T cells to inhibitors of topoisomerases, which are known targets of Schlafen-11 (SLFN11). CD47 mRNA expression positively correlated with schlafen-11 mRNA expression in a subset of human cancers but not the corresponding non-malignant tissues. CD47 mRNA expression was also negatively correlated with *SLFN11* promoter methylation in some cancers. CD47 knockdown, gene disruption, or treatment with a CD47 function-blocking antibody decreased SLFN11 expression in Jurkat cells. The CD47 signaling ligand thrombospondin-1 also suppressed schlafen-11 expression in wild type but not CD47-deficient T cells. Re-expressing SLFN11 restored radiosensitivity to a CD47-deficient Jurkat cells. Disruption of CD47 in PC3 prostate cancer cells similarly decreased schlafen-11 expression and was associated with a CD47-dependent decrease in acetylation and increased methylation of histone H3 in the *SLFN11* promoter region. The ability of histone deacetylase or topoisomerase inhibitors to induce SLFN11 expression in PC3 cells was lost when *CD47* was targeted in these cells. Disrupting CD47 in PC3 cells increased resistance

OPEN ACCESS

Edited by:
Ira Ida Skvortsova, Innsbruck Medical University, Austria

Reviewed by:
Jih-Hwa Guh, National Taiwan University, Taiwan
Katerina Smesny Trtkova, Palacký University, Czechia

***Correspondence:**
David D. Roberts
droberts@mail.nih.gov

[†] *These authors have contributed equally to this work*

[‡] ***Present address:***
Anthony L. Schwartz, Morphiex Biotherapeutics, Boston, MA, United States
David R. Soto-Pantoja, Wake Forest School of Medicine, Winston-Salem, NC, United States

Specialty section:
This article was submitted to Radiation Oncology, a section of the journal Frontiers in Oncology

Received: *15 August 2019*
Accepted: *16 September 2019*
Published: *01 October 2019*

Citation:
Kaur S, Schwartz AL, Jordan DG, Soto-Pantoja DR, Kuo B, Elkahloun AG, Mathews Griner L, Thomas CJ, Ferrer M, Thomas A, Tang S-W, Rajapakse VN, Pommier Y and Roberts DD (2019) Identification of Schlafen-11 as a Target of CD47 Signaling That Regulates Sensitivity to Ionizing Radiation and Topoisomerase Inhibitors. Front. Oncol. 9:994. doi: 10.3389/fonc.2019.00994

to etoposide but, in contrast to Jurkat cells, not to ionizing radiation. These data identify CD47 as a context-dependent regulator of *SLFN11* expression and suggest an approach to improve radiotherapy and chemotherapy responses by combining with CD47-targeted therapeutics.

Keywords: radioresistance, epigenetics, CD47, thrombospondin-1, DNA damage response, schlafen-11, prostate cancer

INTRODUCTION

CD47 is a widely expressed cell surface molecule in higher vertebrates (1, 2). CD47 plays a physiological role in recognition of self by serving as a counter-receptor for the inhibitory receptor SIRPα on macrophages and dendritic cells (3). CD47-like proteins acquired by *Poxviridae* also bind SIRPα and may have similar roles in protecting infected cells from host innate immunity (4, 5). Correspondingly, over-expression of CD47 in some cancers can protect tumors from innate immune surveillance (3, 6, 7). This has led to the development of therapeutic antibodies and decoy molecules that inhibit the CD47-SIRPα interaction and their entry into multiple clinical trials for cancer patients as potential innate immune checkpoint inhibitors (8–10).

In addition to the passive role of CD47 in self-recognition, cell-intrinsic signaling functions of CD47 have been identified in some tumor cells as well as in vascular and immune cells in the tumor microenvironment (11–13). CD47 signaling is induced by binding of its secreted ligand thrombospondin-1 (TSP1 encoded by *THBS1*), which modulates CD47 association with heterotrimeric G-proteins as well as lateral interactions of CD47 with specific integrins and tyrosine kinase receptors (1). In vascular cells, ligation of CD47 modulates calcium, nitric oxide, cAMP, and cGMP signaling (13). TSP1 also inhibits NK cell activation (14) and T cell receptor signaling in a CD47-dependent manner (15, 16). Genetic disruption or antisense suppression of CD47 enhances cytotoxic T cell killing of target tumor cells *in vitro* and suppresses tumor growth *in vivo* when combined with local tumor irradiation or cytotoxic chemotherapy (17, 18). In addition to enhancing their antitumor efficacy, blockade of CD47 signaling protects non-malignant tissues from the off-target effects of these genotoxic therapies by enhancing autophagy pathways, stem cell self-renewal, and broadly enhancing metabolic pathways to repair cell damage caused by ionizing radiation (19–21).

Here we utilized a high throughput screen of drug sensitivity to identify pathways that contribute to the radioresistance and chemoresistance of CD47-deficient cells. CD47-deficient cells exhibited significant resistance to topoisomerase and class I histone deacetylase (HDAC) inhibitors. Global differences in gene expression in WT Jurkat T cells and a CD47-deficient mutant and following siRNA knockdown of CD47 were examined to identify specific genes through which therapeutic targeting of CD47 could modulate radioresistance and chemoresistance. One of the genes that showed consistent down-regulation in CD47-deficient cells was *schlafen-11* (*SLFN11*), which in human cancers is positively correlated with sensitivity of cytotoxic agents including topoisomerase inhibitors (22–28). Loss of SLFN11 expression in cancer cells involves both hypermethylation of its promoter and epigenetic changes in histone modification (29, 30). Correspondingly, expression of *SLFN11* in some resistant cancer cell lines can be induced by class I HDAC inhibitors and restores their sensitivity, whereas knockdown of *SLFN11* confers resistance (29). The mechanism by which SLFN11 regulates sensitivity to DNA damaging agents includes limiting expression of the kinases ATM and ATR (31). Other evidence indicates that SLFN11 blocks DNA replication in stressed cells upon recruitment to the replication fork independent of ATR (32). Parallels between the effects of SLFN11 and CD47 on resistance to genotoxic stress suggested that SLFN11 may be an effector mediating the selective cytoprotective effects of CD47 knockdown, prompting us to examine the regulation of *SLFN11* and its orthologs by CD47 and the potential implications for combining CD47-targeted therapeutics with genotoxic cancer therapies.

MATERIALS AND METHODS

Reagents and Cell Culture

Entinostat and rocilinostat were obtained from the NCI Division of Cancer Treatment and Diagnosis. Etoposide was from Bedford Laboratories. Doxorubicin was from Sigma-Aldrich.

PC3 and Jurkat T cells were purchased from the American Type Culture Collection and maintained at 37°C with 5% CO_2 using RPMI 1640 medium supplemented with 10% FBS, glutamine, penicillin and streptomycin (Thermo Fisher Scientific, USA). The CD47-deficient Jurkat T cell mutant (clone JinB8) was from (33) and cultured as described previously (34). WT and CD47-deficient Jurkat cells were maintained at 2–5 × 10^5 cells per ml to prevent activation.

For transient SLFN11 over-expression, 1 × 10^6 JinB8 cells were transfected with 2 μg of SLFN11 expression vector (29) or control plasmid using an Amaxa nucleofection kit (Lonza) 48 h before irradiation. To assess cell viability Jurkat and JinB8 cells were plated at 2 × 10^4 cells/well and irradiated with a single dose of 20 Gy radiation (operating at kV/10 mA with 2-mm aluminum filter, Precision X-Ray, East Haven, CT) or treated with etoposide. Cells were incubated for an additional 48–72 h at 37°C. Cell viability was determined by 3-(4,5-dimethylthiazol-2-yl)-5-(3-carboxymethoxyphenyl)-2-(4-sulfophenyl)-2H-tetrazolium, inner salt (MTS) reduction using the CellTiter 96 Aqueous One Solution proliferation assay (Promega). Absorbance was read at 490 nm on a microplate spectrophotometer.

PC3 cells and CD47-null CRISPR edited cells (2,000/well) were either unlabeled or labeled with Rapid Red Dye (Sartorius) and were plated in triplicate in 96-well plates (Corning, USA) and cultured overnight. The cells were treated as indicated in the figure legends, and cell proliferation was measured by Phase object Confluence (%) analysis using the IncuCyte instrument. Similarly, Jurkat and JinB8 T cells (5,000/well) were plated on 96 well plates for 1 h. The cells were treated with anti-human CD47 (B6H12, 1 μg/ml) as indicated in the figure legends.

400,000 WT and CD47 null PC3 cells were plated using 6 well plates in 2 ml of complete RPMI medium. The plates were irradiated with 20 Gy at a dose rate of 0.6 Gy/min using a GammaCell 40 Irradiator. PC3 cells were treated with entinostat, etoposide, doxorubicin, and rocilinostat at a concentration of 300 nM for 24 h for IncuCyte assays or for 72 h plated at 2,000 cells/well for MTS proliferation assays. Absorbance of untreated WT and CD47-null PC3 cells was normalized to 100%, and IC_{50} values were calculated using IC50 Calculator | AAT Bioquest software. Control and treated cells were also harvested for RNA extraction and real-time PCR.

H2AX Assay

Jurkat and JinB8 cells or Jurkat cells pretreated with B6H12 antibody, were irradiated at 10 Gy, and then incubated for 0–6 h before fixing with paraformaldehyde for 15 min and washing 2 times with PBS. Cells were permeabilized using 0.14% Triton X-100 in PBS and 3% BSA for 5 min and washed three times for 5 min each. Then, cells were stained with H2AX primary antibody 1:300 for 60 min and secondary antibody 1:600 Alexa-fluor 488 (ebiosciences) for 60 min. Cells were washed three times with PBS and mounted using DAPI VECTASHIELD® Mounting Medium (Vector Laboratories, Inc, Burlingame, CA). Images were acquired using Zeiss 710 or Zeiss 780 microscopes with a 63x objective. High throughput antibody screening or quantification of FITC and DAPI was acquired on a Mirrorball instrument (TTP Labtech).

Comet Assay

DNA fragmentation in WT and $CD47^{-}$ Jurkat cells 24 h after irradiation at 10 Gy was assessed using a single cell gel electrophoresis (Comet) assay essentially as described (35).

Real-Time PCR

Total RNA was extracted using the Trizol method (11, 34) or NucleoSpin RNA isolation kit (Clonetech), and the concentration and quality of RNA was measured using Nanodrop. First strand cDNA was generated using the Maxima First Strand cDNA Synthesis Kit for RT-qPCR, with dsDNase. All RNA samples were subjected to treatment with DNAse-1 prior to first strand cDNA synthesis according to the manufacturer's instructions (Thermo Fisher Scientific). Real-time PCR was performed using SYBR Green detection on a Bio-Rad CFX instrument as described previously (36).

For assessing responses to irradiation, total RNA was extracted as described above using TriPure isolation reagent (Roche). The concentration of RNA was measured using Nanodrop. Hundred nanogram and 1 μg of RNA was used to generate First strand cDNA using the Maxima First Strand cDNA Synthesis Kit for RT-qPCR, with dsDNase. mRNA expression of SLNF11 was amplified using SLFN11-F 5′-GGCCCAGACCAAGCCTTAAT-3′ and SLFN11-R, 5′-CACTGAAAGCCAGGGCAAAC-3′ primers with 1 μg of RNA template, while 18S and actin were amplified using 100 ng RNA. The relative expression is normalized to control untreated samples.

Confocal Microscopy

PC3 cells (WT, low CD47, and CD47-null cells) were plated on 4-well ibidi chambers overnight. The next day, the cells were treated with Rocilinostat or Entinostat for 24 h. The cells were fixed with 4% paraformaldehyde (Sigma Aldrich), and immunostaining was performed using antibodies against CD47 (Proteintech Group, Inc) and SLFN11 (Santa Cruz Biotechnologies) as described previously (36). The images were captured using a Zeiss 710 microscope with an oil immersion 63x objective. Cells were treated with 300 nM of Rocilinostat, or Entinostat, or etoposide for 24 h, and the cells were immunostained using anti-SLFN11 as described above. The images were captured using a Zeiss 780 microscope with an oil immersion 63X objective. All the images were captured with 5 and 10 μm scale bars as indicated in the legends.

CD47 Knockdown and Microarray Analysis

CD47 knockdown was performed using Jurkat T cells with CD47-siRNA as described earlier (34). Oligofectamine transfection reagent alone was used as mock control. Total RNA was extracted using the Trizol method. The quality of RNA was checked using a RNA Bioanalyzer (Agilent Inc). Global expression analysis was performed using Affymetrix microarray protocols as described previously (34, 36). Disruption of CD47 in PC3 cells was performed using a human CD47 gRNA targeting the first exon, 5′-CAGCAACAGCGCCGCTACCAGGG (37) using Cas9-GFP plasmid from Addgene (Cambridge, MA). The CRISPR plasmid was transfected using Oligofectamine (Thermo Fisher Scientific) according to the manufacturer's instructions. The cells were sorted based on CD47 expression to isolate CD47-low and CD47-null populations using CD47-PE antibody (Biolegend). The cells were expanded, and CD47 expression was re-validated by flow cytometry analysis using CD47-APC (Biolegend). CD47 Human siRNA Oligo Duplex (Locus ID 961) was purchased from OriGene and transfected using Oligofectamine (Thermo Fisher Scientific) into PC3 cells for 24 h using a 15 nanomolar concentration of the pooled CD47-siRNAs. After 24 h, the medium was removed, the cells were washed with PBS, and the cells were lysed using Tri Pure Isolation reagents. The knockdown of CD47-siRNA was assessed using real time PCR with the following primers: CD47-F (GGTTTGAGTATCTTAGCTCTAGCA), Long CD47-R (TCTACAGCTTTCCTAGGA) and short CD47-R (CCATCACTTCACTTCAGTCAGTTATTC).

Human Tumor Expression Data

The Cancer Genome Atlas (TCGA) data was analyzed using cBioPortal tools to determine correlations between SLFN11 and CD47 mRNA expression in human tumors with sufficient

RNAseq data (38, 39). Additional TCGA SLFN11 vs. CD47 mRNA expression plots and correlations were derived using log2(x + 1) transformed RSEM normalized count data obtained from the TCGA data portal (prostate adenocarcinoma and normal prostate tissue, invasive breast carcinoma and normal breast tissue, lung squamous cell carcinoma tissue). For some cancer types, correlations between SLFN11 or CD47 mRNA expression and *SLFN11* promoter DNA methylation were evaluated using TCGA methylation data derived using the Illumina HumanMethylation450 (HM450) BeadChip.

Quantitative High-Throughput Drug Sensitivity Screen

Wild type Jurkat T cells and the CD47-deficient mutant JinB8 cells were seeded into 1,536-well plates at 500 cells per well, in 5 μL of medium. A library of FDA approved small molecule drugs and late preclinical stage compounds were added at multiple doses ranging from 0.8 nM to 46 μM. Cell viability was assessed after 48-h incubation at 37°C by adding 3 μL of CellTiter-Glo reagent (Promega) and measuring luminescence (RLU) after a 15 min incubation at 25°C, with ViewLux (PerkinElmer). Data from the high throughput screening assays was analyzed as previously described (18). Differential activity of each compound between the wild type and CD47 deficient cell lines was determined by calculating a difference in the maximum response or $\log IC_{50}$ (concentration giving 50% of maximal inhibition) for each compound.

Chromatin Immunoprecipitation (ChIP)

WT CD47-low and CD47-null PC3 cells were plated overnight in 6-Well plates. The cells were fixed using Paraformaldehyde solution (Sigma), and chromatin was extracted using Chromatin Isolation kit (Abcam). Genomic DNA was sheared using 34 pulses of 10–12 s each at level by sonication with Disruptor sonication System from (Diagenode). ChIP was performed following instructions from ChIP Kit—One Step (Abcam). The Anti-Histone H3 (tri methyl K27) antibody, Anti-Histone H3 (di methyl K4) antibody and Anti-Histone H3 (acetyl K18) antibodies (Abcam) was incubated overnight for 4°C. The genomic SLFN11 primers were designed by using genomic DNA region of hg38_dna range=chr17:35373531-35374940 using UCSC Genome Browser. The following primers were designed using the Primer 3 program: SLFN-838 (CCGTCACGCTGCTAGTGATA), SLFN-968 (GAGTTGGCCAAAGACAGGAG), SLFN-949 (CTCCTGTCTTTGGCCAACTC), SLFN-1076 (CTCCGCATCAGTGAGAAGTG). SLFN11 level of eluted CHIP-DNA was measured using real-time genomic *SLFN11* primers with control GAPDH (Abcam). Enrichment in the ChIP assay was calculated by normalizing to the input.

Statistical Analysis

Two-sample t-test assuming equal variances was used for cell viability assays to quantify statistical significance (* for p-value $<$ 0.05 and *** for $p < 0.001$). Two-factor with replication ANOVA was used for real-time PCR analysis (* for p-value < 0.05 and *** for $p < 0.001$).

RESULTS

CD47 Mutation or Antibody Engagement Modulates the DNA Damage Response

We previously reported that non-malignant cells and Jurkat T cells lacking CD47 are protected from genotoxic stress induced by ionizing radiation (19, 21). This protection is mediated in part by an enhanced protective autophagy response in cells lacking CD47 or with reduced CD47 expression (19). Radioresistance in the CD47-deficient mutant is associated with global metabolic stabilization, including induction of anabolic metabolites that mediate repair of DNA damage induced by ionizing radiation (21). To evaluate whether CD47 also regulates the repair of genomic DNA damage caused by ionizing radiation, we assessed nuclear H2AX foci in WT and CD47$^-$ Jurkat T cells 1 h after irradiation at 10 Gy (**Figure 1A**). Notably, the CD47$^-$ cells showed a stronger H2AX response at this time. Quantitative analysis of the kinetics of foci formation in WT cells showed a maximal response at 2 h and subsequent decline by 6 h (**Figure 1B**). Previous studies of WT Jurkat cells subjected to this dose of radiation demonstrated metabolic collapse at 8 h followed by cell death (21), but treating WT cells with the CD47 function-blocking antibody B6H12 protected cells from radiation-induced death (40). Consistent with these results, subjecting the WT T cells to 10 Gy irradiation in the presence of B6H12 resulted in accelerated but less intense H2AX foci formation that resolved by 6 h (**Figure 1B**). A comet assay to assess DNA fragmentation in the CD47$^-$ T cells 24 h after irradiation at 10 Gy showed no detectable DNA fragments, whereas DNA fragmentation at 24 h remained extensive in the irradiated WT cells (**Figure 1C**). Therefore, loss of CD47 or blocking its function improves the ability of these cells to restore genomic integrity after damage caused by ionizing radiation.

Lack of CD47 Protects T Cells From Topoisomerase and HDAC Inhibitors

Non-malignant cells lacking CD47 are also protected from genotoxic stress induced by the anthracycline doxorubicin (18), which causes DNA damage by multiple mechanisms including redox stress and inhibition of topoisomerase activity (41). A quantitative high-throughput screen of drug sensitivity was performed using the WT and CD47$^-$ Jurkat T cell lines to identify additional drugs that may exhibit CD47-dependent cytotoxic activities and the resistance pathways they target. In addition to increased resistance to anthracyclines in the CD47-deficient cells, analysis of the 72 drugs that exhibited significantly decreased potencies (>3-fold) in CD47-deficient cells identified significant enrichments of topoisomerase I (TOP1), topoisomerase II (TOP2), and HDAC1 inhibitors (**Figure 2A**). Topoisomerase I inhibitors exhibited 5- to 100-fold increases in their IC_{50} values in the CD47-deficient cells (**Figures 2B–E**, **Supplementary Data File 1**). These included camptothecin, its therapeutic analogs topotecan and irinotecan, and the highly active irinotecan metabolite SN-38. Resistance of the CD47$^-$ T cells extended to several drugs in the anthracycline family including idarubicin and mitoxantrone (**Figures 2F,G**).

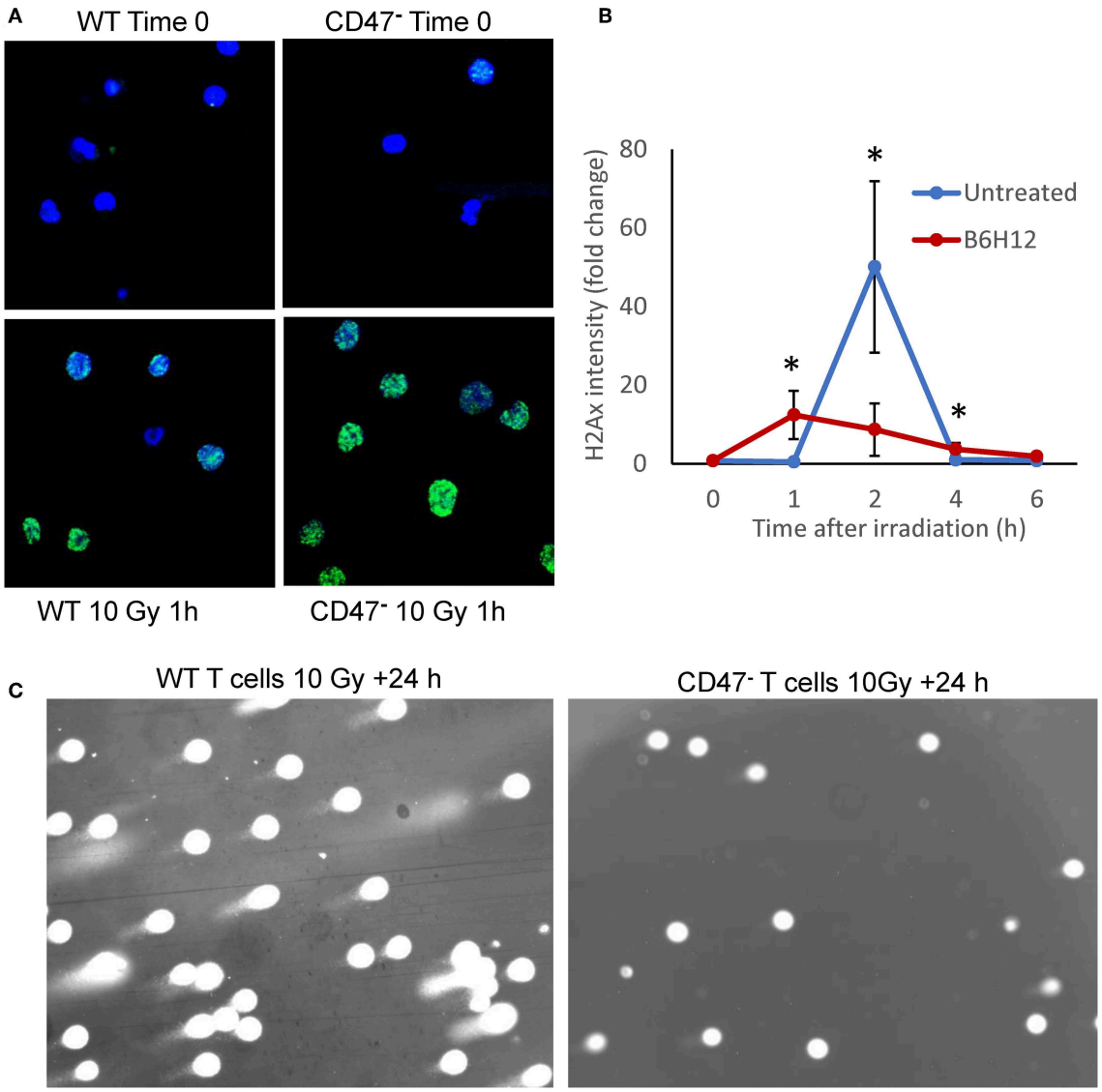

FIGURE 1 | Mutation or blockade of CD47 improves the DNA damage response to ionizing radiation in Jurkat T cells. **(A)** Nuclear H2AX foci (green) stained in WT and CD47$^-$ Jurkat T cells 1 h after irradiation at 10 Gy. **(B)** Modulation of the kinetics of H2AX foci formation by the CD47 antibody B6H12 in WT T cells after 10 Gy irradiation. **(C)** Comet Assay to detect DNA fragmentation in WT and CD47$^-$ T cells 24 h after irradiation at 10 Gy. *$p < 0.05$.

CD47$^-$ cells exhibited enhanced resistance to 16 HDAC1 inhibitors in the screen (**Supplementary Data File 1**). One of these, the class I HDAC inhibitor entinostat (HDAC1>HDAC3), was previously shown to restore SLFN11 expression and sensitivity to DNA damage in resistant cancer cell lines (29). The IC_{50} value for entinostat was 3.2-fold higher for the CD47$^-$ cells compared to WT cells in the CellTiter Glo assay (**Figure 3A**) and was confirmed to be less potent for inhibiting proliferation of CD47$^-$ cells (**Figure 3C**). However, the class I HDAC inhibitor Romidepsin, which was shown to similarly induce SLFN11 (29), did not show differential activity in CD47$^-$ vs. WT cells (**Supplementary Data File 1**). Conversely, the selective HDAC6 inhibitor Rocilinostat, which did not induce SLFN11 in K562 chronic myelogenous leukemia or HT1080 fibrosarcoma cells (29), was 1.51-fold less potent for CD47$^-$ vs. WT cells in the CellTiter Glo assay (**Figure 3B**) and was less potent for inhibiting proliferation of CD47$^-$ cells (**Figure 3D**). Therefore, some but not all of the differences in drug sensitivities between WT and CD47$^-$ Jurkat cells are consistent with the previously reported effects of these drugs on SLFN11 expression.

CD47 Correlation With *SLFN11* Gene Expression

Two independent microarray analyses of the same WT and CD47-deficient T cell lines identified 8.7- and 10-fold decreased expression of SLFN11 mRNA in the CD47-deficient Jurkat

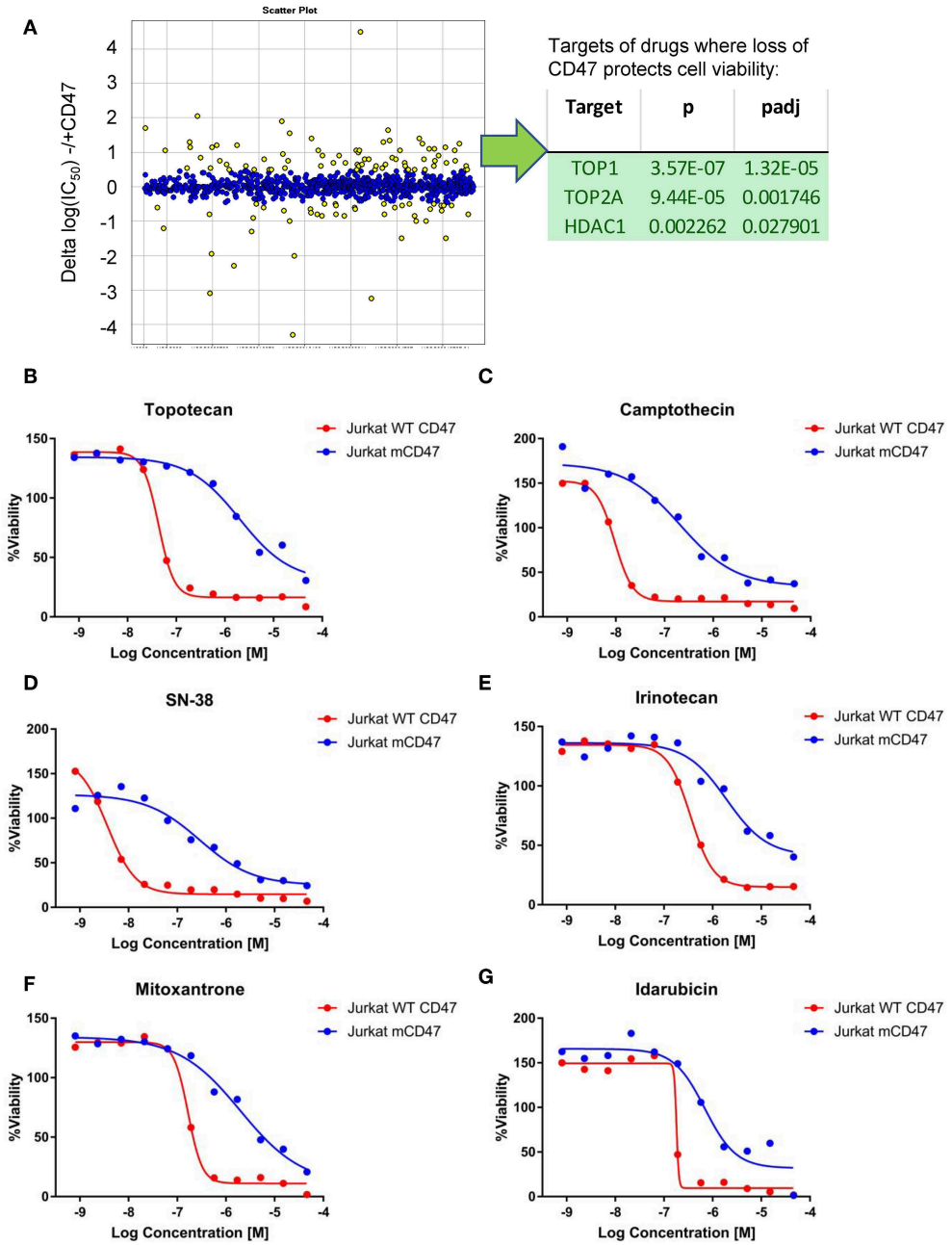

FIGURE 2 | Loss of CD47 confers selective cytoprotection against cytotoxic drugs. **(A)** High throughput screen of FDA-approved and late stage development drugs. Cumulative data is presented as log(IC_{50}) values comparing treated cells lacking or expressing CD47. Yellow points indicate compounds where the IC_{50} values differ significantly, and those with positive values indicate compounds where the absence of CD47 protects cell viability. The table lists the identified significant target classes for 72 compounds that exhibited >3-fold decreased potency (ΔIC_{50} for compounds with Curve Response Class −1.n and −2.n) in CD47-deficient Jurkat T cells compared to WT cells. **(B–G)** Representative dose response curves for WT Jurkat T cells (red) and CD47- mutant cells (blue). CellTiter Glo signal assessing cellular ATP levels is plotted as a function of Log(concentration) for topotecan **(B)**, camptothecin **(C)**, SN38 **(D)**, Irinotecan **(E)**, mitoxantrone **(F)**, and Idarubicin **(G)**.

mutant ($p<0.05$, **Figure 4A**). No other *Schlafen* gene family members showed a significant difference in expression between WT and CD47-deficient cells using a 2-fold cutoff. Decreased SLFN11 mRNA in the $CD47^{-}$ mutant was confirmed using real-time qPCR (**Figure 4B**).

Reexamination of our published microarray data comparing primary lung endothelial cells from WT and $cd47^{-/-}$ mice [GSE43133, (20)] identified a 3.6-fold decrease in mRNA expression of *Slfn9*, a presumed murine ortholog of the *SLFN11* gene (42), in $cd47^{-/-}$ cells, suggesting that CD47 regulation

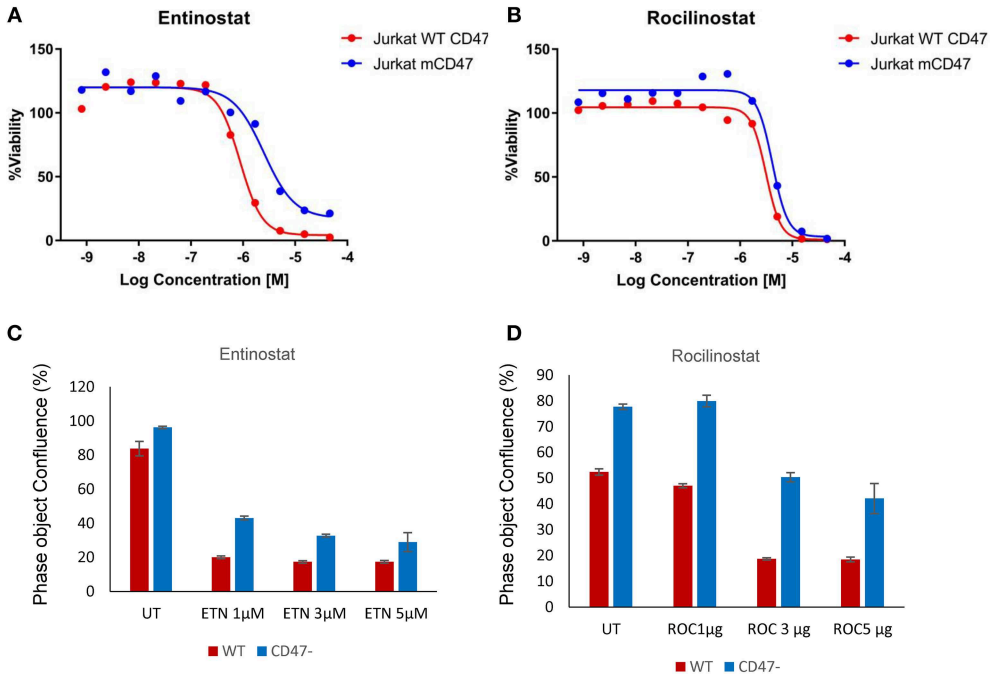

FIGURE 3 | Loss of CD47 in Jurkat T cells increases resistance to selective HDAC1 and HDAC6 inhibitors. **(A,B)** WT (red) and CD47^{-} Jurkat T cells (blue) were treated with the indicated concentrations of Entinostat (HDAC1 selective) or Rocilinostat (HDAC6 selective), and cellular ATP was assessed using the CellTiter Glo reagent. **(C,D)** WT and CD47^{-} Jurkat T cells were treated with the indicated concentrations of Entinostat or Rocilinostat, and cell proliferation after 3 days was assessed by object counting using the IncuCyte live cell analysis instrument.

of mRNA expression for *SLFN11* orthologs is conserved across species (**Figure 4A**). However, RNAseq analysis of unstimulated mouse NK cells (GSE113980) revealed increased *Slfn4* and *Slfn14* in *cd47*$^{-/-}$ NK cells but no significant difference in *Slfn9* mRNA expression comparing sorted Lin^{-}NK1.1^{+}NKp46^{+} cells isolated from naïve *cd47*$^{-/-}$ and *cd47*$^{+/+}$ mouse spleens (43) (**Figure 4A**), suggesting that CD47 regulation of murine *Slfn9* expression is cell type-specific.

CD47 Positively Regulates SLFN11 Expression

The decreased expression of SLFN11 in the CD47^{-} mutant T cells suggested that CD47 signaling regulates the expression of SLFN11. To establish causality and exclude the potential for secondary mutations in the Jurkat somatic mutant suppressing SLFN11 expression, we examined whether acute CD47 knockdown decreases schalfen-11 expression (**Figures 4A,C**, **Supplementary Data File 2**). siRNA knockdown of CD47 in the WT cells resulted in a 1.4-fold decrease in SLFN11 ($p = 0.046$). If loss of SLFN11 contributes to the radioresistance of the CD47^{-} cells, forced expression of SLFN11 should restore sensitivity. Transient transfection of the CD47^{-} cells with a SLFN11 expression vector increased SLFN mRNA expression (**Figure 4D**) and decreased the viability of CD47^{-} cells subjected to 20 Gy irradiation relative to untreated cells or cells transfected with the control plasmid (**Figure 4E**).

CD47 Ligands Alter SLFN11 Expression

TSP1 signaling in T cells can be mediated by several cell surface receptors (44, 45), but at concentrations < 5 nM signaling is primarily CD47-dependent (15, 16). Correspondingly, treatment of WT but not CD47-deficient Jurkat T cells with 2.2 nM TSP1 time-dependently suppressed *SLFN11* mRNA expression (**Figure 5A**). Treatment of WT Jurkat T cells with TSP1 decreased SLFN11 mRNA as early as 30 min. after addition. Inhibition was maximal by 1–3 h and decreased thereafter. This time-dependence is consistent with the known uptake and degradation of TSP1 by T cells (45). No inhibition of SLFN11 mRNA expression by TSP1 was observed in the CD47^{-} mutant, indicating that the inhibitory effect of TSP1 on SLFN11 expression is CD47-dependent.

The function modifying CD47 antibody B6H12 has been used extensively as an antagonist of CD47 signaling through SIRPα in preclinical studies and demonstrated tumor suppressing activities in many xenograft models (3). However, some effects of B6H12 on cancer cells may be independent of inhibiting binding of CD47 ligands (11). B6H12 at 1 µg/ml rapidly suppressed SLFN11 mRNA expression in Jurkat cells, with variable recovery at later time points in repeated experiments (**Figure 5A**). This is consistent with the attenuated DNA damage response following irradiation of Jurkat cells in the presence of B6H12 in **Figure 1B** and the known ability of B6H12 treatment to preserve proliferative capacity in irradiated Jurkat cells (40).

A

Gene	Cell type	Fold change	Comparison	Reference
huSLFN11	Jurkat T cells	-8.69	JinB8/WT	Microarray, GSE132646
huSLFN11	Jurkat T cells	-1.43	CD47siRNA/WT	Microarray, this work
mmSlfn9	Lung endothelial cells	-3.62	*Cd47*$^{-/-}$/WT	Microarray, GSE43133
mmSlfn5	Lung endothelial cells	-6.21	*Cd47*$^{-/-}$/WT	Microarray, GSE43133
mmSlfn10-ps	Lung endothelial cells	-2.52	*Cd47*$^{-/-}$/WT	Microarray, GSE43133
mmSlfn4	Natural killer cells	3.68	*Cd47*$^{-/-}$/WT	RNAseq, GSE113980
mmSlfn14	Natural killer cells	10.2	*Cd47*$^{-/-}$/WT	RNAseq, GSE113980

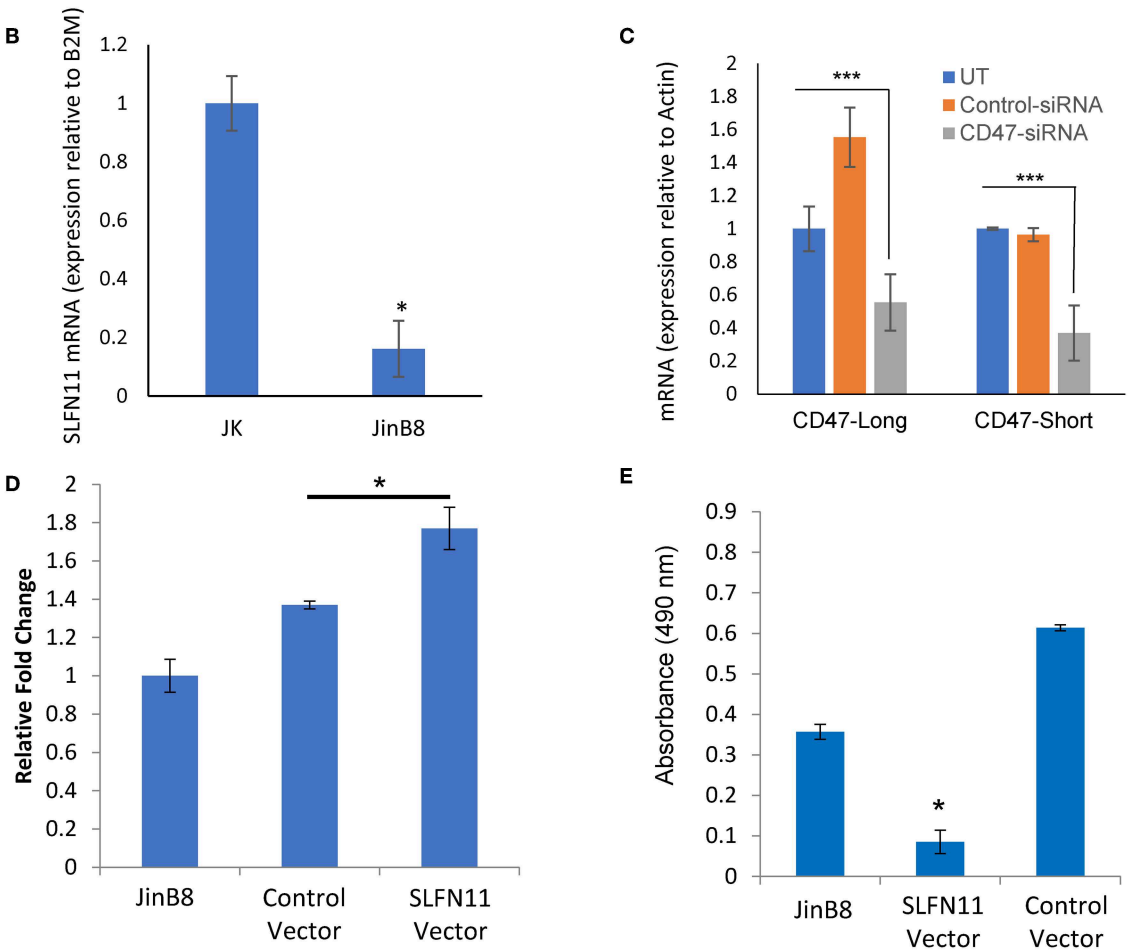

FIGURE 4 | CD47-dependent *Schlafen* gene expression in human and murine cells. **(A)** Genes listed from the cited microarray and RNAseq studies scored *P*-value < 0.05. **(B)** RT-qPCR validation of reduced SLFN11 mRNA expression in WT and CD47^{-} JinB8 Jurkat T cells. **(C)** RT-qPCR confirmation of siRNA knockdown of the long and short CD47 mRNA transcripts. **(D)** RT-qPCR confirmation of transient over-expression of SLFN11 by plasmid transfection. **(E)** Radioresistance was assessed by MTS assay after irradiation at 20 Gy of CD47^{-} JinB8 cells transfected as indicated in **(D)**. *$p < 0.05$, ***$p < 0.001$.

A proliferation assay was used to examine whether the suppression of SLFN11 by B6H12 also alters the sensitivity of Jurkat cells to doxorubicin. A concentration of doxorubicin was selected that is suboptimal for directly inhibiting growth of the cells (**Figures 5B,C**). B6H12 alone at 1 μg/ml significantly inhibited cell proliferation, whereas an isotype-matched control antibody was inactive. Combining B6H12 with 100 nM doxorubicin resulted in more inhibition of

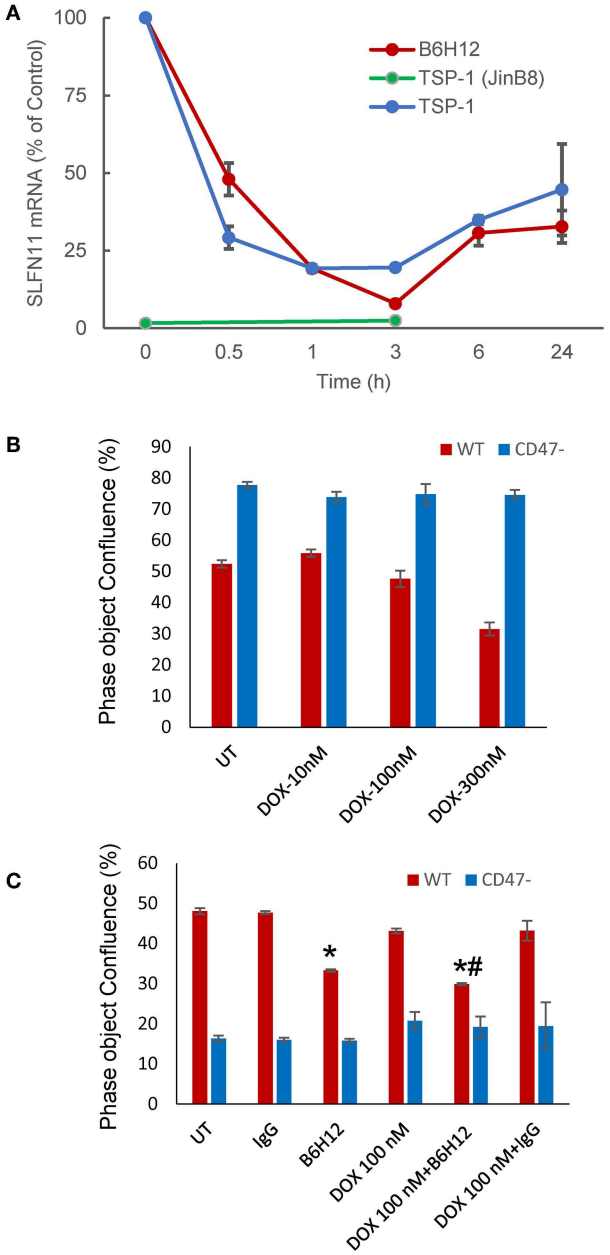

FIGURE 5 | Modulation of SLFN11 expression and cell resistance by CD47 ligands. **(A)** TSP1 and CD47 antibody B6H12 inhibit SLFN11 expression. **(B)** Resistance of CD47-deficient Jurkat cells to the anti-proliferative activities of doxorubicin. Proliferation was assessed after 3 days by object confluence on the IncuCyte. **(C)** The CD47 antibody B6H12 increases sensitivity to doxorubicin. Proliferation was assessed after 4.5 days by object confluence on the IncuCyte live cell analysis system. Significance: * = vs. untreated, # = vs. B6H12 alone.

cell growth, consistent with an additive effect ($p = 0.001$, **Figure 5C**). Therefore, this CD47 antibody can protect Jurkat cells from genotoxic stress induced by ionizing radiation or cytotoxic chemotherapy.

TABLE 1 | Co-expression of SLFN11 and CD47 mRNA in human cancers.

SLFN11/CD47	Spearman's Correlation	*p*-Value	*q*-Value	*n*
Pediatric acute lymphoid leukemia	0.447	2.37×10^{-11}	**1.19×10^{-9}**	203
Bladder urothelial carcinoma	0.440	8.75×10^{-21}	**2.21×10^{-19}**	408
Lung squamous	0.407	2.25×10^{-21}	**1.14×10^{-19}**	501
Renal papillary cell carcinoma	0.355	4.51×10^{-10}	**1.07×10^{-8}**	291
Cutaneous melanoma	0.338	4.35×10^{-14}	**6.44×10^{-13}**	472
Prostate adenocarcinoma	0.329	5.01×10^{-14}	**1.28×10^{-12}**	498
Glioblastoma multiforme	0.269	4.52×10^{-4}	**2.37×10^{-3}**	166
Hepatocellular carcinoma	0.257	4.82×10^{-7}	**6.91×10^{-6}**	373
Esophageal carcinoma	0.256	4.28×10^{-4}	**3.34×10^{-3}**	185
Invasive breast carcinoma	0.245	1.70×10^{-16}	**1.59×10^{-15}**	1100
Acute myeloid leukemia	0.232	2.10×10^{-3}	**6.45×10^{-3}**	173
Soft tissue sarcoma	0.215	4.37×10^{-4}	**2.17×10^{-3}**	263
Renal CCC	0.169	8.88×10^{-5}	**4.05×10^{-4}**	534
Uterine endometrial carcinoma	0.165	0.0280	0.086	177
Pancreatic adenocarcinoma	0.160	0.0324	0.138	179
Brain lower grade glioma	0.086	0.048	0.072	530
Head and neck SCC	0.072	0.102	0.151	522
Colorectal adenocarcinoma	0.046	0.371	0.615	382
Lung adenocarcinoma	−0.006	0.892	0.926	517
Ovarian serous	−0.094	0.0985	0.234	307
Pediatric neuroblastoma	−0.097	0.251	0.445	143
Papillary thyroid carcinoma	−0.224	3.43×10^{-7}	**1.01×10^{-6}**	509

RNAseq data from the indicated TCGA provisional datasets (except TARGET datasets for pediatric ALL and pediatric neuroblastoma) were analyzed using cBioPortal tools. q-values were derived from the Benjamini-Hochberg FDR correction procedure. Significant q-values are indicated in bold font.

Correlation Between CD47 and SLFN11 Expression in Human Cancers

An initial survey of TCGA cancer datasets with sufficient RNAseq data indicated that the positive correlation between CD47 and SLFN11 mRNA expression observed in Jurkat T cells extends to a subset of human cancers (**Table 1**). The most significant positive correlations were found for bladder urothelial carcinoma ($r = 0.44$, $p = 8.75 \times 10^{-21}$) and lung squamous cell carcinoma ($r = 0.41$, $p = 2.2 \times 10^{-21}$, **Supplementary Figure 1A**). Additional cancers with significant correlation included pediatric acute lymphoid leukemia, cutaneous melanoma, prostate adenocarcinoma, glioblastoma multiforme, hepatocellular carcinoma, esophageal carcinoma, invasive breast carcinoma, acute myeloid leukemia, soft tissue

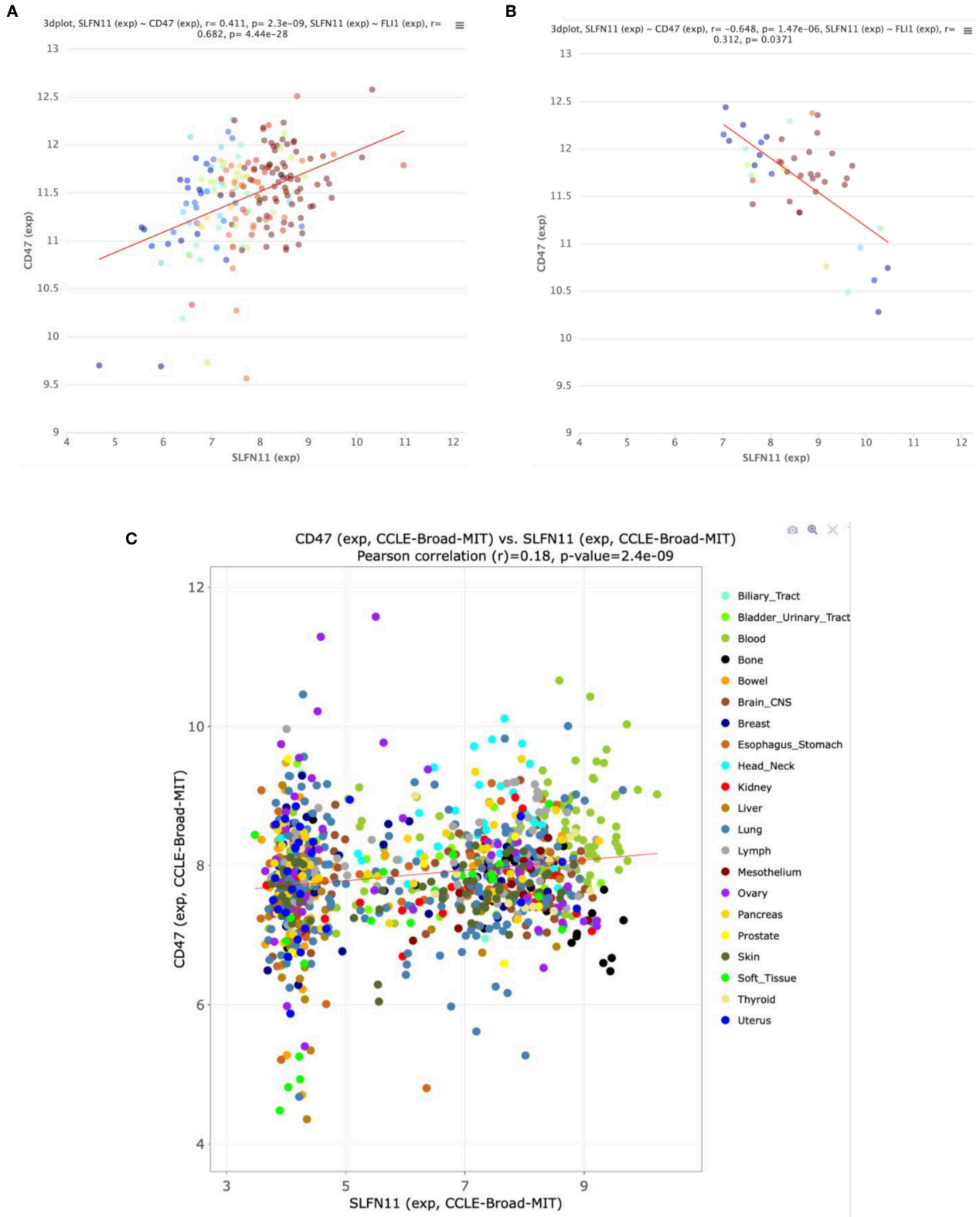

FIGURE 6 | Correlation between CD47 and SLFN11 mRNA expression determined by RNAseq analysis of prostate cancers **(A)** and normal prostate tissues **(B)** in TCGA. Point colors indicate expression of FLI1, a known driver of *SLFN11* expression (26). **(C)** Scatter plot of CD47 and SLFN11 mRNA expression in the Cancer Cell Line Encyclopedia cell lines. Colors identify the indicated cancer origins. The data is publicly available at http://discover.nci.nih.gov/cellminercdb.

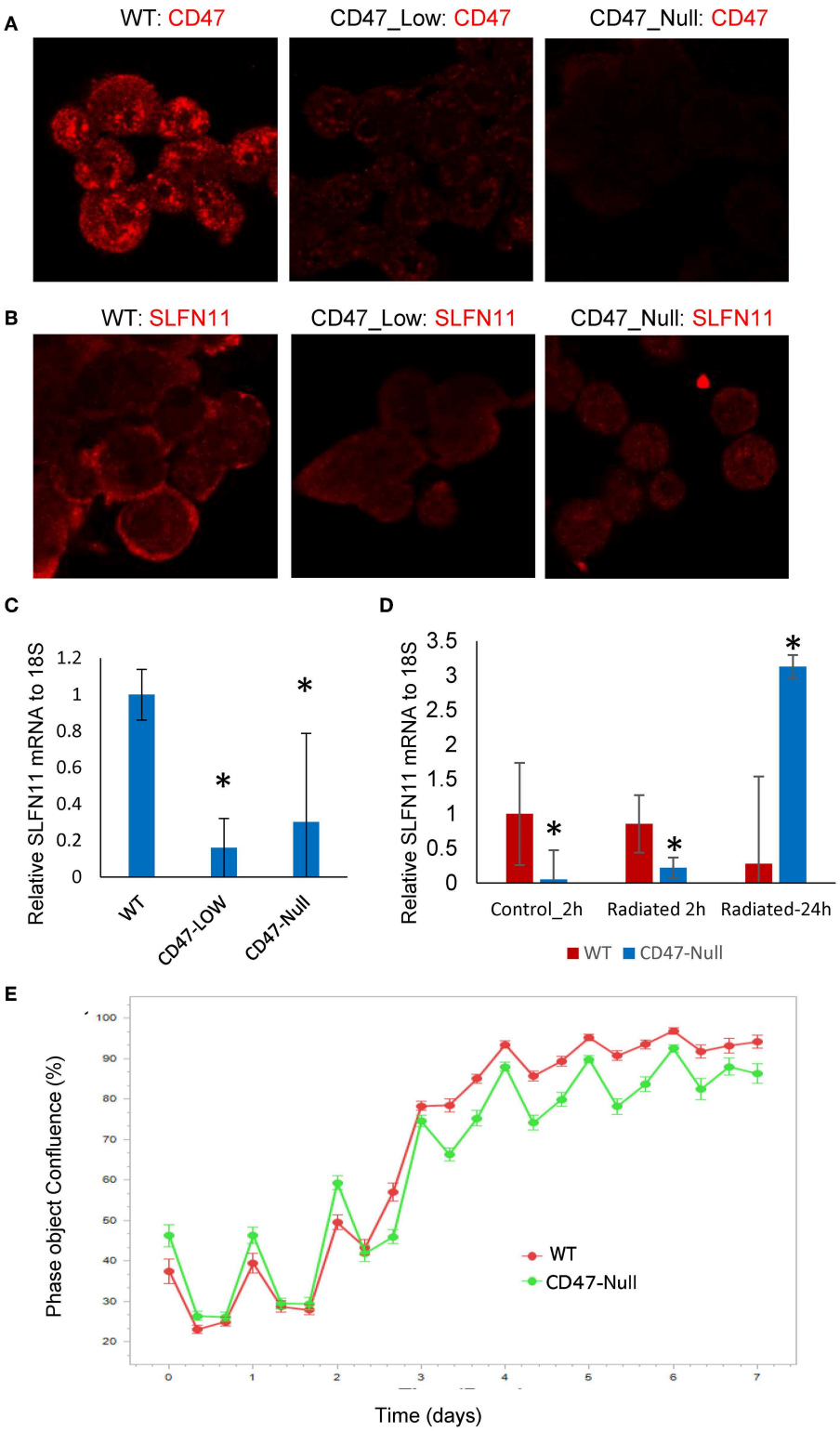

FIGURE 7 | Generation and characterization of CD47-deficient PC3 prostate cancer cells. **(A)** Analysis of CD47 expression in CD47-CRISPR-targeted PC3 cells sorted based on low or absent cell surface CD47 expression. **(B)** SLFN11 expression in WT, Low-CD47, and CD47-null PC3 cells. **(C)** Quantitative analysis of data in **B**. **(D)** RT-qPCR analysis of SLFN11 mRNA expression in WT and CD47-null PC3 cells and the respective cells 2 or 24 h after irradiation at 20 Gy. **(E)** Proliferation of irradiated WT and CD47-null PC3 cells by object confluence on the IncuCyte live cell analysis system. *$p < 0.05$.

TABLE 2 | Drug sensitivities of WT and CD47-null PC3 cells.

Drug	WT IC_{50} (μM)	CD47-null IC_{50} (μM)
Etoposide	0.18	0.58
Doxorubicin	0.91	0.47
Rocilinostat	0.25	>0.30

sarcoma, and renal clear cell carcinoma. The strong positive Spearman's correlation for lung squamous carcinoma contrasted with a lack of correlation for lung adenocarcinoma ($r = -0.01$, $p = 0.89$), further suggesting that the relationship between CD47 and SLFN11 expression is cancer type specific. Eight cancer types with adequate RNAseq expression data showed no significant correlation, and a significant negative correlation between CD47 and SLFN11 mRNA was observed for papillary thyroid carcinoma ($r = -0.22$, $p = 3.4 \times 10^{-7}$).

Further analysis of the TCGA data for prostate cancers showed a positive correlation between CD47 and SLFN11 mRNA expression in the tumors but not in normal prostate tissues (**Figures 6A,B**). Normal breast tissue similarly lacked the positive correlation between CD47 and SLFN11 observed in invasive breast carcinomas (**Supplementary Figures 1B,C**). These data further indicate that CD47 regulation of SLFN11 mRNA expression is cell type-specific and differs between normal and malignant tissues.

A positive correlation between CD47 and SLFN11 was also found for the cell lines in the Cancer Cell Line Encyclopedia (Spearman's correlation 0.193, $p = 1.6 \times 10^{-9}$, $q = 2.6 \times 10^{-8}$, **Figure 6C**). These data suggest that the underlying mechanism for these positive correlations is at least partially intrinsic to the cancer cells. SLFN11 mRNA expression in the CCLE was bimodal. Segregating high vs. low expressing cell lines with a mean cutoff showed higher CD47 in the SLFN11 high cell lines (log ratio 0.35, $p = 3.1 \times 10^{-8}$). Of the 7 prostate cancer cell lines in the CCLE, LNCAP and 22RV1 were high SLFN11 expressers, PC3 was moderate, and the remaining 4 were low expressers.

Loss of CD47 Regulates SLFN11 Expression in Prostate Cancer Cells

We chose the PC3 line to examine whether CD47 also regulates SLFN11 expression and sensitivity to genotoxic stress in prostate cancer cells. CD47 was targeted using CRISPR/Cas9, and pools of mutant PC3 cells with low residual CD47 or completely lacking CD47 were isolated by fluorescence activated cell sorting. Lack of or decreased CD47 expression was confirmed by flow cytometry and visualized by immunofluorescent staining (**Figure 7A**). The CD47-null PC3 cells proliferated at a somewhat slower rate that the WT PC3 cells (**Supplementary Figure 2**). Loss or absence of CD47 expression in PC3 cells was accompanied by decreased SLFN11protein expression (**Figures 7B,C**). SLFN11 mRNA expression was also reduced in the CD47-null PC3 cells (**Figure 7D**).

Loss of CD47 Differentially Regulates Drug and Radiation Sensitivities in Prostate Cancer Cells

Although loss of CD47 in Jurkat cells consistently protects these cells from ionizing radiation [present results and (19, 21, 40)], this was not the case when CD47 was disrupted in PC3 cells (**Figure 7E**). The initial loss and recovery of WT and CD47-null PC3 cells after irradiation at 20 Gy were similar. SLFN11 mRNA remained lower 2 h post-irradiation in the CD47-null cells but rose above that in irradiated WT PC3 cells at 24 h (**Figure 7D**).

Consistent with their lower SLFN11 and with the Jurkat cell results, CD47-null PC3 cells were less sensitive to rocilinostat and etoposide than were the WT PC3 cells (**Table 2**, **Supplementary Figure 3**). In contrast, CD47-null PC3 cells were moderately more sensitive than WT cells to entinostat and doxorubicin.

Treating WT PC3 cells with a sublethal concentrations of rocilinostat, entinostat, or etoposide for 24 h increased SLFN11 protein levels as detected by immunofluorescence (**Figure 8A**). In contrast, SLFN11 expression in CD47-null PC3 cells was not significantly induced by the same treatments. Induction of SLFN11 protein by rocilinostat, entinostat was paralleled by increased SLFN11 mRNA at 24 h in WT PC3 cells (**Figure 8B**). No elevation in SLFN11 mRNA was observed at the same time point in WT PC3 cells treated with etoposide. However, a time course for treatment with 300 nM etoposide indicated acute induction of SLFN11 mRNA at 2 h following the initial decrease (**Figure 8C**), which may account for the elevation of SLFN11 protein seen at 24 h in **Figure 8A**. Notably, SLFN11 mRNA was up-regulated at 24 h in the CD47-null cells treated with rocilinostat or etoposide. These data suggest a CD47 context-dependent effect of HDAC inhibition on SLFN11 expression in PC3 cells.

Tumor Type-Specific Correlation of CD47 Expression With *SLFN11* Promoter Methylation

Previous studies have identified roles for promoter methylation and epigenetic regulation in the loss of SLFN11 expression in various cancers (24, 29, 30). We further analyzed TCGA prostate cancer data to evaluate a potential role of CD47 in these two mechanisms for regulating *SLFN11* transcription. Consistent with the data in **Figure 6A**, prostate tumors with low SLFN11 mRNA (z-score <0) were enriched in the quadrant with low CD47 mRNA (34% CD47 z-score <0 vs. 26% *z*-score >0, **Figure 9A**). As reported previously for a broad collection of cancer cell lines (29), SLFN11 mRNA in prostate tumors was negatively correlated with methylation of the *SLFN11* promoter ($p = 4.5 \times 10^{-31}$, **Figure 9B**). A weaker negative correlation between CD47 mRNA expression and *SLFN11* promoter methylation ($p = 4.6 \times 10^{-19}$) suggested that the regulation of SLFN11 expression in human prostate cancers by CD47 is mediated in part by this mechanism (**Figure 9C**). However, another subset of the prostate cancers with low SLFN11 expression had low promoter methylation (**Figure 9B**),

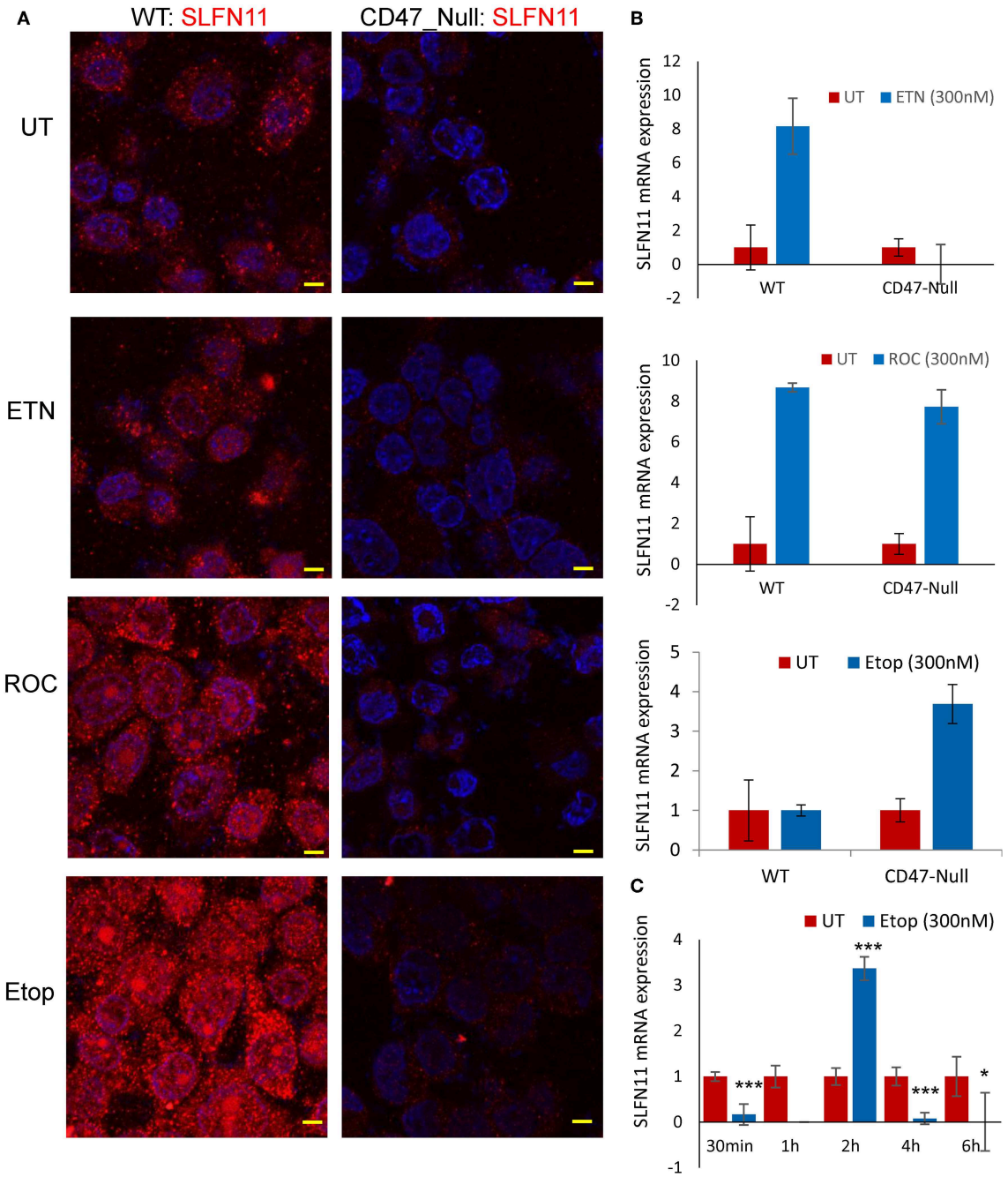

FIGURE 8 | Stress induces SLFN11 expression in WT but not in CD47-null PC3 cells. **(A)** Immunofluorescent imaging of SLFN11 protein expression in untreated WT and CD47-null PC3 cells (UT), and cells treated 24 h with 300 nM entinostat (ETN), rocilinostat (ROC), or etoposide (Etop). **(B)** SLFN11 mRNA expression in cells following the respective treatments for 24 h. Expression was normalized to actin and to one for the untreated WT and CD47-null PC3 cells. **(C)** WT PC3 cells (∼100,000/well) were plated overnight using complete RPM1 medium. After 24 h the cells were treated with 300 nM etoposide or an equal volume of PBS as control. The cells were harvested at the indicated time points, and 1 μg of total RNA per treatment was used to generate cDNA for RT-qPCR analysis. Relative SLFN11 mRNA expression was calculated using 18S RNA primer control and normalized to untreated controls for each time point (* for p-value < 0.05 and *** for $p < 0.001$).

which was previously demonstrated using a diverse panel of cancer cell lines to predict epigenetic regulation of *SLFN11* (29).

TCGA data for additional cancer types in **Table 1** were examined to determine the specificity of the correlation between CD47 expression and *SLFN11* promoter methylation. In all the cancer types where adequate methylation data was available, SLFN11 mRNA expression was negative correlated with *SLFN11* promoter methylation (**Supplementary Figure 4**, left panels). Consistent with the mRNA correlations in **Table 1**, CD47 mRNA expression in breast carcinomas was negatively correlated

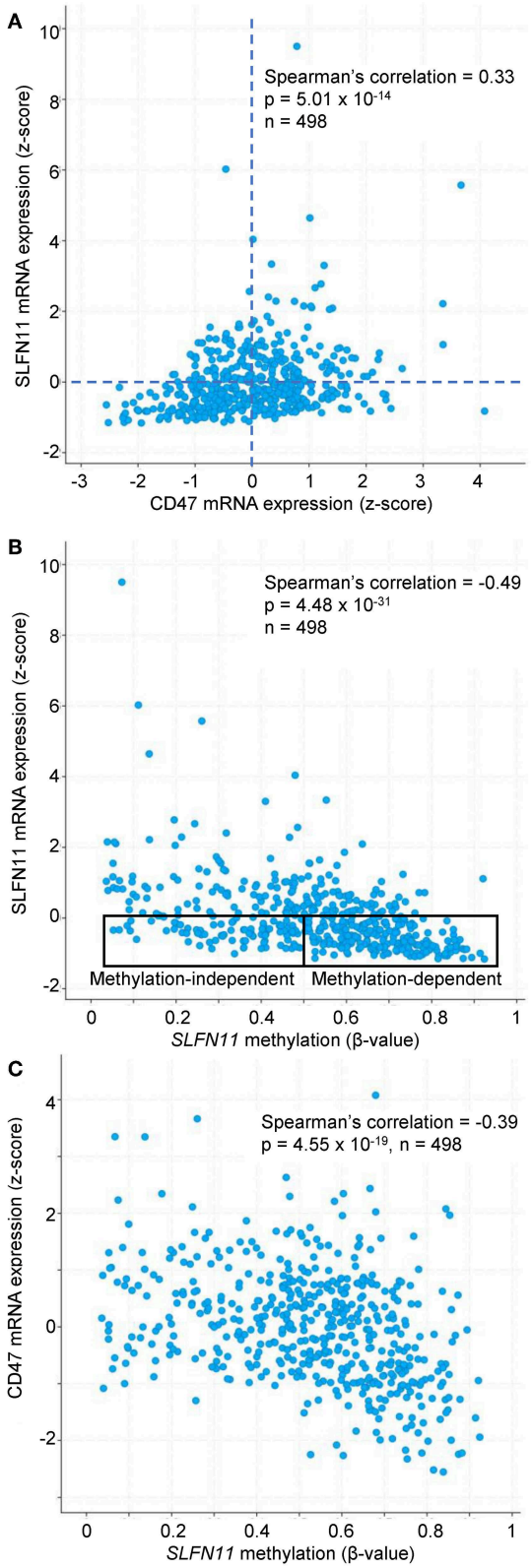

FIGURE 9 | *SLFN11* promoter methylation in human prostate carcinomas correlates with SLFN11 and CD47 expression. TCGA data were analyzed using cBioPortal tools. **(A)** Positive correlation between z-scores for SLFN11 and CD47 mRNA expression determined by RNAseq analysis. **(B)** *z*-scores for SLFN11 mRNA expression are negatively correlated with β-values for *SLFN11* promoter methylation data from the Illumina HumanMethylation450 (HM450) BeadChip. The indicated subsets with low SLFN11 mRNA ($z < 0$) are predicted to be promoter methylation-dependent or -independent based on the previous *in vitro* analysis of tumor cell lines (29). **(C)** *SLFN11* promoter methylation is negatively correlated with CD47 mRNA expression.

with *SLFN11* methylation ($p = 3.6 \times 10^{-14}$), and colorectal carcinoma lacked a significant correlation ($p = 0.62$). In contrast, the positive correlation between CD47 and SLFN11 expression for melanomas in **Table 1** ($p = 4.4 \times 10^{-14}$) diverged from the weak negative correlation between CD47 expression and *SLFN11* methylation in these tumors ($p = 3.1 \times 10^{-3}$). Furthermore, soft tissue sarcomas exhibited low levels of *SLFN11* methylation that were independent of CD47 expression ($p = 0.27$), but had a significant positive correlation between CD47 and SLFN11 expression ($p = 4.4 \times 10^{-4}$), consistent with epigenetic cross-regulation independent of *SLFN11* promoter methylation in these tumors.

Epigenetic Regulation of SLFN11 by CD47

The ability of selective HDAC1 inhibitors to restore SLFN11 expression in some resistant cancer cell lines (29) and the subset of prostate cancers in the TCGA data with low SLFN11 expression despite low promoter methylation suggested a potential epigenetic mechanism by which CD47 signaling could alter SLFN11 expression in prostate cancer. To examine potential epigenetic mechanisms for regulation of *SLFN11* gene expression by CD47 in prostate cancer cells, we performed chromosome immunoprecipitation in WT and CD47-null PC3 cells using acetylated H3K18, trimethylated H3K4, and trimethylated H3K27 antibodies and analyzed their enrichment in a region upstream from *SLFN11* that was identified based on ENCODE data to contain a high abundance of histone H3K27Me3 modification (**Supplementary Figure 5**). Consistent with the low *SLFN11* expression in the CD47-null PC3 cells, H3K18Ac enrichment was markedly decreased at 838–968 and 949–1,076 (**Figures 10A,B**). However, H3K18Ac enrichment did not show a corresponding decrease consistent with the decrease in SLFN11 mRNA expression in the CD47-low pool. In contrast, enrichment of trimethylated H3K4 and H3K27 was dose-dependent with decreasing CD47 expression (**Figures 10C–F**).

DISCUSSION

Previous studies have identified SLFN11 expression as a major determinant of cancer cell sensitivity to DNA-damaging chemotherapeutic agents and patient outcomes for several cancers (22–26, 29, 46). The present data extends this role to regulating the sensitivity of cells to ionizing radiation. We further identify a role for SLFN11 in the regulation by CD47 of the sensitivity of cells to radiotherapy and chemotherapy. Decreased expression of CD47 or its engagement by physiological or pharmacological ligands suppresses SLFN11 expression, and

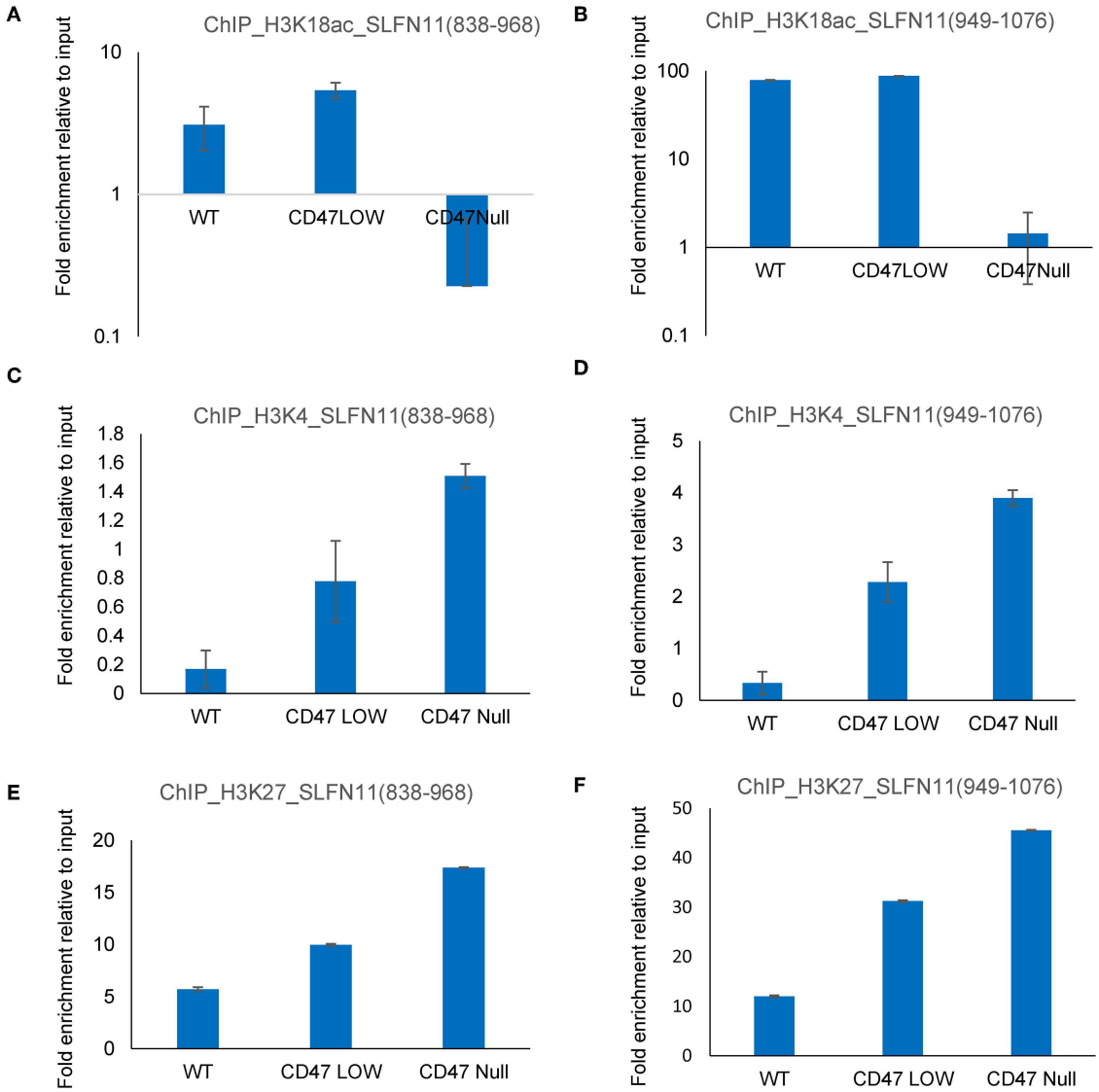

FIGURE 10 | Epigenetic regulation of the *SLFN11* promoter in PC3 cells with altered CD47 expression. Chromosome immunoprecipitation from WT and CD47-null PC3 cells was performed using acetylated H3K18 **(A,B)**, trimethyl H3K4 **(C,D)**, and trimethylated H3K27 antibodies **(E,F)**. Immune precipitates were analyzed by PCR using primers to amplify 838–968 **(A,C,E)** or 949–1,076 bp **(B,D,F)** 5′ from hg38_dna range=chr17:35373531-35374940 5'pad in the *SLFN11* promoter. Results are expressed as fold enrichment relative to input.

re-expression of SLFN11 in some cells with low CD47 expression is sufficient to restore their sensitivity to DNA damage. Previous studies have identified other cytoprotective pathways regulated by CD47 that are probably independent of SLFN11 including upregulation of autophagy (19, 47), anabolic metabolites (21), and transcription factors that support asymmetric stem cell self-renewal (20), but SLFN11 regulation by CD47 provides a complementary mechanism to more proximally regulate the DNA damage response.

Loss or blockade of CD47 in non-transformed cells and tissues and in the Jurkat T cell line consistently protects cells from genotoxic and ischemic stresses (1). However, some of the underlying protective mechanisms are lost or lead to different outcomes in cancer cells. For example, the protective autophagy response in non-transformed CD47-deficient cells exposed to ionizing radiation manifests as a non-protective mitophagy response in breast cancer cells (18). Similarly, blockade of CD47 signaling that preserves non-transformed stem cells results in differentiation of breast and hepatocellular carcinoma and stem cells (11, 12, 48). The present data demonstrate a similar divergence in regulation of the SLFN11 pathway in different cell lines. Loss of CD47 coincides with loss of expression for *SLFN11* or its presumed murine ortholog Slfn9 in non-transformed cells, and at least in human Jurkat cells this contributes to protection from genotoxic stress induced by ionizing radiation or cytotoxic chemotherapy. Transient over-expression of SLFN11 is sufficient

to resensitize CD47-deficient Jurkat cells to ionizing radiation. Conversely, ligation of CD47 by a CD47 antibody, which is known to confer cytoprotection in WT Jurkat cells (40), rapidly decreases SLFN11 expression in these cells. The physiological CD47 signaling ligand TSP1 similarly induces a decrease in SLFN11 expression.

The positive regulation of *SLFN11* expression by CD47 extends to prostate cancer cells, and correlative data in human tumors extends this relationship to a subset of human cancers. Our PC3 cell data indicates that CD47 regulation of *SLFN11* and responses to stress is more restricted in this cancer cell line. The decreased SLFN11 in CD47-null PC3 cells was not sufficient to protect these cells from ionizing radiation, but resistance to the anti-proliferative effects of etoposide and rocilinostat were observed. The latter resistance is consistent with the inability of rocilinostat to induce SLFN11 protein expression in the CD47-null PC3 cells.

To interpret the differences in *SLFN11* regulation in WT and CD47-deficient cells following exposure to ionizing radiation, DNA damaging agents, or HDAC inhibitors, it is important to recognize the temporal differences in their action. DNA strand breaks are induced rapidly by radiation and locally produced ROS, and all damage occurs over a few minutes. In contrast, doxorubicin causes cumulative DNA damage by several mechanisms including intercalation, ROS-induced strand breaks, and inhibition of topoisomerase activity. Etoposide is a more specific inhibitor of topoisomerase activity, but this activity is similarly sustained for the duration of treatment. Our data show that sustained exposure to doxorubicin or etoposide results in a CD47-dependent accumulation of SLFN11 over 24 h. The HDAC inhibitors similarly induce SLFN11 in a CD47-dependent manner. Looking only at 24 h, radiation appears to induce the opposite response. SLFN11 mRNA was induced in CD47-null PC3 cells but not in irradiated WT cells. Considering the noted temporal differences in the respective genotoxic stresses, the observed CD47-dependence for *SLFN11* regulation by these stresses may be consistent.

The detailed molecular mechanism by which CD47 signaling regulates SLFN11 mRNA and protein levels remains to be determined. The high throughput drug screen identified a significant resistance of $CD47^{-}$ Jurkat cells to class I HDAC inhibitors including the selective HDAC1 entinostat. On the other hand, lack of differential activity for romidepsin and differential inhibition of the $CD47^{-}$ and WT cells by the selective HDAC6 inhibitor rocilinostat suggested that the regulation of SLFN11 by CD47 may not exclusively involve HDAC1. Consistent with the drug screening data, ChIP data identified CD47-dependent regulation of histone modification in the *SLFN11* promoter in prostate cancer cells. Loss of CD47 in PC3 cells was associated with increased histone H3 K4 methylation and K27 methylation and decreased H3K18 acetylation at this locus. The observed epigenetic effects of CD47 signaling on *SLFN11* could also account for the differential resistance of CD47-deficient Jurkat T cells to several HDAC inhibitors in the drug screening. However, the ability of etoposide and rocilinostat to induce SLFN11 mRNA without a corresponding increase in protein expression in CD47-null cells suggests that CD47 positively controls SLFN11 expression by a post-transcriptional mechanism.

Analysis of tumor data in TCGA also implicated CD47 regulation of *SLFN11* promoter methylation in a subset of cancers that includes prostate adenocarcinoma. However, *SLFN11* promoter methylation is independent of CD47 expression in some cancer types that exhibit a positive correlation between SLFN11 and CD47 mRNA expression. Further studies will be required to define the relative importance of these two mechanisms in the cross talk between CD47 and SLFN11 in each cancer type. These data could guide the design of clinical trials combining CD47-targeted therapeutics with anticancer drugs that target DNA methylation or histone modification to maximize therapeutic responses in each cancer.

DATA AVAILABILITY STATEMENT

All datasets generated for this study are included in the manuscript/**Supplementary Files**.

ETHICS STATEMENT

Ethical review and approval was not required for the study on human participants in accordance with the local legislation and institutional requirements. The patients/participants provided their written informed consent to participate in this study.

AUTHOR CONTRIBUTIONS

SK, AS AT, S-WT, YP, and DR contributed to conception and design of the study. SK, AS, DJ, DS-P, BK, AE, LM, CT, MF, VR, YP, and DR performed acquisition, analysis, or interpretation of data. SK, AS, and AE performed the statistical analysis. SK, AS, and DR wrote the first draft of the manuscript. DS-P wrote sections of the manuscript. All authors contributed to manuscript revision, read, and approved the submitted version.

FUNDING

This work was supported by the Intramural Research Programs of the NIH/NCI (DR: ZIA SC 009172, YP: Z01-BC-006150) and NHGRI (AE: Z01 HG200365-09), the CCR Drug Development Collaborative (DR), the National Center for Advancing Translational Sciences (NCATS) (MF, CT), and a NCI Career Transition Award K22 (1K22CA181274-01A1) and the Metavivor Foundation Young Investigator Award (DS-P).

ACKNOWLEDGMENTS

We thank Dr. Kun Dong for assisting BK with ligation of gCD47 into the CAS9GFP vector.

SUPPLEMENTARY MATERIAL

The Supplementary Material for this article can be found online at: https://www.frontiersin.org/articles/10.3389/fonc.2019.00994/full#supplementary-material

REFERENCES

1. Soto-Pantoja DR, Kaur S, Roberts DD. CD47 signaling pathways controlling cellular differentiation and responses to stress. *Crit Rev Biochem Mol Biol*. (2015) 50:212–30. doi: 10.3109/10409238.2015.1014024
2. Roberts DD, Frazier WA. Thrombospondins and their receptors: evolving functions. In: Keeley FW, Mecham RP, editors. *Evolution of Extracellular Matrix*. Berlin; Heidelberg: Springer (2013). p. 221–42. doi: 10.1007/978-3-642-36002-2_8
3. Matlung HL, Szilagyi K, Barclay NA, van den Berg TK. The CD47-SIRPalpha signaling axis as an innate immune checkpoint in cancer. *Immunol Rev*. (2017) 276:145–64. doi: 10.1111/imr.12527
4. Hughes AL. Origin and evolution of viral interleukin-10 and other DNA virus genes with vertebrate homologues. *J Mol Evol*. (2002) 54:90–101. doi: 10.1007/s00239-001-0021-1
5. Cameron CM, Barrett JW, Mann M, Lucas A, McFadden G. Myxoma virus M128L is expressed as a cell surface CD47-like virulence factor that contributes to the downregulation of macrophage activation *in vivo*. *Virology*. (2005) 337:55–67. doi: 10.1016/j.virol.2005.03.037
6. Willingham SB, Volkmer JP, Gentles AJ, Sahoo D, Dalerba P, Mitra SS, et al. The CD47-signal regulatory protein alpha (SIRPa) interaction is a therapeutic target for human solid tumors. *Proc Natl Acad Sci USA*. (2012) 109:6662–7. doi: 10.1073/pnas.1121623109
7. Murata Y, Saito Y, Kotani T, Matozaki T. CD47-signal regulatory protein alpha signaling system and its application to cancer immunotherapy. *Cancer Sci*. (2018) 109:2349–57. doi: 10.1111/cas.13663
8. Advani R, Flinn I, Popplewell L, Forero A, Bartlett NL, Ghosh N, et al. CD47 Blockade by Hu5F9-G4 and rituximab in non-Hodgkin's lymphoma. *N Engl J Med*. (2018) 379:1711–21. doi: 10.1056/NEJMoa1807315
9. Lin GHY, Chai V, Lee V, Dodge K, Truong T, Wong M, et al. TTI-621 (SIRPalphaFc), a CD47-blocking cancer immunotherapeutic, triggers phagocytosis of lymphoma cells by multiple polarized macrophage subsets. *PLoS ONE*. (2017) 12:e0187262. doi: 10.1371/journal.pone.0187262
10. Kauder SE, Kuo TC, Harrabi O, Chen A, Sangalang E, Doyle L, et al. ALX148 blocks CD47 and enhances innate and adaptive antitumor immunity with a favorable safety profile. *PLoS ONE*. (2018) 13:e0201832. doi: 10.1371/journal.pone.0201832
11. Kaur S, Elkahloun AG, Singh SP, Chen QR, Meerzaman DM, Song T, et al. A function-blocking CD47 antibody suppresses stem cell and EGF signaling in triple-negative breast cancer. *Oncotarget*. (2016) 7:10133–52. doi: 10.18632/oncotarget.7100
12. Lee TK, Cheung VC, Lu P, Lau EY, Ma S, Tang KH, et al. Blockade of CD47-mediated cathepsin S/protease-activated receptor 2 signaling provides a therapeutic target for hepatocellular carcinoma. *Hepatology*. (2014) 60:179–91. doi: 10.1002/hep.27070
13. Roberts DD, Kaur S, Isenberg JS. Regulation of cellular redox signaling by matricellular proteins in vascular biology, immunology, and cancer. *Antioxid Redox Signal*. (2017) 27:874–911. doi: 10.1089/ars.2017.7140
14. Nath PR, Pal-Nath D, Mandal A, Cam M, Schwartz AL, Roberts DD. Natural killer cell recruitment and activation are regulated by CD47 expression in the tumor microenvironment. *Cancer Immunol Res*. (2019) 7:1547–61. doi: 10.1158/2326-6066.CIR-18-0367
15. Kaur S, Kuznetsova SA, Pendrak ML, Sipes JM, Romeo MJ, Li Z, et al. Heparan sulfate modification of the transmembrane receptor CD47 is necessary for inhibition of T cell receptor signaling by thrombospondin-1. *J Biol Chem*. (2011) 286:14991–5002. doi: 10.1074/jbc.M110.179663
16. Miller TW, Kaur S, Ivins-O'Keefe K, Roberts DD. Thrombospondin-1 is a CD47-dependent endogenous inhibitor of hydrogen sulfide signaling in T cell activation. *Matrix Biol*. (2013) 32:316–24. doi: 10.1016/j.matbio.2013.02.009
17. Soto-Pantoja DR, Terabe M, Ghosh A, Ridnour LA, DeGraff WG, Wink DA, et al. CD47 in the tumor microenvironment limits cooperation between antitumor T-cell immunity and radiotherapy. *Cancer Res*. (2014) 74:6771–83. doi: 10.1158/0008-5472.CAN-14-0037-T
18. Feliz-Mosquea YR, Christensen AA, Wilson AS, Westwood B, Varagic J, Melendez GC, et al. Combination of anthracyclines and anti-CD47 therapy inhibit invasive breast cancer growth while preventing cardiac toxicity by regulation of autophagy. *Breast Cancer Res Treat*. (2018) 172:69–82. doi: 10.1007/s10549-018-4884-x
19. Soto-Pantoja DR, Miller TW, Pendrak ML, Degraff WG, Sullivan C, Ridnour LA, et al. CD47 deficiency confers cell and tissue radioprotection by activation of autophagy. *Autophagy*. (2012) 8:1628–42. doi: 10.4161/auto.21562
20. Kaur S, Soto-Pantoja DR, Stein EV, Liu C, Elkahloun AG, Pendrak ML, et al. Thrombospondin-1 signaling through CD47 inhibits self-renewal by regulating c-Myc and other stem cell transcription factors. *Sci Rep*. (2013) 3:1673. doi: 10.1038/srep01673
21. Miller TW, Soto-Pantoja DR, Schwartz AL, Sipes JM, DeGraff WG, Ridnour LA, et al. CD47 globally regulates metabolic pathways that control resistance to ionizing radiation. *J Biol Chem*. (2015) 290:24858–74. doi: 10.1074/jbc.M115.665752
22. Zoppoli G, Regairaz M, Leo E, Reinhold WC, Varma S, Ballestrero A, et al. Putative DNA/RNA helicase Schlafen-11 (SLFN11) sensitizes cancer cells to DNA-damaging agents. *Proc Natl Acad Sci USA*. (2012) 109:15030–5. doi: 10.1073/pnas.1205943109
23. Rees MG, Seashore-Ludlow B, Cheah JH, Adams DJ, Price EV, Gill S, et al. Correlating chemical sensitivity and basal gene expression reveals mechanism of action. *Nat Chem Biol*. (2016) 12:109–16. doi: 10.1038/nchembio.1986
24. Gardner EE, Lok BH, Schneeberger VE, Desmeules P, Miles LA, Arnold PK, et al. Chemosensitive relapse in small cell lung cancer proceeds through an EZH2-SLFN11 axis. *Cancer Cell*. (2017) 31:286–99. doi: 10.1016/j.ccell.2017.01.006
25. Lok BH, Gardner EE, Schneeberger VE, Ni A, Desmeules P, Rekhtman N, et al. PARP inhibitor activity correlates with SLFN11 expression and demonstrates synergy with Temozolomide in small cell lung cancer. *Clin Cancer Res*. (2017) 23:523–35. doi: 10.1158/1078-0432.CCR-16-1040
26. Tang SW, Bilke S, Cao L, Murai J, Sousa FG, Yamade M, et al. SLFN11 is a transcriptional target of EWS-FLI1 and a determinant of drug response in Ewing sarcoma. *Clin Cancer Res*. (2015) 21:4184–93. doi: 10.1158/1078-0432.CCR-14-2112
27. Sousa FG, Matuo R, Tang SW, Rajapakse VN, Luna A, Sander C, et al. Alterations of DNA repair genes in the NCI-60 cell lines and their predictive value for anticancer drug activity. *DNA Repair*. (2015) 28:107–15. doi: 10.1016/j.dnarep.2015.01.011
28. Deng Y, Cai Y, Huang Y, Yang Z, Bai Y, Liu Y, et al. High SLFN11 expression predicts better survival for patients with KRAS exon 2 wild type colorectal cancer after treated with adjuvant oxaliplatin-based treatment. *BMC Cancer*. (2015) 15:833. doi: 10.1186/s12885-015-1840-6
29. Tang SW, Thomas A, Murai J, Trepel JB, Bates SE, Rajapakse VN, et al. Overcoming resistance to DNA-targeted agents by epigenetic activation of Schlafen 11 (SLFN11) expression with class I histone deacetylase inhibitors. *Clin Cancer Res*. (2018) 24:1944–53. doi: 10.1158/1078-0432.CCR-17-0443
30. Nogales V, Reinhold WC, Varma S, Martinez-Cardus A, Moutinho C, Moran S, et al. Epigenetic inactivation of the putative DNA/RNA helicase SLFN11 in human cancer confers resistance to platinum drugs. *Oncotarget*. (2016) 7:3084–97. doi: 10.18632/oncotarget.6413
31. Li M, Kao E, Malone D, Gao X, Wang JYJ, David M. DNA damage-induced cell death relies on SLFN11-dependent cleavage of distinct type II tRNAs. *Nat Struct Mol Biol*. (2018) 25:1047–58. doi: 10.1038/s41594-018-0142-5
32. Murai J, Tang SW, Leo E, Baechler SA, Redon CE, Zhang H, et al. SLFN11 blocks stressed replication forks independently of ATR. *Mol Cell*. (2018) 69:371–84 e376. doi: 10.1016/j.molcel.2018.01.012
33. Reinhold MI, Green JM, Lindberg FP, Ticchioni M, Brown EJ. Cell spreading distinguishes the mechanism of augmentation of T cell activation by integrin-associated protein/CD47 and CD28. *Int Immunol*. (1999) 11:707–18. doi: 10.1093/intimm/11.5.707
34. Kaur S, Singh SP, Elkahloun AG, Wu W, Abu-Asab MS, Roberts DD. CD47-dependent immunomodulatory and angiogenic activities of extracellular vesicles produced by T cells. *Matrix Biol*. (2014) 37:49–59. doi: 10.1016/j.matbio.2014.05.007
35. Singh NP, McCoy MT, Tice RR, Schneider EL. A simple technique for quantitation of low levels of DNA damage in individual cells. *Exp Cell Res*. (1988) 175:184–91. doi: 10.1016/0014-4827(88)90265-0
36. Kaur S, Elkahloun AG, Singh SP, Arakelyan A, Roberts DD. A function-blocking CD47 antibody modulates extracellular vesicle-mediated intercellular signaling between breast carcinoma cells and endothelial cells. *J Cell Commun Signal*. (2018) 12:157–70. doi: 10.1007/s12079-017-0428-0

37. Ma D, Liu S, Lal B, Wei S, Wang S, Zhan D, et al. Extracellular matrix protein tenascin C increases phagocytosis mediated by CD47 loss of function in glioblastoma. *Cancer Res*. (2019) 79:2697–708. doi: 10.1158/0008-5472.CAN-18-3125
38. Cerami E, Gao J, Dogrusoz U, Gross BE, Sumer SO, Aksoy BA, et al. The cBio cancer genomics portal: an open platform for exploring multidimensional cancer genomics data. *Cancer Discov*. (2012) 2:401–4. doi: 10.1158/2159-8290.CD-12-0095
39. Gao J, Aksoy BA, Dogrusoz U, Dresdner G, Gross B, Sumer SO, et al. Integrative analysis of complex cancer genomics and clinical profiles using the cBioPortal. *Sci Signal*. (2013) 6:pl1. doi: 10.1126/scisignal.2004088
40. Maxhimer JB, Soto-Pantoja DR, Ridnour LA, Shih HB, DeGraff WG, Tsokos M, et al. Radioprotection in normal tissue and delayed tumor growth by blockade of CD47 signaling. *Sci Transl Med*. (2009) 1:3ra7. doi: 10.1126/scitranslmed.3000139
41. Gewirtz DA. A critical evaluation of the mechanisms of action proposed for the antitumor effects of the anthracycline antibiotics adriamycin and daunorubicin. *Biochem Pharmacol*. (1999) 57:727–41. doi: 10.1016/S0006-2952(98)00307-4
42. de la Casa-Esperon E. From mammals to viruses: the Schlafen genes in developmental, proliferative and immune processes. *Biomol Concepts*. (2011) 2:159–69. doi: 10.1515/bmc.2011.018
43. Nath PR, Gangaplara A, Pal-Nath D, Mandal A, Maric D, Sipes JM, et al. CD47 expression in natural killer cells regulates homeostasis and modulates immune response to lymphocytic choriomeningitis virus. *Front Immunol*. (2018) 9:2985. doi: 10.3389/fimmu.2018.02985
44. Li Z, Calzada MJ, Sipes JM, Cashel JA, Krutzsch HC, Annis D, et al. Interactions of thrombospondins with a4b1 integrin and CD47 differentially modulate T cell behavior. *J Cell Biol*. (2002) 157:509–19. doi: 10.1083/jcb.200109098
45. Li SS, Liu Z, Uzunel M, Sundqvist KG. Endogenous thrombospondin-1 is a cell surface ligand for regulation of integrin dependent T lymphocyte adhesion. *Blood*. (2006) 108:3112–20. doi: 10.1182/blood-2006-04-016832
46. Barretina J, Caponigro G, Stransky N, Venkatesan K, Margolin AA, Kim S, et al. The Cancer Cell Line Encyclopedia enables predictive modelling of anticancer drug sensitivity. *Nature*. (2012) 483:603–7. doi: 10.1038/nature11003
47. Soto-Pantoja DR, Ridnour LA, Wink DA, Roberts DD. Blockade of CD47 increases survival of mice exposed to lethal total body irradiation. *Sci Rep*. (2013) 3:1038. doi: 10.1038/srep01038
48. Kaur S, Roberts DD. Divergent modulation of normal and neoplastic stem cells by thrombospondin-1 and CD47 signaling. *Int J Biochem Cell Biol*. (2016) 81:184–94. doi: 10.1016/j.biocel.2016.05.005

Conflict of Interest: AS is Chief Executive Officer and a shareholder of Morphiex Biotherapeutics.

The remaining authors declare that the research was conducted in the absence of any commercial or financial relationships that could be construed as a potential conflict of interest.

Copyright © 2019 Kaur, Schwartz, Jordan, Soto-Pantoja, Kuo, Elkahloun, Mathews Griner, Thomas, Ferrer, Thomas, Tang, Rajapakse, Pommier and Roberts. This is an open-access article distributed under the terms of the Creative Commons Attribution License (CC BY). The use, distribution or reproduction in other forums is permitted, provided the original author(s) and the copyright owner(s) are credited and that the original publication in this journal is cited, in accordance with accepted academic practice. No use, distribution or reproduction is permitted which does not comply with these terms.

frontiers in Oncology

REVIEW
published: 10 October 2019
doi: 10.3389/fonc.2019.01009

Altering DNA Repair to Improve Radiation Therapy: Specific and Multiple Pathway Targeting

Julian Biau[1,2,3,4,5,6*], *Emmanuel Chautard*[5,7], *Pierre Verrelle*[1,6,8,9] *and Marie Dutreix*[1,2,3,4]

[1] Institut Curie, PSL Research University, Centre de Recherche, Paris, France, [2] UMR3347, CNRS, Orsay, France, [3] U1021, INSERM, Orsay, France, [4] Université Paris Sud, Orsay, France, [5] Université Clermont Auvergne, INSERM, U1240 IMoST, Clermont Ferrand, France, [6] Radiotherapy Department, Université Clermont Auvergne, Centre Jean Perrin, Clermont-Ferrand, France, [7] Pathology Department, Université Clermont Auvergne, Centre Jean Perrin, Clermont-Ferrand, France, [8] U1196, INSERM, UMR9187, CNRS, Orsay, France, [9] Radiotherapy Department, Institut Curie Hospital, Paris, France

Radiation therapy (RT) is widely used in cancer care strategies. Its effectiveness relies mainly on its ability to cause lethal damage to the DNA of cancer cells. However, some cancers have shown to be particularly radioresistant partly because of efficient and redundant DNA repair capacities. Therefore, RT efficacy might be enhanced by using drugs that can disrupt cancer cells' DNA repair machinery. Here we review the recent advances in the development of novel inhibitors of DNA repair pathways in combination with RT. A large number of these compounds are the subject of preclinical/clinical studies and target key enzymes involved in one or more DNA repair pathways. A totally different strategy consists of mimicking DNA double-strand breaks via small interfering DNA (siDNA) to bait the whole DNA repair machinery, leading to its global inhibition.

Keywords: DNA damage, repair systems, radiotherapy, radioresistance, inhibition

OPEN ACCESS

Edited by:
Paul N. Span, Radboud University Nijmegen Medical Centre, Netherlands

Reviewed by:
Michael Wayne Epperly, University of Pittsburgh, United States
Bevin P. Engelward, Massachusetts Institute of Technology, United States

***Correspondence:**
Julian Biau
Julian.biau@clermont.unicancer.fr

Specialty section:
This article was submitted to Radiation Oncology, a section of the journal Frontiers in Oncology

Received: *15 July 2019*
Accepted: *19 September 2019*
Published: *10 October 2019*

Citation:
Biau J, Chautard E, Verrelle P and Dutreix M (2019) Altering DNA Repair to Improve Radiation Therapy: Specific and Multiple Pathway Targeting. Front. Oncol. 9:1009. doi: 10.3389/fonc.2019.01009

INTRODUCTION

Radiation therapy (RT), in conjunction with surgery and systemic therapies (chemotherapy, targeted therapies, immunotherapy…), is a cornerstone of cancer care. About 50% of cancer patients receive RT (1). The primary objective of RT is to increase the amount of radiation delivered to the tumor to ensure local control and reduce the amount of radiation in adjacent healthy tissues. Advanced developments such as image-guided RT (IGRT) or intensity-modulated RT (IMRT) have led to the enhancement of this therapeutic ratio (2). Despite such improvements, many patients still experience local recurrence of the disease after RT. Clinical factors such as tumor stage, frequently associated with increased hypoxia, can explain some of the failures, but it is clear that biological characteristics play a key part in successful treatment (3–5). RT-induced cell death is mostly due to DNA damage, especially to double-strand breaks (DSBs) (6, 7). Consequently, tumor cells with highly efficient DNA repair are radioresistant (8), whereas deficiencies in pathways that repair DSBs are particularly detrimental to the cells (9). Therefore, therapies that inhibit the DNA repair machinery have the potential to enhance RT efficacy (10, 11). Inhibiting DNA repair offers an opportunity to target genetic differences between tumor and normal cells, as DNA repair is often dysregulated in tumor cells (10, 12–14). Tumor cells divide rapidly because of unregulated cell cycle control. Thus, they have less time to repair DNA damage as compared to normal cells that are not dividing or will stop dividing after activation of key checkpoints induced by RT (15, 16). Beside altered cell cycle control, cancer cells may also present defects in their DNA repair system, inducing dependence on specific repair pathways and/or overexpression of alternative pathways

(16, 17). Furthermore, cancer cells often develop under stress conditions, thus raising the frequency of endogenous DNA damage (18, 19). This review will firstly focus on the distinct categories of DNA lesions induced by RT and the DNA repair pathways required for their repair. Subsequently, it will present the approaches that are currently being developed to enhance RT efficacy by modulating DNA repair.

RT-INDUCED DNA DAMAGE RESPONSE

DNA lesions induced by RT activate the DNA damage response (DDR), which essentially involves post-translational modifications of proteins to activate downstream signaling pathways (20). DDR is based on an intricate network of proteins that work together to manage DNA repair and cell cycle coordination. DDR interrupts the cell cycle, thereby inhibiting the spread of DNA damage to daughter cells and facilitating repair. Cell division arrest is mainly controlled by the checkpoint kinases CHK1 and CHK2, which are activated by the phosphatidylinsositol-3-kinases (PI3K) of the DDR machinery (15). DDR signaling is also essential for triggering apoptosis when repair is unsuccessful, notably through modifications to the p53 protein (20).

RT induces a variety of DNA lesions. Approximately 10,000 damaged bases, 1,000 single strand breaks (SSBs) and 40 DSBs are produced per gray per cell (21, 22). Such lesions, if not corrected, can lead to cell death by mitotic catastrophe and apoptosis. DSBs are the most lethal to the cells despite their low proportion, as one single unrepaired DSB can trigger cell death (7). DSBs are produced directly and indirectly by RT. Indirect DSBs most often occur during replication if the initial damage is unrepaired. As an example, when a replication fork encounters an unrepaired SSB, the fork is blocked and leads to the conversion of this SSB into a DSB (10, 23, 24). The resulting DSB can directly trigger cell death or activate DDR, which induces cell cycle arrest and promotes DNA repair. This repair is usually error-free, allowing the cell to survive without genetic consequences. It can also be error-prone, leading either to cell death if the error is not viable or mutation and chromosomic aberrations (25).

DNA REPAIR OF RT-INDUCED DAMAGE

Following RT, damaged bases induced by oxidative stress are repaired by the base excision repair pathway (BER) (26–31). In BER, damaged bases are excised by DNA glycosylases, resulting in apurinic (AP) sites. Subsequently; these AP sites are cleaved by apurinic endonuclease 1 (APE1) or an AP-lyase activity, leading to SSBs. SSBs are repaired by the part of the BER pathway called single strand break repair (SSBR) (**Figure 1A**) (12, 32). Either short-patch or long-patch SSBR can then proceed, depending on several factors such as type of lesion and cell cycle state. Single nucleotide insertion by DNA polymerase (Pol) β and ligation by DNA ligase III are described as short-patch SSBR, and interact with the protein X-ray repair cross-complementing 1 (XRCC1). Long-patch SSBR involves the removal of a larger DNA segment, which requires several DNA replication factors such as proliferating cell nuclear antigen (PCNA), Pol δ/ϵ, flap endonuclease 1 (FEN1), and DNA ligase I. Concerning SSBs detection, poly-ADP-ribose polymerase (PARP1 or PARP2) are required (28, 33–37). The binding of PARP to SSB activates its auto-PARylation, and leads to the recruitment of BER/SSBR proteins. PARP-1 was also reported as a regulator of DNA repair gene expression through the E2F1 pathway (38). Unrepaired SSB or a damaged base can block the replication forks, resulting in fork collapse and DSB (23). The great majority of oxidative damage induced by ionizing radiation is corrected by BER. However, under hypoxic conditions, IR causes the formation of cyclodeoxynucleosides that can be only removed by nucleotide excision repair (NER). Several results suggest that NER may be involved in the repair of oxidized DNA damage. In addition, ionizing-radiation breast cancer risk has been related to polymorphism in ERCC2 (one of the main NER enzymes) (39).

Two major pathways repair DSBs: homologous recombination (HR) and non-homologous end joining (NHEJ) (40). However, both mismatch repair (MMR) and NER pathways have been reported to affect both HR- and NHEJ-mediated DSB repair efficacy to a lesser extent (41). The formation of DSBs triggers the activation of three key enzymes from the PIKK family: ataxia telangiectasia mutated kinase (ATM), ATM-related kinase (ATR), and DNA-dependent protein kinase (DNA-PK). This leads to the phosphorylation of many proteins, signaling damage and initiating DNA repair. One of the early steps is the phosphorylation of histone H2AX (γ-H2AX), which signals the presence of DSB to repair proteins where they aggregate in ionizing radiation-induced foci (IRIF) (42). Besides their crucial roles in DDR signaling, the kinases ATR and ATM are also involved in maintaining replication fork stability (14) and fork reversal in case of fork-stalling lesions, notably through SMARCAL1 (43).

In mammalian cells, c-NHEJ (classical NHEJ, **Figure 1B**) is the most efficient DSB repair mechanism. It acts by directly ligating the broken DNA ends (44). c-NHEJ can occur during the entire cell cycle. It is frequently accompanied by small deletions at the repair break site and is considered to be the main cause of DSB error-prone repair. The first step of NHEJ is the binding of the heterodimer Ku70/Ku80 at the end of the DSB (45), allowing the recruitment of catalytic subunit DNA-PKcs forming the protein complex DNA-PK (46). DNA-PK, bounded to DNA, is activated and phosphorylates numerous proteins including H2AX (47), Artemis (48), X-ray repair cross-complementing 4 (XRCC4) and ligase IV complex (49), and XLF (XRCC4-like factor) (50) that are recruited on the site of the DSB and participate in its repair. When c-NHEJ is impaired, an alternative pathway called a-EJ (alternative EJ) or MHEJ (Micro Homology End Joining) (**Figure 1C**) is activated (51). At the initial breaking site, a deletion of 5–25 nucleotides is necessary to reveal micro-homologies to realize a-EJ (52), while a maximum of 4 deleted nucleotides is necessary for c-NHEJ (44). The micro-homologies that are slightly longer in the case of a-EJ could partly explain the higher number of large deletions and other genomic rearrangements that occur (53, 54). The a-EJ pathway is differentiated from c-NHEJ by the fact that it is independent

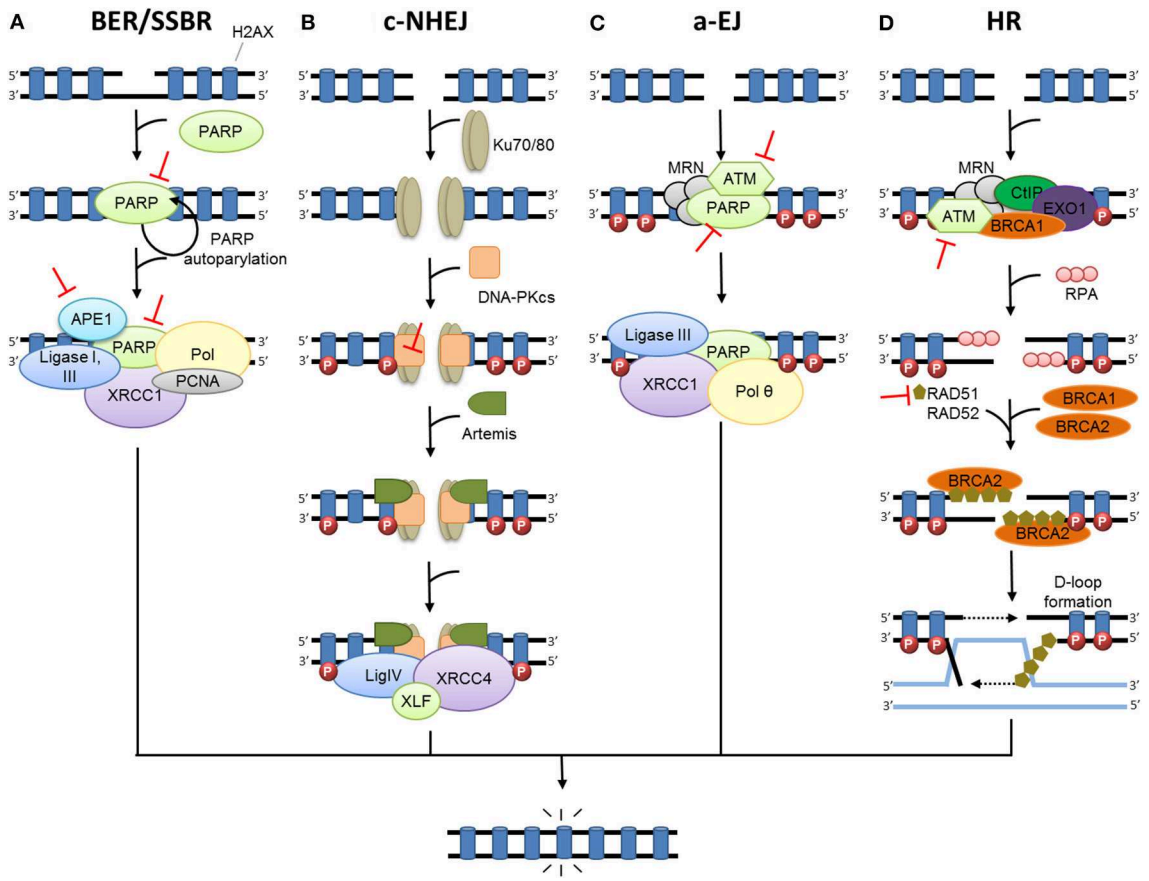

FIGURE 1 | DNA damage repair after radiation therapy. In irradiated cells, a number of DNA lesions are induced including single (SSB) and double-strand breaks (DSB). **(A)** SSBs are corrected by the part of base excision repair (BER) known as single-strand break repair (SSBR). The binding of PARP to SSB activates its auto-PARylation and leads to the recruitment of BER/SSBR proteins including AP endonucleases (APE1), XRCC1 (helper protein), PCNA, FEN, PNK, and DNA polymerases (Pol; damage processing) and DNA ligases. **(B)** In c-NHEJ, DSB is recognized by the Ku80-Ku70 heterodimer, which leads to DNA-dependent protein kinase catalytic subunit DNA-PKcs recruitment, gathering the DNA-PK complex and activating its kinase activity. This leads to the involvement of repair proteins (XRCC4, DNA ligase IV and others), which perform the processing and final junction reaction. **(C)** When c-NHEJ is impaired, an alternative pathway called a-EJ (alternative EJ) takes place and involves mainly PARP1, XRCC1, ligase III, MRN complex and the DNA polymerase θ. **(D)** In HR, after ATM activation, the DSB site is bounded by the MRE11-RAD50-NBS1 complex (MRN). The consequence is the phosphorylation of a set of targets including H2AX (γ-H2AX), localized at the site of DSB. HR uses the sister chromatid as a model to repair DSB. First, the resection of the DNA at DSB results in a 3′ single-strand DNA, which is then coated by proteins of replication A (RPA). Subsequently, proteins of the RAD family are recruited and mediate the invasion of the homologous strand of the sister chromatid, leading to the formation of Holliday junctions. DNA polymerases can then synthetize across the missing regions. The Holliday junctions are finally resolved by cleavage and followed by ligation of adjacent ends. ⊣ Represents inhibitors of DNA repair in preclinical or clinical development.

of Ku proteins (52). a-EJ involves mainly PARP1, XRCC1, ligase III (LIGIII), and the MRE11/RAD50/NBS1 (MRN) complex (55, 56). DNA polymerase theta (Pol θ or PolQ) is specifically involved in nucleotide incorporation in the a-EJ mechanism through the TMEJ (theta-mediated end joining) pathway (57).

HR is an alternative pathway for repairing DSBs that uses the sister chromatid as a model, restricting this mechanism to the S and G2 cell cycle phases (**Figure 1D**) (40). HR is the most conservative and least error-prone repair mechanism. It necessitates the presence of BRCA proteins, defects of which increase susceptibility to breast or ovarian cancer. The DSB site is bounded by several factors such as the MRN complex, EXO1 (exonuclease 1), DNA2-BLM (Bloom syndrome), BRCA1 and CTIP (CtBP-interacting protein) that contribute to DNA resection and formation of a 3′ single-strand DNA (58–60), which is then coated by proteins of replication A (RPA). After the RPA protein's displacement by RAD51, BRCA2 together with the localizer of BRCA2 (PALB2), RAD54, and BARD1 (BRCA1-associated RING domain protein 1) mediates the nucleoprotein filament invasion of the homologous strand of the sister chromatid and creates the "D-loop" (61). DNA polymerases can then synthetize across the missing regions. The resulting Holliday junctions are finally resolved by cleavage and followed by ligation of adjacent ends (62). However, HR can sometimes be error-prone, especially if template switching occurs, e.g., in repeat sequences (63).

The choice between the two major mechanisms for DSB repair (NHEJ and HR pathways) seems to be linked to several factors

such as cell-cycle phase, chromatin context, or availability of key actors such as the Ku complex, 53BP1 or RAD51 (64, 65).

CURRENT STRATEGIES INVOLVED IN DDR INHIBITION IN COMBINATION WITH RT

Targeting Key Enzymes Involved in a Specific DNA Repair Pathway

Inhibiting BER/SSBR

BER and SSBR pathways repair damaged bases and SSBs. Inhibiting BER/SSBR may lead to unrepaired damages that are converted to DSBs when encountering a replication fork (23). Therefore, in cells already defective for HR, such as BRCA$^{-/-}$ breast or ovarian cancer tumors, the inhibition of BER by PARP inhibitors leads to unrepaired DSBs and cell death (14). This effect, called synthetic lethality, has been extensively described (17, 66, 67) and studied in numerous clinical trials (68–70). Since the majority of RT-induced damages are repaired by BER/SSBR, inhibition of this pathway should highly sensitize cells to RT even in HR-proficient cells (29). The preclinical evaluation of PARP inhibitors has shown enhanced RT efficacy both *in vitro* and *in vivo* (71–73). Several PARP inhibitors have already been tested in or entered into numerous clinical trials in association with RT for brain metastases, ovarian cancer, breast cancer, rectal cancer, or glioblastoma, among others (**Table 1**). However, early data did not demonstrate convincing and coherent proof of synergy, although neither did they demonstrate unexpected toxic effects (74, 75). Another strategy for the inhibition of BER/SSBR is the development of APE1 inhibitors. APE1 is crucial for BER/SSBR and is commonly overexpressed in cancer cells (80, 81), giving to this strategy some tumor specificity. APE1 inhibitors have shown efficacy in combination with RT in preclinical studies (82). Lucanthone, an APE1 inhibitor, combined with temozolomide, has recently been tested in a phase 2 clinical trial in glioblastoma (**Table 1**). The results are not yet published.

Inhibiting NHEJ

DNA-PK, a key enzyme in NHEJ, is a member of the PI3K family that performs a central role in many cellular functions (83). Selective DNA-PK inhibitors have led to radiosensitization in preclinical studies (84–86). Three phase 1 trials are currently testing the safety and tolerability of a DNA-PK inhibitor (M3814) in combination with palliative RT +/- immunotherapy in advanced solid tumors (NCT02516813 and NCT03724890) and curative-intent radiotherapy in locally advanced rectal cancer (NCT03770689) (**Table 1**). Such strategies, which are not based on a selective effect on the tumor, are considered promising by some (14) though they have been criticized by others (87). Early reports of the clinical combination of M3814 and palliative RT showed enhanced normal tissue reactions including dysphagia, prolonged mucosal inflammation/stomatitis, and skin injury (87, 88). Inhibition of Ku subunits could also result in reduced DNA-PK activity and NHEJ. This is consistent with the existing data reporting that shRNA depletion of Ku70 or Ku80 showed cytotoxicity and radiosensitization in pancreatic cancer cells (89, 90). CC-115, a dual inhibitor of DNA-PK and mammalian target of rapamycin (mTOR), is being tested; preliminary anti-tumor activity has been reported, although whether these responses are attributable to activity against DNA-PK or mTOR is unclear (14, 91). A phase 1 trial testing CC-115 in combination with RT and temozolomide in the treatment of glioblastoma is ongoing (NCT02977780). NHEJ can also be indirectly inhibited via the EGFR pathway (see below).

Inhibiting HR

Cancer cells are known to be more proliferative than normal cells (92). Inhibitors of replication-associated processes such as HR exploit this specificity to enhance the therapeutic ratio. Nevertheless, there are few specific inhibitors of HR. It has been shown that RAD51 expression and functional HR can be reduced using imatinib during experimental RT, leading to increased radiosensitization (13, 93). Indirect inhibition of HR can also be obtained via cell cycle checkpoint targeting (see below).

Targeting Key Enzymes Involved in Multiple Repair Pathways

DNA damage detection and signaling is the first step common to all DNA repair pathways. Acting on this step will alter several pathways. Therefore, several approaches have been tested to disable part or all of the DNA damage recognition/signaling steps.

Inhibiting ATM

ATM is one of the key enzymes in DNA damage signaling of DSBs for HR but also NHEJ (94). Defective cells in ATM are extremely radiosensitive, independent of their p53 status (95). ATM inhibitors have shown radiosensitization in preclinical studies (96–98). A single 15Gy RT dose suppressed tumor growth in a preclinical model when ATM was deleted in cancer cells vs. when deleted in endothelial cells (99), underlining the interest in testing ATM inhibitors in combination with highly conformal RT. Like DNA-PK, ATM is part of the PI3K family and has many cellular functions. A phase 1 study is currently testing an ATM inhibitor (AZD1390) in combination with RT in brain tumors including glioblastoma and brain metastases (NCT03423628). Indirectly, inhibition of the TGFβ-signaling or mitogen-activated protein kinase (MAPK) pathway can lead to reduced ATM activation and increased tumor cell radiosensitivity through reduced DSB repair (100–102).

Inhibiting ATR

ATR is a critical kinase that is activated in reaction to replication stress and blocked replication forks. ATR is one of the key enzymes in DNA damage signaling of DSBs (103). Cancer cells, which exhibit relatively elevated levels of replication stress, are more susceptible to dependence on ATR signaling for survival (104). An ATR inhibitor (AZD6738) has given encouraging preclinical results (67, 105) and is currently in phase I trials as monotherapy or in combination with olaparib, RT (NCT02223923), carboplatin and immunotherapy agents. Another ATR inhibitor (M6620) is being tested in three phase 1 trials with radiotherapy in esophageal cancer (NCT03641547),

TABLE 1 | Examples of clinical trials of inhibitors of the DNA damage response in combination with radiation therapy.

DNA repair pathway(s)	Target	Inhibitor	Cancer type	Phase	References/trial identifier
Targeting key enzymes involved in a specific pathway					
BER/SSBR	APE1	Lucantone	Glioblastoma	Phase 2	NCT01587144
	PARP	Iniparib	Glioblastoma	Phase 1/2	NCT00687765
			Brain metastases	Phase 1	NCT01551680
		Veliparib	Rectal	Phase 1	NCT01589419
			Breast	Phase 1	NCT01477489
			Peritoneal carcinomatosis	Phase 1	(74)
			Brain metastasis	Phase 2	(75)
NHEJ	DNA-PK	M3814	Solid tumors	Phase 1	NCT02516813
		M3814	Rectal	Phase 1b	NCT03770689
		M3814	Solid tumors	Phase 1	NCT03724890
HR	RAD51	Imatinib	High grade glioma	Phase 1/2	(76)
Targeting key enzymes involved in multiple pathways					
NHEJ/HR	ATM	AZD1390	Brain tumors	Phase 1	NCT03423628
	ATR	AZD6737	Solid tumors	Phase 1	NCT02223923
		M6620	Esophageal	Phase 1	NCT03641547
		M6620	Head and neck	Phase 1	NCT02567422
		M6620	Brain metastases	Phase 1	NCT02589522
Targeting chromatin dynamics via epigenetic modifications					
	HDAC	Vorinostat	Gastrointestinal	Phase 1	(77)
			High grade glioma	Phase 2/3	NCT01236560
		Valproic acid	Cervical	Phase 2	(78)
Baiting DNA-break recognition					
BER/SSBR NHEJ/HR	PARP DNA-PK	Dbait	Melanoma	Phase 1	(79)
Targeting cell cycle checkpoints					
	CHK1/2	Prexsertib	Head and neck	Phase 1	NCT02555644
	WEE1	Adavosertib	Glioblastoma	Phase 1	NCT01849146
		Adavosertib	Cervical	Phase 1	NCT03345784
		Adavosertib	Head and neck	Phase 1	NCT03028766

locally advanced head and neck squamous cell carcinoma (NCT02567422) and brain metastases (NCT02589522).

Inhibiting MRN Complex

Mirin is an inhibitor of MRE11 endonuclease and thus of HR function. However, MRE11 is also upstream of NHEJ, and so mirin inhibits NHEJ and its effects are not specific to HR (16, 106, 107). It might be of particular interest in combination with RT.

Baiting DNA Breaks Signaling

This approach developed recently is represented by the molecules called Dbait/AsiDNA^{TM}. Dbait/AsiDNA^{TM} consist of double-strand oligonucleotides that mimic DNA strand breaks and consequently bind and trap the signaling and repair proteins DNA-PK (24, 108, 109) and PARP (110), leading to inhibition of both SSB and DSB repair. In preclinical studies, the proof of concept that a RT-Dbait association could be used in treating melanoma (24) and high-grade glioma (111) has been established. A first-in-man phase 1 trial was conducted combining Dbait/AsiDNA^{TM} in combination with palliative RT in in-transit metastases of melanoma (79) (**Table 1**). In this trial, no dose-limiting toxicity was reported and the maximum tolerated dose was not met.

Targeting Chromatin Dynamics via Epigenetic Modifications

Epigenetics is an emerging field in cancer biology (112). It focuses on functionally relevant genome modifications that do not modify the nucleotide sequence. Such modifications include DNA methylation or histone modifications that may regulate gene expression but do not alter the associated DNA sequence. These modifications could also affect DNA repair ability. The loss of ARID1A, a piece of the SWI/SNF chromatin remodeling complex, was recently reported to induce a selective vulnerability to combined RT and PARP inhibitor therapy (113).

Inhibiting Histone Deacetylases (HDACs)

HDAC inhibitors are epigenetic therapeutics. They have the capacity to lower RT-induced damage repair both at the level of damage signaling, via inhibition of the ATM or MRN complex, and by directly affecting proteins involved in NHEJ and HR

(112, 114–117). Several clinical trials have been carried out for various cancer types (77, 78) (**Table 1**).

Inhibition of Kinases Involved in DDR-Related Survival Pathways

Sorafenib, a multi-kinase inhibitor, is currently utilized in the clinic for the treatment of hepatocellular and renal cancers. It inhibits MAPK signaling together with additional intracellular Ser/Thr kinases, leading to both NHEJ and HR inhibition. Sorafenib has shown a radiosensitization effect in preclinical studies (118). Dasatinib is another multi-kinase inhibitor inhibiting ABL and SRC tyrosine kinases. In preclinical studies, it has shown a radiosensitization effect partly due to blocking of DNA repair pathways involved in DSB repair (119). Sorafenib and dasatinib are clinically evaluated in association with RT. Because of their large spectrum of targets, most of these inhibitors may show high toxicity, which prevents them from being used at the dosage required to be efficient in combination with RT in the management of aggressive tumors that overexpress some of their targets (120, 121).

After RT, EGFR has been found to translocate into the nucleus and modulate DNA repair (especially NHEJ) through association with DNA-PKcs (122, 123). A current in-clinic approach is using the monoclonal antibody cetuximab to inhibit this nuclear translocation of EGFR. Cetuximab combined with RT has improved patients' overall survival in a phase III trial in head and neck cancer (124). Furthermore, EGFR signaling may be interrupted by small-molecule tyrosine kinase inhibitors such as erlotinib or gefitinib, especially in the case of specific EGFR mutation; these are currently being tested in combination with RT (125, 126).

Targeting Cell Cycle Checkpoints

Checkpoint dysfunction represents a common molecular defect acquired during tumorigenesis (15, 127), underlying the importance of its regulation in cancer development. Interfering with cell cycle checkpoint signaling is an alternative approach to modulating DNA repair activity and potentially improving the therapeutic ratio. The induction of DNA lesions by RT in normal cells stops their progression in the cell cycle, thereby avoiding the accumulation of other lesions and their damaging effects (20). This cell cycle arrest is subtly correlated with DNA repair to fine-tune cell cycle restart with the disappearance of damage. In cancer cells with an altered G1 checkpoint, cell cycle progression goes on relentlessly and, as a result, the removal of the G2 block increases unrepaired damage and its transfer to the daughter cells. This finally causes the loss of essential genetic material and cell death, a process that strengthens checkpoint inhibition strategies. Combination of RT with a dual CHK1 and CHK2 inhibitors (AZD7762 and prexsertib) showed a radiosensitization effect with an increase in mitotic catastrophe in different cancer cell lines and xenografts (128–130). A phase 1b trial was completed that combined prexsertib with RT and cisplatin or cetuximab in locally advanced head and neck cancer (NCT02555644), the results of which are not yet published. However, in addition to checkpoint activation, CHK1 is also involved in HR (131, 132) and it is uncertain if this is only a result of checkpoint inhibition or if it is partly due to HR inhibition (133).

Another target is the WEE1 kinase, which has been shown to be a major regulator of the G2-M checkpoint (134). This tyrosine kinase inhibits the entrance in mitosis by adding an inhibitory phosphorylation to Cdc2 (the human homolog of tyrosine kinase 1[Cdk1]) to tyrosine 15 (Y15). As a consequence, the Cdc2/cyclin B complex becomes inactivated, which stops the cells in G2-M and allows DNA repair. Preclinical studies have shown the potential use of WEE 1 inhibitors as radiosentizers (135, 136). Several ongoing clinical trials are testing WEE1 inhibitors with RT. In addition, several phase 1 trials are currently testing the WEE1 inhibitor adavosertib (AZD1775) in combination with RT and temozolomide in the treatment of glioblastoma (NCT01849146), with RT and cisplatin in cervical, vaginal or uterine cancer (NCT03345784), or in combination with RT and cisplatin in advanced head and neck cancer (NCT03028766 and NCT02585973).

Combining DNA Repair Targeting, Immunotherapy, and Radiotherapy

DNA repair proteins preserve the integrity of the genome; therefore, DNA repair targeting may enhance the tumor mutational burden, which may lead to the production of neoantigens and increased activity of anti-cancer T cells. Some clinical trials have been set to investigate the use of immune checkpoint inhibitors, notably by combining Dravulumab (anti-PD-L1) with PARP (NCT02484404), ATR (NCT02264678) or WEE1 inhibition (NCT02617277). To date, the interplay between radiation and the immune system is far from being completely deciphered, but several interesting facts have been reported. The cytotoxic action of radiotherapy on tumor cells provides T lymphocytes with tumor neoantigens and releases pro-inflammatory cytokines, thus promoting the immune response (137). The cell death inducing this type of immune response is called immunogenic cell death. Combining immunotherapy with radiotherapy (several recent trials: NCT02707588, NCT02952586, NCT02999087) could increase the ability to cause immunogenic cell death by removing locks that block the immune system (138). The non-overlapping toxicities of DNA repair targeting and immune checkpoint inhibitors render the use of combinations of these agents with radiotherapy appealing (14, 139).

CONCLUSION

Targeted therapies are beginning to demonstrate activity across a number of tumor types. The most promising approach toward improving the efficiency of a treatment and gaining a reliable response is to develop therapy combinations that decrease the chance of resistance and to treat resistance when it emerges. There has been a considerable renewed emphasis on new targeted treatments such as radiosensitizers that do not cause overlapping dose-limiting toxicities. Selection of appropriate targeted agents represents a challenge. As predicted, during preclinical and clinical trials, particular attention was paid to proteins involved

in DNA repair pathways. Various strategies have been explored, ranging from specific protein targeting to global inhibition, and many DNA repair inhibitors have been developed. Up until now, only a few of them have reached the clinical stage, while even fewer have been tested in combination with RT. The several clinical trials currently underway will tell whether these new compounds can be tolerable and efficient.

RT-induced lesions can be corrected by various DNA repair pathways. The intricacy of crosstalk between DNA repair pathways suggests that biomarker assays to determine the status of multiple DNA repair pathways could provide essential information on the sensitivity and resistance of cancer cells to repair inhibitors. Understanding these DNA repair pathways and identifying effective stratification biomarkers from the various DNA repair pathways that are specifically altered in some tumors would be required to characterize patients' responses to specific DNA repair inhibitors.

AUTHOR CONTRIBUTIONS

JB and EC analyzed the literature and wrote the manuscript. PV and MD gave important intellectual input and carefully revised the manuscript. All authors approved the final manuscript for submission.

REFERENCES

1. Delaney G, Jacob S, Featherstone C, Barton M. The role of radiotherapy in cancer treatment: estimating optimal utilization from a review of evidence-based clinical guidelines. *Cancer*. (2005) 104:1129–37. doi: 10.1002/cncr.21324
2. Elshaikh M, Ljungman M, Ten Haken R, Lichter AS. Advances in radiation oncology. *Annu Rev Med*. (2006) 57:19–31. doi: 10.1146/annurev.med.57.121304.131431
3. Fertil B, Malaise EP. Intrinsic radiosensitivity of human cell lines is correlated with radioresponsiveness of human tumors: analysis of 101 published survival curves. *Int J Radiat Oncol Biol Phys*. (1985) 11:1699–707. doi: 10.1016/0360-3016(85)90223-8
4. Taghian A, Ramsay J, Allalunis-Turner J, Budach W, Gioioso D, Pardo F, et al. Intrinsic radiation sensitivity may not be the major determinant of the poor clinical outcome of glioblastoma multiforme. *Int J Radiat Oncol Biol Phys*. (1993) 25:243–9. doi: 10.1016/0360-3016(93)90345-V
5. Gerweck LE, Vijayappa S, Kurimasa A, Ogawa K, Chen DJ. Tumor cell radiosensitivity is a major determinant of tumor response to radiation. *Cancer Res*. (2006) 66:8352–5. doi: 10.1158/0008-5472.CAN-06-0533
6. Khanna KK, Jackson SP. DNA double-strand breaks: signaling, repair and the cancer connection. *Nat Genet*. (2001) 27:247–54. doi: 10.1038/85798
7. Radford IR. The level of induced DNA double-strand breakage correlates with cell killing after X-irradiation. *Int J Radiat Biol Relat Stud Phys Chem Med*. (1985) 48:45–54. doi: 10.1080/09553008514551051
8. Jeggo P, Lavin MF. Cellular radiosensitivity: how much better do we understand it? *Int J Radiat Biol*. (2009) 85:1061–81. doi: 10.3109/09553000903261263
9. O'Driscoll M, Jeggo PA. The role of double-strand break repair - insights from human genetics. *Nat Rev Genet*. (2006) 7:45–54. doi: 10.1038/nrg1746
10. Helleday T, Petermann E, Lundin C, Hodgson B, Sharma RA. DNA repair pathways as targets for cancer therapy. *Nat Rev Cancer*. (2008) 8:193–204. doi: 10.1038/nrc2342
11. Stover EH, Konstantinopoulos PA, Matulonis UA, Swisher EM. Biomarkers of response and resistance to DNA repair targeted therapies. *Clin Cancer Res*. (2016) 22:5651–60. doi: 10.1158/1078-0432.CCR-16-0247
12. Begg AC, Stewart FA, Vens C. Strategies to improve radiotherapy with targeted drugs. *Nat Rev Cancer*. (2011) 11:239–53. doi: 10.1038/nrc3007
13. Thoms J, Bristow RG. DNA repair targeting and radiotherapy: a focus on the therapeutic ratio. *Semin Radiat Oncol*. (2010) 20:217–22. doi: 10.1016/j.semradonc.2010.06.003
14. Pilié PG, Tang C, Mills GB, Yap TA. State-of-the-art strategies for targeting the DNA damage response in cancer. *Nat Rev Clin Oncol*. (2019) 16:81–104. doi: 10.1038/s41571-018-0114-z
15. Kastan MB, Bartek J. Cell-cycle checkpoints and cancer. *Nature*. (2004) 432:316–23. doi: 10.1038/nature03097
16. Curtin NJ. DNA repair dysregulation from cancer driver to therapeutic target. *Nat Rev Cancer*. (2012) 12:801–17. doi: 10.1038/nrc3399
17. Shaheen M, Allen C, Nickoloff JA, Hromas R. Synthetic lethality: exploiting the addiction of cancer to DNA repair. *Blood*. (2011) 117:6074–82. doi: 10.1182/blood-2011-01-313734
18. Kryston TB, Georgiev AB, Pissis P, Georgakilas AG. Role of oxidative stress and DNA damage in human carcinogenesis. *Mutat Res*. (2011) 711:193–201. doi: 10.1016/j.mrfmmm.2010.12.016
19. Nowsheen S, Wukovich RL, Aziz K, Kalogerinis PT, Richardson CC, Panayiotidis MI, et al. Accumulation of oxidatively induced clustered DNA lesions in human tumor tissues. *Mutat Res*. (2009) 674:131–6. doi: 10.1016/j.mrgentox.2008.09.010
20. Jackson SP, Bartek J. The DNA-damage response in human biology and disease. *Nature*. (2009) 461:1071–8. doi: 10.1038/nature08467
21. Ward JF. DNA damage and repair. *Basic Life Sci*. (1991) 58:403–15; discussion 415–21. doi: 10.1007/978-1-4684-7627-9_15
22. Burkart W, Jung T, Frasch G. Damage pattern as a function of radiation quality and other factors. *C R Acad Sci III, Sci Vie*. (1999) 322:89–101. doi: 10.1016/S0764-4469(99)80029-8
23. Kuzminov A. Single-strand interruptions in replicating chromosomes cause double-strand breaks. *Proc Natl Acad Sci USA*. (2001) 98:8241–6. doi: 10.1073/pnas.131009198
24. Biau J, Devun F, Jdey W, Kotula E, Quanz M, Chautard E, et al. A preclinical study combining the DNA repair inhibitor Dbait with radiotherapy for the treatment of melanoma. *Neoplasia*. (2014) 16:835–44. doi: 10.1016/j.neo.2014.08.008
25. Jalal S, Earley JN, Turchi JJ. DNA repair: from genome maintenance to biomarker and therapeutic target. *Clin Cancer Res*. (2011) 17:6973–84. doi: 10.1158/1078-0432.CCR-11-0761
26. Krokan HE, Bjørås M. Base excision repair. *Cold Spring Harb Perspect Biol*. (2013) 5:a012583. doi: 10.1101/cshperspect.a012583
27. van Loon B, Markkanen E, Hübscher U. Oxygen as a friend and enemy: how to combat the mutational potential of 8-oxo-guanine. *DNA Repair*. (2010) 9:604–16. doi: 10.1016/j.dnarep.2010.03.004
28. Visnes T, Grube M, Hanna BMF, Benitez-Buelga C, Cázares-Körner A, Helleday T. Targeting BER enzymes in cancer therapy. *DNA Repair*. (2018) 71:118–26. doi: 10.1016/j.dnarep.2018.08.015
29. Vens C, Begg AC. Targeting base excision repair as a sensitization strategy in radiotherapy. *Semin Radiat Oncol*. (2010) 20:241–9. doi: 10.1016/j.semradonc.2010.05.005
30. Hyun J-W, Cheon G-J, Kim H-S, Lee Y-S, Choi E-Y, Yoon B-H, et al. Radiation sensitivity depends on OGG1 activity status in human leukemia cell lines. *Free Radic Biol Med*. (2002) 32:212–20. doi: 10.1016/S0891-5849(01)00793-6
31. Yang N, Galick H, Wallace SS. Attempted base excision repair of ionizing radiation damage in human lymphoblastoid cells produces lethal and mutagenic double strand breaks. *DNA Repair*. (2004) 3:1323–34. doi: 10.1016/j.dnarep.2004.04.014
32. Fortini P, Dogliotti E. Base damage and single-strand break repair: mechanisms and functional significance of short- and long-patch repair subpathways. *DNA Repair*. (2007) 6:398–409. doi: 10.1016/j.dnarep.2006.10.008

33. Carter RJ, Parsons JL. Base excision repair, a pathway regulated by posttranslational modifications. *Mol Cell Biol*. (2016) 36:1426–37. doi: 10.1128/MCB.00030-16
34. Wallace SS. Base excision repair: a critical player in many games. *DNA Repair*. (2014) 19:14–26. doi: 10.1016/j.dnarep.2014.03.030
35. Limpose KL, Corbett AH, Doetsch PW. BERing the burden of damage: pathway crosstalk and posttranslational modification of base excision repair proteins regulate DNA damage management. *DNA Repair*. (2017) 56:51–64. doi: 10.1016/j.dnarep.2017.06.007
36. Jacobs AL, Schär P. DNA glycosylases: in DNA repair and beyond. *Chromosoma*. (2012) 121:1–20. doi: 10.1007/s00412-011-0347-4
37. Dizdaroglu M. Oxidatively induced DNA damage and its repair in cancer. *Mutat Res Rev Mutat Res*. (2015) 763:212–45. doi: 10.1016/j.mrrev.2014.11.002
38. Schiewer MJ, Mandigo AC, Gordon N, Huang F, Gaur S, de Leeuw R, et al. PARP-1 regulates DNA repair factor availability. *EMBO Mol Med*. (2018) 10:e8816. doi: 10.15252/emmm.201708816
39. Rajaraman P, Bhatti P, Doody MM, Simon SL, Weinstock RM, Linet MS, et al. Nucleotide excision repair polymorphisms may modify ionizing radiation-related breast cancer risk in US radiologic technologists. *Int J Cancer*. (2008) 123:2713–6. doi: 10.1002/ijc.23779
40. Wyman C, Kanaar R. DNA double-strand break repair: all's well that ends well. *Annu Rev Genet*. (2006) 40:363–83. doi: 10.1146/annurev.genet.40.110405.090451
41. Zhang Y, Rohde LH, Wu H. Involvement of nucleotide excision and mismatch repair mechanisms in double strand break repair. *Curr Genomics*. (2009) 10:250–8. doi: 10.2174/138920209788488544
42. Belyaev IY. Radiation-induced DNA repair foci: spatio-temporal aspects of formation, application for assessment of radiosensitivity and biological dosimetry. *Mutat Res*. (2010) 704:132–41. doi: 10.1016/j.mrrev.2010.01.011
43. Cortez D. Replication-coupled DNA repair. *Mol Cell*. (2019) 74:866–76. doi: 10.1016/j.molcel.2019.04.027
44. Pannunzio NR, Watanabe G, Lieber MR. Nonhomologous DNA end-joining for repair of DNA double-strand breaks. *J Biol Chem*. (2018) 293:10512–23. doi: 10.1074/jbc.TM117.000374
45. Britton S, Coates J, Jackson SP. A new method for high-resolution imaging of Ku foci to decipher mechanisms of DNA double-strand break repair. *J Cell Biol*. (2013) 202:579–95. doi: 10.1083/jcb.201303073
46. Gottlieb TM, Jackson SP. The DNA-dependent protein kinase: requirement for DNA ends and association with Ku antigen. *Cell*. (1993) 72:131–42. doi: 10.1016/0092-8674(93)90057-W
47. Park E-J, Chan DW, Park J-H, Oettinger MA, Kwon J. DNA-PK is activated by nucleosomes and phosphorylates H2AX within the nucleosomes in an acetylation-dependent manner. *Nucleic Acids Res*. (2003) 31:6819–27. doi: 10.1093/nar/gkg921
48. Ma Y, Pannicke U, Schwarz K, Lieber MR. Hairpin opening and overhang processing by an Artemis/DNA-dependent protein kinase complex in nonhomologous end joining and V(D)J recombination. *Cell*. (2002) 108:781–94. doi: 10.1016/S0092-8674(02)00671-2
49. Nick McElhinny SA, Snowden CM, McCarville J, Ramsden DA. Ku recruits the XRCC4-ligase IV complex to DNA ends. *Mol Cell Biol*. (2000) 20:2996–3003. doi: 10.1128/MCB.20.9.2996-3003.2000
50. Ahnesorg P, Smith P, Jackson SP. XLF interacts with the XRCC4-DNA ligase IV complex to promote DNA nonhomologous end-joining. *Cell*. (2006) 124:301–13. doi: 10.1016/j.cell.2005.12.031
51. Sallmyr A, Tomkinson AE. Repair of DNA double-strand breaks by mammalian alternative end-joining pathways. *J Biol Chem*. (2018) 293:10536–46. doi: 10.1074/jbc.TM117.000375
52. McVey M, Lee SE. MMEJ repair of double-strand breaks (director's cut): deleted sequences and alternative endings. *Trends Genet*. (2008) 24:529–38. doi: 10.1016/j.tig.2008.08.007
53. Boboila C, Jankovic M, Yan CT, Wang JH, Wesemann DR, Zhang T, et al. Alternative end-joining catalyzes robust IgH locus deletions and translocations in the combined absence of ligase 4 and Ku70. *Proc Natl Acad Sci USA*. (2010) 107:3034–9. doi: 10.1073/pnas.0915067107
54. Yan CT, Boboila C, Souza EK, Franco S, Hickernell TR, Murphy M, et al. IgH class switching and translocations use a robust non-classical end-joining pathway. *Nature*. (2007) 449:478–82. doi: 10.1038/nature06020
55. Haince J-F, McDonald D, Rodrigue A, Déry U, Masson J-Y, Hendzel MJ, Poirier GG. PARP1-dependent kinetics of recruitment of MRE11 and NBS1 proteins to multiple DNA damage sites. *J Biol Chem*. (2008) 283:1197–208. doi: 10.1074/jbc.M706734200
56. El-Khamisy SF, Masutani M, Suzuki H, Caldecott KW. A requirement for PARP-1 for the assembly or stability of XRCC1 nuclear foci at sites of oxidative DNA damage. *Nucleic Acids Res*. (2003) 31:5526–33. doi: 10.1093/nar/gkg761
57. Kent T, Chandramouly G, McDevitt SM, Ozdemir AY, Pomerantz RT. Mechanism of microhomology-mediated end-joining promoted by human DNA polymerase θ. *Nat Struct Mol Biol*. (2015) 22:230–7. doi: 10.1038/nsmb.2961
58. Lavin MF. The Mre11 complex and ATM: a two-way functional interaction in recognising and signaling DNA double strand breaks. *DNA Repair*. (2004) 3:1515–20. doi: 10.1016/j.dnarep.2004.07.001
59. Sartori AA, Lukas C, Coates J, Mistrik M, Fu S, Bartek J, et al. Human CtIP promotes DNA end resection. *Nature*. (2007) 450:509–14. doi: 10.1038/nature06337
60. Prakash R, Zhang Y, Feng W, Jasin M. Homologous recombination and human health: the roles of BRCA1, BRCA2, and associated proteins. *Cold Spring Harb Perspect Biol*. (2015) 7:a016600. doi: 10.1101/cshperspect.a016600
61. Heyer W-D, Li X, Rolfsmeier M, Zhang X-P. Rad54: the Swiss Army knife of homologous recombination? *Nucleic Acids Res*. (2006) 34:4115–25. doi: 10.1093/nar/gkl481
62. Solinger JA, Heyer WD. Rad54 protein stimulates the postsynaptic phase of Rad51 protein-mediated DNA strand exchange. *Proc Natl Acad Sci USA*. (2001) 98:8447–53. doi: 10.1073/pnas.121009898
63. Rodgers K, McVey M. Error-prone repair of DNA double-strand breaks. *J Cell Physiol*. (2016) 231:15–24. doi: 10.1002/jcp.25053
64. Scully R, Panday A, Elango R, Willis NA. DNA double-strand break repair-pathway choice in somatic mammalian cells. *Nat Rev Mol Cell Biol*. (2019). doi: 10.1038/s41580-019-0152-0. [Epub ahead of print].
65. Fattah F, Lee EH, Weisensel N, Wang Y, Lichter N, Hendrickson EA. Ku regulates the non-homologous end joining pathway choice of DNA double-strand break repair in human somatic cells. *PLoS Genet*. (2010) 6:e1000855. doi: 10.1371/journal.pgen.1000855
66. Chan DA, Giaccia AJ. Harnessing synthetic lethal interactions in anticancer drug discovery. *Nat Rev Drug Discov*. (2011) 10:351–64. doi: 10.1038/nrd3374
67. Brown JS, O'Carrigan B, Jackson SP, Yap TA. Targeting DNA repair in cancer: beyond PARP inhibitors. *Cancer Discov*. (2017) 7:20–37. doi: 10.1158/2159-8290.CD-16-0860
68. Gelmon KA, Tischkowitz M, Mackay H, Swenerton K, Robidoux A, Tonkin K, et al. Olaparib in patients with recurrent high-grade serous or poorly differentiated ovarian carcinoma or triple-negative breast cancer: a phase 2, multicentre, open-label, non-randomised study. *Lancet Oncol*. (2011) 12:852–61. doi: 10.1016/S1470-2045(11)70214-5
69. Kaye SB, Lubinski J, Matulonis U, Ang JE, Gourley C, Karlan BY, et al. Phase II, open-label, randomized, multicenter study comparing the efficacy and safety of olaparib, a poly (ADP-ribose) polymerase inhibitor, and pegylated liposomal doxorubicin in patients with BRCA1 or BRCA2 mutations and recurrent ovarian cancer. *J Clin Oncol*. (2012) 30:372–9. doi: 10.1200/JCO.2011.36.9215
70. Ledermann J, Harter P, Gourley C, Friedlander M, Vergote I, Rustin G, et al. Olaparib maintenance therapy in platinum-sensitive relapsed ovarian cancer. *N Engl J Med*. (2012) 366:1382–92. doi: 10.1056/NEJMoa1105535
71. Calabrese CR, Almassy R, Barton S, Batey MA, Calvert AH, Canan-Koch S, et al. Anticancer chemosensitization and radiosensitization by the novel poly(ADP-ribose) polymerase-1 inhibitor AG14361. *J Natl Cancer Inst*. (2004) 96:56–67. doi: 10.1093/jnci/djh005
72. Dungey FA, Löser DA, Chalmers AJ. Replication-dependent radiosensitization of human glioma cells by inhibition of poly(ADP-Ribose) polymerase: mechanisms and therapeutic potential. *Int J Radiat Oncol Biol Phys*. (2008) 72:1188–97. doi: 10.1016/j.ijrobp.2008.07.031
73. Donawho CK, Luo Y, Luo Y, Penning TD, Bauch JL, Bouska JJ, et al. ABT-888, an orally active poly(ADP-ribose) polymerase inhibitor that potentiates

DNA-damaging agents in preclinical tumor models. *Clin Cancer Res*. (2007) 13:2728–37. doi: 10.1158/1078-0432.CCR-06-3039

74. Reiss KA, Herman JM, Armstrong D, Zahurak M, Fyles A, Brade A, et al. A final report of a phase I study of veliparib (ABT-888) in combination with low-dose fractionated whole abdominal radiation therapy (LDFWAR) in patients with advanced solid malignancies and peritoneal carcinomatosis with a dose escalation in ovarian and fallopian tube cancers. *Gynecol Oncol*. (2017) 144:486–90. doi: 10.1016/j.ygyno.2017.01.016
75. Chabot P, Hsia T-C, Ryu J-S, Gorbunova V, Belda-Iniesta C, Ball D, et al. Veliparib in combination with whole-brain radiation therapy for patients with brain metastases from non-small cell lung cancer: results of a randomized, global, placebo-controlled study. *J Neurooncol*. (2017) 131:105–15. doi: 10.1007/s11060-016-2275-x
76. Pollack IF, Jakacki RI, Blaney SM, Hancock ML, Kieran MW, Phillips P, et al. Phase I trial of imatinib in children with newly diagnosed brainstem and recurrent malignant gliomas: a pediatric brain tumor consortium report. *Neuro-oncology*. (2007) 9:145–60. doi: 10.1215/15228517-2006-031
77. Ree AH, Dueland S, Folkvord S, Hole KH, Seierstad T, Johansen M, et al. Vorinostat, a histone deacetylase inhibitor, combined with pelvic palliative radiotherapy for gastrointestinal carcinoma: the Pelvic Radiation and Vorinostat (PRAVO) phase 1 study. *Lancet Oncol*. (2010) 11:459–64. doi: 10.1016/S1470-2045(10)70058-9
78. Candelaria M, Cetina L, Pérez-Cárdenas E, de la Cruz-Hernández E, González-Fierro A, Trejo-Becerril C, et al. Epigenetic therapy and cisplatin chemoradiation in FIGO stage IIIB cervical cancer. *Eur J Gynaecol Oncol*. (2010) 31:386–91.
79. Le Tourneau C, Dreno B, Kirova Y, Grob JJ, Jouary T, Dutriaux C, et al. First-in-human phase I study of the DNA-repair inhibitor DT01 in combination with radiotherapy in patients with skin metastases from melanoma. *Br J Cancer*. (2016) 114:1199–205. doi: 10.1038/bjc.2016.120
80. Tell G, Fantini D, Quadrifoglio F. Understanding different functions of mammalian AP endonuclease (APE1) as a promising tool for cancer treatment. *Cell Mol Life Sci*. (2010) 67:3589–608. doi: 10.1007/s00018-010-0486-4
81. Naidu MD, Mason JM, Pica RV, Fung H, Peña LA. Radiation resistance in glioma cells determined by DNA damage repair activity of Ape1/Ref-1. *J Radiat Res*. (2010) 51:393–404. doi: 10.1269/jrr.09077
82. Xiang D-B, Chen Z-T, Wang D, Li M-X, Xie J-Y, Zhang Y-S, et al. Chimeric adenoviral vector Ad5/F35-mediated APE1 siRNA enhances sensitivity of human colorectal cancer cells to radiotherapy *in vitro* and *in vivo*. *Cancer Gene Ther*. (2008) 15:625–35. doi: 10.1038/cgt.2008.30
83. Mohiuddin IS, Kang MH. DNA-PK as an emerging therapeutic target in cancer. *Front Oncol*. (2019) 9:635. doi: 10.3389/fonc.2019.00635
84. Ismail IH, Mårtensson S, Moshinsky D, Rice A, Tang C, Howlett A, McMahon G, Hammarsten O. SU11752 inhibits the DNA-dependent protein kinase and DNA double-strand break repair resulting in ionizing radiation sensitization. *Oncogene*. (2004) 23:873–82. doi: 10.1038/sj.onc.1207303
85. Shinohara ET, Geng L, Tan J, Chen H, Shir Y, Edwards E, et al. DNA-dependent protein kinase is a molecular target for the development of noncytotoxic radiation-sensitizing drugs. *Cancer Res*. (2005) 65:4987–992. doi: 10.1158/0008-5472.CAN-04-4250
86. Davidson D, Amrein L, Panasci L, Aloyz R. Small molecules, inhibitors of DNA-PK, targeting DNA repair, and beyond. *Front Pharmacol*. (2013) 4:5. doi: 10.3389/fphar.2013.00005
87. Brown JM. beware of clinical trials of DNA repair inhibitors. *Int J Radiat Oncol Biol Phys*. (2019) 103:1182–3. doi: 10.1016/j.ijrobp.2018.11.063
88. Mau-Sorensen M, van Bussel M, Kuipers M, Nielsen DL, Verheul HM, Aftimos P, et al. 1845PSafety, clinical activity and pharmacological biomarker evaluation of the DNA-dependent protein kinase (DNA-PK) inhibitor M3814: results from two phase I trials. *Ann Oncol*. (2018) 29. doi: 10.1093/annonc/mdy303.015
89. Li Y-H, Wang X, Pan Y, Lee D-H, Chowdhury D, Kimmelman AC. Inhibition of non-homologous end joining repair impairs pancreatic cancer growth and enhances radiation response. *PLoS ONE*. (2012) 7:e39588. doi: 10.1371/journal.pone.0039588
90. Gavande NS, VanderVere-Carozza PS, Hinshaw HD, Jalal SI, Sears CR, Pawelczak KS, et al. DNA repair targeted therapy: The past or future of cancer treatment? *Pharmacol Ther*. (2016) 160:65–83. doi: 10.1016/j.pharmthera.2016.02.003
91. Munster PN, Mahipal A, Nemunaitis JJ, Mita MM, Paz-Ares LG, Massard C, et al. Phase I trial of a dual TOR kinase and DNA-PK inhibitor (CC-115) in advanced solid and hematologic cancers. *JCO*. (2016) 34:2505. doi: 10.1200/JCO.2016.34.15_suppl.2505
92. Hanahan D, Weinberg RA. The hallmarks of cancer. *Cell*. (2000) 100:57–70. doi: 10.1016/S0092-8674(00)81683-9
93. Qiao B, Kerr M, Groselj B, Teo MTW, Knowles MA, Bristow RG, et al. Imatinib radiosensitizes bladder cancer by targeting homologous recombination. *Cancer Res*. (2013) 73:1611–20. doi: 10.1158/0008-5472.CAN-12-1170
94. Shrivastav M, De Haro LP, Nickoloff JA. Regulation of DNA double-strand break repair pathway choice. *Cell Res*. (2008) 18:134–47. doi: 10.1038/cr.2007.111
95. Westphal CH, Hoyes KP, Canman CE, Huang X, Kastan MB, Hendry JH, et al. Loss of atm radiosensitizes multiple p53 null tissues. *Cancer Res*. (1998) 58:5637–9.
96. Rainey MD, Charlton ME, Stanton RV, Kastan MB. Transient inhibition of ATM kinase is sufficient to enhance cellular sensitivity to ionizing radiation. *Cancer Res*. (2008) 68:7466–74. doi: 10.1158/0008-5472.CAN-08-0763
97. Hickson I, Zhao Y, Richardson CJ, Green SJ, Martin NMB, Orr AI, et al. Identification and characterization of a novel and specific inhibitor of the ataxia-telangiectasia mutated kinase ATM. *Cancer Res*. (2004) 64:9152–9. doi: 10.1158/0008-5472.CAN-04-2727
98. Golding SE, Rosenberg E, Adams BR, Wignarajah S, Beckta JM, O'Connor MJ, et al. Dynamic inhibition of ATM kinase provides a strategy for glioblastoma multiforme radiosensitization and growth control. *Cell Cycle*. (2012) 11:1167–73. doi: 10.4161/cc.11.6.19576
99. Torok JA, Oh P, Castle KD, Reinsvold M, Ma Y, Luo L, et al. Deletion of Atm in tumor but not endothelial cells improves radiation response in a primary mouse model of lung adenocarcinoma. *Cancer Res*. (2019) 79:773–82. doi: 10.1158/0008-5472.CAN-17-3103
100. Andarawewa KL, Paupert J, Pal A, Barcellos-Hoff MH. New rationales for using TGFbeta inhibitors in radiotherapy. *Int J Radiat Biol*. (2007) 83:803–11. doi: 10.1080/09553000701711063
101. Kirshner M, Rathavs M, Nizan A, Essers J, Kanaar R, Shiloh Y, et al. Analysis of the relationships between ATM and the Rad54 paralogs involved in homologous recombination repair. *DNA Repair*. (2009) 8:253–61. doi: 10.1016/j.dnarep.2008.11.005
102. Golding SE, Rosenberg E, Neill S, Dent P, Povirk LF, Valerie K. Extracellular signal-related kinase positively regulates ataxia telangiectasia mutated, homologous recombination repair, and the DNA damage response. *Cancer Res*. (2007) 67:1046–53. doi: 10.1158/0008-5472.CAN-06-2371
103. Minchom A, Aversa C, Lopez J. Dancing with the DNA damage response: next-generation anti-cancer therapeutic strategies. *Ther Adv Med Oncol*. (2018) 10:1758835918786658. doi: 10.1177/1758835918786658
104. Rundle S, Bradbury A, Drew Y, Curtin NJ. Targeting the ATR-CHK1 axis in cancer therapy. *Cancers*. (2017) 9:E41. doi: 10.3390/cancers9050041
105. Vendetti FP, Lau A, Schamus S, Conrads TP, O'Connor MJ, Bakkenist CJ. The orally active and bioavailable ATR kinase inhibitor AZD6738 potentiates the anti-tumor effects of cisplatin to resolve ATM-deficient non-small cell lung cancer *in vivo*. *Oncotarget*. (2015) 6:44289–305. doi: 10.18632/oncotarget.6247
106. Dupré A, Boyer-Chatenet L, Sattler RM, Modi AP, Lee J-H, Nicolette ML, et al. A forward chemical genetic screen reveals an inhibitor of the Mre11-Rad50-Nbs1 complex. *Nat Chem Biol*. (2008) 4:119–25. doi: 10.1038/nchembio.63
107. Kuroda S, Urata Y, Fujiwara T. Ataxia-telangiectasia mutated and the Mre11-Rad50-NBS1 complex: promising targets for radiosensitization. *Acta Med Okayama*. (2012) 66:83–92. doi: 10.18926/AMO/48258
108. Quanz M, Berthault N, Roulin C, Roy M, Herbette A, Agrario C, et al. Small-molecule drugs mimicking DNA damage: a new strategy for sensitizing tumors to radiotherapy. *Clin Cancer Res*. (2009) 15:1308–16. doi: 10.1158/1078-0432.CCR-08-2108
109. Quanz M, Chassoux D, Berthault N, Agrario C, Sun J-S, Dutreix M. Hyperactivation of DNA-PK by double-strand break mimicking

molecules disorganizes DNA damage response. *PLoS ONE*. (2009) 4:e6298. doi: 10.1371/journal.pone.0006298
110. Croset A, Cordelières FP, Berthault N, Buhler C, Sun J-S, Quanz M, et al. Inhibition of DNA damage repair by artificial activation of PARP with siDNA. *Nucleic Acids Res*. (2013) 41:7344–55. doi: 10.1093/nar/gkt522
111. Biau J, Chautard E, Berthault N, de Koning L, Court F, Pereira B, et al. Combining the DNA repair inhibitor Dbait with radiotherapy for the treatment of high grade glioma: efficacy and protein biomarkers of resistance in preclinical models. *Front Oncol*. (2019) 9:549. doi: 10.3389/fonc.2019.00549
112. Groselj B, Sharma NL, Hamdy FC, Kerr M, Kiltie AE. Histone deacetylase inhibitors as radiosensitisers: effects on DNA damage signalling and repair. *Br J Cancer*. (2013) 108:748–54. doi: 10.1038/bjc.2013.21
113. Park Y, Chui MH, Suryo Rahmanto Y, Yu Z-C, Shamanna RA, Bellani MA, et al. Loss of ARID1A in tumor cells renders selective vulnerability to combined ionizing radiation and PARP inhibitor therapy. *Clin Cancer Res*. (2019) 25:5584–94. doi: 10.1158/1078-0432.CCR-18-4222
114. Blattmann C, Oertel S, Ehemann V, Thiemann M, Huber PE, Bischof M, et al. Enhancement of radiation response in osteosarcoma and rhabdomyosarcoma cell lines by histone deacetylase inhibition. *Int J Radiat Oncol Biol Phys*. (2010) 78:237–45. doi: 10.1016/j.ijrobp.2010.03.010
115. Lee J-H, Choy ML, Ngo L, Foster SS, Marks PA. Histone deacetylase inhibitor induces DNA damage, which normal but not transformed cells can repair. *Proc Natl Acad Sci USA*. (2010) 107:14639–44. doi: 10.1073/pnas.1008522107
116. Konsoula Z, Cao H, Velena A, Jung M. Adamantanyl-histone deacetylase inhibitor H6CAHA exhibits favorable pharmacokinetics and augments prostate cancer radiation sensitivity. *Int J Radiat Oncol Biol Phys*. (2011) 79:1541–8. doi: 10.1016/j.ijrobp.2010.11.057
117. Munshi A, Tanaka T, Hobbs ML, Tucker SL, Richon VM, Meyn RE. Vorinostat, a histone deacetylase inhibitor, enhances the response of human tumor cells to ionizing radiation through prolongation of gamma-H2AX foci. *Mol Cancer Ther*. (2006) 5:1967–74. doi: 10.1158/1535-7163.MCT-06-0022
118. Yu W, Gu K, Yu Z, Yuan D, He M, Ma N, et al. Sorafenib potentiates irradiation effect in hepatocellular carcinoma *in vitro* and *in vivo*. *Cancer Lett*. (2013) 329:109–17. doi: 10.1016/j.canlet.2012.10.024
119. Raju U, Riesterer O, Wang Z-Q, Molkentine DP, Molkentine JM, Johnson FM, et al. Dasatinib, a multi-kinase inhibitor increased radiation sensitivity by interfering with nuclear localization of epidermal growth factor receptor and by blocking DNA repair pathways. *Radiother Oncol*. (2012) 105:241–9. doi: 10.1016/j.radonc.2012.08.010
120. Khurshid H, Dipetrillo T, Ng T, Mantripragada K, Birnbaum A, Berz D, et al. A phase I study of dasatinib with concurrent chemoradiation for stage III non-small cell lung cancer. *Front Oncol*. (2012) 2:56. doi: 10.3389/fonc.2012.00056
121. Kroeze SGC, Fritz C, Hoyer M, Lo SS, Ricardi U, Sahgal A, et al. Toxicity of concurrent stereotactic radiotherapy and targeted therapy or immunotherapy: a systematic review. *Cancer Treatment Rev*. (2017) 53:25–37. doi: 10.1016/j.ctrv.2016.11.013
122. Liccardi G, Hartley JA, Hochhauser D. EGFR nuclear translocation modulates DNA repair following cisplatin and ionizing radiation treatment. *Cancer Res*. (2011) 71:1103–14. doi: 10.1158/0008-5472.CAN-10-2384
123. Ang KK, Berkey BA, Tu X, Zhang H-Z, Katz R, Hammond EH, et al. Impact of epidermal growth factor receptor expression on survival and pattern of relapse in patients with advanced head and neck carcinoma. *Cancer Res*. (2002) 62:7350–6.
124. Bonner JA, Harari PM, Giralt J, Azarnia N, Shin DM, Cohen RB, et al. Radiotherapy plus cetuximab for squamous-cell carcinoma of the head and neck. *N Engl J Med*. (2006) 354:567–78. doi: 10.1056/NEJMoa 053422
125. Martins RG, Parvathaneni U, Bauman JE, Sharma AK, Raez LE, Papagikos MA, et al. Cisplatin and radiotherapy with or without erlotinib in locally advanced squamous cell carcinoma of the head and neck: a randomized phase II trial. *J Clin Oncol*. (2013) 31:1415–21. doi: 10.1200/JCO.2012.46.3299
126. Sato Y, Ebara T, Sunaga N, Takahashi T, Nakano T. Interaction of radiation and gefitinib on a human lung cancer cell line with mutant EGFR gene *in vitro*. *Anticancer Res*. (2012) 32:4877–81.
127. Aziz K, Nowsheen S, Pantelias G, Iliakis G, Gorgoulis VG, Georgakilas AG. Targeting DNA damage and repair: embracing the pharmacological era for successful cancer therapy. *Pharmacol Ther*. (2012) 133:334–50. doi: 10.1016/j.pharmthera.2011.11.010
128. Mitchell JB, Choudhuri R, Fabre K, Sowers AL, Citrin D, Zabludoff SD, et al. *In vitro* and *in vivo* radiation sensitization of human tumor cells by a novel checkpoint kinase inhibitor, AZD7762. *Clin Cancer Res*. (2010) 16:2076–84. doi: 10.1158/1078-0432.CCR-09-3277
129. Zabludoff SD, Deng C, Grondine MR, Sheehy AM, Ashwell S, Caleb BL, et al. AZD7762, a novel checkpoint kinase inhibitor, drives checkpoint abrogation and potentiates DNA-targeted therapies. *Mol Cancer Ther*. (2008) 7:2955–66. doi: 10.1158/1535-7163.MCT-08-0492
130. Zeng L, Beggs RR, Cooper TS, Weaver AN, Yang ES. Combining Chk1/2 inhibition with cetuximab and radiation enhances *in vitro* and *in vivo* cytotoxicity in head and neck squamous cell carcinoma. *Mol Cancer Ther*. (2017) 16:591–600. doi: 10.1158/1535-7163.MCT-16-0352
131. Goldstein M, Kastan MB. The DNA damage response: implications for tumor responses to radiation and chemotherapy. *Annu Rev Med*. (2015) 66:129–43. doi: 10.1146/annurev-med-081313-121208
132. Ciccia A, Elledge SJ. The DNA damage response: making it safe to play with knives. *Mol Cell*. (2010) 40:179–204. doi: 10.1016/j.molcel.2010.09.019
133. Morgan MA, Parsels LA, Zhao L, Parsels JD, Davis MA, Hassan MC, et al. Mechanism of radiosensitization by the Chk1/2 inhibitor AZD7762 involves abrogation of the G2 checkpoint and inhibition of homologous recombinational DNA repair. *Cancer Res*. (2010) 70:4972–81. doi: 10.1158/0008-5472.CAN-09-3573
134. Mueller S, Haas-Kogan DA. WEE1 kinase as a target for cancer therapy. *JCO*. (2015) 12:3159–64. doi: 10.1200/JCO.2015.62.2290
135. Bridges KA, Hirai H, Buser CA, Brooks C, Liu H, et al. MK-1775, a novel Wee1 kinase inhibitor, radiosensitizes p53-defective human tumor cells. *Clin Cancer Res*. (2011) 17:5638–48. doi: 10.1158/1078-0432.CCR-11-0650
136. Caretti V, Hiddingh L, Lagerweij T, Schellen P, Koken PW, Hulleman E, et al. WEE1 kinase inhibition enhances the radiation response of diffuse intrinsic pontine gliomas. *Mol Cancer Ther*. (2013) 12:141–50. doi: 10.1158/1535-7163.MCT-12-0735
137. Ko EC, Formenti SC. Radiation therapy to enhance tumor immunotherapy: a novel application for an established modality. *Int J Radiat Biol*. (2019) 95:936–9. doi: 10.1080/09553002.2019.1623429
138. Golden EB, Apetoh L. Radiotherapy and immunogenic cell death. *Semin Radiat Oncol*. (2015) 25:11–7. doi: 10.1016/j.semradonc.2014.07.005
139. Ahmad SS, Crittenden MR, Tran PT, Kluetz PG, Blumenthal GM, Bulbeck H, et al. Clinical development of novel drug-radiotherapy combinations. *Clin Cancer Res*. (2019) 25:1455–61. doi: 10.1158/1078-0432.CCR-18-2466

Conflict of Interest: MD is the cofounder of DNA Therapeutics/Onxeo, which is involved in DT01 development.

The remaining authors declare that the research was conducted in the absence of any commercial or financial relationships that could be construed as a potential conflict of interest.

Copyright © 2019 Biau, Chautard, Verrelle and Dutreix. This is an open-access article distributed under the terms of the Creative Commons Attribution License (CC BY). The use, distribution or reproduction in other forums is permitted, provided the original author(s) and the copyright owner(s) are credited and that the original publication in this journal is cited, in accordance with accepted academic practice. No use, distribution or reproduction is permitted which does not comply with these terms.

frontiers in Oncology

REVIEW
published: 05 November 2019
doi: 10.3389/fonc.2019.01152

Optical Imaging Approaches to Investigating Radiation Resistance

*Sina Dadgar and Narasimhan Rajaram**

Department of Biomedical Engineering, University of Arkansas, Fayetteville, AR, United States

Radiation therapy is frequently the first line of treatment for over 50% of cancer patients. While great advances have been made in improving treatment response rates and reducing damage to normal tissue, radiation resistance remains a persistent clinical problem. While hypoxia or a lack of tumor oxygenation has long been considered a key factor in causing treatment failure, recent evidence points to metabolic reprogramming under well-oxygenated conditions as a potential route to promoting radiation resistance. In this review, we present recent studies from our lab and others that use high-resolution optical imaging as well as clinical translational optical spectroscopy to shine light on the biological basis of radiation resistance. Two-photon microscopy of endogenous cellular metabolism has identified key changes in both mitochondrial structure and function that are specific to radiation-resistant cells and help promote cell survival in response to radiation. Optical spectroscopic approaches, such as diffuse reflectance and Raman spectroscopy have demonstrated functional and molecular differences between radiation-resistant and sensitive tumors in response to radiation. These studies have uncovered key changes in metabolic pathways and present a viable route to clinical translation of optical technologies to determine radiation resistance at a very early stage in the clinic.

Keywords: raman spectroscopy, diffuse reflectance spectroscopy, optical metabolic imaging, nonlinear optical microscopy, mitochondrial organization, radiation resistance

OPEN ACCESS

Edited by:
Ira Ida Skvortsova,
Innsbruck Medical University, Austria

Reviewed by:
Nikolaos Patsoukis,
Harvard Medical School,
United States
Pavithra Viswanath,
University of California, San Francisco,
United States

****Correspondence:***
Narasimhan Rajaram
nrajaram@uark.edu

Specialty section:
This article was submitted to Radiation Oncology, a section of the journal Frontiers in Oncology

Received: *29 July 2019*
Accepted: *16 October 2019*
Published: *05 November 2019*

Citation:
Dadgar S and Rajaram N (2019) Optical Imaging Approaches to Investigating Radiation Resistance. Front. Oncol. 9:1152. doi: 10.3389/fonc.2019.01152

INTRODUCTION

About half of cancer patients from all cancer types are treated with radiation therapy either followed by or concurrently with surgery, chemotherapy, or other forms (1). However, despite the recent advances in targeted radiation therapy, several patients subsequently experience loco-regional recurrence due to acquired or intrinsic radiation resistance. The current standard of care to determine radiation response is an anatomical assessment of tumor volume shrinkage. This evaluation is typically performed 6–8 weeks after completion of treatment using X-ray Computed Tomography (CT) or Magnetic Resonance Imaging (MRI). There are currently no methods to determine radiation response either during or immediately after treatment. An early determination of radiation resistance could help physicians modify the radiation dosage to improve response rates and hence quality of life. The development of methods to identify radiation-resistant tumors early requires a better understanding of the biological mechanisms promoting radiation resistance.

Ionizing radiation functions by producing free radicals in cancer cells either directly in the DNA or indirectly in other molecules, primarily water (H_2O). These radiation-induced free radicals, in the presence of O_2, can generate peroxy radicals (DNA-OO·) capable of breaking chemical bonds

and initiating a series of events which lead to DNA modification, and cell death (damage fixation). In contrast, lack of O_2 leads to the reduction of free radicals in DNA and restoration of the original form of DNA (DNA-H) leading to cancer cell survival (2–4). Landmark studies in clinical head and neck cancer and soft-tissue sarcoma found that pre-treatment oxygenation levels were predictive of treatment response and disease-free survival (5–7). This important role of oxygen is the rationale for fractionated radiation therapy (2 Gy/day for 6–7 weeks), which is believed to re-oxygenate and radio-sensitize former hypoxic cells and hence, cause cell death via damage fixation (8–10). However, recent work has started to uncover a possible role for radiation-induced reoxygenation in also promoting radiation resistance through hypoxia-inducible factor (HIF).

Hypoxia leads to stabilization of HIF-1 (11). While HIF-1 expression is inhibited under oxygenated conditions via prolyl hydroxylases (PHDs), its transcription is significantly upregulated under hypoxic conditions (3, 12, 13). However, radiation-induced tumor reoxygenation can lead to activation of HIF-1 as well-through accumulation of reactive oxygen species (ROS), which is necessary and sufficient to stabilize HIF-1 (14). Nuclear accumulation of HIF-1 in response to ROS has been shown to promote endothelial cell survival and hence promote radiation resistance (15, 16). In a tumor bearing window chamber model, Moeller et al. demonstrated an increase in ROS during radiation-induced reoxygenation. Additionally, they showed that injecting hydrogen peroxide (H_2O_2) into the window chamber lead to an increase in HIF-1 expression (15). HIF-1 directly targets several glycolytic genes and leads to increased glucose catabolism under oxygenated conditions (17–20). HIF-1 transactivates pyruvate dehydrogenase kinase (PDK), which inhibits pyruvate dehydrogenase and shunts pyruvate away from the mitochondria resulting in glucose catabolism to lactate even under oxygenated conditions (17, 18). Inhibition of HIF-1 and subsequent inhibition of PDK-1 restores glucose flux toward mitochondria and increases O_2 consumption (21). Other studies have shown that HIF-1 and pyruvate kinase M2 exist in a positive feedback loop that enhances glycolysis under aerobic conditions (19, 20).

Zhong et al. demonstrated that scavenging ROS resulted in a reduction in post-radiation aerobic glycolysis without reducing the magnitude of reoxygenation (22).

The switch to increased glucose catabolism can promote radiation resistance through utilization of the pentose phosphate shunt (PPP) to maintain the NADPH-glutathione buffer and hence scavenge radiation-induced ROS. Inhibition of glucose flux through the PPP in combination with 2 Gy of radiation treatment significantly decreased cancer cell proliferation, especially in radiation-resistant cells (23). Increased glucose catabolism can also lead to increased production of lactate, an important ROS scavenger, leading to decreased radiation sensitivity (24, 25). Thus, in addition to being key hallmarks in the development of cancer, tumor oxygenation (or hypoxia) and metabolism play a significant role in the development of radiation resistance. Technologies that are sensitive to these key hallmarks and that can measure them both at the "bench" and "bedside" can provide powerful tools to shed light on radiation resistance.

Optical imaging can provide non-destructive and quantitative methods to reveal morphological and biochemical changes within cells and tissue across length scales in response to radiation therapy. Due to its non-destructive nature, optical imaging can be used to longitudinally monitor dynamic biological changes with high resolution to investigate the underlying mechanisms that promote radiation resistance. Given the low cost and non-ionizing nature of the light used, optical techniques are also well-positioned for clinical translation, especially for accessible tumors of breast, skin, oral cavity, and uterine-cervix. In addition, same instrumentation and quantitative models are frequently used to extract meaningful information from pre-clinical animal models. This review highlights recent work that used non-linear optical microscopy and diffuse optical spectroscopy to shed light on differences between radiation-resistant and sensitive cancer cells. Specifically, we highlight studies that identified differences in oxygenation or reoxygenation trends post-radiation therapy as well as those that investigate metabolic and molecular changes in the post-radiation tumor milieu. These studies encompass models ranging from *in vitro* cell culture to *in vivo* animal studies and indicate the great potential of optical imaging in the sphere of biological investigations of radiation resistance and the development of clinically translational optical technologies to benefit patients receiving radiation therapy.

OPTICAL MICROSCOPY

Non-linear microscopy approaches, such as two-photon microscopy present numerous advantages over conventional single-photon microscopy (26). Because autofluorescence is generated through simultaneous absorption of two photons, the excitation wavelengths used are at twice the single-photon excitation wavelength and half the energy. Doubling the single-photon excitation wavelength usually places the non-linear excitation wavelength in the near-infrared range, which allows light to penetrate deeper within tissue (27). Additionally, the localization of autofluorescence to just the focal point of the objective provides an efficient method for rejecting out-of-focus light and minimizing photodamage to the sample. In this review, we discuss how two-photon excited fluorescence (TPEF) from two key metabolic cofactors—nicotinamide and flavin adenine dinucleotides (NADH and FAD, respectively), can provide a non-destructive metabolic profile of cells and how these approaches have been utilized to study the metabolic response to therapy in radiation-resistant and sensitive cancer cells.

Cellular Metabolism

Non-linear optical microscopy is well-suited to provide non-invasive high-resolution 3D images of mitochondrial structure and function within live cells, tissues, and animals (27, 28). Through two-photon excited fluorescence (TPEF), the intrinsic fluorescence of nicotinamide and flavin adenine dinucleotides (NADH and FAD, respectively) can be detected without the aid of exogenous dyes (26, 29). Based on the autofluorescence of NADH and FAD, the optical reduction-oxidation (or redox) state of cells can be quantified as FAD/(NADH+FAD). This optical

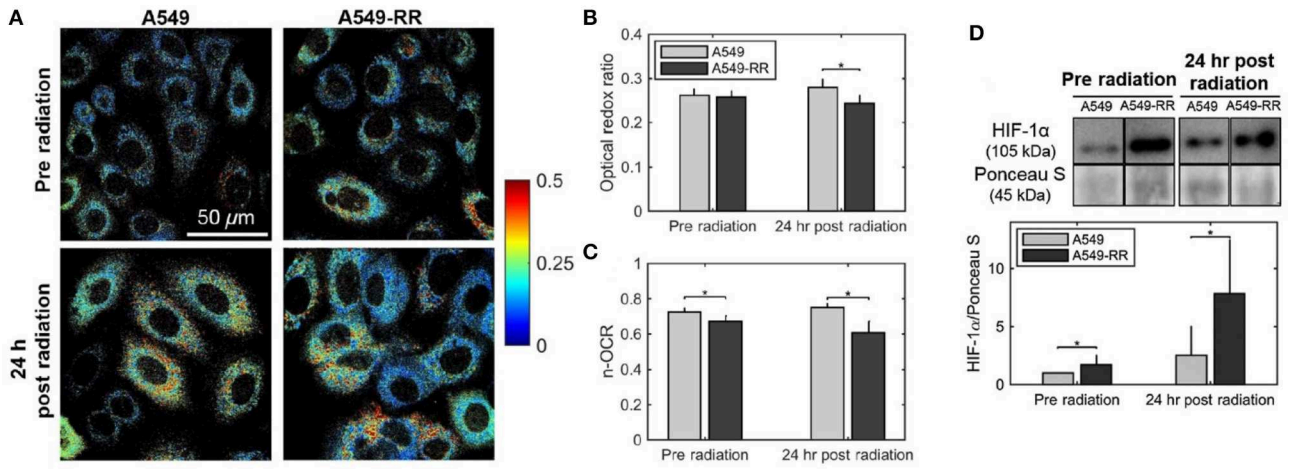

FIGURE 1 | Optical redox ratio is sensitive to radiation-induced changes in cellular metabolism. Radiation causes a decrease in the optical redox ratio after 24 h in the radiation-resistant cells, indicating increased glycolytic metabolism. **(A)** Representative redox images of parental and radiation resistant A549 cells at baseline prior to radiation and 24 h after 2 Gy of radiation. **(B)** Quantification of redox ratio images indicates a statistically significant decrease in the optical redox ratio 24 h after radiation in the A549-RR cells compared with the parental A549 cells ($p = 0.01$). **(C)** Differences in the n-OCR (calculated as OCR/PPR) are consistent with the optical redox ratio. PPR refers to the proton production rate, which is equivalent to the extracellular acidification rate (ECAR). **(D)** Radiation causes a significant increase in HIF-1 in the radiation-resistant cells 24 h after radiation. Western blots of HIF-1 protein expression demonstrate statistically significant differences between A549 and A549-RR cells at baseline and 24 h after radiation, indicating reoxygenation-induced HIF-1 expression in the A549-RR cells. Asterisks placed above bars indicate statistical significance. Error bars in **(B,C)**, and **(D)** represent standard deviation of the mean plate value. Adapted with permission from Alhallak et al. (38).

redox ratio (ORR) has been shown to be significantly correlated with mass spectrometry-based measurements of $NAD^+/(NAD^+ + NADH)$, and can thus reveal the specific metabolic pathways engaged within a cell (30). Specifically, an increase in ORR has been attributed to increased oxidative phosphorylation because of the oxidation of NADH to non-fluorescent NAD^+ and $FADH_2$ to fluorescent FAD. On the other hand, hypoxia-like conditions that drive a buildup of NADH due to the inability to convert to NAD^+ and increased glucose catabolism has been shown to decrease the ORR (30, 31). Recent work from separate groups has demonstrated that the optical redox ratio is sensitive to dynamic changes in oxygen consumption and can provide metabolic assessments comparable to those of the Seahorse metabolic flux analyzer (32, 33). The optical redox ratio has been used to create metabolic image maps of key organs (34), such as the heart and brain, identify metabolic changes associated with cancer progression (35, 36), determine cellular response to therapy (37–39), and discover a relationship between metastatic potential and cellular metabolism (32, 40, 41).

Alhallak et al. determined the early metabolic alterations in response to radiation in human A549 lung cancer cells and an isogenic radiation-resistant clone (38). This clone was obtained by repeated exposure of parental radiation-sensitive human lung cancer cell line (A549) to ionizing radiation (25 fractions of 2.2 Gy every 3 days). Although there was no significant difference in ORR of radiation-resistant and -sensitive cells prior to administration of radiation, there was a significant decrease in ORR of radiation-resistant cells 24 h after radiation, which was consistent with Seahorse-based quantification of the normalized oxygen consumption rate (n-OCR) (**Figure 1**). The observed results indicate that the radiation-resistant cancer cells have decreased levels of oxygen consumption both at baseline and post-radiation and resort to increased glucose catabolism after radiation to potentially reduce ROS-induced toxicity. Interestingly, this radiation-induced decrease in the optical redox ratio was also associated with a large increase in the HIF-1 expression in the radiation-resistant A549 clone.

A subsequent by Lee et al. investigated metabolic changes in response to HIF-1 inhibition to determine if the changes in optical redox ratio post-radiation were indeed mediated by HIF-1 and a mechanism to avoid ROS-induced toxicity (39). They used multiphoton microscopy to determine the ORR of A549-RR prior to and post-treatment with YC-1, an established HIF-1 inhibitor. Treatment with YC-1 for 24 h resulted in a significant increase in the ORR compared with baseline, with a concomitant increase in mitochondrial ROS (**Figure 2**), a decrease in reduced glutathione and a decrease in glucose uptake (39). These results support the conclusion also reached by Furdui and colleagues who found increased glucose uptake that was utilized within the pentose phosphate pathway (PPP) to maintain the NADPH-glutathione buffer. This buffer helps scavenge radiation-induced ROS and hence promote radiation resistance (23). These results demonstrate the enormous potential of autofluorescence microscopy to not only provide clinically translational biomarkers of cellular response to therapy but also create opportunities for investigating radiation biology in live cells and animals at very high resolution.

Lifetime Imaging

Fluorescent lifetime imaging microscopy (FLIM) measures the average time that a molecule spends in an excited state prior to emission. One significant advantage of FLIM over measurements

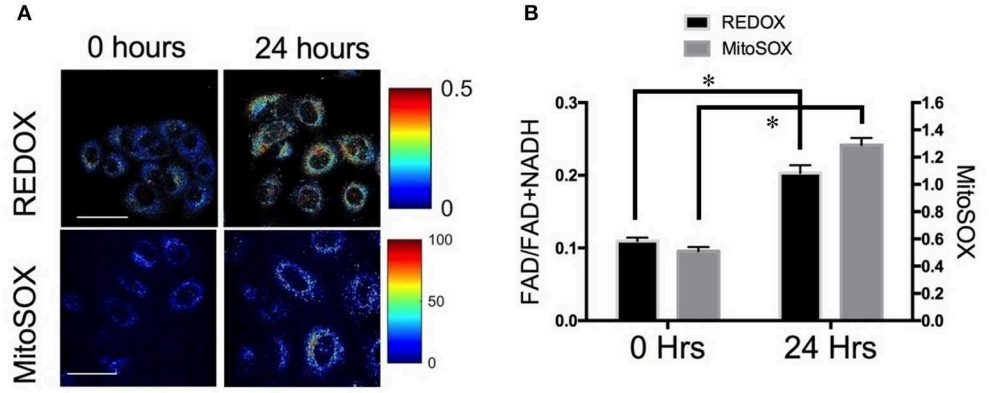

FIGURE 2 | Optical redox ratio (ORR) is sensitive to changes in reactive oxygen species (ROS) **(A)** Representative images and **(B)** quantification of redox ratio and MitoSOX, a fluorescent reporter of mitochondrial ROS illustrates significant differences before and 24 h after treatment with YC-1. *$p < 0.05$. Adapted with permission from Lee et al. (39).

of endogenous autofluorescence is that lifetime is independent of the fluorophore concentration. The lifetime of fluorophores, such as NADH and FAD depend on whether they are free or bound to a protein complex. For instance, the lifetime of NADH autofluorescence is shorter (∼0.4 ns) when free and longer (∼1 ns) when bound to protein complexes, such as malate dehydrogenase and lactate dehydrogenase while the lifetime of FAD autofluorescence is longer when free and shorter when bound to protein complexes, such as alpha-lipoamide dehydrogenase (42–46). By quantifying the ratio of free to protein-bound NADH and their respective lifetimes, FLIM can be used to identify the metabolic state of cells and tissue (42, 47–49). A recent study investigated the application of FLIM in radiation research (50). Campos et al. first treated human cancer cells and normal oral keratinocytes (NOK) with 10 Gy of radiation and recorded the resultant metabolic changes using FLIM. As early as 30 min post treatment, there was a significant decrease in NADH lifetime of cancer cells while there was no change in NADH lifetime of the NOK cells.

Mitochondrial Organization

In addition to being the powerhouse of the cell, mitochondria are also critical to cell death pathways. The energy demands of a cell are maintained by a delicate balance between the rate of oxidative phosphorylation, tricarboxylic acid (TCA) cycle activity, structural changes to the mitochondrial network, and mitochondrial biogenesis. Mitochondria are continuously changing their organization through fission and fusion allowing for adaptation to different functional demands (51, 52). This dynamic mitochondrial network is sensitive to cell differentiation as well as oxygen and nutrient availability (30, 53–55). Fission is critical for mitochondrial biogenesis, cell division, and mitochondrial autophagy and manifests as numerous mitochondrial fragments. Fusion helps to maintain functionality through the sharing of proteins, genetic material, and metabolites and leads to the generation of interconnected mitochondria (56). Alterations to fusion-fission dynamics and hence the mitochondrial organization have been shown to be associated with several pathological conditions, including hypoxia-reoxygenation injury (57–59). Hypoxia-reoxygenation has been shown to result in a decrease in mitochondrial fusion and subsequent changes in length and shape of mitochondria (60). Targeting the changes in mitochondrial fusion and fission has been shown to protect cells from the effects of hypoxia-reoxygenation injury (61, 62). These studies of changes to mitochondrial structure in response to hypoxia-reoxygenation injury are highly relevant to radiation therapy due to the similarity in mechanisms generating oxidative stress. Radiation therapy leads to reoxygenation of previously hypoxic cells, thereby triggering a large production of mitochondrial ROS. The NADH autofluorescence images, which are used to calculate the optical redox ratio, can also be used to evaluate mitochondrial organization and specifically, fission and fusion. Specifically, Fourier-based power spectral density analysis of NADH autofluorescence images has been used to compute a metric termed mitochondrial clustering to quantify mitochondrial organization (30, 63). An increase in mitochondrial clustering was found during periods of increased glucose catabolism, such as hypoxia, resulting in more fragmented, or fissioned mitochondria. On the other hand, glutaminolysis was found to be associated with a decrease in mitochondrial clustering or more networked mitochondria (fusion). The same method was used to investigate mitochondrial structural dynamics in human skin *in vivo* (53). A recent study used an improved image processing method in the spatial domain to rapidly quantify the local fractal dimension (FD) within individual cells in response to radiation therapy (64). This analysis found a significant decrease in FD (or an increase in mitochondrial clustering) of radiation-resistant lung cancer cells between 12- and 24-h post-radiation compared with pre-radiation measurements. There were no significant changes in the radiation-sensitive cell population in response to radiation at any time point (**Figure 3**). The increased mitochondrial clustering observed here is consistent with the decreased optical redox ratio and increased glucose catabolism observed by Alhallak et al. using the same cancer cells (**Figure 1**) (38, 39).

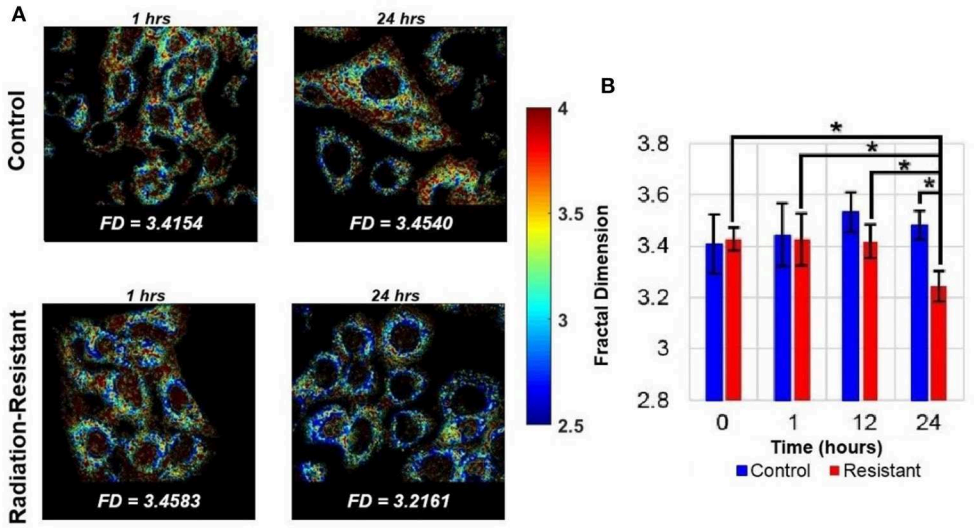

FIGURE 3 | Quantifying mitochondrial organization from NADH autofluorescence. **(A)** Representative FD maps corresponding to lung cancer cells of both control and radiation-resistant groups. The images were obtained at time periods of 1- and 24-h post radiation. **(B)** Summary data demonstrates significant temporal changes in the mitochondrial organization of radiation resistant cell line at 24 h [Reproduced with permission from Vargas et al. (64)]. *$p < 0.0001$.

OPTICAL SPECTROSCOPY

Optical spectroscopy is a fiber-based approach using non-ionizing radiation to non-destructively and non-invasively examine tissue of interest. Their low cost and small footprint make "optical spectroscopy methods" an excellent tool for conducting pilot studies in animal models of cancer and in humans. Since optical measurements using the fiber optic probe are non-invasive or minimally invasive (depending on the tissue site), the same subject can be monitored multiple times a day or over weeks to evaluate response to treatment. In addition to its obvious benefits as a clinical adjunct to existing clinical imaging modalities that cannot be used every day on patients, optical spectroscopy obviates the need for sacrificing large numbers of animals at several time points in longitudinal studies to evaluate treatment response. Here, we describe two specific techniques—diffuse reflectance and Raman spectroscopy—that have demonstrated potential for monitoring radiation response in tumors and studying the differences between resistant and sensitive tumors.

Diffuse Reflectance Spectroscopy

Diffuse reflectance or elastic scattering spectroscopy is an optical fiber- based technique for non-invasive interrogation of tissue. DRS uses optical fibers to deliver low-power non-ionizing light from a broad-band light source (400–650 nm) to tissue surface. The incident weak light undergoes multiple scattering and absorption events and is remitted back to the tissue surface as diffusely reflected light. Since the collected light has interacted non-destructively with the tissue, it provides a wealth of quantitative information about absorption and scattering, a combination of which is used for tissue pathology. Using models of light-tissue interaction that simulate the travel of photons within a scattering and absorbing medium, it is possible to quantify the diffusely reflected light and extract meaningful information related to tissue scattering as well as prominent tissue absorbers, such as oxygenated and deoxygenated hemoglobin (65–70). By exploiting the differences in light absorption spectra of oxygenated and deoxygenated hemoglobin, we can quantify the vascular oxygen content in tissue and obtain volume-averaged estimates of hemoglobin concentration. Measurements of vascular oxygenation have been shown to be concordant with microelectrode-based determinations of tissue oxygenation (71, 72) and immunohistochemical measurements of tumor hypoxia (73). Cell nuclei, mitochondria, and collagen are among the major contributors to light scattering in tissue and are known to undergo significant changes during disease progression (74). Taking advantage of these non-invasive and quantitative measurements, DRS has been used in several studies, with an eye toward clinical translation, for early cancer detection (75–77), prediction of response to therapy (78–80), and evaluation of tumor surgical margins (81). Given the importance of tumor oxygenation in radiation therapy, DRS can provide a non-invasive approach to quantify the biological response to radiation. Vishwanath et al. used DRS to longitudinally monitor tumor oxygenation and determine whether vascular oxygenation can identify treatment outcome earlier than tumor growth assays in a murine model of head and neck cancer treated with single dose of 39 Gy radiation. As early as 5 days post-radiation, radiation-responsive tumors exhibited faster and greater increase in vascular oxygenation compared with non-responding tumors (82). A more recent study from the same group found similar large increases in vascular oxygenation in both locally controlled and locally recurring tumors when the radiation dosage was split into five daily doses instead of a single

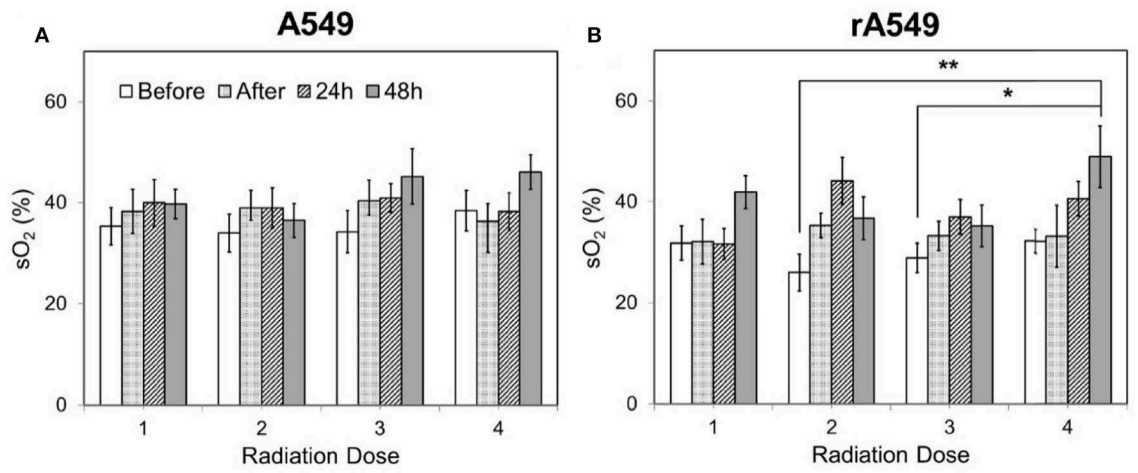

FIGURE 4 | Changes in vascular oxygen saturation across all four doses of radiation for radiation-sensitive **(A)** and resistant tumors **(B)**. Each radiation dose presents the mean sO_2 value for the following time points: 0 h, immediately after, 24 and 48 h post radiation. Data shown as mean ± SEM. *indicates $p < 0.05$ and **$p<0.01$. Adapted with permission from Diaz et al. (84).

dose. Additionally, the study also found that within the locally recurring group of tumors, a faster increase in reoxygenation during therapy was negatively correlated with recurrence time (83). Diaz et al. recently used DRS to study short-term changes in vascular oxygen saturation and hemoglobin concentration in radiation-sensitive and resistant A549 tumors treated with 4 dose fractions of 2 Gy (84), and also found significantly higher reoxygenation in radiation-resistant tumors 24 and 48 h after treatment (**Figure 4**).

This study was the first to report changes in reoxygenation kinetics measured in tumors which were established from a matched model of radiation-resistance. A matched model of radiation-resistance allows direct comparison of resistance-related features due to similar genetic background. While further studies are necessary to fully understand the mechanism of reoxygenation in the radiation-resistant tumors, results from other studies conducted using the same matched model of radiation resistance hint at the possibility of reduced oxygen consumption as a possible reason for the appearance of increased vascular oxygenation within the radiation-resistant tumors. Although the studies by Hu et al. (83) and Diaz et al. (84) used different cell lines in formation of tumor xenografts and treated them with different doses of radiation, they both showed that radiation-resistant tumors reoxygenate in response to radiation. These results are in agreement with a clinical study by Dietz et al. that used oxygen-sensing microelectrodes to measure pO_2 in the cervical lymph nodes of head and neck cancer patients and found that increased reoxygenation correlated with poor radiation response (85). This suggests that DRS is a sensitive detector of reoxygenation and can provide valuable information about radiation response.

Raman Spectroscopy

Raman spectroscopy offers the ability to probe biomolecular changes and visualize the complex molecular heterogeneity directly from cells and tissues (86, 87). Spontaneous Raman spectroscopy relies on the inelastic scattering of light, arising from its interactions with the biological specimen, to quantify the unique vibrational modes of molecules within its native context (88, 89). This exquisite chemical specificity of Raman spectroscopy has been exploited primarily within the realm of early detection of cancers of the oral cavity (90, 91), breast (92–98), cervix (99–101), and the brain (88, 102).

Recent studies have shown the presence of radiation-induced alterations in Raman spectral features and biochemical changes in cell lines with varying radiosensitivity (103, 104). The radiation response of single living cells has been studied to demonstrate dose-dependent changes in spectral features using principle component analysis (105, 106). In a series of human cancer cell lines treated with clinically relevant doses of radiation (<10 Gy), Matthews et al. found radiation-induced accumulation of intracellular glycogen in relatively radiation-resistant breast and lung cancer cell lines (107). Recent Raman spectroscopic studies on *ex vivo* lung and breast tumor xenografts have also identified elevated levels of glycogen in tumors exposed to a single, high radiation dose of 15 Gy (108, 109). These findings are of interest because separate non-imaging studies have identified a critical role for glycogen synthase kinase (GSK-3β) in the development of radiation resistance (110).

Radiation-induced changes in Raman spectra of excised cervical tumors have been shown to differentiate radiation responders from non-responders while pretreatment Raman spectra were incapable of predicting radiation response (111). In a recent study, Paidi et al. investigated whether radiation induced biomolecular changes detected by Raman spectroscopy could differentiate between radiation-resistant and sensitive tumors (112). They treated radiation-resistant and sensitive human head and neck (HN) and lung tumor xenografts with 2 Gy of radiation twice weekly for 2 weeks and conducted chemometric

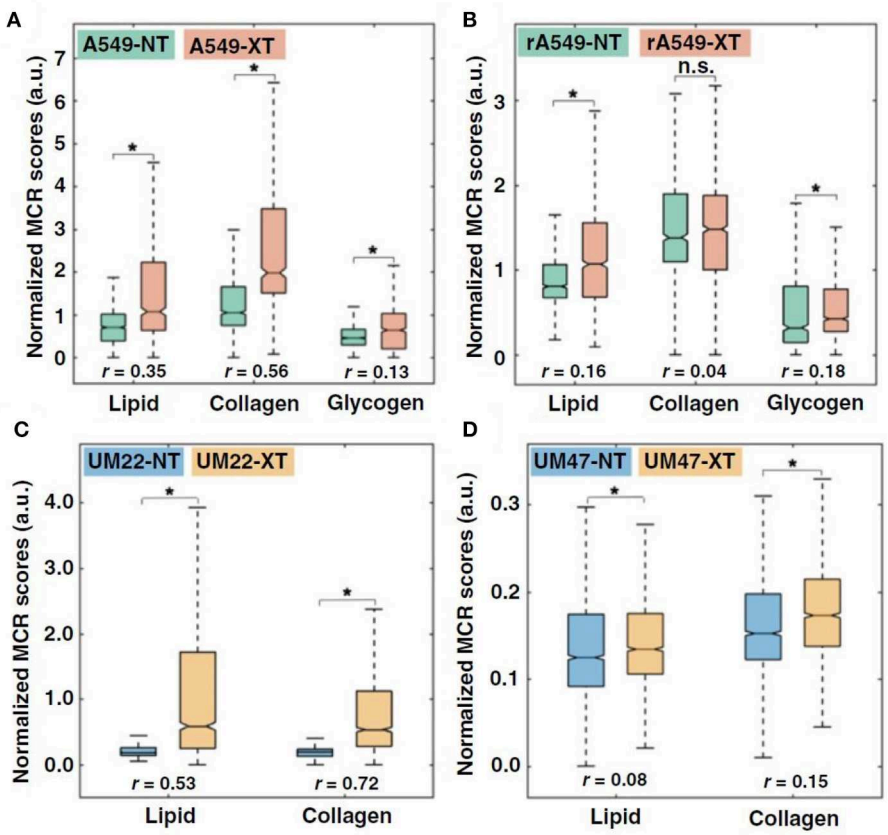

FIGURE 5 | Quantitative MCR-ALS analysis of Raman spectra. **(A,B)**, Boxplots of normalized scores of lipid-rich, collagen-rich, and glycogen-rich MCR-ALS loadings showing radiation-induced differences in sensitive lung tumors (A549-NT vs. A549-XT) (NT: not treated, XT: X-ray treated) **(A)** and radiation-induced differences in resistant lung tumors (rA549-NT vs. rA549-XT) **(B)**. **(C,D)**, Boxplots of normalized scores of lipid-rich and collagen-rich MCR-ALS loadings showing radiation-induced differences in sensitive head and neck tumors (UM-SCC-22B-NT vs. UM-SCC-22B-XT) **(C)** and radiation-induced differences in resistant head and neck tumors (UM-SCC-47-NT vs. UM-SCC-47-XT) **(D)**. The effect size (*r*), characterizing magnitude of differences between groups, is provided for each comparison. *$p < 0.001$. Adapted with permission from Paidi et al. (112).

analysis using multivariate curve resolution-alternating least squares (MCR-ALS) to uncover biomolecular changes in the tumor microenvironment. MCR-ALS recovers the pure spectral profiles of the chemical constituents of the tissue specimen without a priori information of the composition of the specimen (113). Paidi et al. found an increase in lipid, collagen, and glycogen (lung only) levels for both sensitive and resistant lung and head neck tumors that were treated with radiation, with a much larger increase in the lipid-rich and collagen-rich signatures in the radiation-sensitive tumors (**Figure 5**) (112). Comparison of the treated tumors alone (RS-XT vs. RR-XT) pointed to a significantly higher collagen content in the sensitive tumors compared to their resistant counterparts in both lung and HN models, which could be attributed to radiation-induced fibrosis (114, 115). The lipid results are intriguing due to other studies that have found elevated levels of fatty acid synthase (FASN) in radiation-resistant cells (23). These findings demonstrate that clear spectral distinctions exist between radiation-resistant and sensitive tumors, and that these distinctions are consistent with recent work seeking to uncover the molecular mechanisms of radiation resistance.

DISCUSSION AND FUTURE DIRECTION

The use of optical microscopy and diffuse optical spectroscopy presents exciting avenues for exploring radiation-induced changes across different length scales in cells and tissue. The technologies discussed in this review paper (summarized in **Table 1**)—although limited to superficial layers—are sensitive to two key hallmarks of tumors that play a critical role in radiation resistance—tumor hypoxia and metabolic reprogramming. While two-photon excited fluorescence from NADH and FAD can provide valuable information about specific metabolic pathways preferred by cells in response to radiation and the effect of such preferences on radiation resistance, Raman spectroscopy (or microscopy) can shed light on hitherto unknown biomolecular species in the tumor microenvironment that play a role in radiation resistance. Such studies have the potential to lead to new technologies

TABLE 1 | Comparison of optical microscopy and spectroscopy techniques for investigating radiation biology.

Technology	Source of contrast	Quantitative endpoints	Advantages	Limitations
Diffuse reflectance spectroscopy	Absorption and elastic scattering	Vascular oxygenation, vessel diameter, absorber concentration, tissue scattering	Non-invasive, low cost, portable	Limited penetration depth (1–2 mm); volume-averaged information
Raman spectroscopy	Raman (in-elastic) scattering	Contributions of individual molecular species (tissue-dependent)	High biomolecular specificity	Complex data analysis to extract meaningful biological information; limited penetration depth (1–2 mm)
Non-linear optical microscopy	Autofluorescence from NADH and FAD	Cellular redox state and local fractal dimension	High resolution, minimal out-of-focus photodamage	High cost, limited portability for clinical applications
	Fluorescence lifetime	Cellular redox state and protein-binding of NADH and FAD (bound vs. free)	Independent of fluorophore concentration	

centered on specific biomarkers for continuous monitoring during radiation treatment. Additionally, these studies can lead to the identification of novel therapeutic targets that can be exploited to possibly reverse radiation resistance. While optical spectroscopy has been at the forefront of optical technologies attempting to break into the clinical workflow, more work is required to establish baseline optical endpoints and the accuracy and reproducibility of these measurements. In addition, it will be necessary to associate these changes with specific outcomes corresponding to treatment response or failure. Optical spectroscopy has faced challenges with clinical translation, with attempts at early detection of cancer, discrimination between benign and malignant cancer, and demarcation of surgical margins not acquiring enough traction. The principal concerns in these clinical workflows was the perception that optical spectroscopy could never replace pathology, which is currently standard-of-care for these clinical problems. A possible advantage of advancing optical spectroscopy for measuring tumor response to therapy is the complete lack of any imaging technology or treatment biopsies that currently evaluate treatment response during the treatment regimen. While other imaging modalities such as optoacoustic imaging (OAI) can measure tumor oxygenation (116, 117), they have not yet been used in the context of radiation resistance. If decisions to escalate or de-escalate treatment for exceptional treatment responders or non-responders are to be made based on endpoints provided by optical techniques, near-perfect identification of treatment response within the first 1–2 weeks will be necessary to effect meaningful change. Tromberg et al. have demonstrated the ability of optical spectroscopy to provide an early indicator of chemotherapy response in breast cancer (78–80). Recent work has also significantly advanced the translation of non-linear optical microscopy from a laboratory-only method to the clinic for imaging the skin (118). The ability to translate two-photon excited autofluorescence from NADH and FAD to clinically compatible technologies, such as fiber optic probes could allow simultaneous determination of cellular redox state and mitochondrial fractal dimension *in vivo*. When combined with other information from DRS and RS, such as vascular oxygenation and biomolecular content, optical techniques could provide a powerful addition to a clinical workflow that could greatly benefit patients by improving response rates and quality of life.

AUTHOR CONTRIBUTIONS

SD and NR wrote the manuscript.

FUNDING

This work was supported by grants from the Arkansas Biosciences Institute and the National Science Foundation (1847347).

REFERENCES

1. Delaney G, Jacob S, Featherstone C, Barton M. The role of radiotherapy in cancer treatment. *Cancer*. (2005) 104:1129–37. doi: 10.1002/cncr.21324
2. Bertout JA, Patel SA, Simon MC. The impact of O2 availability on human cancer. *Nat Rev Cancer*. (2008) 8:967–75. doi: 10.1038/nrc2540
3. Brown JM. Tumor hypoxia in cancer therapy. *Methods Enzymol*. (2007) 435:297–321. doi: 10.1016/S0076-6879(07)35015-5
4. Gray LH, Conger AD, Ebert M, Hornsey S, Scott OC. The concentration of oxygen dissolved in tissues at the time of irradiation as a factor in radiotherapy. *Br J Radiol*. (1953) 26:638–48. doi: 10.1259/0007-1285-26-312-638
5. Brizel DM, Scully SP, Harrelson JM, Layfield LJ, Bean JM, Prosnitz LR, Dewhirst MW. Tumor oxygenation predicts for the likelihood of distant metastases in human soft tissue sarcoma. *Cancer Res*. (1996) 56:941–3.
6. Nordsmark M, Overgaard M, Overgaard J. Pretreatment oxygenation predicts radiation response in advanced squamous cell carcinoma of the head and neck. *Radiother Oncol*. (1996) 41:31–9. doi: 10.1016/S0167-8140(96)91811-3
7. Brizel DM, Dodge RK, Clough RW, Dewhirst MW. Oxygenation of head and neck cancer: changes during radiotherapy and impact on treatment outcome. *Radiother Oncol*. (1999) 53:113–7. doi: 10.1016/S0167-8140(99)00102-4
8. Fowler J. The rational of dose fractionation. In: Veath JM, editor. The *Relationship of Time and Dose in the Radiation Therapy of Cancer*. San Francisco, CA: Karger Publishers (1967). p. 6–23.
9. Kallman RF. The phenomenon of reoxygenation and its implications for fractionated radiotherapy. *Radiology*. (1972) 105:135–42. doi: 10.1148/105.1.135
10. Withers HR. The 4 Rs of radiotherapy. *Adv Radiat Biol*. (1975) 5:241–71. doi: 10.1016/B978-0-12-035405-4.50012-8

11. Wang GL, Semenza GL. General involvement of hypoxia-inducible factor 1 in transcriptional response to hypoxia. *Proc Natl Acad Sci USA*. (1993) 90:4304–8. doi: 10.1073/pnas.90.9.4304
12. Balamurugan K. HIF-1 at the crossroads of hypoxia, inflammation, and cancer. *Int J Cancer*. (2016) 138:1058–66. doi: 10.1002/ijc.29519
13. Semenza GL. Targeting HIF-1 for cancer therapy. *Nat Rev Cancer*. (2003) 3:721–32. doi: 10.1038/nrc1187
14. Chandel NS, McClintock DS, Feliciano CE, Wood TM, Melendez JA, Rodriguez AM, et al. Reactive oxygen species generated at mitochondrial Complex III stabilize hypoxia-inducible factor-1α during hypoxia: A mechanism of O2 sensing. *J Biol Chem*. (2000) 279:25130–8. doi: 10.1074/jbc.M001914200
15. Moeller BJ, Cao Y, Li CY, Dewhirst MW. Radiation activates HIF-1 to regulate vascular radiosensitivity in tumors: role of reoxygenation, free radicals, and stress granules. *Cancer Cell*. (2004) 5:429–41. doi: 10.1016/S1535-6108(04)00115-1
16. Moeller BJ, Dreher MR, Rabbani ZN, Schroeder T, Cao Y, Li CY, et al. Pleiotropic effects of HIF-1 blockade on tumor radiosensitivity. *Cancer Cell*. (2005) 8:99–110. doi: 10.1016/j.ccr.2005.06.016
17. Kim JW, Tchernyshyov I, Semenza GL, Dang C V. HIF-1-mediated expression of pyruvate dehydrogenase kinase: a metabolic switch required for cellular adaptation to hypoxia. *Cell Metab*. (2006) 3:177–85. doi: 10.1016/j.cmet.2006.02.002
18. Papandreou I, Cairns RA, Fontana L, Lim AL, Denko NC. HIF-1 mediates adaptation to hypoxia by actively downregulating mitochondrial oxygen consumption. *Cell Metab*. (2006) 3:187–97. doi: 10.1016/j.cmet.2006.01.012
19. Luo W, Hu H, Chang R, Zhong J, Knabel M, O'Meally R, et al. Pyruvate kinase M2 is a PHD3-stimulated coactivator for hypoxia-inducible factor 1. *Cell*. (2011) 145:732–44. doi: 10.1016/j.cell.2011.03.054
20. Sun Q, Chen X, Ma J, Peng H, Wang F, Zha X, et al. Mammalian target of rapamycin up-regulation of pyruvate kinase isoenzyme type M2 is critical for aerobic glycolysis and tumor growth. *Proc Natl Acad Sci USA*. (2011) 108:4129–34. doi: 10.1073/pnas.1014769108
21. Cairns RA, Papandreou I, Sutphin PD, Denko NC. Metabolic targeting of hypoxia and HIF1 in solid tumors can enhance cytotoxic chemotherapy. *Proc Natl Acad Sci USA*. (2007) 104:9445–50. doi: 10.1073/pnas.0611662104
22. Zhong J, Rajaram N, Brizel DM, Frees AE, Ramanujam N, Batinic-Haberle I, et al. Radiation induces aerobic glycolysis through reactive oxygen species. *Radiother Oncol*. (2013) 106:390–6. doi: 10.1016/j.radonc.2013.02.013
23. Mims J, Bansal N, Bharadwaj MS, Chen X, Molina AJ, Tsang AW, et al. Energy metabolism in a matched model of radiation resistance for head and neck squamous cell cancer. *Radiat Res*. (2015) 183:291–304. doi: 10.1667/RR13828.1
24. Quennet V, Yaromina A, Zips D, Rosner A, Walenta S, Baumann M, et al. Tumor lactate content predicts for response to fractionated irradiation of human squamous cell carcinomas in nude mice. *Radiother Oncol*. (2006) 81:130–5. doi: 10.1016/j.radonc.2006.08.012
25. Sattler U, Meyer S, Quennet V, Hoerner C, Knoerzer H, Fabian C, et al. Glycolytic metabolism and tumour response to fractionated irradiation. *Radiother Oncol*. (2010) 94:102–9. doi: 10.1016/j.radonc.2009.11.007
26. Georgakoudi I, Quinn KP. Optical imaging using endogenous contrast to assess metabolic state. *Annu Rev Biomed Eng*. (2012) 14:351–67. doi: 10.1146/annurev-bioeng-071811-150108
27. Denk W, Strickler JH, Webb WW. Two-photon laser scanning fluorescence microscopy. *Science*. (1990) 248:73–6. doi: 10.1126/science.2321027
28. Zipfel WR, Williams RM, Christie R, Nikitin AY, Hyman BT, Webb WW. Live tissue intrinsic emission microscopy using multiphoton-excited native fluorescence and second harmonic generation. *Proc Natl Acad Sci USA*. (2003) 100:7075–80. doi: 10.1073/pnas.0832308100
29. Kolenc OI, Quinn KP. Evaluating cell metabolism through autofluorescence imaging of NAD(P)H and FAD. *Antioxid Redox Signal*. (2019) 30:875–89. doi: 10.1089/ars.2017.7451
30. Quinn KP, Sridharan GV, Hayden RS, Kaplan DL, Lee K, Georgakoudi I. Quantitative metabolic imaging using endogenous fluorescence to detect stem cell differentiation. *Sci Rep*. (2013) 3:1–10. doi: 10.1038/srep03432
31. Varone A, Xylas J, Quinn KP, Pouli D, Sridharan G, McLaughlin-Drubin ME, et al. Endogenous two-photon fluorescence imaging elucidates metabolic changes related to enhanced glycolysis and glutamine consumption in precancerous epithelial tissues. *Cancer Res*. (2014) 4:3067–75. doi: 10.1158/0008-5472.CAN-13-2713
32. Alhallak K, Rebello LG, Muldoon TJ, Quinn KP, Rajaram N. Optical redox ratio identifies metastatic potential-dependent changes in breast cancer cell metabolism. *Biomed Opt Exp*. (2016) 7:4364–74. doi: 10.1364/BOE.7.004364
33. Hou J, Wright HJ, Chan N, Tran R, Razorenova OV, Potma EO, et al. Correlating two-photon excited fluorescence imaging of breast cancer cellular redox state with seahorse flux analysis of normalized cellular oxygen consumption. *J Biomed Opt*. (2016) 21:60503. doi: 10.1117/1.JBO.21.6.060503
34. Barlow CH, Harden WR, Harken AH, Simson MB, Haselgrove JC, Chance B, et al. Fluorescence mapping of mitochondrial redox changes in heart and brain. *Crit Care Med*. (1979) 7:402–6. doi: 10.1097/00003246-197909000-00011
35. Skala M, Ramanujam N. Multiphoton redox ratio imaging for metabolic monitoring *in vivo*. *Methods Mol Biol*. (2010) 594:155–62. doi: 10.1007/978-1-60761-411-1_11
36. Skala MC, Squirrell JM, Vrotsos KM, Eickhoff JC, Gendron-Fitzpatrick A, Eliceiri KW, et al. Multiphoton microscopy of endogenous fluorescence differentiates normal, precancerous, and cancerous squamous epithelial tissues. *Cancer Res*. (2005) 65:1180–6. doi: 10.1158/0008-5472.CAN-04-3031
37. Walsh AJ, Cook RS, Sanders ME, Aurisicchio L, Ciliberto G, Arteaga CL, et al. Quantitative optical imaging of primary tumor organoid metabolism predicts drug response in breast cancer. *Cancer Res*. (2014) 74:5184–94. doi: 10.1158/0008-5472.CAN-14-0663
38. Alhallak K, Jenkins SV, Lee DE, Greene NP, Quinn KP, Griffin RJ, et al. Optical imaging of radiation-induced metabolic changes in radiation- sensitive and resistant cancer cells. *J Biomed Opt*. (2017) 22:60502. doi: 10.1117/1.JBO.22.6.060502
39. Lee DE, Alhallak K, Jenkins SV, Vargas I, Greene NP, Quinn KP, et al. A radiosensitizing inhibitor of HIF-1 alters the optical redox state of human lung cancer cells *in vitro*. *Sci Rep*. (2018) 8:8815. doi: 10.1038/s41598-018-27262-y
40. Li LZ, Zhou R, Xu HN, Moon L, Zhong T, Kim EJ, et al. Quantitative magnetic resonance and optical imaging biomarkers of melanoma metastatic potential. *Proc Natl Acad Sci USA*. (2009) 106:6608–13. doi: 10.1073/pnas.0901807106
41. Xu HN, Nioka S, Glickson JD, Chance B, Li LZ. Quantitative mitochondrial redox imaging of breast cancer metastatic potential. *J Biomed Opt*. (2010) 106:6608–13. doi: 10.1117/1.3431714
42. Skala MC, Riching KM, Gendron-Fitzpatrick A, Eickhoff J, Eliceiri KW, White JG, ET AL. *In vivo* multiphoton microscopy of NADH and FAD redox states, fluorescence lifetimes, and cellular morphology in precancerous epithelia. *Proc Natl Acad Sci USA*. (2007) 104:19494–9. doi: 10.1073/pnas.0708425104
43. Kunz WS, Kunz W. Contribution of different enzymes to flavoprotein fluorescence of isolated rat liver mitochondria. *Biochim Biophys Acta*. (1985) 841:237–46. doi: 10.1016/0304-4165(85)90064-9
44. Nakashima N, Yoshihara K, Tanaka F, Yagi K. Picosecond fluorescence lifetime of the coenzyme of D-amino acid oxidase. *J Biol Chem*. (1980) 255:5261–3.
45. Lakowicz JR, Szmacinski H, Nowaczyk K, Johnson ML. Fluorescence lifetime imaging of free and protein-bound NADH. *Proc Natl Acad Sci USA*. (1992) 89:1271–5. doi: 10.1073/pnas.89.4.1271
46. Becker W. Fluorescence lifetime imaging - techniques and applications. *J Microsc*. (2012) 247:119–36. doi: 10.1111/j.1365-2818.2012.03618.x
47. Skala MC, Riching KM, Bird DK, Gendron-Fitzpatrick A, Eickhoff J, Eliceiri KW, et al. *In vivo* multiphoton fluorescence lifetime imaging of protein-bound and free nicotinamide adenine dinucleotide in normal and precancerous epithelia. *J Biomed Opt*. (2007) 12:024014. doi: 10.1117/1.2717503
48. Jones JD, Ramser HE, Woessner AE, Quinn KP. *In vivo* multiphoton microscopy detects longitudinal metabolic changes associated with delayed skin wound healing. *Commun Biol*. (2018) 1:198. doi: 10.1038/s42003-018-0206-4
49. Bird DK, Yan L, Vrotsos KM, Eliceiri KW, Vaughan EM, Keely PJ, et al. Metabolic mapping of MCF10A human breast cells via multiphoton

fluorescence lifetime imaging of the coenzyme NADH. *Cancer Res*. (2005) 65:8766–73. doi: 10.1158/0008-5472.CAN-04-3922
50. Addendum: Campos D, Peeters W, Nickel K, Burkel B, Bussink J, et al. Radiation promptly alters cancer live cell metabolic fluxes: an *in vitro* demonstration. *Radiat Res*. (2016) 185:496–504. doi: 10.1667/RR14093.1
51. Babbar M, Sheikh MS. Metabolic stress and disorders related to alterations in mitochondrial fission or fusion. *Mol Cell Pharmacol*. (2013) 5:109–133.
52. Chan DC. Mitochondria: dynamic organelles in disease, aging, and development. *Cell*. (2006) 125:1241–52. doi: 10.1016/j.cell.2006.06.010
53. Pouli D, Balu M, Alonzo CA, Liu Z, Quinn KP, Rius-Diaz F, et al. Imaging mitochondrial dynamics in human skin reveals depth-dependent hypoxia and malignant potential for diagnosis. *Sci Transl Med*. (2016) 8:367ra169. doi: 10.1126/scitranslmed.aag2202
54. Xylas J, Varone A, Quinn KP, Pouli D, McLaughlin-Drubin ME, Thieu HT, et al. Noninvasive assessment of mitochondrial organization in three-dimensional tissues reveals changes associated with cancer development. *Int J Cancer*. (2015) 136:322–32. doi: 10.1002/ijc.28992
55. Gao AW, Cantó C, Houtkooper RH. Mitochondrial response to nutrient availability and its role in metabolic disease. *EMBO Mol Med*. (2014) 6:580–9. doi: 10.1002/emmm.201303782
56. Westermann B. Mitochondrial fusion and fission in cell life and death. *Nat Rev Mol Cell Biol*. (2010) 11:872–84. doi: 10.1038/nrm3013
57. Murphy E, Steenbergen C. Mechanisms underlying acute protection from cardiac ischemia-reperfusion injury. *Physiol Rev*. (2008) 88:581–609. doi: 10.1152/physrev.00024.2007
58. Cao W, Carney JM, Duchon A, Floyd RA, Chevion M. Oxygen free radical involvement in ischemia and reperfusion injury to brain. *Neurosci Lett*. (1988) 88:233–8. doi: 10.1016/0304-3940(88)90132-2
59. Serracino-Inglott F, Habib NA, Mathie RT. Hepatic ischemia-reperfusion injury. *Am J Surg*. (2001) 6:122–8. doi: 10.1016/j.ijsu.2016.05.050
60. Liu X, Hajnóczky G. Altered fusion dynamics underlie unique morphological changes in mitochondria during hypoxia-reoxygenation stress. *Cell Death Differ*. (2011) 18:1561–72. doi: 10.1038/cdd.2011.13
61. Ong SB, Subrayan S, Lim SY, Yellon DM, Davidson SM, Hausenloy DJ. Inhibiting mitochondrial fission protects the heart against ischemia/reperfusion injury. *Circulation*. (2010) 121:2012–22. doi: 10.1161/CIRCULATIONAHA.109.906610
62. Cui M, Tang X, Christian WV, Yoon Y, Tieu K. Perturbations in mitochondrial dynamics induced by human mutant PINK1 can be rescued by the mitochondrial division inhibitor mdivi-1. *J Biol Chem*. (2010) 285:11740–52. doi: 10.1074/jbc.M109.066662
63. Xylas J, Quinn KP, Hunter M, Georgakoudi I. Improved Fourier-based characterization of intracellular fractal features. *Opt Exp*. (2012) 20:23442–55. doi: 10.1364/OE.20.023442
64. Vargas I, Alhallak K, Kolenc OI, Jenkins SV, Griffin RJ, Dings RPM, et al. Rapid quantification of mitochondrial fractal dimension in individual cells. *Biomed Opt Exp*. (2018) 9:5269–79. doi: 10.1364/BOE.9.005269
65. Rajaram N, Nguyen TH, Tunnell JW. Lookup table–based inverse model for determining optical properties of turbid media. *J Biomed Opt*. (2008) 13:050501. doi: 10.1117/1.2981797
66. Nichols BS. Performance of a lookup table-based approach for measuring tissue optical properties with diffuse optical spectroscopy. *J Biomed Opt*. (2012) 17:057001. doi: 10.1117/1.JBO.17.5.057001
67. Palmer GM, Ramanujam N. Monte Carlo-based inverse model for calculating tissue optical properties. Part II: application to breast cancer diagnosis. *Appl Opt*. (2006) 45:1072–8. doi: 10.1364/AO.45.001072
68. Palmer GM, Ramanujam N. Monte Carlo-based inverse model for calculating tissue optical properties. Part I: theory and validation on synthetic phantoms. *Appl Opt*. (2006) 45:1062–71. doi: 10.1364/AO.45.001062
69. Farrell TJ, Patterson MS, Wilson B. A diffusion theory model of spatially resolved, steady-state diffuse reflectance for the noninvasive determination of tissue optical properties *in vivo*. *Med Phys*. (1992) 19:879–88. doi: 10.1118/1.596777
70. Zonios G, Perelman LT, Backman V, Manoharan R, Fitzmaurice M, Van Dam J, et al. Diffuse reflectance spectroscopy of human adenomatous colon polyps *in vivo*. *Appl Opt*. (1999) 38:6628–37. doi: 10.1364/AO.38.006628
71. Palmer GM, Viola RJ, Schroeder T, Yarmolenko PS, Dewhirst MW, Ramanujam N. Quantitative diffuse reflectance and fluorescence spectroscopy: tool to monitor tumor physiology *in vivo*. *J Biomed Opt*. (2012) 14:024010. doi: 10.1117/1.3103586
72. Wang HW, Putt ME, Emanuele MJ, Shin DB, Glatstein E, Yodh AG, et al. Treatment-induced changes in tumor oxygenation predict photodynamic therapy outcome. *Cancer Res*. (2004) 64:7553–61. doi: 10.1158/0008-5472.CAN-03-3632
73. Dadgar S, Troncoso JR, Rajaram N. Optical spectroscopic sensing of tumor hypoxia. *J Biomed Opt*. (2018) 23:1–10. doi: 10.1117/1.JBO.23.6.067001
74. Drezek R, Guillaud M, Collier T, Boiko I, Malpica A, Macaulay C, et al. Light scattering from cervical cells throughout neoplastic progression: influence of nuclear morphology, DNA content, and chromatin texture. *J Biomed Opt*. (2003) 8:7. doi: 10.1117/1.1528950
75. Rajaram N, Reichenberg JS, Migden MR, Nguyen TH, Tunnell JW. Pilot clinical study for quantitative spectral diagnosis of non-melanoma skin cancer. *Lasers Surg Med*. (2010) 42:716–27. doi: 10.1002/lsm.21009
76. Rajaram N, Aramil TJ, Lee K, Reichenberg JS, Nguyen TH, Tunnell JW. Design and validation of a clinical instrument for spectral diagnosis of cutaneous malignancy. *Appl Opt*. (2010) 49:142–52. doi: 10.1364/AO.49.000142
77. Brown JQ, Wilke LG, Geradts J, Kennedy SA, Palmer GM, Ramanujam N. Quantitative optical spectroscopy: a robust tool for direct measurement of breast cancer vascular oxygenation and total hemoglobin content *in vivo*. *Cancer Res*. (2009) 69:2919–26. doi: 10.1158/0008-5472.CAN-08-3370
78. Ueda S, Roblyer D, Cerussi A, Durkin A, Leproux A, Santoro Y, et al. Baseline tumor oxygen saturation correlates with a pathologic complete response in breast cancer patients undergoing neoadjuvant chemotherapy. *Cancer Res*. (2012) 72:4318–28. doi: 10.1158/0008-5472.CAN-12-0056
79. Roblyer D, Ueda S, Cerussi A, Tanamai W, Durkin A, Mehta R, et al. Optical imaging of breast cancer oxyhemoglobin flare correlates with neoadjuvant chemotherapy response one day after starting treatment. *Proc Natl Acad Sci USA*. (2011) 108:14626–31. doi: 10.1073/pnas.1013103108
80. Tromberg BJ, Zhang Z, Leproux A, O'Sullivan TD, Cerussi AE, Carpenter PM, et al. Predicting responses to neoadjuvant chemotherapy in breast cancer: ACRIN 6691 trial of diffuse optical spectroscopic imaging. *Cancer Res*. (2016) 76:5933–44. doi: 10.1158/0008-5472.CAN-16-0346
81. Wilke LG, Brown JQ, Bydlon TM, Kennedy SA, Richards LM, Junker MK, et al. Rapid noninvasive optical imaging of tissue composition in breast tumor margins. *Am J Surg*. (2009) 198:566–74. doi: 10.1016/j.amjsurg.2009.06.018
82. Vishwanath K, Klein D, Chang K, Schroeder T, Dewhirst MW, Ramanujam N. Quantitative optical spectroscopy can identify long-term local tumor control in irradiated murine head and neck xenografts. *J Biomed Opt*. (2009) 14:054051. doi: 10.1117/1.3251013
83. Hu F, Vishwanath K, Salama JK, Erkanli A, Peterson B, Oleson JR, et al. Oxygen and perfusion kinetics in response to fractionated radiation therapy in FaDu head and neck cancer xenografts are related to treatment outcome. *Int J Radiat Oncol Biol Phys*. (2016) 96:462–9. doi: 10.1016/j.ijrobp.2016.06.007
84. Diaz PM, Jenkins S V, Alhallak K, Semeniak D, Griffin RJ, Dings RPM, et al. Quantitative diffuse reflectance spectroscopy of short-term changes in tumor oxygenation after radiation in a matched model of radiation resistance. *Biomed Opt Exp*. (2018) 9:3794. doi: 10.1364/BOE.9.003794
85. Dietz A, Vanselow B, Rudat V, Conradt C, Weidauer H, Kallinowski F, et al. Prognostic impact of reoxygenation in advanced cancer of the head and neck during the initial course of chemoradiation or radiotherapy alone. *Head Neck*. (2003) 25:50–8. doi: 10.1002/hed.10177
86. Freudiger CW, Min W, Saar BG, Lu S, Holtom GR, He C, et al. Label-free biomedical imaging with high sensitivity by stimulated raman scattering microscopy. *Science*. (2008) 322:1857–61. doi: 10.1126/science.1165758
87. Matousek P, Stone N. Development of deep subsurface Raman spectroscopy for medical diagnosis and disease monitoring. *Chem Soc Rev*. (2016) 45:1794–802. doi: 10.1039/C5CS00466G
88. Jermyn M, Mok K, Mercier J, Desroches J, Pichette J, Saint-Arnaud K, et al. Intraoperative brain cancer detection with Raman spectroscopy in humans. *Sci Transl Med*. (2015) 7:274ra19. doi: 10.1126/scitranslmed.aaa2384

89. Matthäus C, Krafft C, Dietzek B, Brehm BR, Lorkowski S, Popp J. Noninvasive imaging of intracellular lipid metabolism in macrophages by Raman microscopy in combination with stable isotopic labeling. *Anal Chem*. (2012) 84:8549–56. doi: 10.1021/ac3012347
90. Krishna H, Majumder SK, Chaturvedi P, Sidramesh M, Gupta PK. *In vivo* Raman spectroscopy for detection of oral neoplasia: a pilot clinical study. *J Biophotonics*. (2014) 7:690–702. doi: 10.1002/jbio.201300030
91. Singh SP, Deshmukh A, Chaturvedi P, Murali Krishna C. *In vivo* Raman spectroscopic identification of premalignant lesions in oral buccal mucosa. *J Biomed Opt*. (2012) 17:105002. doi: 10.1117/1.JBO.17.10.105002
92. Abramczyk H, Surmacki J, Brozek-Płuska B, Morawiec Z, Tazbir M. The hallmarks of breast cancer by Raman spectroscopy. *J Mol Struct*. (2009) 924:175–82. doi: 10.1016/j.molstruc.2008.12.055
93. Haka AS, Shafer-Peltier KE, Fitzmaurice M, Crowe J, Dasari RR, Feld MS. Diagnosing breast cancer by using Raman spectroscopy. *Proc Natl Acad Sci USA*. (2005) 102:12371–6. doi: 10.1073/pnas.0501390102
94. Saha A, Barman I, Dingari NC, McGee S, Volynskaya Z, Galindo LH, et al. Raman spectroscopy: a real-time tool for identifying microcalcifications during stereotactic breast core needle biopsies. *Biomed Opt Exp*. (2011) 2:2792–803. doi: 10.1364/BOE.2.002792
95. Barman I, Dingari NC, Saha A, McGee S, Galindo LH, Liu W, et al. Application of raman spectroscopy to identify microcalcifications and underlying breast lesions at Stereotactic core needle biopsy. *Cancer Res*. (2013) 73:3206–15. doi: 10.1158/0008-5472.CAN-12-2313
96. Zheng C, Shao W, Paidi SK, Han B, Fu T, Wu D, et al. Pursuing shell-isolated nanoparticle-enhanced Raman spectroscopy. (SHINERS) for concomitant detection of breast lesions and microcalcifications. *Nanoscale*. (2015) 7:16960–8. doi: 10.1039/C5NR05319F
97. Frank CJ, McCreary RL, Redd D. Raman spectroscopy of normal and diseased human breast tissues. *Anal Chem*. (1995) 67:777–83. doi: 10.1021/ac00101a001
98. Haka AS, Volynskaya Z, Gardecki JA, Nazemi J, Lyons J, Hicks D, Fitzmaurice M, et al. *In vivo* margin assessment during partial mastectomy breast surgery using Raman spectroscopy. *Cancer Res*. (2006) 66:3317–22. doi: 10.1158/0008-5472.CAN-05-2815
99. Jess PRT, Smith DDW, Mazilu M, Dholakia K, Riches AC, Herrington CS. Early detection of cervical neoplasia by Raman spectroscopy. *Int J Cancer*. (2007) 121:2723–8. doi: 10.1002/ijc.23046
100. Krishna CM, Prathima NB, Malini R, Vadhiraja BM, Bhatt RA, Fernandes DJ, et al. Raman spectroscopy studies for diagnosis of cancers in human uterine cervix. *Vib Spectrosc*. (2006) 41:136–41. doi: 10.1016/j.vibspec.2006.01.011
101. Kanter EM, Vargis E, Majumder S, Keller MD, Woeste E, Rao GG, et al. Application of Raman spectroscopy for cervical dysplasia diagnosis. *J Biophotonics*. (2009) 2:81–90. doi: 10.1002/jbio.200910001
102. Kirsch M, Schackert G, Salzer R, Krafft C. Raman spectroscopic imaging for *in vivo* detection of cerebral brain metastases. *Anal Bioanal Chem*. (2010) 398:1707–13. doi: 10.1007/s00216-010-4116-7
103. Matthews Q, Jirasek A, Lum JJ, Brolo AG. Biochemical signatures of *in vitro* radiation response in human lung, breast and prostate tumour cells observed with Raman spectroscopy. *Phys Med Biol*. (2011) 56:6839–55. doi: 10.1088/0031-9155/56/21/006
104. Yasser M, Shaikh R, Chilakapati MK, Teni T. Raman spectroscopic study of radioresistant oral cancer sublines established by fractionated ionizing radiation. *PLoS ONE*. (2014) 9:e97777. doi: 10.1371/journal.pone.0097777
105. Matthews Q, Brolo AG, Lum J, Duan X, Jirasek A. Raman spectroscopy of single human tumour cells exposed to ionizing radiation *in vitro*. *Phys Med Biol*. (2011) 56:19–38. doi: 10.1088/0031-9155/56/1/002
106. Harder SJ, Matthews Q, Isabelle M, Brolo AG, Lum JJ, Jirasek A. A Raman spectroscopic study of cell response to clinical doses of ionizing radiation. *Appl Spectrosc*. (2015) 69:193–204. doi: 10.1366/14-07561
107. Matthews Q, Isabelle M, Harder SJ, Smazynski J, Beckham W, Brolo AG, et al. Radiation-induced glycogen accumulation detected by single cell raman spectroscopy is associated with radioresistance that can be reversed by metformin. *PLoS ONE*. (2015) 10:e0135356. doi: 10.1371/journal.pone.0135356
108. Harder SJ, Isabelle M, Devorkin L, Smazynski J, Beckham W, Brolo AG, et al. Raman spectroscopy identifies radiation response in human non-small cell lung cancer xenografts. *Sci Rep*. (2016) 6:21006. doi: 10.1038/srep21006
109. Van Nest SJ, Nicholson LM, DeVorkin L, Brolo AG, Lum JJ, Jirasek A. Raman spectroscopic signatures reveal distinct biochemical and temporal changes in irradiated human breast adenocarcinoma xenografts. *Radiat Res*. (2018) 189:497–504. doi: 10.1667/RR15003.1
110. Shimura T. Acquired radioresistance of cancer and the AKT/GSK3β/cyclin D1 overexpression Cycle. *J Radiat Res*. (2011) 52:539–44. doi: 10.1269/jrr.11098
111. Vidyasagar MS, Maheedhar K, Vadhiraja BM, Fernendes DJ, Kartha VB, Krishna CM. Prediction of radiotherapy response in cervix cancer by Raman spectroscopy: a pilot study. *Biopolymers*. (2008) 89:530–7. doi: 10.1002/bip.20923
112. Paidi SK, Monterroso Diaz P, Dadgar S, Jenkins S V, Quick CM, Griffin RJ, et al. Label-free Raman spectroscopy reveals signatures of radiation resistance in the tumor microenvironment. *Cancer Res*. (2019) 79:2054–64. doi: 10.1158/0008-5472.CAN-18-2732
113. Felten J, Hall H, Jaumot J, Tauler R, De Juan A, Gorzsás A. Vibrational spectroscopic image analysis of biological material using multivariate curve resolution-alternating least squares. (MCR-ALS). *Nat Protoc*. (2015) 10:217–40. doi: 10.1038/nprot.2015.008
114. Gilkes DM, Bajpai S, Chaturvedi P, Wirtz D, Semenza GL. Hypoxia-inducible factor 1. (HIF-1) promotes extracellular matrix remodeling under hypoxic conditions by inducing P4HA1, P4HA2, and PLOD2 expression in fibroblasts. *J Biol Chem*. (2013) 288:10819–29. doi: 10.1074/jbc.M112.442939
115. Hofbauer KH, Gess B, Lohaus C, Meyer HE, Katschinski D, Kurtz A. Oxygen tension regulates the expression of a group of procollagen hydroxylases. *Eur J Biochem*. (2003) 207:4515–22. doi: 10.1046/j.1432-1033.2003.03846.x
116. Tomaszewski MR, Gonzalez IQ, O'Connor JPB, Abeyakoon O, Parker GJM, Williams KJ, et al. Oxygen enhanced Optoacoustic Tomography. (OE-OT) reveals vascular dynamics in murine models of prostate cancer. *Theranostics*. (2017) 7:2900–13. doi: 10.7150/thno.19841
117. Tomaszewski MR, Gehrung M, Joseph J, Quiros-Gonzalez I, Disselhorst JA, Bohndiek SE. Oxygen-enhanced and dynamic contrast-enhanced optoacoustic tomography provide surrogate biomarkers of tumor vascular function, hypoxia, and necrosis. *Cancer Res*. (2018) 78:5980–91. doi: 10.1158/0008-5472.CAN-18-1033
118. Balu M, Mikami H, Hou J, Potma EO, Tromberg BJ. Rapid mesoscale multiphoton microscopy of human skin. *Biomed Opt Exp*. (2016) 7:4375–87. doi: 10.1364/BOE.7.004375

Conflict of Interest: The authors declare that the research was conducted in the absence of any commercial or financial relationships that could be construed as a potential conflict of interest.

Copyright © 2019 Dadgar and Rajaram. This is an open-access article distributed under the terms of the Creative Commons Attribution License (CC BY). The use, distribution or reproduction in other forums is permitted, provided the original author(s) and the copyright owner(s) are credited and that the original publication in this journal is cited, in accordance with accepted academic practice. No use, distribution or reproduction is permitted which does not comply with these terms.

frontiers in Oncology

REVIEW
published: 12 November 2019
doi: 10.3389/fonc.2019.01213

Difference in Acquired Radioresistance Induction Between Repeated Photon and Particle Irradiation

Katsutoshi Sato[1], *Takashi Shimokawa*[2] *and Takashi Imai*[3]*

[1] Division of Hematology and Medical Oncology, Icahn School of Medicine at Mount Sinai, The Tisch Cancer Institute, New York, NY, United States, [2] Department of Accelerator and Medical Physics, National Institute of Radiological Sciences, National Institutes for Quantum and Radiological Sciences and Technology, Chiba, Japan, [3] Medical Databank, Department of Radiation Medicine, QST Hospital, National Institutes for Quantum and Radiological Science and Technology, Chiba, Japan

In recent years, advanced radiation therapy techniques, including stereotactic body radiotherapy and carbon–ion radiotherapy, have progressed to such an extent that certain types of cancer can be treated with radiotherapy alone. The therapeutic outcomes are particularly promising for early stage lung cancer, with results matching those of surgical resection. Nevertheless, patients may still experience local tumor recurrence, which might be exacerbated by the acquisition of radioresistance after primary radiotherapy. Notwithstanding the risk of tumors acquiring radioresistance, secondary radiotherapy is increasingly used to treat recurrent tumors. In this context, it appears essential to comprehend the radiobiological effects of repeated photon and particle irradiation and their underlying cellular and molecular mechanisms in order to achieve the most favorable therapeutic outcome. However, to date, the mechanisms of acquisition of radioresistance in cancer cells have mainly been studied after repeated *in vitro* X-ray irradiation. By contrast, other critical aspects of radioresistance remain mostly unexplored, including the response to carbon-ion irradiation of X-ray radioresistant cancer cells, the mechanisms of acquisition of carbon-ion resistance, and the consequences of repeated *in vivo* X-ray or carbon-ion irradiation. In this review, we discuss the underlying mechanisms of acquisition of X-ray and carbon-ion resistance in cancer cells, as well as the phenotypic differences between X-ray and carbon-ion-resistant cancer cells, the biological implications of repeated *in vivo* X-ray or carbon-ion irradiation, and the main open questions in the field.

Keywords: cancer, radioresistance, acquisition, X-ray radiation, carbon-ion radiation, repeated irradiation, DNA repair, aggressiveness

OPEN ACCESS

Edited by:
Ira I. Skvortsova, Innsbruck Medical University, Austria

Reviewed by:
Zhongxing Liao, University of Texas MD Anderson Cancer Center, United States
Michael W. Epperly, University of Pittsburgh, United States

***Correspondence:**
Takashi Imai
imai.takashi@qst.go.jp

Specialty section:
This article was submitted to Radiation Oncology, a section of the journal Frontiers in Oncology

Received: *14 August 2019*
Accepted: *23 October 2019*
Published: *12 November 2019*

Citation:
Sato K, Shimokawa T and Imai T (2019) Difference in Acquired Radioresistance Induction Between Repeated Photon and Particle Irradiation. Front. Oncol. 9:1213. doi: 10.3389/fonc.2019.01213

INTRODUCTION

The previous decade has seen significant developments in the techniques used in radiotherapy, and advanced radiotherapy has become increasingly adopted. Among advanced radiotherapy techniques, stereotactic body radiation therapy (SBRT) relies on a small irradiation field to precisely deliver high doses of radiation, typically above 10 Gy per fraction, to local tumors. SBRT has been applied to the treatment of various cancers, including lung (1), liver (2), and prostate cancer (3).

The therapeutic outcomes of SBRT are particularly promising for early stage lung cancers, with local control rates exceeding 80% (1, 4) and clinical outcomes comparable to those of surgical resection (5, 6).

In addition to SBRT, particle-beam therapy, such as carbon-ion (C-ion) radiotherapy (CIRT), has demonstrated excellent therapeutic outcomes in various types of cancer (7). CIRT has both physical and biological advantages compared with X-ray therapy. With CIRT, tumors are irradiated with C-ions of relativistic energy, which means that C-ions penetrate the body with lower ionization that significantly increases toward the end of the beam path. This radiophysical feature is commonly referred to as the "Bragg-peak" and contributes to increasing the radiation dose delivered to the tumor while minimizing the radiation dose delivered to the skin and surrounding healthy tissues. Furthermore, CIRT has a relative biological effectiveness, which is defined as the ratio of a dose of radiation to the dose of X-ray radiation producing the same biological effects that is >2. Another important feature of CIRT is its effectiveness against conventional X-ray radiotherapy resistant cancers, including melanoma (8) and bone and soft-tissue sarcoma (9–11). Furthermore, CIRT reportedly works as an alternative ablative treatment for early stage lung cancer, in particular for elderly and inoperable patients (12).

Nevertheless, recent studies show that local recurrence can still occur after advanced radiotherapy. For example, an incidence of local recurrence ranging from 4.9 to 19% in patients who received SBRT for lung cancer treatment was reportedly dependent on treatment regimen, tumor stage, and follow-up periods (13–18). Furthermore, 23.3% of patients who received CIRT for the treatment of stage I non-small cell lung cancer also exhibited local recurrence (19).

In cases of tumor recurrence after primary radiotherapy, patients can rarely be treated again with the same radiation regimen, because the tumor might acquire radioresistance, and it is possible that healthy surrounding tissues will not tolerate additional irradiation. Nevertheless, recent studies report that SBRT and CIRT can be used for re-irradiation of recurrent tumors, taking into account both the dose tolerance of healthy tissues and location of the recurrent tumor (20–23). However, several issues related to re-irradiation with SBRT or CIRT still need to be considered. First, only a few studies have reported the clinical outcomes of repeated irradiation, and second, the characteristics of recurrent tumor after primary radiotherapy are largely unknown. In this review, we focus on the biological aspects of acquired X-ray and C-ion resistance in cancer cells and discuss the differences between the consequences of *in vitro* and *in vivo* repeated irradiation, the possible mechanisms of acquired resistance in cancer cells, and issues that must be addressed in this research field.

ACQUISITION OF PHOTON RADIORESISTANCE *IN VITRO*

Radioresistance acquisition in cancer cells and its underlying mechanisms have been mainly studied using radioresistant cell lines established through repeated *in vitro* photon (e.g., X-ray or γ-ray) irradiation. Because conventional radiotherapy usually relies on a total dose of ∼60 Gy applied in 2-Gy fractions, many studies adopted similar radiation regimens in order to establish radioresistant cell lines (**Table 1**) (24–41). Importantly, most of these studies showed that the survival of repeatedly irradiated cells was significantly higher than that of the parental cells, which indicated that *in vitro*, various cell lines could acquire radioresistance following multiple rounds of X-ray irradiation.

Cellular Processes Involved in the Acquisition of Radioresistance Following Repeated Photon Irradiation

The mechanisms of acquisition of radioresistance in cancer cells have been associated with a variety of biological processes (**Table 1**). However, in many cases, the acquisition of radioresistance can be reasonably explained by the induction of epithelial-to-mesenchymal transition (EMT), which is defined as phenotypic and molecular alterations that result in the loss of epithelial-cell characteristics and the gain of mesenchymal-cell characteristics. As cancer cells undergo EMT, epithelial markers, such as E-cadherin, ZO-1, and cytokeratin, are downregulated, whereas mesenchymal markers, such as N-cadherin, vimentin, snail, and twist, are upregulated, and in some cases, morphological changes lead to the appearance of spindle-shaped cells (42). The most prominent characteristics acquired by cancer cells after EMT are migratory and invasive properties, conferring them a significant metastatic potential, and resistance to chemotherapeutic drugs and ionizing radiation. Indeed, several studies report that EMT in cancer cells, which was defined by reduced E-cadherin protein levels, increased N-cadherin protein levels, and enhanced migration potential, could be induced by single X-ray irradiation (43, 44). Furthermore, Shintani et al. (39) showed that repeated X-ray irradiation of A549 cells (2 Gy weekly for >6 months) induced significant radioresistance and typical EMT (i.e., decreased E-cadherin and increased N-cadherin mRNA and protein levels). Collectively, these data support the notion that EMT induction following X-ray irradiation is a contributing factor in the acquisition of radioresistance.

Another factor involved in the acquisition of radioresistance following repeated X-ray irradiation is an enrichment in cancer stem cells (CSCs), which are known to exhibit higher DNA-repair potential (45) and resistance to reactive oxygen species-induced cytotoxicity (46, 47). CSCs are also often found to be in the G0 phase (48), a quiescent state outside the normal cell cycle and associated with reduced cell proliferation. All of these characteristics are recognized for their role in cellular radioresistance. Additionally, CSCs are important in radioresistance acquisition because of their impact on the heterogeneity of the cell population within a tumor. Indeed, in the hierarchy model, CSCs produce a more differentiated non-CSC progeny exhibiting significant cell-proliferation potential but lacking stem cell properties. Notwithstanding their reduced proliferation rate as compared with their non-CSC progeny, CSCs can self-renew, and maintaining their stemness. Notably,

TABLE 1 | Repeated photon irradiation regimen for the establishment of radioresistant cancer cells.

Author (year)	Single dose (Gy)	Total dose (Gy)	Regimen	Parental cell line	Main findings	References
Kuwahara et al. (2009, 2011)	0.5	>1,600	2 Gy of α-ray, 0.5 Gy/12 h	HepG2	• Promoted DNA repair • Decreased autophagic cell death	(24, 25)
Lee et al. (2010)	2	80	Over 5 months	H460	• Decreased reactive oxygen species production • TP53I3 downregulation	(26)
Lin et al. (2010)	2	60	(*1)	OECM1 KB SAS	• GP96 upregulation	(27)
Luo et al. (2017)	2	30	(*1)	TE-1 Eca-109	• Concomitant increase in CDDP resistance	(28)
Lynam-Lennon et al. (2010)	2	50	(*1)	OE33	• Promoted DNA repair	(29)
Mitsuhashi et al. (1996)	6.37	63.7	(*1)	NMT-1	• (*2)	(30)
Pearce et al. (2001)	2–4	40–60	Weekly	MDA-MB-231	• (*2)	(31)
Post et al. (2018)	1–4	64	4 Gy/2 weeks, 4 times/week	MCF7	• (*2)	(32)
Russell et al. (1995)	2	50	Every 5–7 days	IMR32	• Promoted DNA repair	(33)
Sato et al. (2014, 2017)	10, 5 (*3)	60, 30 (*3)	Every 2 weeks	NR-S1	• Promoted DNA repair • Resistance to C-ion radiation • Increased phosphorylation of mTOR	(34, 35)
Shimura et al. (2010, 2014, 2017)	0.5	31–62	Every 12–24 h	Hela HepG2	• Activation of the DNA-PK-Akt-Cyclin D1 pathway	(36–38)
Shintani et al. (2011)	2	60	Over 6 months	A549	• Induction of epithelial to mesenchymal transition	(39)
You et al. (2014)	2	80	40 times over 5 months	A549 H157 H358	• Increased phosphorylation of JAK2 and STAT3 • Increased levels of Bcl2 and Bcl2-XL	(40)
Zhou et al. (2010)	6.37	76.44	12 times over 6 months	Hep2	• Increased fraction of cells in the G0 phase • Increased telomerase activity	(41)

*(*1) There is no description about treatment regimen.*
*(*2) There is no significant finding other than radioresistance acquisition.*
*(*3) 5 Gy and 30 Gy of single and total dose is that of C-ion irradiation.*

the non-CSC population displays higher radiosensitivity than the CSC population. Consequently, radiation treatment can increase the relative abundance of CSCs in the tumor, which promotes asymmetric cell proliferation and, therefore, an enrichment in CSCs.

Lagadec et al. (49) reported enrichment in $CD44^{high}/CD24^{low}$ breast CSCs following repeated X-ray irradiation of human breast cancer MCF7 and T47D cells, with irradiated cells displaying increased sphere-formation potential. Furthermore, they found that repeated irradiations led CSCs in the G0 phase to reenter the cell cycle, thereby promoting their proliferation, whereas the non-CSC population underwent apoptosis according to the increased fraction of cells in the sub-G1 phase (49). Additionally, Ghisolfi et al. (50) showed that single X-ray irradiation of cancer cells with a dose of 2 Gy to 10 Gy increased the expression of the pluripotency markers *OCT3/4* and *SOX2* and promoted the enrichment of a CSC subpopulation. Moreover, Mani et al. (51) established a link between EMT and CSCs by demonstrating that TGF-β-induced EMT generated a subpopulation with CSC properties, including characteristic CSC markers, such as $CD44^{high}/CD24^{low}$ and elevated sphere- and mammosphere-formation potential.

To the best of our knowledge, a definitive mechanism responsible for the induction of CSCs remains unclear; however, DNA damage or chromosomal aberration can enhance CSC induction along with increased oncogene activity. Liang et al. (52) showed that DNA damage from UV irradiation and the chromosomal aberrations induced by *Mad2* overexpression also increased by *Myc* and *SOX2* expression in human nasopharyngeal carcinoma CNE cell lines and promoted cell dye-exclusion, colony formation, and sphere-formation capacities. These data suggest that the accumulation of DNA damage by repeated X-ray irradiation induces not only EMT but also enrichment of CSCs with increasing oncogenic activity, whereas secondary induction of a CSC subpopulation by EMT (known as cancer plasticity) further contributes to the development of radioresistance.

Molecular Processes Involved in the Acquisition of Radioresistance Following Repeated Photon Irradiation

We and others have independently reported that repeated X-ray irradiation can result in enhanced DNA-repair capacity (24, 29,

33, 34). In our study, the mouse squamous cell carcinoma NR-S1 cell line was irradiated with a total dose of 60 Gy of X-ray radiation applied in 10-Gy fractions in order to establish the X60 radioresistant cancer cell line (**Figure 1**). Notably, the D10 value (i.e., the radiation dose required to decrease the survival to 10% of the non-irradiated condition) and cell survival after 10 Gy of X-ray radiation were 1.6- and 3.8-fold higher, respectively, for X60 cells than for parental NR-S1 cells (34). Furthermore, 24 h after exposure to 10 Gy X-ray radiation, the number of S139 phosphorylated-H2AX (γ-H2AX) foci, a marker of DNA double-strand breaks (DSBs), was 2.5-fold lower in X60 cells than in NR-S1 cells, indicating that DSBs were repaired more efficiently in X60 cells than in NR-S1 cells (34). Indeed, the collected results of numerous studies (**Table 1**) further demonstrate that enhanced DNA-repair capacity is a common feature of radioresistant cancer cells arising from repeated X-ray irradiation.

As part of the investigation of the molecular mechanisms underlying the acquisition of radioresistance, several groups have highlighted a relationship between DNA repair and pro-survival signaling pathways, such as the Akt and mechanistic target of rapamycin (mTOR) pathways. Shimura et al. (36) suggested a potential molecular mechanism for the acquisition of radioresistance induced by repeated X-ray irradiation, showing that *cyclin D1* expression and Akt phosphorylation levels were increased in X-ray-resistant derivatives of HeLa and HepG2 cells established following repeated irradiation. These radioresistant cancer cell lines also displayed constitutively elevated levels of DSBs, as measured by H2AX and ataxia telangiectasia mutated (ATM) phosphorylation, relative to those in parental cell lines. Strikingly, downregulation of cyclin D1 in radioresistant HeLa and HepG2 derivatives decreased H2AX-, ATM-, and Akt-phosphorylation levels, as well as cell survival, after further X-ray irradiation. Therefore, they proposed that repeated X-ray irradiation triggered *cyclin D1* overexpression and forced cell cycle progression, which in turn caused further DNA damage and led to the activation of both Akt signaling and DNA-dependent protein kinase activity, a central component in the non-homologous end joining DSB-repair pathway. Eventually, these signals promoted further *cyclin D1* overexpression as part of a positive-feedback loop that likely resulted in the acquisition of radioresistance (36, 38, 53, 54).

In addition to Akt signaling, mTOR signaling has been associated with the acquisition of X-ray resistance in cancer cells. Chang et al. (55) established radioresistant derivatives of PC-3, DU145, and LNCaP cells following repeated X-ray irradiation with a dose of 2 Gy/day for 5 consecutive days (55) and showed that these radioresistant cancer cell lines exhibited both mesenchymal and CSC phenotypic traits. Interestingly, they found that radioresistant cells treated with BEZ235, a specific inhibitor of the phosphoinositide 3 (PI3) and mTOR kinases, displayed decreased expression of mesenchymal (N-cadherin, vimentin, and snail) and CSC (OCT3/4, SOX2, and CD44) markers, increased expression of the epithelial marker E-cadherin, and reduced cell survival. They further showed that BEZ235, the PI3-kinase inhibitor BKM120, and the mTOR-kinase inhibitor rapamycin, suppressed the expression

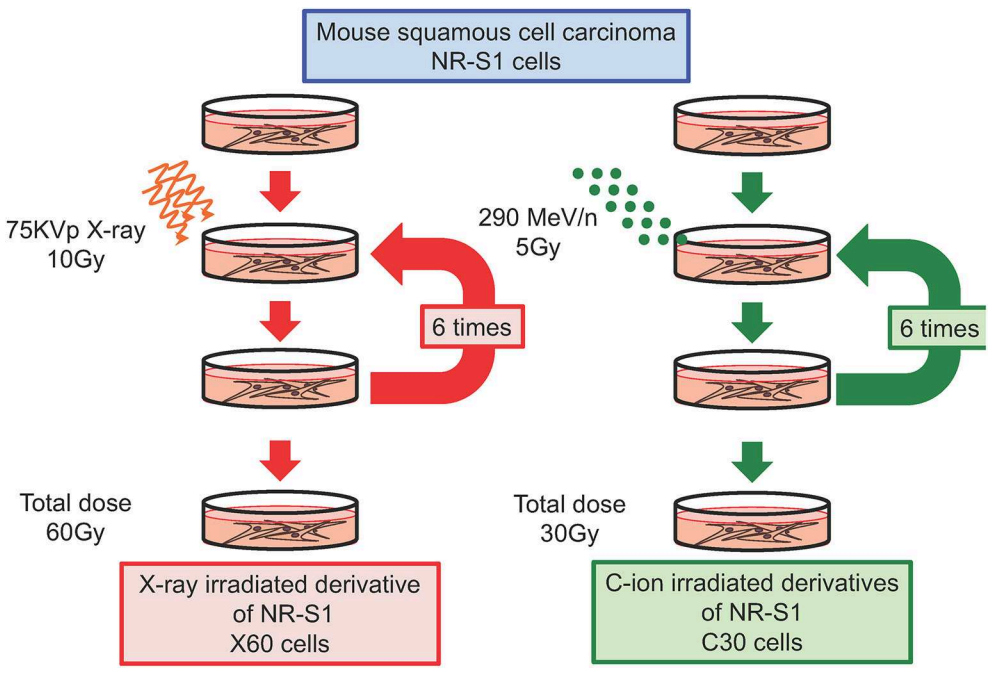

FIGURE 1 | Diagram describing the establishment of radioresistant cancer cells through repeated X-ray or C-ion irradiation. Mouse squamous cell carcinoma NR-S1 cells were irradiated six times at 2-week intervals with 10 Gy of X-ray radiation (left) or 5 Gy of C-ion radiation (left). The radioresistant derivative cell lines exposed to total doses of 60 Gy of X-ray radiation and 30 Gy of C-ion radiation were denoted as X60 and C30 cells, respectively (34, 35).

of DNA-repair proteins induced by X-ray irradiation, including Ku80, BCRA1, and BRCA2 (56). Moreover, we independently demonstrated that mTOR signaling was enhanced in X60 radioresistant cancer cells as compared with parental NR-S1 cells, whereas rapamycin treatment decreased their radioresistant phenotype (35). Importantly, rapamycin also suppresses both non-homologous end joining and homologous recombination (HR) DSB-repair pathways (57). Collectively, these results indicate that activation of the pro-survival Akt and mTOR signaling pathways can eventually increase the DNA-repair capacity of repeatedly irradiated cancer cells and thereby promote the acquisition of radioresistance.

ACQUISITION OF C-ion RADIORESISTANCE *IN VITRO*

Acquisition of C-Ion Resistance Following Repeated X-Ray Irradiation

In clinical practice, CIRT is an effective treatment for locally recurrent tumors after primary radiotherapy, likely because cell killing by C-ion radiation is independent of various cellular or tumor characteristics, including p53 status (58), cell cycle phase (59, 60), and hypoxia (61–63). Although these findings suggest that C-ion radiation should be effective against radioresistant cancer cells arising from repeated X-ray irradiation, no available experimental data supported this hypothesis. Therefore, in a recent study, we determined whether C-ion radiation could efficiently kill X60 radioresistant cancer cells. Contrary to our expectations, we found that compared with parental NR-S1 cells, X60 cells exhibited significant levels of resistance against C-ion radiation (34). Furthermore, 24 h after C-ion irradiation, the number of γ-H2AX foci was 2.5-fold lower in X60 cells than in NR-S1 cells. These observations indicated that repeated X-ray irradiation of cancer cells with a relatively high dose of 10 Gy per fraction could induce not only X-ray resistance but also C-ion resistance (34). We believe that further investigations using such radioresistant cells will likely lead to the discovery of novel mechanisms contributing to C-ion resistance in cancer cells.

To gain further insight into the underlying mechanisms of radioresistance in X60 cells, in a recent study, we compared several biological and morphological traits of X60 cells and parental NR-S1 cells, including cell shape and size, number of heterochromatin domains in the nucleus, and DNA content (34). Additionally, we analyzed the correlation between these factors and X-ray or C-ion resistance. Interestingly, we found that the number of heterochromatin domains was strongly correlated with both X-ray and C-ion resistance, which suggested that heterochromatin components or the dynamics of heterochromatin were also involved in the acquisition of radioresistance.

Indeed, previous studies show that heterochromatin proteins, such as HP1α (64) and CAF1 (65), are directly involved in DNA repair, and recent studies report that DNA damage in heterochromatin domains is mainly repaired by the HR machinery (66, 67). The damaged heterochromatin first move to the periphery of the heterochromatin domain to prevent abnormal recombination or deleterious expansion at satellite or repetitive DNA sequences, after which Rad51, the core component of the HR machinery, accumulates at DNA-damage sites located at the periphery of the heterochromatin domain (66, 67). Although these studies were conducted in *Drosophila* and yeast cells, Jakob et al. (68) observed similar dynamics of damaged heterochromatin and DNA-repair following heavy ion-beam irradiation of mammalian cells, finding that immediately after irradiation, DSBs were formed in the heterochromatin along the uranium ion-beam track. Within 30 min, the DSB sites relocated to the periphery of the heterochromatin domain, and replication protein A, a marker of DNA-end resection during HR repair, accumulated at these DSB sites (68). In agreement with these findings, our preliminary results showed that 1 h after X-ray or C-ion irradiation, X60 cells displayed an increased number of Rad51 foci as compared with NR-S1 cells (**Figure 2**). Because Rad51 is a central factor in the HR machinery, Rad51 foci are commonly considered to represent sites of ongoing DSB repair by HR.

Furthermore, several studies report that HR repair can remove complex DNA lesions, including clustered DNA damage (69) and DNA-protein crosslinks (70, 71). Given that X60 cells exhibit increased numbers of heterochromatin domains and radiation-induced Rad51 foci as compared with NR-S1 cells (**Figure 2**), it appears conceivable that enhanced HR-repair capacity and heterochromatin dynamics contribute to X-ray and C-ion resistance in X60 cells. Whether such a mechanism of acquisition of radioresistance could be specific to X60 cells or shared by other radioresistant cancer cell lines remains to be explored. Nevertheless, future studies focusing on further our understanding of the underlying mechanisms of DSB repair in heterochromatin domains could, therefore, represent a significant breakthrough toward elucidating the mechanisms of acquisition of radioresistance in cancer cells and identifying novel therapeutic strategies for the treatment of radioresistant tumors.

Acquisition of C-Ion Resistance Following Repeated C-Ion Irradiation

To date, only a limited number of studies have investigated the acquisition of C-ion resistance, and it remains unclear whether repeated C-ion irradiation can lead to radioresistance in cancer cells. To address this question, in a recent study, we irradiated NR-S1 cells with a total dose of 30 Gy of C-ion radiation applied in 5-Gy fractions in order to establish a C30 radioresistant cancer cell line (**Figure 1**). This C-ion irradiation regimen is biologically equivalent to the X-ray irradiation regimen used to establish the X60 cell line, because NR-S1 cells exhibit comparable survival following exposure to 5 Gy and 10 Gy of C-ion and X-ray radiation, respectively. Interestingly, when we assessed the X-ray and C-ion radiation sensitivity of C30 cells using a colony formation assay, we found that C30 cells displayed moderate resistance to C-ion radiation but not to X-ray radiation (35).

Although it remains unclear why repeated X-ray irradiation but not repeated C-ion irradiation conferred significant C-ion-resistance to NR-S1 derivative-cells, we believe that enrichment

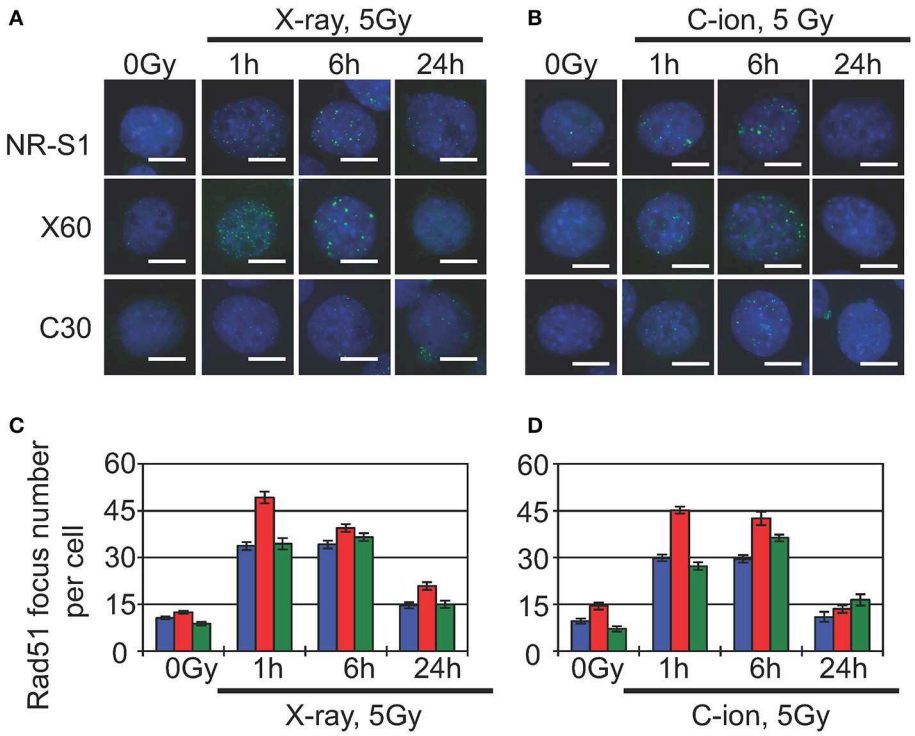

FIGURE 2 | Analysis of Rad51-foci formation in parental NR-S1 cells and radioresistant X60 and C30 cells. **(A,B)** Representative immunofluorescence images of NR-S1, X60, and C30 cells irradiated with 10 Gy of X-ray radiation **(A)** or 5 Gy of C-ion radiation **(B)**, as previously described (51, 56). At the indicated time after irradiation, cells were fixed and labeled with anti-Rad51 antibodies (green) using standard procedures (34, 35). Nuclei were counterstained by Hoechest33342 (blue). Scale bars, 10 μm. **(C,D)** Histograms showing the average number of Rad51 foci per cell following X-ray **(C)** and C-ion **(D)** irradiation of NR-S1 (blue), X60 (red), and C30 (green) cells. Data represent the mean ± standard deviation.

in CSCs might be a contributing factor. Indeed, it is widely recognized that CSCs are more resistant to X-ray radiation and anticancer drugs than more differentiated cancer cells. Furthermore, as noted, several studies report that repeated X-ray irradiation can increase the CSC fraction within a cancer cell population (49, 50, 72–74). Conversely, Cui et al. (75) showed that C-ion radiation could efficiently kill CSCs both *in vitro* and *in vivo*. Therefore, it is conceivable that repeated X-ray irradiation but not repeated C-ion irradiation could contribute to enriching a radioresistant subpopulation with CSC-like characteristics. However, there is one element in contradiction to this hypothesis. Because most CSCs are in a G0 quiescent state (45), the non-CSC subpopulation might proliferate faster; therefore, if the primary factor in the acquisition of X-ray and C-ion resistance is enrichment in CSCs, the level of radioresistance of a growing X60 cell population, for example, could gradually decrease over time, which was not observed (34, 35).

Collectively, these findings indicate that CSC enrichment and other mechanisms, such as genetic alterations and mutations (76), might jointly contribute to the acquisition of both X-ray and C-ion resistance in cancer cells. Although further investigations are required to elucidate these mechanisms, the current body of evidence suggests that C-ion irradiation does not induce radioresistance and can be used for the treatment of locally recurrent tumors arising after primary CIRT.

EFFECTS OF *IN VIVO* REPEATED PHOTON OR C-ion IRRADIATION

Numerous studies are focused on translating results obtained with *in vitro* models of radioresistant cancer cells into clinical practice. Therefore, it appears essential to determine whether phenotypic changes resulting from repeated photon or particle irradiation also occur *in vivo*. However, to the best of our knowledge, the effects of *in vivo* repeated photon or particle irradiation on the acquisition of radioresistance in cancer cells has not been reported.

To address this question and examine whether the characteristics of repeatedly irradiated tumors differ from those of parental tumors, we recently established *in vivo* models of regrown irradiated tumors (77). To this end, NR-S1-derived tumors engrafted into C3H/He mice were irradiated with single doses of γ-ray (30 Gy) or C-ion (15 Gy) radiation, which have comparable effects on tumor growth. Two weeks after irradiation, we harvested the irradiated tumors and transplanted them into healthy mice, and 2 weeks later, the regrown tumors were irradiated again, with this irradiation/regrowth/transplant process repeated six times in total. The resulting repeatedly irradiated tumors were exposed to total doses of 180 Gy of γ-ray radiation and 90 Gy of C-ion radiation and denoted as G180 and C90 *in vivo* regrown tumor models, respectively

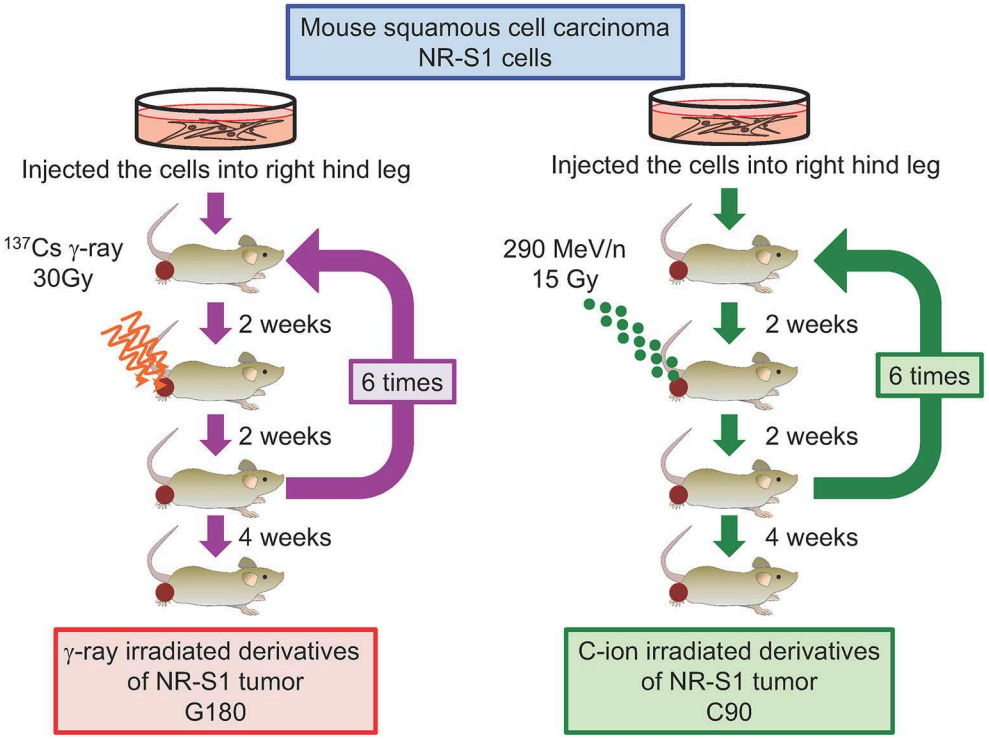

FIGURE 3 | Diagram describing the establishment of regrown tumor models through repeated γ-ray or C-ion irradiation. Mouse squamous cell carcinoma NR-S1 cells were injected into the right hind leg of healthy C3H/He mice. Upon reaching ∼10 mm in diameter, tumors derived from NR-S1 cells were irradiated with 30 Gy of γ-ray radiation or 15 Gy of C-ion radiation and allowed to regrow for 2 weeks before transplant into the right hind leg of healthy mice. The irradiation/regrow/transplant procedure was performed six times in total, resulting in regrown tumors exposed to total doses of 180 Gy of γ-ray radiation and 90 Gy of C-ion radiation, respectively. The tumors were finally harvested for analysis 4 weeks after the final irradiation (77).

(**Figure 3**). We then examined differences in tumor-growth potential, spontaneous metastasis from the primary site to the lung surface, tumor-grafted mouse survival, and radiosensitivity between non-irradiated NR-S1-derived tumors and G180 and C90 tumors.

Notably, G180 tumors displayed drastically increased tumor-growth rates and metastatic potential compared with those of non-irradiated tumors, and mice grafted with G180 tumors displayed significantly shorter survival than those grafted with non-irradiated tumors. By contrast, the characteristics of the C90 tumors remained comparable to those of non-irradiated tumors. Importantly, X-ray and C-ion irradiation of G180 and C90 tumors did not affect the relative tumor-growth rates, spontaneous lung metastasis, and survival of tumor-grafted mice as compared with non-irradiated tumors. Furthermore, colony formation assays performed using cells isolated from non-irradiated, G180, and C90 tumors showed that they all added similar sensitivity to X-ray and C-ion radiation (77). Moreover, compared with non-irradiated and C90 tumors, G180 tumors harbored numerous microvessels and expressed genes associated with angiogenesis and metastasis, including *VEGFA*, *HIF1A*, *FN1*, *MMP2*, *MMP9*, *PAI1*, and *PLAU*. Together, these data indicated that, contrary to repeated *in vitro* irradiation, repeated *in vivo* γ-ray and C-ion irradiation did not lead to the acquisition of radioresistance in regrown tumors. However, repeated photon irradiation but not particle irradiation appeared to enhance tumor growth and metastasis, resulting in an increased aggressiveness of regrown tumors.

These findings could suggest that repeated irradiation affects the tumor microenvironment rather than the tumor itself or its CSC subpopulation. Although our investigations could not determine whether repeated photon irradiation enriched the CSC subpopulation in regrown tumors, our data showed that G180 tumor cells in suspension culture had a significantly higher sphere-formation potential than their non-irradiated and C90 counterparts (77). Because CSCs are characterized by significant resistance to cytotoxic agents, including radiation and anticancer drugs, we believe that G180 tumors are likely enriched in tumor-initiating cells (TICs) that differ from a typical CSC subpopulation. To date, such phenomena have not been reported, and further studies will be required to determine which cells among cancer and stromal cells are mostly affected by repeated *in vivo* irradiation and what mechanisms lead to increased aggressiveness in repeatedly irradiated tumors.

Crucially, these findings also demonstrated that repeated C-ion irradiation was far less prone to induce acquisition of radioresistance and enhance tumor aggressiveness, as assessed by tumor growth, metastatic potential, and prognosis of

tumor-grafted mice. Although it remains necessary to ascertain why C-ion radiation effectively suppressed tumor aggressiveness and TIC or CSC subpopulations, we believe that the accumulated evidence supports CIRT as a promising treatment for local recurrent tumors.

RELATIONSHIP BETWEEN THE 4Rs OF RADIOTHERAPY AND RADIORESISTANCE ACQUISITION

Tumor shrinkage by fractionated radiotherapy has been explained by the "4Rs" of radiotherapy, where each "R" represents "Repair," "Repopulation," "Redistribution," and "Reoxygenation" (78). "Repair" denotes the difference in cell survival of tumor cells and normal tissue between single or fractionated irradiation at the same radiation dose (79) and is basically measured by colony formation assay, followed by calculation of α and β values using a linear-quadratic model to quantify the radiosensitivity of each cell (80). "Repopulation" describes regeneration of normal tissue, such as skin and mucosal tissue (81). This concept relies on experimental results showing that the recovery of skin and mucosal tissue occurs faster than regrowth of gross tumor mass, and that each fractionation regime of radiotherapy can be determined based on these differences. Because α and β values and difference in recovery between tumor and normal tissue are used for treatment planning of radiotherapy, they are recognized as important therapeutic components. "Redistribution" indicates synchronization of the cell cycle in cells exposed to radiation. The tumor harbors multiple cell types exhibiting various cell cycle phases (82). Upon treatment of the tumor with radiotherapy, the relatively radiosensitive cell fractions, such as those in the G2/M phase, will die first, whereas the relatively radioresistant cell fractions, such as those in the G1 and S phases, will survive. However, cells surviving the first round of irradiation will enter a radiosensitive phase of the cell cycle during subsequent rounds and eventually will subsequently be efficiently killed. "Reoxygenation" describes changes in well-oxygenated areas of an irradiated tumor (83). Partial oxygen pressure in the peripheral tumor is higher than that in the center, because nutrition and oxygen at the periphery is well-supplied by tumor blood vessels (78). The partial oxygen pressure enhances the cell-killing effect, because radiation-induced reactive oxygen species, such as OH radical, initiated DNA breakage (84). Therefore, well-oxygenated areas of a tumor (i.e., the periphery) are killed first, followed by vascularization of the central tumor along with tumor shrinkage. Repetition of this process enhances the efficacy of radiotherapy. The 4Rs reasonably describe the process of tumor shrinkage during radiotherapy and are useful for recognizing tumor and environmental conditions the determine radioresistance or radiosensitivity.

On the other hand, our previous results suggest the possibility that use of the 4Rs might not be appropriate for planning secondary radiotherapy. At the very least, using the same definitions as those used to determine primary radiotherapy might not be suitable for secondary radiotherapy. If the tumor targeted for secondary radiotherapy has acquired radioresistance via EMT, the total dose required to control the tumor should be increased. This suggests that the α and β values of the tumor cells and the dose fractionation used to prevent normal-tissue complications should be changed. Therefore, this suggests that "Repair" and "Repopulation" should be properly adjusted in the planning of secondary radiotherapy. In cases where primary radiotherapy fails to control tumor growth, followed by tumor regrowth within the irradiation field, this suggests that radioresistant cancer cells, such as CSCs, likely exist in the target area. If these tumors are treated with another round of irradiation, "Reoxygenation" might not be suitable for interpreting tumor radiosensitivity, because the CSCs might be in a quiescent state and capable of surviving within the hypoxic area. In addition to the induction of the radioresistant cancer cells, our data showed that repeated photon irradiation *in vivo* promoted acquisition of a more aggressive phenotype in the tumors. These characteristic changes do not fit the classical 4Rs of radiotherapy. Although our results were obtained by experiments using mouse cancer cell lines rather that human specimens, and the results *in vitro* did not match those obtained *in vivo*, they indicated that other hallmarks are required to interpret possible radioresistant or aggressive fractions in target tumors for planning secondary radiotherapy targeting regrown tumors. Given that hypoxic areas are primary niches of CSCs (85), and the tumor vasculature clearly changes after irradiation (86), imaging techniques used to identify hypoxic areas and well-vascularized areas in target tumors will likely be useful for planning secondary radiotherapy. Indeed, drugs targeting hypoxic areas have been developed (87, 88), and tumor blood vessels can be visualized by contrast-enhanced magnetic resonance imaging (89).

WHAT ARE THE MAIN OPEN QUESTIONS IN THE FIELD?

Although numerous studies show that repeated X-ray irradiation can lead to increased radioresistance in various cancer cells, the primary source of radioresistant cancer cells remains elusive. Therefore, it is imperative to determine whether the selection of inherently radioresistant cells or emergence of radioresistant cells due to *de novo* genetic alterations is the primary cause of the acquisition of radioresistance in order to prevent the appearance of radioresistance and improve patient care. With the recent development of genetic barcoding techniques (90–93), we can now label a large number of cells within a given population. Combined with high-throughput DNA sequencing, genetic barcoding could be used to track and identify the type(s) of cells that can survive and proliferate following repeated irradiation.

Although extensive efforts have been made to investigate the mechanisms of acquisition of radioresistance in cancer cells using *in vitro* models, the radiobiological effects of repeated *in vivo* irradiation remain poorly understood. Tumors are complex ecosystems comprising various cell types, including cancer, stromal, and immune cells. Furthermore, the tumor environment is partly heterogeneous, with hypoxic or nutrient-deprived areas. In this regard, our *in vivo* data suggest that changes in the tumor microenvironment, including angiogenesis,

might be critical for the prognosis of mice bearing regrown tumors after repeated irradiation.

In addition to the limited amount of data available concerning the effects of repeated *in vivo* irradiation, the differences between photon and particle irradiation remain largely unknown. Indeed, photon and particle radiation have distinct physical properties, and their resulting biological effects might be very different. For example, particle radiation produces a high density of reactive oxygen species and clustered DNA damage along the particle-beam track (94). Nevertheless, there is, to date, no sensible theory linking the physical characteristics of radiation to their biological effects, including high relative biological effectiveness in cell-survival assays and suppression of metastasis both *in vitro* and *in vivo*.

Answers to these questions would definitely promote the understand of why repeated C-ion irradiation does not appear to induce significant radioresistance in cancer cells, whereas repeated X-ray irradiation leads to significant resistance to both X-ray and C-ion radiation in NR-S1 cells. The identification of potential targets to enhance or elicit radiosensitization could facilitate the development of novel therapeutic strategies for the treatment of radioresistant tumors and recurrent tumors after primary radiotherapy.

CONCLUDING REMARKS

To date, few reports have been published describing the acquisition of radioresistance in repeatedly irradiated tumor cells, particularly after particle irradiation. A series of experiments using models of tumors repeatedly irradiated with either photon or particle radiation show that repeated *in vitro* irradiation with relatively high doses of X-ray radiation can induce significant resistance to both X-ray and C-ion radiation. By contrast, repeated *in vitro* irradiation with relative biological effectiveness doses of C-ion radiation does not contribute to the acquisition of X-ray or C-ion resistance in tumor cells. Somewhat surprisingly, repeated X-ray or C-ion irradiation of *in vivo* regrown tumor models does not increase their radioresistance; however, repeated photon irradiation but not C-ion irradiation increased tumor aggressiveness. Because the evidence was limited to a single tumor cell type, further studies are required to conclusively determine the effects of repeated irradiation on the acquisition of radioresistance in tumors.

AUTHOR CONTRIBUTIONS

KS contributed to the design and wrote the manuscript. TS and TI rewrote and made edits. TI conducted the final review.

FUNDING

This work was supported by JPSP KAKENHI Grant Nos. 15K15467 and 24591857, and by the Center of Innovation Program (COI stream from JST) and P-CREATE grant from AMED, and was performed as a research project with heavy ions at NIRS-HIMAC (No. 15J183).

ACKNOWLEDGMENTS

The authors would like to thank their colleagues in ex-Research Center for Charged Particle Therapy at the National Institute of Radiological Sciences. This research was supported in part by the Research Project Heavy Ions at NIRS-HIMAC. We also thank Editage (www.editage.com) for English language editing.

REFERENCES

1. Ohnishi H, Shirato H, Nagata Y, Hiraolka M, Fujino M, Gomi K, et al. Hypofractinated stereoptactic radiotherapy (HypoFXSRT) for stage I non-small cell lung cancer: updated results of 257 patients in a Japnese multi-institutional study. *J Thorac Oncol.* (2007) 2:S94–100. doi: 10.1097/JTO.0b013e318074de34
2. Sanuki N, Takeda A, Oku Y, Mizuno T, Aoki Y, Eriguchi T, et al. Stereotactic body radiotherapy for small hepatocellular carcinoma: a retrospective outcome analysis in 185 patients. *Acta Oncol.* (2014) 53:399–404. doi: 10.3109/0284186X.2013.820342
3. Freeman DE, King CR. Stereotactic body radiotherapy for low-risk prostate cancer: five-year outcomes. *Radio Oncol.* (2011) 6:3. doi: 10.1186/1748-717X-6-3
4. Shioyama Y, Onishi H, Takayama K, Matsuo Y, Takeda A, Yamashita H, et al. Clinical outcomes of stereotactic body radiotherapy for patients with stage I small-cell lung cancer: analysis of a subset of the Japanese radiological society multi-institutional SBRT study group database. *Technol Cancer Res Treat.* (2018). 17:1533033818783904. doi: 10.1177/1533033818783904
5. Kastelijn EA, El Sharouni SY, Hofman FN, Van Putte BP, Monninkhof EM, Van Vulpen M, et al. Clinical outcomes in early-stage NSCLC treated with stereotactic body radiotherapy versus surgical resection. *Anticancer Res.* (2015) 35:5607–14.
6. Ackerson BG, Tong BC, Hong JC, Gu L, Chino J, Trotter JW, et al. Stereotactic body radiation therapy versus sublobar resection for stage I NSCLC. *Lung Cancer.* (2018) 125:185–91. doi: 10.1016/j.lungcan.2018.09.020
7. Kamada T, Tsujii H, Blakely EA, Debus J, De Neve W, Durante M, et al. Carbon ion radiotherapy in Japan: an assessment of 20 years of clinical experience. *Lancet Oncol.* (2015). 16:e93–e100. doi: 10.1016/S1470-2045(14)70412-7
8. Tsuji H, Ishikawa H, Yanagi T, Hirasawa N, Kamada T, Mizoe JE. Carbon-ion radiotherapy for locally advanced or unfavorably located choroidal melanoma: a Phase I/II dose-escalation study. *Int J Radiat Oncol Biol Phys.* (2007) 67:857–62. doi: 10.1016/j.ijrobp.2006.09.022
9. Imai R, Kamada T, Tsuji H, Yanagi T, Baba M, Miyamoto T, et al. Carbon ion radiotherapy for unresectable sacral chordomas. *Clin Cancer Res.* (2004) 10:5741–6. doi: 10.1158/1078-0432.CCR-04-0301
10. Jingu K, Tsujii H, Mizoe JE, Hasegawa A, Bessho H, Takagi R, et al. Carbon ion radiation therapy improves the prognosis of unresectable adult bone and soft-tissue sarcoma of the head and neck. *Int J Radiat Oncol Biol Phys.* (2012) 82:2125–31. doi: 10.1016/j.ijrobp.2010.08.043
11. Serizawa I, Kagei K, Kamada T, Imai R, Sugahara S, Okada T, et al. Carbon ion radiotherapy for unresectable retroperitoneal sarcomas. *Int J Radiat Oncol Biol Phys.* (2009). 75:1105–10. doi: 10.1016/j.ijrobp.2008.12.019
12. Takahashi W, Nakajima M, Yamamoto N, Tsujii H, Kamada T, Tsujii H. Carbon ion radiotherapy in a hypofractionation regimen for stage I non-small-cell lung cancer. *J Radiat Res.* (2014) 55:i26–7. doi: 10.1093/jrr/rrt216
13. Spratt DE, Wu AJ, Adeseye V, Din SU, Shaikh F, Woo KM, et al. Recurrence patterns and second primary lung cancers after stereotactic body radiation therapy for early-stage non-small-cell lung cancer: implications for surveillance. *Clin Lung Cancer.* (2016) 17:177–83.e2. doi: 10.1016/j.cllc.2015.09.006

14. Giuliani ME, Hope A, Mangona V, Guckenberger M, Mantel F, Peulen H, et al. Predictors and patterns of regional recurrence following lung SBRT: a report from the elekta lung research group. *Clin Lung Cancer*. (2017) 18:162–8. doi: 10.1016/j.cllc.2016.10.006
15. Hobbs CJ, Ko SJ, Paryani NN, Accurso JM, Olivier KR, Garces Y, et al. Stereotactic body radiotherapy for medically inoperable stage I-II non-small cell lung cancer: the Mayo clinic experience. *Mayo Clin Proc Innov Qual Outcomes*. (2017) 2:40–8. doi: 10.1016/j.mayocpiqo.2017.11.001
16. Samson P, Rehman S, Juloori A, DeWees T, Roach M, Bradley J, et al. Local control for clinical stage I non-small cell lung cancer treated with 5-fraction stereotactic body radiation therapy is not associated with treatment schedule. *Pract Radiat Oncol*. (2018) 8:404–13. doi: 10.1016/j.prro.2018.04.004
17. von Reibnitz D, Shaikh F, Wu AJ, Treharne GC, Dick-Godfrey R, Foster A, et al. Stereotactic body radiation therapy (SBRT) improves local control and overall survival compared to conventionally fractionated radiation for stage I non-small cell lung cancer (NSCLC). *Acta Oncol*. (2018) 57:1567–73. doi: 10.1080/0284186X.2018.1481292
18. Shintani T, Matsuo Y, Iizuka Y, Mitsuyoshi T, Mizowaki T. A Retrospective long-term follow-up study of stereotactic body radiation therapy for non-small cell lung cancer from a single institution: incidence of late local recurrence. *Int J Radiat Oncol Biol Phys*. (2018) 100:1228–36. doi: 10.1016/j.ijrobp.2018.01.050
19. Koto M, Miyamoto T, Yamamoto N, Nishimura H, Yamada S, Tsujii H. Local control and recurrence of stage I non-small cell lung cancer after carbon ion radiotherapy. *Radiother Oncol*. (2004) 71:147–56. doi: 10.1016/j.radonc.2004.02.007
20. Høyer M. Re-irradiation with stereotactic body radiation therapy (SBRT). *Chin Clin Oncol*. (2017) 6 (Suppl. 2):S15. doi: 10.21037/cco.2017.07.01
21. Ogawa Y, Shibamoto Y, Hashizume C, Kondo T, Iwata H, Tomita N, et al. Repeat stereotactic body radiotherapy (SBRT) for local recurrence of non-small cell lung cancer and lung metastasis after first SBRT. *Radiat Oncol*. (2018) 13:136. doi: 10.1186/s13014-018-1080-4
22. Shirai K, Ohno T, Saitoh JI, Okamoto M, Katoh H, Murata K, et al. Prospective study of isolated recurrent tumor re-irradiation with carbon-ion beams. *Front Oncol*. (2019) 9:181. doi: 10.3389/fonc.2019.00181
23. Milano MT, Kong FS, Movsas B. Stereotactic body radiotherapy as salvage treatment for recurrence of non-small cell lung cancer after prior surgery or radiotherapy. *Transl Lung Cancer Res*. (2019) 8:78–87. doi: 10.21037/tlcr.2018.08.15
24. Kuwahara Y, Li L, Baba T, Nakagawa H, Shimura T, Yamamoto Y, et al. Clinically relevant radioresistant cells efficiently repair DNA double-strand breaks induced by X-rays. *Cancer Sci*. (2009) 100:747–52. doi: 10.1111/j.1349-7006.2009.01082.x
25. Kuwahara Y, Oikawa T, Ochiai Y, Roudkenar MH, Fukumoto M, Shimura T, et al. Enhancement of autophagy is a potential modality for tumors refractory to radiotherapy. *Cell Death Dis*. (2011) 2:e177. doi: 10.1038/cddis.2011.56
26. Lee YS, Oh JH, Yoon S, Kwon MS, Song CW, Kim KH, et al. Differential gene expression profiles of radioresistant non-small-cell lung cancer cell lines established by fractionated irradiation: tumor protein p53-inducible protein 3 confers sensitivity to ionizing radiation. *Int J Radiat Oncol Biol Phys*. (2010) 77:858–66. doi: 10.1016/j.ijrobp.2009.12.076
27. Lin TY, Chang JT, Wang HM, Chan SH, Chiu CC, Lin CY, et al. Proteomics of the radioresistant phenotype in head-and-neck cancer: Gp96 as a novel prediction marker and sensitizing target for radiotherapy. *Int J Radiat Oncol Biol Phys*. (2010) 78:246–56. doi: 10.1016/j.ijrobp.2010.03.002
28. Luo J, Wang W, Tang Y, Zhou D, Gao Y, Zhang Q, et al. mRNA and methylation profiling of radioresistant esophageal cancer cells: the involvement of Sall2 in acquired aggressive phenotypes. *J Cancer*. (2017) 8:646–56. doi: 10.7150/jca.15652
29. Lynam-Lennon N, Reynolds JV, Pidgeon GP, Lysaght J, Marignol L, Maher SG. Alterations in DNA repair efficiency are involved in the radioresistance of esophageal adenocarcinoma. *Radiat Res*. (2010) 174:703–11. doi: 10.1667/RR2295.1
30. Mitsuhashi N, Takahashi T, Sakurai H, Nozaki M, Akimoto T, Hasegawa M, et al. A radioresistant variant cell line, NMT-1R, isolated from a radiosensitive rat yolk sac tumour cell line, NMT-1: differences of early radiation-induced morphological changes, especially apoptosis. *Int J Radiat Biol*. (1996) 69:329–36. doi: 10.1080/095530096145887
31. Pearce AG, Segura TM, Rintala AC, Rintala-Maki ND, Lee H. The generation and characterization of a radiation-resistant model system to study radioresistance in human breast cancer cells. *Radiat Res*. (2001) 156:739–50. doi: 10.1667/0033-7587(2001)156[0739:TGACOA]2.0.CO;2
32. Post AEM, Smid M, Nagelkerke A, Martens JWM, Bussink J, Sweep FCGJ, et al. Interferon-stimulated genes are involved in cross-resistance to radiotherapy in tamoxifen-resistant breast cancer. *Clin Cancer Res*. (2018) 24:3397–408. doi: 10.1158/1078-0432.CCR-17-2551
33. Russell J, Wheldon TE, Stanton P. A radioresistant variant derived from a human neuroblastoma cell line is less prone to radiation-induced apoptosis. *Cancer Res*. (1995) 55:4915–4921.
34. Sato K, Imai T, Okayasu R, Shimokawa T. Heterochromatin domain number correlates with X-ray and carbon-ion radiation resistance in cancer cells. *Radiat Res*. (2014) 182:408–19. doi: 10.1667/RR13492.1
35. Sato K, Azuma R, Imai T, Shimokawa T. Enhancement of mTOR signaling contributes to acquired X-ray and C-ion resistance in mouse squamous carcinoma cell line. *Cancer Sci*. (2017) 108:2004–10. doi: 10.1111/cas.13323
36. Shimura T, Kakuda S, Ochiai Y, Nakagawa H, Kuwahara Y, Takai Y, et al. Acquired radioresistance of human tumor cells by DNA-PK/AKT/GSK3beta-mediated cyclin D1 overexpression. *Oncogene*. (2010) 29:4826–37. doi: 10.1038/onc.2010.238
37. Shimura T, Noma N, Sano Y, Ochiai Y, Oikawa T, Fukumoto M, et al. AKT-mediated enhanced aerobic glycolysis causes acquired radioresistance by human tumor cells. *Radiother Oncol*. (2014) 112:302–7. doi: 10.1016/j.radonc.2014.07.015
38. Shimura T. Targeting the AKT/cyclin D1 pathway to overcome intrinsic and acquired radioresistance of tumors for effective radiotherapy. *Int J Radiat Biol*. (2017) 93:381–5. doi: 10.1080/09553002.2016.1257832
39. Shintani Y, Okimura A, Sato K, Nakagiri T, Kadota Y, Inoue M, et al. Epithelial to mesenchymal transition is a determinant of sensitivity to chemoradiotherapy in non-small cell lung cancer. *Ann Thorac Surg*. (2011) 92:1794–804. doi: 10.1016/j.athoracsur.2011.07.032
40. You S, Li R, Park D, Xie M, Sica GL, Cao Y, et al. Disruption of STAT3 by niclosamide reverses radioresistance of human lung cancer. *Mol Cancer Ther*. (2014) 13:606–16. doi: 10.1158/1535-7163.MCT-13-0608
41. Zhou FX, Xiong J, Luo ZG, Dai J, Yu H J, Liao ZK, et al. cDNA expression analysis of a human radiosensitive-radioresistant cell line model identifies telomere function as a hallmark of radioresistance. *Radiat Res*. (2010) 174:550–7. doi: 10.1667/RR1657.1
42. Thiery JP. Epithelial-mesenchymal transitions in tumour progression. *Nat Rev Cancer*. (2012) 2:442–54. doi: 10.1038/nrc822
43. Jung JW, Hwang SY, Hwang JS, Oh ES, Park S, Han IO. Ionising radiation induces changes associated with epithelial-mesenchymal transdifferentiation and increased cell motility of A549 lung epithelial cells. *Eur J Cancer*. (2007) 43:1214–24. doi: 10.1016/j.ejca.2007.01.034
44. Zhou YC, Liu JY, Li J, Zhang J, Xu YQ, Zhang HW, et al. Ionizing radiation promotes migration and invasion of cancer cells through transforming growth factor-beta-mediated epithelial-mesenchymal transition. I*nt J Radiat Oncol Biol Phys*. (2011) 81:1530–7. doi: 10.1016/j.ijrobp.2011.06.1956
45. Maugeri-Saccà M, Bartucci M, De Maria R. DNA damage repair pathways in cancer stem cells. *Mol Cancer Ther*. (2012) 11:1627–36. doi: 10.1158/1535-7163.MCT-11-1040
46. Diehn M, Cho RW, Lobo NA, Kalisky T, Dorie MJ, Kulp AN. Association of reactive oxygen species levels and radioresistance in cancer stem cells. *Nature*. (2009) 458:780–3. doi: 10.1038/nature07733
47. Ishimoto T, Nagano O, Yae T, Tamada M, Motohara T, Oshima H, et al. CD44 variant regulates redox status in cancer cells by stabilizing the xCT subunit of system xc(-) and thereby promotes tumor growth. *Cancer Cell*. (2011) 19:387–400. doi: 10.1016/j.ccr.2011.01.038
48. Cheung TH, Rando TA. Molecular regulation of stem cell quiescence. *Nat Rev Mol Cell Biol*. (2013) 14:329–40. doi: 10.1038/nrm3591
49. Lagadec C, Vlashi E, Della Donna L, Meng Y, Dekmezian C, Kim K, et al. Survival and self-renewing capacity of breast cancer initiating cells during fractionated radiation treatment. *Breast Cancer Res*. (2010) 12:R13. doi: 10.1186/bcr2479
50. Ghisolfi L, Keates AC, Hu X, Lee DK, Li CJ. Ionizing radiation induces stemness in cancer cells. *PLoS ONE*. (2012) 7:e43628. doi: 10.1371/journal.pone.0043628

51. Mani SA, Guo W, Liao MJ, Eaton EN, Ayyanan A, Zhou AY, et al. The epithelial-mesenchymal transition generates cells with properties of stem cells. *Cell*. (2008) 133:704–15. doi: 10.1016/j.cell.2008.03.027
52. Liang Y, Zhong Z, Huang Y, Deng W, Cao J, Tsao G, et al. Stem-like cancer cells are inducible by increasing genomic instability in cancer cells. *J Biol Chem*. (2010) 285:4931–40. doi: 10.1074/jbc.M109.048397
53. Shimura T. Acquired radioresistance of cancer and the AKT/GSK3b/cyclin D1 overexpression cycle. *J Radiat Res*. (2011) 52:539–44. doi: 10.1269/jrr.11098
54. Shimura T, Ochiai Y, Noma N, Oikawa T, Sano Y, Fukumoto M. Cyclin D1 overexpression perturbs DNA replication and induces replication-associated DNA double-strand breaks in acquired radioresistant cells. *Cell Cycle*. (2013) 12:773–82. doi: 10.4161/cc.23719
55. Chang L, Graham PH, Hao J, Ni J, Bucci J, Cozzi PJ, et al. Acquisition of epithelial-mesenchymal transition and cancer stem cell phenotypes is associated with activation of the PI3K/Akt/mTOR pathway in prostate cancer radioresistance. *Cell Death Dis*. (2013) 4:e875. doi: 10.1038/cddis.2013.407
56. Chang L, Graham PH, Hao J, Ni J, Bucci J, Cozzi PJ, et al. PI3K/Akt/mTOR pathway inhibitors enhance radiosensitivity in radioresistant prostate cancer cells through inducing apoptosis, reducing autophagy, suppressing NHEJ and HR repair pathways. *Cell Death Dis*. (2014) 5: e1437. doi: 10.1038/cddis.2014.415
57. Chen H, Ma Z, Vanderwaal RP, Feng Z, Gonzalez-Suarez I, Wang S, et al. The mTOR inhibitor rapamycin suppresses DNA double-strand break repair. *Radiat Res*. (2011) 175:214–24. doi: 10.1667/RR2323.1
58. Takahashi A, Matsumoto H, Yuki K, Yasumoto J, Kajiwara A, Aoki M, et al. High-LET radiation enhanced apoptosis but not necrosis regardless of p53 status. *Int J Radiat Oncol Biol Phys*. (2004) 60:591–7. doi: 10.1016/j.ijrobp.2004.05.062
59. Schlaff CD, Krauze A, Belard A, O'Connell JJ, Camphausen KA. Bringing the heavy: carbon ion therapy in the radiobiological and clinical context. *Radiat Oncol*. (2014) 9:88. doi: 10.1186/1748-717X-9-88
60. Okayasu R. Repair of DNA damage induced by accelerated heavy ions-A mini review. *Int J Cancer*. (2012) 130:991–1000. doi: 10.1002/ijc.26445
61. Hirayama R, Uzawa A, Takase N, Matsumoto Y, Noguchi M, Koda K, et al. Evaluation of SCCVII tumor cell survival in clamped and non-clamped solid tumors exposed to carbon-ion beams in comparison to X-rays. *Mutat Res*. (2013) 756:146–51. doi: 10.1016/j.mrgentox.2013.05.008
62. Tinganelli W, Ma NY, Von Neubeck C, Maier A, Schicker C, Kraft-Weyrather W, et al. Influence of acute hypoxia and radiation quality on cell survival. *J Radiat Res*. (2013) 54 (Suppl. 1):i23–30. doi: 10.1093/jrr/rrt065
63. Tinganelli W, Durante M, Hirayama R, Krämer M, Maier A, Kraft-Weyrather W, et al. Kill-painting of hypoxic tumours in charged particle therapy. *Sci Rep*. (2015) 5:17016. doi: 10.1038/srep17016
64. Luijsterburg MS, Dinant C, Lans H, Stap J, Wiernasz E, Lagerwerf S, et al. Heterochromatin protein 1 is recruited to various types of DNA damage. *J Cell Biol*. (2009) 185:577–86. doi: 10.1083/jcb.200810035
65. Baldeyron C, Soria G, Roche D, Cook AJ, Almouzni G. HP1alpha recruitment to DNA damage by p150CAF-1 promotes homologous recombination repair. *J Cell Biol*. (2011) 193:81–95. doi: 10.1083/jcb.201101030
66. Chiolo I, Minoda A, Colmenares SU, Polyzos A, Costes SV, Karpen GH. Double-strand breaks in heterochromatin move outside of a dynamic HP1a domain to complete recombinational repair. *Cell*. (2011) 144:732–44. doi: 10.1016/j.cell.2011.02.012
67. Ryu T, Spatola B, Delabaere L, Bowlin K, Hopp H, Kunitake R, et al. Heterochromatic breaks move to the nuclear periphery to continue recombinational repair. *Nat Cell Biol*. (2015) 17:1401–11. doi: 10.1038/ncb3258
68. Jakob B, Splinter J, Conrad S, Voss KO, Zink D, Durante M, et al. DNA double-strand breaks in heterochromatin elicit fast repair protein recruitment, histone H2AX phosphorylation and relocation to euchromatin. *Nucleic Acids Res*. (2011) 39:6489–99. doi: 10.1093/nar/gkr230
69. Hada M, Georgakilas AG. Formation of clustered DNA damage after high-LET irradiation: a review. *J Radiat Res*. (2008) 49:203–10. doi: 10.1269/jrr.07123
70. Ide H, Shoulkamy MI, Nakano T, Miyamoto-Matsubara M, Salem AM. Repair and biochemical effects of DNA-protein crosslinks. *Mutat Res*. (2011) 711:113–22. doi: 10.1016/j.mrfmmm.2010.12.007
71. Culard F, Bouffard S, Charlier M. High-LET irradiation of a DNA- binding protein: protein-protein and DNA-protein crosslinks. *Radiat Res*. (2005) 164:774–80. doi: 10.1667/RR3456.1
72. López J, Poitevin A, Mendoza-Martínez V, Pérez-Plasencia C, García-Carrancá A. Cancer-initiating cells derived from established cervical cell lines exhibit stem-cell markers and increased radioresistance. *BMC Cancer*. (2012) 12:48. doi: 10.1186/1471-2407-12-48
73. Desai A, Webb B, Gerson SL. CD133+ cells contribute to radioresistance via altered regulation of DNA repair genes in human lung cancer cells. *Radiother Oncol*. (2014) 110:538–45. doi: 10.1016/j.radonc.2013.10.040
74. Sun L, Moritake T, Zheng YW, Suzuki K, Gerelchuluun A, Hong Z, et al. *In vitro* stemness characterization of radio-resistant clones isolated from a medulloblastoma cell line ONS-76. *J Radiat Res*. (2013) 54:61–9. doi: 10.1093/jrr/rrs078
75. Cui X, Oonishi K, Tsujii H, Yasuda T, Matsumoto Y, Furusawa Y, et al. Effects of carbon ion beam on putative colon cancer stem cells and its comparison with X-rays. *Cancer Res*. (2011) 71:3676–87. doi: 10.1158/0008-5472.CAN-10-2926
76. Durante M, Bedford JS, Chen DJ, Conrad S, Cornforth MN, Natarajan AT, et al. From DNA damage to chromosome aberrations: joining the break. *Mutat Res*. (2013) 756:5–13. doi: 10.1016/j.mrgentox.2013.05.014
77. Sato K, Nitta N, Aoki I, Imai T, Shimokawa T. Repeated photon and C-ion irradiations *in vivo* have different impact on alteration of tumor characteristics. *Sci Rep*. (2018) 8:1458. doi: 10.1038/s41598-018-19422-x
78. Withers HR. The four R's of radiotherapy. In: Lett JT, Adler H, editors. *Advances in Radiation Biology, Vol 5*. Cambridge, MA: Academic Press, Inc. (1975). p. 241–71.
79. Elkind MM. Fractional dose radiotherapy and its relationship to survival curve shape. *Cancer Treat Rev*. (1976) 3:1–15. doi: 10.1016/S0305-7372(76)80014-X
80. Brenner DJ. The linear-quadratic model is an appropriate methodology for determining isoeffective doses at large doses per fraction. *Semin Radiat Oncol*. (2008) 18:234–9. doi: 10.1016/j.semradonc.2008.04.004
81. Hall EJ, Giaccia AJ, editors. Time, dose, and fractionation in radiotherapy. In: *Radiobiology for Radiologists*. Philadelphia, PA: Lippincottt Williams & Wilkins (2011). p. 391–418.
82. Withers HR. Cell cycle redistribution as a factor in multifraction irradiation. *Radiology*. (1975) 114:199–202. doi: 10.1148/114.1.199
83. van Putten LM, Kallman RF. Oxygenation status of a transplantable tumor during fractionated radiation therapy. *J Natl Cancer Inst*. (1968) 40:441–5. doi: 10.1097/00007890-196808000-00017
84. Hirayama R, Ito A, Noguchi M, Matsumoto Y, Uzawa A, Kobashi G, et al. OH radicals from the indirect actions of X-rays induce cell lethality and mediate the majority of the oxygen enhancement effect. *Radiat Res*. (2013) 180:514–23. doi: 10.1667/RR13368.1
85. Peitzsch C, Perrin R, Hill RP, Dubrovska A, Kurth I. Hypoxia as a biomarker for radioresistant cancer stem cells. *Int J Radiat Biol*. (2014) 90:636–52. doi: 10.3109/09553002.2014.916841
86. Crokart N, Jordan BF, Baudelet C, Ansiaux R, Sonveaux P, Grégoire V, et al. Early reoxygenation in tumors after irradiation: determining factors and consequences for radiotherapy regimens using daily multiple fractions. *Int J Radiat Oncol Biol Phys*. (2005) 63:901–10. doi: 10.1016/j.ijrobp.2005.02.038
87. Stieb S, Eleftheriou A, Warnock G, Guckenberger M, Riesterer O. Longitudinal PET imaging of tumor hypoxia during the course of radiotherapy. *Eur J Nucl Med Mol Imaging*. (2018) 45:2201–17. doi: 10.1007/s00259-018-4116-y
88. Hirata K, Yamaguchi S, Shiga T, Kuge Y, Tamaki N. The Roles of hypoxia imaging using ^{18}F-fluoromisonidazole positron emission tomography in glioma treatment. *J Clin Med*. (2019) 24:E1088. doi: 10.3390/jcm8081088
89. Nitta N, Takakusagi Y, Kokuryo D, Shibata S, Tomita A, Higashi T, et al. Intratumoral evaluation of 3D microvasculature and nanoparticle distribution

using a gadolinium-dendron modified nano-liposomal contrast agent with magnetic resonance micro-imaging. *Nanomedicine*. (2018) 14:1315–24. doi: 10.1016/j.nano.2018.03.006
90. Bhang HE, Ruddy DA, Krishnamurthy Radhakrishna V, Caushi JX, Zhao R, Hims MM, et al. Studying clonal dynamics in response to cancer therapy using high-complexity barcoding. *Nat Med*. (2015). 21:440–8. doi: 10.1038/nm.3841
91. Kalhor R, Mali P, Church GM. Rapidly evolving homing CRISPR barcodes. *Nat Methods*. (2017) 14:195–200. doi: 10.1038/nmeth.4108
92. Guernet A, Mungamuri SK, Cartier D, Sachidanandam R, Jayaprakash A, Adriouch S, et al. CRISPR-barcoding for intratumor genetic heterogeneity modeling and functional analysis of oncogenic driver mutations. *Mol Cell*. (2016) 63:526–38. doi: 10.1016/j.molcel.2016.06.017
93. Nguyen LV, Pellacani D, Lefort S, Kannan N, Osako T, Makarem M, et al. Barcoding reveals complex clonal dynamics of *de novo* transformed human mammary cells. *Nature*. (2015) 528: 267–71. doi: 10.1038/nature15742
94. Tobias F, Durante M, Taucher-Scholz G, Jakob B. Spatiotemporal analysis of DNA repair using charged particle radiation. *Mutat Res*. (2010) 704:54–60. doi: 10.1016/j.mrrev.2009.11.004

Conflict of Interest: The authors declare that the research was conducted in the absence of any commercial or financial relationships that could be construed as a potential conflict of interest.

Copyright © 2019 Sato, Shimokawa and Imai. This is an open-access article distributed under the terms of the Creative Commons Attribution License (CC BY). The use, distribution or reproduction in other forums is permitted, provided the original author(s) and the copyright owner(s) are credited and that the original publication in this journal is cited, in accordance with accepted academic practice. No use, distribution or reproduction is permitted which does not comply with these terms.

frontiers in Oncology

PERSPECTIVE
published: 13 November 2019
doi: 10.3389/fonc.2019.01174

Targeting the Innate Immune Kinase IRAK1 in Radioresistant Cancer: Double-Edged Sword or One-Two Punch?

Peter H. Liu [1,2] *and Samuel Sidi* [1,2,3]*

[1] Division of Hematology and Medical Oncology, Icahn School of Medicine at Mount Sinai, Tisch Cancer Institute, New York, NY, United States, [2] Department of Cell, Developmental and Regenerative Biology, The Graduate School of Biomedical Sciences, Icahn School of Medicine at Mount Sinai, New York, NY, United States, [3] Department of Oncological Sciences, Icahn School of Medicine at Mount Sinai, New York, NY, United States

OPEN ACCESS

Edited by:
Paul N. Span, Radboud University Nijmegen Medical Centre, Netherlands

Reviewed by:
James W. Jacobberger, Case Western Reserve University, United States
Marleen Ansems, Radboud Institute for Molecular Life Sciences, Netherlands

***Correspondence:**
Samuel Sidi
samuel.sidi@mssm.edu

Specialty section:
This article was submitted to Radiation Oncology, a section of the journal Frontiers in Oncology

Received: *17 July 2019*
Accepted: *18 October 2019*
Published: *13 November 2019*

Citation:
Liu PH and Sidi S (2019) Targeting the Innate Immune Kinase IRAK1 in Radioresistant Cancer: Double-Edged Sword or One-Two Punch? Front. Oncol. 9:1174. doi: 10.3389/fonc.2019.01174

Antitumor immunity has emerged as a favorable byproduct of radiation therapy (RT), whereby tumor-associated antigens released from irradiated cells unleash innate and adaptive attacks on tumors located both within and outside the radiation field. RT-induced immune responses further provide actionable targets for overcoming tumor resistance to RT (R-RT); immunotherapy (IT) with checkpoint inhibitors or Toll-like receptor (TLR) agonists can markedly improve, if not synergize with, RT in preclinical models, and several of these drugs are currently investigated as radiosensitizers in patients. In an unbiased chemical-genetic screen in a zebrafish model of tumor R-RT, we unexpectedly found that Interleukin 1 Receptor-Associated Kinase 1 (IRAK1), a core effector of TLR-mediated innate immunity, also functions in live fish and human cancer models to counter RT-induced cell death mediated by the PIDDosome complex (PIDD-RAIDD-caspase-2). IRAK1 acting both as a driver of intrinsic tumor R-RT and as an effector of RT-induced antitumor immunity would, at first glance, pose obvious therapeutic conundrums. IRAK1 inhibitors would be expected to sensitize the irradiated tumor to RT but simultaneously thwart RT-induced antitumor immunity as initiated by stromal dendritic cells. Conversely, TLR agonist-based immunotherapy would be expected to intensify RT-induced antitumor immunity but at the expense of fueling IRAK1-mediated cell survival in the irradiated tumor. We discuss how IRAK1's differential reliance on catalytic activity in the radiation vs. TLR responses might help overcome these hurdles, as well as the crucial importance of developing IRAK1 inhibitors that lack activity against IRAK4, the kinase activity of which is essential for IRAK1 activation in both pathways.

Keywords: IRAK1, irak4, radiation therapy, immunotherapy, radiosensitiser

IRAK1: A CORE EFFECTOR IN IL-1R/TLR INNATE IMMUNE SIGNALING

IRAK1 is a conserved death domain (DD)-containing protein kinase whose *Drosophila* homolog, pelle, transduces dorso-ventral patterning and microbial cues recognized by the transmembrane receptor, Toll (1–6). The discovery of a Toll-like receptor (TLR) family of proteins in humans (3), composed of 10 TLRs, was soon followed by the finding that, as in flies, TLRs are responsible for the innate response to microbial infection through binding to *p*athogen- and *d*amage-associated molecular patterns (PAMPs and DAMPs) and viral/bacterial nucleic acids in the intracellular space (endosomal TLRs). These discoveries were awarded the 2011 Nobel Prize in Physiology or Medicine (3).

Upon ligation, TLRs and IL-1R receptor (IL-1R/TLR) signal proinflammatory and cell survival responses, the majority of which through IRAK1/4 kinases and attendant downstream signaling cascades such as NF-kB, p38/MAPK, and JNK (3, 7) (**Figure 1A**). IRAK1 and IRAK4 are recruited to the ligated receptor by the Toll/IL-1R homology (TIR) and DD-containing adaptor protein, Myeloid Differentiation Primary Response 88 (MyD88) (8). MyD88 engages in homotypic TIR:TIR and DD:DD interactions with IL-1R/TLR and IRAK1/4, respectively, mobilizing the kinases to the receptor and resulting in the formation of the "MyDDosome" (9) complex (MyD88-IRAK4-IRAK1) (10) (**Figure 1A**). Only once in the MyDDosome, comprising six MyD88, four IRAK4, and four IRAK1 subunits (11), can IRAK4 dimerize. This proximity-induced dimerization of IRAK4 is the key initiating step in IRAK1 activation, with most (10, 12–16) but not all (17) models involving *trans* autophosphorylation of IRAK4 and ultimately phosphorylation of T209 on IRAK1 by fully active IRAK4. Once primed for activation by T209 phosphorylation, IRAK1 autophosphorylates on T387 in its activation loop, resulting in full activation, dissociation from the complex, and activation of downstream pathways (**Figure 1A**) (10, 13). IRAK1 activation also notably involves the peptidyl prolyl *cis/trans* isomerase PIN1, whose binding to IRAK1 is required for activation within, and dissociation from, the MyDDosome, and is overall essential for TLR signaling (**Figure 1A**) (18). Surprisingly, whether the catalytic activity of IRAK1 is required at *any* step for its function remains unclear (5, 17, 19), with genetic studies involving kinase-dead variants questioning reliance on catalytic activity (4, 6, 19–23). Consistent with this, engagement of three major signaling branches downstream of IRAK1, namely NF-κB, p38/MAPK, and JNK, relies on physical contact between activated IRAK1 and TNF receptor-associated factor 6 (TRAF6), independently of IRAK1 catalytic activity (**Figure 1A**) (3, 4, 21, 24). The relative importance of catalytic vs. structural functionalities of IRAK1 is an important consideration for the development of IRAK1 inhibitors for clinical use, particularly in radioresistant cancer, and will be discussed in detail in the closing sections of this review.

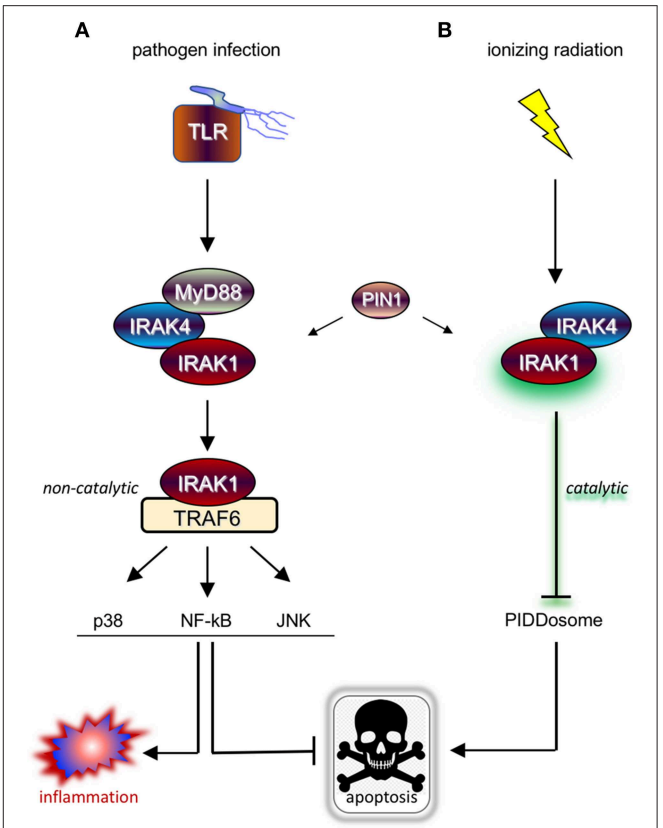

FIGURE 1 | IRAK1 kinase drives distinct prosurvival responses to microbial infection and ionizing radiation. **(A)** Diagram of the TLR signaling cascade which stimulates immune cell survival and inflammation in response to pathogen sensing. Ligated TLRs recruit MyD88 to trigger Myddosome (MyD88-IRAK4-IRAK1) formation, resulting in the activation of IRAK1 and release of the kinase from the complex. In turn, the activated form of IRAK1 binds TRAF6 to enable TRAF6-mediated activation of multiple pathways involved in anti-apoptotic and pro-inflammatory signaling. **(B)** Diagram of the newly identified IRAK1 signaling pathway triggered by IR, which involves IRAK4 but not MyD88 and antagonizes apoptosis through a different route involving inhibition of PIDDosome formation. Note that while IRAK1 catalytic activity is required in the radiation response (as symbolized by a green glare), it is dispensable for microbial responses relying on TRAF6 as signaling intermediate downstream of IRAK1.

IL-1R/TLR SIGNALING CONTRIBUTES TO RT-INDUCED ANTITUMOR IMMUNITY AND DEFINES A TARGET FOR RT+IT-BASED RADIOSENSITIZATION STRATEGIES

While predominantly activated by microbes, IL-1R/TLR signaling is also notably engaged by stromal dendritic cells (DCs) and macrophages located in the vicinity of irradiated tumors (**Figures 2A,B**). Indeed, many of the molecules released by irradiated cancer cells (i.e., damaged/apoptotic/necrotic cancer cells) are bona fide ligands for IL-1R/TLR, including IL-1β itself and a number of DAMPs such as heat shock proteins, high mobility group protein 1 (HMGB1) and tumor DNA/RNA fragments (25–34). In response to IL-1R/TLR ligation, DCs

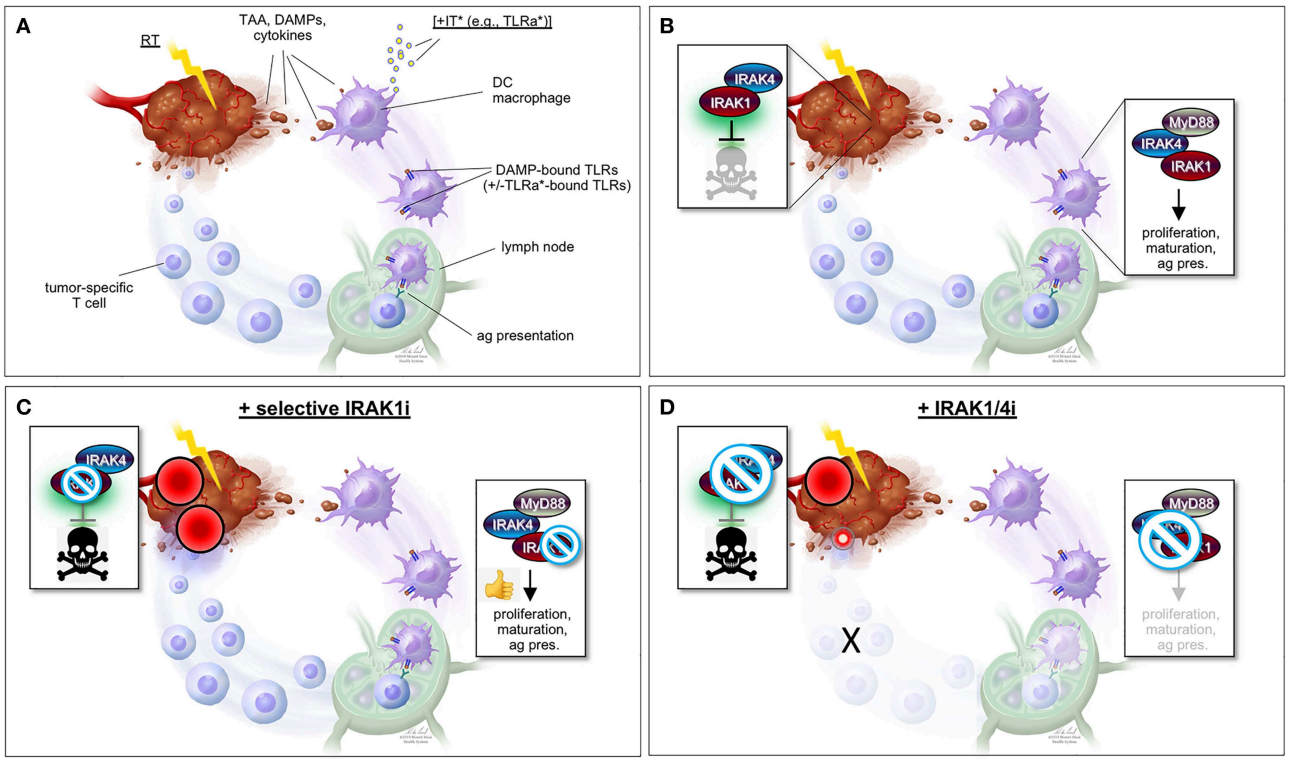

FIGURE 2 | "One-two punch" vs. "double-edged sword" scenarios for tumor radiosensitization strategies exploiting IRAK1 inhibitors. **(A)** Simplified view of RT-induced antitumor immunity. DAMPs and cytokines (i.e., IL-1β) released by irradiated tumor cells are recognized by cell surface IL-1R/TLRs on surrounding stromal DCs and macrophages, stimulating their activation, maturation, and antigen presentation activity toward T-cells in lymph nodes, and ultimately unleashing tumor-specific T-cells against the irradiated tumor (as well as distant tumors not pictured here). TAA, tumor-associated antigen; DAMPs, damage-associated molecular patterns; IT, immunotherapy; TLRa, toll-like receptor agonist; DC, dendritic cell; ag pres., antigen presentation. *IT (with TLRa) is optional and acts as a boost for the immune events otherwise described in the figure. **(B)** Simplified views of the IRAK1-mediated response to RT (left; tumor cell-intrinsic antiapoptotic response) and DAMP-bound TLRs (right, innate immune response). Note that while IRAK1 catalytic activity is required for the tumor response to RT (illustrated by green glare), it is largely dispensable for immune IRAK1 signaling. **(C)** "One-two punch" scenario, as afforded by a highly specific IRAK1 inhibitor with no activity against IRAK4. Such drugs would be expected to both blunt intrinsic tumor radioresistance (which depends on IRAK1 kinase activity) and spare IRAK1 mediated-antitumor immunity (which is less reliant on IRAK1 catalytic activity), resulting in a "one-two punch" on the tumor. The double-punch is illustrated by two red dart target symbols on the tumor. **(D)** "Double-edged sword" scenario, as afforded by a less specific IRAK1i with similar activity against IRAK4. Such IRAK1/4i would be expected to block both the tumor and immune responses to RT (each of which depends on IRAK4 catalytic activity; see text). Thus, in this scenario, intrinsic tumor radiosensitization activity would be retained but at the expense of blunting the immune component. A small, residual "punch" from the immune system on the tumor is indicated to further emphasize the detrimental effects of IRAK1/4i relative to the "one-two punch" effects of specific IRAK1i [compare with **(C)**]. Figure design by Ni-Ka Ford, printed with permission from with permission from ©Mount Sinai Health System.

engage in increased proliferation, maturation, and antigen presentation activity, ultimately triggering T-cell-mediated attacks of tumors located within and outside the radiation field (immune attacks of distant tumors are responsible for the "abscopal" effect of RT long observed in a small subset of patients). The molecules, immune cell types and mechanisms believed to underlie RT-induced, IL-1R/TLR-mediated antitumor immunity are briefly summarized in **Figures 2A,B** but have been extensively investigated and reviewed by expert colleagues (27–29, 31, 34–41).

The notion that RT acts as a trigger for IL-1R/TLR signaling is at the root of emerging RT+IT combination strategies making use of TLR agonists (TLRa) as adjuvant or neoadjuvant therapies (**Figure 2A**). TLRa such as CpG oligodeoxynucleotides (CpG-ODN, TLR9a) and various imidazoquinolines and nucleoside analogs (TLR7a; e.g., imiquimod/Aldara/R-837, resiquimod/R-848, DSR-6434, DSR-29133, 3M-011/854A) have demonstrated substantial efficacy, if not outright synergy, when combined with RT in mouse spontaneous or xenograft models of fibrosarcoma (38, 39), lymphoma (37), colorectal cancer (35, 36, 40), sarcoma (35), breast cancer (42), renal cell carcinoma (36), lung adenocarcinoma (43), pancreatic cancer (40), and metastatic osteosarcoma (36). Success with these preclinical studies has spurred a number of clinical trials of CpG-ODNs in combination with diverse chemo-RT treatment regimens (34, 44–46). Such trials initiated between 2015 and 2018 include NCT03410901, NCT01745354, NCT02254772, and NCT02266147 for the treatment lymphoma; NCT02927964 for the treatment of follicular lymphoma; NCT03322384 for the treatment of advanced solid tumors and lymphoma; and NCT03007732 for the treatment of prostate carcinoma [reviewed in (44)]. Despite mixed results so far,

favorable clinical responses observed in patient subsets warrant further testing (34, 44–46).

IRAK1 ALSO ANCHORS AN ANTIAPOPTOTIC RESPONSE TO RT DISTINCT FROM IRAK1 IMMUNE SIGNALING

As discussed in Introduction, while mammalian IRAK1 is a genuine protein kinase and is a central transducer in IL-1R/TLR signaling, its catalytic activity appears largely dispensable for innate immunity. TLR/IL-1R-independent roles for IRAK1 might explain this paradox, yet until recently no such non-immune IRAK1 function had been reported in vertebrates. In a screen for small molecules that restore RT-induced cell death in otherwise radioresistant *p53* mutant zebrafish (47, 48), we identified the microtubule inhibitor, oxfendazole (47). Surprisingly, target discovery identified IRAK1, and not tubulin, as the key target whose inhibition by oxfendazole was responsible for cell death recovery in irradiated fish (47). The requirement of IRAK1 for cell survival after RT was conserved in multiple human cancer cell lines tested in *vitro* or as tumor xenografts *in vivo*, regardless of *p53* genotype. Overexpression of IRAK1 was sufficient to force cell survival after RT in otherwise radiosensitive cells, in a manner that completely relied on its catalytic activity. Likewise, kinase-dead IRAK1 failed to complement *IRAK1* deficiency in both human and fish models (47). Rather than promoting survival through NF-κB and other attendant pathways, we found that IRAK1 acts to deny RT-induced apoptosis mediated by the PIDDosome complex (PIDD-RAIDD-caspase-2) (47, 49, 50). These observations identified an essential role for *IRAK1* outside of innate immunity as a gene required for the survival of irradiated vertebrate cells. IRAK1's reliance on its catalytic activity and engagement of a distinct antiapoptotic cascade were first clues that it might function in a pathway distinct from the canonical IL-1R/TLR axis (**Figure 1B**) (47).

Further evidence for IRAK1 functioning in a novel pathway came when we asked whether its known upstream proximal regulators, MyD88, IRAK4, and PIN1, were also required for the survival of irradiated cells. While IRAK4 and PIN1 clearly were, MyD88 clearly *was not*, whether in human cells or zebrafish embryos (47). Likewise, while IRAK4 and PIN1 were required for IRAK1 activation after RT, as assessed by T209 phosphorylation, MyD88 was not (47). In summary, RT-induced IRAK1 signaling differs from its canonical counterpart in three fundamental ways: (1) It fully relies on its kinase activity; (2) it acts through distinct downstream antiapoptotic mechanisms; and (3) it does not require MyD88 for activation by IRAK4 and PIN1 (**Figure 1B** vs. **Figure 1A**).

IR-INDUCED IRAK1 SIGNALING AS A DRIVER OF INTRINSIC TUMOR R-RT

Thus far, the case for IR-induced IRAK1 signaling acting as a driver of intrinsic tumor R-RT is four-fold. (i) IRAK1 and PIN1 are both sufficient to force R-RT in otherwise radiosensitive tumor cells (47). (ii) IRAK1 and PIN1 enzymatic activities are required for R-RT in cancer cell lines derived from multiple tumor types including HNSCC, breast cancer, colorectal cancer, and glioblastoma. These requirements for R-RT were verified *in vivo* in a mouse xenograft model of radioresistant HNSCC (47). (iii) IR-induced activation of IRAK1, as assessed by T209 phosphorylation, systematically correlated with tumor cell line sensitivity to RT+IRAK1i (47). (iv) Patients with high-risk HNSCC (HPV^{neg}, mutant *TP53*) whose tumors resisted post-operative RT (51) show evidence of pathway activation, whereby elevated *PIN1* expression levels strongly associate with locoregional recurrence (LRR; $P = 0.006$) and reduced overall survival (OS; $P = 0.007$) (47). Notably, *PIN1* overexpression did not otherwise correlate with metastatic potential, arguing against the notion that PIN1 levels merely reflected an aggressive tumor subtype. While upregulation of *IRAK1* itself failed to correlate with R-RT in this cohort, this is not unexpected given the upstream role played by PIN1 in the pathway (see above; **Figure 1B**). Upregulation of PIN1 would in fact be expected to alleviate selective pressure to overexpress *IRAK1* in this context. Deregulation/amplification at the *IRAK1* locus might also not be a mechanism of choice via which tumors upregulate IRAK1 activity, though *IRAK1* overexpression has been detected in several tumor types (4, 19), with particularly convincing evidence for causality in triple-negative breast cancer (52). Alternative routes to IRAK1 activation include upregulation of upstream positive regulators, such as seen with PIN1 (see above) as well as S100A-7/9 proteins in breast cancers with 1q21.3 amplification (53); mutational inactivation or downregulation of negative regulators such as miR-146a, as seen in del(5q) acute myeloid leukemia (54); and likely additional mechanisms [reviewed in (4, 19)]. Complementing our microarray analyses with that of exome sequence datasets from radioresistant tumors across tumor spectra will further clarify the extent to which IR-induced IRAK1 signaling drives R-RT in human cancer.

TARGETING IRAK1 IN RADIORESISTANT CANCER

As discussed earlier, IRAK1 inhibitors (IRAK1i) were highly effective at suppressing R-RT in live *p53* mutant zebrafish and human cancer cell lines assayed *in vitro* or as mouse xenografts *in vivo* (47). Remarkably, effective doses of IRAK1i in these models caused little to no cell death in non-irradiated controls. This was in stark contrast with the traditional radiosensitizer cisplatin, which failed to overcome R-RT at maximal tolerable doses (47). This data, combined with the previously established viability of $Irak1^{-/-}$ mice (55), suggests that systemic IRAK1i could restore RT sensitivity in patients without affecting healthy tissues outside of the radiation field.

While our work thus outlines a strong rationale for targeting IRAK1 in radioresistant tumors, as based on the projected efficacy and safety of such treatments, the strategy poses an immediate conundrum. Wouldn't systemic inhibition of the kinase simultaneously thwart the patient's immune attack on

the irradiated tumor or the enhancement thereof by means of TLRa-based IT? Our tumor xenograft experiments, which were performed in immunodeficient mice, left this key question unanswered. Neoadjuvant administration of the TLRa (i.e., prior to RT+IRAK1i) or post-treatment delivery thereof might help circumvent the issue. However, our studies indicate that the window for IRAK1i radiosensitizing efficacy is limited to within a few hours of RT (47), and such treatments would thus be expected to come at the cost of blunting any acute immune contribution to the overall tumor response to RT.

However, such a "double-edged sword"-like tradeoff in efficacy is likely to be avoided by virtue of a critical, differential reliance of IRAK1 on catalytic activity when operating in response to IL-1R/TLR vs. when operating in response to RT (**Figures 1A,B**). As outlined earlier, kinase activity is essential for IRAK1 signaling in response to RT in all settings tested, both in zebrafish embryos and human cancer cells (47). In contrast, similar experiments making use of kinase dead IRAK1 variants in human cells (D340N, K239A) or knock-in mice (D359A) have indicated that catalytic activity is largely dispensable for IRAK1 function in IL-1R/TLR signaling (21–23, 56). Specifically, kinase dead IRAK1 retained full NF-κB inducing activity in all tested settings, presumably reflecting the protein's strict structural role when engaging TRAF6 (4, 24, 57). IL-1R/TLR-induced secretion of IL-6, TNFα, and IL-10 were likewise unaffected in bone marrow-derived macrophages from *Irak1*^{D359A} knockin mice (22). Thus, RT+IRAK1i-based radiosensitization strategies, whether alone or in combination with TLRa-based IT, would be expected to largely spare IL-1R/TLR-initiated immune attacks on the tumor, leading to an effective "one-two punch" both from within and outside the irradiated tumor (**Figure 2C**). It should be noted, however, that IRAK1 catalytic activity might not be entirely dispensable for all forms of IL-1R/TLR signaling. In the TLR7/9-IRF7 signaling branch, for instance, an intact IRAK1 kinase domain appears required for the transcriptional activation of IRF7 as well as for the timely induction of interferons by TLR7/9 (56), as further evidenced by a significant delay in IFN-β production by plasmacytoid DCs derived from *Irak1*^{D359A} mice (22). The relative contributions of the IL-1R/TLR-NF-κB (kinase-independent branch) vs. IL-1R/TLR-NF-α/β (partially kinase-dependent branch) to RT-induced antitumor immunity have not been rigorously explored to date and is an important topic for future studies.

The "one-two punch" hypothesis that IRAK1i will both intrinsically sensitize tumor cells to RT while also allowing for RT-induced antitumor immunity to proceed (**Figure 2C**) is further contingent on the use of IRAK1i that are highly specific to IRAK1. Indeed, unlike IRAK1, the catalytic activity of the sister kinase IRAK4 is essential for IRAK1 signaling in *both* the RT and IL-1R/TLR response pathways, in which IRAK4 acts to activate IRAK1 via direct phosphorylation on T209 (4, 13, 47). Thus, any IRAK1i with significant off-target activity against IRAK4 would be expected to radiosensitize the tumor proper but at the expense of affecting its immunogenic attack (**Figure 2D**). We recently confirmed the essential role of IRAK4 in RT-induced IRAK1 signaling *in vivo*, whereby (i) *irak4*-depleted *p53*$^{MK/MK}$ zebrafish embryos recover RT-induced cell death as efficiently as *irak1*-depleted embryos (Liu and Sidi, unpublished observations); and (ii) *irak1*-depleted embryos reconstituted with T209A human *IRAK1* mRNA fail to resist RT-induced cell death, as opposed to embryos complemented with WT *IRAK1* mRNA (Li and Sidi, unpublished observations). Thus, IRAK1i used for radiosentization purposes should, at the very least, demonstrate marked selectivity for IRAK1 over IRAK4 (**Figures 2C,D**).

Of the many IRAK1i developed so far [reviewed in (19)], only one, pacritinib (58), combines clinical efficacy, acceptable safety, and selectivity for IRAK1 over IRAK4. This selectivity is only moderate, however, with IC50s of 6 and 177 nM vs. IRAK1 and IRAK4, respectively (19). In spite of IRAK1 and IRAK4 kinase domains sharing >90% amino-acid sequence identity within the ATP binding pocket as well as identical gatekeeper tyrosine residues, the selectivity—albeit moderate—of pacritinib for IRAK1 indicates that developing a highly specific IRAK1i is feasible in principle. The crystal structure of the human IRAK1 kinase domain bound to a small molecule was recently reported (10), which together with the known structure of the IRAK4 kinase domain (15) should help develop such selective IRAK1i. A very first example of such a compound was recently reported by Buhrlage, Treon, Gray and colleagues (59). The drug, Jh-X-119-01, labels IRAK1 at C302 and shows irreversible inhibition with an IC50 of 9.3 nM against IRAK1 vs. >10 μM vs. IRAK4. Disclosure of the structure of Jh-X-199-01 should spur future efforts to develop IRAK1i suited for use as radiosensitizers.

AUTHOR CONTRIBUTIONS

SS conceived the review and figures. SS and PL wrote the paper.

ACKNOWLEDGMENTS

We thank Julio Aguirre-Ghiso and Jian Jin for helpful discussions and Ni-Ka Ford for the design of **Figure 2**. Our study (47) discussed in this perspective was supported by the National Institutes of Health (RO1CA178162 to SS; F30CA186448 to PL), and awards from the JJR Foundation, Pershing Square Sohn Cancer Research Alliance, New York Community Trust, and Searle Scholars Program to SS.

REFERENCES

1. Jain A, Kaczanowska S, Davila E. IL-1 receptor-associated kinase signaling and its role in inflammation, cancer progression, and therapy resistance. *Front Immunol*. (2014) 5:553. doi: 10.3389/fimmu.2014.00553
2. Janssens S, Beyaert R. Functional diversity and regulation of different interleukin-1 receptor-associated kinase (IRAK) family members. *Mol Cell*. (2003) 11:293–302. doi: 10.1016/S1097-2765(03)00053-4
3. O'Neill LA, Golenbock D, Bowie AG. The history of Toll-like receptors - redefining innate immunity. *Nat Rev Immunol*. (2013) 13:453–60. doi: 10.1038/nri3446

4. Rhyasen GW, Starczynowski DT. IRAK signalling in cancer. *Br J Cancer*. (2015) 112:232–7. doi: 10.1038/bjc.2014.513
5. Flannery S, Bowie AG. The interleukin-1 receptor-associated kinases: critical regulators of innate immune signalling. *Biochem Pharmacol*. (2010) 80:1981–91. doi: 10.1016/j.bcp.2010.06.020
6. Gottipati S, Rao NL, Fung-Leung WP. IRAK1: a critical signaling mediator of innate immunity. *Cell Signal*. (2008) 20:269–76. doi: 10.1016/j.cellsig.2007.08.009
7. Kawasaki T, Kawai T. Toll-like receptor signaling pathways. *Front Immunol*. (2014) 5:461. doi: 10.3389/fimmu.2014.00461
8. Deguine J, Barton GM. MyD88: a central player in innate immune signaling. *F1000Prime Rep*. (2014) 6:97. doi: 10.12703/P6-97
9. Motshwene PG, Moncrieffe MC, Grossmann JG, Kao C, Ayaluru M, Sandercock AM, et al. An oligomeric signaling platform formed by the Toll-like receptor signal transducers MyD88 and IRAK-4. *J Biol Chem*. (2009) 284:25404–11. doi: 10.1074/jbc.M109.022392
10. Wang L, Qiao Q, Ferrao R, Shen C, Hatcher JM, Buhrlage SJ, et al. Crystal structure of human IRAK1. *Proc Natl Acad Sci USA*. (2017) 114:13507–12. doi: 10.1073/pnas.1714386114
11. Lin SC, Lo YC, Wu H. Helical assembly in the MyD88-IRAK4-IRAK2 complex in TLR/IL-1R signalling. *Nature*. (2010) 465:885–90. doi: 10.1038/nature09121
12. Ferrao R, Zhou H, Shan Y, Liu Q, Li Q, Shaw DE, et al. IRAK4 dimerization and trans-autophosphorylation are induced by Myddosome assembly. *Mol Cell*. (2014) 55:891–903. doi: 10.1016/j.molcel.2014.08.006
13. Kollewe C, Mackensen AC, Neumann D, Knop J, Cao P, Li S, et al. Sequential autophosphorylation steps in the interleukin-1 receptor-associated kinase-1 regulate its availability as an adapter in interleukin-1 signaling. *J Biol Chem*. (2004) 279:5227–36. doi: 10.1074/jbc.M309251200
14. Latty SL, Sakai J, Hopkins L, Verstak B, Paramo T, Berglund NA, et al. Activation of Toll-like receptors nucleates assembly of the MyDDosome signaling hub. *Elife*. (2018) 7:e31377. doi: 10.7554/eLife.31377
15. Wang Z, Liu J, Sudom A, Ayres M, Li S, Wesche H, et al. Crystal structures of IRAK-4 kinase in complex with inhibitors: a serine/threonine kinase with tyrosine as a gatekeeper. *Structure*. (2006) 14:1835–44. doi: 10.1016/j.str.2006.11.001
16. Cushing L, Stochaj W, Siegel M, Czerwinski R, Dower K, Wright Q, et al. Interleukin 1/Toll-like receptor-induced autophosphorylation activates interleukin 1 receptor-associated kinase 4 and controls cytokine induction in a cell type-specific manner. *J Biol Chem*. (2014) 289:10865–75. doi: 10.1074/jbc.M113.544809
17. Vollmer S, Strickson S, Zhang T, Gray N, Lee KL, Rao VR, et al. The mechanism of activation of IRAK1 and IRAK4 by interleukin-1 and Toll-like receptor agonists. *Biochem J*. (2017) 474:2027–38. doi: 10.1042/BCJ20170097
18. Tun-Kyi A, Finn G, Greenwood A, Nowak M, Lee TH, Asara JM, et al. Essential role for the prolyl isomerase Pin1 in Toll-like receptor signaling and type I interferon-mediated immunity. *Nat Immunol*. (2011) 12:733–41. doi: 10.1038/ni.2069
19. Singer JW, Fleischman A, Al-Fayoumi S, Mascarenhas JO, Yu Q, Agarwal A. Inhibition of interleukin-1 receptor-associated kinase 1 (IRAK1) as a therapeutic strategy. *Oncotarget*. (2018) 9:33416–39. doi: 10.18632/oncotarget.26058
20. Li X, Commane M, Burns C, Vithalani K, Cao Z, Stark GR. Mutant cells that do not respond to interleukin-1 (IL-1) reveal a novel role for IL-1 receptor-associated kinase. *Mol Cell Biol*. (1999) 19:4643–52. doi: 10.1128/MCB.19.7.4643
21. Maschera B, Ray K, Burns K, Volpe F. Overexpression of an enzymically inactive interleukin-1-receptor-associated kinase activates nuclear factor-kappaB. *Biochem J*. (1999) 339 (Pt 2):227–31. doi: 10.1042/bj3390227
22. Pauls E, Nanda SK, Smith H, Toth R, Arthur JSC, Cohen P. Two phases of inflammatory mediator production defined by the study of IRAK2 and IRAK1 knock-in mice. *J Immunol*. (2013) 191:2717–30. doi: 10.4049/jimmunol.1203268
23. Knop J, Martin MU. Effects of IL-1 receptor-associated kinase (IRAK) expression on IL-1 signaling are independent of its kinase activity. *FEBS Lett*. (1999) 448:81–5. doi: 10.1016/S0014-5793(99)00322-1
24. Jiang Z, Ninomiya-Tsuji J, Qian Y, Matsumoto K, Li X. Interleukin-1 (IL-1) receptor-associated kinase-dependent IL-1-induced signaling complexes phosphorylate TAK1 and TAB2 at the plasma membrane and activate TAK1 in the cytosol. *Mol Cell Biol*. (2002) 22:7158–67. doi: 10.1128/MCB.22.20.7158-7167.2002
25. Candeias SM, Testard I. The many interactions between the innate immune system and the response to radiation. *Cancer Lett*. (2015) 368:173–8. doi: 10.1016/j.canlet.2015.02.007
26. Shan YX, Jin SZ, Liu XD, Liu Y, Liu SZ. Ionizing radiation stimulates secretion of pro-inflammatory cytokines: dose-response relationship, mechanisms and implications. *Radiat Environ Biophys*. (2007) 46:21–9. doi: 10.1007/s00411-006-0076-x
27. Roses RE, Xu M, Koski GK, Czerniecki BJ. Radiation therapy and Toll-like receptor signaling: implications for the treatment of cancer. *Oncogene*. (2008) 27:200–7. doi: 10.1038/sj.onc.1210909
28. Dar TB, Henson RM, Shiao SL. Targeting innate immunity to enhance the efficacy of radiation therapy. *Front Immunol*. (2018) 9:3077. doi: 10.3389/fimmu.2018.03077
29. Apetoh L, Ghiringhelli F, Tesniere A, Obeid M, Ortiz C, Criollo A, et al. Toll-like receptor 4-dependent contribution of the immune system to anticancer chemotherapy and radiotherapy. *Nat Med*. (2007) 13:1050–9. doi: 10.1038/nm1622
30. Yamazaki T, Hannani D, Poirier-Colame V, Ladoire S, Locher C, Sistigu A, et al. Defective immunogenic cell death of HMGB1-deficient tumors: compensatory therapy with TLR4 agonists. *Cell Death Differ*. (2014) 21:69–78. doi: 10.1038/cdd.2013.72
31. Bockel S, Durand B, Deutsch E. Combining radiation therapy and cancer immune therapies: from preclinical findings to clinical applications. *Cancer Radiother*. (2018) 22:567–80. doi: 10.1016/j.canrad.2018.07.136
32. Gallo PM, Gallucci S. The dendritic cell response to classic, emerging, and homeostatic danger signals. Implications for autoimmunity. *Front Immunol*. (2013) 4:138. doi: 10.3389/fimmu.2013.00138
33. Garg AD, Nowis D, Golab J, Vandenabeele P, Krysko DV, Agostinis P. Immunogenic cell death, DAMPs and anticancer therapeutics: an emerging amalgamation. *Biochim Biophys Acta*. (2010) 1805:53–71. doi: 10.1016/j.bbcan.2009.08.003
34. Rodriguez-Ruiz ME, Rodriguez I, Leaman O, Lopez-Campos F, Montero A, Conde AJ, et al. Immune mechanisms mediating abscopal effects in radioimmunotherapy. *Pharmacol Ther*. (2019) 196:195–203. doi: 10.1016/j.pharmthera.2018.12.002
35. Adlard AL, Dovedi SJ, Telfer BA, Koga-Yamakawa E, Pollard C, Honeychurch J, et al. A novel systemically administered Toll-like receptor 7 agonist potentiates the effect of ionizing radiation in murine solid tumor models. *Int J Cancer*. (2014) 135:820–9. doi: 10.1002/ijc.28711
36. Dovedi SJ, Adlard AL, Ota Y, Murata M, Sugaru E, Koga-Yamakawa E, et al. Intravenous administration of the selective toll-like receptor 7 agonist DSR-29133 leads to anti-tumor efficacy in murine solid tumor models which can be potentiated by combination with fractionated radiotherapy. *Oncotarget*. (2016) 7:17035–46. doi: 10.18632/oncotarget.7928
37. Dovedi SJ, Melis MH, Wilkinson RW, Adlard AL, Stratford IJ, Honeychurch J, et al. Systemic delivery of a TLR7 agonist in combination with radiation primes durable antitumor immune responses in mouse models of lymphoma. *Blood*. (2013) 121:251–9. doi: 10.1182/blood-2012-05-432393
38. Mason KA, Ariga H, Neal R, Valdecanas D, Hunter N, Krieg AM, et al. Targeting toll-like receptor 9 with CpG oligodeoxynucleotides enhances tumor response to fractionated radiotherapy. *Clin Cancer Res*. (2005) 11:361–9. Available online at: https://clincancerres.aacrjournals.org/content/11/1/361.long
39. Milas L, Mason KA, Ariga H, Hunter N, Neal R, Valdecanas D, et al. CpG oligodeoxynucleotide enhances tumor response to radiation. *Cancer Res*. (2004) 64:5074–7. doi: 10.1158/0008-5472.CAN-04-0926
40. Scholch S, Rauber C, Tietz A, Rahbari NN, Bork U, Schmidt T, et al. Radiotherapy combined with TLR7/8 activation induces strong immune responses against gastrointestinal tumors. *Oncotarget*. (2015) 6:4663–76. doi: 10.18632/oncotarget.3081
41. Scholch S, Rauber C, Weitz J, Koch M, Huber PE. TLR activation and ionizing radiation induce strong immune responses against multiple tumor

entities. *Oncoimmunology*. (2015) 4:e1042201. doi: 10.1080/2162402X.2015.1042201
42. Dewan MZ, Vanpouille-Box C, Kawashima N, DiNapoli S, Babb JS, Formenti SC, et al. Synergy of topical toll-like receptor 7 agonist with radiation and low-dose cyclophosphamide in a mouse model of cutaneous breast cancer. *Clin Cancer Res*. (2012) 18:6668–78. doi: 10.1158/1078-0432.CCR-12-0984
43. Zhang H, Liu L, Yu D, Kandimalla ER, Sun HB, Agrawal S, et al. An *in situ* autologous tumor vaccination with combined radiation therapy and TLR9 agonist therapy. *PLoS ONE*. (2012) 7:e38111. doi: 10.1371/journal.pone.0038111
44. Smith M, Garcia-Martinez E, Pitter MR, Fucikova J, Spisek R, Zitvogel L, et al. Trial watch: toll-like receptor agonists in cancer immunotherapy. *Oncoimmunology*. (2018) 7:e1526250. doi: 10.1080/2162402X.2018.1526250
45. Kim YH, Gratzinger D, Harrison C, Brody JD, Czerwinski DK, Ai WZ, et al. *In situ* vaccination against mycosis fungoides by intratumoral injection of a TLR9 agonist combined with radiation: a phase 1/2 study. *Blood*. (2012) 119:355–63. doi: 10.1182/blood-2011-05-355222
46. Garg AD, Vara Perez M, Schaaf M, Agostinis P, Zitvogel L, Kroemer G, et al. Trial watch: dendritic cell-based anticancer immunotherapy. *Oncoimmunology*. (2017) 6:e1328341. doi: 10.1080/2162402X.2017.1328341
47. Liu PH, Shah RB, Li Y, Arora A, Ung PM, Raman R, et al. An IRAK1-PIN1 signalling axis drives intrinsic tumour resistance to radiation therapy. *Nat Cell Biol*. (2019) 21:203–13. doi: 10.1038/s41556-018-0260-7
48. Sidi S, Sanda T, Kennedy RD, Hagen AT, Jette CA, Hoffmans R, et al. Chk1 suppresses a caspase-2 apoptotic response to DNA damage that bypasses p53, Bcl-2, and caspase-3. *Cell*. (2008) 133:864–77. doi: 10.1016/j.cell.2008.03.037
49. Tinel A, Tschopp J. The PIDDosome, a protein complex implicated in activation of caspase-2 in response to genotoxic stress. *Science*. (2004) 304:843–6. doi: 10.1126/science.1095432
50. Ando K, Kernan JL, Liu PH, Sanda T, Logette E, Tschopp J, et al. PIDD death-domain phosphorylation by ATM controls prodeath versus prosurvival PIDDosome signaling. *Mol Cell*. (2012) 47:681–93. doi: 10.1016/j.molcel.2012.06.024
51. Skinner HD, Sandulache VC, Ow TJ, Meyn RE, Yordy JS, Beadle BM, et al. TP53 disruptive mutations lead to head and neck cancer treatment failure through inhibition of radiation-induced senescence. *Clin Cancer Res*. (2012) 18:290–300. doi: 10.1158/1078-0432.CCR-11-2260
52. Wee ZN, Yatim SM, Kohlbauer VK, Feng M, Goh JY, Bao Y, et al. IRAK1 is a therapeutic target that drives breast cancer metastasis and resistance to paclitaxel. *Nat Commun*. (2015) 6:8746. doi: 10.1038/ncomms9746
53. Goh JY, Feng M, Wang W, Oguz G, Yatim S, Lee PL, et al. Chromosome 1q21.3 amplification is a trackable biomarker and actionable target for breast cancer recurrence. *Nat Med*. (2017) 23:1319–30. doi: 10.1038/nm.4405
54. Starczynowski DT, Kuchenbauer F, Argiropoulos B, Sung S, Morin R, Muranyi A, et al. Identification of miR-145 and miR-146a as mediators of the 5q- syndrome phenotype. *Nat Med*. (2010) 16:49–58. doi: 10.1038/nm.2054
55. Thomas JA, Allen JL, Tsen M, Dubnicoff T, Danao J, Liao XC, et al. Impaired cytokine signaling in mice lacking the IL-1 receptor-associated kinase. *J Immunol*. (1999) 163:978–84.
56. Uematsu S, Sato S, Yamamoto M, Hirotani T, Kato H, Takeshita F, et al. Interleukin-1 receptor-associated kinase-1 plays an essential role for Toll-like receptor (TLR)7- and TLR9-mediated interferon-{alpha} induction. *J Exp Med*. (2005) 201:915–23. doi: 10.1084/jem.20042372
57. Butler MP, Hanly JA, Moynagh PN. Kinase-active interleukin-1 receptor-associated kinases promote polyubiquitination and degradation of the Pellino family: direct evidence for PELLINO proteins being ubiquitin-protein isopeptide ligases. *J Biol Chem*. (2007) 282:29729–37. doi: 10.1074/jbc.M704558200
58. Singer JW, Al-Fayoumi S, Ma H, Komrokji RS, Mesa R, Verstovsek S. Comprehensive kinase profile of pacritinib, a nonmyelosuppressive Janus kinase 2 inhibitor. *J Exp Pharmacol*. (2016) 8:11–9. doi: 10.2147/JEP.S110702
59. Yang G, Hatcher J, Wang J, Liu X, Munshi M, Chen J. A novel highly selective IRAK1 inhibitor Jh-X-119-01 shows synergistic cell killing with ibrutinib in MYD88 mutated B-cell lymphoma cells. Abstract 719. In: *Oral Presentation at: 59th Annual Meeting & Exposition for the American Society of Hematology*. Atlanta, GA (2017).

Conflict of Interest: The authors declare that the research was conducted in the absence of any commercial or financial relationships that could be construed as a potential conflict of interest.

Copyright © 2019 Liu and Sidi. This is an open-access article distributed under the terms of the Creative Commons Attribution License (CC BY). The use, distribution or reproduction in other forums is permitted, provided the original author(s) and the copyright owner(s) are credited and that the original publication in this journal is cited, in accordance with accepted academic practice. No use, distribution or reproduction is permitted which does not comply with these terms.

frontiers in Oncology

ORIGINAL RESEARCH
published: 15 November 2019
doi: 10.3389/fonc.2019.01259

Radiation-Induced Changes in Tumor Vessels and Microenvironment Contribute to Therapeutic Resistance in Glioblastoma

Yun-Soo Seo[1,2†], In Ok Ko[3†], Hyejin Park[1], Ye Ji Jeong[1], Ji-Ae Park[3], Kwang Seok Kim[1], Myung-Jin Park[1] and Hae-June Lee[1*]*

[1] Division of Radiation Biomedical Research, Korea Institute of Radiological & Medical Sciences, Naju, South Korea, [2] Herbal Medicine Resources Research Center, Korea Institute of Oriental Medicine, Naju, South Korea, [3] Division of Applied RI, Korea Institute of Radiological & Medical Science, Seoul, South Korea

OPEN ACCESS

Edited by:
Ira Ida Skvortsova, Innsbruck Medical University, Austria

Reviewed by:
Yidong Yang, University of Science and Technology of China, China
Sara Pedron, University of Illinois at Urbana-Champaign, United States

***Correspondence:**
Myung-Jin Park
mjpark@kirams.re.kr
Hae-June Lee
hjlee@kirams.re.kr

† These authors have contributed equally to this work

Specialty section:
This article was submitted to Radiation Oncology, a section of the journal Frontiers in Oncology

Received: *18 July 2019*
Accepted: *31 October 2019*
Published: *15 November 2019*

Citation:
Seo Y-S, Ko IO, Park H, Jeong YJ, Park J-A, Kim KS, Park M-J and Lee H-J (2019) Radiation-Induced Changes in Tumor Vessels and Microenvironment Contribute to Therapeutic Resistance in Glioblastoma. Front. Oncol. 9:1259. doi: 10.3389/fonc.2019.01259

Glioblastoma (GBM) is a largely fatal and highly angiogenic malignancy with a median patient survival of just over 1 year with radiotherapy (RT). The effects of RT on GBM remain unclear, although increasing evidence suggests that RT-induced alterations in the brain microenvironment affect the recurrence and aggressiveness of GBM. Glioma stem cells (GSCs) in GBM are resistant to conventional therapies, including RT. This study aimed to investigate the effect of radiation on tumor growth and the GSC microenvironment in a mouse model of glioma. To evaluate the growth-inhibitory effects of ionizing radiation on GSCs, tumor volume was measured via anatomical magnetic resonance imaging (MRI) after the intracranial injection of 1×10^4 human patient-derived GSCs (83NS cells), which exhibit marked radioresistance. When a tumor mass of ∼5 mm^3 was detected in each animal, 10 Gy of cranial irradiation was administered. Tumor progression was observed in the orthotopic xenografted GSC tumor (primary tumor) from a detectable tumor mass (5 mm^3) to a lethal tumor mass (78 mm^3) in ∼7 d in the non-irradiated group. In the RT group, tumor growth was halted for almost 2 weeks after administering 10 Gy cranial irradiation, with tumor growth resuming thereafter and eventually approaching a lethal mass (56 mm^3) 21 d after radiation. Radiation therapy yielded good therapeutic effects, with a 2-fold increase in GSC glioma survival; however, tumor relapse after RT resulted in higher mortality for the mice with a smaller tumor volume ($p = 0.029$) than the non-irradiated tumor-bearing mice. Moreover, tumor regrowth after IR resulted in different phenotypes associated with glioma aggressiveness compared with the non-irradiated mice; the apparent diffusion coefficient by diffusion MRI decreased significantly ($p < 0.05$, 0 Gy vs. 10 Gy) alongside decreased angiogenesis, abnormal vascular dilatation, and upregulated CD34, VWF, AQP1, and AQP4 expression in the tumor. These findings demonstrate that radiation affects GSCs in GBM, potentially resulting in therapeutic resistance by changing the tumor microenvironment. Thus, the results of this study suggest potential therapeutic targets for overcoming the resistance of GBMs to RT.

Keywords: glioblastoma, glioma stem cell, radiotherapy, tumor microenvironment, tumor vessel

INTRODUCTION

Glioblastoma (GBM) is the most malignant and highly angiogenic tumor in the central nervous system (CNS). Due to its aggressiveness, GBM has a very poor prognosis, with a median survival of 14.6 months from diagnosis (1–3). Radiotherapy (RT) is currently used to treat GBM alongside surgical resection and chemotherapy. Highly proliferative cells, including tumor cells, are sensitive to ionizing radiation-induced DNA damage via reactive oxygen species, which causes apoptosis and reduces cell proliferation. Although RT is a locoregional treatment for GBM, RT-induced alterations in the brain microenvironment have been shown to contribute to GBM recurrence and aggressiveness (4). Understanding of the origin of therapeutic resistance in GBM may therefore help to improve patient outcome and survival.

A specific subpopulation of glioma cells, known as glioma stem cells (GSCs), contribute to tumor recurrence during aggressive multimodal therapies. After RT, GBM frequently recurs as focal masses (5), indicating that GSCs are radio-resistant and responsible for relapse (6, 7). GSCs can inherently resist conventional therapy due to their enhanced self-renewal and differentiation potential (8). Recent studies reporting that GSCs maintain GBM (9) have indicated that GSCs interact closely with the vascular niche and promote neovasculogenesis by releasing angiogenic factors (10); however, the underlying mechanisms remain unclear.

GBM patients have poor prognosis due to tumor cells that survive initial treatment and cause relapse or recurrence; thus, failure to inhibit tumor growth at the primary site is a major cause of mortality (11). GBM tumors originate in the brain and interact closely with their unique microenvironment (12). Furthermore, highly aggressive tumors rarely metastasize outside the brain (13), indicating a preference for the brain microenvironment. Cell-cell interactions, tissue dynamics, and cytokines and growth factors constitute a complex microenvironment that is altered in the presence of GBM tumors, promoting tumor invasion, and therapeutic resistance. Therefore, it is important to identify and characterize treatment-resistant tumor cells and whether they influence their microenvironment.

In this study, we investigated the extent of GSC glioma progression after brain irradiation for a specific duration via magnetic resonance imaging (MRI) with an orthotopic xenograft mouse model of GBM established using patient-derived GSCs. Furthermore, we assessed the morphological and molecular phenotypes that may be associated with radioresistance in post-irradiation relapse.

MATERIALS AND METHODS

Cell Culture

The GBM patient-derived GSC line 83NS was maintained in DMEM/F-12 (Corning, 10-090-cvr, Corning, NY, USA) supplemented with B27 (Invitrogen, 17504044, Carlsbad, CA, USA), epidermal growth factor (10 ng/mL; Prospec, cyt-217, Brunswick, NJ, USA), and basic fibroblast growth factor (5 ng/mL; Prospec, cyt-218). 83NS cells were provided by Dr. Ichiro Nakano (University of Alabama at Birmingham, Birmingham, AL, USA) (14). Prior to transplantation, cells were washed with PBS and dissociated. After centrifugation at 1,500 rpm for 5 min, the cell pellet was resuspended in PBS at a density of 1×10^4 cells/3 μL.

Establishment of the Orthotopic Mouse Model of Glioma and Radiotherapy

All animal experiments were conducted in accordance with protocols approved by the Institutional Animal Care and Use Committee (IACUC) of the Korea Institute of Radiological and Medical Sciences (KIRAMS2018-0079). Athymic BALB/c nu/nu mice were purchased from Orient Bio Inc. (Seoul, Korea), housed under specific pathogen-free conditions, and supplied with standard rodent feed and tap water *ad libitum*. The animals' heads were fixed in a stereotactic frame using non-perforating bars, a midline incision was made on the scalp, and a burr hole was drilled 0.1 mm posterior and 2 mm left of the bregma. An 83NS cell suspension (1×10^4 cells) was injected into the left frontal cortex at the coordinate bregma using a stereotactic frame and microinjector. The average tumor size was determined to be 5 mm^3 by MRI. Mice were randomly divided into two subgroups: a control group and an irradiated group. Radiation (a single dose of 10 Gy) was administered to the entire head under anesthesia (30 mg/kg Zoletil and 10 mg/kg Rompun) using an X-Rad320 (Precision X-Ray, East Haven, CT, USA; filter: 2 mm AI; distance: 42 cm; 260 kVp, 10 mA, 10Gy/5 min).

MRI

All MRI was performed using a 9.4-T animal MR system and a specific mouse brain coil (Agilent Technologies, Palo Alto, CA, USA). The incidence and size of the orthotopic glioma were determined radiologically. Cranial irradiation was carried out 12 d after stereotactic 83NS cell transplantation when the tumor volume approached 5 mm^3. To confirm the therapeutic effects of tumor irradiation, MR images were obtained 0, 3, 7, 14, and 21 d after irradiation and tumor size was compared. Before MRI, animals were anesthetized with 2.5% isoflurane in oxygen. A fast spin-echo MR sequence for T2-weighted imaging (T2-WI) was used with the following parameters: repetition time (TR), 2500 ms; effective echo time (TE_{eff}), 30 ms; echo train length (ETL), 4; average number, 4; slice thickness, 0.8 mm; slice number, 6; matrix size, 192 × 192; field-of-view, 25 × 25 mm^2; and total imaging time, 605 s. Tumor volume was measured by summing all voxels within the tumor boundary of the anatomical T2-W images using ImageJ software (NIH Bethesda, MD, USA).

A fast spin-echo MR sequence for diffusion-weighted imaging was used with the following parameters: repetition time (TR), 2000 ms; echo time (TE), 23.5 ms; echo number, 1; average number, 1; slice thickness, 0.8 mm; matrix size, 192 × 192; field-of-view, 25 × 25 mm^2; b-value, 0 and 800 s/mm^2; and total imaging time, 512 s. Apparent diffusion coefficient (ADC) maps and values were processed using the intrinsic VnmrJ 4.0 workstation (Agilent Technologies, Inc.).

Histopathological Analysis

All mice were euthanized by CO_2 inhalation and brain tissue specimens were harvested in accordance with IACUC

guidelines. The harvested brain tissue specimens were fixed in 4% paraformaldehyde, embedded in paraffin, and cut into 5 μm sections using a microtome (Leica, Nussloch, Germany).

Immunofluorescence staining was performed as described previously (15). Briefly, specimens were blocked with blocking buffer (PBS with 1.5% normal horse serum and 0.1% Triton X-100), incubated with anti-Ki-67 (Acris, DRM004, Herford, Germany), anti-CD31 (R&D Systems, AF3628, Minneapolis, MN, USA), anti-CD34 (SantaCruz, sc-74499, Dallas, TX, USA), anti-Von Willebrand factor (VWF; Abcam, ab6994, Cambridge, MA, USA), anti-aquanporin 1 (AQP1; SantaCruz, sc-32737), and anti-aquaporin 4 (AQP4; Novus Biologicals, NBP1-87679, Littleton, CO, USA) antibodies overnight at 4°C, and then incubated with Alexa Fluor 488-, Alexa Fluor 546-, and Alexa Fluor 647-conjugated secondary antibodies (Invitrogen). After washing the sections with PBST, nuclei were counterstained with DAPI and fluorescence visualized was using confocal microscopy (Carl Ziess, Oberkochen, Germany). Fluorescence intensity was measured using ImageJ software (NIH). Briefly, fluorescence positive areas were assessed and the ratio was calculated (16). A TUNEL assay was carried out to evaluate apoptotic glioma cells using an Apoptosis kit (Promega, g3250, Madison, WI, USA) in accordance with the manufacturer's instructions.

Quantitative Reverse Transcription Polymerase Chain Reaction (qRT-PCR) Analysis

Total RNA was isolated from cultured GSCs treated with or without radiation (10 Gy) using an RNeasy Mini kit (Qiagen, Valencia, CA, USA) and 1 μg was reverse-transcribed into cDNA using amfiRivert cDNA Synthesis Platinum Master Mix (GenDEPOT, Barker, TX, USA) in accordance with the manufacturer's protocol. qPCR was carried out in triplicate, using qPCR SYBR green 2× mastermix kit (M Biotech, 18303, Seoul, Korea) with a CXF-96 detection system (Bio-Rad Laboratories, Hercules, CA, USA). Relative gene expression was normalized to that of *Gapdh* using the comparative C_T method with Bio-Rad CFX manager v2.1 (Bio-Rad Laboratories). The following primers were used: *aqp1* (sense: 5′-CGTGACCTTGGTGGCTCAG-3′; anti-sense: 5′-GGACCGAGCAGGGTTAATCC-3′), *aqp4* (sense: 5′-AACGGACTGATGTCACTGGC-3′; anti-sense: 5′-AAAGGATCGGGCGGGATTC-3′), and *Gapdh* (sense: 5′- CATCGCTCAGACACCATG 3′; anti-sense: 5′-TGTAGTTGAGGTCAATGAAGGG-3′).

Statistical Analysis

Data are presented as the mean ± standard deviation (SD). Differences between tumor stages were assessed by one-way ANOVA with statistical significance set at $p < 0.05$. All statistical analyses were carried out using GraphPad Prism Software version 7.0 (GraphPad Software, La Jolla, CA, USA).

RESULTS

Effect of IR on the Survival of Orthotopic GBM Xenograft Model Mice

We assessed the survival of non-IR control and IR mice administered with 83NS cells. GBM xenograft model mice were orthotopically injected with 83NS cells and subjected to whole-brain RT (single 10 Gy dose) 12 d post-injection. As shown in **Figure 1A**, the IR group displayed significantly higher survival than the control group ($p = 0.0035$, Log-rank test) and the median survival of the IR group (32 ± 2.24) was 12.4 d longer than that of the control group (19.6 ± 0.89). We also monitored the body weight of each mouse. In the control group, body weight was maintained for 12 d after injection and then rapidly decreased when the tumors became detectable by MRI (**Figure 1B**). Weight loss in the IR group was temporarily delayed after IR but resumed 2 weeks later, achieving similar levels to the control group.

IR Delayed Orthotopic GSC Glioma Progression

MRI has been widely used to characterize brain tumor growth, progression, and response to various treatments in clinical and

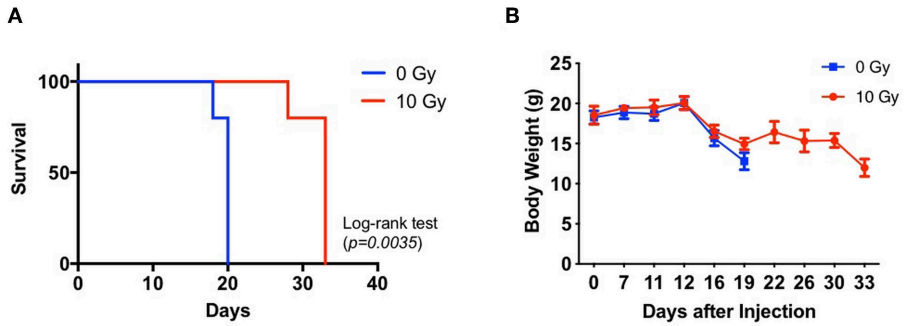

FIGURE 1 | Effects of irradiation (IR) on the tumorigenicity of glioma stem cells (GSCs) in an orthotopic xenograft mouse model of glioma. **(A)** Kaplan-Meier survival graph of mice implanted with 83NS cells and treated with or without radiation ($n = 5$, 1×10^4 cells injected per mouse). IR treatment was administered when tumors grew to their detectable size (12 d, 10 Gy). **(B)** Changes in body weight were monitored.

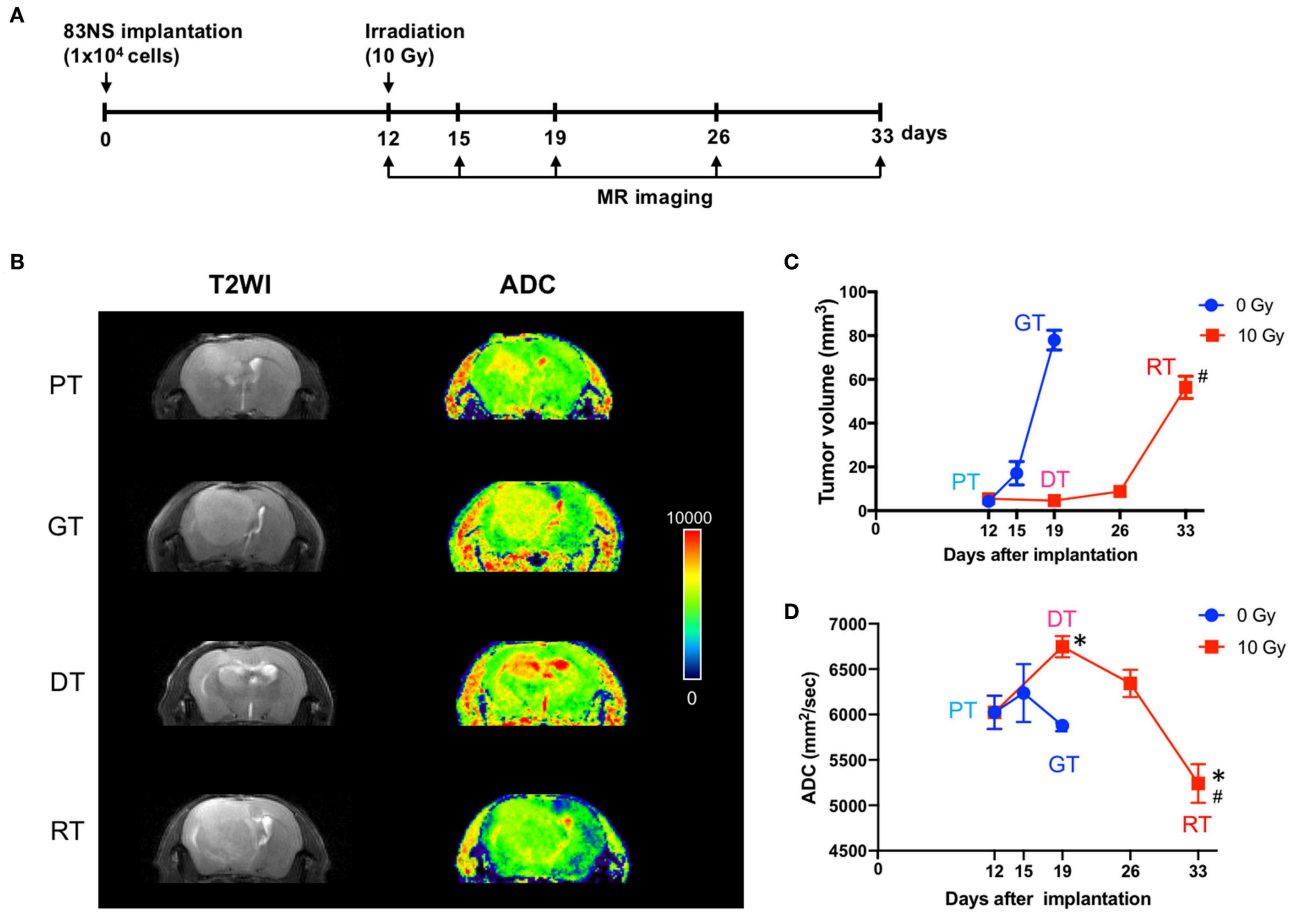

FIGURE 2 | Effects of irradiation (IR) on tumor progression in an orthotopic mouse model of glioma. **(A)** Experimental protocol for IR and magnetic resonance imaging (MRI). **(B)** Representative images of brain imaging by anatomical or diffusion-weighted MRI of an orthotopic xenograft tumor model. **(C)** Graphical representation of changes in glioma volume during tumor progression with or without IR. The volume of each GSC glioma was measured using ImageJ software from anatomical MR images. **(D)** Apparent diffusion coefficient maps generated by diffusion-weighted MRI. Data presented as mean ± standard error of the mean. $^{*}p < 0.05$. Significant differences among the tumor stages compared to PT were determined by one-way ANOVA ($n = 4$–6). $^{\#}p < 0.05$. Significant differences between the GT and RT groups were determined using unpaired *t*-tests ($n = 4$–6). PT; primary tumors detectable by MRI; GT; growing tumors that progressed without IR; DT; delayed tumors after IR; RT; re-grown tumors after IR.

preclinical studies (17, 18). To evaluate the effect of IR on GSC glioma, we recorded whole tumor volume using anatomical MRI. As shown in **Figure 2**, the tumors in the control group progressed in 7 d from a detectable mass of ∼5 mm^3 (5.50 ± 0.94) to a lethal mass of 78 mm^3 (77.95 ± 4.47). In the IR group, tumor growth was temporarily attenuated for 14 d after RT; however, it eventually reverted to a lethal mass of ∼56 mm^3 (56.35 ± 5.12) after a further 7 d. Thereafter, we performed diffusion-weighted MRI (DW-MRI), which quantifies the movement of water within tumors by measuring the ADC, which is negatively correlated with tumor cell density. An increase in ADC values is a quantifiable indicator of antitumor efficacy and thus decreasing angiogenic activity and increasing apoptotic rate (17–19). **Figure 2D** shows that IR increased the ADC by up to 12% during the delay in GSC glioma growth ($p < 0.05$, one-way ANOVA, PT vs. DT), whereas the ADC remained largely unchanged during tumor progression in the non-IR group (+1% at 3 d and −3% at 7 d vs. 0 d). Based on GSC glioma relapse, the ADC was reduced by up to 13% 21 d after IR and was significantly lower than that of the non-irradiated group ($p = 0.044$, unpaired *t*-test, GT vs. RT), although the tumor volume of the relapsed tumor was significantly lower than that of the non-IR group ($p = 0.029$, unpaired *t*-test). Based on these results, increased ADC, which was induced by a decline in cell density and enlarged extracellular space after radiation, was decreased according to tumor relapse to an even greater extent than that in growing tumors (GTs), which suggests that RTs had a higher cell density than GTs. To evaluate the changes induced by IR and to allow additional analysis, the tumors were divided into four groups: primary tumors (PTs) that were detectable by MRI, growing tumors (GTs) that progressed without IR, delayed tumors after IR (DTs), and re-grown tumors after IR (RTs).

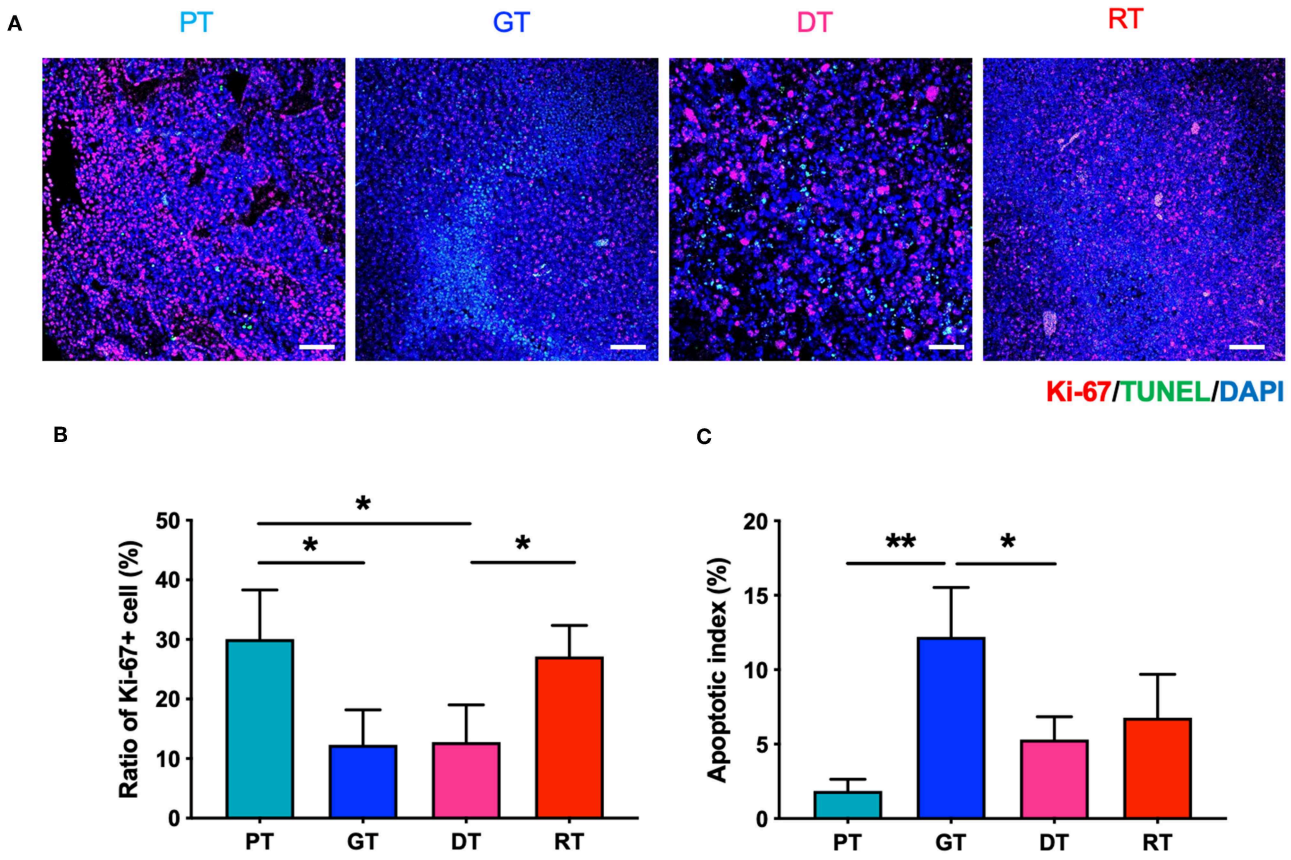

FIGURE 3 | Effects of irradiation (IR) on the proliferation and apoptosis of tumor cells in the orthotopic mouse model of glioma. **(A)** Glioma from the brain tissue of xenografted mice were stained with hematoxylin and eosin to identify tumor regions. **(B)** Proliferative and apoptotic cells were visualized by immunofluorescence staining and TUNEL assays, respectively. Scale bar, 100 μm. **(C)** The percentage of Ki-67+ and TUNEL+ cells of total tumor cells per unit area was determined. $^{*}p < 0.05$ and $^{**}p < 0.01$. Significant differences among the treated groups were determined by analysis of variance followed by Tukey's test for multiple comparisons ($n = 4$–6). PT; primary tumors detectable by MRI, GT; growing tumors that progressed without IR, DT; delayed tumors after IR, RT; re-grown tumors after IR.

IR Temporally Inhibited GSC Proliferation and Attenuated GSC Proliferation During Tumor Progression

To investigate the effect of IR on GSC glioma growth, we enumerated the proliferative and apoptotic cells in the brain tumors. As shown in **Figure 3**, the number of Ki-67-positive proliferative cells decreased gradually in accordance with tumor growth in the GTs compared to the PTs, whilst the number of TUNEL-positive apoptotic cells increased. These results may have occurred due to spatial constraints during the progression of solid tumors which induce cell death and affect the delivery of oxygen and nutrients to the tumor (20). The number of Ki-67-positive cells decreased significantly 7 d after IR in the DTs compared to that in the PTs ($p < 0.05$), corresponding to the delay in tumor growth. These inhibitory effects on tumor growth are consistent with the low tumor cell density representing increased ADC in the DTs (**Figures 2B,D**). The number of Ki-67-positive cells was also significantly increased in RTs compared to that in DTs ($p < 0.05$) during tumor regrowth. Furthermore, no significant differences were observed in the apoptotic index during regrowth from DTs to RTs, unlike the tumor growth from PTs to GTs. Delayed tumor regrowth was accompanied by GSC re-proliferation and a significant decrease in ADC levels compared with GTs, indicating that 10 Gy of IR transiently inhibited GSC growth; however, GSCs regrew with increased aggressiveness.

IR Suppressed Angiogenesis and Structurally Altered Microvasculature in the Late Phase of Tumor Progression

We investigated the effect of RT on GSC glioma angiogenesis by measuring the microvessel density (MVD) of tumors using CD31 as a pan-endothelial cell marker. As shown in **Figure 4**, MVD decreased significantly with tumor progression ($p < 0.01$, PT vs. GT) or re-growth ($p < 0.05$, DT vs. RT). During the early phase of tumor progression, IR slightly but non-significantly inhibited angiogenesis ($p = 0.074$, PT vs. DT), whereas in the late phase of tumor progression IR drastically inhibited MVD in RTs compared with PTs ($p < 0.001$) or DTs ($p < 0.05$). Vessel diameter increased sharply during delayed tumor regrowth compared to ordinary

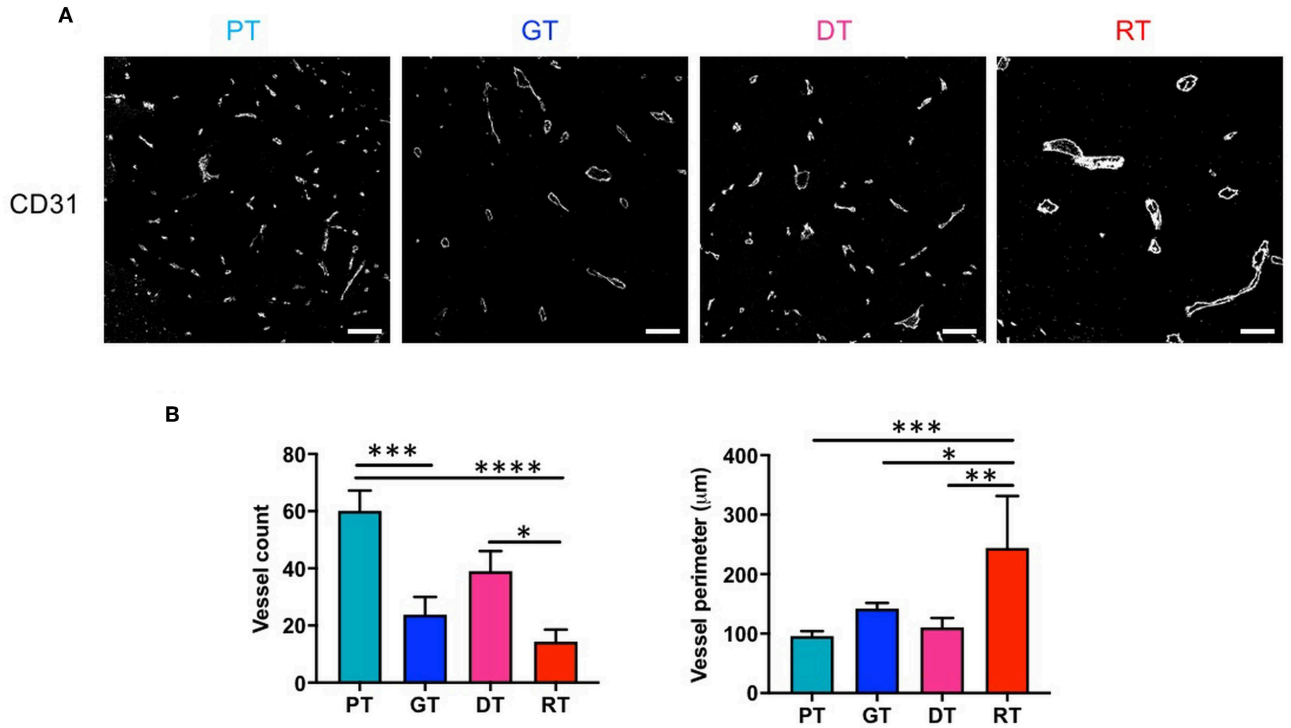

FIGURE 4 | Effects of irradiation on microvessel composition in an orthotopic mouse model of glioma. **(A)** Microvessels in tumor tissues were visualized by immunofluorescence staining using an endothelial-specific anti-CD31 antibody. Scale bar, 100 μm. **(B)** The number and diameter of microvessels were determined. *$p < 0.05$, **$p < 0.01$, ***$p < 0.005$, and ****$p < 0.0001$. Significant differences among the treated groups were determined by analysis of variance followed by Tukey's test for multiple comparisons ($n = 6$). PT; primary tumors detectable by MRI, GT; growing tumors that progressed without IR, DT; delayed tumors after IR, RT; re-grown tumors after IR.

tumor progression from PTs to GTs, consistent with the decrease in ADC (**Figure 2D**). Interestingly, RTs showed a significant increase in vessel diameter compared to that in GTs, which had similar tumor sizes. These results indicate that radiation inhibits angiogenesis and alters the vasculature of GSC gliomas.

IR Altered Vascular Phenotypes in GSC Glioma

To verify the IR-induced morphological microvascular changes, we examined the molecular phenotypes of the tumor vessels by immunofluorescence staining with the additional endothelial cell markers CD34 and VWF during each stage of tumor progression. CD34 is a well-known marker of angiogenesis and endothelial progenitor cells (21, 22), whilst VWF is a multimeric plasma glycoprotein that mediates platelet adhesion to both the subendothelial matrix and endothelial surfaces (23) and is associated with tumor survival and angiogenesis (24, 25). As shown in **Figure 5**, in the non-irradiated group, CD34 and VWF expression were not markedly different in GTs compared to that in PTs. DTs showed only a mild increase in the number of CD34-positive cells and no changes in VWF expression in comparison with PTs, which displayed a similar tumor size. However, IR significantly increased the number of VWF- and CD34-positive cells in GTs compared to RTs. Due to regrowth, the tumors displayed decreased angiogenesis and enlarged vasculature; hence, increased CD34 and VWF may be involved in vascular abnormality rather than angiogenesis.

Since DW-MRI showed significant changes depending on the state of the tumor after IR, we also analyzed two major aquaporins (AQPs), AQP1 and AQP4, which are transmembrane water transporters that are primarily expressed in the brain tissue. In the non-irradiated group, AQP1 and AQP4 were expressed in GSCs at basal levels and no significant changes were observed in their expression during tumor progression. However, both AQPs were significantly upregulated following IR ($p < 0.05$; **Figure 6**). AQP1 is reportedly expressed in normal brain endothelial cells; however, AQP1 displayed a different expression pattern to CD31 (**Figure 6A**). Moreover, AQP4 is generally expressed in astrocytes; however, AQP4 displayed no colocalization with the astrocyte marker GFAP in the tumors (data not shown). We then examined *aqp1* and *aqp4* mRNA expression by qRT-PCR to determine whether IR upregulates AQPs in 83NS GSCs. As shown in **Figure 6C**, both AQPs were directly and significantly upregulated ($p < 0.01$) in 83NS 48 h after IR (10 Gy). These results show that IR directly alters GSCs and influences the microenvironment associated with tumor regrowth and aggressiveness.

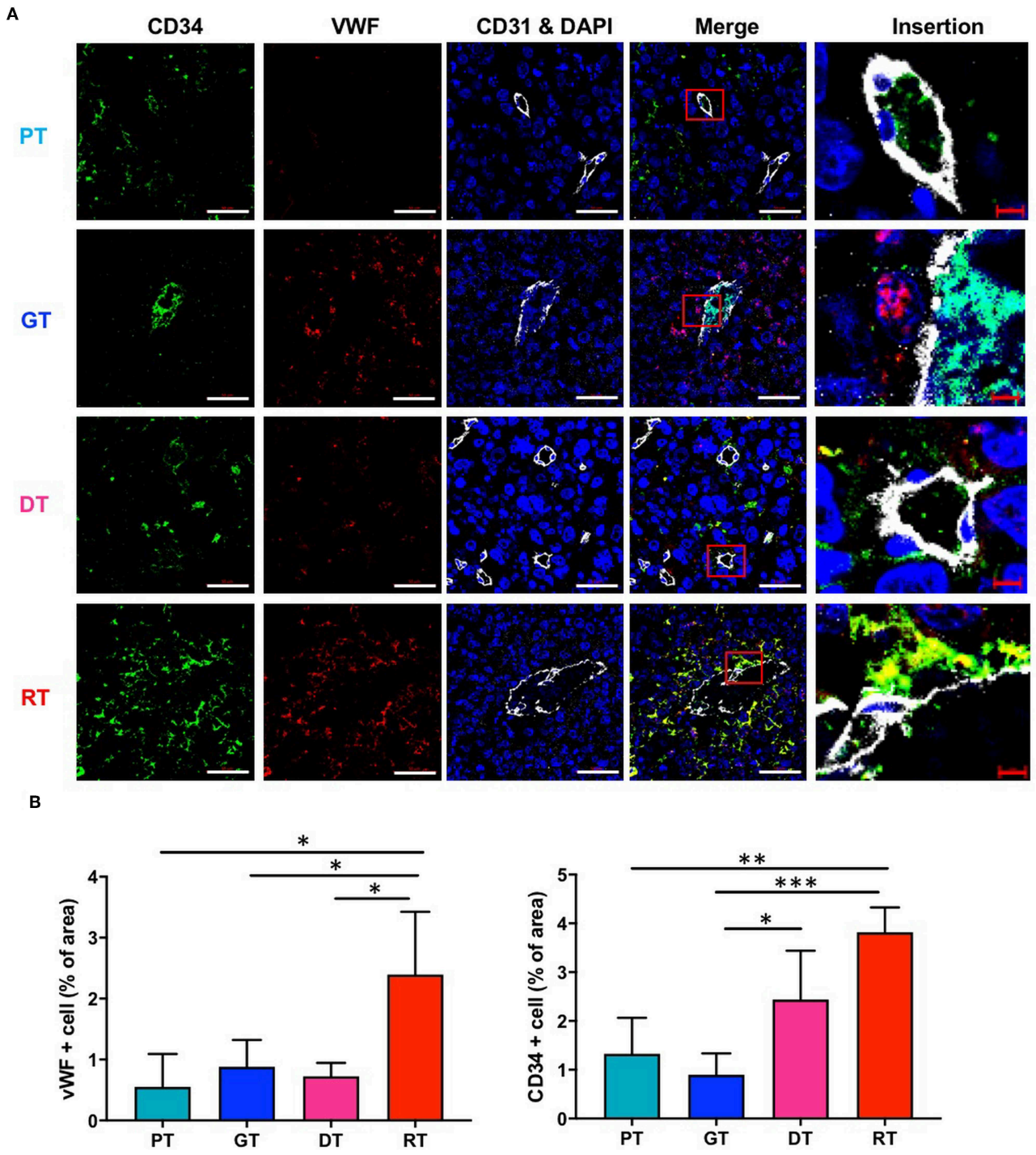

FIGURE 5 | Effects of irradiation on the vascular microenvironment in an orthotopic mouse model of glioma. **(A)** Vascular components in tumor tissue were visualized by immunofluorescence staining using anti-CD34 and anti-VWF antibodies. Scale bar (white), 50 μm. Scale bar (red), 10 μm. **(B)** Proportions of CD34+ and VWF+ cells in tumor tissues were determined using ImageJ software. $^{*}p < 0.05$, $^{**}p < 0.01$, and $^{***}p < 0.005$. Significant differences among the treated groups were determined by analysis of variance followed by Tukey's test for multiple comparisons ($n = 6$). PT; primary tumors detectable by MRI, GT; growing tumors that progressed without IR, DT; delayed tumors after IR, RT; re-grown tumors after IR.

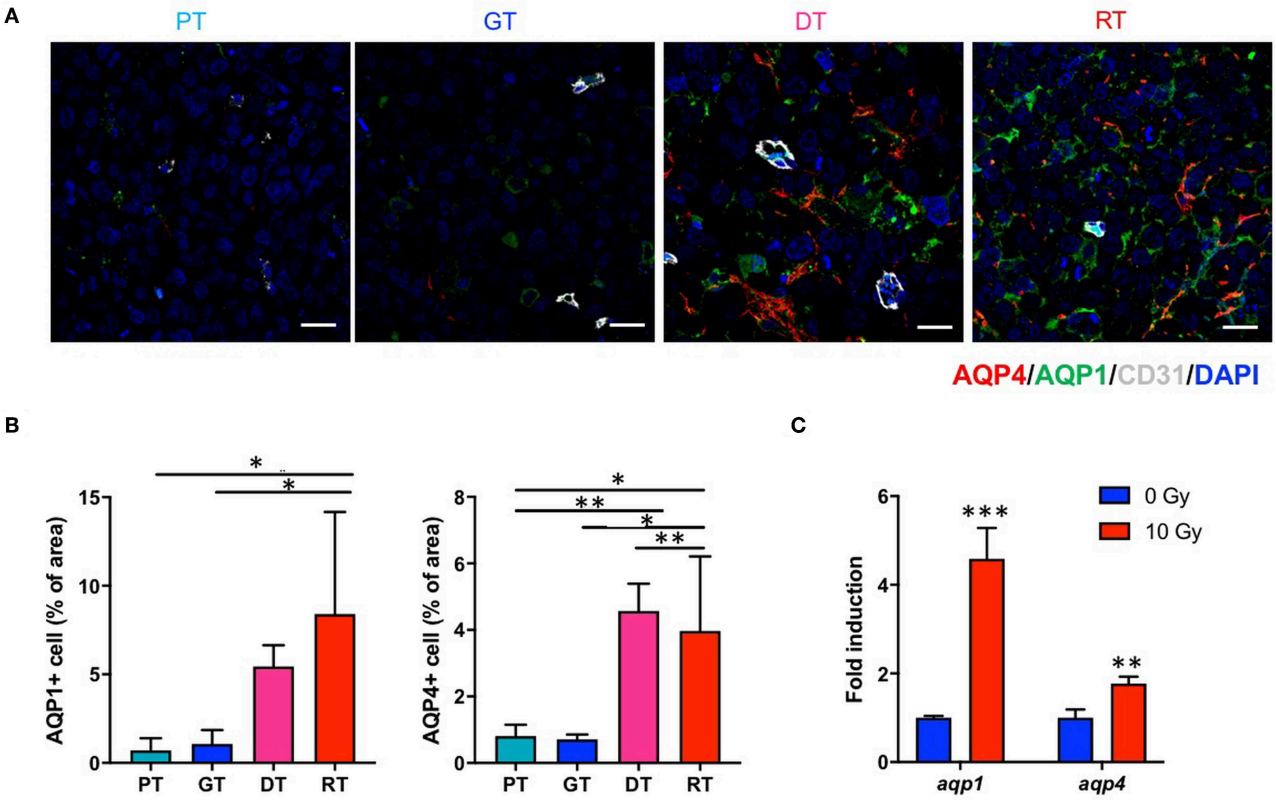

FIGURE 6 | Effects of irradiation (IR) on the AQP expression in an orthotopic mouse model of glioma. **(A)** AQPs in tumor tissues were visualized by immunofluorescence staining using anti-AQP1 and anti-AQP4 antibodies. Scale bar, 100 μm. **(B)** The proportion of AQP1+ and AQP4+ cells in tumor tissues were determined using ImageJ software. $^{*}p < 0.05$ and $^{**}p < 0.01$. Significant differences among the treated groups were determined by analysis of variance followed by Tukey's test for multiple comparisons ($n = 6$). PT; primary tumors detectable by MRI, GT; growing tumors that progressed without IR, DT; delayed tumors after IR, RT; re-grown tumors after IR. **(C)** *aqp1* and *aqp4* mRNA expression levels were quantified by quantitative reverse transcription polymerase chain reaction analysis. 83NS cells were treated with or without IR (10 Gy) $^{**}p < 0.01$ and $^{***}p < 0.005$. Significant differences between the 0 and 10 Gy groups were determined by unpaired *t*-tests ($n = 3$).

DISCUSSION

GBM is one of the most intractable and angiogenic malignant tumors of the CNS. Despite recent advancements in the treatment of solid tumors, the treatment of these malignant gliomas remains essentially palliative since GBMs are extremely resistant to conventional radiation and chemotherapy. Moreover, despite significant technological improvements, radiotherapeutic effects are generally limited due to marked radioresistance in gliomas, particularly GSCs. Specific subpopulations of GSCs underlie this recurrence even when treated with aggressive multimodal therapies (26). In this study, we investigated the effects of therapeutic IR on GSCs in GBM by assessing histological and molecular alterations induced by IR in an orthotopic xenograft mouse model of GBM established using patient-derived GSCs. After IR, tumor progression was temporarily inhibited and the median survival increased for 12.4 days; however, tumors displayed rapid, and aggressive regrowth. Regrown GSC glioma, which displayed a smaller tumor volume than the non-irradiated group, was lethal to mice. Based on comparative histopathological analysis of different stages of tumor growth with or without IR, tumor regrowth after IR occurred alongside significant alterations in the vascular microenvironment. As shown in **Figure 5**, CD34 and VWF were significantly upregulated in regrown tumors with enlarged vessels. Unlike numerous studies reporting that CD34 and VWF are involved in angiogenesis, our study shows that CD34 and VWF expression coincide with reduced tumor vasculature. Consistent with our results, some studies have reported that primary GBM is characterized by increased angiogenesis, while recurrent GBM displays increased vasculogenesis and decreased angiogenic activity after RT (27). Hence, CD34 and VWF upregulation could be involved in abnormal vasculogenesis during tumor regrowth. Unlike ordinary vessel progression from PT to a GT which results from maturation and stabilization, vessel development from a DT to a RT after radiation may occur by vasculogenesis. Loss of angiogenic activity caused by radiation led to an influx of circulating cells which boost vasculogenesis, including endothelial progenitor cells and myeloid cells (3, 28). The increase in CD34+ and VWF+ cells in DTs and RTs caused by the infiltration of circulating cells might increase vessel diameter, which is crucial for tumor recurrence after radiation.

Although CD34 is a marker of vascular endothelial progenitor cells (29, 30) and an optimal marker of microvascular density, a recent study showed that CD34 overexpression was associated with higher WHO glioma grades (III + IV) in 684 patients, suggesting that CD34 is a potential diagnostic and prognostic marker and therapeutic target for gliomas (31). In addition, VWF was only significantly upregulated in the late phase of GSC glioma regrowth; endothelial cell activation and the release of the procoagulatory protein VWF induce platelet aggregation, thus protecting cancer cells from immune cells, including NK cells, which is essential for malignancy (32). Therefore, these IR-induced alterations in the tumor microenvironment could contribute to resistance against further treatments, including RT.

This study demonstrated that IR upregulates AQP1 and AQP4 in GSC glioma tissue and 83NS cells *in vitro*. It has been reported that APQ expression is involved in water diffusion (33). To our knowledge, no studies have yet investigated IR-induced alterations in AQPs in GSCs or GBM. Since AQPs are involved in water transportation and edema, their upregulation in histopathological analysis was inconsistent with the reduced ADC in DW-MRI. In brain cancer, AQP1 expression is associated with brain capillary endothelial cells, which do not express AQP1 in normal brain tissue. The signals that induce AQP1 expression in the endothelium of brain tumors remain unclear but might include signals regulating the production and release of VEGF from cancer cells. As shown in **Figure 6A**, AQP1 was not expressed in tumor endothelial cells in GSC glioma. Hayashi et al. reported that AQP1 induction correlated with tumor cell metabolism and increased glycolysis and lactate dehydrogenase (LDH) activity, with patient GBM tissue exhibiting increased coincident AQP1, LDH, and cathepsin B expression levels which contributed to acidification of the extracellular milieu and glioma cell invasiveness (34). AQP4 is primarily an astroglial membrane protein localized in astrocytic endfeet that serves as a key functional component of the blood-brain barrier and is thought to be involved in brain edema pathogenesis (35). However, immunofluorescence staining and the ADC map of late phase regrown GSC glioma revealed differences compared to previous findings. In GSC glioma tissue, AQP4 was expressed on tumor cells, not tumor endothelial cells, and its expression levels decreased along with ADC levels, thus may not have contributed to edema. Interestingly, AQP4 expression is correlated with the incidence of epileptic seizures in GBM since patients with seizures have higher cell membrane AQP4 levels, suggesting that AQP4 expression is regulated post-transcriptionally (36). Furthermore, Lan et al. reported that AQP4 dissociates from orthogonal particle arrays and is redistributed across the entire surface of glioma cells under tumor conditions; thus, AQP4 expression levels may correlate with tumor grade as AQP4 expression increases in higher glioma grades (37). These previous studies support our finding that increased AQP expression after IR may be associated with GSC glioma malignancy or aggressiveness; however, further studies are required to elucidate the role and underlying mechanism of AQPs involvement in GBM radioresistance.

There are numerous obstacles to improving the therapeutic efficacy of RT and further studies are required to investigate the basic molecular events in GBM. In particular, GSCs are responsible for post-treatment GBM relapse. To understand the molecular events that occur in radioresistant tumors, we used an orthotopic mouse model of glioma implanted with a patient-derived GSC xenograft to monitor tumor progression after RT and alterations in the tumor microenvironment over time. This study shows that CD34, VWF, and AQPs are associated with post-IR GSCs glioma relapse and provides essential insights for the development of treatment regimens for radioresistant tumors.

DATA AVAILABILITY STATEMENT

All datasets generated for this study are included in the article.

ETHICS STATEMENT

The animal study was reviewed and approved by the Institutional Animal Care and Use Committee at the Korea Institute of Radiological & Medical Sciences.

AUTHOR CONTRIBUTIONS

Y-SS: data collection, data analysis, and manuscript writing. IK, HP, and YJ: data collection and data analysis. J-AP: data analysis. KK and M-JP: developed the study concept project development. H-JL: project development, developed the study concept, edited, manuscript writing, and revised the manuscript.

FUNDING

This study was supported by a grants of the National Research Foundation of Korea (2015M2B2B1068627) and a grant from the Korea Institute of Radiological and Medical Sciences funded by the Ministry of Science and ICT (MSIT), Republic of Korea (50531-2019 and 50436-2019).

REFERENCES

1. Stupp R, Mason WP, van den Bent MJ, Weller M, Fisher B, Taphoorn MJ, et al. Radiotherapy plus concomitant and adjuvant temozolomide for glioblastoma. *N Engl J Med.* (2005) 352:987–96. doi: 10.1056/NEJMoa043330
2. Louis DN, Ohgaki H, Wiestler OD, Cavenee WK, Burger PC, Jouvet A, et al. The 2007 WHO classification of tumours of the central nervous system. *Acta Neuropathol.* (2007) 114:97–109. doi: 10.1007/s00401-007-0243-4
3. Brown JM. Vasculogenesis: a crucial player in the resistance of solid tumours to radiotherapy. *Br J Radiol.* (2014) 87:20130686. doi: 10.1259/bjr.20130686
4. Yamanaka R, Hayano A, Kanayama T. Radiation-induced gliomas: a comprehensive review and meta-analysis. *Neurosurg Rev.* (2018) 41:719–31. doi: 10.1007/s10143-016-0786-8
5. Garden AS, Maor MH, Yung WK, Bruner JM, Woo SY, Moser RP, et al. Outcome and patterns of failure following limited-volume irradiation

for malignant astrocytomas. *Radiother Oncol.* (1991) 20:99–110. doi: 10.1016/0167-8140(91)90143-5
6. Calabrese C, Poppleton H, Kocak M, Hogg TL, Fuller C, Hamner B, et al. A perivascular niche for brain tumor stem cells. *Cancer Cell.* (2007) 11:69–82. doi: 10.1016/j.ccr.2006.11.020
7. Zhang C, Hai L, Zhu M, Yu S, Li T, Lin Y, et al. Actin cytoskeleton regulator Arp2/3 complex is required for DLL1 activating Notch1 signaling to maintain the stem cell phenotype of glioma initiating cells. *Oncotarget.* (2017) 8:33353–64. doi: 10.18632/oncotarget.16495
8. Singh SK, Hawkins C, Clarke ID, Squire JA, Bayani J, Hide T, et al. Identification of human brain tumour initiating cells. *Nature.* (2004) 432:396–401. doi: 10.1038/nature03128
9. Ricci-Vitiani L, Pallini R, Biffoni M, Todaro M, Invernici G, Cenci T, et al. Tumour vascularization via endothelial differentiation of glioblastoma stem-like cells. *Nature.* (2010) 468:824–8. doi: 10.1038/nature09557
10. Bao S, Wu Q, Sathornsumetee S, Hao Y, Li Z, Hjelmeland AB, et al. Stem cell-like glioma cells promote tumor angiogenesis through vascular endothelial growth factor. *Cancer Res.* (2006) 66:7843–8. doi: 10.1158/0008-5472.CAN-06-1010
11. Osuka S, Van Meir EG. Overcoming therapeutic resistance in glioblastoma: the way forward. *J Clin Invest.* (2017) 127:415–26. doi: 10.1172/JCI89587
12. Zamecnik J. The extracellular space and matrix of gliomas. *Acta Neuropathol.* (2005) 110:435–42. doi: 10.1007/s00401-005-1078-5
13. Bernstein JJ, Woodard CA. Glioblastoma cells do not intravasate into blood vessels. *Neurosurgery.* (1995) 36:124–32; discussion 32. doi: 10.1227/00006123-199501000-00016
14. Mao P, Joshi K, Li J, Kim SH, Li P, Santana-Santos L, et al. Mesenchymal glioma stem cells are maintained by activated glycolytic metabolism involving aldehyde dehydrogenase 1A3. *Proc Natl Acad Sci USA.* (2013) 110:8644–9. doi: 10.1073/pnas.1221478110
15. Jeong YJ, Jung MG, Son Y, Jang JH, Lee YJ, Kim SH, et al. Coniferyl aldehyde attenuates radiation enteropathy by inhibiting cell death and promoting endothelial cell function. *PLoS ONE.* (2015) 10:e0128552. doi: 10.1371/journal.pone.0128552
16. Jensen EC. Quantitative analysis of histological staining and fluorescence using ImageJ. *Anat Rec.* (2013) 296:378–81. doi: 10.1002/ar.22641
17. Moffat BA, Hall DE, Stojanovska J, McConville PJ, Moody JB, Chenevert TL, et al. Diffusion imaging for evaluation of tumor therapies in preclinical animal models. *MAGMA.* (2004) 17:249–59. doi: 10.1007/s10334-004-0079-z
18. Patterson DM, Padhani AR, Collins DJ. Technology insight: water diffusion MRI–a potential new biomarker of response to cancer therapy. *Nat Clin Pract Oncol.* (2008) 5:220–33. doi: 10.1038/ncponc1073
19. Fayed N, Modrego PJ. The contribution of magnetic resonance spectroscopy and echoplanar perfusion-weighted MRI in the initial assessment of brain tumours. *J Neurooncol.* (2005) 72:261–5. doi: 10.1007/s11060-004-2180-6
20. Lee SY, Ju MK, Jeon HM, Jeong EK, Lee YJ, Kim CH, et al. Regulation of tumor progression by programmed necrosis. *Oxid Med Cell Longev.* (2018) 2018:3537471. doi: 10.1155/2018/3537471
21. Asahara T, Murohara T, Sullivan A, Silver M, van der Zee R, Li T, et al. Isolation of putative progenitor endothelial cells for angiogenesis. *Science.* (1997) 275:964–7. doi: 10.1126/science.275.5302.964
22. Ott I, Keller U, Knoedler M, Gotze KS, Doss K, Fischer P, et al. Endothelial-like cells expanded from CD34+ blood cells improve left ventricular function after experimental myocardial infarction. *FASEB J.* (2005) 19:992–4. doi: 10.1096/fj.04-3219fje
23. Starke RD, Ferraro F, Paschalaki KE, Dryden NH, McKinnon TA, Sutton RE, et al. Endothelial von Willebrand factor regulates angiogenesis. *Blood.* (2011) 117:1071–80. doi: 10.1182/blood-2010-01-264507
24. Tesfamariam B. Involvement of platelets in tumor cell metastasis. *Pharmacol Ther.* (2016) 157:112–9. doi: 10.1016/j.pharmthera.2015.11.005
25. Zanetta L, Marcus SG, Vasile J, Dobryansky M, Cohen H, Eng K, et al. Expression of Von Willebrand factor, an endothelial cell marker, is up-regulated by angiogenesis factors: a potential method for objective assessment of tumor angiogenesis. *Int J Cancer.* (2000) 85:281–8. doi: 10.1002/(SICI)1097-0215(20000115)85:2<281::AID-IJC21>3.0.CO;2-3
26. Caragher SP, Sachdev S, Ahmed A. Radiotherapy and glioma stem cells: searching for chinks in cellular armor. *Curr Stem Cell Rep.* (2017) 3:348–57. doi: 10.1007/s40778-017-0102-8
27. Greenfield JP, Cobb WS, Lyden D. Resisting arrest: a switch from angiogenesis to vasculogenesis in recurrent malignant gliomas. *J Clin Invest.* (2010) 120:663–7. doi: 10.1172/JCI42345
28. Ceradini DJ, Kulkarni AR, Callaghan MJ, Tepper OM, Bastidas N, Kleinman ME, et al. Progenitor cell trafficking is regulated by hypoxic gradients through HIF-1 induction of SDF-1. *Nat Med.* (2004) 10:858–64. doi: 10.1038/nm1075
29. Sidney LE, Branch MJ, Dunphy SE, Dua HS, Hopkinson A. Concise review: evidence for CD34 as a common marker for diverse progenitors. *Stem Cells.* (2014) 32:1380–9. doi: 10.1002/stem.1661
30. Hristov M, Weber C. Endothelial progenitor cells in vascular repair and remodeling. *Pharmacol Res.* (2008) 58:148–51. doi: 10.1016/j.phrs.2008.07.008
31. Kong X, Guan J, Ma W, Li Y, Xing B, Yang Y, et al. CD34 Over-Expression is associated with gliomas' higher WHO grade. *Medicine.* (2016) 95:e2830. doi: 10.1097/MD.0000000000002830
32. Bauer AT, Suckau J, Frank K, Desch A, Goertz L, Wagner AH, et al. von Willebrand factor fibers promote cancer-associated platelet aggregation in malignant melanoma of mice and humans. *Blood.* (2015) 125:3153–63. doi: 10.1182/blood-2014-08-595686
33. Mukherjee A, Wu D, Davis HC, Shapiro MG. Non-invasive imaging using reporter genes altering cellular water permeability. *Nat Commun.* (2016) 7:13891. doi: 10.1038/ncomms13891
34. Hayashi Y, Edwards NA, Proescholdt MA, Oldfield EH, Merrill MJ. Regulation and function of aquaporin-1 in glioma cells. *Neoplasia.* (2007) 9:777–87. doi: 10.1593/neo.07454
35. Maugeri R, Schiera G, Di Liegro CM, Fricano A, Iacopino DG, Di Liegro I. Aquaporins and Brain Tumors. *Int J Mol Sci.* (2016) 17:E1029. doi: 10.3390/ijms17071029
36. Isoardo G, Morra I, Chiarle G, Audrito V, Deaglio S, Melcarne A, et al. Different aquaporin-4 expression in glioblastoma multiforme patients with and without seizures. *Mol Med.* (2012) 18:1147–51. doi: 10.2119/molmed.2012.00015
37. Lan YL, Wang X, Lou JC, Ma XC, Zhang B. The potential roles of aquaporin 4 in malignant gliomas. *Oncotarget.* (2017) 8:32345–55. doi: 10.18632/oncotarget.16017

Conflict of Interest: The authors declare that the research was conducted in the absence of any commercial or financial relationships that could be construed as a potential conflict of interest.

Copyright © 2019 Seo, Ko, Park, Jeong, Park, Kim, Park and Lee. This is an open-access article distributed under the terms of the Creative Commons Attribution License (CC BY). The use, distribution or reproduction in other forums is permitted, provided the original author(s) and the copyright owner(s) are credited and that the original publication in this journal is cited, in accordance with accepted academic practice. No use, distribution or reproduction is permitted which does not comply with these terms.

frontiers in Oncology

ORIGINAL RESEARCH
published: 29 November 2019
doi: 10.3389/fonc.2019.01301

The Dual Cell Cycle Kinase Inhibitor JNJ-7706621 Reverses Resistance to CD37-Targeted Radioimmunotherapy in Activated B Cell Like Diffuse Large B Cell Lymphoma Cell Lines

*Gro Elise Rødland[1], Katrine Melhus[2], Roman Generalov[2], Sania Gilani[1], Francesco Bertoni[3], Jostein Dahle[2], Randi G. Syljuåsen[1] and Sebastian Patzke[1,2]**

[1] Department of Radiation Biology, Institute for Cancer Research, Norwegian Radium Hospital, Oslo University Hospital, Oslo, Norway, [2] Research and Development, Nordic Nanovector ASA, Oslo, Norway, [3] Lymphoma and Genomics Research Program, Institute of Oncology Research, Università Della Svizzera Italiana, Lugano, Switzerland

The CD37 targeting radioimmunoconjugate ^{177}Lu-lilotomab satetraxetan (Betalutin) is currently being evaluated in a clinical phase 2b trial for patients with follicular lymphoma (FL) and in a phase 1 trial for patients with diffuse large B-cell lymphoma (DLBCL). Herein we have investigated the effect of ^{177}Lu-lilotomab satetraxetan in seven activated B-cell like (ABC) DLBCL cell lines. Although the radioimmunoconjugate showed anti-tumor activity, primary resistance was observed in a subset of cell lines. Thus, we set out to identify drugs able to overcome the resistance to ^{177}Lu-lilotomab satetraxetan in two resistant ABC-DLBCL cell lines. We performed a viability-based screen combining ^{177}Lu-lilotomab satetraxetan with the 384-compound Cambridge Cancer Compound Library. Drug combinations were scored using Bliss and Chou-Talalay algorithms. We identified and characterized the dual-specific CDK1/2 and AURA/B kinase inhibitor JNJ-7706621 as compound able to revert the resistance to RIT, alongside topoisomerase and histone deacetylases (HDAC) inhibitors.

Keywords: radioimmunotherapy (RIT), CD37, combination therapy, lymphoma, radiation resistance, aurora kinase, cyclin-dependent kinase, polo-like kinase

OPEN ACCESS

Edited by:
Ira Ida Skvortsova, Innsbruck Medical University, Austria

Reviewed by:
Heng-Hong Li, Georgetown University, United States
Richard Piekarz, National Institutes of Health (NIH), United States

***Correspondence:**
Sebastian Patzke
spatzke@nordicnanovector.com;
sebastip@rr-research.no

Specialty section:
This article was submitted to Radiation Oncology, a section of the journal Frontiers in Oncology

Received: *21 July 2019*
Accepted: *11 November 2019*
Published: *29 November 2019*

Citation:
Rødland GE, Melhus K, Generalov R, Gilani S, Bertoni F, Dahle J, Syljuåsen RG and Patzke S (2019) The Dual Cell Cycle Kinase Inhibitor JNJ-7706621 Reverses Resistance to CD37-Targeted Radioimmunotherapy in Activated B Cell Like Diffuse Large B Cell Lymphoma Cell Lines. Front. Oncol. 9:1301. doi: 10.3389/fonc.2019.01301

INTRODUCTION

Diffuse large B-cell lymphoma (DLBCL) is the most common type of lymphoma, accounting for ∼35% of all newly diagnosed cases. Despite its phenotypical relatively homogenous appearance, DLBCL is a heterogeneous diseases (1). So far, the most commonly used sub-classification is based on the cell-of-origin (COO), identifying the germinal center B-cell (GCB)-type and the activated B-cell (ABC)-like DLBCL subtypes on the basis of gene or protein expression pattern reminiscent of normal germinal center or ABCs, respectively. ABC-DLBCL is associated with a worse outcome than GCB-DLBCL when patients are treated with the standard R-CHOP-like treatment (R-CHOP: a combination of the CD20-targeting antibody rituximab and the chemotherapeutics cyclophosphamide, doxorubicin, prednisolone, and vincristine).

Despite the major improvements in our understanding of the biology of DLBCL and the availability of a large number of novel compounds, no new regimen has shown superiority to R-CHOP (2–4). Recent studies have indeed uncovered a high degree of genetic

heterogeneity even within the GCB and ABC-DLBCL subtypes (5, 6), thus indicating the need to target more specific subgroups of patients. Furthermore, over-expression of MYC and BCL2 proteins in the absence of chromosomal rearrangements identifies a subgroup of cases, the so-called double expressor lymphomas (DEL), with a particularly poor prognosis. DELs are more frequent in ABC than GCB-DLBCL (1, 7). In standard clinical practice first-line R-CHOP-like treatment of DEL includes etoposide in addition to prednisone, vincristine, cyclophosphamide and doxorubicin (R-ECHOP) [reviewed in (1, 8)]. Patients with refractory, relapsed or treatment resistant DLBCL are, if eligible, treated with intensive chemotherapy [in the case of chemoresistance: rituximab in combination with ifosfamide, carboplatin, and etoposide (R-ICE), or dexamethasone, high-dose cytarabine, and cisplatin (R-DHAP)] followed by autologous (or allogeneic) stem cell transplantation (ASCT). Still, the DEL patient group remain a particularly poor prognostic group with 5-year progression free survival (PFS) of <30% after relapse.

Radioimmunotherapy (RIT) is an alternative and target-specific treatment for lymphomas. RIT is based on the conjugation of a short-ranged and short half-lived radioemitter to a lineage-specific monoclonal antibody (9). ^{90}Y-Ibriumomab and ^{131}I-tositumomab are examples of CD20 targeted FDA-approved, first-generation RITs for the treatment of relapsed or refractory follicular lymphoma (r/r-FL) and transformed FL [for a review (10)]. These showed promising results for treatment of FL and DLBCL, but, amongst other, logistic challenges resulted in underusage (11–14). ^{131}I-tositumomab was withdrawn from the market in 2014. CD37 is a transmembrane protein expressed almost exclusively on cells of the immune system, especially in mature B cells and B cell NHL (15), hence being an important alternative for CD20-targeting therapies, to which treatment-resistance can be developed (16). ^{177}Lu-lilotomab satetraxetan (Betalutin®) is a CD37-specific murine monoclonal antibody (clone HH1) that is chelated via a p-SCN-benzyl-DOTA-linker (satetraxetan) to the β-emitting isotope ^{177}Lutetium ($T_{1/2}$ = 6.7 days) (17–19). ^{177}Lu-lilotomab satetraxetan is currently being investigated as a single-injection mono-therapy for treatment of relapsed or refractory (r/r) FL (NCT01796171, Phase 2B) and r/r-DLBCL (NCT02658968, Phase 1), showing a promising overall response rate in r/r-FL of about 65–70% (20). ^{177}Lu-lilotomab satetraxetan may thus have potential in the treatment of high-grade DLBCL, though as in the case of r/r-FL treatment, resistance may occur. To explore and attempt to over-come the potential resistance we chose to investigate the sensitivity to ^{177}Lu-lilotomab in cell lines derived from ABC-DLBCL, the DLBCL subtype that has the lower sensitivity to standard regimens. Subsequently, we conducted a combinatorial drug screen for small molecular anti-cancer compounds preventing ^{177}Lu-lilotomab satetraxetan treatment resistance in the most resistant cell lines. Herein, we report the identification and pre-clinical characterization of a dual CDK1/2 and AURKA/B kinase inhibitor that was identified in the screen as a candidate compound to overcome ^{177}Lu-lilotomab satetraxetan therapy resistance.

RESULTS

Resistance of U-2932 and RIVA to CD37-Targeted ^{177}Lu-Radioimmunotherapy

We initially investigated the sensitivity of seven different ABC-DLBCL cell lines (HBL1, OciLy-3, Oci-Ly10, RIVA [RI-1], SU-DHL-2, TMD-8, U-2932) to treatment with ^{177}Lu-lilotomab satetraxetan. Cells were treated for 18 h with 11 different doses of ^{177}Lu-lilotomab satetraxetan ranging from concentrations of 0.01–20 μg/ml (specific activity: 600 MBq/mg), washed and plated in 96-well plates. Mock treated cells were included as controls. The total DNA content in each well was assessed using the CyQuant reagent as a readout of cell proliferation. Comparative analysis of relative proliferation capacity compared to untreated control cells identified U-2932 and the RIVA cells as the most resistant cell lines, showing over 40% of signal intensity of untreated control cells even after treatment at 20 μg/ml ^{177}Lu-lilotomab satetraxetan (**Figure 1A**). Conversely, Oci-Ly10 cells showed highest sensitivity to treatment with a 70% decreased proliferation capacity in response to treatment with 0.25 μg/ml ^{177}Lu-lilotomab satetraxetan. Notably, *CD37* mRNA and CD37 surface expression were not associated with the resistance to CD37-target RIT (**Table 1**). We confirmed the differential sensitivity of these three cell lines in a metabolic cell viability assay, utilizing MT RealTimeGlo, that allowed the monitoring of cell proliferation throughout a continuous period of 72 h (**Figures 1B,C**). Cells were treated as previously and the luminescent assay substrate added 72 h after plating into micro-well titer plates. All cell lines and control treatment groups showed continuous proliferation throughout the observation period. Addition of cold, non-^{177}Lu chelated lilotomab (HH1-DOTA) did not markedly inhibit proliferation in either cell line. Oci-Ly10 cells were sensitive to even the lowest tested dose of 0.05 μg/ml ^{177}Lu-lilotomab satetraxetan and ceased proliferation at 0.25 μg/ml. Confirming the observed resistance in the CyQuant assay, U-2932 and RIVA retained ∼60 and 40%, respectively, of the proliferation capacity of untreated cells at 5 days after treatment with 2 μg/ml ^{177}Lu-lilotomab satetraxetan. Again, RIVA cells were more sensitive to ^{177}Lu-lilotomab satetraxetan than U-2932 and showed about 60% of the proliferation capacity of control cells at a dose of 0.5 μg/ml, which is half of the dose required in U-2932 cells to reach a similar level of inhibition.

To conclude, U-2932 and RIVA have been shown to be ^{177}Lu-lilotomab satetraxetan treatment resistant ABC-DLBCL cell lines. Furthermore, the resistance of these cell lines to CD37-targeted RIT was not due to a reduced expression of and binding to CD37 on the cell surface.

Combinatorial Drug Screen Identifies Cell Cycle Kinase Inhibitors as Candidate Drugs to Overcome Radioimmunotherapy Resistance

Only two out of seven cell lines of the ABC-DLBCL panel did not respond well to CD37-targeted RIT. These two cell lines, U-2932 and RIVA, may represent models of most challenging to

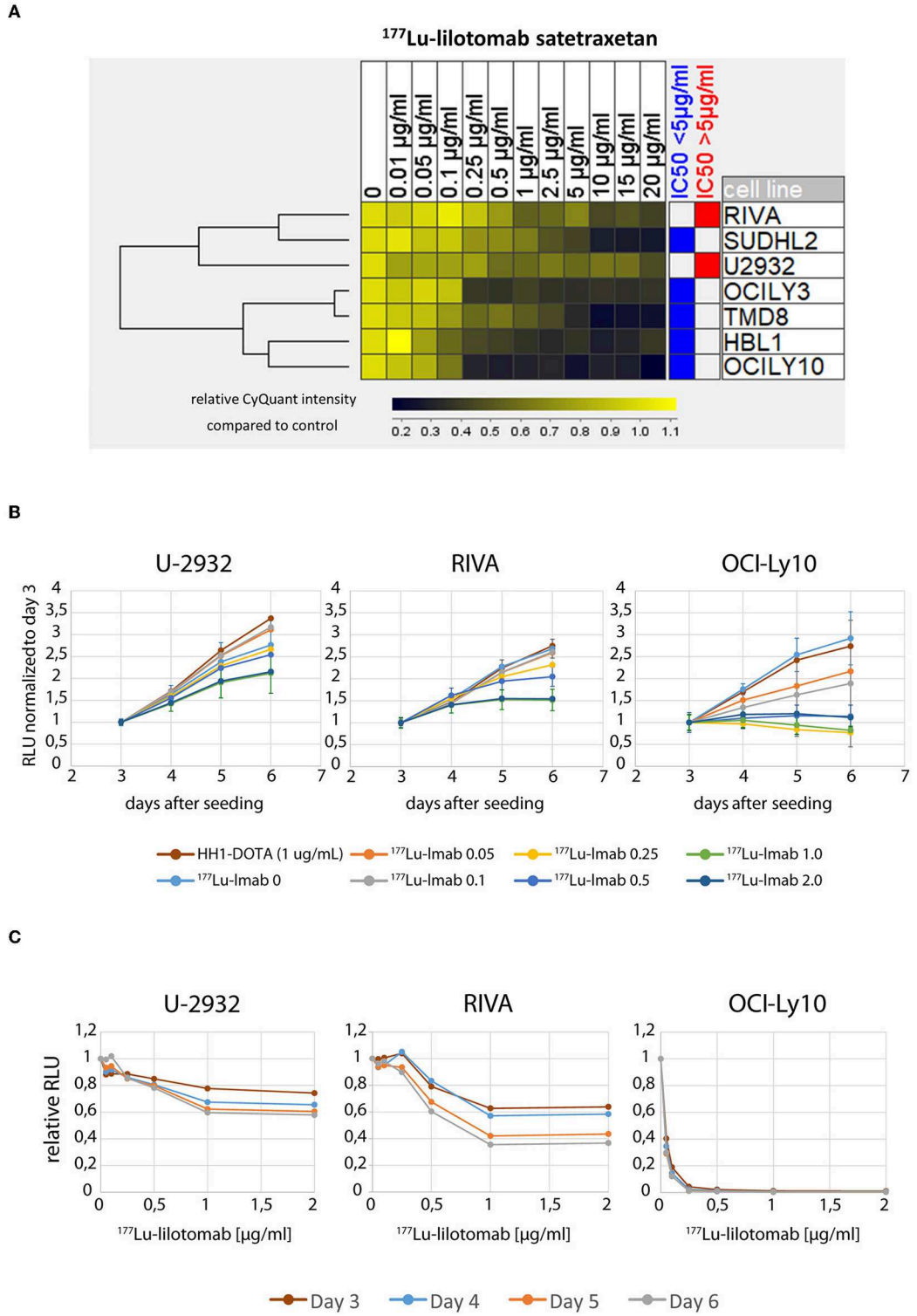

FIGURE 1 | U-2932 and RIVA are resistant to CD37-targeted ^{177}Lu-radioimmunotherapy. **(A)** Cells were treated for 18 h with 11 different doses of ^{177}Lu-lilotomab satetraxetan ranging from 0.01 to 20 µg/mL (specific activity: 600 MBq/mg), washed and plated in 96-well plates. Mock treated cells were included as control. The total DNA content in each well was assessed using the CyQuant reagent as an equivalent of cell proliferation. **(B,C)** Treated as in **(A)** with doses of ^{177}Lu-lilotomab satetraxetan ranging from 0 to 2 µg/mL or cold antibody (HH-1-Dota) and measuring proliferation utilizing MT, RealTime-Glo, adding luminescent assay substrate 72 h after seeding in micro-well titer plates. **(C)** Relative RLU (^{177}Lu-lilotomab satetraxetan to control) of data presented in **(B)**. Error bars: Standard deviation (STDEV) (n = 5 for U-2932 and RIVA, n = 3 OCI-Ly10). Inhibition of cell proliferation on days 5 and 6 were significantly reduced compared to control ($p < 0.001$, 1-way ANOVA) in U-2932 cells at doses ≥ 1 µg/mL, in RIVA at doses ≥ 0.25 µg/mL, and Oci-Ly10 at doses ≥ 0.1 µg/mL.

TABLE 1 | Characteristics of ABC-DLBCL cell lines.

Cell line	IC50 (CyQUANT) [μg/ml]	CD37 mRNA [RPKM]	CD37 mRNA (rel. to RIVA)	CD37 protein MS [counts]	CD37 protein (rel. to RIVA)	CD37 surface HH1-DOTA binding rel. to RIVA	*TP53*	*MYC*	*BCL2*
Oci-Ly10	0.3	10.6	0.9	29.76	0.99	0.32 ± 0.04	Inactive	WT	WT
HBL1	0.6	11.3	1.0	30.83	1.02	n.d.	Inactive	WT	WT
OCI-LY3	1.1	11.5	1.0	31.08	1.03	n.d.	WT	WT	Amp
TMD8	1.1	11	1.0	31.45	1.04	n.d.	WT	WT	WT
SUDHL2	2.5	9.6	0.8	29.34	0.97	n.d.	WT	WT	WT
RIVA	8.6	11.5	1	30.14	1	1	Inactive	T	Amp
U-2932	31.6	9.4	0.8	29.99	1.00	0.55 ± 0.02	Inactive	OE	Amp

WT, wild-type; T, translocated; OE, overexpressed, Amp, amplified; RPKM, Reads per kilo base per million (21–23).

treat DLBCL. To understand and overcome the lack of response to ^{177}Lu-lilotomab satetraxetan treatment, we set out to find combinatorial drug partners for ^{177}Lu-lilotomab satetraxetan capable of reversing CD37-targeted RIT resistance in both cell lines. U-2932 and RIVA cells were treated with 1 and 0.5 μg/ml of ^{177}Lu-lilotomab satetraxetan for 18 h, respectively, washed and seeded onto micro-well plates pre-printed with a library of 384 anti-cancer compounds (Cambridge anti-Cancer Compound library; SelleckChem). Three days post-plating RealTimeGlo reagent was added and luminescence read on three consecutive days to assess the relative amount of metabolically active cells. The screen design is schematically presented in **Figure 2**.

Both cell lines continuously proliferated throughout the observation period, albeit U-2932 cells showed a higher growth rate and stronger resistance to ^{177}Lu-lilotomab satetraxetan monotreatment than RIVA cells in the primary screen (**Supplementary Figure 1**). Three different concentrations of drugs (U-2932: 10/1,000 nM; RIVA: 10/100 nM final concentration) were tested to account for compound-specific differences in potency. Inhibitory compounds were considered as a hit candidate if they: (1) in combination with ^{177}Lu-lilotomab satetraxetan inhibited cell proliferation over two consecutive days to a degree greater than the expected additive effect of the mono-treatments alone (Bliss theorem, see Materials and Methods for details), and (2) the inhibitory effect of the compound alone at the tested concentration was <90% relative to the untreated control. These criteria were met by 53 compounds in U-2932 (11 at 10 nM and 42 at 1 μM) and 27 compounds in RIVA cell lines (8 at 10 nM and 19 at 100 nM) (**Tables 2**, **3**). **Figures 3A,B** summarize the screen results for each cell line and library concentration. Hit candidates are highlighted in dot-plots showing the relative proliferation of cells at day 5 treated with the compound alone vs. its combination with ^{177}Lu-lilotomab satetraxetan (datasets are included as excel spreadsheets in **Supplementary Material**). Topoisomerase inhibitors accounted for 13% of the hits in U-2932 and 23% in RIVA, and histone deacetylase (HDAC) inhibitors for 7% of the hits in U-2932 and 27% in RIVA cells (**Tables 2**, **3**). The enrichment defined topoisomerases and histone deacetylases (HDAC) as prime targets for co-inhibition in both cell lines. A third prominent group of hit candidates comprised inhibitors targeting mitotic cell cycle kinases, including AURKA, AURKB, CDK1, PLK1, and WEE1 (17% of total hits in U-2932; 12% in RIVA).

Since both topoisomerase inhibitors, such as doxorubicin or etoposide, and HDAC inhibitors are known to cause direct or indirect DNA damage, respectively, it is likely they might overcome resistance by potentiating the level of DNA damage in ^{177}Lu-RIT-targeted cells (24–26). Therefore, we focused on the third group of compounds, the mitotic kinase inhibitors, that affect kinases with critical functions for both mitotic entry and exit, and have a role in termination of the DNA damage-induced G_2-checkpoint (27–29). In particular we further explored the combination of ^{177}Lu-lilotomab satetraxetan with the dual CDK1/2-Aurora A/B inhibitor JNJ-7706621, the Aurora A inhibitor alisertib (MLN8237), and the Plk1 inhibitor GSK461364, respectively. JNJ-7706621 and alisertib were hit candidates in both cell lines. GSK461364 did not score as a hit candidate in U-2932 cells only due to its high potency as a mono-therapy.

JNJ-7706621 Synergistically Reduces Viability of DLBCL When Combined With ^{177}Lu-Lilotomab Satetraxetan

To investigate the validity of the synergism observed following ^{177}Lu-Lilotomab satetraxetan with the effect of the cell cycle kinase inhibitors in resistant cell lines, U-2932 cells were treated or not with ^{177}Lu-lilotomab satetraxetan (0.5, 1, and 2 μg/ml) for 18 h, washed and seeded onto 384-well plates pre-printed with 11-step gradients of JNJ-7706621, alisertib, and GSK461364 ranging from 0 to 1,280 nM. Similar to the primary screen, viability was measured by RealTimeGlo. Dose-response profiles were recorded at day 5 and Combination Indexes (CI) calculated to test for a synergistic interaction of ^{177}Lu-Lilotomab satetraxetan-inhibitor combinations (Chou-Thalaly; CompuSyn software). CI values were calculated for combinations within the minimum and maximum effect range of mono-treatment of each inhibitor.

Figure 4 shows dose-response curves for treatment with either drug alone or in combination with different doses of ^{177}Lu-lilotomab satetraxetan. The anti-proliferative effect of the dual CDK1/2-AURKA/B inhibitor JNJ-7706621 was moderate, even at high doses (**Figure 4A**). However, and confirming the

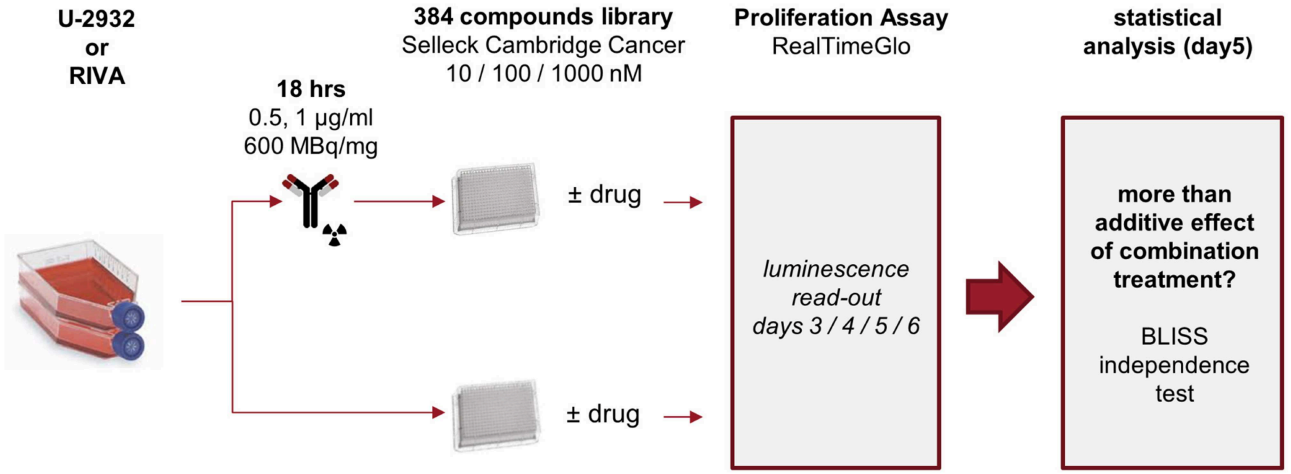

FIGURE 2 | Experimental layout. U-2932 and RIVA cells were treated with 1 or 0.5 µg/mL ^{177}Lu-lilotomab satetraxetan (600 MBq/mg) for 18 h, excess ^{177}Lu-lilotomab satetraxetan removed, and cells seeded onto 384-well plates pre-printed with the 384-compound Cambridge Cancer compound library sourced from Selleckchem at final concentrations of 10 nM, 100 nM, or 1 µM. Untreated control cells were seeded on parallel plates. Viability measurements, using RealTime-Glo, were carried out between day 3 and 6 after seeding. Inhibitory compounds were considered as candidate hits if they: (1) in combination with ^{177}Lu-lilotomab satetraxetan inhibited cell proliferation over two consecutive days to a degree greater than the expected additive effect of the mono-treatments alone (BLISS theorem, see Materials and Methods for details), and (2) drug treatment alone did not reduce viability to <90% of that of untreated control.

primary screen results, the combination with ^{177}Lu-lilotomab satetraxetan led to a greater reduction in the fraction of viable cells than each treatment alone. Synergism (CI < 1) was observed for all tested combinations (blue circles in Fa/CI plots). The AURKA inhibitor alisertib had a bi-phasic dose-response profile, with a decreasing anti-proliferative effect at doses above 160 nM (**Figure 4B**) and synergism was observed within a range of 10–160 nM. U-2932 cells were highly sensitive to treatment with the PLK1 inhibitor GSK461364 with a near complete growth inhibition obtained at 20 nM (**Figure 4C**). At lower doses the sensitivity was greatly reduced, and when combined with ^{177}Lu-lilotomab satetraxetan growth inhibition was, however modestly, potentiated. Weak synergism (CI 0.75–0.95) was observed only at GSK461364 concentrations near the maximum effect (20 and 40 nM; Fa close to 1). Similar CI index profiles were obtained in RIVA cells (**Supplementary Figure 2**). The results of the validation screen identified the dual CDK1/2 and AURKA/B kinase inhibitor JNJ-7706621 as the best hit candidate. We hence controlled first for target-specificity/activity for inhibition of CDK1 and AURKB (**Supplementary Figure 3**). Synergism with ^{177}Lu-lilotomab satetraxetan was then confirmed in two additional combination experiments in U-2932 cells covering the range of 100–10,000 nM JNJ-7706621 (**Figure 4A**, yellow and red circles).

The Dual CDK1/2 and AURKA/B Inhibitor JNJ-7706621 Synergizes With CD37-Targeted RIT by Potentiating Mitotic Slippage and Apoptotic Cell Death

The validation experiments confirmed a synergistic drug interaction of JNJ-7706621 and ^{177}Lu-lilotomab satetraxetan in the inhibition of proliferation of U-2932 and RIVA cells, as assessed by the decreased capacity in reducing the RealTimeGlo substrate. CD37-targeted RIT induced DNA damage and inhibition of CDK1/2 and AURKA/B kinases by JNJ-7706621 are independently of each other expected to result in cell cycle progression defects. For instance, in mitotic shake-off synchronized HeLa cells, inhibition of CDK1/2 and AURKA/B by JNJ-7706621 at a final concentration of 1–3 µM was reported to delay exit from G_1, to arrest cells at G_2/M, and to induce endoreduplication (30). We thus investigated the effects of mono- and combination therapy on cell cycle progression in U-2932 and RIVA cells (**Figure 5**). Cells were treated with or without ^{177}Lu-lilotomab satetraxetan (18 h; U-2932: 1 µg/ml, RIVA 0.5 µg/ml), washed and treated with or without 500 nM JNJ-7706621, a concentration at which strong synergism was observed in both cell lines (**Figure 4** and **Supplementary Figure 2**).

Samples were taken immediately after treatment with ^{177}Lu-lilotomab satetraxetan and at 24, 72, and 144 h after inhibitor addition, and DNA content and cell death assessed by flow cytometry (**Figure 5A**). Medium was replenished (with or without inhibitor) at 72 h to allow for optimal growth conditions throughout the observation period. Treatment with JNJ-7706621 alone induced a prominent but transient accumulation of cells in G_2/M-phase (4n DNA content) after 24 h of treatment in both cell lines (**Figure 5B**). Similarly, pre-treatment with ^{177}Lu lilotomab satetraxetan alone also induced a prominent but transient accumulation of cells in G_2/M-phase in both cell lines. The addition of JNJ-7706621 to ^{177}Lu-lilotomab satetraxetan treated cells strongly reduced the fraction of cells in G_1 phase (2n) at the 24 h time time-point and at later times strongly increased appearance of single cells with <2n or >4n DNA content, indicative of cell death and endoreduplication/cytokinesis failure, respectively. We therefore quantitatively assessed the fraction

TABLE 2 | Hit candidate list from screen in U-2932 cells.

U-2932		
Drug name	**Target**	**Bliss score**
10 nM		
Mitoxantrone Hydrochloride	Topo	0.39
Idarubicin HCl	Topo	0.33
Doxorubicin (Adriamycin)	Topo	0.32
Epirubicin Hydrochloride	Topo	0.25
Flutamide (Eulexin)	Antiandrogen drug	0.16
Barasertib (AZD1152-HQPA)	Aurora	0.15
Daunorubicin HCl (Daunomycin HCl)	DNA	0.19
Oxaliplatin (Eloxatin)	DNA	0.17
Paclitaxel (Taxol)	Microtubule	0.30
Triptolide	NF-κB inhibitor	0.26
Elesclomol	Oxidative stress inducer	0.43
BX-795	PDK1	0.20
PF-3845	FAAH	0.18
Panobinostat	HDAC	0.07
1 μM		
Danusertib (PHA-739358)	Aurora	0.28
VX-680 (MK-0457, Tozasertib)	Aurora	0.19
AMG 900	Aurora	0.18
MLN8237 (Alisertib)	Aurora	0.14
SNS-314	Aurora	0.12
Ponatinib (AP24534)	Abl, PDGFRα, VEGFR2, FGFR1, and Src	0.39
Dasatinib (BMS-354825)	Abl, Src, and c-Kit	0.31
Salinomycin (Procoxacin)	Anti-bacterial	0.09
PCI-32765 (Ibrutinib)	Btk	0.18
PHA-793887	CDK2, CDK5, and CDK7	0.17
JNJ-7706621	pan-CDK	0.39
LY2603618 (IC-83)	Chk1	0.16
Cytarabine	DNA	0.57
Bleomycin sulfate	DNA	0.20
Oxaliplatin (Eloxatin)	DNA	0.14
Decitabine	DNA methyltransferase	0.37
NU7441(KU-57788)	DNA-PK	0.23
SMER 3	E3 ubiquitin ligase	0.34
BIX 01294	G9a histone methyltransferase	0.16
Oxamflatin	HDAC	0.77
Vorinostat (SAHA)	HDAC	0.22
Entinostat (MS-275, SNDX-275)	HDAC	0.22
Mocetinostat (MGCD0103)	HDAC	0.12
TPCA-1	IKK-2	0.18
Pomalidomide	Inhibits LPS-induced TNF-α release	0.15
BI 78D3	JNK	0.35
Mycophenolate mofetil (CellCept)	Monophosphate dehydrogenase I/II	0.52
Sotrastaurin (AEB071)	pan-PKC	0.13
Crenolanib (CP-868596)	PDGFRα/β	0.30
BX-795	PDK1	0.13
GDC-0941	PI3Kα/δ	0.43
PIK-93	PI4KIIIβ	0.18
LY 333531	Protein kinase C	0.25
Pentostatin	Purine analog	0.14
GSK 269962	Rho-associated protein kinase	0.19
GSK 650394	Serum- and glucocorticoid-regulated kinase-1	0.18
SANT-2	Smoothened antagonist	0.19
SKI II	SphK	0.19
Bay 11-7085	TNFα-induced IκBα phosphorylation	0.23
Etoposide (VP-16)	Topo	0.31
Banoxantrone dihydrochloride	Topo	0.19
AZ 23	Trk	0.16
Tivozanib (AV-951)	VEGFR1/2/3	0.14
MK-1775	Wee1	0.38
PD 166285	Wee1/Chk1	0.86

(Continued)

TABLE 2 | Continued

Color-shading indicates increasing Bliss score from yellow to dark green.

of endoreduplication (>4n DNA content), cell death (Pacific blue uptake), as well as cell size (median forward scatter) in both cell lines in two independent experiments (**Figure 6** and **Supplementary Figures 4, 5**). Combination treatment strongly induced the formation of endoreduplicating cells (20- and 12-fold increase in U-2932 and RIVA, respectively; Bliss CI U-2932 = 0.55, RIVA = 0.69; [CI= $((E_{RIT} + E_{JNJ}) - E_{RIT} \times E_{JNJ})/E_{[RIT+JNJ]}$]), which was accompanied by a 2-fold increase in relative cell size, compared to untreated and mono-treated cells. Visual inspection of cells by microscopy confirmed this result, revealing prominent occurrence of multinucleated cells and increased DNA content (**Supplementary Figure 6**). Most importantly, combination treatment led to a 5- and 13-fold increase in cell death compared to untreated cells at the 144 h time point in U-2932 (CI = 0.72) and RIVA (CI = 0.50), respectively. To further explore the mechanistic details behind the anti-tumor activity of JNJ-7706621 and ^{177}Lu-litomab satetraxetan combination treatment, we used the same experimental setup as described in **Figure 5** but now monitored PARP cleavage, a late apoptotic event, and cell growth (**Figure 7**). In accordance with our RealTime-Glo data we found that cells exposed to the combination showed a significantly reduced growth rate between 24 and 72 h post-treatment as compared to control cells and cells receiving monotherapy (**Figure 7A**). The fraction of cells in late apoptosis (cleaved PARP positive cells), was at all tested time-points significantly increased in cells receiving combination therapy as compared to control cells, reaching about 50% after 144 h (**Figure 7B**). Induction of apoptosis was also significantly increased in cells receiving single

TABLE 3 | Hit candidate list from screen in RIVA cells.

RIVA		
Drug name	**Target**	**Bliss score**
10 nM		
Panobinostat	HDAC	0.27
Daunorubicin HCl (Daunomycin HCl)	DNA	0.22
BX-795	PDK1	0.12
GSK461364	Plk1	0.20
Doxorubicin (Adriamycin)	Topo	0.29
Mitoxantrone Hydrochloride	Topo	0.23
Idarubicin HCl	Topo	0.21
Epirubicin Hydrochloride	Topo	0.20
100 nM		
PCI-24781	HDAC	0.40
SB939 (Pracinostat)	HDAC	0.25
Trichostatin A (TSA)	HDAC	0.21
CUDC-101	HDAC	0.19
Belinostat (PXD101)	HDAC	0.15
Mocetinostat (MGCD0103)	HDAC	0.12
MLN8237 (Alisertib)	Aurora	0.13
Cytarabine	DNA	0.25
Mycophenolic (Mycophenolate)	IMP dehydrogenase I/II	0.12
GW3965 HCl	LXR	0.21
Cladribine	Nucleoside analog	0.24
JNJ-7706621	Pan-CDK	0.13
AG14361	PARP1	0.14
MLN2238	Proteasome	0.12
Clofarabine	Ribonucleotide reductase	0.21
Toremifene Citrate (Fareston. Acapodene)	SERM	0.19
Etoposide (VP-16)	Topo	0.27
Irinotecan HCl Trihydrate (Campto)	Topo	0.20
Doxorubicin (Adriamycin)	Topo	0.11
Epirubicin Hydrochloride	Topo	0.14

Color-shading indicates increasing Bliss score from yellow to dark green.

agent therapy at 72 and 144 h time points compared to control. At 144 h, 22% of JNJ-7706621 and 28% ^{177}Lu-litomab satetraxetan treated cells were determined as late apoptotic, indicating an additive effect of the combination treatment. Taken together, these results suggest that the synergistic anti-proliferative effect of the combination of JNJ-7706621 and ^{177}Lu-litomab satetraxetan is a consequence of JNJ-7706621 mediated mitotic infidelity of cells which have over-come the ^{177}Lu-litomab satetraxetan induced G_2-arrest, leading to incompatibility with proliferation and to excessive cell death by apoptosis (**Figure 7C**).

DISCUSSION

Targeted radionuclide delivery for DNA damaging radiation by means of antibody-conjugates has shown promising efficacy in clinical studies in the treatment of hematological cancers. ^{90}Y-Ibriumomab and ^{131}I-tositumomab have demonstrated significant activity in indolent relapsed/refractory NHL. ^{177}Lu-lilotomab satetraxetan is emerging as a potential treatment option for patients with rituximab resistant relapsed/refractory FL as well as R-CHOP resistant (and ASCT in-eligible) DLBCL. Here, we identified two ABC-DLBCL cell lines, U-2932 and RIVA, with primary resistance to CD37-targeting ^{177}Lu-lilotomab satetraxetan treatment, derived from DE ABC-DLBCL with inactive TP53. Subsequently, we used these cell lines to screen for compounds able to prevent the resistance to RIT and we identified and characterized the dual-specific CDK1/2 and AURKA/B kinase inhibitor JNJ-7706621, alongside topoisomerase and HDAC inhibitors. Alike other RITs ^{177}Lu-lilotomab satetraxetan is likely to induce a DNA damage response mediated cell cycle G_2 arrest that resistant cells are required to overcome or adapt to. Our findings may thus be of particular importance as G_1 arrest abrogating subclonal *TP53* mutations were recently found to be predictive of PFS in FL patients treated with CD20-targeting RIT-CHOP (^{131}I Tositumomab), but not R-CHOP (31).

U-2932 and RIVA are notoriously treatment resistant cell line models of ABC-DLBCL, including radiation- and chemotherapy (32, 33). Importantly, loss of or decreased binding to CD37 was excludable as an underlying cause of resistance to CD37-targeting RIT. The unbiased screening for anti-cancer compounds, which in combination with ^{177}Lu-lilotomab satetraxetan synergistically impair proliferation of these cell lines identified three major classes of compounds that may be utilizable to overcome RIT-resistance: topoisomerase inhibitors, HDAC inhibitors, and inhibitors of mitotic cell cycle kinases. Since we tested only a limited set of concentrations in a sequential approach following exposure to RIT, our study might have missed additional compounds that might be beneficial in combination at different concentrations or when given before or concomitantly with RIT, although radiation is persistently delivered through binding of the radioisotope conjugated antibody to CD37.

Interestingly, all Topoisomerase and all HDAC inhibitors within the compound library scored in at least one cell line. Topoisomerase inhibitors, such as doxorubicin and etoposide, are essential constituents of standard and salvage chemotherapy regimens (R-CHOP and R-ICE/R-DHAP) for lymphoma treatment and may synergize with ^{177}Lu-lilotomab satetraxetan by exaggerating the cumulative DNA damage beyond the cell's capacity of repair. HDAC inhibitors have been shown to lead to excessive DNA damage in cancer cells (24), but other downstream aspects within the pleiotropic effects of epigenetic modification may contribute to or be essential for the observed synergistic interaction. They have shown anti-tumor activity especially in T-cell lymphomas and are currently under evaluation in different combination regimens for r/r-DLBCL (34). Hence, both classes of compounds might not only potentiate the amount of DNA damage in ^{177}Lu-RIT-targeted cancer cells but also confer off-targeted DNA damage in untransformed cells due to their systemic administration. We focused on the third enriched group composed of mitotic cell cycle kinases inhibitors, which represent a secondary main (independent) target different from induction of DNA damage. Their inhibition ultimately interferes with balanced segregation of chromosomes as well as

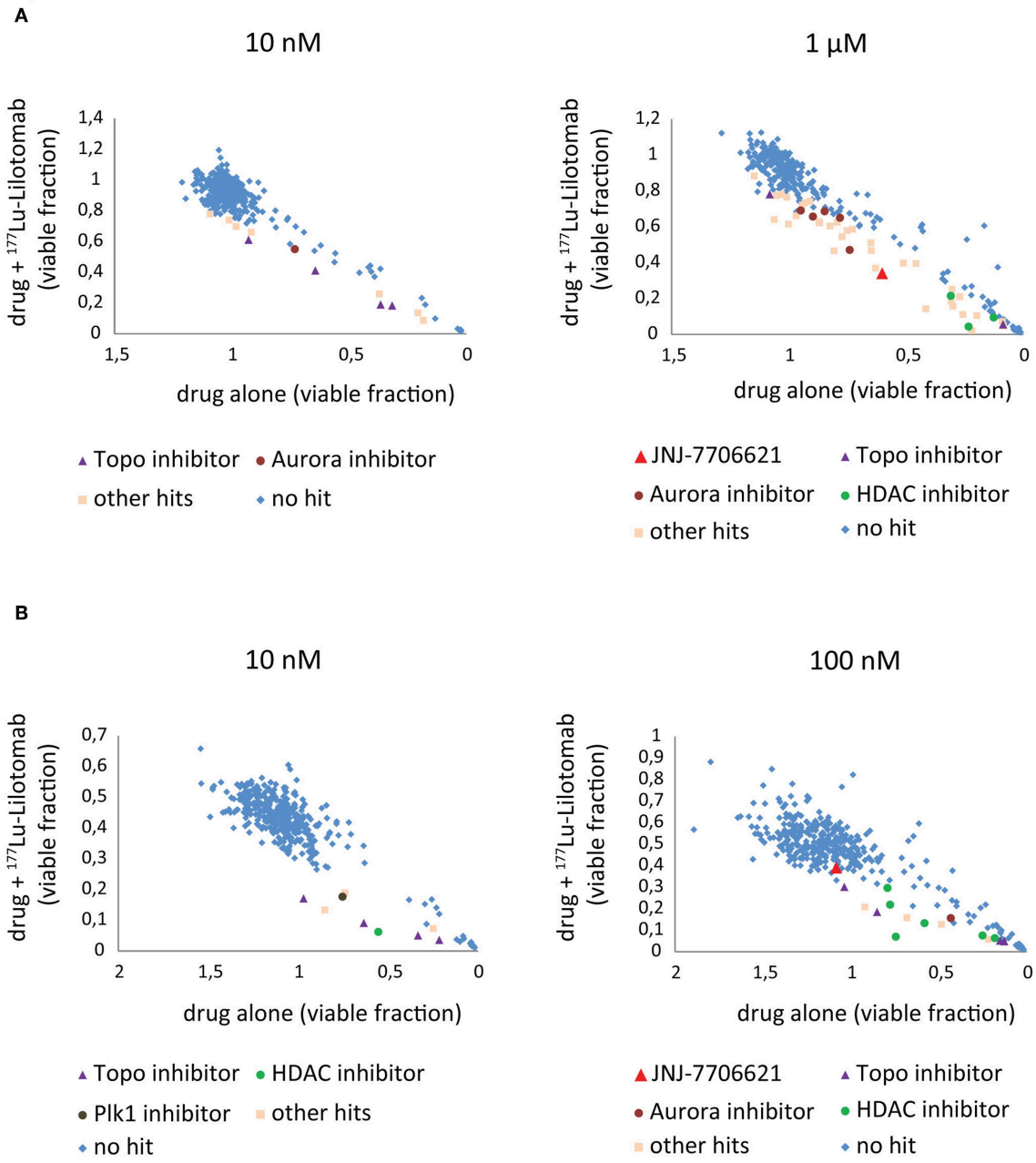

FIGURE 3 | Combination screen for compounds reversing ^{177}Lu-lilotomab satetraxetan resistance in DLBCL. Cells were treated as explained in **Figure 2**. The fraction of viable cells relative to untreated control at day 5 has been plotted for cells treated with drug alone (x-axis) against cells treated with drug combined with ^{177}Lu-lilotomab satetraxetan (y-axis) for the two concentrations of drugs tested in each cell line. **(A)** U-2932 and **(B)** RIVA. In blue are drugs excluded as hits by our statistical criteria (See **Figure 2**). Enriched hits are specified with name of common target and are in separate colors [purple triangles: topoisomerase inhibitors, burgundy circles: aurora kinase inhibitors (including Alisertib) and green circles: histone deacetylase inhibitors]. In red is the pan-CDK1/2 and AuroraA/B inhibitor JNJ-7706621 and in brown the Plk1 inhibitor GSK461364. In light pink are all other hits.

separation of daughter cells, rather than the direct DNA damage induction of replicating cells (27–29). Mitotic kinase inhibitors, including the hit candidate MLN8237 (alisertib), are currently in clinical trials for B cell lymphomas, e.g., Friedberg et al. (35) and Kelly et al. (36) (NCT00807495; NCT00697346). The dual-specific inhibitor of CDK1/2 and AURA/B kinases, JNJ-7706621, outperformed the PLK1 inhibitor GSK461364 and the AURKA inhibitor alisertib in the validation screen on the basis of strong synergism within a broad concentration range, at which mono-treatment with JNJ-7706621 showed little to no anti-proliferative efficacy. In contrast, synergism with PLK1 inhibition was only confirmed at concentrations near the maximum effect of the

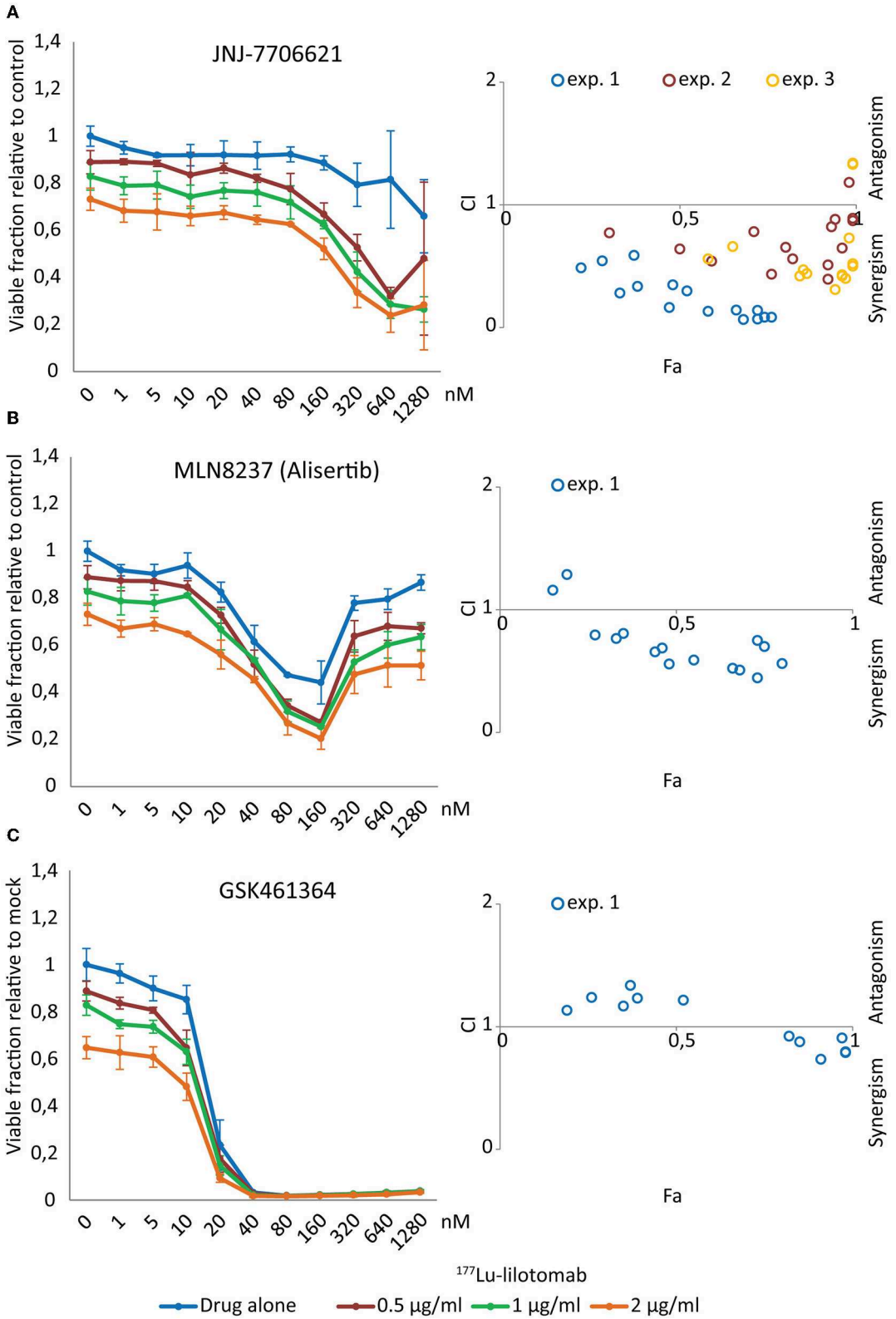

FIGURE 4 | JNJ-7706621 synergistically reduces viability of U-2932 cells when combined with ^{177}Lu-lilotomab satetraxetan. U-2932 cells were treated with 0.5, 1, and 2 µg/mL ^{177}Lu-lilotomab satetraxetan as in **Figure 1** and seeded in 384-well plates pre-printed with JNJ-7706621, Alisertib, and GSK461364 in an 11 step

(Continued)

FIGURE 4 | concentration gradient (0–1,280 nM). Viability was measured as in **Figure 1B**. In left panels the fraction of viable cells relative to untreated control at day 5 are plotted for cells exposed to single treatment or combinations for each drug dose (blue: drug alone, red: drug combined with 0.5 μg/mL ^{177}Lu-lilotomab satetraxetan, green: drug combined with 1 μg/mL ^{177}Lu-lilotomab satetraxetan and orange: drug combined with 2 μg/mL ^{177}Lu-lilotomab satetraxetan) **(A)** JNJ-7706621, **(B)** Alisertib, and **(C)** GSK461364. Right panels show Fa/CIs plots obtained by the Chou-Talaly method using the CompuSyn software. The fraction affected (Fa) is the fraction of non-viable cells relative to untreated control. For each combination with a specific Fa value the CI indicates whether the combined treatment is synergistic (<1) or antagonistic (>1). In blue are data from the same experiment as that shown in left panels, whereas red and yellow circles represent two independent experiments performed in U-2932 with JNJ-7706621. In experiment 2, 100, 266, 707, 1,880, and 5,000 nM of JNJ-7706621 were combined with the same doses of ^{177}Lu-lilotomab satetraxetan as in experiment 1, and in experiment 3 the doses of JNJ-7706621 were; 200, 532, 1,410, 3,760, and 10,000 nM. Error bars: STDEV of triplicate samples.

highly potent GSK461364 inhibitor itself. The high efficacy of GSK461364 alone may suggest its applicability (or that of equivalent PLK1 inhibitors) in mono-therapy for treatment of CD37-targeting RIT-resistant DLBCL or aggressive ABC-DLBCL. Clearly, further pre-clinical evaluation will be required to support this hypothesis. GSK461364 showed dose-related anti-tumor activity in a phase 1 study, but concomitantly lead to a high incidence rate of venous thrombotic emboli (37). Furthermore, acquired resistance due to up-regulation of ATP-binding cassette drug transporters has been reported for GSK461364 and alternative PLK1 inhibitors, including BI2536 and the clinically most advanced BI6727/Volasertib, potentially favoring combination over monotherapy strategies (38–40). Synergism of ^{177}Lu-lilotomab satetraxetan with alisertib was less strong than with JNJ-7706621, and confined to a narrow concentration window, since alisertib demonstrated a loss of efficacy at concentrations above 360 nM. The latter may be a concentration-dependent compound de-activating artifact of formulation in DMSO or a consequence of an antagonistic interaction with a secondary "off-target" inhibited enzyme. *AURKA (STK15)* is a driver and essential gene in DLBCL (41) and the identification of several other AURKA inhibitors in our screening campaign (not validated here) are supportive of further investigations. Pre-clinical and clinical investigations of alisertib in DLBCL treatment strongly suggest the need for combination drug partners, since re-commitment of treatment induced senescent aneuploid cells to cell cycle progression and low mitotic index in primary tumors are apparent causes of treatment resistance (29, 42–44). Hence, a more elaborate analysis of ^{177}Lu-lilotomab satetraxetan with a panel of AURKA inhibitors may prove valuable. This is strongly supported by the robust synergistic interaction of CD37-targeting RIT with JNJ-7706621 reported here. Dual-specificity and activity of JNJ-7706621 against CDK1/2 and AURA/B kinases was shown in TP53 proficient and deficient cell lines (45) and observed in U-2932 and RIVA cells. This inhibitor has shown anti-tumor activity in mouse xenograft models of solid tumors, but not been tested in clinical trials (30, 46). Of note, pre-clinical studies of JNJ-7706621 activity investigated its effect in the μM range, where anti-proliferative activity in monotreatment is evident (30, 45). Here, we showed that even sub-μM concentrations of JNJ-7706621 were sufficiently strong enough to synergize with ^{177}Lu-lilotomab satetraxetan, reducing the potential toxicity-risk of this compound and concomitantly lowering its required active concentration. The *in vivo* synergistic interaction of JNJ-7706621 and CD37-targeting RIT remain, however, to be proven.

Kinetic studies of the effect of mono- and combination therapy of U-2932 and RIVA cells with JNJ-7706621 and ^{177}Lu-lilotomab satetraxetan are suggestive of a model (**Figure 7**) in which radiation damage induced G_2-arrested lymphoma cells eventually enter mitosis (repair or escape) and mitotic entry, progression and exit are impaired by JNJ-7706621 mediated inhibition of CDK1/2 and AURKA/B. DNA damage in mitosis is a known driver of chromosomal instabilities (47, 48). The extended residence-time of cells in mitosis due to chromosome condensation and congression defects as well as spindle and mid-spindle assembly failure is pivotal for the increased sensitivity to persistent ^{177}Lu-lilotomab satetraxetan deposited DNA damage, ultimately promoting cytokinesis failure (multinucleation, aneuploidy, increased cell size) and cell death by apoptosis.

In conclusion, CD37-targeting ^{177}Lu-lilotomab satetraxetan RIT showed activity in several ABC-DLBCL lymphoma cell lines. CD37-independent RIT-resistance was identified in two cell lines representative of aggressive DE ABC-DLBCLs with inactive TP53, and reversed by subsequent inhibition of CDK1/2 and AURKA/B by JNJ-7706621. These findings are of specific relevance for ongoing clinical trials of ^{177}Lu-lilotomab satetraxetan in relapsed, ASCT-non-eligible DLBCL, and may also be more generally applicable to other ^{177}Lu-based RITs and alternative radionuclide utilizing targeted therapies. Future pre-clinical investigations are required to elucidate the potential application of CDK1/2 and AURKA/B inhibitors as a strategy to revert RIT resistance in *TP53* deficient cancers.

MATERIALS AND METHODS

Cells and Reagents

ABC-DLBCL cell lines were maintained in RPMI 1640-GlutaMAX medium (Gibco 61870-044) supplemented with 15% fetal bovine serum (Biowest S181B-050) and 1% penicillin-streptomycin (Gibco 15140-122) at 37°C in a humidified atmosphere containing 5% CO_2. Cell lines were obtained as previously described (21) and their identity was authenticated by short tandem repeat DNA profiling (IDEXX BioResearch, Ludwigsburg, Germany). Real Time Glo was from Promega (G9713). The Selleck Cambridge Cancer Compound library was obtained from and printed onto 384-well plates [384 well, PS, F-bottom, μclear, white, lid, sterile, Greiner Bio-One 781098 (82050-076)] by the High-Throughput Chemical Biology Screening Platform at the Center for Molecular Medicine

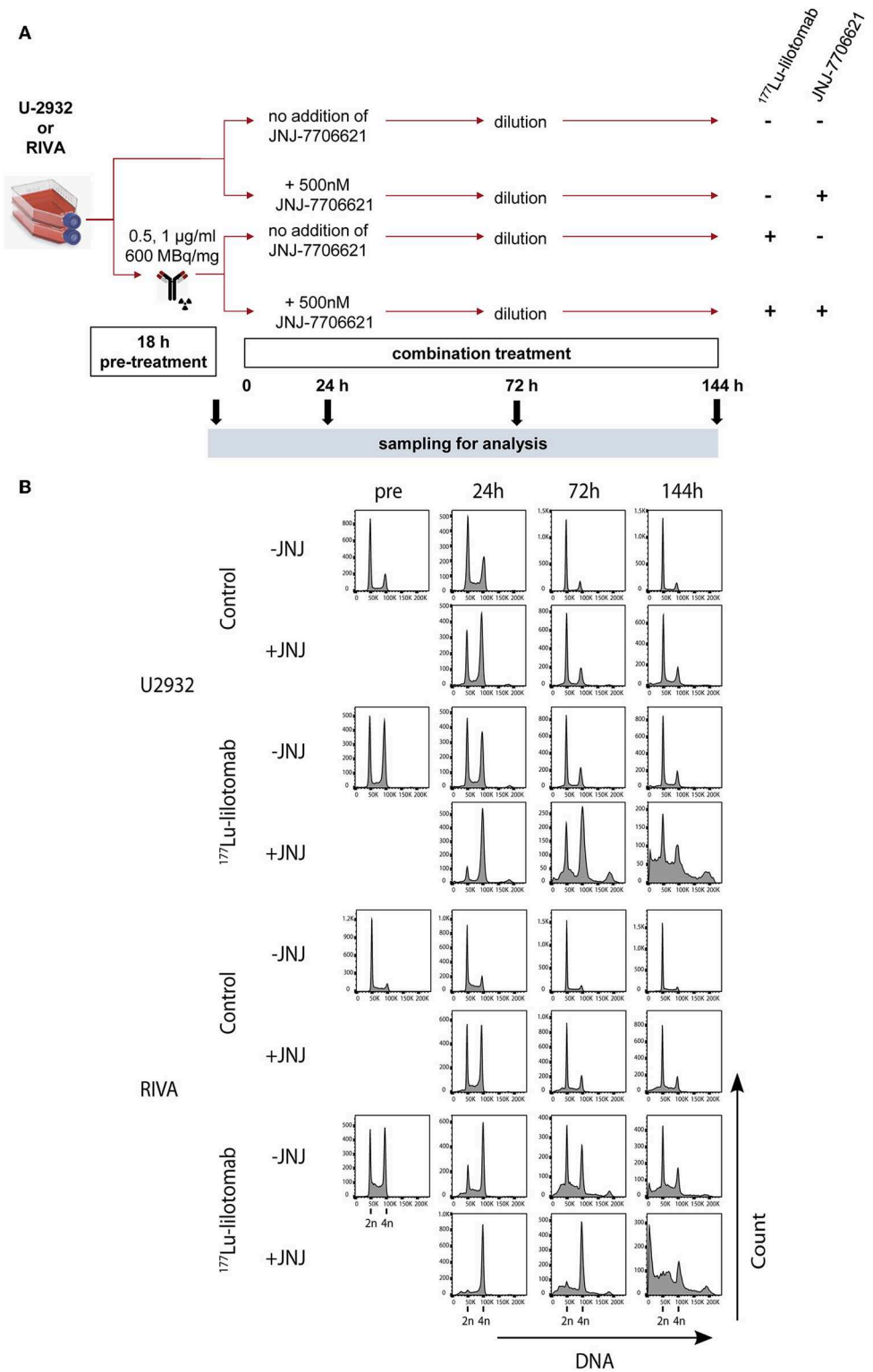

FIGURE 5 | JNJ-7706621 leads to extended G2/M arrest and endoreduplication in ^{177}Lu-lilotomab satetraxetan treated cells. **(A)** Outline of experiment. U-2932 and RIVA cells were treated as in **Figure 1** with indicated doses of ^{177}Lu-lilotomab satetraxetan. JNJ-7706621 was added to treated and untreated cells to a final concentration of 500 nM. Samples were harvested for flow analysis before (pre) and 24, 72, and 144 h after adding inhibitor. After harvesting 72 h sample cultures were replenished with medium containing inhibitor. Before fixation, cells were stained with Pacific Blue in order to discriminate between live and dead cells. FxCycleFar Red was used to stain DNA. **(B)** DNA histograms showing cell cycle distribution in U-2932 (upper panels) and RIVA (lower panels). Data shown are representative of two independent experiments.

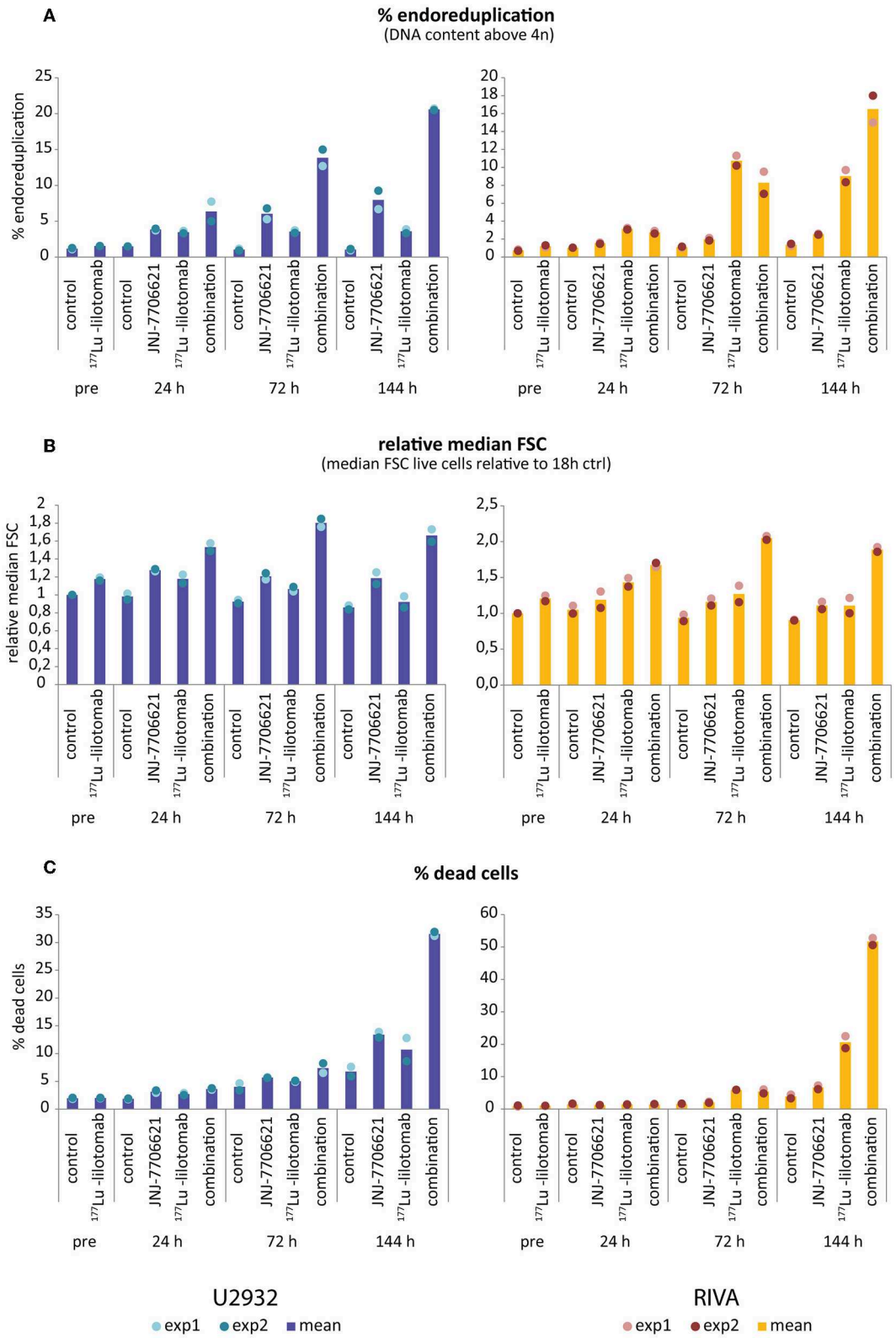

FIGURE 6 | Increase in >4n population and cell size precedes cell death upon combined treatment with JNJ-7706621 and ^{177}Lu-lilotomab satetraxetan. Results are from the same experiment as in **Figure 5** and a parallel experiment. **(A)** Percentage of cells with DNA content above 4n. **(B)** Median forward scatter (FSC) of live cells (gated on Pacific Blue channel), all values are relative to untreated control of 18 h pre-treatment. **(C)** Percentage of dead cells as measured by Pacific blue staining. Bar diagrams show mean of two separate experiments, with individual data indicated with dots. Left panels: U-2932, right panels: RIVA.

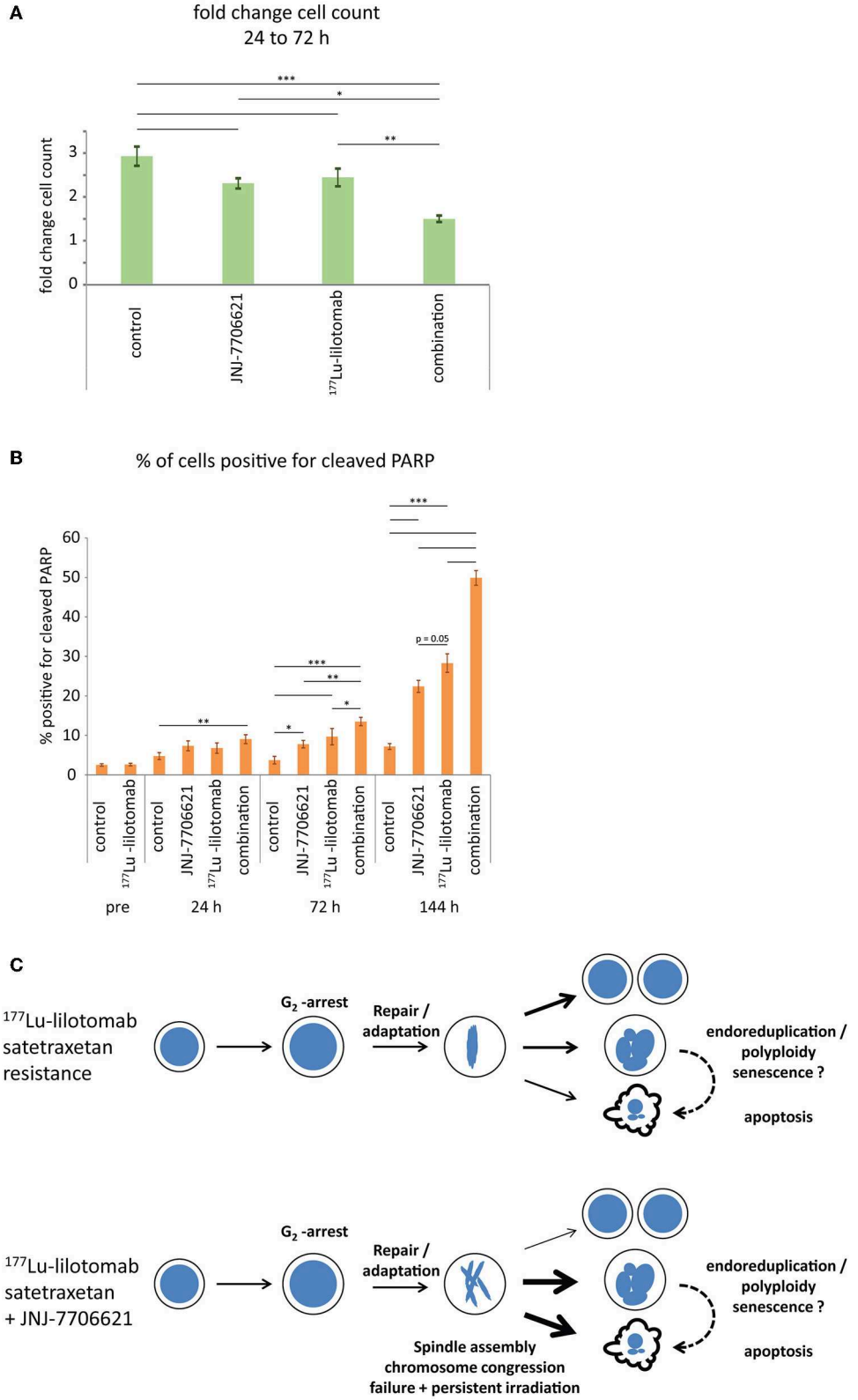

FIGURE 7 | Combined treatment with ^{177}Lu-lilotomab satetraxetan and JNJ-7706621 induces growth delay and apoptotic death. Cells were treated as in **Figure 5**. **(A)** Bar diagram showing relative cell growth of cells between 24 and 72 h after treatment ($n = 4$; error bars represent standard error of the mean). **(B)** Bar diagram

(Continued)

FIGURE 7 | showing percentage of cells positive for cleaved PARP ($n = 4$; error bars represent standard error of mean ($n = 4$). **(A,B)** Statistical significance in differences between treatment groups were tested by One Way ANOVA: $^{*}p < 0.05$, $^{**}p < 0.01$, $^{***}p < 0.001$. **(C)** Model: treatment with ^{177}Lu-lilotomab satetraxetan leads to DNA-damage induced G_2 arrest and apoptotic cell death. Cells resistant to treatment adapt and recover from the arrest. Inhibition of CDK1 and AURKA/B interferes with bipolar- and mid-spindle assembly, causing chromosome congression and cytokinesis defects. Combined treatment with JNJ-7706621 and ^{177}Lu-lilotomab satetraxetan reverses resistance likely by potentiating the effect of persistent radiation due to extended residence time in and failure of mitosis, the cell cycle phase in which repair capacity is low.

Norway (NCMM). Antibodies used were: rabbit-anti-phospho-BRCA2(Ser3291) (AB9986 Millipore), rabbit-anti-Cleaved-PARP (Asp214) Alexa647-conjugate (#6987, Cell Signaling), rabbit-anti-phospho-histone 3-Ser10 (06-570, Millipore), Alexa488 anti-rabbit (A21206, Life Technologies), and Alexa647 donkey-anti-mouse (Jackson ImmunoResearch, UK). The DNA stain FxCycle™ Far Red (200 nM FxCycle and 0.1mg/ml RNase A) (Thermo Fisher Scientific) was used together with Pacific Blue (Thermo Fisher Scientific, P10163) staining, and Hoechst 33258 (Sigma-Aldrich) (1.5 μg/ml) in other experiments.

Labeling of Antibody With ^{177}Lu

The chelator (p-SCN-Bn-DOTA, Macrocyclics, TX, USA) was dissolved in 0.005 M HCl, added to the HH1-DOTA (lilotomab) in a 6:1 ratio and pH-adjusted to ∼8.5 using carbonate buffer. After 45 min of incubation at 37°C, the reaction was stopped by the addition of 50 μL per mg of Ab of 0.2 mol/L glycine solution. To remove free p-SCN-Bn-DOTA, the conjugated antibody was washed using Vivaspin 20 centrifuge tubes (Sartorius Stedim Biotech, Göttingen Germany) 4–5 times with NaCl 0.9%. Before labeling with ^{177}Lu, the pH was adjusted to 5.3 ± 0.3 using 0.25 mol/L ammonium acetate buffer. Between 120 and 220 MBq of ^{177}Lu (ITG, Garching, Germany) was added to 1 mg of satetraxetan-Ab and incubated for 15–30 min at 37°C. The radiochemical purity (RCP) of the conjugate was evaluated using instant thin-layer chromatography. If RCP was below 95% the conjugate was purified by elution through a Sephadex G-25 PD-10 column (GE Healthcare Bio-Sciences AB, Uppsala, Sweden).

Treatment With ^{177}Lu-Lilotomab Satetraxetan (Betalutin)

Cells were treated in 6-well plates (2.5×10^6 cells/mL) without shaking for 18 h with Betalutin (specific activity of ∼600 Mbq/mg) at a final concentration of 1 μg/ml for U2932 and 0.5 μg/ml for RIVA (or as otherwise specified). After treatment, PBS was added to the cells, and the cells pelleted. Cells were first resuspended in 1 ml PBS, then washed twice in PBS and finally diluted in growth medium to desired concentration for the assay applied.

For the initial screening of ABC-DLBCL cell lines cells were incubated in deep well plates (Nunc™ 96-Well Polypropylene DeepWell Storage Plates from Thermo Scientific) with 12 different concentrations of ^{177}Lu-lilotomab satetraxetan, including a control with no treatment, for 18–20 h with shaking. Cells were washed three times with PBS using a plate washer (ELx405 Select Deep Well Washer from BioTek) and seeded in 96-well plates in 0.2 ml medium and incubated at 37°C/5% CO_2. Fifty microliter of fresh medium was added after 72 h. The cytotoxic effect was measured at 144 h using the CyQuant NF Cell Proliferation Assay kit (ThermoFischer) for Ascent FL multiplate reader (ThermoFischer. IC50 were calculated using Prism (GraphPad) and clustering analysis performed in J-Express Pro (49).

Combinatorial Drug Screen

Cells treated with ^{177}Lu-lilotomab satetraxetan and untreated control cells were seeded onto 384-well plates pre-printed with the 384-compound Cambridge Cancer Compound library sourced from SelleckChem. The library was divided onto two plates and a total of 48 no-drug controls were included per plate. Cell seeding densities were 120 000 cells/mL, and a volume of 25 μL was seeded in each well-giving 3,000 cells/well. The drug library was screened at two concentrations for each cell line (10/100 nM for RIVA and 10/1,000 nM for U-2932). Three days after seeding, 25 μL of diluted NanoLuc® luciferase and MT Cell Viability Substrate (RealTime-Glo) was added to each well. Cells were incubated with the reaction mix for 1 h at 37°C before measuring luminescence in a Tecan Spark multimode microplate reader, with integration time set to 1 s. Luminescence readings were repeated each day for three consecutive days. A microplate sample processor (Precision XS, BioTek) was used to facilitate the cell seeding and dispensing of RealTimeGlo reagent. Hit candidates were identified using the Bliss Independence test for synergy. The effect of each drug alone (Fa) at each concentration was calculated as the fraction of dead cells as compared to control cells

$$Fa = 1 - \left(\frac{RLU_{drug}}{averageRLU_{control}}\right)$$

a similar calculation was performed for the average effect of ^{177}Lu-lilotomab satetraxetan alone ($\overline{Fb}$)

$$\overline{Fb} = 1 - \left(\frac{averageRLU_{177Lu-lilotomab}}{averageRLU_{control}}\right)$$

Through the following equations we found the expected additive effect (E) and the measured effect (M) of the combination of drug + ^{177}Lu-lilotomab satetraxetan:

$$E = Fa + \overline{Fb} - Fa{*}\overline{Fb}$$
$$M = 1 - \left(\frac{RLU_{combination}}{averageRLU_{control}}\right)$$

The Bliss score was defined as:

$$Bliss\ score = \frac{M - E}{1 - Fa}$$

The normalization to the fraction of viable cells in samples treated with drug alone (1-Fa in equation above) was carried

out to compensate for the reduced population of cells that could be affected by combined treatment with ^{177}Lu-lilotomab satetraxetan. The standard deviation for the effect of ^{177}Lu-lilotomab satetraxetan alone in the 48 control wells was calculated on each plate as follows:

$$s = \sqrt{\sum_{i=1}^{n} \frac{\left(Fb_i - \overline{Fb}\right)^2}{n-1}}$$

Drugs with a Bliss score two times higher than the standard deviation of ^{177}Lu-lilotomab satetraxetan treated controls were scored as potential hits. Finally, we excluded inhibitory drugs that alone reduced viability by >90% to that of untreated control. Each plate was treated individually. In validation experiments the same procedure was used with the following modifications; Cells were treated in 12-well plates (1.2 ml per well, with 2.5 × 10^6 cells/ml) without shaking for 18 h with ^{177}Lu-lilotomab satetraxetan at final concentrations of 0.5, 1, and 2 μg/ml for U2932 and 0.25, 0.5, and 1 μg/ml for RIVA. After treatment, cells were seeded on 384-well plates pre-printed with JNJ-7706621, Alisertib and GSK461364 in an 11 step concentration gradient (0-1280 nM). A total of 60 no-drug controls were included on each plate. Synergy of drug/^{177}Lu-lilotomab satetraxetan combinations was determined by calculating Combination Indexes (CI) using the Chou-Talaly theorem (CompuSyn software) (50), where CI < 1 represents synergy. In replicates of validation experiment cells were treated with ^{177}Lu-lilotomab satetraxetan in 96 deep-well plates (100 μL per well, with 2.5 × 10^6 cells/ml) for 18 h, diluted to 40 cells/μL and 25 μL transferred to 384-well plates. Immediately after seeding a Tecan D300 Digital dispenser was used to administer drug to wells at 100, 266, 707, 1,880, and 5,000 nM (f.c. experiment 2) or 200, 532, 1,410, 3,760, and 10,000 μM (f.c experiment 3).

Flow Cytometry

For live/dead discrimination, ^{177}Lu-lilotomab satetraxetan treated cells were diluted to 500 000 cells/mL, transferred to T-25 cell culture flasks and inhibitor (JNJ-7706621) added to a final concentration of 500 nM. ^{177}Lu-lilotomab satetraxetan treated and untreated control samples, with or without inhibitor, were harvested for flow cytometry analysis before and at 24, 72, and 144 h after addition of the inhibitor (**Figure 5A**). At 72 h, 6 mL of fresh medium w/wo inhibitor was added to allow continuous growth of the cells that were harvested at the latest timepoint (144 h). Before fixation, cell pellets were resuspended in 200 μL PBS with 18 ng/μL of Pacific Blue and incubated at 4°C for 20 min for live/dead discrimination. One milliliter of PBS was added to the samples, and cells were pelleted and resuspended in 1 mL of ice-cold 70% ethanol for fixation. Samples were stained with FxCycle Far Red for visualization of DNA, and analyzed on an LSR II flow cytometer (BD Biosciences) using FlowJo software. The same experimental setup (omitting Pacific Blue) was followed for assessment of PARP cleavage. Cells were fixed in 1.5% neutral buffered formaldehyde for 5 min at r.t, washed in PBS, and stored in Methanol (−20°C). For analysis, cells were rehydrated and stained with anti-cleaved-PARP-Asp214 and Hoechst. Cell counts in **Figure 7A** were determined in quadruplicates for each time-point using a Countess Automated Cell counter (Thermo Fisher). For testing efficacy of JNJ-7706621, cells were arrested in mitosis by culturing for 16 h in medium containing nocodazol (0.04 μg/ml). Still in the presence of nocodazol, cells were treated with JNJ-7706621 for 1 or 6 h at a final concentration of 250, 500, or 1,000 nM before fixation in ice-cold 70% ethanol. Samples were stained with primary antibodies against CDK and Aurora B targets phospho-BRCA2-Ser3291 and phospho-histone H3-Ser10, respectively.

CD37-expression in U-2932, RIVA and Oci-Ly10 was measured by determination of the binding capacity of cold antibody (HH1-dota). For accurate comparison of different cell lines, we included barcoding with CellTracer stain and pooled the samples from the different cell lines together in a single tube before staining with the CD37 antibody. To this, 2 × 10^{e6} cells were pelleted and resuspended in 1 ml PBS and labeled with CellTrace stain (U-2932: CFSE 1 μM f.c., RIVA: Violet 2 μM f.c., Oci-Ly10: blank) in the dark for 20 min at 37°C with gentle shaking every 3–5 min. Cells were diluted in 5 ml of pre-warmed medium. After 5 min, cells were pelleted and resuspended in 1 ml fresh medium, pooled and an additional 1 ml of medium added. Cells were kept on ice thereafter. The cell mixture was divided into four polystyrene tubes and pelleted. Primary antibody (HH1-dota) was diluted in medium and added to three of the four tubes (no antibody, 1, 2, and 20 μg). Cells were incubated on ice for 20 min, washed twice with cold PBS and resuspended in medium containing Alexa647 donkey-anti-mouse (Jackson ImmunoResearch, UK) at 1 μl/ml. After 20 min incubation on ice, cells were resuspended in 1 ml cold PBS w/1% Fetal Bovine Serum and analyzed on a LSR II flow cytometer.

Microscopy

Cells were imaged using a CellObserver microscope system (Carl Zeiss) equipped with a 20×/0.8 PlanApo Phase 2 lens, a Hamamatsu ORCA-Flash4.0 v3 camera, a temperature controlled XL-chamber, a temperature, humidity and CO_2 controlled stage incubator, a motorized coded X,Y-stage, a Definite Focus system and a HXP120 Metal-Halide illumination unit. Visual inspection of cells prepared for flow cytometry was conducted using 96-well flat-bottom plates (Greiner Bio-One, Kremsmünster, AUT).

DATA AVAILABILITY STATEMENT

All datasets generated for this study are included in the article/**Supplementary Material**.

AUTHOR CONTRIBUTIONS

FB, GR, JD, KM, RS, and SP contributed to the conception and design of the study. GR, KM, RG, SG, and SP performed the experiments presented in the study. Data analysis was carried out by GR, JD, RS, and SP. GR and SP wrote the first draft of the manuscript. FB, GR, JD, RS, and SP contributed to

the manuscript revision. All authors read and approved the submitted version.

ACKNOWLEDGMENTS

The authors wish to express their sincere gratitude to Helene Solhaug (Nordic Nanovector ASA) for technical assistance, and to Idun Dale-Rein and Dr. Trond Stokke at the core facility for flow cytometry (Institute for Cancer Research, Norwegian Radium Hospital, Oslo University Hospital) for their invaluable expert-advice in design and conduction of quantitative multi-color flow cytometry experiments.

SUPPLEMENTARY MATERIAL

The Supplementary Material for this article can be found online at: https://www.frontiersin.org/articles/10.3389/fonc.2019.01301/full#supplementary-material

REFERENCES

1. Liu Y, Barta SK. Diffuse large B-cell lymphoma: 2019 update on diagnosis, risk stratification, and treatment, *Am J Hematol*. (2019) 94:604–16. doi: 10.1002/ajh.25460
2. Iacoboni G, Zucca E, Ghielmini M, Stathis A. Methodology of clinical trials evaluating the incorporation of new drugs in the first-line treatment of patients with diffuse large B-cell lymphoma (DLBCL): a critical review. *Ann Oncol*. (2018) 29:1120–9. doi: 10.1093/annonc/mdy113
3. Vitolo U, Witzig TE, Gascoyne RD, Scott DW, Zhang Q, Jurczak W, et al. ROBUST: first report of phase III randomized study of lenalidomide/R-CHOP (R2-CHOP) vs. placebo/R-CHOP in previously untreated ABC-type diffuse large B-cell lymphoma. *Hematol Oncol*. (2019) 37:36–7. doi: 10.1002/hon.5_2629
4. Younes A, Sehn LH, Johnson P, Zinzani PL, Hong X, Zhu J, et al. Randomized phase III trial of ibrutinib and rituximab plus cyclophosphamide, doxorubicin, vincristine, and prednisone in non-germinal center B-cell diffuse large B-cell lymphoma. *J Clin Oncol*. (2019) 37:1285–95. doi: 10.1200/JCO.18.02403
5. Schmitz R, Wright GW, Huang DW, Johnson CA, Phelan JD, Wang JQ, et al. Genetics and pathogenesis of diffuse large B-cell lymphoma. *N Engl J Med*. (2018) 378:1396–407. doi: 10.1056/NEJMoa1801445
6. Chapuy B, Stewart C, Dunford AJ, Kim J, Kamburov A, Redd RA, et al. Molecular subtypes of diffuse large B cell lymphoma are associated with distinct pathogenic mechanisms and outcomes. *Nat Med*. (2018) 24:679–90. doi: 10.1038/s41591-018-0016-8
7. Riedell PA, Smith SM. Double hit and double expressors in lymphoma: definition and treatment. *Cancer*. (2018) 124:4622–32. doi: 10.1002/cncr.31646
8. Sha C, Barrans S, Cucco F, Bentley MA, Care MA, Cummin T, et al. Molecular high-grade B-cell lymphoma: defining a poor-risk group that requires different approaches to therapy. *J Clin Oncol*. (2019) 37:202–12. doi: 10.1200/JCO.18.01314
9. Pohlman B, Sweetenham J, Macklis RM. Review of clinical radioimmunotherapy. *Expert Rev Anticancer Ther*. (2006) 6:445–61. doi: 10.1586/14737140.6.3.445
10. Green DJ, Press OW. Whither radioimmunotherapy: to be or not to be? *Cancer Res*. (2017) 77:2191–6. doi: 10.1158/0008-5472.CAN-16-2523
11. Friedberg JW, Unger JM, Burack WR, Gopal AK, Raju RN, Nademanee AP, et al. R-CHOP with iodine-131 tositumomab consolidation for advanced stage diffuse large B-cell lymphoma (DLBCL): SWOG S0433. *Br J Haematol*. (2014) 166:382–9. doi: 10.1111/bjh.12906
12. Mondello P, Cuzzocrea S, Navarra M, Mian M. 90 Y-ibritumomab tiuxetan: a nearly forgotten opportunityr. *Oncotarget*. (2016) 7:7597–609. doi: 10.18632/oncotarget.6531
13. Tomblyn M. Radioimmunotherapy for B-cell non-hodgkin lymphomas. *Cancer Control*. (2012) 19:196–203. doi: 10.1177/107327481201900304
14. Vose JM, Carter S, Burns LJ, Ayala E, Press OW, Moskowitz CH, et al. Phase III randomized study of rituximab/carmustine, etoposide, cytarabine, and melphalan (BEAM) compared with iodine-131 tositumomab/BEAM with autologous hematopoietic cell transplantation for relapsed diffuse large B-cell lymphoma: results from the BMT CTN 0401 trial. *J Clin Oncol*. (2013) 31:1662–8. doi: 10.1200/JCO.2012.45.9453
15. Bertoni F, Stathis A. Staining the target: CD37 expression in lymphomas. *Blood*. (2016) 128:3022–3. doi: 10.1182/blood-2016-11-748137
16. Freeman CL, Sehn LH. A tale of two antibodies: obinutuzumab versus rituximab. *Br J Haematol*. (2018) 182:29–45. doi: 10.1111/bjh.15232
17. Dahle J, Repetto-Llamazares AH, Mollatt CS, Melhus KB, Bruland OS, Kolstad A, et al. Evaluating antigen targeting and anti-tumor activity of a new anti-CD37 radioimmunoconjugate against non-Hodgkins lymphoma. *Anticancer Res*. (2013) 33:85–95. Available online at: http://ar.iiarjournals.org/content/33/1/85.full
18. Repetto-Llamazares AH, Larsen RH, Giusti AM, Riccardi E, Bruland OS, Selbo PK, et al. 177Lu-DOTA-HH1, a novel anti-CD37 radio-immunoconjugate: a study of toxicity in nude mice. *PLoS ONE*. (2014) 9:e103070. doi: 10.1371/journal.pone.0103070
19. Repetto-Llamazares AH, Larsen RH, Patzke S, Fleten KG, Didierlaurent D, Pichard A, et al. Targeted cancer therapy with a novel anti-CD37 beta-particle emitting radioimmunoconjugate for treatment of non-hodgkin lymphoma. *PLoS ONE*. (2015) 10:e0128816. doi: 10.1371/journal.pone.0128816
20. Kolstad A, Madsbu U, Beasley M, Bayne M, Illidge TM, ORourke N, et al. LYMRIT 37-01: a phase I/II study of ^{177}Lu-lilotomab satetraxetan (Betalutin®) antibody-radionuclide-conjugate (ARC) for the treatment of relapsed non-hodgkins lymphoma (NHL) — Analysis with 6-month follow-up. *Blood*. (2018) 132:2879. doi: 10.1182/blood-2018-99-110555
21. Spriano F, Chung EYL, Gaudio E, Tarantelli C, Cascione L, Napoli S, et al. The ETS inhibitors YK-4-279 and TK-216 are novel anti-lymphoma agents. *Clin Cancer Res*. (2019) 25:5167–76. doi: 10.1158/1078-0432.CCR-18-2718
22. Cascione L, Benvento M, Gaudio E, Tarantelli C, Spriano F, Arribas A, et al. Abstract 4275: analysis of gene and protein expression in lymphoma cell lines using multiple platforms. *Cancer Res*. (2018) 78:4275. doi: 10.1158/1538-7445.AM2018-4275
23. Tarantelli C, Gaudio E, Arribas AJ, Kwee I, Hillmann P, Rinaldi A, et al. PQR309 is a novel dual PI3K/mTOR inhibitor with preclinical antitumor activity in lymphomas as a single agent and in combination therapy. *Clin Cancer Res*. (2018) 24:120–9. doi: 10.1158/1078-0432.CCR-17-1041
24. Lee JH, Choy ML, Ngo L, Foster SS, Marks PA. Histone deacetylase inhibitor induces DNA damage, which normal but not transformed cells can repair. *Proc Natl Acad Sci USA*. (2010) 107:14639–44. doi: 10.1073/pnas.1008522107
25. Guillem V, Tormo M. Influence of DNA damage and repair upon the risk of treatment related leukemia. *Leuk Lymphoma*. (2008) 49:204–17. doi: 10.1080/10428190701769657
26. Delgado JL, Hsieh CM, Chan NL, Hiasa H. Topoisomerases as anticancer targets. *Biochem J*. (2018) 475:373–98. doi: 10.1042/BCJ20160583
27. Lindqvist A, Rodriguez-Bravo V, Medema RH. The decision to enter mitosis: feedback and redundancy in the mitotic entry network. *J Cell Biol*. (2009) 185:193–202. doi: 10.1083/jcb.200812045
28. Otto T, Sicinski P. Cell cycle proteins as promising targets in cancer therapy. *Nat Rev Cancer*. (2017) 17:93–115. doi: 10.1038/nrc.2016.138
29. Tischer J, Gergely F. Anti-mitotic therapies in cancer. *J Cell Biol*. (2019) 218:10–1. doi: 10.1083/jcb.201808077
30. Emanuel S, Rugg CA, Gruninger RH, Lin R, Fuentes-Pesquera A, Connolly PJ, et al. The *in vitro* and *in vivo* effects of JNJ-7706621: a dual inhibitor of cyclin-dependent kinases and aurora kinases. *Cancer Res*. (2005) 65:9038–46. doi: 10.1158/0008-5472.CAN-05-0882
31. Burack R, Li H, Spence JM, Adlowitz D, Rimsza LM, Braziel RM, et al. Subclonal mutations of TP53 are common in untreated follicular lymphoma

and mutation status is predictive of PFS when CHOP is combined with 131-iodine tositumomab but not with rituximab: an analysis of SWOG S0016. *Blood*. (2018) 132:919. doi: 10.1182/blood-2018-99-111399
32. Li L, Pongtornpipat P, Tiutan T, Kendrick SL, Park S, Persky DO, et al. Synergistic induction of apoptosis in high-risk DLBCL by BCL2 inhibition with ABT-199 combined with pharmacologic loss of MCL1. *Leukemia*. (2015) 29:1702–12. doi: 10.1038/leu.2015.99
33. O'Steen S, Green DJ, Gopal AK, Orozco JJ, Kenoyer AL, Lin Y, et al. Venetoclax synergizes with radiotherapy for treatment of B-cell lymphomas. *Cancer Res*. (2017) 77:3885–93. doi: 10.1158/0008-5472.CAN-17-0082
34. Mann BS, Johnson JR, Cohen MH, Justice R, Pazdur R. FDA approval summary: vorinostat for treatment of advanced primary cutaneous T-cell lymphoma. *Oncologist*. (2007) 12:1247–52. doi: 10.1634/theoncologist.12-10-1247
35. Friedberg JW, Mahadevan D, Cebula E, Persky D, Lossos I, Agarwal AB, et al. Phase II study of alisertib, a selective Aurora A kinase inhibitor, in relapsed and refractory aggressive B- and T-cell non-Hodgkin lymphomas. *J Clin Oncol*. (2014) 32:44–50. doi: 10.1200/JCO.2012.46.8793
36. Kelly KR, Friedberg JW, Park SI, McDonagh K, Hayslip J, Persky D, et al. Phase I study of the investigational aurora A kinase inhibitor alisertib plus rituximab or rituximab/vincristine in relapsed/refractory aggressive B-cell lymphoma. *Clin Cancer Res*. (2018) 24:6150–9. doi: 10.1158/1078-0432.CCR-18-0286
37. Olmos D, Barker D, Sharma R, Brunetto AT, Yap TA, Taegtmeyer AB, et al. Phase I study of GSK461364, a specific and competitive Polo-like kinase 1 inhibitor, in patients with advanced solid malignancies. *Clin Cancer Res*. (2011) 17:3420–30. doi: 10.1158/1078-0432.CCR-10-2946
38. Wu CP, Hsieh CH, Hsiao SH, Luo SY, Su CY, Li YQ, et al. Human ATP-binding cassette transporter ABCB1 confers resistance to volasertib (BI 6727), a selective inhibitor of polo-like kinase 1. *Mol Pharm*. (2015) 12:3885–95. doi: 10.1021/acs.molpharmaceut.5b00312
39. Wu CP, Hsiao SH, Luo SY, Tuo WC, Su CY, Li YQ, et al. Overexpression of human ABCB1 in cancer cells leads to reduced activity of GSK461364, a specific inhibitor of polo-like kinase 1. *Mol Pharm*. (2014) 11:3727–36. doi: 10.1021/mp500492r
40. Wu CP, Hsiao SH, Sim HM, Luo SY, Tuo WC, Cheng HW, et al. Human ABCB1 (P-glycoprotein) and ABCG2 mediate resistance to BI 2536, a potent and selective inhibitor of Polo-like kinase 1. *Biochem Pharmacol*. (2013) 86:904–13. doi: 10.1016/j.bcp.2013.08.004
41. Reddy A, Zhang J, Davis NS, Moffitt AB, Love CL, Waldrop A, et al. Genetic and functional drivers of diffuse large B cell lymphoma. *Cell*. (2017) 171:481–94.e15. doi: 10.1016/j.cell.2017.09.027
42. Mahadevan D, Morales C, Cooke LS, Manziello A, Mount DW, Persky DO, et al. Alisertib added to rituximab and vincristine is synthetic lethal and potentially curative in mice with aggressive DLBCL co-overexpressing MYC and BCL2. *PLoS ONE*. (2014) 9:e95184. doi: 10.1371/journal.pone.0095184
43. Islam S, Qi W, Morales C, Cooke L, Spier C, Weterings E, et al. Disruption of aneuploidy and senescence induced by aurora inhibition promotes intrinsic apoptosis in double hit or double expressor diffuse large B-cell lymphomas. *Mol Cancer Ther*. (2017) 16:2083–93. doi: 10.1158/1535-7163.MCT-17-0089
44. Islam S, Paek AL, Hammer M, Rangarajan S, Ruijtenbeek R, Cooke L, et al. Drug-induced aneuploidy and polyploidy is a mechanism of disease relapse in MYC/BCL2-addicted diffuse large B-cell lymphoma. *Oncotarget*. (2018) 9:35875–90. doi: 10.18632/oncotarget.26251
45. Matsuhashi A, Ohno T, Kimura M, Hara A, Saio M, Nagano A, et al. Growth suppression and mitotic defect induced by JNJ-7706621, an inhibitor of cyclin-dependent kinases and aurora kinases. *Curr Cancer Drug Targets*. (2012) 12:625–39. doi: 10.2174/156800912801784839
46. Danhier F, Ucakar B, Magotteaux N, Brewster ME, Preat V. Active and passive tumor targeting of a novel poorly soluble cyclin dependent kinase inhibitor, JNJ-7706621. *Int J Pharm*. (2010) 392:20–8. doi: 10.1016/j.ijpharm.2010.03.018
47. Bakhoum SF, Kabeche L, Murnane JP, Zaki BI, Compton DA. DNA-damage response during mitosis induces whole-chromosome missegregation. *Cancer Discov*. (2014) 4:1281–9. doi: 10.1158/2159-8290.CD-14-0403
48. Bakhoum SF, Kabeche L, Compton DA, Powell SN, Bastians H. Mitotic DNA damage response: at the crossroads of structural and numerical cancer chromosome instabilities. *Trends Cancer*. (2017) 3:225–34. doi: 10.1016/j.trecan.2017.02.001
49. Stavrum AK, Petersen K, Jonassen I, Dysvik B. Analysis of gene-expression data using J-Express. *Curr Protoc Bioinformatics*. (2008) Chapter 7:Unit 7.3. doi: 10.1002/0471250953.bi0703s21
50. Chou TC, Martin N. *CompuSyn for Drug Combinations: PC Software and Users Guide: A Computer Program for Quantitation of Synergism and Antagonism in Drug Combinations, and the Determination of IC50 and ED50 and LD50 Values* (Paramus, NJ: ComboSyn Inc.) (2005).

Conflict of Interest: SP: Nordic Nanovector ASA: Employment, Patent. KM, RG, and JD: Nordic Nanovector ASA: Employment, Equity Ownership, Patents. GR: Patent. RS: Institutional research funds from Nordic Nanovector ASA, Patent. FB: Institutional research funds from Acerta, ADC Therapeutics, Bayer AG, Cellestia, CTI Life Sciences, EMD Serono, Helsinn, ImmunoGen, Menarini Ricerche, NEOMED Therapeutics 1, Nordic Nanovector ASA, Oncology Therapeutic Development, PIQUR Therapeutics AG; consultancy fee from Helsinn, Menarini; expert statements provided to HTG; travel grants from Amgen, Astra Zeneca, Jazz Pharmaceuticals, PIQUR Therapeutics AG.

The remaining author declares that the research was conducted in the absence of any commercial or financial relationships that could be construed as a potential conflict of interest.

Copyright © 2019 Rødland, Melhus, Generalov, Gilani, Bertoni, Dahle, Syljuåsen and Patzke. This is an open-access article distributed under the terms of the Creative Commons Attribution License (CC BY). The use, distribution or reproduction in other forums is permitted, provided the original author(s) and the copyright owner(s) are credited and that the original publication in this journal is cited, in accordance with accepted academic practice. No use, distribution or reproduction is permitted which does not comply with these terms.

frontiers in Oncology

REVIEW
published: 06 December 2019
doi: 10.3389/fonc.2019.01376

The Extracellular, Cellular, and Nuclear Stiffness, a Trinity in the Cancer Resistome—A Review

Sara Sofia Deville[1,2,3] *and Nils Cordes*[1,2,3,4,5]*

[1] OncoRay – National Center for Radiation Research in Oncology, Faculty of Medicine and University Hospital Carl Gustav Carus, Helmholtz-Zentrum Dresden - Rossendorf, Technische Universität Dresden, Dresden, Germany, [2] Department of Radiation Oncology, University Hospital Carl Gustav Carus, Technische Universität Dresden, Dresden, Germany, [3] Helmholtz-Zentrum Dresden - Rossendorf, Institute of Radiooncology - OncoRay, Dresden, Germany, [4] German Cancer Consortium (DKTK), Dresden, Germany, [5] Germany German Cancer Research Center (DKFZ), Heidelberg, Germany

Alterations in mechano-physiological properties of a tissue instigate cancer burdens in parallel to common genetic and epigenetic alterations. The chronological and mechanistic interrelation between the various extra- and intracellular aspects remains largely elusive. Mechano-physiologically, integrins and other cell adhesion molecules present the main mediators for transferring and distributing forces between cells and the extracellular matrix (ECM). These cues are channeled via focal adhesion proteins, termed the focal adhesomes, to cytoskeleton and nucleus and vice versa thereby affecting the pathophysiology of multicellular cancer tissues. In combination with simultaneous activation of diverse downstream signaling pathways, the phenotypes of cancer cells are created and driven characterized by deregulated transcriptional and biochemical cues that elicit the hallmarks of cancer. It, however, remains unclear how elastostatic modifications, i.e., stiffness, in the extracellular, intracellular, and nuclear compartment contribute and control the resistance of cancer cells to therapy. In this review, we discuss how stiffness of unique tumor components dictates therapy response and what is known about the underlying molecular mechanisms.

Keywords: stiffness, extracellular matrix, cancer resistome, radio(chemo)resistance, cell-extracellular matrix interaction, focal adhesions, solid stress

OPEN ACCESS

Edited by:
Paul N. Span,
Radboud University Nijmegen Medical Centre, Netherlands

Reviewed by:
Jon Humphries,
University of Manchester, United Kingdom
Mirjam Zegers,
Radboud University Medical Center, Netherlands

***Correspondence:**
Nils Cordes
nils.cordes@oncoray.de

Specialty section:
This article was submitted to Radiation Oncology, a section of the journal Frontiers in Oncology

Received: *05 September 2019*
Accepted: *22 November 2019*
Published: *06 December 2019*

Citation:
Deville SS and Cordes N (2019) The Extracellular, Cellular, and Nuclear Stiffness, a Trinity in the Cancer Resistome—A Review. Front. Oncol. 9:1376. doi: 10.3389/fonc.2019.01376

INTRODUCTION

Stiffness refers to the rigidity of a material or the extent to which the material can resist to deformation or deflection in response to an applied force (1). Typically, stiffness depends on properties of the material such as the composition and organization of the building elements. A stiff as compared to a flexible structure is less susceptible to deform under an external load and, consequently, apt to develop greater stress.

Generally, the composition of the extracellular matrix (ECM) determines the stiffness of a tissue (2, 3). Cells are surrounded by ECM providing structural and biochemical support. Eventually, these interactions present the fundamental organization unit of multicellular complex development into tissues. The ECM comprises two classes of macromolecules: polysaccharide chains and fibrillar proteins (4). The polysaccharide chains are covalently bound to transmembrane proteins and assemble into proteoglycans. The fibrillar proteins like collagens, fibronectin, elastin, and laminins have structural functions and serve as ligands for cell adhesion molecules. The proteoglycans

form a gel-like structure in which the fibrillar proteins are embedded. Mesenchymal cells such as fibroblasts are responsible for the production and secretion of ECM proteins (5–8). The ECM is constantly reorganized and its dynamic is modulated by growth factors, cytokines, hormones, and extracorporal factors influencing significantly tissue physiology, morphology, homeostasis, and repair (9). A primary source of ECM restructuring is re-synthesis or proteolytic degradation by matrix metalloproteinases (MMPs) (10, 11). Several studies indicate that the spatio-temporal organization and dynamic re-modulation of the ECM has extensive biological implications for tumorigenesis promotion, progression, and metastasis.

In general, the outgrowth of a tumor produces an additional physical pressure, also defined as stress, on the host tissue and this is reciprocally balanced by the physical stress generated by the host tissue on the tumor. To overcome the stress enforced by the host tissue, tumor stiffening is essential for allowing host tissue displacement and growth in size (12). Tumors modulate their surrounding microenvironment including ECM, which results in alterations of tissue stiffness, porosity, and organization (13). A number of studies demonstrated specific changes in the mechanical properties of tumors over the time of their progression. When measured as single component, cancer cells and their nuclei become softer compared to normal cells (14, 15) suggesting a dis-regulation of cellular signaling pathways, cell proliferation, migration, survival, and treatment resistance (16, 17).

Fundamental for cell stiffness and mechanical forces are focal adhesions, serving as nexus between cytoskeleton and ECM (18–20). Cell adhesion elicits activation of different cytoplasmic signaling pathways for co-regulation of pro-survival mechanisms (5–8). Key mediators of this adhesion are integrins, an essential family among cell adhesion molecules. ECM reorganization drives significant changes in the integrin-mediated signaling pathways fundamental for tumor development and response to chemo- and radiotherapy (21–24). Various studies in normal (e.g., human fibroblasts and keratinocytes) and tumor cells (e.g., glioblastoma, pancreatic carcinomas, bronchial carcinomas, melanomas, breast cancers) documented adhesion to ECM to enhance resistance to ionizing radiation, chemotherapy, and molecular therapies (25, 26). These mechanisms are referred to as cell adhesion-mediated radioresistance (CAM-RR) and cell adhesion-mediated drug resistance (CAM-DR) (**Figure 1**) (25, 27).

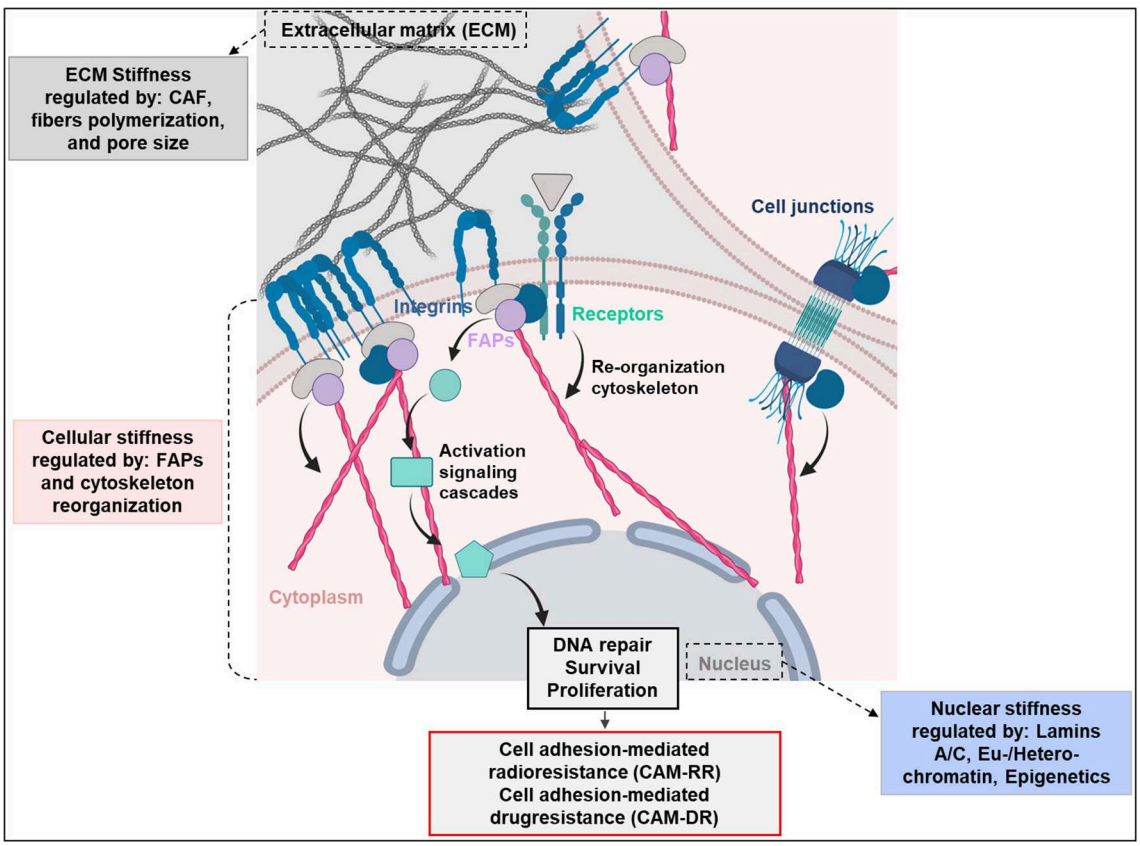

FIGURE 1 | Extracellular matrix (ECM), cellular end nuclear stiffness are regulated by several factors. The ECM remodeling is highly dependent on cancer associated fibroblasts (CAFs). The cell stiffness instead is regulated by integrins and focal adhesion proteins (FAPs), which contribute to cancer radio- and drug-resistance by mediating cell adhesion to the extracellular matrix. Upon cell adhesion to ECM, integrins induce pro-survival signaling cascades mediating radiotherapy- and drug-resistance (CAM-RR and CAM-DR). Finally, the nuclear stiffness is regulated by the levels of lamin-A/C and chromatin condensation. Created with BioRender.

This review gives insights into recent findings of how tissue, cellular, and nuclear stiffness are associated with therapy resistance and discusses the underlying mechanisms.

REGULATION OF CANCER THERAPY RESISTANCE THROUGH ECM REMODELING AND STIFFNESS

During tumor progression, cellular and genomic alterations occur, which are accompanied by changes in mechanical properties in the intracellular- and extracellular environment. The ECM is a key component of the tumor microenvironment, which interacts with cancer cells and regulates signaling cascades through focal adhesion proteins (FAPs) (28–30).

The ECM of tumors, primarily composed of fibrous tissue, becomes stiffer due to an increase of fiber cross-linking (31, 32). This is in line with the development of desmoplasia during carcinogenesis. Desmoplasia is an intense fibrotic response characterized by the formation of dense ECM (31). Tumors with high desmoplasia are considered to be more aggressive and associated with worse prognosis (31). Reports showed cancer-associated fibroblast to (over-)secrete matrix and modulate tumor phenotype and therapy response (31). These dynamic ECM modifications alter the ECM mechanical properties: degradation, re-polymerization, and alignment, contributing to a re-arrangement of ECM fibers and strain-induced stretching (33–38). In order to remodel the matrix, cancer cells and CAFs release enzymes, such as MMP and lysyl oxidases (LOX), which degrade and crosslink the ECM, respectively (**Figure 2A**). A structural analysis of the fibrillary collagen revealed the presence of reorganized collagen in the tumor-stromal interphase (39). Moreover, it was demonstrated that an increased collagen alignment and fiber thickness is a negative prognostic marker for cancer, supporting the significance of ECM dynamic in cancer progression (40–43).

ECM stiffness is related to a high malignant tumor phenotype (16). This can be explained by: (a) limited distribution and penetration of drugs (44) and/or (b) alterations in integrin signaling, focal adhesions, Rho/Rho-associated protein kinase (ROCK) pathway activation, as well as actomyosin- and cytoskeletal-dependent cell contractility and increased Ca^{2+} influx through mechanosensitive channels (28, 45, 46). For instance, integrins respond to the force alteration by rearrangement and aggregation in clusters at the plasma membrane. The cluster is composed of multiple mechanosensors (e.g., talin, vinculin), signaling molecules [e.g., focal adhesion kinase (FAK), proto-oncogene tyrosine-protein kinase Src (SRC), Phosphoinositide 3-kinase (PI3K)], adapter proteins [paxillin, LIM, and senescent cell antigen-like-containing domain protein 1 (PINCH1)], and actin linker proteins (e.g., filamin, alpha-actinin), which physically connect integrins to the cytoskeleton. On stiff substrates, the resistance to cellular tension leads to talin stabilization mediated by vinculin binding and also enhances FAK activation. These are some of the key mediators of the transmission of contractile forces to the cytoskeleton (17).

The higher aggressiveness also originates from matrix stiffness-induced epithelial to mesenchymal transition (EMT) being accompanied by cancer cell migration and invasion due to loss of intercellular adhesions (**Figure 2A**) (47, 48). EMT has been found to be related to treatment resistance (47, 48).

Another feature of the intra-tumoral microenvironment regulated by stiffness is the high interstitial hydrodynamic pressure induced by hypervascularization during tumor development. Such pressures have been found to promote tumor progression by impairing vessel function through constriction, thereby limiting tumor oxygen and nutriment supply, also known as hypoxia (44). Hypoxic tumors are known to be resistant to anticancer therapy, including radiation therapy, chemotherapy, and targeted therapy (44, 49).

Additional determinants of tumor stiffness are genetic mutations as they are not limited to initial driver mutations but encompass a wide genomic variation corresponding to the normal tissue where a tumor arises. High stiffness is correlated with dense collagen matrices resulting in small pore sizes for cells to transverse (50, 51). These events can drive genomic diversity through DNA damaged during migration. Meta-analyses showed that tumors originating from stiff tissues (e.g., lung, skin, bone) have substantially higher somatic mutations and chromosome copy numbers than malignancies originating from soft tissues (e.g., bone marrow, brain) (50). There are three hypotheses stating stiffness to drive genomic instability: (a) stiffness induces cell proliferations, increasing the probability to acquire spontaneous mutations; (b) stiffness increases the frequency of nuclear envelop rupture; (c) invasion of cancer cells through packed-tissue environments causes cell selection with a more aggressive phenotype (50).

Altogether, to gain a better understanding in the dynamics of cancer, it is necessary to uncover the effects cellular and extracellular mechanical properties elicit on tumor growth, metastatic spread and therapy resistance (**Table 1**). The basis of these events is cell behavior, which profoundly depends on mechanical properties and forces controlling signaling pathways involved in cell differentiation, proliferation, migration, and survival mechanisms (64–69).

The role of the ECM in treatment resistance was predominantly investigated for chemotherapeutics, with breast cancer being one of the most frequent models used (**Table 1**). As a matter of fact, one of the early detection methods for this tumor entity was the determination of abnormal stiffness by palpation or using medical devices. By means of an poly(ethylene glycol)-phosphorylcholine (PEG-PC) hydrogel system, Nguyen et al. examined the response of breast cancer cells to the Raf kinase inhibitor sorafenib in different stiffness substrates (55). The efficacy of sorafenib was reduced depending on stiffness and collagen concentration but independent of the commonly associated ROCK activity. Instead, triple negative breast cancer cells sustained an activation of JNK mediating the drug resistance (55). However, the combination of a JNK inhibitor with sorafenib eliminated the stiffness-mediated resistance. Strikingly, they found out that ERK (extracellular-signal-regulated kinase) and p38 (mitogen-activated protein kinases) were not involved in the drug resistance, it was rather regulated by β1 integrin (55).

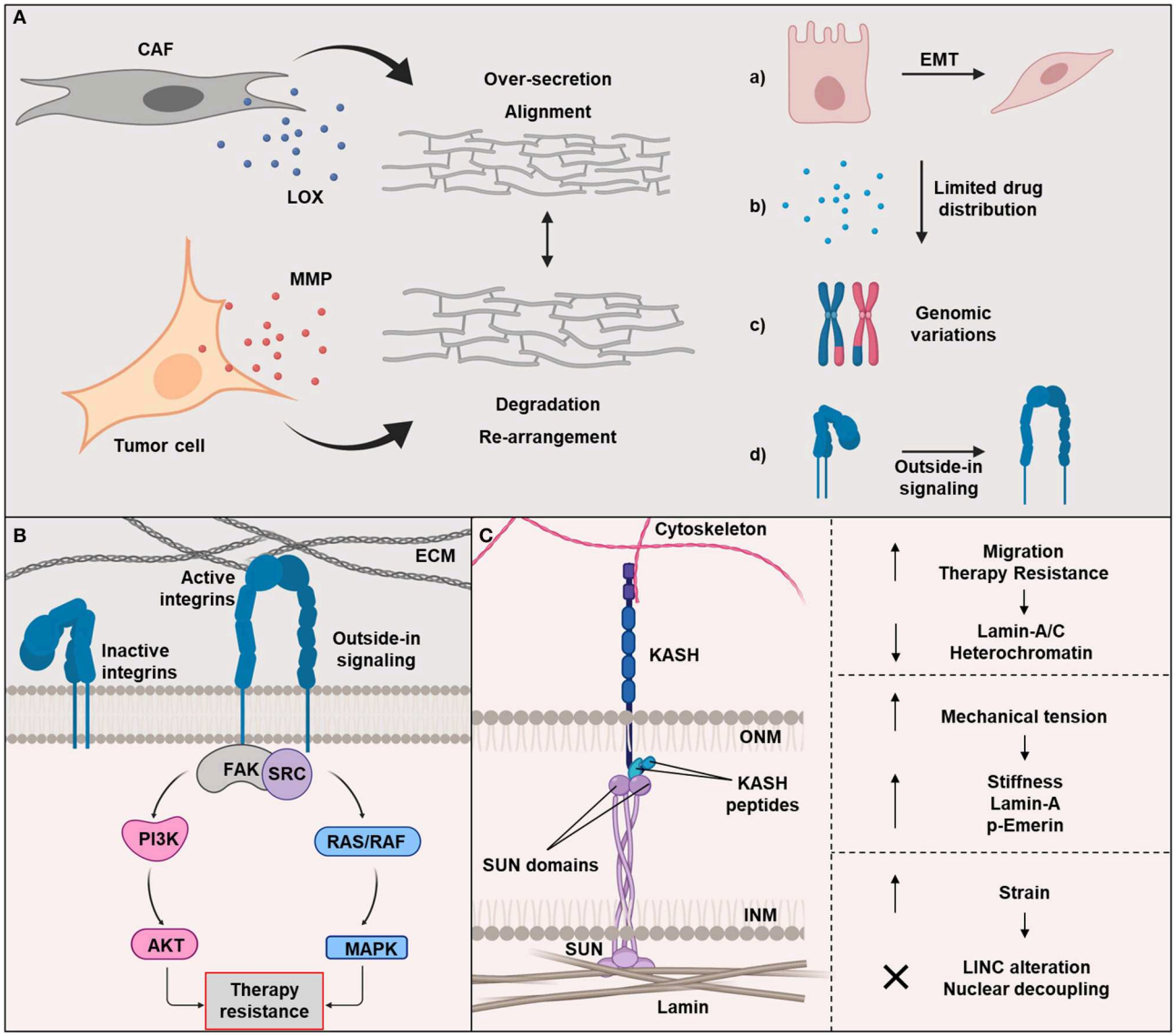

FIGURE 2 | (A) The extracellular matrix (ECM) secretion depends mainly on cancer associated fibroblasts (CAFs). The dynamic reorganization of ECM is regulated by matrix metalloproteinase (MMP)-dependent matrix degradation and lysyl oxidase (LOX)-dependent ECM crosslinking. Changes in ECM and stiffening leads to: (a) epithelial-to-mesenchymal transition (EMT) enhancing cell migration and invasion, (b) limited drugs distribution, (c) genomic alterations resulting in clonogenicity and heterogeneity, and (d) the activation of key adhesion proteins, such as integrin. **(B)** Integrin-dependent outside-in signaling mechanisms regulated cell adhesion to ECM as part of their role in cancer radio- and drug-resistance. Many of these mechanisms involve the focal adhesion kinase (FAK). **(C)** The Linker of Nucleoskeleton and Cytoskeleton (LINC) complex is composed of two families: KASH located at the nuclear membrane exterior (NME) and SUN situated in the nuclear membrane interior (NMI). LINC regulates the physical transmission of forces generated by the ECM and cytoskeleton. Moreover, a low expression levels of lamin-A/C is correlated with a high cell migration and an increase of therapy resistance. Cells adjust to mechanical tensions by enhancing the expression level of lamin-A and phosphorylated emerin. LINC complex detaches from the nucleus and cytoskeleton to maintain DNA integrity when cells fail to manage the tension. Created with BioRender.

Moreover, Joyce et al. showed that extrinsic resistance is associated with matrix stiffness (56). As culture model, an innovative 3D alginate-based hydrogel system enabling dynamic ECM stiffening over time was used. The results displayed a stiffness-dependent response to the chemotherapeutic doxorubicin in triple negative breast cancer cells (MDA-MB-231), while a non-triple negative cell model (MCF7) failed to show the same stiffness-dependent resistance (56). This differential therapeutic response was correlated with a nuclear translocation of YAP, a marker of mesenchymal differentiation. In fact, a higher level of nuclear YAP was found in MDA-MB-231 relative to MCF7 cells (56).

Another example of a cancer entity with poor prognosis that seems to be dependent on ECM stiffness and EMT is pancreatic cancer (62). Pancreatic cancer is one of the stiffest human solid carcinomas characterized by a fibrotic reaction, leading to the

TABLE 1 | Overview of ECM stiffness-mediated resistance in different tumor entities.

Tumor entity	Method	Treatment	Stiffness effects on therapy resistance	References
Hepatocellular carcinoma	Polyacrylamide (PA) gels	Cisplatin	↑stiffness, ↑resistance ↓stiffness, ↑cell dormancy, and stem cells characteristics	(52)
	Alginate gel (ALG) beads	Paclitaxel, 5-FU, and cisplatin	↑stiffness, ↑resistance	(53)
	COL1-coated polyacrylamide gel	Oxaliplatin	↑stiffness, ↑resistance	(54)
	96-well PEG-PC hydrogel platform	Sorafenib	↑stiffness, ↑resistance	(55)
Breast cancer	3D alginate-based hydrogel system	Doxorubicin	↑stiffness, ↑resistance in triple negative cells	(56)
	In vivo: heterozygous col1a1^{tm1Jae} (mCol1a1) mice with excessive collagen I accumulation	Rapamycin	↑stiffness, ↑resistance in lung metastatic cells but not in primary tumor	(57)
Melanoma	PEG hydrogels	PLX4032	Cell line-dependent response, ↓stiffness, ↑apoptosis	(58)
	In vivo serial biopsies	Vemurafenib (Zelboraf®)	↑stiffness, ↑resistance, ↑tumor relapse	(59)
Myeloid leukemias	3D hydrogels, *in vivo*	Several chemotherapeutics	↓stiffness, ↑resistance to standard chemotherapeutics	(60)
Laryngeal squamous cancer	Polyacrylamide (PA) gels	Cisplatin or 5-FU	↓stiffness, ↑resistance	(61)
Pancreatic cancer	Polyacrylamide (PA) gels	Paclitaxel	↑stiffness, ↑resistance	(62)
Glioblastoma	Chitosan–hyaluronic acid scaffolds	Temozolomide	↑stiffness, ↑resistance	(63)

Research methods and treatment are included.

activation of EMT-related and prosurvival signaling pathways (62). Rice et al. reported that *in vitro* PDAC cell lines cultured on varying stiff polyacrylamide gels had different behavior than the corresponding tumors *in vivo*. Resistance to gemcitabine, a therapeutic drug that inhibits DNA synthesis and transcription, was shown to be unchanged with increased rigidity, although matrix rigidity still promoted EMT. In contrast, cells grown on stiff gels showed increased resistance to paclitaxel (a taxane that stabilizes microtubules preventing mitosis) compared with the softer conditions (62).

The second most studied tumor entity, in terms of matrix stiffness, is the hepatocellular carcinoma (HCC) since it often relates to liver fibrosis. Various studies demonstrated resistance to cisplatin, sorafenib, paclitaxel, 5-FU, and oxaliplatin to depend on ECM stiffness (52–55). It was also shown that a large number of cells were dormant and carrying stem cell-like characteristics in HCC when cultivated in low stiffness (52). Liu et al. cultured HCC cells in alginate gel beads with different degrees of stiffness (53). Cells cultured in the stiff matrices resisted to cisplatin, 5-FU, and paclitaxel, whereas cells in the soft environment were sensitive to these agents. Moreover, cells encapsulated in alginate beads highly express ABC transporters and endoplasmatic reticulum-related proteins compared to 2D growth conditions. These proteins are supposed to contribute to drug resistance of solid tumors and treatment failure.

A recent study focused on the matrix stiffness-mediated effects in HCC stem cells (54). In this work, the authors showed that, when the substrate stiffness is increased, HCC cells exhibit an elevated number of CD133(+)/EpCAM(+) positive cells (stem cells markers). The increase in this cell population was accompanied by elevated expression levels of EpCAM, Nanog, and SOX2 (54). Moreover, the phosphorylation levels of Akt and mTOR were upregulated showing a greater self-renewing ability and oxaliplatin resistance. Interestingly, when these populations were subjected to integrin inhibition, all the previous described effects were attenuated, suggesting that integrin β1 may deliver higher stiffness signal inside HCC cells activating stemness associated signaling cascades (54).

Opposite to the results from You et al. (54), human laryngeal squamous cell carcinoma (Hep-2) cells cultured in a low stiffness environment showed an enhanced expression of stem cell markers (61). In addition, under the low stiffness environment, Hep-2 cells underwent less apoptosis to cisplatin and 5-FU. The authors suggested that the observed chemoresistance is related to increased Sox2 levels and an upregulation of the ABCG2 protein, a membrane xenobiotic transporter connected to multi-drug resistance (61). These examples illustrate the diversity of resistance mechanisms in different tumor entities, suggesting that there is no "one-for-all" approach, and thus only tumor-specific studies shed light on the mechanisms.

Tokuda et al. studied the effect of stiffness on the treatment response of melanoma cells, showing a cell-line dependent effect (58). Cells were grown in different PEG hydrogels with variable tensile moduli and treated with a BRaf inhibitor—PLX4032. Cells derived from radial growth phase (WM35) presented stiffness-dependent chemoresistance in contrast to the metastatic melanoma cells (A375) (58). A recent study on therapeutic relapse to another BRaf inhibitor—vemurafenib—used serial biopsies of genetically modified mice (59). Next-generation sequencing and single-cell transcriptomics enabled

TABLE 2 | Cell stiffness and related causes in different tumor entities, together with an overview of the methods for measuring cell stiffness.

Tumor entity	Method	Treatment	Stiffness effects on therapy resistance	References
Breast cancer	Optical tweezers	Different stiffness substrates	↓ECM stiffness, ↑cellular stiffness	(82)
	Atomic Force Microscopy (AFM)	Soft and stiff gels//EGFR inhibitor (Cetuximab)	↑stiffness when cultured on stiffer substrates//↑stiffness upon EGFR inhibition	(83)
Prostate cancer	Magnetic twisting cytometry	Paclitaxel	↑stiffness, ↑resistance, ↑fluid-like behavior	(84)
Ovarian cancer	Atomic Force Microscopy (AFM)	Cisplatin	↑stiffness, ↑resistance	(85)
	Filtration device depending on cellular pressure driven deformation	Cisplatin	↓stiffness, ↑resistance	(86)
Liver cancer	Atomic Force Microscopy (AFM)	Different shear stresses (parallel plated flow chamber)	↑shear stress, ↓stiffness	(87)
Leukemia	Microfluidic system for cell sorting and Atomic Force Microscopy (AFM)	Daunorubicin	↓stiffness, ↑resistance	(88)
Transformed mesenchymal stem cells	Atomic Force Microscopy (AFM)	Hypermethylation of cancer 1 (HIC1) and Ras-association domain family member 1A (RassF1A)	↓stiffness, ↑tumor aggressiveness	(89)

tracking of the evolution of multiple cellular "compartments" within individual lesions during first-line treatment response, relapse, and second-line therapeutic interventions (59). It became clear that tumor relapse is genetically stable, while differentiation state and ECM contribute significantly to the resistant phenotype. The result from *in vitro* experiments presented a correlation between cell state changes and ECM remodeling, suggesting an increased tumor stiffness modulates tumor cell fate and reduces treatment responses (59).

For glioblastoma, the most common brain tumor in adults (70), no physiologically relevant model is currently available for exploring effects of cellular stiffness. The majority of investigations on stiffness applied 2D cultures system. Erickson et al. suggested a newly developed and characterized Chitosan-Hyaluronic Acid scaffold with varying stiffness for glioblastoma cell culture (63). They showed glioblastoma cells to form large spheroids in stiff scaffolds exhibiting a higher degree of drug resistance and a more invasive phenotype relative to 2D models (63).

Altogether, we conclude that an increase of ECM stiffness leads to enhanced therapy resistance, with some exceptions that might be tumor- or substrate/matrix-dependent. ECM stiffness, therefore, might be used as a physical marker for the prediction of tumor therapy resistance. Certain contradictory issues, especially in terms of stemness, need to be clarified. Cancer stem cells are a well-known factor of therapy resistance and more studies are necessary to understand how these subpopulations behave in different stiffness substrates.

REGULATION OF CANCER RESISTANCE THROUGH CELLULAR STIFFNESS

Regulation of cellular stiffness is typically dictated by a variety of factors such as cytoskeleton organization, number of focal adhesion clusters, and nuclear deformability. Generally, cancer cells tend to be softer than their normal counterpart (= tissue of origin) depending on the status of their malignant transformation (35, 71–77).

Using magnetic tweezers to probe cellular resistance to physical force, a study in ovarian cancer cells demonstrated that the migration and invasion potential are inversely proportional to cellular stiffness. Moreover, some treatments such as pharmacological myosin II inhibitors reduce cellular stiffness and, therefore, convert cancer cells into a more invasive phenotype (75, 78). Pathways regulating these mechanical cues may potentially serve as targets for molecular cancer therapy.

Cellular stiffness is also determined by particular membrane proteins found in focal adhesions. FAPs assemble into protein complexes and act as connecting and adaptor proteins between ECM and the cellular interior (18–20). The complexes transmit extracellular signaling and mediate a strong interaction with the actin cytoskeleton. In many cancers, these proteins are de-regulated, resulting in abnormal cell-cell and cell-ECM adhesion. Integrins are commonly overexpressed in tumors and affect growth rate, cellular morphology, and invasiveness (28, 79, 80). Integrin activation triggers cytoskeletal re-arrangements through the regulation of signaling cascades like Src- and FAK and their downstream signaling pathways for therapy resistance (81).

The effects of cellular biophysical properties fundamental for therapy resistance remain to be clarified (**Table 2**). Liu et al. used a microfluidic platform to evaluate cancer cell transportability and invasiveness in heterogeneous breast cancer cells (90). Cell transportability is determined by cellular stiffness and cell surface frictional property, allowing the discrimination between more and less invasive phenotypes (90). The same principle was applied in another study. Leukemic cells treated with daunorubicin were sorted according to their cellular stiffness using a microfluidic device (88) uncovering cellular physics to serve as distinctive features between chemoresistant and -sensitive cells. Softer cells

showed an alteration in multiple mechanisms related to drug resistance, including decreased sensitivity to apoptosis induction, enhanced metabolic activity, and regulation of key genes involved in extrusion of drugs such as CYP supergene family typically involved in drug resistance (88).

Using lab on chip technology, several studies investigated the influence of cell deformability on the chemotherapeutical response of ovarian, breast, and prostate cancer. It became clear that cisplatin-resistant ovarian cancer cells have more elastic deformation capability relative to cisplatin-sensitive cell populations (86). Although these results seem exciting, they are in contrast to the study of Sharma et al. showing that cisplatin-resistant ovarian cancer cells are stiffer than their normal counterpart. This stiff phenotype is characterized by cytoskeletal long actin stress fibers mediated by Rho GTPases (85).

In line with this, paclitaxel-resistant prostate cancer cells were shown to be stiffer than the non-resistant counterpart. Kim et al. showed that paclitaxel-resistant cells gain mobility and invasiveness through increased EMT (84). Moreover, enhanced cell migration and invasion of paclitaxel-resistant cells was facilitated by increased cytoskeleton remodeling dynamics, stiffness, traction forces, and by a repression of keratin 8/18/19. In this work, the authors observed that resistant prostate cancer cells, despite being stiffer than the non-resistant cells, showed a more fluid-like behavior leading to a higher invasion capability (84).

In another study, matrices of different stiffness were used to understand the cellular behavior of different breast cancer cell lines (82). Interestingly, the most aggressive cells (MDA-MB-231) were softer when cultured on glass substrate, but when these cells were cultured on soft matrices they presented a stiffer phenotype compared to the other cell lines cultured in the same matrix. This is a good example of how the environment modulates cellular mechanical properties (82).

A similar work on breast cancer cells using matrices of different rigidity discovered a direct correlation between migration capacity and increase of matrix stiffness (83). Moreover, cells treated with cetuximab, an epidermal growth factor receptor (EGFR) inhibitor, had an increased elastic modulus followed by a decrease in migration ability. Here, the authors explained that cell mechanics are not only regulated by mechanical cues of the ECM but also by biochemical signals mediated through membrane receptors, such as EGFR (83).

Another study investigating environmental effects on liver cancer stem cells is from Sun et al. The authors investigated the effects of shear stress on cancer stem cell signaling regulating cellular migration, proliferation, and differentiation (87). It was found that certain shear stresses promote cell migration through activation of FAK and ERK1/2 signaling pathways. Moreover, shear stresses were responsible for lowering cellular stiffness in line with disrupted F-actin organization (87).

Environmental factors can also regulate epigenetic signatures such as methylation (89). Using cell lines with methylated tumor suppressor genes (e.g., hypermethylated in cancer 1—HIC1, Ras-association domain family member 1A—RassF1A), a Taiwanese group investigated cell stiffness changes depending on the methylation status and found that the stiffness of the methylated cells was lost, followed by a decrease of tubulin expression and F-actin disorganization (89). Further experiments involving cellular relaxation after cell compression showed that cancerous cells also have increased acto-myosin cortex contractility as compared to corresponding healthy cells (74, 91). Moreover, the higher the invasive level, the greater the cellular recovery behavior.

In contrast to ECM stiffness, cellular stiffness seems not to correlate with treatment resistance. Although there is a prevalence that a decrease cellular stiffness leads to an increase resistance, this assumption is often uncertain due to several factors: (1) measurement technique, (2) cell culture methodology, and (3) tumor entity/heterogeneity.

INTEGRINS BRIDGING BETWEEN ECM AND CELLULAR STIFFNESS: EFFECTS ON THE RESISTOME

After years of research, it became obvious that cell adhesion is fundamental for cell survival (92). Furthermore, a number of studies showed that cell adhesion is associated with the refractory to cancer treatments (92, 93). The principles of treatment resistance of cancer modulated by cell adhesion were proposedly categorized into: (i) cell adhesion mediated radioresistance (CAM-RR) and (ii) cell adhesion mediated drug resistance (CAM-DR) (**Figure 1**). Diverse adhesion resistomes composed of integrins, adaptor proteins, kinases, and cytoskeleton mainly contribute to both resistance mechanisms (92, 93). Interestingly, the components of the adhesion resistomes are widely heterogeneous depending on tumor entities. These might be also related to the tissue of origin.

To form multicellular structures or tissues, cells need to attach to adjacent cells via cell-cell contacts and anchor to the ECM through the transmembrane adhesion receptors known as integrins. An integrin receptor is a non-covalent heterodimer consisting of an α and a β integrin subunit. To date, there are 18 α and 8 β integrin subunits allowing the formation of 24 different integrin receptors. These α and β combinations determine the binding specificity of the integrin (29). Essentially, integrins consist of a big extracellular ectodomain, a transmembrane domain and a short cytoplasmic tail (29).

In the last two decades, substantial studies on cell adhesion to ECM primarily focused on integrins. Integrins and their downstream FAPs are known as mechano-sensors and mechano-transducers that sense and transduce mechanical signals into chemical signals. Generally, normal tissues weakly express integrins and FAPs. In contrast, cells start to express them when cells are grown in an *in vitro* tissue culture surfaces, indicating that cell culture stiffness highly impacts on the expression of these proteins (94).

Most integrins are not constitutively active and are located at the cell surface in an inactive state. Integrins are bi-directional signal receptors stimulated in two ways: the inside-out and outside-in activation (95). Both activation pathways are based on a conformational change in the ectodomain of the integrin (**Figure 2B**). The ability of integrins to signal in an inside-out and outside-in manner may be exquisite in normal cells but it is

deleterious in cancer cells (92). The outside-in signaling is better understood with regard to its role in the cell adhesion resistome to elicit CAM-DR and CAM-RR compared to the inside-out signaling, which is rarely investigated in cancer cells (96–107).

During the inside-out signaling, the cytoplasmic domain of the integrin binds and stimulates intracellular proteins such as kindlin or talin. By integrin conformational changes, there is an increased binding affinity for extracellular ligands. This activation mechanism controls, among other things, the migration of cells. With the help of outside-in activation, which is mainly dictated by ECM properties, integrins can introduce information into the cell. The extracellular binding of a ligand also leads to conformational changes of the integrin and activation of intracellular signaling pathways (**Figure 2B**). Often this signaling pathway recruits and activates kinases such as FAK and SCR, and also the RAS-MAPK (mitogen-activated protein kinase) and PI3K (phosphoinositide 3-kinase)—AKT (RAC-alpha serine/threonine Protein kinase) signaling nodes (42). Moreover, both signaling pathways, inside-out and outside-in, are powerful and can activate each other (108–114).

Binding of integrins to ECM proteins is mediated by short amino acid sequences. Motifs that can bind these sequences are (1) the RGD (arginine-glycine-aspartate) motif in fibronectin and laminin or (2) the DGEA (aspartate-glycine-glutamic acid-alanine)—and the GFOGER (glycine-phenylalanine-glycine-glutamic acid-arginine) motif in collagen (29, 115). Intracellular adapter proteins such as paxillin, parvin, or talin link integrins to the actin cytoskeleton, generating a bridge between ECM and cytoskeleton. Although integrins do not have intrinsic kinase activity, they recruit and activate a large spectrum of kinases to the cytoplasmic subunit. As a result, important cellular processes such as proliferation, apoptosis, differentiation, migration, or cell survival regulated (**Figures 1**, **2B**) (92, 116–119).

Beta-1 integrins are the largest subgroup of integrin adhesion receptors (29). Inhibition of β1 integrins, leads to an inactivation of a variety of integrin receptors such as for laminins, fibronectin, and collagens. This property, as well as the upregulated expression of β1 integrins in a variety of tumors, make β1 integrins a promising target molecule for cancer therapy (92, 120). The resistance of tumors to radiation and chemotherapy is dependent on the β1 integrin adhesion to ECM proteins. A collection of studies showed the importance of β1 integrin-mediated pathways for radiation resistance and survival, differentiation and proliferation, as well as for tumor progression and metastasis (34, 100, 101, 106, 107, 121–126).

In clinical trials, some inhibitors against β1 integrin receptors have been used. These include three inhibitors against the fibronectin receptor α5β1 integrin: ATN-161, Volociximab (M200) and JSM6427. ATN-161 is a peptide, which acts as an antagonist of the α5β1 integrin and blocks the receptor. Phase I studies showed that the use of ATN-161 had no risks or side effects (127). Volociximab, a humanized monoclonal antibody, has been reported as an angiogenesis inhibitor developed for solid tumors. Treatment with volociximab was in Phase I and no adverse reactions nor dose-related toxicity was observed (127). Further clinical studies in metastatic melanoma and renal cell carcinoma have shown promising effects upon volociximab treatment (128). The third α5β1 integrin inhibitor is the small molecule JSM6427 which inhibits angiogenesis and fibrosis and has so far only been tested in preclinical studies (127, 129).

Therefore, preclinical examinations have already described the importance of β1 integrin-mediated adhesion to ECM for survival of tumor cells after irradiation. Studies in several tumor entities were able to demonstrate that the inhibition of β1 integrin leads to radiation sensitization in glioblastoma cells (81, 130), lung carcinoma cells (131), colon carcinoma cells (132), breast carcinoma cells (133, 134), and HNSCC cells (121, 135). *In vitro* data from 3D cultured cells and data from xenograft tumors confirmed that inhibition of β1 integrins reduces significantly the radiation resistance of tumors (121, 134).

Depending on the integrin receptor and the tumor entity, integrins activate different survival-promoting signaling pathways. In breast cancer cells, the PI3K-AKT signaling pathway is mainly activated leading to adhesion-mediated radiation resistance (134). Integrins modulate the FADD (caspase-8/Fas-associated protein with death domain) signaling pathway, which is of importance for cell survival, resulting in the resistance to radiation induced cell death in leukemia cells (136). In HNSCC, FAK is the central signaling molecule for the β1 integrin-mediated signaling pathways and plays an essential role for cell survival after irradiation (116, 121). Data from our group showed that the inhibition of β1 integrin dephosphorylates FAK, causing the FAK/cortactin complex dissociation. This leads to the inactivation of JNK1 and the radio-sensitization of tumor cells (121). FAK consists of an N-terminal FERM (protein 4.1, ezrin, radixin, moesin homology) domain, a kinase domain, and a FAT (focal-adhesion targeting) domain (137, 138). The FERM domain mediates various interactions of FAK, e.g., with the EGFR. The FAT domain is responsible for the recruitment of FAK to the focal adhesion site. It binds integrin-associated adapter proteins such as talin or paxillin. In addition, FAK contains three proline-rich ones Regions (PRR1-3) that help proteins target a SH3 (SRC-homology 3) domain contained as e.g., p130Cas (139).

FAK can be phosphorylated on various tyrosine residues (139). The autophosphorylation of the tyrosine 397 site is triggered through the bond of β1 integrin to the ECM. In HNSCC cells, inhibition of β1 integrins leads to the dephosphorylation of FAK on tyrosine 397. This phosphorylation site is therefore used as a control of a functional β1 integrin inhibition (121). Interestingly, Lim and colleagues identified that FAK plays an important role in the nucleus. They showed that p53 binds to the FERM domain of FAK, thereby modulating cell survival and proliferation (140, 141). This observed function in the nucleus suggested that FAK has additional nuclear functions and, thus, might contribute to the rectification of radiation-induced DSB. In line, our group demonstrated that the non-homologous end-joining DNA double strand break repair pathway is partially co-controlled by β1 integrins via the FAK/JNK1 signaling axis (100). The significance of integrins in DNA repair processes was further emphasized by Christmann and colleagues. They observed that the αV/β3 integrin signaling axis coordinates the homologous recombination repair pathway in glioblastomas (142). Upon simultaneous temozolomide treatment and αV/β3

integrin knockdown, glioblastoma cells presented increased DNA double strand breaks and a depletion of Rad51 expression, indicating an impaired homologous recombination (142).

Furthermore, we have shown that β1 integrin targeting leads to an induction of the EGFR signaling cascade and the double targeting of β1 integrin and EGFR achieved a greater radiosensitization compared to the single targeting approaches *in vitro* and *in vivo* (101). This suggests a more efficient suppression of FAK/ERK (extracellular-signal-regulated kinase) prosurvival signaling upon the combination treatment of anti-β1 integrin/anti-EGFR treatment than the single therapy.

To date, only a few studies attempted to investigate the crosstalk between integrins and receptor tyrosine kinases (RTK) and its effect on cancer cell therapy resistance. Therefore, more studies are needed to identify the therapeutic potential of such combination therapy approaches. One of our recent study showed that HNSCC cells, which basically poorly respond to EGFR and β1 integrin blockage, were radiosensitized by the inhibition of targets identified from a whole exome sequencing (123). Briefly, we identified different gene mutation profiles in the non-responder HNSCC cell lines to EGFR and β1 integrin inhibition compared to the responder HNSCC cell lines. These profiles would allow the stratification of HNSCC patients and the identification of potential targets to address the treatment resistance. Kelch Like ECH Associated Protein 1 (KEAP1) and Mammalian target of rapamycin (mTOR) were identified as key targets. The pharmacological inhibition of KEAP1 or mTOR together with β1 integrin and EGFR effectively increased non-responder radiosensitization (123). The study suggested a therapeutic approach to identify a potential combination therapy and to promote identifications of novel targets.

In summary, we can assert that integrins and FAPs essentially contribute to therapy resistance and the possibility of targeting these proteins could be developed as a therapeutical option in combination with radiotherapy and chemotherapy.

REGULATION OF CANCER RESISTANCE THROUGH NUCLEAR STIFFNESS

During tumorigenesis, in addition to altered ECM stiffness, contractility of the cytoskeleton, and cell adhesion, stiffness of the cell's nucleus actively or passively adjusts to the process of malignant transformation. A growing number of studies report a modified nuclear envelope structure and composition in cancer cells (143). The nuclear envelope, consisting mainly of lamins and nuclear pore complexes, was identified as the major structure that is modulated in cancer (143, 144). The nuclear envelope contributes to cellular mechanical properties and functions and determines nuclear deformability (145). It is also involved in mechano-transduction and transmission of forces to the nucleus. Cancer progression promotes modifications in the composition of the nuclear envelope generating softer and highly lobulated nuclei, which consequently allow cancer cells to invade dense tissues more easily (143, 146). The nuclear stiffness is predominantly modulated by mechano-signals communicating between ECM and nucleus. Physical interactions of nucleus and cytoskeleton are essential for cytoskeletal organization and cellular polarization, which influence cell migration for metastasis (147). Moreover, the interaction seems to induce rearrangements in chromatin structure and lamin expression via intranuclear signaling cascades (143, 144, 146).

A study using a microfluidic channel with a narrow constriction to investigate the stiffness of prostate cancer nuclei showed that the nuclear rigidity is reduced in more malignant phenotypes. Furthermore, prostate cancer cells expressed a more aggressive phenotype when a low expression level of lamin-A/C and a decreased chromatin condensation were present (148). This supports the hypothesis that cancer cells with softer nuclei metastasize more efficiently. The importance of nuclear stiffness in cellular migration was also shown in lung carcinoma and glioblastoma multiforme. Generally, lamin-Bs are more stably expressed than lamin-A, of which the expression level widely varies among normal and cancerous solid tissue cells. In this study, cells with low levels of lamin-A expression showed the most pronounced increase in 3D migration. Of key importance was the finding that the cellular migration was biphasic in lamin-A expressing cells as wildtype lamin-A protects cells against stress-induced cell death. In fact, knockout of lamin-A caused broad defects in stress resistance. Therefore, lamins impede 3D migration but also promote survival against migration-induced stress (149).

Remodeling of the nuclear structures is associated with mechanical stress transmitted via the ECM/FAPs/cytoskeleton/nuclear envelop protein axis. The mechanical stress transmission axis promotes the epigenetic changes and the modification of chromatin dynamics that influence on the nuclear behavior (150). FAPs, however, can become activated independent of ECM in certain cases e.g., in breast cancer cells (151, 152). During tumor progression, microenvironmental control of nuclear organization seems to be impaired but still dependent on β1 integrin signaling (152).

Of great interest is a finding showing that DNA repair proteins are mechanosensitive factors leading to a new field of mechano-genomics (153). The group of Discher focuses on the spatiotemporal changes of endogenous DNA damage and repair factors in cells migrating through rigid micropores and on the lasting perturbations to the genome. The study showed that multiple DNA repair proteins avoid mechanical stress upon pore migration, resulting in a cytoplasmic mislocalization sustained for many hours, which leads to delayed repair and consequently DNA sequence alteration (154, 155).

In the previous section, we discussed about signaling cascades activated from the integrin axis. These mechanical signals are then transduced to the nucleus though mechanosignaling, in other words biochemical mechanotransduction pathways. In addition to the mechanosignaling, there is a faster way to transmit physical signals directly to the nucleus possibly through the physical anchoring of the cytoskeleton with the nuclear lamina via the linker of nucleoskeleton and cytoskeleton (LINC) complex (17). This complex is composed of two family members, which are SUN (Sad1p, UNC-84) and KASH (Klarsicht/ANC-1/Syne Homology) located at the interior and the exterior of the nuclear membrane, respectively (**Figure 2C**).

Typically, SUN is connected with the nuclear intermediate filament lamins, whereas, KASH interacts with cytoskeletal proteins, such as intermediate filaments, actin filaments and microtubules. SUN and KASH proteins interact within the perinuclear space forming a bridge between cytoskeleton and nucleoskeleton (156). Guilluy and colleagues studied the association of LINC complex with mechanical tension. They showed that an isolated nucleus adapts to mechanical tension induced by magnetic tweezers, which results in increased nuclear stiffness. The stiffening of the nucleus did not involve structural modification of chromatin or nuclear actin, but required an intact nuclear lamina and phosphorylation of emerin, a protein of the inner nuclear membrane (157).

In a recent study from the Swift group, the response of cells to cyclic tensile strain mimicking the dynamics of the microenvironment *in vivo* was investigated (158). A series of strains with different intensities was applied to cells. They observed that cells subjected to low levels of strain responded similar to cells exposed to an increased stiffness. In case cells were exposed to the high intensities, the composition of LINC complex was altered, specifically the SUN domain containing the SUN2 protein. This domain was significantly affected by protein levels and posttranslational modifications leading to a strain induced breakpoint in the linker complex. As a result, cells were able to detach the nucleus from the cytoskeleton in case of excess stress, conferring a protection to DNA (158).

Collectively, nuclear stiffness is associated with tumor aggressiveness, especially in migration and metastasis. However, more studies are required to understand the underlying mechanisms and to validate whether nuclear stiffness can be used as a predictive biomarker of therapy response.

CONCLUDING REMARKS AND PERSPECTIVE

We discussed recent studies showing how the tumor creates a microenvironment favorable for proliferation, invasion and treatment resistance. Cellular, nuclear, and ECM stiffness play essential and intertwined roles in the cancer response to therapy. Despite many investigations performed with regard to the impact of stiffness on chemotherapy response, it remains open if these results are similar and can be translated to the response to radiotherapy. We have shown that the presence of a 3D environment and matrix composition affects radiotherapy response upon the activation of FAPs (CAM-RR) (**Figure 1**) for pro-survival signaling. FAPs and extracellular matrices have been defined as important determinants of the hallmarks of cancer (30, 101, 159–161). In our previous studies, we demonstrated different growth conditions to modulate chromatin structure, DNA repair and cell survival upon radiation exposure (100, 162). Obviously, force transmission and mechanotransduction are mediated by FAPs to enable control over nuclear processes including therapy resistance. Together, the current body of literature strongly supports the concept of mechanical characteristics of the cellular environment to critically regulate the epigenetic and genetic landscape driving cancer cell radiochemoresistance.

Clearly, the matrix stiffness is a main element in cancer therapy resistance, especially in chemotherapy. Radiotherapy typically induces fibrotic reactions that, consequently, amplify tissue stiffening. This causes complications in normal tissues such as lung fibrosis. A combination of multiple factors like fibroblast activation, vascular damage, and leakage, etc., promotes ECM remodeling and excess matrix deposition (163–165). To date, it remains to be understood to what extent these therapy-induced changes contribute to tumor progression, resistance, and metastasis.

The role of stiffness in resistance and the potential of ECM, cellular, and nuclear stiffness as a biomarker for therapy response are still elusive. This ambiguity is also due to the heterogeneous set of data, which may sometimes be conflicting (**Table 2** provides some examples). Therefore, an optimized and standardized approach for the study of stiffness is necessary. Moreover, it would be of great benefit for the community to collaboratively standardize experimental setups and measurement techniques.

Despite the number of research groups studying cell behavior on different substrates with different stiffness, the impact of these matrices on cell function and therapy response has only recently been appreciated. Future efforts may focus on (1) how stiffness sensing occurs in different macro-micro-nano-scales (ECM/tissue, cell, nucleus) and (2) whether stiffness is a promising biomarker for therapy response or even a therapeutic target.

AUTHOR CONTRIBUTIONS

SD and NC formulated the topic of the review and drafted and approved the manuscript.

FUNDING

This project has received funding from the European Union's Horizon 2020 research and innovation program under the Marie Skłodowska-Curie Grant Agreement No. 642623 (to NC).

REFERENCES

1. Roylance D. *Mechanical Properties of Materials*. Massachusetts, MA: MIT (2008).
2. Muiznieks LD, Keeley FW. Molecular assembly and mechanical properties of the extracellular matrix: a fibrous protein perspective. *Biochim Biophys Acta Mol Basis Dis*. (2013) 1832:866–75. doi: 10.1016/j.bbadis.2012.11.022
3. Yue B. Biology of the extracellular matrix: an overview NIH public access. *J Glaucoma*. (2014) 23:S20–3. doi: 10.1097/IJG.0000000000000108
4. Mouw JK, Ou G, Weaver VM. Extracellular matrix assembly: a multiscale deconstruction HHS Public Access. *Nat Rev Mol Cell Biol*. (2014) 15:771–85. doi: 10.1038/nrm3902
5. Bosman FT, Stamenkovic I. Functional structure and composition of the extracellular matrix. *J Pathol*. (2003) 200:423–8. doi: 10.1002/path.1437

6. Frantz C, Stewart KM, Weaver VM. The extracellular matrix at a glance. *J Cell Sci*. (2010) 123:4195–200. doi: 10.1242/jcs.023820
7. Guo W, Giancotti FG. Integrin signalling during tumour progression. *Nat Rev Mol Cell Biol*. (2004) 5:816–26. doi: 10.1038/nrm1490
8. Kalluri R. Basement membranes: structure, assembly and role in tumour angiogenesis. *Nat Rev Cancer*. (2003) 3:422–33. doi: 10.1038/nrc1094
9. McLeod CM, Mauck RL. High fidelity visualization of cell-to-cell variation and temporal dynamics in nascent extracellular matrix formation. *Sci Rep*. (2016) 6:38852. doi: 10.1038/srep38852
10. Labat-Robert J. Age-dependent remodeling of connective tissue: role of fibronectin and laminin. *Pathol Biol*. (2003) 51:563–8. doi: 10.1016/j.patbio.2003.09.006
11. Mott JD, Werb Z. Regulation of matrix biology by matrix metalloproteinases. *Curr Opin Cell Biol*. (2004) 16:558–64. doi: 10.1016/j.ceb.2004.07.010
12. Malanchi I. Tumour cells coerce host tissue to cancer spread. *Bonekey Rep*. (2013) 2:371. doi: 10.1038/bonekey.2013.105
13. Lu P, Weaver VM, Werb Z. The extracellular matrix: a dynamic niche in cancer progression. *J Cell Biol*. (2012) 196:395–406. doi: 10.1083/jcb.201102147
14. Lin H-H, Lin H-K, Lin I-H, Chiou Y-W, Chen H-W, Liu C-Y, et al. Mechanical phenotype of cancer cells: cell softening and loss of stiffness sensing. *Oncotarget*. (2015) 6:20946–58. doi: 10.18632/oncotarget.4173
15. Alibert C, Goud B, Manneville JB, Baptiste J. Are cancer cells really softer than normal cells? *Biol Cell*. (2017) 109:167–89. doi: 10.1111/boc.201600078
16. Gkretsi V, Stylianopoulos T. Cell adhesion and matrix stiffness: coordinating cancer cell invasion and metastasis. *Front Oncol*. (2018) 8:145. doi: 10.3389/fonc.2018.00145
17. Northcott JM, Dean IS, Mouw JK, Weaver VM. Feeling stress: the mechanics of cancer progression and aggression. *Front Cell Dev Biol*. (2018) 6:17. doi: 10.3389/fcell.2018.00017
18. Legate KR, Wickström SA, Fässler R. Genetic and cell biological analysis of integrin outside-in signaling. *Genes Dev*. (2009) 23:397–418. doi: 10.1101/gad.1758709
19. Ringer P, Colo G, Fässler R, Grashoff C. Sensing the mechano-chemical properties of the extracellular matrix. *Matrix Biol*. (2017) 64:6–16. doi: 10.1016/j.matbio.2017.03.004
20. Sun Z, Costell M, Fässler R. Integrin activation by talin, kindlin and mechanical forces. *Nat Cell Biol*. (2019) 21:25–31. doi: 10.1038/s41556-018-0234-9
21. Eke I, Cordes N. Dual targeting of EGFR and focal adhesion kinase in 3D grown HNSCC cell cultures. *Radiother Oncol*. (2011) 99:279–86. doi: 10.1016/j.radonc.2011.06.006
22. Eke I, Cordes N. Radiobiology goes 3D: how ECM and cell morphology impact on cell survival after irradiation. *Radiother Oncol*. (2011) 99:271–8. doi: 10.1016/j.radonc.2011.06.007
23. Larsen M, Artym VV, Green JA, Yamada KM. The matrix reorganized: extracellular matrix remodeling and integrin signaling. *Curr Opin Cell Biol*. (2006) 18:463–71. doi: 10.1016/j.ceb.2006.08.009
24. Werb Z, Chin JR. Extracellular matrix remodeling during morphogenesisa. *Ann N Y Acad Sci*. (1998) 857:110–8. doi: 10.1111/j.1749-6632.1998.tb10111.x
25. Cordes N, Meineke V. Cell adhesion-mediated radioresistance (CAM-RR). Extracellular matrix-dependent improvement of cell survival in human tumor and normal cells *in vitro*. *Strahlenther Onkol*. (2003) 179:337–44. doi: 10.1007/s00066-003-1074-4
26. Cordes N, Blaese MA, Plasswilm L, Rodemann HP, Van Beuningen D. Fibronectin and laminin increase resistance to ionizing radiation and the cytotoxic drug Ukrain® in human tumour and normal cells *in vitro*. *Int J Radiat Biol*. (2003) 79:709–20. doi: 10.1080/09553000310001610240
27. Damiano JS, Cress AE, Hazlehurst LA, Shtil AA, Dalton WS. Cell adhesion mediated drug resistance (CAM-DR): role of integrins and resistance to apoptosis in human myeloma cell lines. *Blood*. (1999) 93:1658–67. doi: 10.1182/blood.V93.5.1658
28. Eke I, Cordes N. Focal adhesion signaling and therapy resistance in cancer. *Semin Cancer Biol*. (2015) 31:65–75. doi: 10.1016/j.semcancer.2014.07.009
29. Hynes RO. Integrins: bidirectional, allosteric signaling machines. *Cell*. (2002) 110:673–87. doi: 10.1016/S0092-8674(02)00971-6
30. Pickup MW, Mouw JK, Weaver VM. The extracellular matrix modulates the hallmarks of cancer. *EMBO Rep*. (2014) 15:1243–53. doi: 10.15252/embr.201439246
31. Cox TR, Erler JT. Remodeling and homeostasis of the extracellular matrix: implications for fibrotic diseases and cancer. *Dis Model Mech*. (2011) 4:165–78. doi: 10.1242/dmm.004077
32. Levental KR, Yu H, Kass L, Lakins JN, Egeblad M, Erler JT, et al. Matrix crosslinking forces tumor progression by enhancing integrin signaling. *Cell*. (2009) 139:891–906. doi: 10.1016/j.cell.2009.10.027
33. Alini M, Losa GA. Partial characterization of proteoglycans isolated from neoplastic and nonneoplastic human breast tissues. *Cancer Res*. (1991) 51:1443–7.
34. Paszek MJ, Zahir N, Johnson KR, Lakins JN, Rozenberg GI, Gefen A, et al. Tensional homeostasis and the malignant phenotype. *Cancer Cell*. (2005) 8:241–54. doi: 10.1016/j.ccr.2005.08.010
35. Plodinec M, Loparic M, Monnier CA, Obermann EC, Zanetti-Dallenbach R, Oertle P, et al. The nanomechanical signature of breast cancer. *Nat Nanotechnol*. (2012) 7:757–65. doi: 10.1038/nnano.2012.167
36. Vader D, Kabla A, Weitz D, Mahadevan L. Strain-induced alignment in collagen gels. *PLoS ONE*. (2009) 4:e5902. doi: 10.1371/journal.pone.0005902
37. Vijayagopal P, Figueroa JE, Levine EA. Altered composition and increased endothelial cell proliferative activity of proteoglycans isolated from breast carcinoma. *J Surg Oncol*. (1998) 68:250–4. doi: 10.1002/(SICI)1096-9098(199808)68:4<250::AID-JSO9>3.0.CO;2-3
38. Yang CM, Chien CS, Yao CC, Hsiao L, Der Huang YC, Wu CB. Mechanical strain induces collagenase-3 (MMP-13) expression in MC3T3-E1 osteoblastic cells. *J Biol Chem*. (2004) 279:22158–65. doi: 10.1074/jbc.M401343200
39. Provenzano PP, Eliceiri KW, Campbell JM, Inman DR, White JG, Keely PJ. Collagen reorganization at the tumor-stromal interface facilitates local invasion. *BMC Med*. (2006) 4:38. doi: 10.1186/1741-7015-4-38
40. Drifka CR, Loeffler AG, Mathewson K, Keikhosravi A, Eickhoff JC, Liu Y, et al. Highly aligned stromal collagen is a negative prognostic factor following pancreatic ductal adenocarcinoma resection. *Oncotarget*. (2016) 7:76197–213. doi: 10.18632/oncotarget.12772
41. Drifka CR, Loeffler AG, Esquibel CR, Weber SM, Eliceiri KW, Kao WJ. Human pancreatic stellate cells modulate 3D collagen alignment to promote the migration of pancreatic ductal adenocarcinoma cells. *Biomed Microdevices*. (2016) 18:105. doi: 10.1007/s10544-016-0128-1
42. Hamidi H, Ivaska J. Every step of the way: integrins in cancer progression and metastasis. *Nat Rev Cancer*. (2018) 18:533–48. doi: 10.1038/s41568-018-0038-z
43. Laklai H, Miroshnikova YA, Pickup MW, Collisson EA, Kim GE, Barrett AS, et al. Genotype tunes pancreatic ductal adenocarcinoma tissue tension to induce matricellular fibrosis and tumor progression. *Nat Med*. (2016) 22:497–505. doi: 10.1038/nm.4082
44. Broders-Bondon F, Ho-Bouldoires THN, Fernandez-Sanchez M-E, Farge E. Mechanotransduction in tumor progression: the dark side of the force. *J Cell Biol*. (2018) 217:1571–87. doi: 10.1083/jcb.201701039
45. Wei L, Surma M, Shi S, Lambert-Cheatham N, Shi J. Novel insights into the roles of rho kinase in cancer. *Arch Immunol Ther Exp*. (2016) 64:259–78. doi: 10.1007/s00005-015-0382-6
46. Yoneda A, Morgan-Fisher M, Wewer UM. Regulation of ROCK activity in cancer. *J Histochem Cytochem*. (2013) 61:185–98. doi: 10.1369/0022155412470834
47. Brabletz T, Kalluri R, Angela Nieto M, Weinberg RA. EMT in cancer. *Nat Rev Cancer*. (2018) 18:128–34. doi: 10.1038/nrc.2017.118
48. Le Bras GF, Taubenslag KJ, Andl CD. The regulation of cell-cell adhesion during epithelial-mesenchymal transition, motility and tumor progression. *Cell Adh Migr*. (2012) 6:365–73. doi: 10.4161/cam.21326
49. Karakashev SV, Reginato MJ. Cancer Management and Research Progress toward overcoming hypoxia-induced resistance to solid tumor therapy. *Cancer Manag Res*. (2015) 7:253–264. doi: 10.2147/CMAR.S58285
50. Pfeifer CR, Alvey CM, Irianto J, Discher DE. Genome variation across cancers scales with tissue stiffness – An invasion-mutation mechanism and implications for immune cell infiltration. *Curr Opin Syst Biol*. (2017) 2:103–14. doi: 10.1016/j.coisb.2017.04.005

51. Yang Y-L, Leone LM, Kaufman LJ. Elastic moduli of collagen gels can be predicted from two-dimensional confocal microscopy. *Biophys J*. (2009) 97:2051–60. doi: 10.1016/j.bpj.2009.07.035
52. Schrader J, Gordon-Walker TT, Aucott RL, van Deemter M, Quaas A, Walsh S, et al. Matrix stiffness modulates proliferation, chemotherapeutic response, and dormancy in hepatocellular carcinoma cells. *Hepatology*. (2011) 53:1192–205. doi: 10.1002/hep.24108
53. Liu C, Liu Y, Xie HG, Zhao S, Xu XX, Fan LX, et al. Role of three-dimensional matrix stiffness in regulating the chemoresistance of hepatocellular carcinoma cells. *Biotechnol Appl Biochem*. (2015) 62:556–62. doi: 10.1002/bab.1302
54. You Y, Zheng Q, Dong Y, Xie X, Wang Y, Wu S, et al. Matrix stiffness-mediated effects on stemness characteristics occurring in HCC cells. *Oncotarget*. (2016) 7:32221–31. doi: 10.18632/oncotarget.8515
55. Nguyen TV, Sleiman M, Moriarty T, Herrick WG, Peyton SR. Sorafenib resistance and JNK signaling in carcinoma during extracellular matrix stiffening. *Biomaterials*. (2014) 35:5749–59. doi: 10.1016/j.biomaterials.2014.03.058
56. Joyce MH, Lu C, James ER, Hegab R, Allen SC, Suggs LJ, et al. Phenotypic basis for matrix stiffness-dependent chemoresistance of breast cancer cells to doxorubicin. *Front Oncol*. (2018) 8:337. doi: 10.3389/fonc.2018.00337
57. Shea MP, O'Leary KA, Wegner KA, Vezina CM, Schuler LA. High collagen density augments mTOR-dependent cancer stem cells in ERα+ mammary carcinomas, and increases mTOR-independent lung metastases. *Cancer Lett*. (2018) 433:1–9. doi: 10.1016/j.canlet.2018.06.025
58. Tokuda EY, Leight JL, Anseth KS. Modulation of matrix elasticity with PEG hydrogels to study melanoma drug responsiveness. *Biomaterials*. (2014) 35:4310–8. doi: 10.1016/j.biomaterials.2014.01.063
59. Long JE, Wongchenko MJ, Nickles D, Chung WJ, Wang B, Riegler J, et al. Therapeutic resistance and susceptibility is shaped by cooperative multi-compartment tumor adaptation. *Cell Death Differ*. (2019) 26:2416–29. doi: 10.1038/s41418-019-0310-0
60. Shin J-W, Mooney DJ. Extracellular matrix stiffness causes systematic variations in proliferation and chemosensitivity in myeloid leukemias. *Proc Natl Acad Sci USA*. (2016) 113:12126–31. doi: 10.1073/pnas.1611338113
61. Hui L, Zhang J, Ding X, Guo X, Jiang X. Matrix stiffness regulates the proliferation, stemness and chemoresistance of laryngeal squamous cancer cells. *Int J Oncol*. (2017) 50:1439–47. doi: 10.3892/ijo.2017.3877
62. Rice AJ, Cortes E, Lachowski D, Cheung BCH, Karim SA, Morton JP, et al. Matrix stiffness induces epithelial-mesenchymal transition and promotes chemoresistance in pancreatic cancer cells. *Oncogenesis*. (2017) 6:1–9. doi: 10.1038/oncsis.2017.54
63. Erickson AE, Lan Levengood SK, Sun J, Chang FC, Zhang M. Fabrication and characterization of chitosan–hyaluronic acid scaffolds with varying stiffness for glioblastoma cell culture. *Adv Healthc Mater*. (2018) 7:e1800295. doi: 10.1002/adhm.201800295
64. Assoian RK, Klein EA. Growth control by intracellular tension and extracellular stiffness. *Trends Cell Biol*. (2008) 18:347–52. doi: 10.1016/j.tcb.2008.05.002
65. Kumar S, Weaver VM. Mechanics, malignancy, and metastasis: the force journey of a tumor cell. *Cancer Metastasis Rev*. (2009) 28:113–27. doi: 10.1007/s10555-008-9173-4
66. Mammoto A, Ingber DE. Cytoskeletal control of growth and cell fate switching. *Curr Opin Cell Biol*. (2009) 21:864–70. doi: 10.1016/j.ceb.2009.08.001
67. Nelson CM, Gleghorn JP. Sculpting organs: mechanical regulation of tissue development. *Annu Rev Biomed Eng*. (2012) 14:129–54. doi: 10.1146/annurev-bioeng-071811-150043
68. Peyton SR, Ghajar CM, Khatiwala CB, Putnam AJ. The emergence of ECM mechanics and cytoskeletal tension as important regulators of cell function. *Cell Biochem Biophys*. (2007) 47:300–20. doi: 10.1007/s12013-007-0004-y
69. West-Foyle H, Robinson DN. Cytokinesis mechanics and mechanosensing. *Cytoskeleton*. (2012) 69:700–9. doi: 10.1002/cm.21045
70. Wen PY, Kesari S. Malignant Gliomas in Adults. *N Engl J Med*. (2008) 359:492–507. doi: 10.1056/NEJMra0708126
71. Cross SE, Jin YS, Rao J, Gimzewski JK. Nanomechanical analysis of cells from cancer patients. *Nat Nanotechnol*. (2007) 2:780–3. doi: 10.1038/nnano.2007.388
72. Fuhrmann A, Staunton JR, Nandakumar V, Banyai N, Davies PCW, Ros R. AFM stiffness nanotomography of normal, metaplastic and dysplastic human esophageal cells. *Phys Biol*. (2011) 8:015007. doi: 10.1088/1478-3975/8/1/015007
73. Guck J, Schinkinger S, Lincoln B, Wottawah F, Ebert S, Romeyke M, et al. Optical deformability as an inherent cell marker for testing malignant transformation and metastatic competence. *Biophys J*. (2005) 88:3689–98. doi: 10.1529/biophysj.104.045476
74. Jonas O, Mierke CT, Käs JA. Invasive cancer cell lines exhibit biomechanical properties that are distinct from their noninvasive counterparts. *Soft Matter*. (2011) 7:11488–95. doi: 10.1039/c1sm05532a
75. Katira P, Bonnecaze RT, Zaman MH. Modeling the mechanics of cancer: effect of changes in cellular and extra-cellular mechanical properties. *Front Oncol*. (2013) 3:145. doi: 10.3389/fonc.2013.00145
76. Remmerbach TW, Wottawah F, Dietrich J, Lincoln B, Wittekind C, Guck J. Oral cancer diagnosis by mechanical phenotyping. *Cancer Res*. (2009) 69:1728–32. doi: 10.1158/0008-5472.CAN-08-4073
77. Suresh S. Biomechanics and biophysics of cancer cells. *Acta Mater*. (2007) 55:3989–4014. doi: 10.1016/j.actamat.2007.04.022
78. Swaminathan V, Mythreye K, Tim O'Brien E, Berchuck A, Blobe GC, Superfine R. Mechanical Stiffness grades metastatic potential in patient tumor cells and in cancer cell lines. *Cancer Res*. (2011) 71:5075–80. doi: 10.1158/0008-5472.CAN-11-0247
79. Paredes J, Albergaria A, Oliveira JT, Jeronimo C, Milanezi F, Schmitt FC. P-cadherin overexpression is an indicator of clinical outcome in invasive breast carcinomas and is associated with CDH3 promoter hypomethylation. *Clin Cancer Res*. (2005) 11:5869–77. doi: 10.1158/1078-0432.CCR-05-0059
80. Ribeiro AS, Albergaria A, Sousa B, Correia AL, Bracke M, Seruca R, et al. Extracellular cleavage and shedding of P-cadherin: a mechanism underlying the invasive behaviour of breast cancer cells. *Oncogene*. (2010) 29:392–402. doi: 10.1038/onc.2009.338
81. Eke I, Storch K, Kästner I, Vehlow A, Faethe C, Mueller-Klieser W, et al. Three-dimensional invasion of human glioblastoma cells remains unchanged by X-ray and carbon ion irradiation *in vitro*. *Int J Radiat Oncol Biol Phys*. (2012) 84:e515–23. doi: 10.1016/j.ijrobp.2012.06.012
82. Yousafzai MS, Coceano G, Bonin S, Niemela J, Scoles G, Cojoc D. Investigating the effect of cell substrate on cancer cell stiffness by optical tweezers. *J Biomech*. (2017) 60:266–9. doi: 10.1016/j.jbiomech.2017.06.043
83. Azadi S, Tafazzoli-Shadpour M, Soleimani M, Warkiani ME. Modulating cancer cell mechanics and actin cytoskeleton structure by chemical and mechanical stimulations. *J Biomed Mater Res Part A*. (2019) 107:1569–81. doi: 10.1002/jbm.a.36670
84. Kim JJ, Yin B, Christudass CS, Terada N, Rajagopalan K, Fabry B, et al. Acquisition of paclitaxel resistance is associated with a more aggressive and invasive phenotype in prostate cancer. *J Cell Biochem*. (2013) 114:1286–93. doi: 10.1002/jcb.24464
85. Sharma S, Santiskulvong C, Rao J, Gimzewski JK, Dorigo O. The role of Rho GTPase in cell stiffness and cisplatin resistance in ovarian cancer cells. *Integr Biol*. (2014) 6:611–7. doi: 10.1039/C3IB40246K
86. Gill NK, Nyberg KD, Lee L, Qi D, Rowat AC, Ly C, et al. A scalable filtration method for high throughput screening based on cell deformability. *Lab Chip*. (2019) 19:343–57. doi: 10.1039/C8LC00922H
87. Sun J, Luo Q, Liu L, Song G. Low-level shear stress promotes migration of liver cancer stem cells via the FAK-ERK1/2 signalling pathway. *Cancer Lett*. (2018) 427:1–8. doi: 10.1016/j.canlet.2018.04.015
88. Islam M, Mezencev R, McFarland B, Brink H, Campbell B, Tasadduq B, et al. Microfluidic cell sorting by stiffness to examine heterogenic responses of cancer cells to chemotherapy. *Cell Death Dis*. (2018) 9:239. doi: 10.1038/s41419-018-0266-x
89. Chen CC, He BC, Chen YL, Lee KD, Tung CH, Hsu CC, et al. HIC1 and RassF1A methylation attenuates tubulin expression and cell stiffness in cancer. *Int J Mol Sci*. (2018) 19:E2884. doi: 10.3390/ijms19102884
90. Liu Z, Lee Y, Jang JH, Li Y, Han X, Yokoi K, et al. Microfluidic cytometric analysis of cancer cell transportability and invasiveness. *Sci Rep*. (2015) 5:14272. doi: 10.1038/srep14272

91. Kraning-Rush CM, Califano JP, Reinhart-King CA. Cellular traction stresses increase with increasing metastatic potential. *PLoS ONE*. (2012) 7:e32572. doi: 10.1371/journal.pone.0032572
92. Dickreuter E, Cordes N. The cancer cell adhesion resistome: mechanisms, targeting and translational approaches. *Biol Chem*. (2017) 398:721–35. doi: 10.1515/hsz-2016-0326
93. Seguin L, Desgrosellier JS, Weis SM, Cheresh DA. Integrins and cancer: regulators of cancer stemness, metastasis, and drug resistance. *Trends Cell Biol*. (2015) 25:234–40. doi: 10.1016/j.tcb.2014.12.006
94. Yeh YC, Ling JY, Chen WC, Lin HH, Tang MJ. Mechanotransduction of matrix stiffness in regulation of focal adhesion size and number: reciprocal regulation of caveolin-1 and β1 integrin. *Sci Rep*. (2017) 7:15008. doi: 10.1038/s41598-017-14932-6
95. Coppolino MG, Dedhar S. Bi-directional signal transduction by integrin receptors. *Int J Biochem Cell Biol*. (2000) 32:171–88. doi: 10.1016/S1357-2725(99)00043-6
96. Thamilselvan V, Craig DH, Basson MD. FAK association with multiple signal proteins mediates pressure-induced colon cancer cell adhesion *via* a Src-dependent PI3K/Akt pathway. *FASEB J*. (2007) 21:1730–41. doi: 10.1096/fj.06-6545com
97. Vellon L, Menendez JA, Lupu R. A bidirectional "αvβ3 integrin-ERK1/ERK2 MAPK" connection regulates the proliferation of breast cancer cells. *Mol Carcinog*. (2006) 45:795–804. doi: 10.1002/mc.20242
98. Cordes N, Meineke V. Modification of the cellular radiation survival and proliferation response by cell-matrix interactions: implications for integrin targeting in therapeutic approaches for radiation accident patients. *Br J Radiol Suppl.* (2005) 27:152–6. doi: 10.1259/bjr/55705431
99. Cordes N, Seidler J, Durzok R, Geinitz H, Brakebusch C. β1-integrin-mediated signaling essentially contributes to cell survival after radiation-induced genotoxic injury. *Oncogene.* (2006) 25:1378–90. doi: 10.1038/sj.onc.1209164
100. Dickreuter E, Eke I, Krause M, Borgmann K, Van Vugt MA, Cordes N. Targeting of β1 integrins impairs DNA repair for radiosensitization of head and neck cancer cells. *Oncogene.* (2016) 35:1353–62. doi: 10.1038/onc.2015.212
101. Eke I, Zscheppang K, Dickreuter E, Hickmann L, Mazzeo E, Unger K, et al. Simultaneous β1 integrin-EGFR targeting and radiosensitization of human head and neck cancer. *J Natl Cancer Inst*. (2015) 107:dju419. doi: 10.1093/jnci/dju419
102. Hou S, Isaji T, Hang Q, Im S, Fukuda T, Gu J. Distinct effects of β1 integrin on cell proliferation and cellular signaling in MDA-MB-231 breast cancer cells. *Sci Rep*. (2016) 6:18430. doi: 10.1038/srep18430
103. Lock R, Debnath J. Extracellular matrix regulation of autophagy. *Curr Opin Cell Biol*. (2008) 20:583–8. doi: 10.1016/j.ceb.2008.05.002
104. Rozzo C, Chiesa V, Ponzoni M. Integrin up-regulation as marker of neuroblastoma cell differentiation: correlation with neurite extension. *Cell Death Differ*. (1997) 4:713–24. doi: 10.1038/sj.cdd.4400304
105. Song J, Zhang J, Wang J, Wang J, Guo X, Dong W. β1 integrin mediates colorectal cancer cell proliferation and migration through regulation of the Hedgehog pathway. *Tumor Biol*. (2015) 36:2013–21. doi: 10.1007/s13277-014-2808-x
106. Vehlow A, Klapproth E, Storch K, Dickreuter E, Seifert M, Dietrich A, et al. Adhesion- and stress-related adaptation of Glioma radiochemoresistance is circumvented by β1 integrin/JNK cotargeting. *Oncotarget*. (2017) 8:49224–37. doi: 10.18632/oncotarget.17480
107. Wang H, Zhu Y, Zhao M, Wu C, Zhang P, Tang L, et al. miRNA-29c suppresses lung cancer cell adhesion to extracellular matrix and metastasis by targeting integrin β1 and matrix metalloproteinase2 (MMP2). *PLoS ONE*. (2013) 8:e70192. doi: 10.1371/journal.pone.0070192
108. Bouvard D, Pouwels J, De Franceschi N, Ivaska J. Integrin inactivators: balancing cellular functions *in vitro* and *in vivo*. *Nat Rev Mol Cell Biol*. (2013) 14:432–44. doi: 10.1038/nrm3599
109. Calderwood DA, Campbell ID, Critchley DR. Talins and kindlins: partners in integrin-mediated adhesion. *Nat Rev Mol Cell Biol*. (2013) 14:503–17. doi: 10.1038/nrm3624
110. Gahmberg CG, Fagerholm SC, Nurmi SM, Chavakis T, Marchesan S, Grönholm M. Regulation of integrin activity and signalling. *Biochim Biophys Acta Gen Subj*. (2009) 1790:431–44. doi: 10.1016/j.bbagen.2009.03.007
111. Luo BH, Springer TA. Integrin structures and conformational signaling. *Curr Opin Cell Biol*. (2006) 18:579–86. doi: 10.1016/j.ceb.2006.08.005
112. Oxvig C, Lu C, Springer TA. Conformational changes in tertiary structure near the ligand binding site of an integrin I domain. *Proc Natl Acad Sci USA*. (1999) 96:2215–20. doi: 10.1073/pnas.96.5.2215
113. Shattil SJ, Kim C, Ginsberg MH. The final steps of integrin activation: the end game. *Nat Rev Mol Cell Biol*. (2010) 11:288–300. doi: 10.1038/nrm2871
114. Shimaoka M, Takagi J, Springer TA. Conformational regulation of integrin structure and function. *Annu Rev Biophys Biomol Struct*. (2002) 31:485–516. doi: 10.1146/annurev.biophys.31.101101.140922
115. Brakebusch C, Fässler R. β 1 integrin function *in vivo*: adhesion, migration and more. *Cancer Metastasis Rev*. (2005) 24:403–11. doi: 10.1007/s10555-005-5132-5
116. Hehlgans S, Haase M, Cordes N. Signalling via integrins: implications for cell survival and anticancer strategies. *Biochim Biophys Acta Rev Cancer.* (2007) 1775:163–80. doi: 10.1016/j.bbcan.2006.09.001
117. Miyamoto S, Teramoto H, Coso OA, Gutkind JS, Burbelo PD, Akiyama SK, et al. Integrin function: molecular hierarchies of cytoskeletal and signaling molecules. *J Cell Biol*. (1995) 131:791–805. doi: 10.1083/jcb.131.3.791
118. Shibue T, Weinberg RA. Integrin β1-focal adhesion kinase signaling directs the proliferation of metastatic cancer cells disseminated in the lungs. *Proc Natl Acad Sci USA*. (2009) 106:10290–5. doi: 10.1073/pnas.0904227106
119. Yamada KM, Miyamoto S. Integrin transmembrane signaling and cytoskeletal control. *Curr Opin Cell Biol*. (1995) 7:681–9. doi: 10.1016/0955-0674(95)80110-3
120. Eriksen. JG, Steiniche T, Sogaard H, Overgaard J. Expression of integrins and E-cadherin in squamous cell carcinomas of the head and neck. *APMIS*. (2004) 112:560–8. doi: 10.1111/j.1600-0463.2004.apm1120902.x
121. Eke I, Deuse Y, Hehlgans S, Gurtner K, Krause M, Baumann M, et al. β1 Integrin/FAK/cortactin signaling is essential for human head and neck cancer resistance to radiotherapy. *J Clin Invest*. (2012) 122:1529–40. doi: 10.1172/JCI61350
122. Imanishi Y, Hu B, Jarzynka MJ, Guo P, Elishaev E, Bar-Joseph I, et al. Angiopoietin-2 stimulates breast cancer metastasis through the α5β1 integrin-mediated pathway. *Cancer Res*. (2007) 67:4254–63. doi: 10.1158/0008-5472.CAN-06-4100
123. Klapproth E, Dickreuter E, Zakrzewski F, Seifert M, Petzold A, Dahl A, et al. Whole exome sequencing identifies mTOR and KEAP1 as potential targets for radiosensitization of HNSCC cells refractory to EGFR and β1 integrin inhibition. *Oncotarget.* (2018) 9:18099–114. doi: 10.18632/oncotarget.24266
124. Kren A, Baeriswyl V, Lehembre F, Wunderlin C, Strittmatter K, Antoniadis H, et al. Increased tumor cell dissemination and cellular senescence in the absence of β1-integrin function. *EMBO J*. (2007) 26:2832–42. doi: 10.1038/sj.emboj.7601738
125. Nam J-M, Chung Y, Hsu HC, Park CC. β1 integrin targeting to enhance radiation therapy. *Int J Radiat Biol*. (2009) 85:923–8. doi: 10.3109/09553000903232876
126. White DE, Kurpios NA, Zuo D, Hassell JA, Blaess S, Mueller U, et al. Targeted disruption of β1-integrin in a transgenic mouse model of human breast cancer reveals an essential role in mammary tumor induction. *Cancer Cell.* (2004) 6:159–70. doi: 10.1016/j.ccr.2004.06.025
127. Barkan D, Chambers AF. β1-integrin: a potential therapeutic target in the battle against cancer recurrence. *Clin Cancer Res*. (2011) 17:7219–23. doi: 10.1158/1078-0432.CCR-11-0642
128. Goodman SL, Picard M. Integrins as therapeutic targets. *Trends Pharmacol Sci*. (2012) 33:405–12. doi: 10.1016/j.tips.2012.04.002
129. Cox D, Brennan M, Moran N. Integrins as therapeutic targets: lessons and opportunities. *Nat Rev Drug Discov*. (2010) 9:804–20. doi: 10.1038/nrd3266
130. Cordes N, Hansmeier B, Beinke C, Meineke V, van Beuningen D. Irradiation differentially affects substratum-dependent survival, adhesion, and invasion of glioblastoma cell lines. *Br J Cancer.* (2003) 89:2122–32. doi: 10.1038/sj.bjc.6601429
131. Cordes N, Blaese MA, Meineke V, Van Beuningen D. Ionizing radiation induces up-regulation of functional β1-integrin in human lung tumour cell lines *in vitro*. *Int J Radiat Biol*. (2002) 78:347–57. doi: 10.1080/09553000110117340

132. Meineke V, Gilbertz KP, Schilperoort K, Cordes N, Sendler A, Moede T, et al. Ionizing radiation modulates cell surface integrin expression and adhesion of COLO-320 cells to collagen and fibronectin *in vitro*. *Strahlentherapie Und Onkol*. (2002) 178:709–14. doi: 10.1007/s00066-002-0993-9
133. Nam JM, Onodera Y, Bissell MJ, Park CC. Breast cancer cells in three-dimensional culture display an enhanced radioresponse after coordinate targeting of integrin α5β1 and fibronectin. *Cancer Res*. (2010) 70:5238–48. doi: 10.1158/0008-5472.CAN-09-2319
134. Park CC, Zhang HJ, Yao ES, Park CJ, Bissell MJ. β1 integrin inhibition dramatically enhances radiotherapy efficacy in human breast cancer xenografts. *Cancer Res*. (2008) 68:4398–405. doi: 10.1158/0008-5472.CAN-07-6390
135. Eke I, Dickreuter E, Cordes N. Enhanced radiosensitivity of head and neck squamous cell carcinoma cells by β1 integrin inhibition. *Radiother Oncol*. (2012) 104:235–42. doi: 10.1016/j.radonc.2012.05.009
136. Estrugo D, Fischer A, Hess F, Scherthan H, Belka C, Cordes N. Ligand bound β1 integrins inhibit procaspase-8 for mediating cell adhesion-mediated drug and radiation resistance in human leukemia cells. *PLoS ONE*. (2007) 2:e269. doi: 10.1371/journal.pone.0000269
137. Frame MC, Patel H, Serrels B, Lietha D, Eck MJ. The FERM domain: organizing the structure and function of FAK. *Nat Rev Mol Cell Biol*. (2010) 11:802–14. doi: 10.1038/nrm2996
138. Sulzmaier FJ, Jean C, Schlaepfer DD. FAK in cancer: mechanistic findings and clinical applications. *Nat Rev Cancer*. (2014) 14:598–610. doi: 10.1038/nrc3792
139. Mitra SK, Hanson DA, Schlaepfer DD. Focal adhesion kinase: in command and control of cell motility. *Nat Rev Mol Cell Biol*. (2005) 6:56–68. doi: 10.1038/nrm1549
140. Lim STS. Nuclear FAK: a new mode of gene regulation from cellular adhesions. *Mol Cells*. (2013) 36:1–6. doi: 10.1007/s10059-013-0139-1
141. Lim ST, Chen XL, Lim Y, Hanson DA, Vo TT, Howerton K, et al. Nuclear FAK promotes cell proliferation and survival through FERM-enhanced p53 degradation. *Mol Cell*. (2008) 29:9–22. doi: 10.1016/j.molcel.2007.11.031
142. Christmann M, Diesler K, Majhen D, Steigerwald C, Berte N, Freund H, et al. Integrin αVβ3 silencing sensitizes malignant glioma cells to temozolomide by suppression of homologous recombination repair. *Oncotarget*. (2017) 8:27754–71. doi: 10.18632/oncotarget.10897
143. Chow K-H, Factor RE, Ullman KS. The nuclear envelope environment and its cancer connections. *Nat Rev Cancer*. (2012) 12:196–209. doi: 10.1038/nrc3219
144. Alvarado-Kristensson M, Rosselló CA. The biology of the nuclear envelope and its implications in cancer biology. *Int J Mol Sci*. (2019) 20:2586. doi: 10.3390/ijms20102586
145. Dahl KN, Kahn SM, Wilson KL, Discher DE. The nuclear envelope lamina network has elasticity and a compressibility limit suggestive of a molecular shock absorber. *J Cell Sci*. (2004) 117:4779–86. doi: 10.1242/jcs.01357
146. Denais C, Lammerding J. Nuclear mechanics in cancer. *Adv Exp Med Biol*. (2014) 773:435–70. doi: 10.1007/978-1-4899-8032-8_20
147. Isermann P, Lammerding J. Nuclear mechanics and mechanotransduction in health and disease. *Curr Biol*. (2013) 23:R1113–21. doi: 10.1016/j.cub.2013.11.009
148. Khan ZS, Santos JM, Hussain F. Aggressive prostate cancer cell nuclei have reduced stiffness. *Biomicrofluidics*. (2018) 12:014102. doi: 10.1063/1.5019728
149. Harada T, Swift J, Irianto J, Shin J-W, Spinler KR, Athirasala A, et al. Nuclear lamin stiffness is a barrier to 3D migration, but softness can limit survival. *J Cell Biol*. (2014) 204:669–82. doi: 10.1083/jcb.201308029
150. Storch K, Cordes N. Focal adhesion-chromatin linkage controls tumor cell resistance to radio- and chemotherapy. *Chemother Res Pract*. (2012) 2012:319287. doi: 10.1155/2012/319287
151. Madrazo E, Conde AC, Redondo-Muñoz J. Inside the cell: integrins as new governors of nuclear alterations? *Cancers*. (2017) 9:82. doi: 10.3390/cancers9070082
152. Maya-Mendoza A, Bartek J, Jackson DA, Streuli CH. Cellular microenvironment controls the nuclear architecture of breast epithelia through β1-integrin. *Cell Cycle*. (2016) 15:345–56. doi: 10.1080/15384101.2015.1121354
153. Discher DE, Smith L, Cho S, Colasurdo M, García AJ, Safran S. Matrix mechanosensing: from scaling concepts in 'omics data to mechanisms in the nucleus, regeneration, and cancer. *Annu Rev Biophys*. (2017) 46:295–315. doi: 10.1146/annurev-biophys-062215-011206
154. Irianto J, Pfeifer CR, Bennett RR, Xia Y, Ivanovska IL, Liu AJ, et al. Nuclear constriction segregates mobile nuclear proteins away from chromatin. *Mol Biol Cell*. (2016) 27:4011–20. doi: 10.1091/mbc.E16-06-0428
155. Irianto J, Xia Y, Pfeifer CR, Athirasala A, Ji J, Alvey C, et al. DNA damage follows repair factor depletion and portends genome variation in cancer cells after pore migration. *Curr Biol*. (2017) 27:210–23. doi: 10.1016/j.cub.2016.11.049
156. Guilluy C, Burridge K. Nuclear mechanotransduction: forcing the nucleus to respond. *Nucleus*. (2015) 6:19–22. doi: 10.1080/19491034.2014.1001705
157. Guilluy C, Osborne LD, Van Landeghem L, Sharek L, Superfine R, Garcia-Mata R, et al. Isolated nuclei adapt to force and reveal a mechanotransduction pathway in the nucleus. *Nat Cell Biol*. (2014) 16:376–81. doi: 10.1038/ncb2927
158. Gilbert HTJ, Mallikarjun V, Dobre O, Jackson MR, Pedley R, Gilmore AP, et al. Nuclear decoupling is part of a rapid protein-level cellular response to high-intensity mechanical loading. *Nat Commun*. (2019) 10:4149. doi: 10.1038/s41467-019-11923-1
159. Ganguly KK, Pal S, Moulik S, Chatterjee A. Integrins and metastasis. *Cell Adh Migr*. (2013) 7:251–61. doi: 10.4161/cam.23840
160. Glukhova MA, Streuli CH. How integrins control breast biology. This review comes from a themed issue on Cell adhesion and migration. *Curr Opin Cell Biol*. (2013) 25:633–41. doi: 10.1016/j.ceb.2013.06.010
161. Marelli UK, Rechenmacher F, Sobahi TRA, Mas-Moruno C, Kessler H. Tumor targeting via integrin ligands. *Front Oncol*. (2013) 3:222. doi: 10.3389/fonc.2013.00222
162. Storch K, Eke I, Borgmann K, Krause M, Richter C, Becker K, et al. Three-dimensional cell growth confers radioresistance by chromatin density modification. *Cancer Res*. (2010) 70:3925–34. doi: 10.1158/0008-5472.CAN-09-3848
163. Calvo F, Ege N, Grande-Garcia A, Hooper S, Jenkins RP, Chaudhry SI, et al. Mechanotransduction and YAP-dependent matrix remodelling is required for the generation and maintenance of cancer-associated fibroblasts. *Nat Cell Biol*. (2013) 15:637–46. doi: 10.1038/ncb2756
164. Hirata E, Sahai E. Tumor microenvironment and differential responses to therapy. *Cold Spring Harb Perspect Med*. (2017) 7:a026781. doi: 10.1101/cshperspect.a026781
165. Yarnold J, Vozenin Brotons M-C. Pathogenetic mechanisms in radiation fibrosis. *Radiother Oncol*. (2010) 97:149–61. doi: 10.1016/j.radonc.2010.09.002

Conflict of Interest: The authors declare that the research was conducted in the absence of any commercial or financial relationships that could be construed as a potential conflict of interest.

Copyright © 2019 Deville and Cordes. This is an open-access article distributed under the terms of the Creative Commons Attribution License (CC BY). The use, distribution or reproduction in other forums is permitted, provided the original author(s) and the copyright owner(s) are credited and that the original publication in this journal is cited, in accordance with accepted academic practice. No use, distribution or reproduction is permitted which does not comply with these terms.

frontiers in Oncology

ORIGINAL RESEARCH
published: 10 January 2020
doi: 10.3389/fonc.2019.01470

Biological Determinants of Chemo-Radiotherapy Response in HPV-Negative Head and Neck Cancer: A Multicentric External Validation

*Martijn van der Heijden[1,2], Paul B. M. Essers[1,3], Monique C. de Jong[3], Reinout H. de Roest[4], Sebastian Sanduleanu[5], Caroline V. M. Verhagen[1,2], Olga Hamming-Vrieze[2], Frank Hoebers[5], Philippe Lambin[6], Harry Bartelink[3], C. René Leemans[4], Marcel Verheij[1,3,7], Ruud H. Brakenhoff[4], Michiel W. M. van den Brekel[2,8] and Conchita Vens[1,3]**

[1] Division of Cell Biology, The Netherlands Cancer Institute, Amsterdam, Netherlands, [2] Department of Head and Neck Oncology and Surgery, The Netherlands Cancer Institute, Amsterdam, Netherlands, [3] Department of Radiation Oncology, The Netherlands Cancer Institute, Amsterdam, Netherlands, [4] Amsterdam UMC, Vrije Universiteit Amsterdam, Otolaryngology/Head and Neck Surgery, Cancer Center Amsterdam, Amsterdam, Netherlands, [5] Department of Radiation Oncology (MAASTRO), GROW—School for Oncology and Developmental Biology, Maastricht University Medical Centre, Maastricht, Netherlands, [6] The D-Lab and The M-Lab, Department of Precision Medicine, GROW—School for Oncology and Developmental Biology, Maastricht University, Maastricht, Netherlands, [7] Department of Radiation Oncology, Radboud University Medical Center, Nijmegen, Netherlands, [8] Department of Oral and Maxillofacial Surgery, Amsterdam UMC, Academic Medical Center, Amsterdam, Netherlands

OPEN ACCESS

Edited by:
Ira Ida Skvortsova, Innsbruck Medical University, Austria

Reviewed by:
Panagiotis Balermpas, University Hospital Zürich, Switzerland
Raghvendra Mohan Srivastava, Memorial Sloan Kettering Cancer Center, United States

***Correspondence:**
Conchita Vens
c.vens@nki.nl

Specialty section:
This article was submitted to Radiation Oncology, a section of the journal Frontiers in Oncology

Received: *21 August 2019*
Accepted: *09 December 2019*
Published: *10 January 2020*

Citation:
van der Heijden M, Essers PBM, de Jong MC, de Roest RH, Sanduleanu S, Verhagen CVM, Hamming-Vrieze O, Hoebers F, Lambin P, Bartelink H, Leemans CR, Verheij M, Brakenhoff RH, van den Brekel MWM and Vens C (2020) Biological Determinants of Chemo-Radiotherapy Response in HPV-Negative Head and Neck Cancer: A Multicentric External Validation. Front. Oncol. 9:1470. doi: 10.3389/fonc.2019.01470

Purpose: Tumor markers that are related to hypoxia, proliferation, DNA damage repair and stem cell-ness, have a prognostic value in advanced stage HNSCC patients when assessed individually. Here we aimed to evaluate and validate this in a multifactorial context and assess interrelation and the combined role of these biological factors in determining chemo-radiotherapy response in HPV-negative advanced HNSCC.

Methods: RNA sequencing data of pre-treatment biopsy material from 197 HPV-negative advanced stage HNSCC patients treated with definitive chemoradiotherapy was analyzed. Biological parameter scores were assigned to patient samples using previously generated and described gene expression signatures. Locoregional control rates were used to assess the role of these biological parameters in radiation response and compared to distant metastasis data. Biological factors were ranked according to their clinical impact using bootstrapping methods and multivariate Cox regression analyses that included clinical variables. Multivariate Cox regression analyses comprising all biological variables were used to define their relative role among all factors when combined.

Results: Only few biomarker scores correlate with each other, underscoring their independence. The different biological factors do not correlate or cluster, except for the two stem cell markers CD44 and SLC3A2 ($r = 0.4$, $p < 0.001$) and acute hypoxia prediction scores which correlated with T-cell infiltration score, $CD8^+$ T cell abundance and proliferation scores ($r = 0.52$, 0.56, and 0.6, respectively with $p < 0.001$).

Locoregional control association analyses revealed that chronic (Hazard Ratio (HR) = 3.9) and acute hypoxia (HR = 1.9), followed by stem cell-ness (CD44/SLC3A2; HR = 2.2/2.3), were the strongest and most robust determinants of radiation response. Furthermore, multivariable analysis, considering other biological and clinical factors, reveal a significant role for EGFR expression (HR = 2.9, $p < 0.05$) and T-cell infiltration ($CD8^+$T-cells: HR = 2.2, $p < 0.05$; $CD8^+$T-cells/Treg: HR = 2.6, $p < 0.01$) signatures in locoregional control of chemoradiotherapy-treated HNSCC.

Conclusion: Tumor acute and chronic hypoxia, stem cell-ness, and $CD8^+$ T-cell parameters are relevant and largely independent biological factors that together contribute to locoregional control. The combined analyses illustrate the additive value of multifactorial analyses and support a role for EGFR expression analysis and immune cell markers in addition to previously validated biomarkers. This external validation underscores the relevance of biological factors in determining chemoradiotherapy outcome in HNSCC.

Keywords: HNSCC, chemoradiotherapy, radiation resistance, hypoxia, immune cell infiltration, expression profile analysis, head and neck cancer, radiation oncology

INTRODUCTION

In this study we set out to perform multifactorial analyses to gain understanding of the role and dependence of biological factors that have shown to influence tumor radiation response in preclinical studies and to be associated with radiotherapy response in clinical studies (1, 2). Chemo-radiotherapy is the primary treatment option for advanced head and neck squamous cell carcinoma (HNSCC). Cure and locoregional failure rates of around 50 and 25%, respectively, facilitate the evaluation of biological determinants of radiation response. Using biological characteristics of the tumors, outcome association studies revealed many potential determinants of prognosis and treatment response in HNSCC (3–7). This study evaluates complementarity and hierarchy of radiation response determining "HNSCC biology."

Head and neck squamous cell carcinoma (HNSCC) is the 6th most common cancer in the world, with smoking, alcohol and HPV infection as the main risk factors. Around two thirds of the patients present with advanced stage disease and have a poor prognosis with 5 year overall survival rates around 50% (8, 9). Allowing for organ preservation, curative treatment for advanced stage hypopharyngeal, laryngeal and HPV-negative oropharyngeal carcinomas shifted from extensive surgery to concomitant cisplatin-based chemo-radiotherapy in the last decades (10). Around two third of all HNSCC patients receive radiotherapy as part of their treatment. Among these, those with HPV-positive oropharyngeal tumors have a particularly good prognosis, reason to consider them as a new entity in the new TNM staging (11). As revealed by gene expression and mutational analyses, these tumors are also biologically very different (12, 13). HPV-negative HNSCC, in contrast, are characterized by poor prognosis. They exhibit frequent amplifications and mutations in proto-oncogenes (EGFR, MYC, HRAS) and in cell cycle genes that drive and support tumor proliferation (14–16). p53 is affected in almost all HPV-negative HNSCC.

Early radiobiology studies revealed determinants of tumor radiation response. Hypoxia, repopulation, driven by tumor cell proliferation, tumor stem cell density (i.e., clonogenic cell density) and cellular radiosensitivity (as for example determined by cellular DNA damage repair capacity) were shown to be among the most relevant biological factors that affect radiation or fractionated radiotherapy response in preclinical models of different cancers (1, 2). In recent years, increased interest emerged in immune response related markers and immune cells due to novel immunotherapeutic options (17–21). A series of preclinical and clinical studies highlight the potential relevance of immune-related markers in HNSCC [reviewed in (5, 6, 19, 22–24)].

HNSCC outcome association studies using many different biomarkers, demonstrated the clinical importance of some of these pre-clinically assessed tumor biology parameters (1, 5–7). HPV and hypoxia are indeed the best studied biology related prognostic markers in HNSCC. Within the HPV-negative patients, tumor hypoxia marks patients with a poor prognosis (25–29). Confirming its role above marking poor prognosis patients, hypoxia biomarkers also predict response to hypoxia modification therapy (25, 30–33). Elaborating on a gene expression profile that captures the cellular changes caused by acute hypoxia, we recently showed the relevance of acute hypoxia in addition to chronic hypoxia (29). As predicted by the process they capture, these two classifications did not necessarily overlap in the samples and also reveal different outcome associations in HNSCC that result from a prominent role of acute hypoxia.

While the success of accelerated radiotherapy schedules (34) highlight the important role of tumor repopulation in HNSCC, there is a lack of biomarker data showing a link to cellular proliferation (35). Based on genetic mutation data, we find a small role for co-occurring CCND1 and CDKN2A mutations

in HPV-negative chemo-radiotherapy treated HNSCC that was however not visible in the locoregional control endpoints (36). Yet, the combination of radiotherapy with the epidermal growth factor receptor (EGFR) binding antibody cetuximab has shown efficacy and EGFR expression has been associated with poor survival, preferentially in non-accelerated schedules arguing for a role in tumor repopulation (37–40). The role of EGFR and cellular proliferation in radiotherapy response needs to be further elaborated (41–43). However proliferation, as determined by the proliferation marker by Starmans et al. has been linked to aggressive disease or disease progression in multiple cancer types; unfortunately this was not assessed in HNSCC (44).

Originated from CD44 expression data from de Jong et al. (45) in laryngeal cancer and confirmed in resected and chemo-radiotherapy treated HNSCC for CD44 and SLC3A2 (27, 46) in subsequent studies, it also became clear that tumor "stem cell-ness" is important in radiotherapy outcomes since these stem cell related biomarkers were associated with poor prognosis (35, 47–49).

The consistent effect of $CD8^+$ T cell depletion on radiation induced tumor growth delays in preclinical studies expose the relevance of certain immune cell populations in radiation response and resistance (50, 51). Evidence in clinic of a possible interaction is less strong and current studies focus on strategies to optimize combinations with immune response modulators to improve radiotherapy outcomes (6, 18, 20, 21, 23, 27, 52–55). Interestingly, Mandal et al. recently showed that markers for regulatory Tcells (Treg), NK cells and $CD8^+$ T cells are prognostic in head and neck cancer (56) in the TCGA dataset. Despite these interesting initial reports, the prognostic value of these gene expression based immune markers is still unknown for chemo-radiotherapy treated patients since all patients in the TCGA dataset have been treated with primary surgery. Immunohistochemically (IHC) determined high $CD8^+$ T-cell counts are associated with good prognosis in postoperative chemo-radiotherapy treated patients, further indicating its relevance for HNSCC (57). A good prognosis association with IHC $CD8^+$ TIL density was found in patients with oropharyngeal squamous cell carcinoma treated with surgery or (chemo) radiotherapy and in a similarly mixed treatment cohort of hypopharyngeal SCC patients (58–60).

Our previous studies emphasized the important role of functional and genetic DNA crosslink repair defects in HNSCC (61, 62) and provided the basis for machine learning generated models that predicted such DNA repair defects in clinical samples (63). The expression based DNA repair defect prediction models revealed an association with metastasis in HNSCC and linked DNA repair defects to migratory and invasive behavior in HNSCC cell lines (63). Given the relevance of Epithelial to Mesenchymal Transition (EMT) in many cancer types, we also developed a HNSCC-specific EMT model that classifies HNSCC according to epithelial or mesenchymal characteristics (64). The strong prognostic value of this HNSCC-EMT model also suggests an important role in radiation response.

Taken together, the individual roles of some of these biological factors important in radiation response have not been validated and the interrelation of these biological factors has not been investigated in the clinical setting. We therefore studied the role of the aforementioned biological factors in the context of head and neck cancer and chemo-radiotherapy. Previously published gene expression based signatures were used to detect these factors. In a set of nearly 200 patients with advanced stage HPV-negative HNSCC treated with chemo-radiotherapy, we used univariate and multivariate outcome analyses to examine these factors while also considering correlation and dependence to delineate their relative roles.

MATERIALS AND METHODS

Patient Data and Material

This retrospective study included material and data from patients that were diagnosed between 2001 and 2014 and treated with definitive cisplatin-based chemo-radiotherapy within three centers: the Netherlands Cancer Institute (Amsterdam, NL), the Amsterdam University Medical Center (Amsterdam, NL) or the MAASTRO clinic/MUMC+ (Maastricht, NL). Selection criteria for this gene expression study cohort were (i) concomitant radiotherapy and cisplatin treatment of unresected HNSCC, (ii) hypopharyngeal, laryngeal or HPV-negative oropharyngeal (iii) no prior treatment with chemotherapy or radiotherapy in the head and neck area. To minimize the number of variables, AJCC disease staging, summarizing TNM stage, was used to classify HNSCC patients after determining whether this classification also represented N-staging and its known association with survival well (**Supplementary Figure 1**). Received radiotherapy regimens were 70 Gy over 35 fractions (up to 77 Gy in ARTFORCE patients) in 7 or 6 weeks (DAHANCA scheme). All patients were treated with either of four different cisplatin regimens: daily [25 × 6 mg/m^2 Body Surface Area (BSA)], weekly (7 × 40 mg/m^2 BSA) or 3-weekly (3 × 100 mg/m^2 BSA) intravenous administration or weekly intra-arterial administration [4 × 150 mg/m^2 BSA, for 8 patients according to the RADPLAT trial protocol (65)]. Not all patients completed the full chemotherapy scheme. Therefore, cumulative cisplatin doses were calculated and patients were classified into $<$ or $\geq$ or 200 mg/m^2 BSA cisplatin, according to literature (66, 67). Survival data was calculated from the start of treatment until the first event was detected. The primary outcome measure is loco-regional control (LRC) and implies absence of recurrences in the radiotherapy targeted regions of the head and neck area. Patient characteristics are provided in **Supplementary Table 1**. Institutional Review Boards at the Netherlands Cancer Institute, the Amsterdam University Medical Center and the MAASTRO clinic/MUMC+ approved biopsies and collection of fresh-frozen HNSCC tumor material and the use of genetic and clinical data from patients at their respective centers after anonymization. All patients granted written informed consent for biopsy, material use and data use. Pre-treatment tumor biopsy material available for the DESIGN study or collected from the NKI ARTFORCE (68) or RADPLAT trial patients were used for RNA preparation and sequencing. HPV-status of all oropharyngeal carcinomas was determined by immunohistochemical assessment of p16 by a dedicated head and neck pathologist (69) followed by a HPV

DNA test on the p16-immunopositive cases and/or confirmed using RNA-sequencing data.

Material Preparation and RNA-Sequencing

Fresh-frozen tumor samples were sectioned, collected for RNA preparation and in part subjected to tumor percentage evaluation by revision of HE stained coupes by senior head and neck pathologist Dr. S.M. Willems. Only samples with a tumor percentage of >40% proceeded to RNA-sequencing. RNA was isolated using the AllPrep DNA/RNA mini kit (Qiagen). Quality and quantity of total RNA was assessed by the 2100 Bioanalyzer using a Nano chip (Agilent, Santa Clara, CA). Only total RNA samples having RIN>7 were used for library preparation. Strand-specific libraries were generated using the TruSeq Stranded mRNA sample preparation kit (Illumina Inc., San Diego, RS-122-2101/2) according to the manufacturer's instructions (Illumina, Part # 15031047 Rev. E). The libraries were analyzed on a 2100 Bioanalyzer using a 7500 chip (Agilent, Santa Clara, CA), diluted and pooled equimolar into a 10 nM multiplex sequencing pool and sequenced with 65 base single reads on a HiSeq2500 using V4 chemistry (Illumina Inc., San Diego). Reads were mapped against the GRCh38 human genome using TopHat2.1 (70), with options "fr-firststrand," "transcriptome-index," and "prefilter multi-hits." Read counts were determined using HTSeq-count (71) with options "stranded" and mode "union."

Expression and Patient Outcome Analyses

All analyses were performed in R 3.4.3 using Rstudio 1.1. Samples were classified and scored for the different analyzed biological characteristics using different gene expression profiles according to the protocols described in the original publication. If not possible due to the lack of original reference data, GSVA, a Bioconductor package for R, was used on raw read counts to calculate gene expression profile scores (72). Transcripts per million (TPM) was used for individual gene expression analyses. Patient outcome analyses were performed using Cox proportional hazard model. Time to event was defined as the time between the first day of treatment and the day the event was detected. Events in the locoregional control data (LRC) were defined by recurrences in the radiotherapy targeted region. Distant metastasis (DM) events were defined by tumors detected outside the head and neck area. A patient's death prior to a possible event led to censoring in the LRC and DM data and no event was recorded. Progression free survival (PFS) was defined as the time from the start of treatment to the day the patient died, had a locoregional recurrence or distant metastasis. Tests were considered significant when $p < 0.05$. A spearman correlation coefficient was computed between continuous variables.

In order to obtain a robust cut-off when transforming a continuous variable into a dichotomous variable we used the bootstrap procedure as described in Linge et al. (28). In brief, 197 sample values were randomly assigned into one bootstrap cohort (from the cohort of 197 patients) while data from the same patient could be chosen multiple times. This procedure was repeated to obtain 10.000 randomized cohorts. At each possible cut-off value of the marker of interest, the individual cohorts were split into a "low" and "high" group and Cox proportional hazards models were fit based on these splits. These models included, next to the newly grouped marker of interest, all clinical variables that were found to be significantly associated with the outcome of interest [Locoregional Control (LRC), Distant Metastasis (DM), Overall Survival (OS) or Progression Free Survival (PFS)]. The fraction of cohorts for which the marker of interest was significantly associated with survival ($p < 0.05$) was recorded for each cutoff. The values of nine adjacent cutoffs were averaged to smoothen the data. The cutoff with the highest fraction of significant associations was chosen for further analysis. Cutoffs that would result in patient subgroups with <10% of the patients were not considered to maintain statistical power. Note that, this analysis was repeated for each endpoint resulting in different cut-offs.

To reduce the number of possible variables included in multivariable analysis we used a backward selection procedure. The most frequent level of each variable was used as the reference level for this analysis. A Cox proportional hazard model was fit containing all biological markers and clinical variables. Then, each individual variable was removed from the model and improvements in model performance by this process were assessed using the Akaike Information Criterion (AIC) from the "stats" package in R. The best model (lowest AIC) was selected for further analysis in the multivariate Cox regression analysis. This process was repeated until removing variables from the model did no longer result in an improved model.

RESULTS

Role of Clinical Factors and Patient Characteristics in Chemo-Radiotherapy Outcome

In this retrospective multicenter study, 197 patients met all inclusion criteria and had sufficient tumor material available. All patients were treated with definitive cisplatin-based chemo-radiotherapy for advanced stage HPV-negative oropharyngeal, hypopharyngeal, or laryngeal carcinoma. Patient characteristics are shown in **Table 1**. The median age in this patient cohort is 62 years and there is a male: female ratio of 3:1. Most patients reported ongoing or a history of alcohol and/or tobacco use. The largest subsite representation is oropharyngeal tumors with 85 patients, then hypopharyngeal with 78 and laryngeal carcinoma with 34 patients. Except for two patients, all patients had stage III/IV classified tumors. As expected, outcomes and survival curves differ according to stage (**Supplementary Figure 2**). Tumor volume data as determined by delineation on RT planning CT images were available for 166 patients with a median volume of 23.2 cm^3. Not all patients finished chemotherapy, but 126 patients (63%) received a cumulative dose of and above 200 mg/m^2 body surface area. Locoregional recurrences occurred in 23.8% ($N = 49$) of cases and distant metastasis in 19.8% ($N = 39$).

Clinical factors were tested for their association with locoregional control and other survival outcomes (**Supplementary Figure 1**, **Supplementary Table 1**). Consistent with previous reports we find that locoregional control (LRC) is influenced by cumulative cisplatin dose levels (66, 67). The

TABLE 1 | HNSCC patients and tumor characteristics.

Variable		#Patients (total 197)
Median Age at diagnosis (Range)		61 years (40–80.23)
Sex	Female	55
	Male	142
Alcohol	No	22
	Former alcoholic	22
	Yes	146
	Missing	7
Tobacco	Never	5
	Former smoker	30
	Yes	156
	Missing	6
Tumor subsite	Larynx	34
	Hypopharynx	78
	Oropharynx	85
Median tumor volume (Range)		23.2 cm^3 (1.03–752.2)
	Missing	31
Stage	IVB	20
	III	40
	II	2
	IVA	135
Cumulative cisplatin dose	<200 mg/cm^2	67
	≥200 mg/cm^2	126
	Missing	4
Median Follow-up		5.24 years (4.59–5.86)
Locoregional Recurrences		49
Distant Metastasis		39

cumulative cisplatin dose of < 200 mg/m^2 BSA was significantly associated with LRC failure (HR = 2.57, $p = 0.0012$). Female sex shows a trend toward better locoregional control (HR = 0.52, $p = 0.072$). This could however been confounded by the less prominent alcohol consumption characteristics or other differences in lifestyle in this particular patient group. More female patients reported to abstain from alcohol compared to male patients (21.8 vs. 7.4%, $p = 0.019$), which was however not the case for tobacco use ($p = 0.66$). Heavy past or ongoing alcohol consumption was associated with an increased risk for LRC failure (HR = 2.16, $p = 0.041$). Interestingly, age, tobacco, tumor subsite and AJCC stage is not significantly associated with LRC in our patient cohort. The other clinical outcomes (DM, PFS or OS) showed significant associations with sex, tumor volume, stage and cisplatin (**Supplementary Figure 1**, **Supplementary Table 1**).

Tumor Biology Assessment and (in)Dependence in HPV-Negative HNSCC

Preclinical radiobiology studies and clinical biomarker studies exposed many different determinants of radiation response. The number of variables that can be included in statistical analyses are however limited by the cohort size and number of events. Thus, in order to evaluate the relative role of different tumor biology parameters in clinic, we prioritized those with a reported clinical outcome association. The following 12 gene expression signatures were therefore selected to characterize the clinical samples using pretreatment HNSCC transcriptomic data: The Toustrup (1) and Seigneuric (2) expression signatures were used to assess the level of chronic (1) and acute (2) hypoxia, respectively (25, 73). Linked to tumor stem cell richness SLC3A2 (3) and CD44 (4) gene expression values (in TPM) were included since both have been reported to be associated with outcome in chemo-radiotherapy treated patients (74). Economopoulou et al. (5) EGFR expression (in TPM) and (6) the Starmans et al. "proliferation" expression signature (44) were selected as cellular proliferation markers which could influence tumor repopulation between radiotherapy fractions. To cover immune-related factors we further included expression signatures from Senbabaoglu et al. (75) that originated from Bindea et al. (76) and assess (7) 'T-cell infiltration score' (TIS), (8) $CD8^+$ T-cells, (9) $CD56^{dim}$ natural killer (NK) cells abundance while considering the (10) $CD8^+$ vs. T regulatory (Treg) cell ratios. This immune status gene expression signature selection is based on the reported outcome association in resected HNSCC (56). Our own studies conducted in HPV-negative advanced HNSCC revealed an important role for EMT and DNA crosslink (CL) repair defects in treatment outcome and these prediction models for mesenchymal characteristics and tumor cell DNA crosslink repair defects (11). "HNSCC-EMT" and (12) "MMConly," were therefore included in this analysis and are referred to as "EMT" and "DNA CL repair" in this manuscript (63, 64). Most of these biological factors have been tested individually, predominantly in univariable analyses and in different settings in previous studies; however their mutual correlations and possible dependence between them are unknown.

The goal of this study is to pinpoint biological factors that are important for (chemo)-radiotherapy treatment failure and thus might validate their independent role in radioresistance. We therefore calculated scores for all aforementioned markers. **Supplementary Figure 3** shows the frequency of the scores and their distribution over the patient cohort. Next, we performed hierarchical clustering to investigate the presence of HNSCC subsets as defined by these characteristics. Tumor volume was included in this analysis as it promotes chronic hypoxia or may be associated with high proliferation scores. Despite the coexistence and correlation of some factors this does however not reveal any prominent clusters (**Figures 1A,B**). Surprisingly, we find that the acute hypoxia profile score correlates with the Starmans proliferation score ($r = 0.58, p < 0.001$) (**Figure 1C**) but also with the T-cell Infiltration Score (TIS) and the $CD8^+$ T cell scores ($r = 0.51$ and $r = 0.54, p < 0.001$).

Within their own category, stem cell related markers, CD44 and SLC3A2 ($r = 0.57$, $p < 0.001$), and the immune cell related markers correlate with each other. While the correlation of acute and chronic hypoxia is significant, it is fairly weak ($R = 0.26$, $p < 0.001$) and was in line with previous reports (29). EGFR expression and the proliferation score are correlated to some extent ($r = 0.26$, $p < 0.01$). The $CD8^+$ T cell to regulatory T cell ratio ($CD8^+$/Treg) as determined by the expression signature scores is negatively associated with the abundance of $CD56^{dim}$

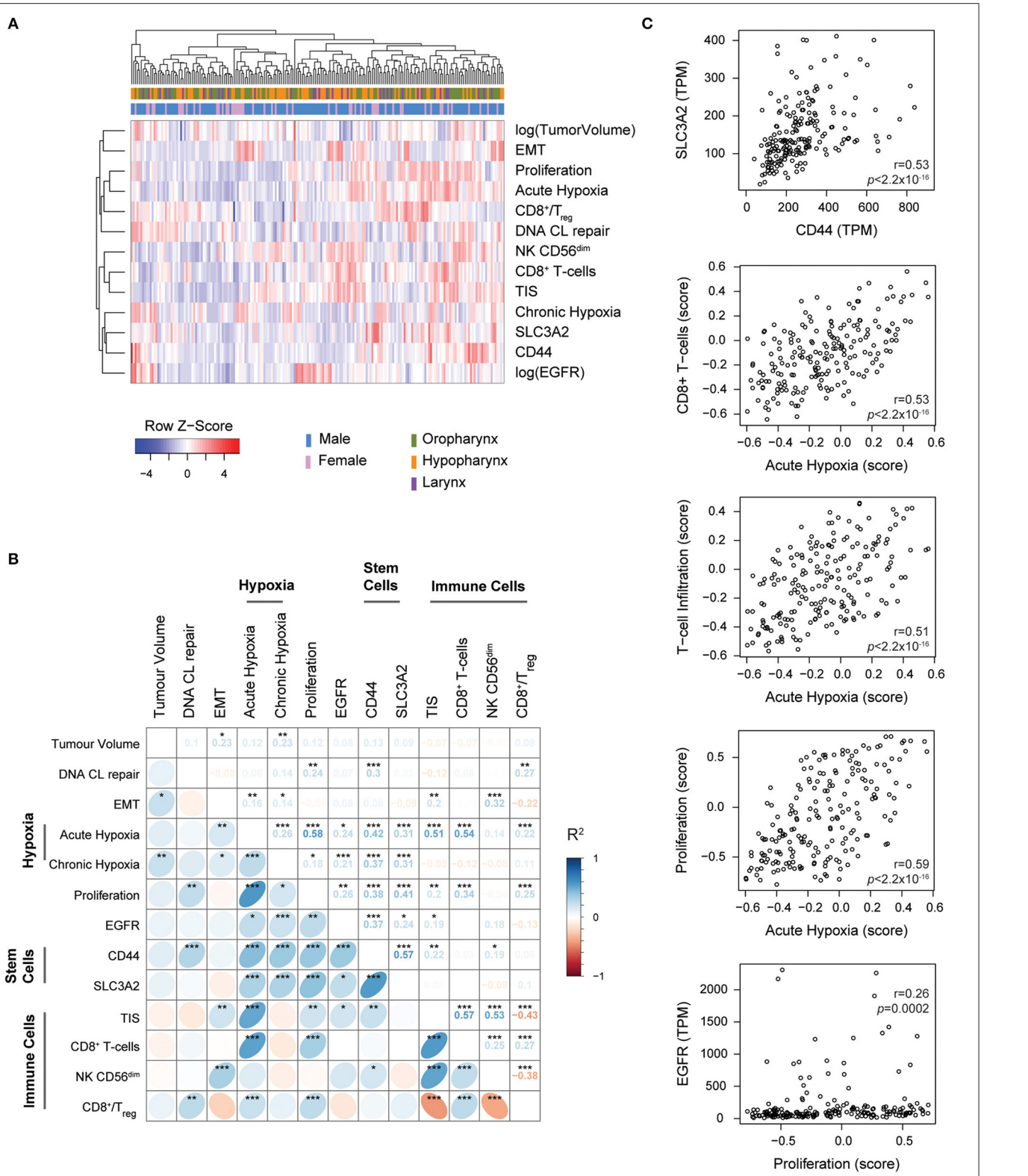

FIGURE 1 | Interrelation and dependence of biological markers. **(A)** Heatmap showing hierarchical clustering of patients based on the selected biological markers. Tumor volume and EGFR expression were log-transformed to prevent clustering to be dominated by few samples with high values. **(B)** Correlation plot with spearman's ranked correlation values between all biological marker scores. Markers were grouped by tumor biology class where appropriate. $^{*}p < 0.05$, $^{**}p < 0.01$, $^{***}p < 0.001$, not corrected for multiple testing. **(C)** Scatterplots with Spearman's coefficients and *p*-values for correlations of interest.

natural killer (NK) cells and the TIS signature. While the link between tumor volume and chronic hypoxia ($R = 0.23$, $p < 0.01$) is expected, tumor volume is also associated with EMT ($R = 0.23$, $p < 0.05$). With a maximum variance inflation factor value of 3.3, correlations were not strong enough to exclude parameters from subsequent analyses. None of these markers show strong associations with any of the clinical factors. Among all, we find that the most independent tumor characteristics are the presence of DNA CL repair defects and tumor EMT status (and tumor volumes).

Role of Individual Biological Factors in Locoregional Control by Chemo-Radiotherapy in HNSCC

Since we aimed to evaluate tumor characteristics with respect to radiation resistance and response, we initially focused on locoregional control outcome values that are mainly determined by the success of the "local" radiotherapy treatment. Given the lack of strong correlations, all markers were individually tested for their association with locoregional failure. A 10.000 times bootstrapping method was employed to (a) determine a potential role for the biomarker across different cutoffs and (b) to identify a clinically robust cut-off for each so to compare the biomarkers among each other. In brief, each marker was tested for their association with the selected survival outcome for all possible cutoffs. This analysis was performed using a multivariable Cox proportional hazard model with all relevant clinical factors included, as determined above. Consequently, clinical variables were included according to outcome type: sex and cumulative cisplatin dose for LRC; sex, subsite and cumulative cisplatin dose for OS; stage, subsite and cisplatin dose for PFS; and sex and alcohol use for DM. Based on the results of these 10.000 bootstrap repeats (**Figure 2A**), we find that the hypoxia and stem cell related markers are most robustly associated with LRC across different score cut-offs. Proliferation, EGFR and immune cell signatures merely provide significant associations with LRC in a fraction of the randomly created cohorts and tested cut-offs.

Cut-offs with the most stable clinical association were selected for each biomarker for further analysis as depicted in **Figure 2A** and listed in **Supplementary Table 2**. These analyses confirm that both, chronic and acute hypoxia, are strongly associated with locoregional control. Using these calculated cut-offs in multivariable analyses with clinical factors, we find that among all chronic hypoxia is most strongly associated with a failure of locoregional control (HR = 3.95, $p = 0.0038$) followed by acute hypoxia (HR = 1.9, $p = 0.03$) and stem cell related, SLC3A2 (HR = 2.31, $p = 0.026$) and CD44 (HR = 2.03, $p = 0.043$; **Figures 2B**, **3**; **Supplementary Table 3**). Although not significantly, larger tumor volumes showed a trend toward worse locoregional control with a hazard ratio (HR = 1.63, $p = 0.11$) that is comparable to those previously reported by others (27). It should be however noted that most tumors in this cohort are relatively large and stage III/IV. This and the fact that the LRC measure also includes regional recurrences, may together affect the specific HR values. Trends toward a worse LRC prognosis were observed in patient groups with tumors with high proliferation and CD8+ T cell scores (HR = 1.89, $p = 0.067$ and HR = 2.35, $p = 0.071$, respectively) (**Supplementary Figure 4** and **Supplementary Table 3**).

To delineate this from general poor prognosis pattern and to investigate the radiation response link further, we repeated these analyses and compared the role of these biomarkers for overall survival, progression free survival and distant metastasis (**Figure 3**). Cut-off values were defined by the bootstrapping method described above for each biomarker; and multivariable Cox proportional hazard analyses with clinical factors were performed. Notably, gene expression signature scores or expression value cut-offs, as determined by their potential relevance in the 10,000x bootstrapping method, resulted to be different in some of the biomarkers such as "acute hypoxia," "chronic hypoxia," "EGFR," "TIS," "NK $CD56^{dim}$." and "CD8+/Treg" (**Supplementary Figures 4–6** and **Supplementary Table 2**).

Most markers show an association with several of the outcome parameters. We find that distant metastasis is associated with EMT (HR = 3.14, $p = 0.0086$), acute hypoxia score (HR = 2.44, $p = 0.0086$), NK $CD56^{dim}$ score (HR = 2.47, $p = 0.019$) and EGFR expression (HR = 2.07, $p = 0.032$) (**Supplementary Figure 5**, **Supplementary Table 3**). Poor overall survival is associated with increased tumor volume (HR = 2.12, $p = 0.00054$), EMT score (HR = 2.15, $p = 0.002$), DNA CL repair defect (HR = 1.97, $p = 0.0043$), acute hypoxia (HR = 1.62, $p = 0.023$) and EGFR expression (HR = 1.68, $p = 0.014$) (**Supplementary Figure 6**, **Supplementary Table 3**). High EMT (HR = 2.19, $p = 0.0014$), EGFR (HR = 1.82, $p = 0.0038$), acute hypoxia (HR = 1.64, $p = 0.017$), DNA CL repair defect (HR = 1.8, $p = 0.0085$) and chronic hypoxia scores (HR = 1.7, $p = 0.015$) and tumor volumes (HR = 1.72, $p = 0.036$) are associated with a worse progression free survival (PFS) (**Supplementary Figure 7**; **Supplementary Table 3**). Interestingly, when comparing the distant metastasis and locoregional control failure data, locoregional control is increased in tumors with higher EGFR expression or containing few $CD56^{dim}$ NK cells while high values in both result in an increased risk of DM. It should be noted, however, that the bootstrapping defined cut-offs were different in both. Yet, as evident from the bootstrapping data chronic hypoxia was not linked to DM but LRC at many cut-offs. On the contrary, the similar shape of the results from the acute hypoxia bootstrapping supports its relevance in both, LRC and DM (**Figure 2** and **Supplementary Figure 5**).

Taken together, for biomarkers which have been previously reported to be prognostic in HNSCC these analyses validate their role in an independent data set. Most biological factors as determined by the selected biomarkers are significantly associated with PFS thereby confirming their relevance. Overall, we find a prominent role for acute and chronic hypoxia and CD44 and SCL3A2 in our cohorts. We show that, from all, chronic hypoxia appears to be the most specific to LRC. In contrast, HR values from EMT and proliferation based splits are greater when assessing DM. Furthermore, these data reveal a role for

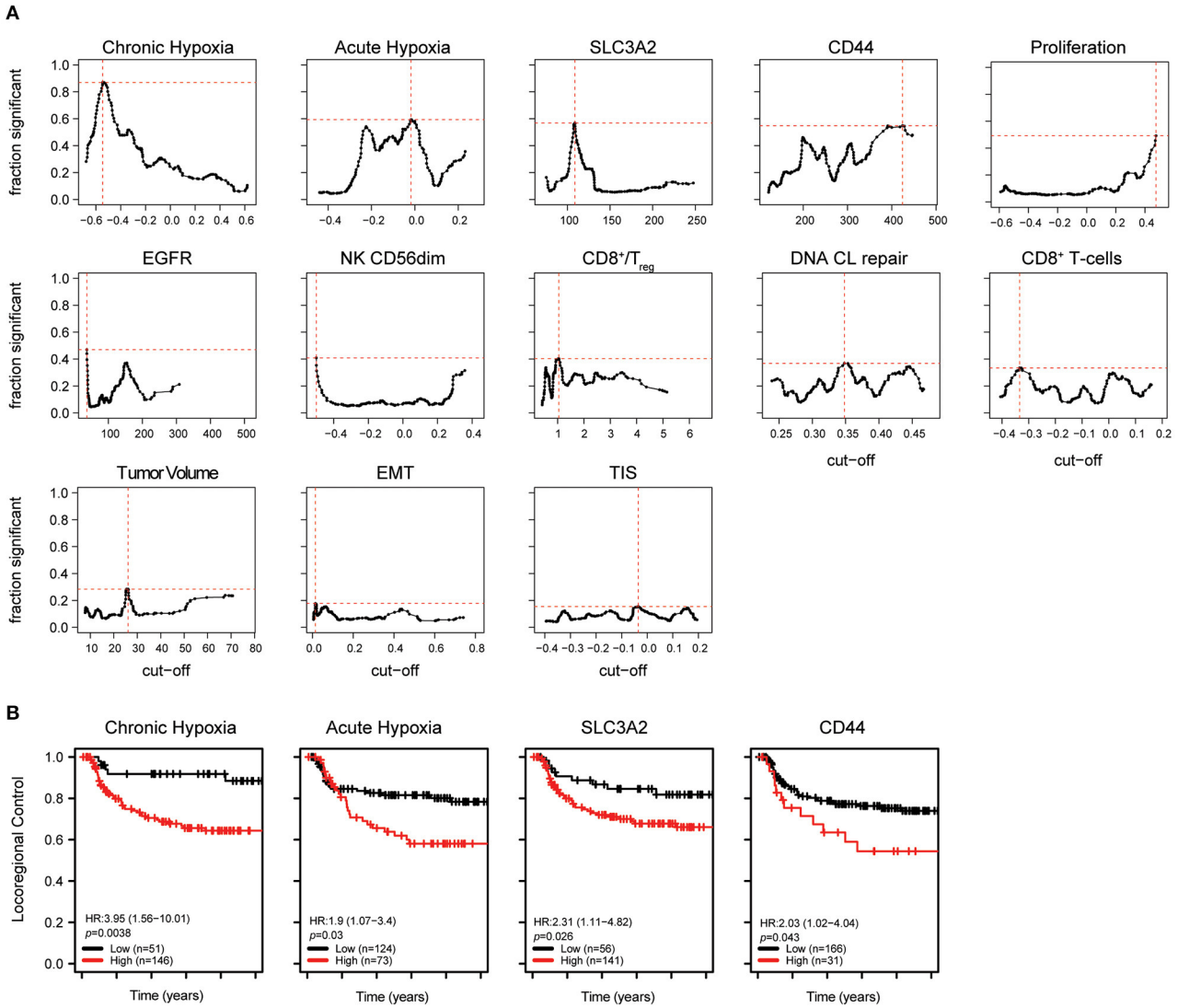

FIGURE 2 | Role of individual biological factors for locoregional control. **(A)** Results of individual bootstrap analysis (see methods) including important clinical factors. The fraction of randomized cohorts with a significant association with locoregional control is shown for each cut-off and biological marker. Markers are ordered by the magnitude of the maximum fraction of significant Cox proportional hazard tests at the best cut-off. The best cutoff is indicated with dotted red lines. **(B)** For each marker, the cohort was split into a high and low group at the best cutoff determined in A. Hazard ratios for recurrences and corresponding *p*-values were obtained with a multivariate Cox proportional hazard analysis using the same variables as those used to determine the cutoff.

the immune cell and proliferation related biomarkers in HNSCC outcome after definitive chemo-radiotherapy.

The Relative Role of Biological Factors in Chemo-Radiotherapy Outcomes in HNSCC

The biological markers have been tested independently of each other and most are significantly associated with patient outcome thereby supporting their role in HNSCC and treatment response. However, tumor biology and determinants of radioresistance are multifactorial and may depend on the context and relation to each other. We therefore aimed to identify the most relevant markers in a multivariable analysis. To this end we used a backward selection method. This method creates a Cox proportional hazard model using all available factors. It then iteratively eliminates the least relevant factor until no further decrease in AIC, a measure of model performance, is possible. From these analyses (**Supplementary Table 4**), we conclude that chronic hypoxia, EGFR expression, CD8+/Treg, T-cell infiltration, and CD44 are the most relevant biological factors that are associated with locoregional control. Multivariable analyses (**Figure 4**) also demonstrate that they are independent from relevant clinical factors such as cumulative cisplatin dose or sex. Cisplatin dose, age and sex are the clinical factors most associated with locoregional control in this cohort (**Figure 4**

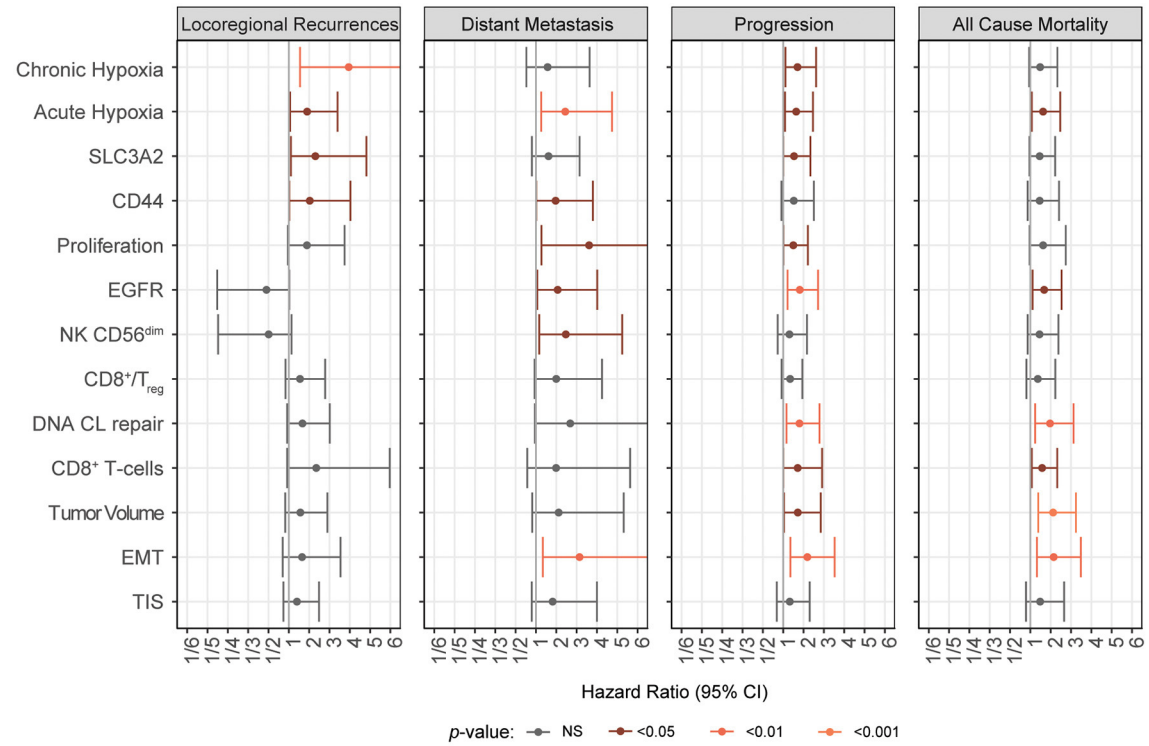

FIGURE 3 | Relevance of biological markers for HNSCC chemo-radiotherapy outcomes. Forest plots comparing individual biological markers across different outcome endpoints are shown. Hazard Ratios for locoregional recurrences, distant metastasis, disease progression and death are from multivariate Cox proportional hazard analyses of the dichotomized cohorts using bootstrap analysis defined cut-offs for all outcomes analyzed in this study. For each marker the "low" score or low expression group was used as reference. Each individual model contained the same clinical variables as those used to determine the cut-off. Only the biological markers are shown.

and **Supplementary Table 4**). Broadly consistent with the results from the multivariate analyses that were performed on the biomarkers on an individual basis, EGFR and immune cell related factors remain important in instituting an increased risk for distant metastasis, while chronic hypoxia and CD44 are less relevant. Instead, tumor EMT and proliferation affects progression free survival most profoundly and independent of other important factors such as tumor volume or cisplatin dose (**Supplementary Figure 8** and **Supplementary Table 4**). The consistent worse prognosis and distant metastasis association of patients with tumors that score high in the $CD8^+$ T cells and related gene expression signatures is remarkable. High $CD8^+$ T cell scores, as determined by these signatures or by immunohistochemistry, have been reported to be linked to good prognosis in other heterogeneous HNSCC cohorts (6, 56, 77) and prompted us to analyze this further (**Supplementary Figures 9**, **10**). These analyses suggest that the lack of a good prognosis association could be based on the absence of HPV-positive HNSCC which show overall higher CD8 expression and $CD8^+$ T-cell signature scores in the TCGA cohort (**Supplementary Figure 9A**). Within the HPV-positive group, high CD8 expression is strongly associated with good prognosis (**Supplementary Figure 9B**). Notably, CD8A/B expression and $CD8^+$ T-cell signature values do not correlate well (**Supplementary Figure 10**). Interestingly, the observed outcome associations in HPV-negative HNSCC appear to be dependent on cumulative cisplatin dose (**Supplementary Figure 10**).

The obvious divergence in the biomarker associations with local treatment outcomes compared to DM development risks prompted us to investigate this further. Unable to classify patients according to "true" biological parameter classes, we relied on bootstrapping methods to provide cut-offs for each outcome endpoints. As described above those resulted to be largely different in some cases such as for EGFR expression and pointed to a different influence in the respective biological mechanisms. We therefore compared the biological markers with respect to their influence in locoregional control or DM risk in a less cutoff-dependent manner by computing the AUC of the hazard ratio plots from multivariable regression analysis with clinical variables (**Supplementary Figure 11**). **Figure 5** shows an overview of the impact of the individual biological parameters on locoregional control or distant metastasis risk. This analysis highlights the difference in the collection of the most relevant survival determinants for each outcome endpoint. Notably, locoregional control is mainly determined by chronic hypoxia, but also acute hypoxia. CD44 expression and $CD8^+$ T-cell/Treg ratio are more relevant to LRC than DM, whereas distant

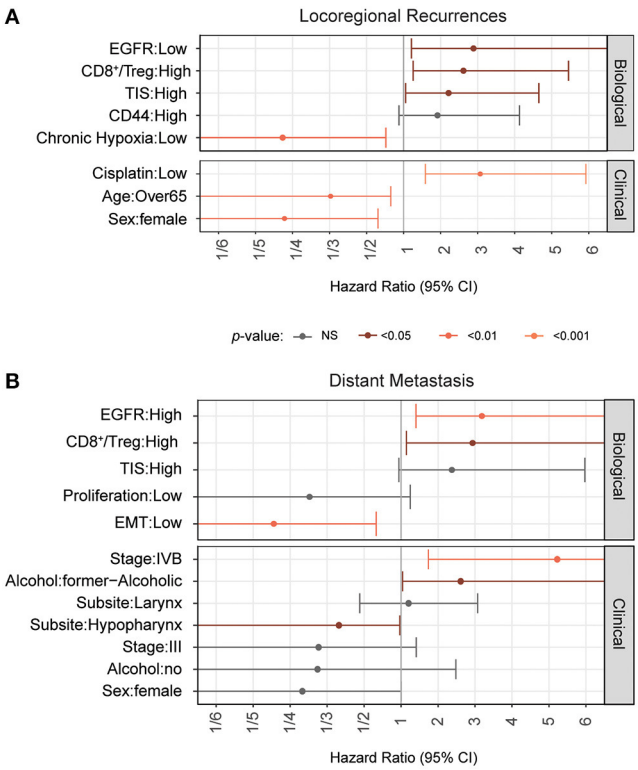

FIGURE 4 | Relative role of biological markers in combined analyses. Forest plots with results from full multivariate Cox Proportional Hazards models are shown. The model was generated using a backward selection procedure. The most frequent level was used as the reference level for this analysis. A Cox proportional hazard model was fit that included all biological markers and clinical variables. Then, each variable was individually eliminated from the model and improvements in model performance were assessed. This process was repeated with the best performing models until the removal of variables did no longer improve the models. Hazard ratios for locoregional recurrences **(A)** and distant metastasis **(B)** as determined by the final model are shown.

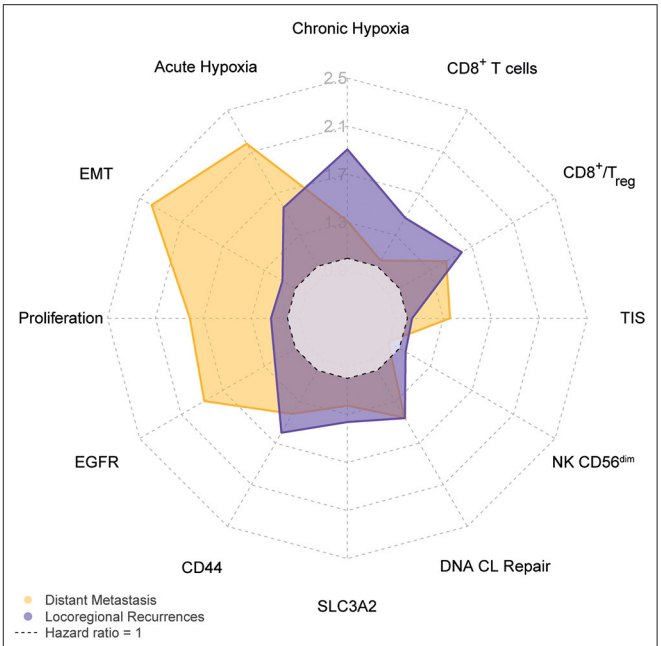

FIGURE 5 | Divergence in biological parameter role for locoregional or distant control. The spider plot depicts the average hazard ratio as obtained after testing all possible cutoffs in a multivariable Cox proportional hazard analysis that included relevant clinical factors as shown in **Supplementary Figure 8** and described in Materials and Methods. Hazard ratios for locoregional recurrences are shown in purple and distant metastasis hazard ratios in yellow.

metastasis is predominantly influenced by EMT, acute hypoxia, proliferation and EGFR status.

DISCUSSION

Here, we aimed to evaluate the relevance and interrelation of biological factors known to influence radiation response as determined in preclinical studies. Limited by the size of the study cohort, we restricted the study to markers for which discriminative power has been reported in clinical data in HNSCC and added clinical or biological factors that have shown an important association with radiotherapy outcomes. Using RNA-sequencing data from a large and relative uniform cohort of 197 HPV-negative advanced stage HNSCC patients that were all treated with cisplatin-based chemo-radiotherapy, we find an important role of immune cell (T cell) markers in locoregional control which suggests a role in radiation response. We also show that chronic and acute hypoxia are robustly associated with locoregional control. Similarly, we validated the equally important role of CD44 and SCL3A2, in part related to stem cells, in our study cohort. When assessed in combination, hypoxia, immune cells, EGFR are the most discriminating independent factors in LRC. For DM, those also include EMT. Overall, considered in the context of clinical factors and each other, our study underscores the relevance of many of these biological factors in HNSCC chemo-radiotherapy outcomes.

To advance previous findings on determinants of chemo-radiotherapy outcomes and to prioritize prognostic markers for multi-parametric prediction models, we focused on (i) the validation of expression-based prognostic markers in the chemo-radiotherapy setting and (ii) the evaluation of their complementarity and (iii) the assessment of any dependence to important clinical or other biologic factors. Many HNSCC studies highlight the role of biology for outcome (3–6, 78). A major drawback however for many of such studies is the heterogeneity of the HNSCC patient cohorts or a lack of contextual analyses (78). If focused on tumor site they often encompass many different treatments or if focused on treatment they combine different tumor sites, HPV-negative and positive. Large multicentric studies are therefore valuable contributions to the field (12, 13, 15, 16, 57) that provide insights to the biology of HNSCC and its link to patient outcome (5, 6, 27, 28, 79, 80). Clinical factors are important (81, 82) but are often not considered in multivariable analyses (78, 83). A lack of tumor volume data for example, even though clearly linked to LRC (81, 84–86), impedes the assessment of a role for or a bias from tumor volumes in such analyses. To minimize such treatment or tumor site related bias due to possible interactions; we deliberately

excluded the biologically distinct oral cavity and HPV-positive oropharyngeal HNSCC (14, 16, 87–90) in our study. Our cohort also solely comprises definitive chemo-radiotherapy-treated advanced HNSCC. In contrast to predetermined gene sets in nanostring technologies, the availability of full transcriptomic data by RNA-Seq allowed us to test selected gene expressions and signatures related to the biological processes that we queried. Together we were able to show that most of the selected markers or marker categories are not related, are independently linked to outcome and that outcome associations are not based on links with known important clinical factors. Overall, we observed little or no influence or interactions with clinical factors, with the notable exception of tumor volume and cumulative cisplatin dose, factors often not accounted for in other biomarker studies. While correlations within the immune markers were expected, here we reveal an association with acute hypoxia scores which in turn appears to be linked to proliferation. Such relations or complementarities can alter the prognostic value or impede a discrimination of the true source of the observed outcome relevance. It however highlights the importance to study such markers in the context of each other and within the same cohort. Overall, our study pinpoints expression markers that should be considered as valuable contributors of future multi-parametric prediction models that combine clinical, radiologic, pathological and genetic variables for improved prognosis in advanced HPV-negative HNSCC (91, 92).It is difficult to discern factors that determine tumor radioresistance (83). A comparison of similar patient cohorts treated without or with different doses of radiotherapy would be required to strengthen such a link. Since cisplatin-based chemo-radiotherapy has become a standard treatment for HNSCC to improve quality of life by achieving organ preservation, surgically resected HNSCC patients with similar clinical tumor characteristics are rare, impeding such comparisons. However, in the absence of a comparable but non-radiotherapy treated study cohort, differences in LRC (mostly achieved by radiotherapy) as defined by the biomarker classification, can suggest a role in radiation response. In our study, we assured that important clinical factors that impact patient outcomes have been considered to limit bias or dependence. DM events may have occurred prior to LRC events and could have masked a greater impact in radiation response, such as in the case of acute hypoxia that also shows a strong association with DM. The comparison of LRC with DM further helped to discern a more radiation response specific role from a role in metastasis. Our data here and those reported by us and others do indeed confirm the role of hypoxia in determining radiation response as reflected by the LRC rates (25, 27, 29). In addition, hypoxia has been also implicated in tumor cell invasiveness, facilitating dissemination, and has been therefore associated with metastasis formation, a role that is also evident from our DM analyses. Similarly, we have recently shown that HNSCC cell lines with DNA crosslink repair defects are more migratory and invasive (63), a feature that may explain the association with DM prognosis but could also result in a greater regional spread and failure of locoregional control.

After the initial EGFR studies in clinic and the success of cetuximab combinations (40, 93, 94), cetuximab in HNSCC and the role of EGFR amplification and expression have been disputed since then (95). Most of these studies focused on the very high expressing or used a median cut-off to detect an association with the clinical endpoints analyzed. Here we see a clear role for EGFR in the outcome data when also considering hypoxia and other factors in multivariable analyses. Average to high EGFR expression, is linked to improved LRC when analyzed individually. The association of a low EGFR expressing group with poor LRC however becomes much clearer in the combined multivariable analyses that integrated all relevant biomarkers. It epitomizes the importance of combined analysis, as the prevalence of other, also clinical, factors in the different EGFR expression classified groups may have shifted or masked a possible influence in other studies if not accounted for, as revealed here. Given its role in promoting cell cycle progression, it is conceivable that increased EGFR levels mediate an increase in tumor repopulation between fractions; a radiotherapy response determining process that is counteracted by radiotherapy treatment acceleration or concurrent chemotherapy. This process is therefore limited in our patient population in contrast to some earlier studies that analyzed the influence of EGFR (96). Notably, the association with improved LRC is still discernible (HR = 0.57, $p = 0.067$) when reanalyzing the data using the higher EGFR expression cut-off that was used for the DM data. DM HR values however drop to 0.57 ($p = 0.2$) showing a DM link only in the top 25% EGFR expression group (HR = 3.19, $p = 0.0056$). This more aggressive nature of highly EGFR expressing tumors is consistent with other reports in HNSCC and other cancer types (97).

Our study is limited by statistical constraints due to the cohort size. This enforced us to limit the biological variables and apply selection processes such as the bootstrapping analyses. Yet, it becomes evident that the prognostic value of many of the factors could be validated in our cohort and withstood multivariable analyses with the important clinical variables. Among the clinical variables, we observe a trend toward poor outcomes in current smokers, however this does not reach significance in our cohort. Low numbers in the former smoker category but also the lack of more accurate smoking status values may have decreased the power to reveal the reported association with smoking (79, 98, 99). Since we focused on known determinants of radiation response, other biomarkers were not included despite their relevance or prognostic value in HNSCC (5, 6, 16, 100–106). Some, such as tumor mutational burden (TMB) are prevalent in laryngeal and HPV-negative pharyngeal HNSCC (14) but require DNA sequencing data. TMB was found to be associated with poor prognosis in HPV-negative chemo-radiotherapy treated patients in our previous study (36) and more strongly so in a cohort of patients that also included oral cavity cancers and HPV-positive oropharyngeal (107). Interestingly, low immune cell infiltration or CD8+ T cell values, as assessed by gene expression, have been assigned to HNSCC high in TMB or mutational signatures related to smoking (56, 107).

Other limitations result from technical challenges. Here we detect different biological processes and factors in clinical samples by using published and validated expression signatures—that are linked to these processes. These gene expression signatures may not be perfect identification tools for

the specific biology in question (83); however they often reflect the abundance of certain biological elements well (108, 109). The DNA CL repair defect prediction model has for example been generated using functional endpoints and then validated in independent cell line panels or by genetic modification. On the other hand, markers such as CD44 are less clear defined. CD44 expression is associated with stem cell-ness in tumor cells (110), but it is also expressed under hypoxic conditions or in epithelial cells and is a marker for effector memory T cells (45). Therefore, it is particularly interesting to observe the correlation with SLC3A2 another stem cell related marker in our samples which confirms its link to tumor stem cell abundance. Notably, we find a correlation between acute hypoxia and TIS or $CD8^+$ T-cell scores, suggesting a higher T-cell content in acute hypoxic areas or tumors which could be proposed to be driven by hypoxia induced inflammatory cytokine release (111). This T-cell/acute hypoxia correlation may in part also be responsible for the consistent poor outcome association of the $CD8^+$ T-cell gene expression signatures. Reiterating the role of technical limitations, it should be noted that these gene expression signatures were based on transcriptional profiles of purified immune cell subsets. Through multiple adaptation steps, they evolved to markers that allowed further discrimination in the context of colorectal carcinoma and HNSCC (56, 75, 76). In terms of identification accuracy there are potential challenges with such technical approaches that can also explain discrepancies with immunohistochemistry determined factors. It is evident that the tumor context affects gene expression of the immune cells and, on the other hand, tumor gene expression features, if present in these signatures, can compound the identification. For instance, the $CD8^+$ T cell signature includes ZEB1 expression, a protein involved in EMT and a poor prognostic factor in HNSCC (56, 76, 112–115). We therefore assessed CD8A and B gene expression in our samples as a simple surrogate for $CD8^+$ T cells and show its limited complementarity with the $CD8^+$ T cell signature score and associations with outcome. The better LRC outcome of patients with CD8 positive tumors in the low cumulative cisplatin patient category is in line with previous report based on IHC (116) The lack of an association with outcome in patients that received high cisplatin doses however demonstrates treatment dependence and explains the discrepancy to other studies (6, 77) when considering this clinical variable in our cisplatin treated cohort. Despite a significant but weak correlation with CD8A expression, high $CD8^+$ T cell signature values are associated with poor outcomes, demonstrating the influence of the other features in this discriminating signature. Immune cell identification by gene expression may not be flawless. Yet, together, our data indicate a prognosis association that is linked to this particular patient treatment. One could speculate that hematologic toxicities associated with cisplatin administration could contribute to this pattern by abolishing the benefit from an immune cell rich tumor status in these individuals. On the other hand, recent studies suggest an enhancement of antitumor immunity by cisplatin that could also diminish the impact of the pre-treatment immune status (117, 118). While the primary emphasis for prognostic biomarkers lays in the discriminatory power to predict patient outcome, the focus of biomarkers for targeting opportunities is the achievement of an accurate representation of the marked biological process or elements. The signatures used here were selected based on their reported association with both immune cell infiltration and prognosis in HNSCC (56, 76). Yet the question remains whether they reflect $CD8^+$ T cell infiltration well.

Interestingly, we did find a seemingly independent and consistent role for $CD8^+$, non-regulatory, T cells in our study cohort. Observed for resected HNSCC in overall survival outcome data before, here we show an association with both, LRC and DM, in chemo-radiotherapy treated HNSCC patients indicating those with a high abundance of such T cells to have a worse prognosis. To our knowledge this poor prognosis association with radiation response has not been reported previously (6, 77, 119). As detailed above, this discrepancy with other studies is only in part explained by the used technology (116, 120) (IHC CD8 expression vs. gene expression signatures) since the signatures showed a good prognosis association in the Mandal et al. (56). Careful inspection of the TCGA data revealed increased $CD8^+$ T-cell gene expression signature scores in the HPV-positive oropharyngeal that drive the good prognosis association. A pattern observed in other studies as well (56, 77, 121–124). Mandal et al. adjusted for HPV-associated outcome differences, which does not account for a possible interaction between the two variables (56). The CD8A and B expression HR plots in our analyses however suggest a stronger effect in the HPV-positive subgroup. Despite obvious evaluation challenges when using the different techniques and associated cut-offs, a similar argument applies to other studies based on immunohistochemistry determined $CD8^+$ T cell infiltration values. A significant HPV status association got lost in multivariable analyses that indicated a good prognosis association of $CD8^+$ T cells in oropharyngeal squamous cell carcinoma patients (59). Yet, some studies also show a good prognosis association with TIS or $CD8^+$ T cells in HPV-negative patients using other scorings, cut offs and expression signatures (125). Since the effect size can be small, patient treatment associations with survival are often not significant in small studies. Treatment could however alter prognosis in subsets of patients. For instance, patients with tumors with DNA crosslink repair defects benefit most from a high cumulative cisplatin dose (63). Similarly, possible immune cell infiltration links could depend on treatment. Despite worse PFS in cases that lack or show minimal CD8A or CD8B expression, we cannot observe the previously reported poor prognosis link in $CD8^+$ T cell signature low patients in our cohort. No associations between TIS or $CD8^+$ scores and clinical variables were found; and outcome association links derived from the correlation with acute hypoxia should have been accounted for by the multivariable analyses. Together, our data suggest a role for HNSCC treatment, in particular cisplatin, in immune cell infiltration determined outcomes. Early cancer immunotherapy trials in HNSCC with immune checkpoint inhibitors demonstrate a benefit and underscore the potential value of immune response and chemo-radiotherapy relevant biomarkers to identify patients that will benefit from such treatments (24, 126–134). Larger comparative studies are

therefore needed to disentangle the role of $CD8^+$ T cells in the individual genetic HNSCC context and the important clinical variables connected to its role in patient outcome (78, 83, 135).

Our patient cohort is fairly unique in that it consists of definitive chemoradiotherapy treated advanced HNSCC patients. Based exclusively on resected HNSCC, these cases are unfortunately not present in the TCGA data. Supported by the detailed clinical data and follow up, this allowed us to elaborate on the role of biological determinants of chemoradiotherapy response. A quarter of the patients suffered from loco regional recurrences after treatment; a treatment success rate that further stresses the relevance of the biological factors found to determine treatment failure. This study does not provide or test clinically applicable prognostic markers. It was designed to compare the individual factors in relation to each other to assess and understand their influence in HNSCC outcome. Optimal cutoffs identified by the bootstrapping method and illustrated in the hazard ratio plots require validation for further development into true prognostic markers. Based on our results, future studies should focus on the elaboration of prognostic models that incorporate these biological markers together with important clinical factors. The multivariable outcome association results and the lack of correlations suggest that these future models should include all biological factors. Discrepancy in the optimal cutoff values further points to the value of non-dichotomized variables in such efforts and also reveals a possible cause of incongruent outcome associations in previous studies. The value of the clinical factors is exemplified by the fact that some biological markers (i.e., DNA CL repair or $CD8^+$ T cells) lose their strength in patients groups with a high cumulative cisplatin dose.

While tumor stem cell targeting agents are still under development, some of the other biological factors are targetable. Next to high-dose alkylating agents, PARP inhibitors may help to exploit DNA CL repair defects (62) and different immunotherapy options are currently being tested in the HNSCC setting (136). The value of such biological markers in personalized treatments remains to be determined; however our study demonstrates that those patients are in need of improved therapy options.

In conclusion, this multicentric external validation study confirms the important and independent role of biological factors that embody hypoxia, stem cell-ness, tumor growth, EMT and DNA repair for locoregional control in chemoradiotherapy treated patients. The multifactorial analyses results highlight the need to consider these biomarkers in the context of each other and also revealed an important role for immune cell abundance in HNSCC treatment outcome.

DATA AVAILABILITY STATEMENT

The data in this study is available the European Genome-phenome Archive (https://www.ebi.ac.uk/ega/) with the accession numbers: EGAD00001005721, EGAD00001005715, EGAD00001005716, EGAD00001005717, and study number EGAS00001004090.

ETHICS STATEMENT

The studies involving human participants were reviewed and approved by Institutional Review Board The Netherlands Cancer Institute, Amsterdam, The Netherlands; Institutional Review Board VuMC, Amsterdam, The Netherlands; Institutional Review Board Maastro, Maastricht, The Netherlands. The patients/participants provided their written informed consent to participate in this study.

AUTHOR CONTRIBUTIONS

CVen, MH, PE, and MJ contributed to the conception and design of the study. MH, RR, CVer, OH-V, FH, PL, HB, CL, MV, RB, and MB contributed to the acquisition of data. MH, RR, and FH established and/or curated databases. PE, MH, and SS performed data analysis. MH, CVen, PE, and MJ contributed to data interpretation. CVen, MH, and PE wrote the first draft of the manuscript. All authors contributed to manuscript revisions and approved the submitted version.

FUNDING

Authors acknowledge financial support from the Dutch Cancer Society (KWF-A6C7072, acronym DESIGN), from the EU 7th framework program (no 257144, acronym ARTFORCE) and the ERC advanced grant (no 694812, acronym Hypoximmuno).

ACKNOWLEDGMENTS

The authors are grateful for financial support from Brunel and Verwelius and would like to thank the NKI Genomics Core Facility for performing RNA sequencing, the NKI RHPC facility for providing computational resources and the Core Facility-Molecular Pathology and Biobank (CFMPB) for collecting and preparing tissue samples.

SUPPLEMENTARY MATERIAL

The Supplementary Material for this article can be found online at: https://www.frontiersin.org/articles/10.3389/fonc.2019.01470/full#supplementary-material

REFERENCES

1. Baumann M, Krause M, Overgaard J, Debus J, Bentzen SM, Daartz J, et al. Radiation oncology in the era of precision medicine. *Nat Rev Cancer*. (2016) 16:234–49. doi: 10.1038/nrc.2016.18
2. van der Kogel A. *Basic Clinical Radiobiology, 4th edn*. London: CRC Press (2009). doi: 10.1201/b13224
3. Alsahafi E, Begg K, Amelio I, Raulf N, Lucarelli P, et al. Clinical update on head and neck cancer: molecular biology and ongoing challenges. *Cell Death Dis*. (2019) 10:540. doi: 10.1038/s41419-019-1769-9

4. Leemans CR, Braakhuis BJM, Brakenhoff RH. The molecular biology of head and neck cancer. *Nat Rev Cancer*. (2011) 11:9–22. doi: 10.1038/nrc2982
5. Economopoulou P, de Bree R, Kotsantis I, Psyrri A. Diagnostic tumor markers in head and neck squamous cell carcinoma (HNSCC) in the clinical setting. *Front Oncol*. (2019) 9:827. doi: 10.3389/fonc.2019.00827
6. Budach V, Tinhofer I. Novel prognostic clinical factors and biomarkers for outcome prediction in head and neck cancer: a systematic review. *Lancet Oncol*. (2019) 20:e313–26. doi: 10.1016/S1470-2045(19)30177-9
7. Kang H, Kiess A, Chung CH. Emerging biomarkers in head and neck cancer in the era of genomics. *Nat Rev Clin Oncol*. (2015) 12:11–26. doi: 10.1038/nrclinonc.2014.192
8. Petersen JF, Timmermans AJ, van Dijk BAC, Overbeek LIH, Smit LA, Hilgers FJM, et al. Trends in treatment, incidence and survival of hypopharynx cancer: a 20-year population-based study in the Netherlands. *Eur Arch Oto Rhino Laryngol*. (2018) 275:181–9. doi: 10.1007/s00405-017-4766-6
9. Timmermans AJ, van Dijk BAC, Overbeek LIH, van Velthuysen M-LF, van Tinteren H, Hilgers FJM, et al. Trends in treatment and survival for advanced laryngeal cancer: a 20-year population-based study in The Netherlands. *Head Neck*. (2015) 38 (Suppl. 1):E1247–55. doi: 10.1002/hed.24200
10. Price KAR, Cohen EE. Current treatment options for metastatic head and neck cancer. *Curr Treat Options Oncol*. (2012) 13:35–46. doi: 10.1007/s11864-011-0176-y
11. Huang SH, O'Sullivan B. Overview of the 8th Edition TNM classification for head and neck cancer. *Curr Treat Options Oncol*. (2017) 18:40. doi: 10.1007/s11864-017-0484-y
12. Lawrence MS, Sougnez C, Lichtenstein L, Cibulskis K, Lander E, Gabriel SB, et al. Comprehensive genomic characterization of head and neck squamous cell carcinomas. *Nature*. (2015) 517:576–82. doi: 10.1038/nature14129
13. Stransky N, Egloff AM, Tward AD, Kostic AD, Cibulskis K, Sivachenko A, et al. The mutational landscape of head and neck squamous cell carcinoma. *Science*. (2011) 333:1157–60. doi: 10.1126/science.1208130
14. Vossen DM, Verhagen CVM, Verheij M, Wessels LFA, Vens C, van den Brekel MWM. Comparative genomic analysis of oral versus laryngeal and pharyngeal cancer. *Oral Oncol*. (2018) 81:35–44. doi: 10.1016/j.oraloncology.2018.04.006
15. Agrawal N, Frederick MJ, Pickering CR, Bettegowda C, Chang K, Li RJ, et al. Exome sequencing of head and neck squamous cell carcinoma reveals inactivating mutations in NOTCH1. *Science*. (2011) 333:1154–7. doi: 10.1126/science.1206923
16. Dogan S, Xu B, Middha S, Vanderbilt CM, Bowman AS, Migliacci J, et al. Identification of prognostic molecular biomarkers in 157 HPV-positive and HPV-negative squamous cell carcinomas of the oropharynx. *Int J Cancer*. (2019) 145:3152–62. doi: 10.1002/ijc.32412
17. Theelen WSME, Peulen HMU, Lalezari F, van der Noort V, de Vries JF, Aerts JGJV, et al. Effect of pembrolizumab after stereotactic body radiotherapy vs pembrolizumab alone on tumor response in patients with advanced non–small cell lung cancer. *JAMA Oncol*. (2019) 5:1276–82. doi: 10.1001/jamaoncol.2019.1478
18. Ngwa W, Irabor OC, Schoenfeld JD, Hesser J, Demaria S, Formenti SC. Using immunotherapy to boost the abscopal effect. *Nat Rev Cancer*. (2018) 18:313–22 doi: 10.1038/nrc.2018.6
19. Tinhofer I, Budach V, Johrens K, Keilholz U. The rationale for including immune checkpoint inhibition into multimodal primary treatment concepts of head and neck cancer. *Cancers Head Neck*. (2016) 1:8. doi: 10.1186/s41199-016-0009-6
20. Bristow RG, Alexander B, Baumann M, Bratman SV, Brown JM, Camphausen K, et al. Combining precision radiotherapy with molecular targeting and immunomodulatory agents: a guideline by the American Society for Radiation Oncology. *Lancet Oncol*. (2018) 19:e240–51. doi: 10.1016/S1470-2045(18)30096-2
21. Swart M, Verbrugge I, Beltman JB. Combination approaches with immune-checkpoint blockade in cancer therapy. *Front Oncol*. (2016) 6:233. doi: 10.3389/fonc.2016.00233
22. Canning M, Guo G, Yu M, Myint C, Groves MW, Byrd JK, Cui Y. Heterogeneity of the head and neck squamous cell carcinoma immune landscape and its impact on immunotherapy. *Front Cell Dev Biol*. (2019) 7:52. doi: 10.3389/fcell.2019.00052
23. Economopoulou P, Agelaki S, Perisanidis C, Giotakis EI, Psyrri A. The promise of immunotherapy in head and neck squamous cell carcinoma. *Ann Oncol Off J Eur Soc Med Oncol*. (2016) 27:1675–85. doi: 10.1093/annonc/mdw226
24. Solomon B, Young RJ, Rischin D. Head and neck squamous cell carcinoma: genomics and emerging biomarkers for immunomodulatory cancer treatments. *Semin Cancer Biol*. (2018) 52:228–40. doi: 10.1016/j.semcancer.2018.01.008
25. Toustrup K, Sørensen BS, Nordsmark M, Busk M, Wiuf C, Alsner J, Overgaard J. Development of a hypoxia gene expression classifier with predictive impact for hypoxic modification of radiotherapy in head and neck cancer. *Cancer Res*. (2011) 71:5923–31. doi: 10.1016/S0167-8140(11)70012-3
26. Tawk B, Schwager C, Deffaa O, Dyckhoff G, Warta R, Linge A, et al. Comparative analysis of transcriptomics based hypoxia signatures in head-and neck squamous cell carcinoma. *Radiother Oncol*. (2016) 118:350–8. doi: 10.1016/j.radonc.2015.11.027
27. Linge A, Lohaus F, Löck S, Nowak A, Gudziol V, Valentini C, et al. HPV status, cancer stem cell marker expression, hypoxia gene signatures and tumour volume identify good prognosis subgroups in patients with HNSCC after primary radiochemotherapy: A multicentre retrospective study of the German Cancer Consortium Radiation. *Radiother Oncol*. (2016) 121:364–73. doi: 10.1016/j.radonc.2016.11.008
28. Linge A, Lock S, Gudziol V, Nowak A, Lohaus F, von Neubeck C, et al. Low cancer stem cell marker expression and low hypoxia identify good prognosis subgroups in HPV(-) HNSCC after postoperative radiochemotherapy: a multicenter study of the DKTK-ROG. *Clin Cancer Res*. (2016) 22:2639–49. doi: 10.1158/1078-0432.CCR-15-1990
29. van der Heijden M, de Jong MC, Verhagen CVM, de Roest RH, Sanduleanu S, Hoebers F, et al. Acute hypoxia profile is a stronger prognostic factor than chronic hypoxia in advanced stage head and neck cancer patients. *Cancers*. (2019) 11:E583. doi: 10.3390/cancers11040583
30. Rademakers SE, Hoogsteen IJ, Rijken PF, Oosterwijk E, Terhaard CH, Doornaert PA, et al. Pattern of CAIX expression is prognostic for outcome and predicts response to ARCON in patients with laryngeal cancer treated in a phase III randomized trial. *Radiother Oncol*. (2013) 108:517–22. doi: 10.1016/j.radonc.2013.04.022
31. Thomson D, Yang H, Baines H, Miles E, Bolton S, West C, et al. NIMRAD - A phase III trial to investigate the use of nimorazole hypoxia modification with intensity-modulated radiotherapy in head and neck cancer. *Clin Oncol*. (2014) 26:344–7. doi: 10.1016/j.clon.2014.03.003
32. Kaanders JHAM, Bussink J, Van der Kogel AJ. ARCON: a novel biology-based approach in radiotherapy. *Lancet Oncol*. (2002) 3:728–37. doi: 10.1016/S1470-2045(02)00929-4
33. Overgaard J. Hypoxic modification of radiotherapy in squamous cell carcinoma of the head and neck - A systematic review and meta-analysis. *Radiother Oncol*. (2011) 100:22–32. doi: 10.1016/S0167-8140(11)70167-0
34. Overgaard J, Hansen HS, Specht L, Overgaard M, Grau C, Andersen E, et al. Five compared with six fractions per week of conventional radiotherapy of squamous-cell carcinoma of head and neck: DAHANCA 6&7 randomised controlled trial. *Lancet*. (2003) 362:933–40. doi: 10.1016/S0140-6736(03)14361-9
35. Bentzen SM, Thames HD. Clinical evidence for tumor clonogen regeneration: interpretations of the data. *Radiother Oncol*. (1991) 22:161–6. doi: 10.1016/0167-8140(91)90019-D
36. Vossen DM, Verhagen CVM, Van Der Heijden M, Essers PBM, Bartelink H, Verheij M, et al. Genetic factors associated with a poor outcome in head and neck cancer patients receiving definitive chemoradiotherapy. *Cancers*. (2019) 11:E445. doi: 10.3390/cancers11040445
37. Ang KK. Multidisciplinary management of locally advanced SCCHN: optimizing treatment outcomes. *Oncologist*. (2008) 13:899–910. doi: 10.1634/theoncologist.2007-0157
38. Bonner JA, Harari PM, Giralt J, Cohen RB, Jones CU, Sur RK, et al. Radiotherapy plus cetuximab for locoregionally advanced head and neck cancer. *Lancet Oncol*. (2010) 11:21–8. doi: 10.1016/S1470-2045(09)70311-0
39. Bentzen SM, Atasoy BM, Daley FM, Dische S, Richman PI, Saunders MI, et al. Epidermal growth factor receptor expression in pretreatment biopsies from head and neck squamous cell carcinoma as a predictive factor for a

benefit from accelerated radiation therapy in a randomized controlled trial. *J Clin Oncol*. (2005) 23:5560–7. doi: 10.1200/JCO.2005.06.411
40. Bossi P, Resteghini C, Paielli N, Licitra L, Pilotti S, Perrone F. Prognostic and predictive value of EGFR in head and neck squamous cell carcinoma. *Oncotarget*. (2016) 7:74362–79. doi: 10.18632/oncotarget.11413
41. Xu MJ, Johnson DE, Grandis JR. EGFR-targeted therapies in the post-genomic era. *Cancer Metastasis Rev*. (2017) 36:463–73. doi: 10.1007/s10555-017-9687-8
42. Juergens RA, Bratman SV, Tsao M-S, Laurie SA, Sara Kuruvilla M, Razak ARA, Hansen AR. Biology and patterns of response to EGFR-inhibition in squamous cell cancers of the lung and head & neck. *Cancer Treat Rev*. (2017) 54:43–57. doi: 10.1016/j.ctrv.2017.01.003
43. Taberna M, Oliva M, Mesia R. Cetuximab-containing combinations in locally advanced and recurrent or metastatic head and neck squamous cell carcinoma. *Front Oncol*. (2019) 9:383. doi: 10.3389/fonc.2019.00383
44. Starmans MHW, Krishnapuram B, Steck H, Horlings H, Nuyten DSA, Van De Vijver MJ, et al. Robust prognostic value of a knowledge-based proliferation signature across large patient microarray studies spanning different cancer types. *Br J Cancer*. (2008) 99:1884–90. doi: 10.1038/sj.bjc.6604746
45. De Jong MC, Pramana J, Van Der Wal JE, Lacko M, Peutz-Kootstra CJ, De Jong JM, et al. CD44 expression predicts local recurrence after radiotherapy in larynx cancer. *Clin Cancer Res*. (2010) 16:5329–38. doi: 10.1158/1078-0432.CCR-10-0799
46. Linge A, Schmidt S, Lohaus F, Krenn C, Bandurska-Luque A, Platzek I, et al. Independent validation of tumour volume, cancer stem cell markers and hypoxia-associated gene expressions for HNSCC after primary radiochemotherapy. *Clin Transl Radiat Oncol*. (2019) 16:40–7. doi: 10.1016/j.ctro.2019.03.002
47. Baumann M, Krause M, Hill R. Exploring the role of cancer stem cells in radioresistance. *Nat Rev Cancer*. (2008) 8:545–54. doi: 10.1038/nrc2419
48. Krause M, Dubrovska A, Linge A, Baumann M. Cancer stem cells: radioresistance, prediction of radiotherapy outcome and specific targets for combined treatments. *Adv Drug Deliv Rev*. (2017) 109:63–73. doi: 10.1016/j.addr.2016.02.002
49. Krause M, Yaromina A, Eicheler W, Koch U, Baumann M. Cancer stem cells: targets and potential biomarkers for radiotherapy. *Clin Cancer Res*. (2011) 17:7224–9. doi: 10.1158/1078-0432.CCR-10-2639
50. Chen H-Y, Xu L, Li L-F, Liu X-X, Gao J-X, Bai Y-R. Inhibiting the CD8 + T cell infiltration in the tumor microenvironment after radiotherapy is an important mechanism of radioresistance. *Sci Rep*. (2018) 8:11934. doi: 10.1038/s41598-018-30417-6
51. Gupta A, Probst HC, Vuong V, Landshammer A, Muth S, Yagita H, et al. Radiotherapy promotes tumor-specific effector CD8 + T cells via dendritic cell activation. *J Immunol*. (2012) 189:558–66. doi: 10.1158/1538-7445.TUMIMM2012-B1
52. Ran X, Yang K. Inhibitors of the PD-1/PD-L1 axis for the treatment of head and neck cancer: current status and future perspectives. *Drug Des Devel Ther*. (2017) 11:2007–14. doi: 10.2147/DDDT.S140687
53. Moskovitz J, Moy J, Ferris RL. Immunotherapy for head and neck squamous cell carcinoma. *Curr Oncol Rep*. (2018) 20:22. doi: 10.1007/s11912-018-0654-5
54. Economopoulou P, Kotsantis I, Psyrri A. Checkpoint inhibitors in head and neck cancer: rationale, clinical activity, and potential biomarkers. *Curr Treat Options Oncol*. (2016) 17:40. doi: 10.1007/s11864-016-0419-z
55. Van Limbergen EJ, De Ruysscher DK, Pimentel VO, Marcus D, Berbee M, Hoeben A, et al. Combining radiotherapy with immunotherapy: the past, the present and the future. *Br J Radiol*. (2017) 90:20170157. doi: 10.1259/bjr.20170157
56. Mandal R, Senbabaoglu Y, Desrichard A, Havel JJ, Dalin MG, Riaz N, et al. The head and neck cancer immune landscape and its immunotherapeutic implications. *JCI Insight*. (2016) 1:e89829. doi: 10.1172/jci.insight.89829
57. Balermpas P, Rodel F, Rodel C, Krause M, Linge A, Lohaus F, et al. CD8+ tumour-infiltrating lymphocytes in relation to HPV status and clinical outcome in patients with head and neck cancer after postoperative chemoradiotherapy: a multicentre study of the German cancer consortium radiation oncology group (DKTK-ROG). *Int J Cancer*. (2016) 138:171–81. doi: 10.1002/ijc.29683
58. Ono T, Azuma K, Kawahara A, Akiba J, Kakuma T, Chitose S, et al. Pre-treatment CD8(+) tumour-infiltrating lymphocyte density predicts distant metastasis after definitive treatment in patients with stage III/IV hypopharyngeal squamous cell carcinoma. *Clin Otolaryngol*. (2018) 43:1312–20. doi: 10.1111/coa.13171
59. De Meulenaere A, Vermassen T, Aspeslagh S, Deron P, Duprez F, Laukens D, et al. Tumor PD-L1 status and CD8(+) tumor-infiltrating T cells: markers of improved prognosis in oropharyngeal cancer. *Oncotarget*. (2017) 8:80443–52. doi: 10.18632/oncotarget.19045
60. De Meulenaere A, Vermassen T, Aspeslagh S, Zwaenepoel K, Deron P, Duprez F, et al. Prognostic markers in oropharyngeal squamous cell carcinoma: focus on CD70 and tumour infiltrating lymphocytes. *Pathology*. (2017) 49:397–404. doi: 10.1016/j.pathol.2017.02.002
61. Verhagen CVM, Vossen DM, Borgmann K, Hageman F, Grénman R, Verwijs-Janssen M, et al. Fanconi anemia and homologous recombination gene variants are associated with functional DNA repair defects *in vitro* and poor outcome in patients with advanced head and neck squamous cell carcinoma. *Oncotarget*. (2018) 9:18198–213. doi: 10.18632/oncotarget.24797
62. Verhagen CVM, De Haan R, Hageman F, Oostendorp TPD, Carli ALE, O'Connor MJ, et al. Extent of radiosensitization by the PARP inhibitor olaparib depends on its dose, the radiation dose and the integrity of the homologous recombination pathway of tumor cells. *Radiother Oncol*. (2015) 116:358–65. doi: 10.1016/j.radonc.2015.03.028
63. Essers PBM, van der Heijden M, Verhagen CVM, Ploeg EM, de Roest RH, Leemans CR, et al. Drug sensitivity prediction models reveal link between DNA repair defects and poor prognosis in HNSCC. *Cancer Res*. (2019) 79:5597–611. doi: 10.1158/0008-5472.CAN-18-3388
64. Van der Heijden M, Essers P, Verheij M, Van den Brekel M, Vens C. OC-0487: EMT signatures as a prognostic marker for metastasis in HPV-negative HNSCC. *Radiother Oncol*. (2018) 127:S250–1. doi: 10.1016/S0167-8140(18)30797-7
65. Balm AJM, Rasch CRN, Schornagel JH, Hilgers FJM, Keus RB, Schultze-Kool L, et al. High-dose superselective intra-arterial cisplatin and concomitant radiation (radplat) for advanced head and neck cancer. *Head Neck*. (2004) 26:485–93. doi: 10.1002/hed.20006
66. Al-Mamgani A, de Ridder M, Navran A, Klop WM, de Boer JP, Tesselaar ME. The impact of cumulative dose of cisplatin on outcome of patients with head and neck squamous cell carcinoma. *Eur Arch Oto Rhino Laryngol*. (2017) 274:3757–65. doi: 10.1007/s00405-017-4687-4
67. Spreafico A, Huang SH, Xu W, Granata R, Liu CS, Waldron JN, et al. Impact of cisplatin dose intensity on human papillomavirus-related and -unrelated locally advanced head and neck squamous cell carcinoma. *Eur J Cancer*. (2016) 67:174–82. doi: 10.1016/j.ejca.2016.08.013
68. Heukelom J, Hamming O, Bartelink H, Hoebers F, Giralt J, Herlestam T, et al. Adaptive and innovative Radiation Treatment FOR improving Cancer treatment outcomE (ARTFORCE); a randomized controlled phase II trial for individualized treatment of head and neck cancer. *BMC Cancer*. (2013) 13:84. doi: 10.1186/1471-2407-13-84
69. Lewis JS, Chernock RD, Ma XJ, Flanagan JJ, Luo Y, Gao G, et al. Partial p16 staining in oropharyngeal squamous cell carcinoma: extent and pattern correlate with human papillomavirus RNA status. *Mod Pathol*. (2012) 25:1212–20. doi: 10.1038/modpathol.2012.79
70. Kim D, Pertea G, Trapnell C, Pimentel H, Kelley R, Salzberg SL. TopHat2: accurate alignment of transcriptomes in the presence of insertions, deletions and gene fusions. *Genome Biol*. (2013) 14:R36. doi: 10.1186/gb-2013-14-4-r36
71. Anders S, Pyl PT, Huber W. HTSeq-A Python framework to work with high-throughput sequencing data. *Bioinformatics*. (2015) 31:166–9. doi: 10.1093/bioinformatics/btu638
72. Hänzelmann S, Castelo R, Guinney J. GSVA: gene set variation analysis for microarray and RNA-Seq data. *BMC Bioinform*. (2013) 14:7. doi: 10.1186/1471-2105-14-7
73. Seigneuric R, Starmans MHW, Fung G, Krishnapuram B, Nuyten DSA, van Erk A, et al. Impact of supervised gene signatures of early hypoxia on patient survival. *Radiother Oncol*. (2007) 83:374–82. doi: 10.1016/j.radonc.2007.05.002
74. Lohaus F, Linge A, Tinhofer I, Budach V, Gkika E, Stuschke M, et al. HPV16 DNA status is a strong prognosticator of loco-regional control

after postoperative radiochemotherapy of locally advanced oropharyngeal carcinoma: results from a multicentre explorative study of the German Cancer Consortium Radiation Oncology Group. *Radiother Oncol*. (2014) 113:317–23. doi: 10.1016/j.radonc.2014.11.011

75. Senbabaoglu Y, Winer AG, Gejman RS, Liu M, Luna A, Ostrovnaya I, et al. The landscape of {T} cell infiltration in human cancer and its association with antigen presenting gene expression. *bioRxiv*. (2015). doi: 10.1101/025908
76. Bindea G, Mlecnik B, Tosolini M, Kirilovsky A, Waldner M, Obenauf AC, et al. Spatiotemporal dynamics of intratumoral immune cells reveal the immune landscape in human cancer. *Immunity*. (2013) 39:782–95. doi: 10.1016/j.immuni.2013.10.003
77. De Meulenaere A, Vermassen T, Aspeslagh S, Vandecasteele K, Rottey S, Ferdinande L. TILs in head and neck cancer: ready for clinical implementation and Why (Not)? *Head Neck Pathol*. (2017) 11:354–63. doi: 10.1007/s12105-016-0776-8
78. Kim KY, McShane LM, Conley BA. Designing biomarker studies for head and neck cancer. *Head Neck*. (2014) 36:1069–75. doi: 10.1002/hed.23444
79. Lassen P, Lacas B, Pignon J-P, Trotti A, Zackrisson B, Zhang Q, et al. Prognostic impact of HPV-associated p16-expression and smoking status on outcomes following radiotherapy for oropharyngeal cancer: The MARCH-HPV project. *Radiother Oncol*. (2018) 126:107–15. doi: 10.1016/j.radonc.2017.10.018
80. O'Sullivan B, Huang SH, Su J, Garden AS, Sturgis EM, Dahlstrom K, et al. Development and validation of a staging system for HPV-related oropharyngeal cancer by the International Collaboration on Oropharyngeal cancer Network for Staging (ICON-S): a multicentre cohort study. *Lancet Oncol*. (2016) 17:440–51. doi: 10.1016/S1470-2045(15)00560-4
81. Hoebers F, Rios E, Troost E, van den Ende P, Kross K, Lacko M, et al. Definitive radiation therapy for treatment of laryngeal carcinoma: impact of local relapse on outcome and implications for treatment strategies. *Strahlentherapie und Onkol Organ der Dtsch Rontgengesellschaft*. (2013) 189:834–41. doi: 10.1007/s00066-013-0414-2
82. Silva P, Homer JJ, Slevin NJ, Musgrove BT, Sloan P, Price P, et al. Clinical and biological factors affecting response to radiotherapy in patients with head and neck cancer: a review. *Clin Otolaryngol*. (2007) 32:337–45. doi: 10.1111/j.1749-4486.2007.01544.x
83. Lucs A, Saltman B, Chung CH, Steinberg BM, Schwartz DL. Opportunities and challenges facing biomarker development for personalized head and neck cancer treatment. *Head Neck*. (2013) 35:294–306. doi: 10.1002/hed.21975
84. Welch ML, McIntosh C, Haibe-Kains B, Milosevic MF, Wee L, Dekker A, et al. Vulnerabilities of radiomic signature development: The need for safeguards. *Radiother Oncol*. (2019) 130:2–9. doi: 10.1016/j.radonc.2018.10.027
85. Strongin A, Yovino S, Taylor R, Wolf J, Cullen K, Zimrin A, et al. Primary tumor volume is an important predictor of clinical outcomes among patients with locally advanced squamous cell cancer of the head and neck treated with definitive chemoradiotherapy. *Int J Radiat Oncol Biol Phys*. (2012) 82:1823–30. doi: 10.1016/j.ijrobp.2010.10.053
86. Knegjens JL, Hauptmann M, Pameijer FA, Balm AJ, Hoebers FJ, de Bois JA, et al. Tumor volume as prognostic factor in chemoradiation for advanced head and neck cancer. *Head Neck*. (2011) 33:375–82. doi: 10.1002/hed.21459
87. Gopinath D, Kunnath Menon R. Unravelling the molecular signatures in HNSCC: is the homogenous paradigm becoming obsolete? *Oral Oncol*. (2018) 82:195. doi: 10.1016/j.oraloncology.2018.05.011
88. Pai SI, Westra WH. Molecular pathology of head and neck cancer: implications for diagnosis, prognosis, and treatment. *Annu Rev Pathol*. (2009) 4:49–70. doi: 10.1146/annurev.pathol.4.110807.092158
89. van Monsjou HS, Balm AJM, van den Brekel MM, Wreesmann VB. Oropharyngeal squamous cell carcinoma: a unique disease on the rise? *Oral Oncol*. (2010) 46:780–5. doi: 10.1016/j.oraloncology.2010.08.011
90. Dogan V, Rieckmann T, Münscher A, Busch CJ. Current studies of immunotherapy in head and neck cancer. *Clin Otolaryngol*. (2018) 43:13–21. doi: 10.1111/coa.12895
91. Caudell JJ, Torres-Roca JF, Gillies RJ, Enderling H, Kim S, Rishi A, et al. The future of personalised radiotherapy for head and neck cancer. *Lancet Oncol*. (2017) 18:e266–73. doi: 10.1016/S1470-2045(17)30252-8
92. Lambin P, Zindler J, Vanneste BGL, Van De Voorde L, Eekers D, Compter I, et al. Decision support systems for personalized and participative radiation oncology. *Adv Drug Deliv Rev*. (2017) 109:131–53. doi: 10.1016/j.addr.2016.01.006
93. Cripps C, Winquist E, Devries MC, Stys-Norman D, Gilbert R. Epidermal growth factor receptor targeted therapy in stages III and IV head and neck cancer. *Curr Oncol*. (2010) 17:37–48. doi: 10.3747/co.v17i3.520
94. Grandis JR, Melhem MF, Gooding WE, Day R, Holst VA, Wagener MM, et al. Levels of TGF-α and EGFR protein in head and neck squamous cell carcinoma and patient survival. *J Natl Cancer Inst*. (1998) 90:824–32. doi: 10.1093/jnci/90.11.824
95. Hutchinson L. Drug therapy: cetuximab or cisplatin in HNSCC? *Nat Rev Clin Oncol*. (2016) 13:66. doi: 10.1038/nrclinonc.2015.235
96. Ang KK, Berkey BA, Tu X, Zhang HZ, Katz R, Hammond EH, et al. Impact of epidermal growth factor receptor expression on survival and pattern of relapse in patients with advanced head and neck carcinoma. *Cancer Res*. (2002) 62:7350–6.
97. Nicholson R., Gee JM., Harper M. EGFR and cancer prognosis. *Eur J Cancer*. (2001) 37:(Suppl. 4):S9–15. doi: 10.1016/S0959-8049(01)00231-3
98. Gillison ML, Zhang Q, Jordan R, Xiao W, Westra WH, Trotti A, et al. Tobacco smoking and increased risk of death and progression for patients with p16-positive and p16-negative oropharyngeal cancer. *J Clin Oncol*. (2012) 30:2102–11. doi: 10.1200/JCO.2011.38.4099
99. Gronhoj C, Jensen JS, Wagner S, Dehlendorff C, Friborg J, Andersen E, et al. Impact on survival of tobacco smoking for cases with oropharyngeal squamous cell carcinoma and known human papillomavirus and p16-status: a multicenter retrospective study. *Oncotarget*. (2019) 10:4655–63. doi: 10.18632/oncotarget.27079
100. Hess J, Unger K, Maihoefer C, Schuttrumpf L, Wintergerst L, Heider T, et al. A five-MicroRNA signature predicts survival and disease control of patients with head and neck cancer negative for HPV infection. *Clin Cancer Res*. (2019) 25:1505–16. doi: 10.1158/1078-0432.CCR-18-0776
101. Glorieux M, Dok R, Nuyts S. Novel DNA targeted therapies for head and neck cancers: clinical potential and biomarkers. *Oncotarget*. (2017) 8:81662–78. doi: 10.18632/oncotarget.20953
102. Bossi P, Alfieri S, Strojan P, Takes RP, Lopez F, Makitie A, et al. Prognostic and predictive factors in recurrent and/or metastatic head and neck squamous cell carcinoma: a review of the literature. *Crit Rev Oncol Hematol*. (2019) 137:84–91. doi: 10.1016/j.critrevonc.2019.01.018
103. Foy J-P, Bazire L, Ortiz-Cuaran S, Deneuve S, Kielbassa J, Thomas E, et al. A 13-gene expression-based radioresistance score highlights the heterogeneity in the response to radiation therapy across HPV-negative HNSCC molecular subtypes. *BMC Med*. (2017) 15:165. doi: 10.1186/s12916-017-0929-y
104. Scott JG, Berglund A, Schell MJ, Mihaylov I, Fulp WJ, Yue B, et al. A genome-based model for adjusting radiotherapy dose (GARD): a retrospective, cohort-based study. *Lancet Oncol*. (2017) 18:202–11. doi: 10.1016/S1470-2045(16)30648-9
105. Hsieh JC-H, Wang H-M, Wu M-H, Chang K-P, Chang P-H, Liao C-T, et al. Review of emerging biomarkers in head and neck squamous cell carcinoma in the era of immunotherapy and targeted therapy. *Head Neck*. (2019) 41 (Suppl. 1):19–45. doi: 10.1002/hed.25932
106. Lim SM, Cho SH, Hwang IG, Choi JW, Chang H, Ahn M-J, et al. Investigating the feasibility of targeted next-generation sequencing to guide the treatment of head and neck squamous cell carcinoma. *Cancer Res Treat*. (2019) 51:300–12. doi: 10.4143/crt.2018.012
107. Eder T, Hess AK, Konschak R, Stromberger C, Johrens K, Fleischer V, et al. Interference of tumour mutational burden with outcome of patients with head and neck cancer treated with definitive chemoradiation: a multicentre retrospective study of the German Cancer Consortium Radiation Oncology Group. *Eur J Cancer*. (2019) 116:67–76. doi: 10.1016/j.ejca.2019.04.015
108. Hoogsteen IJ, Marres HAM, Bussink J, van der Kogel AJ, Kaanders JHAM. Tumor microenvironment in head and neck squamous cell carcinomas: predictive value and clinical relevance of hypoxic markers. A review. *Head Neck*. (2007) 29:591–604. doi: 10.1002/hed.20543
109. Spiegelberg L, Houben R, Niemans R, de Ruysscher D, Yaromina A, Theys J, et al. Hypoxia-activated prodrugs and (lack of) clinical progress: The need for hypoxia-based biomarker patient selection in phase III clinical

trials. *Clin Transl Radiat Oncol*. (2019) 15:62–9. doi: 10.1016/j.ctro.2019.01.005
110. Baumann M, Krause M. CD44: a cancer stem cell-related biomarker with predictive potential for radiotherapy. *Clin Cancer Res*. (2010) 16:5091–3. doi: 10.1158/1078-0432.CCR-10-2244
111. Eltzschig HK, Carmeliet P. Hypoxia and Inflammation. *N Engl J Med*. (2011) 364:656–65. doi: 10.1056/NEJMra0910283
112. Zhang P, Sun Y, Ma L. ZEB1: at the crossroads of epithelial-mesenchymal transition, metastasis and therapy resistance. *Cell Cycle*. (2015) 14:481–7. doi: 10.1080/15384101.2015.1006048
113. Schmalhofer O, Brabletz S, Brabletz T. E-cadherin, beta-catenin, and ZEB1 in malignant progression of cancer. *Cancer Metastasis Rev*. (2009) 28:151–66. doi: 10.1007/s10555-008-9179-y
114. Chen C, Zimmermann M, Tinhofer I, Kaufmann AM, Albers AE. Epithelial-to-mesenchymal transition and cancer stem(-like) cells in head and neck squamous cell carcinoma. *Cancer Lett*. (2013) 338:47–56. doi: 10.1016/j.canlet.2012.06.013
115. Smith A, Teknos TN, Pan Q. Epithelial to mesenchymal transition in head and neck squamous cell carcinoma. *Oral Oncol*. (2013) 49:287–92. doi: 10.1016/j.oraloncology.2012.10.009
116. De Meulenaere A, Vermassen T, Creytens D, Aspeslagh S, Deron P, Duprez F, et al. Importance of choice of materials and methods in PD-L1 and TIL assessment in oropharyngeal squamous cell carcinoma. *Histopathology*. (2018) 73:500–9. doi: 10.1111/his.13650
117. Tran L, Allen CT, Xiao R, Moore E, Davis R, Park S-J, et al. Cisplatin alters antitumor immunity and synergizes with PD-1/PD-L1 inhibition in head and neck squamous cell carcinoma. *Cancer Immunol Res*. (2017) 5:1141–51. doi: 10.1158/2326-6066.CIR-17-0235
118. Kroon P, Frijlink E, Iglesias-Guimarais V, Volkov A, van Buuren MM, Schumacher TN, et al. Radiotherapy and cisplatin increase immunotherapy efficacy by enabling local and systemic intratumoral T-cell activity. *Cancer Immunol Res*. (2019) 7:670–82. doi: 10.1158/2326-6066.CIR-18-0654
119. de Ruiter EJ, Ooft ML, Devriese LA, Willems SM. The prognostic role of tumor infiltrating T-lymphocytes in squamous cell carcinoma of the head and neck: a systematic review and meta-analysis. *Oncoimmunology*. (2017) 6:e1356148. doi: 10.1080/2162402X.2017.1356148
120. Hendry S, Salgado R, Gevaert T, Russell PA, John T, Thapa B, et al. Assessing tumor-infiltrating lymphocytes in solid tumors: a practical review for pathologists and proposal for a standardized method from the international immuno-oncology biomarkers working group: part 2: TILs in melanoma, gastrointestinal tract carcinom. *Adv Anat Pathol*. (2017) 24:311–35. doi: 10.1097/PAP.0000000000000161
121. Spector ME, Bellile E, Amlani L, Zarins K, Smith J, Brenner JC, et al. Prognostic value of tumor-infiltrating lymphocytes in head and neck squamous cell carcinoma. *JAMA Otolaryngol Head Neck Surg*. (2019) 145:1012–19. doi: 10.1001/jamaoto.2019.2427
122. Balermpas P, Rodel F, Krause M, Linge A, Lohaus F, Baumann M, et al. The PD-1/PD-L1 axis and human papilloma virus in patients with head and neck cancer after adjuvant chemoradiotherapy: a multicentre study of the German Cancer Consortium Radiation Oncology Group (DKTK-ROG). *Int J Cancer*. (2017) 141:594–603. doi: 10.1002/ijc.30770
123. Ward MJ, Thirdborough SM, Mellows T, Riley C, Harris S, Suchak K, et al. Tumour-infiltrating lymphocytes predict for outcome in HPV-positive oropharyngeal cancer. *Br J Cancer*. (2014) 110:489–500. doi: 10.1038/bjc.2013.639
124. Oguejiofor K, Hall J, Slater C, Betts G, Hall G, Slevin N, et al. Stromal infiltration of CD8 T cells is associated with improved clinical outcome in HPV-positive oropharyngeal squamous carcinoma. *Br J Cancer*. (2015) 113:886–93. doi: 10.1038/bjc.2015.277
125. Hess A-K, Johrens K, Zakarneh A, Balermpas P, Von Der Grun J, Rodel C, et al. Characterization of the tumor immune micromilieu and its interference with outcome after concurrent chemoradiation in patients with oropharyngeal carcinomas. *Oncoimmunology*. (2019) 8:1614858. doi: 10.1080/2162402X.2019.1614858
126. Ghanizada M, Jakobsen KK, Grønhøj C, von Buchwald C. The effects of checkpoint inhibition on head and neck squamous cell carcinoma: a systematic review. *Oral Oncol*. (2019) 90:67–73. doi: 10.1016/j.oraloncology.2019.01.018
127. Seiwert TY, Burtness B, Mehra R, Weiss J, Berger R, Eder JP, et al. Safety and clinical activity of pembrolizumab for treatment of recurrent or metastatic squamous cell carcinoma of the head and neck (KEYNOTE-012): an open-label, multicentre, phase 1b trial. *Lancet Oncol*. (2016) 17:956–65. doi: 10.1016/S1470-2045(16)30066-3
128. Alfieri S, Cavalieri S, Licitra L. Immunotherapy for recurrent/metastatic head and neck cancer. *Curr Opin Otolaryngol Head Neck Surg*. (2018) 26:152–6. doi: 10.1097/MOO.0000000000000448
129. Cohen EEW, Soulieres D, Le Tourneau C, Dinis J, Licitra L, Ahn M-J, et al. Pembrolizumab versus methotrexate, docetaxel, or cetuximab for recurrent or metastatic head-and-neck squamous cell carcinoma (KEYNOTE-040): a randomised, open-label, phase 3 study. *Lancet*. (2019) 393:156–67. doi: 10.1016/S0140-6736(18)31999-8
130. Lee YS, Johnson DE, Grandis JR. An update: emerging drugs to treat squamous cell carcinomas of the head and neck. *Expert Opin Emerg Drugs*. (2018) 23:283–99. doi: 10.1080/14728214.2018.1543400
131. Sato K, Ono T, Sato F, Kawahara A, Azuma K, Kawaguchi T, et al. Different responses to nivolumab therapy between primary and metastatic tumors in a patient with recurrent hypopharyngeal squamous cell carcinoma. *Oral Oncol*. (2019). doi: 10.1016/j.oraloncology.2019.07.009. [Epub ahead of print].
132. Ferris RL, Blumenschein GJ, Fayette J, Guigay J, Colevas AD, Licitra L, et al. Nivolumab for recurrent squamous-cell carcinoma of the head and neck. *N Engl J Med*. (2016) 375:1856–67. doi: 10.1056/NEJMoa1602252
133. Zandberg DP, Algazi AP, Jimeno A, Good JS, Fayette J, Bouganim N, et al. Durvalumab for recurrent or metastatic head and neck squamous cell carcinoma: results from a single-arm, phase II study in patients with >/=25% tumour cell PD-L1 expression who have progressed on platinum-based chemotherapy. *Eur J Cancer*. (2019) 107:142–52. doi: 10.1016/j.ejca.2018.11.015
134. Chow LQM, Haddad R, Gupta S, Mahipal A, Mehra R, Tahara M, et al. Antitumor activity of pembrolizumab in biomarker-unselected patients with recurrent and/or metastatic head and neck squamous cell carcinoma: results from the phase Ib KEYNOTE-012 expansion cohort. *J Clin Oncol*. (2016) 34:3838–45. doi: 10.1200/JCO.2016.68.1478
135. Bedognetti D, Hendrickx W, Ceccarelli M, Miller LD, Seliger B. Disentangling the relationship between tumor genetic programs and immune responsiveness. *Curr Opin Immunol*. (2016) 39:150–8. doi: 10.1016/j.coi.2016.02.001
136. Ferris RL. Immunology and immunotherapy of head and neck cancer. *J Clin Oncol*. (2015) 33:3293–304. doi: 10.1200/JCO.2015.61.1509

Conflict of Interest: The authors declare that the research was conducted in the absence of any commercial or financial relationships that could be construed as a potential conflict of interest.

Copyright © 2020 van der Heijden, Essers, de Jong, de Roest, Sanduleanu, Verhagen, Hamming-Vrieze, Hoebers, Lambin, Bartelink, Leemans, Verheij, Brakenhoff, van den Brekel and Vens. This is an open-access article distributed under the terms of the Creative Commons Attribution License (CC BY). The use, distribution or reproduction in other forums is permitted, provided the original author(s) and the copyright owner(s) are credited and that the original publication in this journal is cited, in accordance with accepted academic practice. No use, distribution or reproduction is permitted which does not comply with these terms.

frontiers in Oncology

REVIEW
published: 17 January 2020
doi: 10.3389/fonc.2019.01563

Ultra-High Dose Rate (FLASH) Radiotherapy: Silver Bullet or Fool's Gold?

Joseph D. Wilson[1†], *Ester M. Hammond*[1†], *Geoff S. Higgins*[1†] *and Kristoffer Petersson*[1,2*†]

[1] Department of Oncology, The Oxford Institute for Radiation Oncology, University of Oxford, Oxford, United Kingdom,
[2] Radiation Physics, Department of Haematology, Oncology and Radiation Physics, Skåne University Hospital, Lund, Sweden

OPEN ACCESS

Edited by:
Ira Ida Skvortsova,
Innsbruck Medical University, Austria

Reviewed by:
Virginie Monceau,
Collège de France, France
Anne-Sophie Wozny,
Université Claude Bernard Lyon 1, France
Marie-Catherine Vozenin,
Lausanne University Hospital (CHUV), Switzerland

***Correspondence:**
Kristoffer Petersson
kristoffer.petersson@oncology.ox.ac.uk

†ORCID:
Joseph D. Wilson
orcid.org/0000-0001-8878-5882
Ester M. Hammond
orcid.org/0000-0002-2335-3146
Geoff S. Higgins
orcid.org/0000-0003-3072-909X
Kristoffer Petersson
orcid.org/0000-0003-0300-5790

Specialty section:
This article was submitted to Radiation Oncology, a section of the journal Frontiers in Oncology

Received: 06 September 2019
Accepted: 24 December 2019
Published: 17 January 2020

Citation:
Wilson JD, Hammond EM, Higgins GS and Petersson K (2020) Ultra-High Dose Rate (FLASH) Radiotherapy: Silver Bullet or Fool's Gold? Front. Oncol. 9:1563. doi: 10.3389/fonc.2019.01563

Radiotherapy is a cornerstone of both curative and palliative cancer care. However, radiotherapy is severely limited by radiation-induced toxicities. If these toxicities could be reduced, a greater dose of radiation could be given therefore facilitating a better tumor response. Initial pre-clinical studies have shown that irradiation at dose rates far exceeding those currently used in clinical contexts reduce radiation-induced toxicities whilst maintaining an equivalent tumor response. This is known as the FLASH effect. To date, a single patient has been subjected to FLASH radiotherapy for the treatment of subcutaneous T-cell lymphoma resulting in complete response and minimal toxicities. The mechanism responsible for reduced tissue toxicity following FLASH radiotherapy is yet to be elucidated, but the most prominent hypothesis so far proposed is that acute oxygen depletion occurs within the irradiated tissue. This review examines the tissue response to FLASH radiotherapy, critically evaluates the evidence supporting hypotheses surrounding the biological basis of the FLASH effect, and considers the potential for FLASH radiotherapy to be translated into clinical contexts.

Keywords: FLASH, radiotherapy, hypoxia, normal tissue, immune

INTRODUCTION

In the UK, almost 30% of diagnosed tumors are treated with radiotherapy (RT) (1). External beam RT is a non-invasive procedure whereby tumors are targeted with ionizing radiation causing lethal damage to cancer cells resulting in cell death. However, RT also inflicts acute and chronic toxicities to the normal tissue surrounding the tumor (2–6). These radiation-induced toxicities limit the dose of radiation that can be delivered and subsequently limits the extent to which RT can be curative. Furthermore, as the number of long-term cancer survivors increases, late onset toxicities resulting from RT are emerging that significantly impact the quality of life of those patients. Consequently, there is a need for novel RT strategies that maintain the anti-tumor effect whilst limiting the extent of toxicities induced in the surrounding healthy tissue. Limiting the induction of toxicities to normal tissue would subsequently increase the therapeutic index of RT regimes (7). A number of recent studies have demonstrated that irradiation at ultra-high dose rates (FLASH) diminishes the severity of toxicities in normal tissues compared to irradiation at the conventional dose rates (CONV) currently used in clinical practice (8–18). Notably, limited data also shows that FLASH-RT reduces normal tissue toxicities whilst maintaining the anti-tumor response of CONV-RT (8–10, 15, 17, 19). FLASH-RT delivery uses irradiators with a high radiation output that allows for the entire RT treatment, or large fraction doses, to be delivered in parts of a second, compared to several minutes for CONV-RT. The short treatment times used in

FLASH-RT, often shorter than 0.1 s, have the added value of minimizing treatment delivery uncertainties caused by intra-fraction motion. Carefully implemented, this would allow for smaller treatment margins and therefore smaller volumes of normal tissue being unnecessarily irradiated. Given both the radiobiological advantageous FLASH effect and its potential to "freeze" physiological motion (15, 20), FLASH-RT has the potential to be an important evolutionary step in cancer treatment. The biology underpinning the FLASH effect, however, remains unknown.

FLASH-RT LIMITS NORMAL TISSUE TOXICITY

Investigation of the dose rate at which RT is delivered harks back to the 1960s, when it was demonstrated that non-cancerous mammalian cells irradiated at ultra-high dose rates had greater viability than those irradiated at conventional dose rates (21). More recently, this toxicity-limiting property of ultra-high dose rate was rediscovered and named FLASH by Favaudon et al. (10). In their study, they demonstrated that thoracic irradiation of mice with a single fraction of 17 Gy at conventional dose rates (0.03 Gy/s) induced "moderate" and "severe" regions of pulmonary fibrosis at 36 weeks post-irradiation. In contrast, when mice received the same dose at ultra-high dose rates (40–60 Gy/s) the induction of pulmonary fibrosis was starkly reduced. A greater dose of 30 Gy delivered by FLASH-RT was required to induce comparable levels of pulmonary fibrosis as seen following CONV-RT (10). Whilst exploring this reduction in pulmonary fibrosis following FLASH-RT, the same group investigated any changes in the induction of the transforming growth factor beta (TGFβ) signaling cascade—a well-documented molecular marker of radiation-induced pulmonary fibrosis (22). In accordance with their prior findings, CONV-RT of 17 Gy significantly induced TGFβ signaling; this signaling was reduced in mice that had been subjected to FLASH-RT. Once again, a greater dose of 30 Gy delivered by FLASH-RT was required to induce TGFβ signaling to the equivalent extent as seen following irradiation with CONV-RT (10). Limited TGFβ signaling following FLASH-RT has also been shown *in vitro* (23): this study demonstrated that even 24 h post-irradiation, CONV-RT induced 3-fold greater TGFβ signaling compared to FLASH-RT.

In addition to thoracic irradiation, it has been shown in several studies that whole brain irradiation using FLASH-RT confers neuroprotection compared to CONV-RT (13, 14, 24, 25). In one such study, mice were exposed to varying dose rates, ranging from 0.1 Gy/s to 10 Gy delivered in a single 1.8 μs pulse; at all dose rates mice were exposed to 10 Gy in a single fraction (14). Any radiation-induced neurotoxicity was measured by a novel object recognition test 2 months post-irradiation. Analysis of these data showed that mice irradiated at 0.1 Gy/s performed significantly worse on the novel object recognition test compared to the non-irradiated control. Notably, as dose rate increased, mice performed significantly better in the recognition test when irradiated at dose rates $\geq$ 30 Gy/s. Furthermore, there was no statistical difference in novel object recognition between mice irradiated at dose rates exceeding 100 Gy/s and non-irradiated mice (14).

In earlier studies, it was observed in rodent models that radiation-induced skin reactions could be significantly reduced at ultra-high dose rates (26, 27). Specifically, it was shown in a rat model that irradiation at 67 Gy/s induced less severe skin reactions, e.g., reddening, moist desquamation, and skin breakdown, in the short and long term compared to rats irradiated at either 1 or 0.03 Gy/s. This study also measured the deformity of the irradiated feet 6 months post-irradiation; consistent with the induction of skin reactions, the extent of deformation was less in the rats irradiated at 67 Gy/s compared to the two lower dose rates (26). Pre-clinical FLASH-RT studies have also been extended from rodent models to higher mammals such as mini-pigs and cats (16). As recently and succinctly reviewed (28), this study irradiated ten 26 mm in diameter circular patches of skin on the back of a single mini-pig to five different dose levels from 22 to 34 Gy (in 3 Gy increments), with either FLASH-RT at a dose rate of 300 Gy/s, or CONV-RT at 0.083 Gy/s. Examination 48 weeks post-irradiation showed that FLASH-RT had been well-tolerated, with only mild cutaneous depigmentation at the site of irradiation (16). In contrast, sites subjected to CONV-RT presented with clear fibronecrotic lesions. By way of extension, this study used FLASH-RT to treat six cats, all presenting with squamous cell carcinoma of the nasal planum, to a total dose ranging from 25 to 41 Gy. All six cats responded extremely well to treatment with complete remission of tumors with minimal toxicity; cats treated with the largest doses of radiation exhibited moist desquamation around the site of irradiation (16). An obvious limitation of this study is the lack of a parallel arm of cat subjects treated with CONV-RT.

Many pre-clinical studies have reported a successful FLASH normal tissue sparing effect, but it cannot be overlooked that there have also been several studies reporting no significant sparing of normal tissues following irradiation at ultra-high dose rates (29–33). For example, Smyth et al. delivered whole and partial body (abdominal or head) synchrotron irradiation to mice, at ultra-high dose rates of 37–41 Gy/s in the hope of characterizing the equivalent CONV-RT dose (32). However, comparing TD_{50} values (dose predicted to cause toxicity, i.e., >15–20% weight loss, severe diarrhea, moribund behavior, in 50% of the animals), this study did not observe any differential sparing between broad beam irradiation of ultra-high and conventional dose rates. A similar study by Montay-Gruel et al. delivering whole brain synchrotron irradiation at a dose rate of 37 Gy/s to mice, did however show significant neurocognitive sparing compared to conventional X-ray irradiation (24). Synchrotron irradiation beams are very flat, several cm in width but with a height on the μm-mm scale, requiring the irradiated sample to be scanned through this beam slice. For studies investigating the FLASH effect with synchrotron irradiation, the dose rate within the beam slice is likely the most important parameter. So even though the average dose rate was similar in these two studies, and probably just high enough for a FLASH sparing effect (14), the height of the beam slice through which the mice were scanned was different by a factor 20 (50 μm compared

to 1 mm), corresponding to the same difference in dose rate in the slice (12 000 Gy/s compared to 600 Gy/s) (14, 32). This difference in beam slice dose rate, and of course the difference in the investigated end-points, could explain why one study found a FLASH sparing effect whilst the other study did not. A summary of *in vivo* studies investigating the tissue response to FLASH-RT compared to CONV-RT, across a range of tissue types, are shown in **Tables 1**, **2**, many of which have demonstrated a reduction in radiation-induced toxicities for FLASH-RT (10–16, 24–27, 34).

SIMILAR ANTI-TUMOR RESPONSE WITH FLASH-RT AS CONV-RT

In addition to limiting toxicities, there have also been reports of FLASH-RT maintaining the same tumor response as seen following CONV-RT (8, 10, 17, 19, 35). In one such study, breast cancer, and head and neck carcinoma xenografts were established in mice (10). Both tumor models were then exposed to either FLASH-RT or CONV-RT; tumor volume was controlled independent of dose rate in breast, and head and neck xenografts. In the same study, mouse lung carcinoma luciferase-positive (luc+) TC-1 cells were transpleurally injected to generate an orthotopic lung tumor model. Thoracic irradiation of the mice with either CONV-RT or FLASH-RT, and subsequent evaluation of tumor growth using bioluminescence, showed no difference in treatment efficacy (10). Similarly in another study, human glioblastoma (GBM) were engrafted to nude mice and locally irradiated with either FLASH-RT or CONV-RT, resulting in similar tumor growth retardation (19). In the study by Bourhis et al. H454-luc+ murine GBM cells were implanted orthotopically in the striatum of nude mice. This

TABLE 1 | Summary of irradiation parameters and outcomes for *in vivo* studies investigating the FLASH effect in normal tissues (organized in order of model species and targeted tissue, as well as color coded by radiation modality).

***In vivo* studies**			**Irradiation delivery technique**			
Model	**Assay**	**FLASH dose modification factor (Bold if >1)**	**Total dose (Gy)**	**Dose rate (Gy/s)**	**Pulse rate (Hz)**	**Modality of radiation**
Zebrafish embryo (16)	Fish length	**1.2–1.5**	10–12	10^6-10^7	Single pulse	Electron
Zebrafish embryo (29)	Fish length, survival, and rate of oedema	1	0–43	100	0.106×10^9	Proton
Whole body irradiation of mice (34)	LD50	**1.1**	8–40	17–83	400	Electron
Thoracic irradiation of mice (10)	TGFβ signaling induction	**1.8**	17	40–60	100–150	Electron
Thoracic irradiation of mice (18)	Number of proliferating cells, DNA damage, expression of inflammatory genes	**>1 Significant Differences**	17	40–60	100–150	Electron
Abdominal irradiation of mice (33)	Survival	<1 Significant Difference	16	35	Likely 300	Electron
Abdominal irradiation of mice (12)	LD50	**1.2**	22	70–210	100–300	Electron
Abdominal irradiation of mice (17)	Survival, stool formation, regeneration in crypts, apoptosis, and DNA damage in crypt cells	**>1 Significant Differences**	12–16	216	108	Electron
Whole brain irradiation of mice (25)	Novel object recognition and object location tests	**>1 Significant Differences**	30	200, 300	108, 180	Electron
Whole brain irradiation of mice (13)	Variety of neurocognitive tests	**>1 Significant Differences**	10	$5.6 \cdot 10^6$	Single pulse	Electron
Whole brain irradiation of mice (14)	Novel object recognition test	**>1 Significant Differences**	10	$30–5.6 \cdot 10^6$	100 or single pulse	Electron
Whole brain irradiation of mice (8)	Novel object recognition test	**≥1.4**	10	$5.6–7.8 \cdot 10^6$	single pulse	Electron
Whole brain irradiation of mice (24)	Novel object recognition test	**>1 Significant Difference**	10	37	1,300	X-ray
Total body and partial body irradiation of mice (32)	TD50	1	3.6–28	37–41	1,388	X-ray
Thoracic irradiation of mice (11)	lung fibrosis, skin dermatitis, and survival	**>1 Significant Difference**	15, 17.5, 20	40	?	Proton
Irradiation of mouse tail skin (49)	Necrosis ND50	**1.4**	30 and 50	17–170	50	Electron
Irradiation of mouse skin (27)	Early skin reaction score	**1.1–1.6**	50–75	2.5 mean, 3×10^4 in the pulse	23–80	Electron
Irradiation of rat skin (26)	Early skin reaction score	**1.4–1.8**	25–35	67	400	Electron
Irradiation of mini-pig skin (15)	Skin toxicity	**≥1.4**	22–34	300	100	Electron

TABLE 2 | Summary of irradiation parameters and outcomes for *in vivo* studies investigating the FLASH effect in tumor tissues (organized in order of model species and targeted tissue, as well as color coded by radiation modality).

***In vivo* studies**			**Irradiation delivery technique**			
Model	**Assay**	**FLASH dose modification factor (Bold if >1)**	**Total dose (Gy)**	**Dose rate (Gy/s)**	**Pulse rate (Hz)**	**Modality of radiation**
Thoracic irradiation of orthotopic engrafted non-small cell lung cancer (Lewis lung carcinoma) in mice (36)	Tumor size and T-cell Infiltration	**>1 Differences in tumor size (significant) and T-cell infiltration**	18	40	?	Proton
Thoracic irradiation of orthotopic engrafted mouse lung carcinoma TC-1 Luc+ in mice (10)	Survival and tumor Growth Delay	1	15-28	60	100–150	Electron
Abdominal irradiation of mice (17)	Number of tumors, tumor weights	1	12–16	216	108	Electron
Whole brain irradiation of nude mice with orthotopic engrafted H454 murine glioblastoma (8)	Tumor Growth Delay	1	10–25	$2.8–5.6{\cdot}10^6$	Single pulse	Electron
Local irradiation of subcutaneous engrafted Human breast cancer HBCx-12A and head and neck carcinoma HEp-2 in nude mice (10)	Tumor Growth Delay	1	15–25	60	100–150	Electron
Local irradiation of subcutaneous engrafted U87 human glioblastoma in nude mice (8)	Tumor Growth Delay	1	0–35	$125–5.6{\cdot}10^6$	100 or single pulse	Electron
Local irradiation of subcutaneous engrafted U87 human glioblastoma in nude mice (19)	Tumor Growth Delay	1	10–30	$125–5.6{\cdot}10^6$	100 or single pulse	Electron
Local irradiation of subcutaneous engrafted Human hypopharyngeal squamous cell carcinoma ATCC HTB-43 in nude mice (35)	Tumor Growth Delay in irradiated Mice and RBE	1	20	0.008 mean, $\approx 10^9$ in pulse	<<1	Proton
Treatment of locally advanced squamous cell carcinoma (SCC) in cat patients (15)	Tumor response and survival	1 Similar response as in published studies with CONV-RT	25–41	130–390	100	Electron
Treatment of CD30+ T-cell cutaneous lymphoma T3 N0 M0 B0 in human patient (9)	Tumor response	1 Similar response as previous treatments with CONV-RT	15	167	100	Electron

was subsequently followed by whole brain irradiation 3 days post-implantation with either single pulse (1.8 μs) FLASH-RT or CONV-RT (0.1 Gy/s) (8). The mice were irradiated with a 10 Gy single fraction, 3 times 8 Gy, or 5 times 5 Gy, with 24 h in-between fractions. Using bioluminescence to assess the tumor burden, no significant difference could be seen between FLASH-RT and CONV-RT for any of the fractionation schemes (8). In a study by Rama et al. Lewis Lung Carcinoma (LLC) cells were inoculated into the left lung of C57Bl/6J mice (36). Two weeks post-inoculation, the whole lungs of tumor-bearing mice were irradiated with a single fraction dose of 18 Gy, using a clinical pencil beam scanning proton system. One week post treatment, CT-scans were performed to measure tumor size. Tumor size was also measured with a caliper after the mice had been sacrificed 10 days post-treatment. Surprisingly, the tumors of the mice treated with proton FLASH-RT were smaller than the tumors of the mice treated with proton CONV-RT. Moreover, immuno?uorescent staining on harvested tumor sections showed an improved recruitment of T lymphocytes into the tumor microenvironment for tumors treated with FLASH-RT compared to CONV-RT (36). Evidentially in some cases, the anti-tumor response to FLASH-RT might even be better than that of CONV-RT.

WHAT FACTORS INFLUENCE THE FLASH EFFECT?

An important caveat of the pre-clinical studies investigating FLASH-RT is the lack of consistency between variables that could potentially influence the induction of the FLASH effect such as: dose rate, total dose, pulse rate, fractionation, and modality of radiation (**Tables 1**, **2**). The study by Montay-Gruel et al. using a wide range of dose rates has helped to elucidate the extent to which dose rate modulates the FLASH effect (14). As previously described, a neuroprotective FLASH effect was apparent at dose rates ≥ 30 Gy/s with a maximal FLASH effect

induced at dose rates ≥ 100 Gy/s. This relationship is important to consider when examining studies such as those by Favaudon et al. (10), and Vozenin et al. (15, 16), which used 40–60 and 300 Gy/s, respectively when administering FLASH-RT. In contrast to previously mentioned studies, a recent interesting study by Venkatesulu et al. showed a higher toxicity for FLASH-RT delivered at 35 Gy/s than for CONV-RT delivered at 0.1 Gy/s (33). This dose rate is probably on the low side for a sparing effect to occur but that does not explain the highly unexpected increased toxicity they found for FLASH-RT in all of their experiments, especially the increased toxicity of a factor 1.3–1.4 for their *in vitro* data. There could be many reasons for these results, e.g., the dose-rate needed for a FLASH sparing effect might not be universal but rather tissue-specific, model and/or assay specific, or there could be dosimetric differences between the two delivery modes/setups, all of which highlights the challenge in performing studies at these dose rates, finding, and exploring a beneficial FLASH effect (33). Furthermore, there is a large degree of variation in the total dose of radiation used in pre-clinical FLASH-RT studies. Compounding this, the majority of studies administer FLASH-RT in single fractions of 10 Gy or more; in many clinical situations, these are currently considered to be extremely large and unattainable fraction doses.

The source of radiation must also be considered when evaluating the FLASH effect. The FLASH effect has been predominantly observed following FLASH-RT using dedicated electron linear accelerators as the source of radiation (10, 14, 15, 18, 37). However, recent studies have expanded the FLASH field and include observations of a FLASH effect following proton (11, 23, 36) and X-ray (24) irradiation. Again, it must be noted that there have been a couple of studies that have been unable to induce a FLASH effect using proton and X-ray sources (**Table 1**). The reason for one X-ray study showing a FLASH effect and one study not showing an effect was discussed above. The proton study compared quasi-continuous proton beam delivery at a CONV-RT dose rate of 5 Gy/min to FLASH-RT of 100 Gy/s, without seeing any toxicity difference for zebrafish embryos (29). A reason for the absent FLASH effect might be the quasi-continuous proton beam delivery with several orders of magnitude lower dose rates within each micro-pulse (≈ 10^3 Gy/s) than the FLASH electron studies macro-pulses (≈ 10^6 Gy/s) (29). So, further to mean dose rate, total dose, and the source of radiation, the pulsatile nature of irradiation may also influence the FLASH effect. In order to induce a FLASH effect, it seems that the irradiation beam should ideally be pulsed at a frequency in the order of 100 Hz (**Figure 1**). Furthermore, within each pulse; irradiation should be delivered at sufficiently high dose-per-pulse, and dose rate within the pulse (≥ 1 Gy and ≥ 10^6 Gy/s, respectively). Together, resulting in a total treatment delivery time of maximum a few tenths of a second (**Table 1**). The range of variables and outcomes seen to date warrants further investigation to confirm that these are the key parameters for inducing the FLASH effect (**Figure 1**).

HYPOTHESES TO EXPLAIN THE FLASH EFFECT

Oxygen Depletion Hypothesis

The biological mechanism responsible for the reduction in normal tissue toxicities following irradiation at FLASH dose rates is not currently understood, yet several non-mutually exclusive hypotheses have been proposed. Some researchers have suggested that the differential response between FLASH-RT and CONV-RT may be due to the radiochemical depletion of oxygen at ultra-high dose rates and subsequent radioresistance conferred to the irradiated tissue (32, 38, 39). It is widely accepted that hypoxic tissues are more radioresistant than well-oxygenated tissues. This is because in the presence of molecular oxygen there is fixation of indirect radiation-induced DNA damage. Indirect damage, the predominant mechanism by which low linear energy transfer (LET) radiation induces DNA damage, occurs when

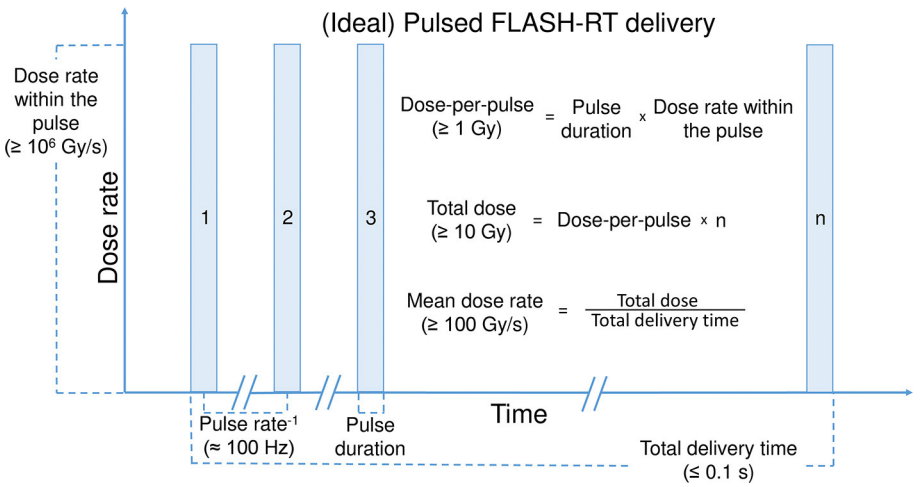

FIGURE 1 | (Ideal) Pulsed FLASH-RT delivery. A schematic view of a pulsed beam delivery, specifying some parameters which seems to be important for inducing the FLASH effect.

radiation results in the radiolysis of water molecules and the subsequent generation of free radicals. Free radicals are then incorporated into DNA, causing damage—yet this can be easily resolved. However, if a free radical reacts with molecular oxygen, this yields a peroxyl radical. Peroxyl radicals have the potential to induce permanent damage, and are therefore a more efficacious DNA damaging agent. Hence, a lack of oxygen in the immediate environment of a cell limits the extent of radiation-induced DNA damage (40).

When considering the oxygen depletion theory, it is important to note the nature of physiologically relevant oxygen concentrations, or "physoxia" (41). Normal tissues *in vivo* are perfused at much lower oxygen concentrations than *in vitro* cell lines cultured in atmospheric oxygen concentrations. Depending on tissue type, physoxia generally lies between 3.4 and 6.8% oxygen (42). Especially relevant for current treatment with FLASH-RT limited to superficial tissues, physoxia in skin increases with depth from the surface of the skin to the dermis, from around 1.1–4.6% (43). Considering physoxia, and given the critical relationship between oxygen concentration and radiosensitivity radiochemical oxygen depletion has the potential to significantly dampen the radiobiological response.

A relationship between dose rate and oxygen consumption was proposed by Dewey and Boag in 1959 (44). They demonstrated that bacteria irradiated at ultra-high dose rates had greater survival compared to bacteria irradiated at what we now consider to be conventional dose rates. The survival curve generated following ultra-high dose rate irradiation was indicative of bacteria irradiated in a hypoxic environment. The authors hypothesized at the time that this response was a consequence of oxygen depletion following a large dose of radiation in such a short timeframe; the time for which the bacteria were irradiated for was shorter than the time required for oxygen to diffuse and restore the oxygen that had been depleted. Given that molecular oxygen is depleted as it reacts with free radicals generated from the radiolysis of water, irradiation at ultra-high dose rates is able to significantly deplete oxygen before it can replenish. This gives rise to a small window of radiobiological hypoxia.

The oxygen-depletion hypothesis has been strengthened by work demonstrating that as dose rate is increased, cellular survival mimics that of cells irradiated in an increasingly hypoxic environment (45, 46). Furthermore, it was subsequently shown in mammalian cells that the oxygen-dependent fixation of indirect DNA damage could be dampened at ultra-high dose rates (47). Importantly, the total dose at which these cells exhibited a hypoxic-like response was linear with respect to increasing the oxygen concentration in which the cells were cultured. The range of oxygen concentrations used in this study was relatively narrow (0.44–0.7% O_2) and therefore the phenomenon could have been limited to cells already in hypoxic environments. However, the recent *in vitro* study by Adrian et al. used physiologically relevant oxygen concentrations (1.6–8.3% O_2) and showed that the sparing effect of FLASH irradiation is dependent on oxygen concentration (48). An *in vivo* mouse model has also shown that irradiation of mouse tails at ultra-high dose rates induced radioresistance indicative of oxygen depletion (49).

Together, these data suggest that the irradiation of tissues with FLASH-RT results in radiochemical oxygen depletion, giving rise to an extremely acute period of hypoxia within the irradiated tissue and consequently a transient radioresistance (**Figure 2**). This phenomenon is not seen following irradiation with CONV-RT as radiation is delivered with much smaller pulses and over a longer timeframe. Hence during CONV-RT, oxygen depletion is limited, and there is sufficient time for oxygen to diffuse into the irradiated region to replace oxygen that has been lost. Therefore, oxygen concentration within the irradiated tissue is maintained.

There is growing interest surrounding other oxygen-based radicals as a potential mechanism bridging the local oxygen depletion observed following irradiation at ultra-high dose rates, and reduced toxicities to normal tissue. A recent study proposes that oxygen depletion at ultra-high dose rates promotes the protection of normal tissue by limiting the production of reactive oxygen species (ROS) (13). This study repeated previous work, demonstrating that whole brain irradiation of C57Bl6/J mice with FLASH-RT did not induce cognitive impairments at dose rates exceeding 100 Gy/s compared to non-irradiated controls. Moreover, in support of a critical role for oxygen in the FLASH effect, increasing the local oxygen concentration in mice brains through carbogen breathing reversed the cognitive protection conferred by FLASH-RT. Furthermore, zebrafish embryos were subjected to either FLASH-RT or CONV-RT in the presence or absence of two well-documented ROS scavengers: *N*-acetyl-cysteine (NAC), and amifostine (13). Giving weight to the involvement of ROS in the FLASH effect, zebrafish embryos exposed to FLASH-RT in combination with a ROS scavenger had no effect on zebrafish length 5 days post-irradiation. However, zebrafish embryos exposed to CONV-RT alone were significantly shorter than those exposed to CONV-RT in combination with a ROS scavenger (13). This provides crude but encouraging evidence suggesting that toxicities arising from CONV-RT are in part due to the generation of ROS, and that the generation of these species is reduced following FLASH-RT. The largest limitation of this study is that there are no direct measurements of ROS in a physiological context. Instead, water containing 4% aqueous oxygen was irradiated at either ultra-high or conventional dose rates; conventional dose rates generated significantly greater ROS than ultra-high dose rates (13). Despite this short fall, the interesting findings detailed upon irradiation in combination with antioxidants merits further exploration into the role of ROS for the FLASH effect.

The oxygen depletion hypothesis seems to explain the reduced toxicity of FLASH-RT to normal tissue. However, it does not easily explain how FLASH-RT can maintain tumor response relative to CONV-RT. Although tumors are more hypoxic compared to their normal tissue counterparts, most are not completely anoxic (42). Therefore, following FLASH-RT, there will also be radiochemical depletion of oxygen within the tumor, hence it would be expected that this would confer radioresistance to the tumor. In contrast to experimental data (8, 10, 19), one would subsequently expect to observe reduced tumor control following FLASH-RT relative to CONV-RT. Though, for highly hypoxic tumor models the reduced tumor control would be expected to be minimal (**Figure 2**). A possible explanation for the

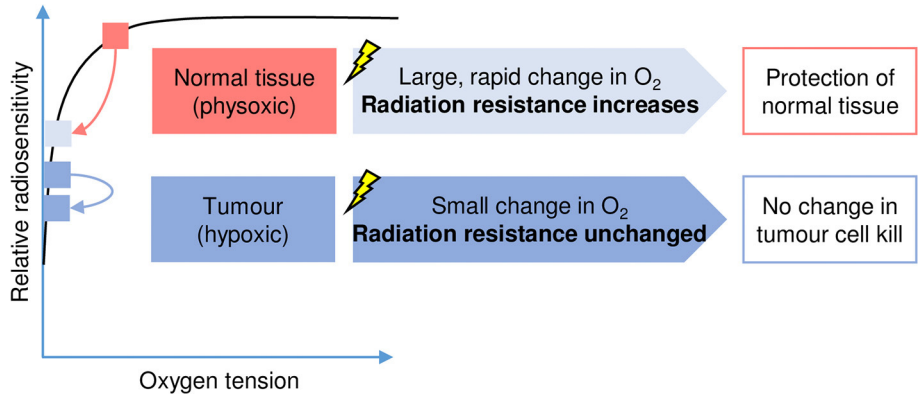

FIGURE 2 | The oxygen depletion hypothesis. The relationship between oxygen tension (horizontal axis) and radiation sensitivity (vertical axis) is shown schematically and has been widely reported (40, 41). In response to FLASH-RT, the physiological level of oxygen (physoxic) found in normal tissues decreases rapidly (pink arrow) and has an important impact on radiation sensitivity. This temporary or transient hypoxia protects the normal tissues as radiation resistance increases. In contrast, oxygen levels are low (hypoxic) in tumor tissues and consequently FLASH-RT has less of an impact on radiation sensitivity.

maintained tumor control is proposed in a recent paper by Spitz et al. They hypothesized that higher levels of redox-active iron (labile iron) in tumor compared to normal tissue and differences in oxidative metabolism between normal and tumor tissues, with the more rapid removal and decay of the organic hydroperoxides and free radicals derived from peroxidation chain reactions in normal tissue, defines the beneficial therapeutic index of the FLASH effect (50). Interestingly, a recent computational model of oxygen depletion induced by FLASH-RT concluded that radiochemical oxygen depletion at an expected rate of 0.42 mmHg/Gy would be sufficient to confer radioresistance (51). However, this conclusion was predicated on the basis that radioresistance would only be conferred to already hypoxic tissues. To explore this, it would be interesting to compare the DNA repair proficiency of normal tissue relative to tumor tissue; perhaps radioresistance induced in tumor tissue by oxygen depletion is compensated for by a lower ability of DNA repair compared to normal tissue. Regions of hypoxia occur in the majority of solid tumors as opposed to the physoxia found in the surrounding normal tissue. This may well be relevant to the relative repair of DNA damage induced by FLASH-RT as exposure to hypoxia has also been described to lead to the repression of the DNA repair pathways including homologous recombination (HR), non-homologous end joining (NHEJ), and base excision repair (BER) (52, 53). To test this hypothesis, the rate of DNA repair, assayed for example by determining the appearance and resolution of 53BP1 foci, should be measured in both normal and tumor cells after exposure to FLASH-RT.

The vast majority of data pertaining to the oxygen depletion theory has been extrapolated from cell survival responses following irradiation at different dose rates (44–47, 49, 54). Therefore, there must be more direct measurements of any potential oxygen flux in tissues following irradiation at ultra-high dose rates. However, given the supposed brevity of any hypoxia induced by FLASH-RT, this is extremely difficult; it has been inferred that reoxygenation by diffusion of a tissue following FLASH-RT occurs after just 10^{-3} s (54). Hypoxia for such a brief moment can certainly not be detected by measuring markers of a hypoxia-mediated transcriptional response, which would be observed following a longer period of hypoxia (41). However, it is unknown whether a chemical marker of hypoxia, such as pimonidazole (55) is sufficiently sensitive to detect such an acute period of hypoxia.

Immune Hypothesis

A modified immune response following FLASH-RT relative to CONV-RT has also been proposed as a potential mechanism for the FLASH effect (9, 38). The fractionated RT regimes commonly used in CONV-RT, result in the irradiation of a greater proportion of circulating lymphocytes compared to total dose delivered in a single fraction (56). Following a standard regime of thirty fractions of 2 Gy, 98.8% of the blood pool has been exposed to more than 0.5 Gy. Additionally, it has been reported that the induction of chromosomal aberrations in the circulating blood pool is dependent on the total volume of the blood pool irradiated (57). Therefore, in accordance with the short irradiation time, characteristic of FLASH-RT, it would follow that fewer lymphocytes would be irradiated and subsequently reduced induction of chromosomal aberrations (9, 38, 56). However, FLASH-RT would expose lymphocytes to a greater dose of radiation, albeit much fewer of them, in comparison to CONV-RT. If a modified immune response contributes to the FLASH effect, one would expect a fractionated FLASH-RT regime to, at least in part, reduce any protection conferred by the FLASH effect.

This hypothesis has been strengthened recently by a study that carried out genome-wide microarray analysis on mice following FLASH-RT and CONV-RT (11). This study reported that immune system wide activation and maturation was dampened in mice following FLASH-RT relative to CONV-RT. Also as mentioned above, the study by Rama et al. showed an improved recruitment of T lymphocytes into the tumor microenvironment for tumors treated with FLASH-RT compared to CONV-RT, which gives merit to this hypothesis

(36). In several studies, immunocompromised animals were used to compare treatment efficacy of FLASH-RT and CONV-RT with no observed difference in tumor response (**Table 2**), which could be interpreted to further strengthen the hypothesis (7, 8, 10, 35). It is worth noting however, that any evidence linking an immune role to the FLASH effect is correlative rather than causative; it is unclear whether any differential immune response following irradiation at ultra-high dose rates contributes to the FLASH effect, or is a consequence of it. Additionally, since the FLASH effect has been observed *in vitro* in bacterial and cell culture models, which are devoid of a functioning immune system, any immunological component is likely to be responsible for only part of the underlying mechanism. More studies are needed to clarify if the immune response or other biological responses like DNA damage response or inflammation is different following FLASH-RT compared to CONV-RT, and if they are part of the underlying mechanism resulting in the FLASH effect.

CLINICAL APPLICATIONS OF FLASH-RT

The obvious endpoint of investigation into the FLASH effect is the translation of FLASH-RT to the clinic. FLASH-RT could be translated to the clinic to serve two general purposes. Firstly, the FLASH effect could be exploited to allow for escalation of total dose in the treatment of radioresistant tumors that are currently associated with poorer patient outcomes (8). In this case, it is hypothesized that a greater dose of radiation could be delivered to the tumor without inducing as severe toxicities to the normal surrounding tissue as would be expected following CONV-RT. Secondly, FLASH-RT could be used in situations in which RT confers good levels of tumor control but is associated with severe normal tissue toxicity—the same total dose would be administered, but hypothetically FLASH-RT would induce less severe toxicities compared to CONV-RT.

Despite these exciting potential applications of FLASH-RT, the extent to which it is clinically viable in practice is questionable. As reviewed above, there are some inconsistencies in the results from the pre-clinical studies. Furthermore, a proportion of these studies are designed with significant limitations, such as using a single subject and a lack of controls irradiated at conventional dose rates (15). Moreover, the results emerging from pre-clinical studies put into question the suitability of FLASH-RT in many clinical situations. Independent studies that have successfully observed a FLASH effect report a dose-modifying factor of about 20–40% in favor of FLASH-RT relative to CONV-RT (**Table 1**). However, these same studies only report a FLASH effect at total doses of 10 Gy or more. This point is particularly well-illustrated in the recent study by Vozenin et al. (16). In a zebrafish model, whereby zebrafish embryos were irradiated with FLASH-RT or CONV-RT at doses ranging from 5 to 12 Gy, increasing in 1 Gy increments, zebrafish length was recorded 5 days post-irradiation as a measure of radiation-induced toxicity. A significant difference in morphology between those irradiated with FLASH-RT or CONV-RT was only apparent at doses $\geq$ 10 Gy. Even when accounting for the dose modifying factor of FLASH-RT, an equivalent dose per fraction of 6–8 Gy given by CONV-RT may still be considered as too large a dose in various clinical scenarios (58–60), such as in the treatment of larger, locally advanced tumors. A previous phase I dose escalation study in locally advanced non-small cell lung cancer (NSCLC) utilized hypofractionated treatment with doses per fraction well-below those required for a FLASH effect (58). Six patients developed late onset, grade 4–5 toxicities that were attributed to damage to the proximal bronchial tree, ergo highlighting the need for caution when employing hypofractionated regimes. Hypofractionation is nevertheless getting more widely used in the clinic for a variety of treatments sites (59, 61–64), and could be proven even more useful together with FLASH-RT and its (potentially) lower level of normal tissue toxicity.

One of the most interesting advancements in the FLASH field is the first human patient treated with FLASH-RT (9). A 75-year-old male presenting with multiresistant CD30+ T cell cutaneous lymphoma was offered the opportunity to be first human subject of FLASH-RT. A 35 mm lesion was exposed to a dose rate exceeding 10^6 Gy/s in each of ten discreet 1 μs pulses to a total dose of 15 Gy. This equates to a mean dose rate of 167 Gy/s, and 1.5 Gy per pulse. Following treatment, shrinkage of the lesion was observed 10 days post-irradiation culminating in a complete tumor response 36 days post-irradiation which was maintained for the following 5 months. From the point at which the lesion initially began to shrink, the patient presented with redness and mild (grade 1) oedema and epithelitis around the site of irradiation. This was starkly different to the patient's other lesions treated with CONV-RT that resulted in high-grade acute reactions to the surrounding skin that took ∼3–4 months to heal (9). Despite the promising outcome for this patient, this should not be considered evidence confirming that FLASH-RT can be successfully translated to the clinic. This study was performed in a single patient that only allowed for limited comparison of the differential response between FLASH-RT and CONV-RT. An appropriately powered, randomized controlled trial with FLASH-RT and CONV-RT arms would be required to definitively show whether FLASH-RT is associated with superior clinical outcomes. At the very least, a positive phase II, single-arm study of FLASH-RT in a sample of participants truly representative of real-world patients is required before the routine adoption of FLASH-RT can be seriously entertained. If 4.5–20 MeV electron beams are to be used for the clinical trials, they would be limited to treating surficial tumors or treating tumors with intra-operative radiation therapy (IORT). Currently, FLASH-RT clinical trials on deep-seated tumors can only be performed with proton beams (**Table 3**). However, to treat tumors with a proton beam in a clinical trial, the beam needs to be scattered or scanned to cover the target volume which reduces the average dose rate (65). So before performing clinical trial, pre-clinical studies are needed to ensure that the FLASH effect is not lost due to either the increased LET in the Bragg peak or to the required scattering/scanning of the beam.

As previously mentioned, most studies showing a FLASH effect has dedicated electron linear accelerators as the source of radiation (9, 10, 14, 15, 18, 37). Recent studies have shown that clinical linear accelerators can be modified to deliver FLASH-RT with electrons, largely increasing the potential availability

TABLE 3 | Some relevant advantages and disadvantages of current and prospective FLASH radiotherapy sources (color coded by radiation modality).

Radiation source	Modality of radiation	Advantages (+)	Disadvantages (–)	Currently available for FLASH-RT clinical studies, with which main limitations?
Conventional electron linear accelerator (10, 14, 66, 67)	1–25 MeV Electrons	Inexpensive. Minor beam size limitation.	Poor depth penetration. Wide penumbra.	Yes, Limited to treating superficial tumors.
Very High Energy Electron linear accelerator (68, 69) or Laser plasma accelerators (70, 71)	100–250 MeV Electrons	Good depth penetration. Electromagnetic steering and focusing. Not sensitive to tissue heterogeneity.	Low pulse rate (1–10 Hz) for Laser plasma accelerators. Limited beam size.	No
Laser plasma accelerators (75)	1–45 MeV Protons	Compact design possible. Electromagnetic steering possible.	Poor depth penetration. Low pulse rate (1–10 Hz). Very sensitive to tissue. heterogeneity. Higher LET in Bragg peak. Beam contamination. Stability issues. Limited beam size.	No
Cyclotrons, synchrotrons or Synchrocyclotron (11, 76)	100–250 MeV Protons	Good depth penetration. Electromagnetic steering possible. Limited dose-bath. Electromagnetic steering.	Large expensive sources. Sensitive to tissue heterogeneity. Higher LET in Bragg peak. Beam scanning or scattering required to cover target volumes	Yes, FLASH effect might be lost with beam scanning and/or higher LET.
X-ray tube (72)	50–250 keV X-rays	Inexpensive. Compact design.	Very limited depth penetration. Limited beam size. High entrance dose.	Yes, Limited to treating small and very superficial tumors.
Synchrotron (24, 32)	50–600 keV X-rays	Microbeam Radiation Therapy possible.	Very large. Very expensive. Limited depth penetration. Very limited availability. Limited beam size requires scanning of sample/target.	Yes, Very limited availability.
Electron linear accelerator with high density target (20)	6–10 MV X-rays	Good depth penetration. Narrow penumbra. Minor beam size limitation.	Multiple beam angles required.	No

of FLASH-RT devices and facilitating the translation to clinical trials (66, 67). However, an obvious limitation is the depth penetration with 4.5–20 MeV electron beams, only reaching to a few cm depths in tissue (**Table 3**). Consequently, other treatment devices/techniques are needed for FLASH-RT to be clinically useful for more than superficial treatments with external beam RT or IORT. A solution to the limited depth penetration would be to use electron beams of higher energy, so called Very High Energy Electron (VHEE) beams, with beam energies of 100–250 MeV. Such beams have good depth penetration, sharp beam penumbra, and are less sensitive to tissue heterogeneity than conventional X-ray beams (68, 69). Also, using electromagnets, the beam can *in theory* be focused to the tumor volume, resulting in dose-to-target conformity with a single beam comparable to that of modern X-ray treatment techniques, e.g., intensity-modulated radiation therapy (IMRT) and volumetric modulated arc therapy (VMAT). A single beam delivery might prove essential for retaining the FLASH effect in clinical trials. Unfortunately, these beams are currently limited to research accelerators which are either rather large (linear accelerator) or suffers from a low pulse rate, a small beam size, and stability issues (laser-based accelerators) (68–71). A recent paper showed (using a 160 kV X-ray beam) that conventional X-ray tubes could potentially be used for FLASH-RT studies (72). This is interesting as such systems are small, relatively inexpensive and clinically available (**Table 3**). Similar however to the electron linear accelerators, the depth penetration is a limiting factor making it useful only down to a few mm depth in tissue, an additional limitation is the beam size of only a few cm. Synchrotron sources has similar beam energies as X-ray tubes but has the added advantage of the possibility of using spatially fractionated ultra-high dose rate microbeam radiation therapy (MRT). MRT is characterized by arrays of quasi-parallel micro-planar beams with a width of 25–100 μm, typically separated by 100–400 μm (32). Since its invention in 1992, numerous pre-clinical studies have shown extraordinary tolerance of normal organs and blood vessels exposed to fractionated radiation doses in excess of 100 Gy in-beam (peak) doses, with dose rates exceeding several hundred Gy/s. The combined effect of spatially fractionated microbeams and FLASH dose rates have been shown in small animal models to achieve therapeutic ratios that clearly exceed those obtained by conventional X-ray with

a homogeneous dose distribution and CONV-RT dose rates, in a range of malignancies, including gliomas, gliosarcomas, human squamous cell carcinomas, and glioblastomas (73). The disadvantage of this technique is the requirement of synchrotrons, which are very large, expensive, and therefore of limited availability. A platform that might solve both the size and stability issue of VHEE beams and also allow for the production of 6–10 MV FLASH X-ray beams, is PHASER (Pluridirectional High-energy Agile Scanning Electronic Radiotherapy). The PHASER concept has been presented by Maxim et al. and might be an ideal way for introducing FLASH into the clinic (20). Included in the concept is a novel and quick image-guided technique. New or highly adapted image-guidance techniques are needed for the clinical treatment of deep-seated tumors with FLASH-RT, regardless of radiation modality. The PHASER is reliant on technical advances and novel innovations in linear accelerator technology, radiofrequency science and medical physics, which in turn requires time and funding for research and development. Therefore, it is still under development (**Table 3**). Alternative concepts of producing 6–10 MV FLASH X-ray beams would be to use multiple synchronized linear accelerators or a powerful recirculating accelerator (74). Albeit large and expensive, a clinically available system for treating deep-seated tumors with FLASH-RT is with proton beams (75, 76). Clinical proton beams have good depth penetration, are often electromagnetically steered, and can produce conformal dose distributions with a single to a few beams (65). There have been studies (published and unpublished) with mixed reports on a FLASH effect with protons but significant resources have now been put into research on proton FLASH-RT by the principal vendors for proton RT devices, which should expedite the translation of proton FLASH-RT into clinical trials (77–79).

CONCLUSION

The FLASH effect is an extremely interesting radiobiological phenomenon that confers some degree of protection compared to CONV-RT. The FLASH effect has now been observed across a range of animal models, and more recently has been suggested in a human patient for the first time. Of equal importance, limited data would suggest that FLASH-RT maintains a similar tumor response to CONV-RT. Together, this raises the prospect that FLASH-RT will allow patients to receive a greater total dose of radiation prior to the induction of unacceptable toxicities that currently limit RT regimes.

There has been much speculation regarding the biological mechanism(s) underpinning the FLASH effect. It is well-established that irradiation results in the radiochemical depletion of oxygen; this is particularly prevalent at ultra-high dose rates. From the data currently available, we can safely conclude that oxygen depletion contributes, at least in part, to the FLASH effect. However, the extent of its contribution remains unknown and therefore warrants further investigation. Aside from oxygen depletion, an immune modulatory role has been broadly implicated in the FLASH effect, yet evidence to support this is currently sparse and preliminary. Likewise, any potential immune-mediated contribution to the FLASH effect requires much greater exploration.

Aside from mechanistic insights, the overarching question remains of the translational potential of FLASH-RT to clinical environments. Despite independent studies concluding that FLASH-RT confers a dose modifying factor of 20–40%, the repeated finding that the FLASH effect is only evident at total doses of 10 Gy or more means that FLASH-RT would not be suitable in many clinical cases. As a result of further investigation into the biological basis of the FLASH effect, it may eventually be possible to generate a FLASH effect at smaller doses, therefore further increasing the clinical potential of FLASH-RT. Another limiting factor in translating FLASH-RT to the clinic is the availability of radiation sources, capable of producing beams suitable for treatment of deep-seated as well as superficial tumors with ultra-high dose rates. In summary, with shorter treatment times and lower levels of toxicity, FLASH-RT may 1 day have the potential to be a paradigm shift in the field of RT. For this to be the case, however, there is a real need to identify the mechanism(s) behind the FLASH effect. The currently available data more than justifies this further investigation.

AUTHOR CONTRIBUTIONS

JW and KP wrote the article. EH and GH contributed ideas to, read, and edited the article.

FUNDING

JW was grateful for support from the Royal College of Radiologists, and Oriel College, Oxford.

REFERENCES

1. NCRAS, CRUK. *Chemotherapy, Radiotherapy and Tumour Resection By Tumour & Patient Characteristics in England, 2013–2015.* National Cancer Registration & Analysis Service and Cancer Research UK (2018).
2. Siddiqui F, Movsas B. Management of radiation toxicity in head and neck cancers. *Semin Radiat Oncol.* (2017) 27:340–9. doi: 10.1016/j.semradonc.2017.04.008
3. Nicholas S, Chen L, Choflet A, Fader A, Guss Z, Hazell S, et al. Pelvic radiation and normal tissue toxicity. *Semin Radiat Oncol.* (2017) 27:358–69. doi: 10.1016/j.semradonc.2017.04.010
4. Smart D. Radiation toxicity in the central nervous system: mechanisms and strategies for injury reduction. *Semin Radiat Oncol.* (2017) 27:332–9. doi: 10.1016/j.semradonc.2017.04.006
5. Jelonek K, Pietrowska M, Widlak P. Systemic effects of ionizing radiation at the proteome and metabolome levels in the blood of cancer patients treated with radiotherapy: the influence of inflammation and radiation toxicity. *Int J Radiat Biol.* (2017) 93:683–96. doi: 10.1080/09553002.2017.1304590
6. Simone CB. Thoracic radiation normal tissue injury. *Semin Radiat Oncol.* (2017) 27:370–7. doi: 10.1016/j.semradonc.2017.04.009
7. Montay-Gruel P, Meziani L, Yakkala C, Vozenin MC. Expanding the therapeutic index of radiation therapy by normal tissue protection. *Br J Radiol.* (2018). doi: 10.1259/bjr.20180008. [Epub ahead of print].

8. Bourhis J, Montay-Gruel P, Goncalves Jorge P, Bailat C, Petit B, Ollivier J, et al. Clinical translation of FLASH radiotherapy: why and how? *Radiother Oncol.* (2019) 139:11–7. doi: 10.1016/j.radonc.2019.04.008
9. Bourhis J, Sozzi WJ, Jorge PG, Gaide O, Bailat C, Duclos F, et al. Treatment of a first patient with FLASH-radiotherapy. *Radiother Oncol.* (2019) 139:18–22. doi: 10.1016/j.radonc.2019.06.019
10. Favaudon V, Caplier L, Monceau V, Pouzoulet F, Sayarath M, Fouillade C, et al. Ultrahigh dose-rate FLASH irradiation increases the differential response between normal and tumor tissue in mice. *Sci Transl Med.* (2014) 6:245ra293. doi: 10.1126/scitranslmed.3008973
11. Girdhani S, Abel E, Katsis A, Rodriquez A, Senapati S, KuVillanueva A, et al. Abstract LB-280: FLASH: A novel paradigm changing tumor irradiation platform that enhances therapeutic ratio by reducing normal tissue toxicity and activating immune pathways. *Cancer Res.* (2019) 79(13 Suppl):LB-280. doi: 10.1158/1538-7445.AM2019-LB-280
12. Loo BW, Schuler E, Lartey FM, Rafat M, King GJ, Trovati S, et al. (P003) Delivery of ultra-rapid flash radiation therapy and demonstration of normal tissue sparing after abdominal irradiation of mice. *Int J Radiat Oncol Biol Phys.* (2017) 98:E16. doi: 10.1016/j.ijrobp.2017.02.101
13. Montay-Gruel P, Acharya MM, Petersson K, Alikhani L, Yakkala C, Allen BD, et al. Long-term neurocognitive benefits of FLASH radiotherapy driven by reduced reactive oxygen species. *Proc Natl Acad Sci USA.* (2019) 116:10943–51. doi: 10.1073/pnas.1901777116
14. Montay-Gruel P, Petersson K, Jaccard M, Boivin G, Germond JF, Petit B, et al. Irradiation in a flash: unique sparing of memory in mice after whole brain irradiation with dose rates above 100Gy/s. *Radiother Oncol.* (2017) 124:365–9. doi: 10.1016/j.radonc.2017.05.003
15. Vozenin MC, De Fornel P, Petersson K, Favaudon V, Jaccard M, Germond JF, et al. The advantage of FLASH radiotherapy confirmed in mini-pig and cat-cancer patients. *Clin Cancer Res.* (2019) 25:35–42. doi: 10.1158/1078-0432.CCR-17-3375
16. Vozenin MC, Hendry JH, Limoli CL. Biological benefits of ultra-high dose rate FLASH radiotherapy: sleeping beauty awoken. *Clin Oncol.* (2019) 31:407–15. doi: 10.1016/j.clon.2019.04.001
17. Levy K, Natarajan S, Wang J, Chow S, Eggold J, Loo P, et al. FLASH irradiation enhances the therapeutic index of abdominal radiotherapy in mice. *bioRxiv [Prepint].* (2019). doi: 10.1101/2019.12.12.873414
18. Fouillade C, Curras-Alonso S, Giuranno L, Quelennec E, Heinrich S, Bonnet-Boissinot S, et al. FLASH irradiation spares lung progenitor cells and limits the incidence of radio-induced senescence. *Clin Cancer Res.* (2019). doi: 10.1158/1078-0432.CCR-19-1440
19. Montay - Gruel P, Petit B, Bochud F, Favaudon V, Bourhis J, Vozenin MC. PO-0799: normal brain, neural stem cells and glioblastoma responses to FLASH radiotherapy. *Radiother Oncol.* (2015) 115:S400–1. doi: 10.1016/S0167-8140(15)40791-1
20. Maxim PG, Tantawi SG, Loo BW. PHASER: a platform for clinical translation of FLASH cancer radiotherapy. *Radiother Oncol.* (2019) 139:28–33. doi: 10.1016/j.radonc.2019.05.005
21. Berry RJ, Hall EJ, Forster DW, Storr TH, Goodman MJ. Survival of mammalian cells exposed to x rays at ultra-high dose-rates. *Br J Radiol.* (1969) 42:102–7. doi: 10.1259/0007-1285-42-494-102
22. Rube CE, Uthe D, Schmid KW, Richter KD, Wessel J, Schuck A, et al. Dose-dependent induction of transforming growth factor beta (TGF-beta) in the lung tissue of fibrosis-prone mice after thoracic irradiation. *Int J Radiat Oncol.* (2000) 47:1033–42. doi: 10.1016/S0360-3016(00)00482-X
23. Buonanno M, Grilj V, Brenner DJ. Biological effects in normal cells exposed to FLASH dose rate protons. *Radiother Oncol.* (2019) 139:51–5. doi: 10.1016/j.radonc.2019.02.009
24. Montay-Gruel P, Bouchet A, Jaccard M, Patin D, Serduc R, Aim W, et al. X-rays can trigger the FLASH effect: Ultra-high dose-rate synchrotron light source prevents normal brain injury after whole brain irradiation in mice. *Radiother Oncol.* (2018) 129:582–8. doi: 10.1016/j.radonc.2018.08.016
25. Simmons DA, Lartey FM, Schüler E, Rafat M, King G, Kim A, et al. Reduced cognitive deficits after FLASH irradiation of whole mouse brain are associated with less hippocampal dendritic spine loss and neuroinflammation. *Radiother Oncol.* (2019) 139:4–10. doi: 10.1016/j.radonc.2019.06.006
26. Field SB, Bewley DK. Effects of dose-rate on the radiation response of rat skin. *Int J Radiat Biol Relat Stud Phys Chem Med.* (1974) 26:259–67. doi: 10.1080/09553007414551221
27. Inada T, Nishio H, Amino S, Abe K, Saito K. High dose-rate dependence of early skin reaction in mouse. *Int J Radiat Biol Relat Stud Phys Chem Med.* (1980) 38:139–45. doi: 10.1080/09553008014551031
28. Harrington KJ. Ultrahigh dose-rate radiotherapy: next steps for FLASH-RT. *Clin Cancer Res.* (2019) 25:3–5. doi: 10.1158/1078-0432.CCR-18-1796
29. Beyreuther E, Brand M, Hans S, Hideghéty K, Karsch L, Leßmann E, et al. Feasibility of proton FLASH effect tested by zebrafish embryo irradiation. *Radiother Oncol.* (2019) 139:46–50. doi: 10.1016/j.radonc.2019.06.024
30. Beyreuther E, Karsch L, Laschinsky L, Leßmann E, Naumburger D, Oppelt M, et al. Radiobiological response to ultra-short pulsed megavoltage electron beams of ultra-high pulse dose rate. *Int J Radiat Biol.* (2015) 91:643–52. doi: 10.3109/09553002.2015.1043755
31. Oppelt M, Baumann M, Bergmann R, Beyreuther E, Brüchner K, Hartmann J, et al. Comparison study of in vivo dose response to laser-driven versus conventional electron beam. *Radiat Environ Biophys.* (2015) 54:155–66. doi: 10.1007/s00411-014-0582-1
32. Smyth LML, Donoghue JF, Ventura JA, Livingstone J, Bailey T, Day LRJ, et al. Comparative toxicity of synchrotron and conventional radiation therapy based on total and partial body irradiation in a murine model. *Sci Rep.* (2018) 8:12044. doi: 10.1038/s41598-018-30543-1
33. Venkatesulu BP, Sharma A, Pollard-Larkin JM, Sadagopan R, Symons J, Neri S, et al. Ultra high dose rate (35 Gy/sec) radiation does not spare the normal tissue in cardiac and splenic models of lymphopenia and gastrointestinal syndrome [published online ahead of print 2019/11/22]. *Sci Rep.* (2019) 9:17180. doi: 10.1038/s41598-019-53562-y
34. Hornsey S, Bewley DK. Hypoxia in mouse intestine induced by electron irradiation at high dose-rates. *Int J Radiat Biol Relat Stud Phys Chem Med.* (1971) 19:479–83. doi: 10.1080/09553007114550611
35. Zlobinskaya O, Siebenwirth C, Greubel C, Hable V, Hertenberger R, Humble N, et al. The effects of ultra-high dose rate proton irradiation on growth delay in the treatment of human tumor xenografts in nude mice. *Radiat Res.* (2014) 181:177–83. doi: 10.1667/RR13464.1
36. Rama N, Saha T, Shukla S, Goda C, Milewski D, Mascia AE, et al. Improved tumor control through t-cell infiltration modulated by ultra-high dose rate proton FLASH using a clinical pencil beam scanning proton system. *Int J Radiat Oncol Biol Phys.* (2019) 105:S164–5. doi: 10.1016/j.ijrobp.2019.06.187
37. Jaccard M, Durán MT, Petersson K, Germond JF, Liger P, Vozenin MC, et al. High dose-per-pulse electron beam dosimetry: commissioning of the Oriatron eRT6 prototype linear accelerator for preclinical use. *Med Phys.* (2018) 45:863–74. doi: 10.1002/mp.12713
38. Durante M, Bräuer-Krisch E, Hill M. Faster and safer? FLASH ultra-high dose rate in radiotherapy. *Br J Radiol.* (2018) 91:20170628. doi: 10.1259/bjr.20170628
39. Wilson P, Jones B, Yokoi T, Hill M, Vojnovic B. Revisiting the ultra-high dose rate effect: implications for charged particle radiotherapy using protons and light ions. *Br J Radiol.* (2012) 85:e933–9. doi: 10.1259/bjr/17827549
40. Hall EJ, Giaccia AJ. *Radiobiology for the Radiologist, 8th Ed.* Philadelphia, PA: Lippincott Williams & Wilkins (2018).
41. Hammond EM, Asselin MC, Forster D, O'Connor JP, Senra JM, Williams KJ. The meaning, measurement and modification of hypoxia in the laboratory and the clinic. *Clin Oncol.* (2014) 26:277–88. doi: 10.1016/j.clon.2014.02.002
42. McKeown SR. Defining normoxia, physoxia and hypoxia in tumours-implications for treatment response. *Br J Radiol.* (2014) 87:20130676. doi: 10.1259/bjr.20130676
43. Carreau A, El Hafny-Rahbi B, Matejuk A, Grillon C, Kieda C. Why is the partial oxygen pressure of human tissues a crucial parameter? Small molecules and hypoxia. *J Cell Mol Med.* (2011) 15:1239–53. doi: 10.1111/j.1582-4934.2011.01258.x
44. Dewey DL, Boag JW. Modification of the oxygen effect when bacteria are given large pulses of radiation. *Nature.* (1959) 183:1450–1. doi: 10.1038/1831450a0
45. Ewing D. Breaking survival curves and oxygen removal times in irradiated bacterial spores. *Int J Radiat Biol Relat Stud Phys Chem Med.* (1980) 37:321–9. doi: 10.1080/09553008014550371
46. Weiss H, Epp ER, Heslin JM, Ling CC, Santomasso A. Oxygen depletion in cells irradiated at ultra-high dose-rates and at conventional

dose-rates. *Int J Radiat Biol Relat Stud Phys Chem Med.* (1974) 26:17–29. doi: 10.1080/09553007414550901
47. Michaels HB, Epp ER, Ling CC, Peterson EC. Oxygen sensitization of CHO cells at ultrahigh dose rates: prelude to oxygen diffusion studies. *Radiat Res.* (1978) 76:510–21. doi: 10.2307/3574800
48. Adrian G, Konradsson E, Lempart M, Bäck S, Ceberg C, Petersson K. The FLASH effect depends on oxygen concentration. *Br J Radiol.* (2019). doi: 10.1259/bjr.20190702. [Epub ahead of print].
49. Hendry JH, Moore JV, Hodgson BW, Keene JP. The constant low oxygen concentration in all the target cells for mouse tail radionecrosis. *Radiat Res.* (1982) 92:172–81. doi: 10.2307/3575852
50. Spitz DR, Buettner GR, Petronek MS, St-Aubin JJ, Flynn RT, Waldron TJ, et al. An integrated physico-chemical approach for explaining the differential impact of FLASH versus conventional dose rate irradiation on cancer and normal tissue responses. *Radiother Oncol.* (2019) 139:23–7. doi: 10.1016/j.radonc.2019.03.028
51. Pratx G, Kapp DS. A computational model of radiolytic oxygen depletion during FLASH irradiation and its effect on the oxygen enhancement ratio. *Phys Med Biol.* (2019) 64:185005. doi: 10.1088/1361-6560/ab3769
52. Chan N, Bristow RG. "Contextual" synthetic lethality and/or loss of heterozygosity: tumor hypoxia and modification of DNA repair. *Clin Cancer Res.* (2010) 16:4553–60. doi: 10.1158/1078-0432.CCR-10-0527
53. Leszczynska KB, Göttgens EL, Biasoli D, Olcina MM, Ient J, Anbalagan S, et al. Mechanisms and consequences of ATMIN repression in hypoxic conditions: roles for p53 and HIF-1. *Sci Rep.* (2016) 6:21698. doi: 10.1038/srep21698
54. Ling CC, Michaels HB, Epp ER, Peterson EC. Oxygen diffusion into mammalian cells following ultrahigh dose rate irradiation and lifetime estimates of oxygen-sensitive species. *Radiat Res.* (1978) 76:522–32. doi: 10.2307/3574801
55. Varia MA, Calkins-Adams DP, Rinker LH, Kennedy AS, Novotny DB, Fowler WC, et al. Pimonidazole: a novel hypoxia marker for complementary study of tumor hypoxia and cell proliferation in cervical carcinoma. *Gynecol Oncol.* (1998) 71:270–7. doi: 10.1006/gyno.1998.5163
56. Yovino S, Kleinberg L, Grossman SA, Narayanan M, Ford E. The etiology of treatment-related lymphopenia in patients with malignant gliomas: modeling radiation dose to circulating lymphocytes explains clinical observations and suggests methods of modifying the impact of radiation on immune cells. *Cancer Invest.* (2013) 31:140–4. doi: 10.3109/07357907.2012.762780
57. Durante M, Yamada S, Ando K, Furusawa Y, Kawata T, Majima H, et al. Measurements of the equivalent whole-body dose during radiation therapy by cytogenetic methods. *Phys Med Biol.* (1999) 44:1289–98. doi: 10.1088/0031-9155/44/5/314
58. Cannon DM, Mehta MP, Adkison JB, Khuntia D, Traynor AM, Tomé WA, et al. Dose-limiting toxicity after hypofractionated dose-escalated radiotherapy in non-small-cell lung cancer. *J Clin Oncol.* (2013) 31:4343–8. doi: 10.1200/JCO.2013.51.5353
59. Masucci GL. Hypofractionated radiation therapy for large brain metastases. *Front Oncol.* (2018) 8:379. doi: 10.3389/fonc.2018.00379
60. Shaw E, Scott C, Souhami L, Dinapoli R, Kline R, Loeffler J, et al. Single dose radiosurgical treatment of recurrent previously irradiated primary brain tumors and brain metastases: final report of RTOG protocol 90–05. *Int J Radiat Oncol Biol Phys.* (2000) 47:291–8. doi: 10.1016/S0360-3016(99)00507-6
61. Gupta A, Khan AJ, Yegya-Raman N, Sayan M, Ahlawat S, Ohri N, et al. 5-year results of a prospective phase 2 trial evaluating 3-week hypofractionated whole breast radiation therapy inclusive of a sequential boost. *Int J Radiat Oncol Biol Phys.* (2019) 105:267–74. doi: 10.1016/j.ijrobp.2019.05.063
62. Widmark A, Gunnlaugsson A, Beckman L, Thellenberg-Karlsson C, Hoyer M, Lagerlund M, et al. Ultra-hypofractionated versus conventionally fractionated radiotherapy for prostate cancer: 5-year outcomes of the HYPO-RT-PC randomised, non-inferiority, phase 3 trial. *Lancet.* (2019) 394:385–95. doi: 10.1016/S0140-6736(19)31131-6
63. Milano MT, Mihai A, Kang J, Singh DP, Verma V, Qiu H, et al. Stereotactic body radiotherapy in patients with multiple lung tumors: a focus on lung dosimetric constraints. *Exp Rev Anticancer Ther.* (2019) 17:959–69. doi: 10.1080/14737140.2019.1686980
64. Nabavizadeh N, Waller JG, Fain R, Chen Y, Degnin CR, Elliott DA, et al. Safety and efficacy of accelerated hypofractionation and stereotactic body radiation therapy for hepatocellular carcinoma patients with varying degrees of hepatic impairment. *Int J Radiat Oncol Biol Phys.* (2018) 100:577–85. doi: 10.1016/j.ijrobp.2017.11.030
65. van Marlen P, Dahele M, Folkerts M, Abel E, Slotman BJ, Verbakel WFAR. Bringing FLASH to the clinic: treatment planning considerations for ultrahigh dose-rate proton beams. *Int J Radiat Oncol Biol Phys.* (2019). doi: 10.1016/j.ijrobp.2019.11.011. [Epub ahead of print].
66. Lempart M, Blad B, Adrian G, Bäck S, Knöös T, Ceberg C, et al. Modifying a clinical linear accelerator for delivery of ultra-high dose rate irradiation. *Radiother Oncol.* (2019) 139:40–5. doi: 10.1016/j.radonc.2019.01.031
67. Schüler E, Trovati S, King G, Lartey F, Rafat M, Villegas M, et al. Experimental platform for ultra-high dose rate FLASH irradiation of small animals using a clinical linear accelerator. *Int J Radiat Oncol Biol Phys.* (2017) 97:195–203. doi: 10.1016/j.ijrobp.2016.09.018
68. Bazalova-Carter M, Liu M, Palma B, Dunning M, McCormick D, Hemsing E, et al. Comparison of film measurements and Monte Carlo simulations of dose delivered with very high-energy electron beams in a polystyrene phantom. *Med Phys.* (2015) 42:1606–13. doi: 10.1118/1.4914371
69. Schüler E, Eriksson K, Hynning E, Hancock SL, Hiniker SM, Bazalova-Carter M, et al. Very high-energy electron (VHEE) beams in radiation therapy; Treatment plan comparison between VHEE, VMAT, and PPBS. *Med Phys.* (2017) 44:2544–55. doi: 10.1002/mp.12233
70. Kokurewicz K, Brunetti E, Welsh GH, Wiggins SM, Boyd M, Sorensen A, et al. Focused very high-energy electron beams as a novel radiotherapy modality for producing high-dose volumetric elements. *Sci Rep.* (2019) 9:10837. doi: 10.1038/s41598-019-46630-w
71. Lundh O, Rechatin C, Faure J, Ben-Ismaïl A, Lim J, De Wagter C, et al. Comparison of measured with calculated dose distribution from a 120-MeV electron beam from a laser-plasma accelerator. *Med Phys.* (2012) 39:3501–8. doi: 10.1118/1.4719962
72. Bazalova-Carter M, Esplen N. On the capabilities of conventional x-ray tubes to deliver ultra-high (FLASH) dose rates. *Med Phys.* (2019) 46:5690–5. doi: 10.1002/mp.13858
73. Grotzer MA, Schültke E, Bräuer-Krisch E, Laissue JA. Microbeam radiation therapy: clinical perspectives. *Phys Med.* (2015) 31:564–7. doi: 10.1016/j.ejmp.2015.02.011
74. Dubinov AE, Ochkina EI. Recirculating electron accelerators with noncircular electron orbits as radiation sources for applications (a Review). *Phys Particles Nuclei.* (2018) 49:431–56. doi: 10.1134/S1063779618030048
75. Karsch L, Beyreuther E, Enghardt W, Gotz M, Masood U, Schramm U, et al. Towards ion beam therapy based on laser plasma accelerators. *Acta Oncol.* (2017) 56:1359–66. doi: 10.1080/0284186X.2017.1355111
76. Patriarca A, Fouillade C, Auger M, Martin F, Pouzoulet F, Nauraye C, et al. Experimental set-up for FLASH proton irradiation of small animals using a clinical system. *Int J Radiat Oncol Biol Phys.* (2018) 102:619–26. doi: 10.1016/j.ijrobp.2018.06.403
77. Varian Medical Systems. *FlashForward^{TM} Consortium [Press Release]* (2018).
78. Fiddian-Green RG, Silen W. *First Flash Irradiation Delivered in an IBA Gantry Treatment Room [Press Release]* (2019).
79. Mevion Medical Systems, Inc. *Focus on the Future : FLASH Therapy [Press Release]* (2019).

Conflict of Interest: The authors declare that the research was conducted in the absence of any commercial or financial relationships that could be construed as a potential conflict of interest.

The reviewer M-CV declared a past supervisory role with one of the authors KP to the handling editor.

Copyright © 2020 Wilson, Hammond, Higgins and Petersson. This is an open-access article distributed under the terms of the Creative Commons Attribution License (CC BY). The use, distribution or reproduction in other forums is permitted, provided the original author(s) and the copyright owner(s) are credited and that the original publication in this journal is cited, in accordance with accepted academic practice. No use, distribution or reproduction is permitted which does not comply with these terms.

frontiers in Oncology

ORIGINAL RESEARCH
published: 21 January 2020
doi: 10.3389/fonc.2019.01461

Linking NRP2 With EMT and Chemoradioresistance in Bladder Cancer

Alexander Schulz[1†], Ielizaveta Gorodetska[1†], Rayk Behrendt[2], Susanne Fuessel[3], Kati Erdmann[3], Sarah Foerster[4], Kaustubh Datta[5], Thomas Mayr[4], Anna Dubrovska[1,6,7,8*] and Michael H. Muders[4*]*

[1] Faculty of Medicine and University Hospital Carl Gustav Carus, OncoRay-National Center for Radiation Research in Oncology, Technische Universität Dresden and Helmholtz-Zentrum Dresden-Rossendorf, Dresden, Germany, [2] Faculty of Medicine, Institute for Immunology, Technische Universität Dresden, Dresden, Germany, [3] Department of Urology, Technische Universität Dresden, Dresden, Germany, [4] Rudolf Becker Laboratory for Prostate Cancer Research, Center of Pathology, University of Bonn Medical Center, Bonn, Germany, [5] Department of Biochemistry and Molecular Biology, University of Nebraska Medical Center, Omaha, NE, United States, [6] Helmholtz-Zentrum Dresden - Rossendorf, Institute of Radiooncology – OncoRay, Dresden, Germany, [7] German Cancer Consortium (DKTK), Partner Site Dresden, Dresden, Germany, [8] German Cancer Research Center (DKFZ), Heidelberg, Germany

OPEN ACCESS

Edited by:
Paul N. Span, Radboud University Nijmegen Medical Centre, Netherlands

Reviewed by:
Hyuk-Jin Cha, Seoul National University, South Korea
Michael Wayne Epperly, University of Pittsburgh, United States

***Correspondence:**
Thomas Mayr
Thomas.Mayr@ukbonn.de
Anna Dubrovska
Anna.Dubrovska@OncoRay.de
Michael H. Muders
Michael.Muders@ukbonn.de

[†] *These authors share first authorship*

Specialty section:
This article was submitted to Radiation Oncology, a section of the journal Frontiers in Oncology

Received: *02 August 2019*
Accepted: *05 December 2019*
Published: *21 January 2020*

Citation:
Schulz A, Gorodetska I, Behrendt R, Fuessel S, Erdmann K, Foerster S, Datta K, Mayr T, Dubrovska A and Muders MH (2020) Linking NRP2 With EMT and Chemoradioresistance in Bladder Cancer. Front. Oncol. 9:1461. doi: 10.3389/fonc.2019.01461

Neuropilin-2 (NRP2) is a prognostic indicator for reduced survival in bladder cancer (BCa) patients. Together with its major ligand, vascular endothelial growth factor (VEGF)-C, NRP2 expression is a predictive factor for treatment outcome in response to radiochemotherapy in BCa patients who underwent transurethral resection. Therefore, we investigated the benefit of combining cisplatin-based chemotherapy with irradiation treatment in the BCa cell line RT112 exhibiting or lacking endogenous NRP2 expression in order to evaluate NRP2 as potential therapeutic target. We have identified a high correlation of NRP2 and the glioma-associated oncogene family zinc finger 2 (GLI2) transcripts in the cancer genome atlas (TCGA) cohort of BCa patients and a panel of 15 human BCa cell lines. Furthermore, we used *in vitro* BCa models to show the transforming growth factor-beta 1 (TGFβ1)-dependent regulation of NRP2 and GLI2 expression levels. Since NRP2 was shown to bind TGFβ1, associate with TGFβ receptors, and enhance TGFβ1 signaling, we evaluated downstream signaling pathways using an epithelial-to-mesenchymal transition (EMT)-assay in combination with a PCR profiling array containing 84 genes related to EMT. Subsequent target validation in NRP2 knockout and knockdown models revealed secreted phosphoprotein 1 (SPP1/OPN/Osteopontin) as a downstream target positively regulated by NRP2.

Keywords: bladder cancer, Neuropilin-2 (NRP2), glioma-associated oncogene family zinc finger 2 (GLI2), secreted phosphoprotein 1 (SPP1), osteopontin (OPN), epithelial-to-mesenchymal transition (EMT), RT112, J82

INTRODUCTION

Bladder cancer (BCa) is the 9th most common malignancy in the world with the highest incidence in Europe and North America (1). There are three main stages of this disease, the non-muscle invasive bladder cancer (NMIBC), the muscle invasive bladder cancer (MIBC), and the metastatic BCa. At diagnosis, 70% of the patients present with NMIBC, 20% with MIBC, and 10% with metastatic disease (2). While NMIBC can be treated with good outcome by transurothelial resection

of the bladder tumor (TURBT) and adjuvant intravesical Bacillus Calmette-Guérin (BCG) or chemotherapy, the treatment options for the more aggressive MIBC consist of neoadjuvant and adjuvant cisplatin treatment and radical cystectomy. Despite the aggressive therapy regimen, MIBC has a 50% risk to progress to metastatic disease. The average survival time in these patients is 14–15 months (3), and no curative treatment option is available for these patients. Only recently, immune checkpoint inhibition has become available in patients with metastatic disease. The success rate for this treatment is still uncertain. Nevertheless, new therapy options are urgently needed for this disease stage. Radiochemotherapy has emerged as a promising new option for improving locoregional control and being able to preserve the bladder and hence quality of life (4–6).

Our group previously demonstrated that Neuropilin-2 (NRP2) is a prognostic indicator for reduced survival in BCa patients. Together with its major ligand, vascular endothelial growth factor (VEGF)-C, NRP2 expression is capable of predicting treatment outcome in response to radiochemotherapy in BCa patients who underwent transurethral resection (7). NRP2 is a co-receptor frequently overexpressed in cancers. Because NRP2 expression is significantly associated with poor prognosis in renal cell carcinomas, colorectal carcinomas, gastric carcinomas, osteosarcoma, breast, pancreatic, and bladder cancer (7–13), it has become an attractive target for cancer therapy. This is in part due to the fact that NRP2 is implicated in signaling pathways commonly hijacked by tumor cells.

Hedgehog (Hh) signaling is silenced in many adult tissues; however, during tumorigenesis, it is often reactivated (14). Canonical Hh signaling is induced by sonic, indian, or desert Hh ligands and functions via glioma-associated oncogene family zinc finger (GLI) proteins, the major transcriptional effectors of Hh signaling (14). GLI proteins contain activation (GLI1, GLI2, and GLI3) and repression domains (GLI2 and GLI3) (15), thus differentially affecting their downstream target genes. Hh signaling can also be induced by non-canonical pathways including transforming growth factor (TGF)β-induced signaling (14, 16, 17). Non-canonical Hh signaling by TGFβ (and Wnt) was shown to induce GLI2 expression and activation (14). In another non-canonical pathway, NRP2 also directly enhances Hh signaling in a ligand-independent manner (18).

Epithelial-to-mesenchymal transition (EMT), a complex molecular process, plays an important role in tumor progression, invasion, and metastasis and is induced, among others, by TGFβ (19). EMT signaling is associated with therapy resistance in various tumor entities, including breast cancer (20), pancreatic cancer (21), and BCa (22). Interestingly, TGFβ1-induced EMT highly increased NRP2 protein levels and NRP2 was subsequently identified as a receptor for both the latent and active form of TGFβ1 (23).

Taken together, NRP2 supports a vast number of tumor-promoting events but seems to be less crucial in most healthy tissues, and thus, it has become an attractive target for anti-cancer therapy. In this report, we aimed to elucidate NRP2's role in TGFβ-mediated EMT as well as in radio(chemo)therapy treatment of BCa models.

RESULTS

The Relationship of NRP2 and GLI2 in BCa

Because NRP2 has previously shown to enhance TGFβ signaling, we first aimed to determine the correlation of NRP2 mRNA expression with the expression of other TGFβ regulated genes in bladder tumors. To achieve this aim, we employed data from 408 BCa patients of the provisional BCa cohort from The Cancer Genome Atlas (TCGA) data set. The complete list of genes can be found in **Supplementary Tables 1A,B**. One of the most interesting identified targets was the Hh transcription factor GLI2 ($r = 0.709$). It was more strongly associated with NRP2 expression than its related genes GLI1 ($r = 0.396$) or GLI3 ($r = 0.310$) (**Figure 1A**). Notably, this relation was confirmed in other TCGA data sets of breast and prostate cancer (**Supplementary Figures 1A,B**). Furthermore, we confirmed this strong correlation between NRP2 and GLI2 transcripts by qPCR in a panel of 15 human BCa cell lines (**Figure 1B** and **Supplementary Figure 1C**) and by analysis of NRP2 and GLI2 co-expression in the cell lines of urinary tract ($n = 26$) using RNA-sequencing (RNA-seq) data from the Broad Institute Cell Line Encyclopedia (**Supplementary Figure 1D**). In order to investigate the potential clinical impact of NRP2 and GLI2 expression levels, we compared overall survival of single gene signatures of either NRP2 or GLI2 to the combined NRP2/GLI2 signature in Kaplan–Meier plots with median separation. This analysis demonstrated that combining NRP2 and GLI2 gene expression results in a higher predictive value for overall survival (**Figures 1C–E**). Notably, the same trend was observed for disease-free survival (**Supplementary Figure 2**). This observation, together with the strong correlation of both transcripts, tempted us to investigate the relationship of NRP2 and GLI2 in more detail by selecting two BCa cell lines, namely, J82 and HS853T, showing robust mRNA levels of both NRP2 and GLI2 (**Supplementary Figure 1C**) for knockdown experiments. To further evaluate the role of NRP2 in TGFβ-induced EMT, we treated these cell lines with TGFβ1 in addition to the respective knockdown. siRNA-mediated knockdown of NRP2 resulted in a reduction of GLI2 expression in both cell lines. On the other hand, induction of NRP2 expression by TGFβ1 is impaired following GLI2 knockdown (**Figure 2**). This suggests a co-dependency of both targets based on the ligand initiating the downstream pathways. Notably, we also checked the expression of isoforms NRP2a and NRP2b as well as GLI1, a direct target gene of GLI2 (**Supplementary Figures 3**, **4**). As expected, GLI1 expression was also induced in response to TGFβ1 but to a lesser extent than GLI2. Accordingly, GLI1 levels were reduced following GLI2 knockdown. Isoforms NRP2a and NRP2b were induced similarly in TGFβ1-treated samples and GLI2 knockdown led to a shift of these isoforms in favor of NRP2b. A complete list of all p values for all targets and samples is provided in **Supplementary Table 2**.

In addition to the NPR2 knockdown in these cell lines, we created two NRP2 knockout clones from the cell line RT112. Wild-type (WT) and knockout (KO) cells were subjected to

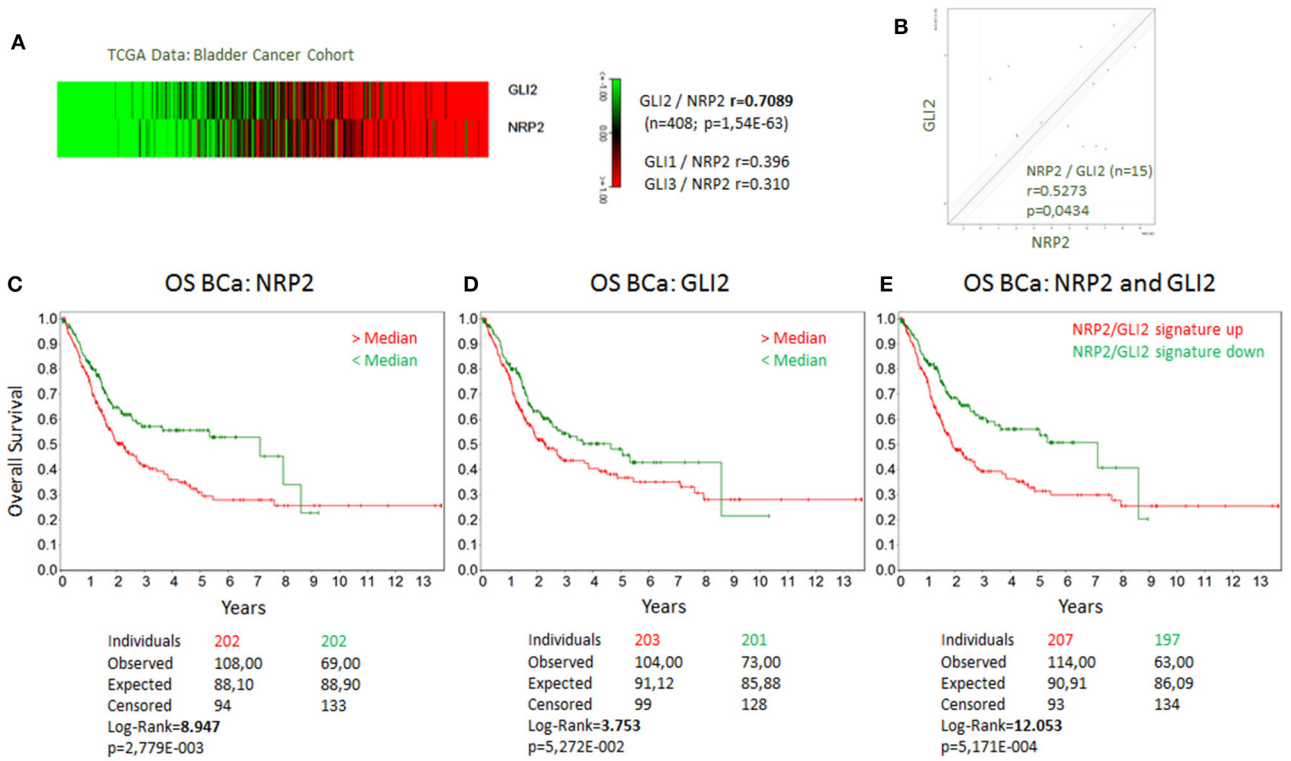

FIGURE 1 | Coexpression of GLI2 and NRP2 genes in BCa cells and correlation of GLI2 and NRP2 gene expression with overall survival of BCa patients. **(A)** Correlation of GLI2 and NRP2 gene expression in a provisional bladder cancer cohort of The Cancer Genome Atlas (TCGA). Correlation coefficient of GLI1 and GLI3 to NRP2 from the same data set is provided for comparison. **(B)** mRNA expression of NRP2 and GLI2 was correlated in a panel of 15 bladder cancer cell lines. Normalized to housekeeping gene HPRT1. Kaplan-Meier plot of overall survival (OS) of bladder cancer (BCa) patients with high (red) compared to low mRNA signature (green) for NRP2 **(C)**, GLI2 **(D),** and combined NRP2/GLI2 **(E)**. Log-Rank value was increased compared to single gene signature. The same applies for disease-free survival shown in **Supplementary Figure 2**.

treatment with TGFβ1 and compared to untreated controls. KO cell lines may still produce NRP2 transcript but the resulting mRNA contains premature translational stop codons on all alleles. While WT cells significantly increased the level of NRP2 mRNA in response to TGFβ1, both KO clones failed to upregulate transcription, potentially hinting to a positive feedback loop of NRP2 enhancing its own transcription upon TGFβ-signaling (**Figure 3A**). Moreover, TGFβ1 highly induced GLI2 in both WT and KO cell lines, suggesting that NRP2 is not upstream of TGFβ1-mediated GLI2 regulation. The mRNA level of GLI2 in WT cells was comparable to both KOs in the untreated state. In the treated samples, TGFβ1 induced GLI2 transcription more prominently in KO cell lines. However, this difference was not significant. Hence, TGFβ1-induced GLI2 expression seems to be independent of NRP2 in this model or cell line.

The fact that NRP2 is induced by more than 5-fold in WT cells raised the question whether upregulation is a direct effect of TGFβ signaling or TGFβ1 leads to faster degradation of NRP2, which may prompt cells to upregulate its transcription for maintaining constant NRP2 protein levels. Therefore, we performed Western blot analysis of WT lysates, which indicated that NRP2 protein was not upregulated significantly in TGFβ1-treated samples compared to untreated samples (**Figures 3B,C** and **Supplementary Figure 5A**). Despite the minor increase on protein level, it is not comparable to the 5-fold upregulation of NRP2 transcript, suggesting that the effect on mRNA level may potentially be a compensatory mechanism.

Knockout of NRP2 Alters Gene Expression of EMT Regulators

To investigate how NRP2 may enhance TGFβ-signaling, cDNA of WT and KO cell lines was analyzed by a PCR array covering 84 genes involved in EMT. By addition of TGFβ1, EMT was successfully and similarly induced in both KO clones and their wild-type parental cell line RT112 as visible by an increase in the EMT marker vimentin (**Supplementary Figure 5B**). With this approach, it was possible to identify four genes whose expression was altered in both KOs compared to WT without TGFβ1 treatment. When all cell lines received TGFβ1 treatment, one gene was found to be deregulated in KOs vs. WT cells (**Figure 4**). Validation of these targets by qPCR in four biological repeats demonstrated that upregulation of Caldesmon 1 (CALD1) and Cadherin 2 (CDH2, N-Cadherin) was not significant but Secreted Phosphoprotein 1 (SPP1) and Six Transmembrane Epithelial

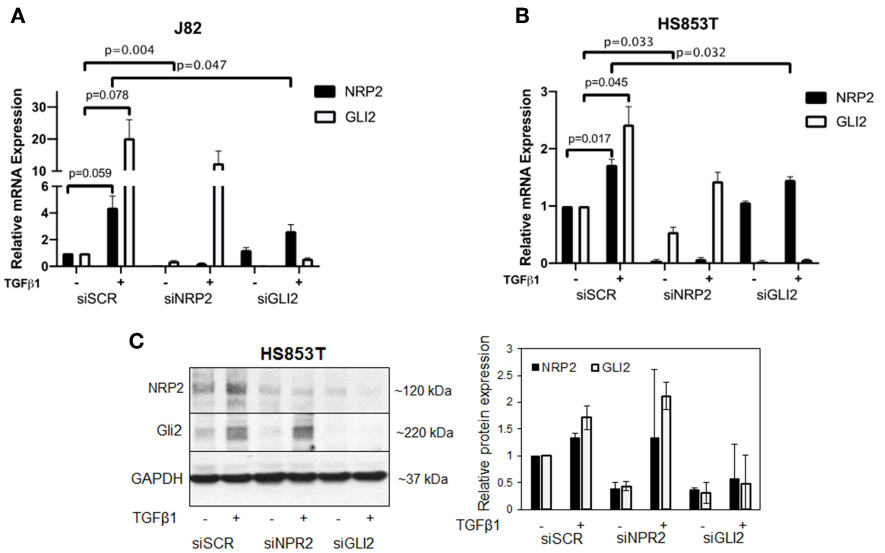

FIGURE 2 | Validation of the relationship of NRP2 and GLI2 in BCa cells after NRP2 and GLI2 knockdown. Quantitative real-time PCR in two cell lines: J82 **(A)** and HS853T **(B)** with robust expression of NRP2 and GLI2 were subjected to knockdown of these gene products (siNRP2 or siGLI2) or scrambled control (siSCR) and treated with 5 ng/ml TGFβ1 or left untreated (±). All transcripts were induced by TGFβ1 treatment. GLI2 levels were reduced after NRP2 knockdown while NRP2 induction by TGFβ1 is inhibited following GLI2 knockdown. Normalized to housekeeping gene HPRT1 and plotted relative to untreated siSCR sample. Significance calculated by two-way ANOVA. Error bars indicate standard error of the mean. $n = 3$. Not all p values are shown. A plot of all targets including NRP2a, NRP2b, and GLI1 is provided in **Supplementary Figure 3**. The figure also contains additional graphs with normalization against two other housekeeping genes ACTB and GAPDH. All p values for all cell lines are provided in **Supplementary Table 2**. **(C)** Western blot analysis of NRP2 and GLI2 expression in HS853T cells in response to GLI2 or NRP2 knockdown. Cells were transfected with gene-specific siRNA (siNRP2 or siGLI2) or siSCR and treated with 5 ng/ml TGFβ1 or left untreated (±). Relative protein expression was normalized to GAPDH. Error bars indicate standard deviation. $n = 2$.

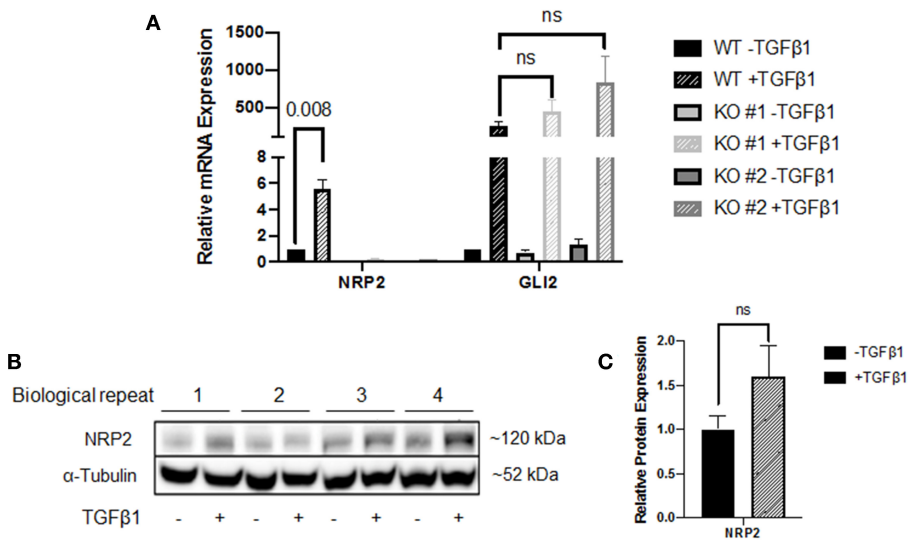

FIGURE 3 | Analysis of the NRP2 and GLI2 relationship in BCa cells after NRP2 knockout. **(A)** mRNA expression of NRP2 and GLI2 transcript in response to TGFβ1 treatment of two independent NRP2 knockout clones (KO #1 and KO #2) and their parental wild-type BCa cell line RT112 (WT). Untreated samples were used as control. NRP2 transcripts are highly induced by TGFβ1 only when NRP2 protein is expressed. Normalized to housekeeping gene HPRT1. Significance calculated by two-way ANOVA. Error bars indicate standard error of the mean. $n = 4$. **(B)** Western blot of WT cell line for NRP2 and α-tubulin as loading control. **(C)** Calculation of optical densitometry. Significance determined by two-tailed, unpaired Student's t test. $n = 4$.

Antigen of Prostate Family Member 1 (STEAP1) mRNA levels were significantly downregulated in KO clones (**Figure 5A**). When cells were treated with TGFβ1, mRNA expression of Secreted Protein Acidic and Cysteine Rich (SPARC) was highly upregulated but remained non-significant (**Figure 5B**). As an example, SPP1 expression as determined by the human EMT

A

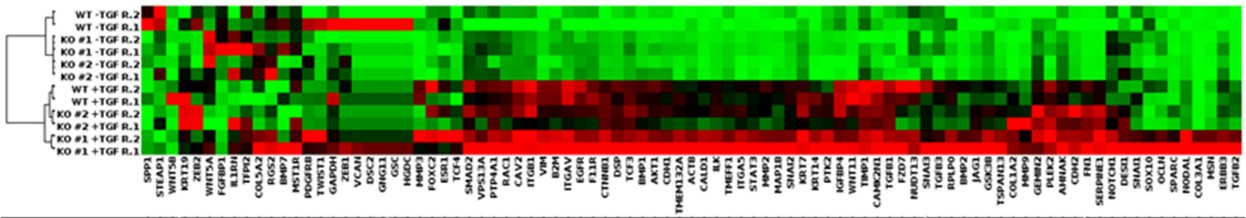

B

Comparison	Gene Symbol	Gene Name	Mean Fold Change	Correlation Coefficient
KOs vs. WT -TGFβ1	CALD1	Caldesmon 1	+3,86	0,823
	CDH2	Cadherin 2 (N-Cadherin)	+3,41	0,517
	SPP1	Secreted Phosphoprotein 1 (Osteopontin)	-5,55	0,413
	STEAP1	Six Transmembrane Epithelial Antigen of Prostate Family Member 1	-2,99	0,255
KOs vs. WT +TGFβ1	SPARC	Secreted Protein Acidic and Cysteine Rich (Osteonectin)	+9,23	0,744

FIGURE 4 | Analysis of the expression levels of EMT-related genes in wild type and NRP2 knockout BCa cells using PCR gene expression array. **(A)** Clustergram for all samples and genes on the PCR array plate extracted from Qiagen data analysis center software. **(B)** Consistently deregulated genes in both KOs vs. WT samples and their correlation based on the TCGA data set. $n = 2$.

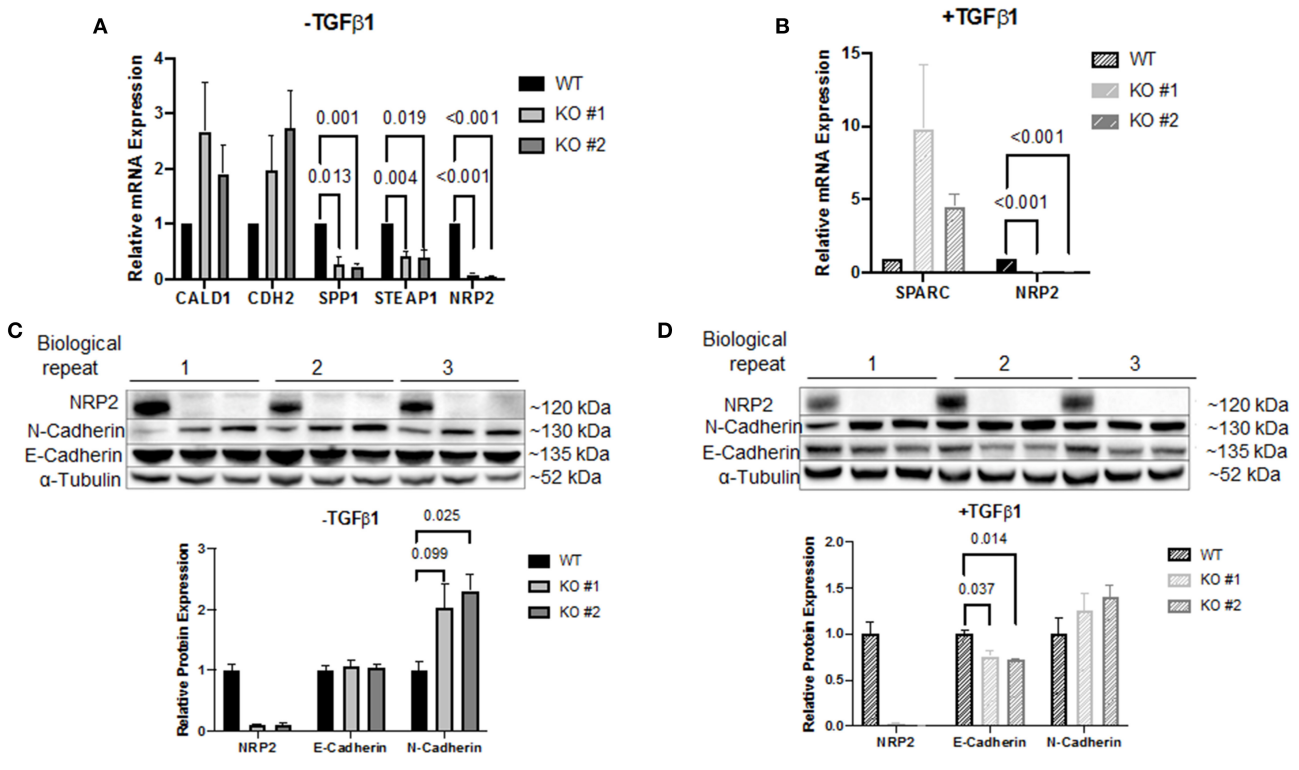

FIGURE 5 | Validation of the PCR array results. Target validation by qPCR in two NRP2 knockout clones (KO #1, KO #2) compared to their parental wild-type cell line RT112 (WT) **(A)** without TGFβ1 treatment or **(B)** including TGFβ1 treatment. Genes SPP1 and STEAP1 were significantly affected by NRP2 knockout in both knockout clones. For other targets, data were either inconsistent or not significant. Data were normalized to housekeeping gene HPRT1. Significance calculated by two-way ANOVA. Error bars indicate standard error of the mean. $n = 4$. **(C)** Western blot of samples that remained untreated for proteins NRP2, N-Cadherin, and E-Cadherin. α-Tubulin served as loading control. Untreated KO cells demonstrated increased N-Cadherin expression. **(D)** Western blot of TGFβ1-treated KO clones did not show a significantly upregulated N-Cadherin expression compared to parental cells but revealed downregulated E-Cadherin on protein level. Significance calculated by two-way ANOVA. Error bars indicate standard error of the mean. $n = 3$.

PCR array is lower in both KO clones compared to the wild-type parental cell line (**Supplementary Figure 6**).

CDH2 was the only target that demonstrated robust mRNA expression in both conditions. Therefore, validation on protein level seemed promising only for this target. Western blot analysis demonstrated that N-Cadherin (gene CDH2) appeared to be upregulated following knockout of NRP2 without TGFβ1 treatment (**Figure 5C**). Since E-Cadherin is known to be an opposing player of N-Cadherin in EMT, we used this target as control. Surprisingly, lysates from TGFβ1-treated samples showed significantly decreased levels of E-Cadherin in KOs compared to WT despite no change in gene expression was detected by the PCR array (**Figure 5D**). qPCR of CDH1 (E-Cadherin) confirmed that this change did not arise from altered transcript levels (**Supplementary Figure 7**). Because EMT-related signaling pathways are involved in the regulation of cancer stem cell (CSC) phenotype and properties in urothelial carcinoma including BCa, we analyzed if the absence of NRP2 has an impact on the CSC-related properties (24). Sphere forming assays revealed that the number of spheres formed by KO cells was significantly reduced (**Supplementary Figure 8A**).

To confirm the aberrant EMT signature in an additional cell line, we used conventional siRNA-mediated knockdown of NPR2 in the BCa cell line J82 and HS853T (**Figures 6A,B** and **Supplementary Figure 8B**). The results show that all except one gene (STEAP1) were significantly altered by NRP2 knockdown (**Figures 6A,B**). Analysis of BCa TCGA dataset also revealed that all validated genes positively correlate with expression of both NRP2 and GLI2 genes (**Supplementary Figure 8C**). However, only one gene transcript was regulated in a similar manner to NRP2 knockout in RT112 as well as NRP2 knockdown in J82 (**Figure 6C**). The SPP1 gene (Osteopontin, OPN) was previously reported to be induced by VEGF (25) and to be associated with decreased survival, disease stage, and grading in BCa (26, 27). Previous findings support the role of SPP1 as one of the key EMT regulators (28). We applied an EMT PCR array to analyze if SPP1 regulates gene expression of EMT regulators in our cell models. We found that SPP1 knockdown in J82 cells decreased expression of a number of key EMT genes including SNAI1, COL1A2, FGFBP1, and STAT3 (**Figure 6D**). In the TCGA BCa cohort, SPP1 expression positively correlated with both NRP2 and GLI2 (**Figure 6E**). Although our data did not confirm that SPP1 might be a regulator of BCa radiosensitivity on its own, analysis of TCGA BCa dataset showed that combined NRP2/SPP1 signature improved predictive value for disease-free but not overall survival compared to single NRP2 gene expression (**Supplementary Figures 8D,E**, **9**, **10**).

The Relevance of NRP2 to Treatment With Radiochemotherapy

The standard curative treatment of BCa is surgery and chemotherapy. Only for progressed stages of disease

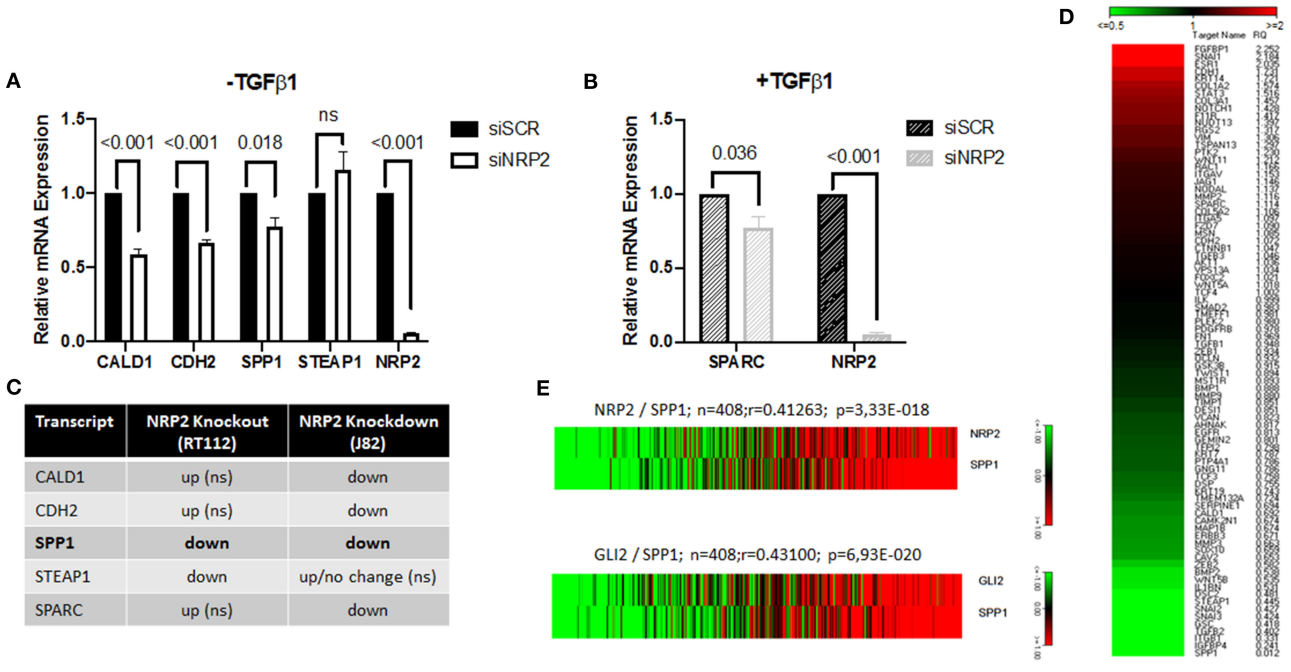

FIGURE 6 | Identification of SPP1 as one of the NRP2-regulated and EMT-associated genes. qPCR of all identified targets following NRP2 knockdown in cell line J82 **(A)** excluding or **(B)** including TGFβ1 treatment. Significance calculated by two-way ANOVA. Error bars indicate standard error of the mean. $n = 3$. **(C)** Comparison of deregulated genes by NRP2 knockout in RT112 or NRP2 knockdown in J82. SPP1 is the only gene reacting the same way to both depletions in two different cell lines. ns = not significant. **(D)** Analysis of J82 cells transfected with siSCR (three pooled biological repeats) and J82 cells transfected with siSPP1 (three pooled biological repeats) with EMT PCR array. **(E)** Correlation of NRP2 with SPP1 and GLI2 with SPP1 in a provisional bladder cancer cohort of The Cancer Genome Atlas (TCGA).

other therapy options like radiochemotherapy and immunotherapy gained importance. Based on the fact that NRP2 and its ligand VEGF-C predicted treatment response to radiochemotherapy in patients (7), we analyzed the response of our KO and WT cell lines to radiotherapy and combined radiochemotherapy with cisplatin (**Figures 7A,B** and **Supplementary Figure 11**). Significances for plating efficacy are shown in **Supplementary Figure 12**, and the alpha–beta ratio defined from interpolation of linear–quadratic cell survival curves are shown in **Supplementary Figures 13A,B**. Our results indicate that there was no immediately visible effect between both KOs and their parental WT cell line. All cell lines responded to additional cisplatin treatment with significantly reduced clonogenic survival and plating efficacy. To identify the potential benefit of chemotherapy in addition to radiation treatment, we calculated the radiobiological enhancement ratio (RER) for each subset. The RER is an indicator of the radiosensitizing effect of any potential agent used as it compares the ratio of the surviving fraction from the radiation only to the radiation in combination with any agent at a specific dose. Analysis of RER showed a higher benefit of radiochemotherapy for KO cells than for WT cells (**Figure 7C** and **Supplementary Figure 13C**).

DISCUSSION

NRP2 and GLI2 Interplay Is Dependent on the Ligand

The close relationship of NRP2 to GLI2 was discovered by correlation of genes in a provisional TCGA BCa data set (**Supplementary Table 1A**). Interestingly, this correlation of GLI2 and NRP2 was even stronger ($r = 0.709$) than the correlation of GLI2 to either GLI1 ($r = 0.555$) or GLI3 ($r = 0.252$). This is surprising because GLI1 is known to be a direct target gene of GLI2 in both the canonical and non-canonical Hh pathway (14, 16, 29, 30) (**Supplementary Table 1B**). We analyzed GLI1 levels for additional functional verification of GLI2 knockdown and could confirm that GLI1 levels were reduced following knockdown with a GLI2-specific siRNA pool. Since GLI1 levels are directly dependent on the expression of GLI2, we cannot fully exclude the possibility that changes in NRP2 could also be mediated through GLI1 or other downstream targets of GLI2 despite the fact that correlation between NRP2 and GLI2 is by far highest compared to GLI1 or GLI3 in a patient cohort. Whether or not this interdependency of the two gene products is a direct or indirect effect was demonstrated in two human BCa cell lines that GLI2 levels are regulated in

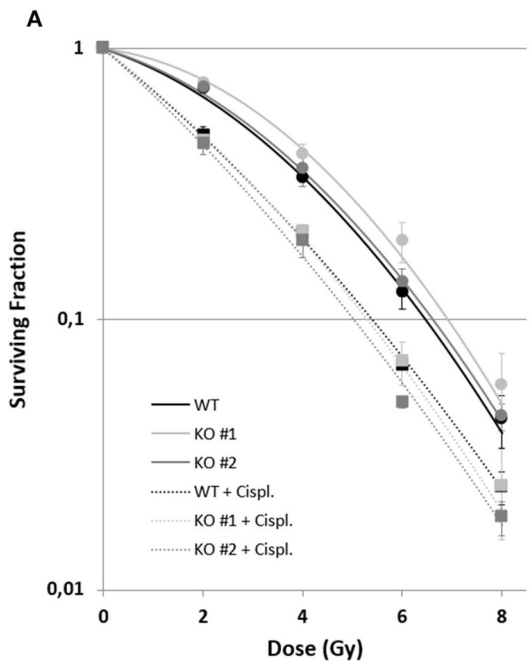

B

Group	Comparison	p-value
Radiotherapy Group	WT- / KO #1-	0.287
	WT- / KO #2-	0.797
	KO #1- / KO #2-	0.465
Radiochemo-therapy Group	WT+ / KO #1+	0.830
	WT+ / KO #2+	0.065
	KO #1+ / KO #2+	0.535
Cell Lines	WT- / WT+	<0.001
	KO #1- / KO #1+	<0.001
	KO #2- / KO #2+	<0.001

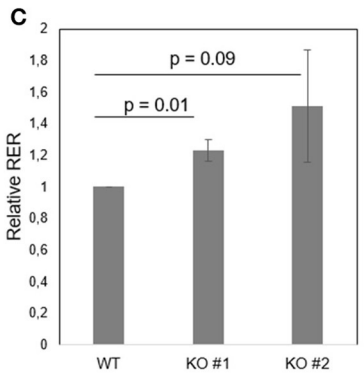

FIGURE 7 | NRP2 regulates BCa radiochemosensitivity. **(A)** Surviving fraction of cell line RT112 either harboring (WT—black) or lacking (KO #1—light gray, KO #2—dark gray) endogenous NRP2 after radiotherapy treatment with doses of 0, 2, 4, 6, and 8 Gy (dots). All cell lines were additionally treated with the chemotherapeutic drug cisplatin (Cispl. IC5 for KO #2 = 1.52 μM) for 24 h prior to radiation (squares). Plotted lines were fitted using the linear quadratic model for both the radiochemotherapy group (dashed lines) and the radiation only group (solid lines). Error bars indicate standard error of the mean. $n = 3$. **(B)** Table of significance of fitted curves. Significance was calculated by SPSS software. –, without cisplatin (Cispl.); +, with cisplatin. **(C)** Radiation enhancement ratios (RERs) were calculated at doses 2, 4, 6, and 8 Gy from interpolation of linear-quadratic cell survival curves using mean values of three independent experiments. Relative RER values for KO #1 and KO #2 were calculated as *RERrel = Average* ([*RER KO*, 2*Gy*]/[*RER WT*, 2*Gy*];[*RER KO*, 4*Gy*]/[*RER WT*, 4*Gy*];[*RER KO*, 6*Gy*]/[*RER WT*, 6*Gy*];[*RER KO*, 8*Gy*]/[*RER WT*, 8*Gy*]). Error bars indicate standard error of the mean. $n = 3$.

part through NRP2 and that NRP2 mRNA levels are partially regulated by GLI2 signaling in a TGFβ1-dependent manner. In contrast to cell lines J82 and HS853T, another cell line (5637) showed no changes in the expression of these genes possibly because TGFβ1 failed to induce their expression. Consequently, the relationship of NRP2 and GLI2 could not be observed in this cell line (**Supplementary Figure 14**). Because prediction of overall and disease-free survival could be improved by combining NRP2 and GLI2 gene expression in the TCGA patient cohort, these results suggest a functional interplay between NRP2 and GLI2 in regulating tumor growth, although the mechanisms of this interplay still remain elusive and merit further investigation. Notably, GLI2 knockdown also changed the ratio of isoforms NRP2a and NRP2b in favor of the latter in two BCa cell lines. It was recently described in a lung cancer model that while NRP2a is almost dispensable for tumor formation and metastasis, NRP2b severely impacted these traits (31). The authors demonstrated that TGFβ1 predominantly upregulated NRP2b and that TGFβ1-dependent stabilization was specifically dedicated to isoform NRP2b. In our model, both NRP2 isoforms were equally increased on mRNA level, but this induction might be the result of compensating for increased protein degradation following TGFβ1 treatment given that the protein level of total NRP2 was not significantly increased.

NRP2 Positively Regulates Osteopontin Expression

The active ligand TGFβ1 is a potent inducer of EMT. For investigating how NRP2 might enhance EMT, we chose a qPCR array containing 84 genes involved in EMT signaling and checked cDNA from two NRP2 knockout cell lines and their parental wild-type cell line RT112. Using this approach, a number of genes were deregulated in both KO clones compared to the parental cell line irrespective of the housekeeping gene used. Validation of these genes in four independent biological repeats confirmed their altered expression, although the change for CALD1, CDH2, and SPARC1 was not significant. Because the expression of CDH2 mRNA was sufficient to detect this target by Western blot, we checked the expression of the corresponding protein N-Cadherin as well as its counterpart E-Cadherin as control in treated and untreated conditions. Although N-Cadherin expression doubled in KO clones without TGFβ1-treatment, only one KO clone showed a significant increase. However, when TGFβ1-treatment was applied, we detected a significant reduction in both KO clones, although the change was less dramatic than for N-Cadherin in the untreated condition. There have been numerous reports in the past stating the significance of cadherin switching in progression and malignancy of BCa pointing to the importance of elucidating the mechanism for targeted therapy (32–37). Moreover, it was already shown that NRP2 and E-Cadherin expression are connected in multiple cancer types (23, 38–41). However, unlike the positive correlation in our model system, all publications reported a negative correlation. It has previously been described for melanoma that Osteonectin (gene SPARC) can downregulate E-Cadherin (42). We could show a 4.5-fold (KO #2) to 9.8-fold (KO #1) upregulation of SPARC compared to WT when treated with TGFβ1. Although this change was not found to be significant, it was still the highest deregulated gene within the panel. Therefore, the reduced E-Cadherin (CDH1) expression might be a direct result of increased SPARC expression. Given that the authors of the cited paper only investigated E-Cadherin by Western blot but not by qPCR and the fact that the change of E-Cadherin in our model was only visible on protein level suggests that SPARC might not control E-Cadherin transcriptionally. Previous studies showed that SPARC induces β-catenin nuclear localization and binding to the transcriptional regulator lymphocyte-enhancer factor-1 (LEF-1) (43, 44), whereas E-Cadherin forms alternative complexes with β-catenin in the adherens junctions (AJ). These AJ complexes prevent β-catenin nuclear localization and transactivation as well as E-Cadherin internalization (45). We can hypothesize that SPARC can induce loss of β-Catenin in the AJ by triggering its nuclear translocation that might result in E-Cadherin endocytosis and degradation. Of note, protein levels of N-Cadherin (CDH2) after TGFβ1-treatment did not change dramatically anymore, potentially indicating that this change is independent of the ligand TGFβ1.

In order to investigate if the identified targets were specific to that cell line or if signaling pathways were deregulated for compensation of complete NRP2 loss in the knockout cells, we used siRNA-mediated depletion of NRP2 in another human cell line (J82). The results confirmed deregulation of all but one gene (STEAP1), but the direction of change was only consistent for one gene (SPP1/Osteopontin/OPN). Thus, changes in other genes are either cell line specific or long-term KO models adapt to missing NRP2 by deregulation of other EMT pathways that were initially downregulated in the short-term knockdown model (for example, CALD1, CDH2, and SPARC). But given that Osteopontin was the only target significantly downregulated in both NRP2 KO and knockdown models in different cell lines, we propose that this dependency might be a general mechanism. To our knowledge, this is the first report linking NRP2 and SPP1/OPN in any tissue or cancer entity by showing that NRP2 acts upstream of SPP1 in a TGFβ1-independent manner. This can be an explanation for the VEGF-induced OPN expression, which was demonstrated in a large number of cases (25). OPN was shown to be upregulated in multiple cancer types including breast and prostate cancer as well as glioblastoma and melanoma (46, 47). Regarding BCa, immunohistochemical staining of OPN demonstrated significant correlation with tumor stage (27). More recently, Wong and colleagues showed that OPN expression correlates with disease stage and grading and that higher OPN expression led to decreased survival in multiple patient cohorts (26). Of note, we could not see the same in our TCGA data set when applying median expression for overall and disease-free survival (**Supplementary Figure 9**). However, combining NRP2 and OPN expression slightly improved prediction of disease-free but not overall survival (**Supplementary Figure 10**). Since OPN is a secreted soluble molecule, it may serve as an attractive non-invasive prognostic marker in serum or urine. One study investigated plasma OPN levels before and after tumor resection in 50 patients with BCa and found significantly higher preoperative OPN levels in patients with muscle invasive tumors despite the relatively low number of patients. OPN levels also increased significantly with T stage when patients had undergone radical cystectomy. The strong

trend of correlation with tumor grade and predicting recurrence did not reach statistical significance, potentially indicating that patient number for this analysis was too low (48). Similar to OPN, the expression pattern of NRP2 was previously reported to be significantly associated with pathological stage and tumor grade in a BCa cohort, suggesting a prominent role of NRP2 in BCa progression (49).

Because OPN is also associated with bone matrix formation, it would be highly interesting to analyze if the connection between NRP2 and OPN is also true for cancer entities like breast and prostate cancer, where bone metastases remain a big challenge.

NRP2 as Target for Radiochemotherapy

Overall and disease-free survival data suggested NRP2 as prognostic indicator for a TCGA BCa cohort. Our group previously showed that expression of NRP2 as well as its ligand VEGF-C could predict treatment outcome of BCa patients following TURBT and radiochemotherapy. This clinical finding prompted us to use our NRP2 KO and WT cell lines for an *in vitro* assay to determine their clonogenicity after radio(chemo)therapeutic treatment. When looking at the radiotherapy group only, no significant differences between both KO and the WT cell lines were found, which confirmed the previous finding that NRP2 expression alone in the patient group receiving only local radiotherapy was not a prognostic factor (7). When the same analysis was applied to the group of patients, which received radiochemotherapy, NRP2 was highly prognostic for overall and cancer-specific survival. In accordance to this clinical observation, we revealed a radiation dose-dependent trend toward higher profit of additional chemotherapy in KO cells, suggesting that NRP2 downregulation results in BCa radiochemosensitization. The exact role of NRP2 for radiochemotherapy in BCa warrants further investigation using additional cell lines and animal models.

Taken together, our study demonstrated that mRNA expression of NRP2 and GLI2 highly correlate in BCa cell lines and the TCGA BCa cohort. They influence each other's expression depending on the presence or absence of TGFβ1, a potent inducer of EMT. Moreover, screening of 84 genes involved in EMT identified SPP1/Osteopontin as a downstream target of NRP2 in two different BCa cell lines using different model systems.

Future research is needed to evaluate the exact mechanism of how NRP2 and GLI2 communicate bidirectionally, how NRP2 modulates SPP1 transcription, and what implications this will have for development and progression of other cancer entities apart from bladder carcinoma.

MATERIALS AND METHODS

Cell Lines and Cell Culture

The cell line RT112 (DSMZ) was maintained in MEM alpha medium with GlutaMAX supplemented with 10% FBS (fetal bovine serum, both Gibco, Life Technologies, Waltham, USA). The cell line and their knockout derivatives were validated to be RT112 by single nucleotide polymorphism (SNP) profiling (performed by Multiplexion GmbH, Friedrichshafen, Germany). Cell line J82 (ATCC) and HS853T (ATCC) were cultured in DMEM medium (4.5 g/L glucose) supplemented with 10% FBS (both Gibco, Life Technologies, Waltham, USA), 1% HEPES solution, and 1% MEM non-essential amino acids (both Sigma-Aldrich, St. Louis, USA). The cell line 5637 (ATCC) was cultured in RPMI supplemented with 10% FBS (both Gibco, Life Technologies, Waltham, USA). All cell lines were subject to regular testing for excluding mycoplasma contamination (last on 2nd April 2019). All cells were maintained at standard conditions in a humidified incubator with 5% CO_2 at 37°C.

CRISPR/Cas9-Mediated Deletion of NRP2 in RT112 Cells

Plasmid-based CRISPR/Cas9 technology was used to generate RT112 cell clones deficient in NRP2 expression according to the protocol established by Ran et al. (50). In brief, DNA double stranded oligonucleotides located in the exon 3 splice acceptor region (NRP2e3gu1-top: 5′-CACCGGATAAAGTCAT ACCTGGGTG-3′, NRP2e3gu1-bottom: 5′-AAACCACCCAGG TATGACTTTATCC-3′) and exon 3 coding region (NRP2e3gu2-top sequence: 5′-CCACCGGGTGAACTTGATGTAGAGCA-3′; NRP2e3gu1-bottom sequence: 5′-AAACTGCTCTACATCAAG TTCACCC-3′) of the NRP2 locus were designed using the Benchling software (San Francisco, USA) and cloned into pSpCas9 BB2A-GFP for gu1 (PX458, Addgene, LGC Standards, UK) or pSpCas9 BB-2A-Puro for gu2 (PX459v2, Addgene). RT112 cells were transfected by calcium phosphate precipitation with a 1:1 ratio of PX458-NRP2e3gu1 and PX459v2-NRP2e3-gu2 for 8 h, kept under puromycin selection (0.5 μg/ml) for 24 h and then seeded at low density. One hundred clones were picked after two weeks, grown and checked for the desired 110 bp deletion in NRP2 exon 3 by PCR on isolated genomic DNA using primers 5′-AGTGCCCTTCGCTTATCCATC-3′ and 5′-TC TAAGACGCCCATCTCCCG-3′. Clones that carried the deletion in the NRP2 locus were further checked for mutations within the corresponding region of the NRP1 locus (primer sequences 5′-GCTGGATGATGCTGGTGTCTA-3′ and 5′-TTCTACCGTA AGCTGTTCACTC-3′) and for Cas9 (primer sequences 5′-CG ACGACAGCCTGACCTTTA-3′ and 5′-TTGATGCCCTCTTC GATCCG-3′) to exclude integration of transfected plasmids. Sanger sequencing of the PCR amplification products verified the deletions. TOPO cloning of DNRP2 PCR products and subsequent Sanger sequencing of single mutated alleles yielded the sequences of individual deletion alleles for NRP2 in two individual RT112 DNRP2 cell clones. Three independent mutant alleles were identified for both RT112 DNRP2 clones, with altered exon 3 splice acceptor sequences and/or introduction of frame shifts due to nucleotide insertions or deletions:

(clone: mutant alleles; mutation; location of mutation in NRP2 exon 3)
#J9 (KO#1): J9high-3 delAG; delCT delAG (−2;−1); delCT (107; 108)
#J9 (KO#1): J9high-2 del111 deletion: −4 to +107
#J9 (KO#1): J9high-1 del111 deletion: −2 to +109
#J32(KO′2): #J32-5 insC; delT insC (−3); delT (107)

#J9 (KO#2): #J32low-1 del110 deletion: −3 to +107
#J9 (KO#1): #J32-P2 del111 deletion: −4 to +107

Both RT112 DNRP2 cell clones were checked for the absence of NRP2 expression by Western blot immunostaining using an anti-NRP2 antibody (R&D Systems, Minneapolis, USA). For reasons of simplicity, the clones are referred to as knockout (KO) #1 (clone #J9) and KO #2 (clone #J32) in this publication.

TGFβ1-Induced EMT

RT112 WT and derived KO cell lines were seeded at 1×10^5 cells per well in a 6-well culture plate containing 2 ml of serum-reduced (5 % FBS) growth medium either including or lacking 5 ng/ml TGFβ1 (Miltenyi Biotec, Bergisch Gladbach, Germany). After 48 h in the incubator, the medium was renewed and cells were incubated for another 24 h before RNA or protein isolation. In total, four independent biological repeats were performed with cells at different passages. RNA of two repeats was used for "RT^2 Profiler PCR Array" for human EMT and all four repeats were used for validation of identified targets by qPCR. Protein was used for immunoblotting.

Transfection of Cell Lines With siRNA

Cell lines J82, HS853T, and 5637 were used for knockdown experiments. 2×10^5 (J82, HS853) or 5×10^5 (5,637) cells per well were seeded in a 6-well culture plate with 2 ml complete growth medium (10% FBS) and incubated 24 h to allow attachment. Next, medium was renewed and liposomal transfection was conducted according to the manufacturer's protocol using 12 µl of Lipofectamine RNAi MAX (Thermo Fisher Scientific, Waltham, USA) and 50 nM siRNA (SMARTpool by Dharmacon, Lafayette, USA). The catalog number of siRNA pools was D-001810-10-20 (siSCR, control), L-017721-00-0010 (siNRP2), L-0066468-00-0005 (siGLI2), and L-012558-00-0005 (SPP1). Cells were treated with TGFβ1 as described above.

RNA Isolation, cDNA Synthesis, and qPCR

RNA was isolated with the RNeasy Plus Mini Kit (Qiagen, Hilden, Germany) by adding 350 µl of lysis buffer RLT Plus supplemented with 1% β-mercaptoethanol (Sigma-Aldrich, St. Louis, USA) to a well of a 6-well plate that was previously rinsed with PBS. Using a scraper, lysed cells were collected from the plate and transferred to a DNA removal column. The following steps were carried out according to the manufacturer's protocol and RNA was eluted from the column by addition of 30 µl of RNase-free water (Qiagen, Hilden, Germany). cDNA from 1,000 ng of total RNA input was synthesized by employing the PrimeScriptTM RT Reagent Kit (Takara Bio Inc., Kusatsu, Japan) according to the manufacturer's instructions. cDNA was diluted 1:5 with RNase-free water before continuing with real-time quantitative polymerase chain reaction (qPCR). qPCR was conducted using the TB GreenTM Premix Ex TaqTM II (Takara Bio Inc., Kusatsu, Japan) according to the manufacturer's protocol for a total reaction volume of 20 µl. The qPCR cycling conditions were set on a StepOnePlus system (Applied Biosystems, Waltham, USA): 94°C for 3 min, 40 cycles: 94°C for 15 s, 58°C 60 s, 72°C 60 s followed by a melt curve to 95°C in steps of 0.3°C. All experiments were conducted using at least two (for housekeeping genes) or three technical replicates (other targets) and most experiments included three different housekeeping genes as control: ACTB, GAPDH, and HPRT1. All primer sequences are listed in **Supplementary Table 3**. cDNA of the following BCa cell lines was used for qPCR analyses of NRP2 and GLI2: 5637 (ATCC), 639V (DSMZ), Cal29 (DSMZ), EJ28 (University Frankfurt), HS853T (ATCC), HT1376 (ATCC), J82 (ATCC), UMUC-3 (ATCC), UMUC-14 (Sigma-Aldrich), UMUC-16 (Sigma-Aldrich), VMCUB (DSMZ), KU1919 (DSMZ), RT112 (DSMZ), T24 (DSMZ), and TCC-SUP (DSMZ). HPRT1 served as housekeeping gene. ΔCt values were used to calculate correlation in SUMO software (http://angiogenesis.dkfz.de/oncoexpress/software/sumo/).

RT^2 Profiler PCR Array for Human EMT

cDNA synthesis was performed following RNA isolation as described above (total volume: 10 µl). For each 96-well plate, a master mix was prepared composed of 1,050 µl of TB Green™ Premix Ex Taq™ II, 42 µl of ROX dye, 1,000 µl of RNase-free water, and 10 µl of cDNA sample. From this master mix, 20 µl was added to each well. The PCR program was identical to the one described above. For the human EMT PCR array (Qiagen, Hilden, Germany), two out of four biological replicates were chosen that displayed values closest to the median. Later, all four biological replicates were evaluated for target validation. Data were extracted using the housekeeping gene HPRT1 from the EMT profiler plate.

Protein Isolation and Immunoblotting

Protein was isolated from 1-well of a 6-well plate by washing cells once with PBS before adding cold 200-µl RIPA buffer (Thermo Fisher Scientific, Waltham, USA) supplemented with Complete inhibitor (Roche, Basel, Switzerland), proteinase, and phosphatase inhibitor (both Thermo Fisher Scientific, Waltham, USA). Lysates were collected with cell scrapers, transferred to a 1.5-ml reaction tube and centrifuged at 10,000 rpm at 4°C for 10 min in a 5415R cooling centrifuge (Eppendorf, Hamburg, Germany). Supernatant was transferred to a new reaction tube and protein was quantified by Pierce™ BCA Protein Assay Kit (Thermo Fisher Scientific, Waltham, USA) according to the manufacturer's protocol. Thirty-five micrograms of total protein lysate was loaded into each pocket of a 12-well Bolt 4–12% Bis-Tris Plus Gel (Thermo Fisher Scientific, Waltham, USA) running in an XCell SureLock™ Electrophoresis Cell (Invitrogen, Carlsbad, USA) at 90 V for 2 h in MOPS buffer (Thermo Fisher Scientific, Waltham, USA). Wet transfer to a methanol-activated 0.2-µm Amersham™ Hybond™ Low Fluorescence PVDF membrane (GE Healthcare, Chicago, USA) was achieved by applying 90 V for 4 h in a cooled Mini-PROTEAN® three transfer tank (Bio-Rad, Hercules, USA). Membranes were washed once with TBS-T before blocking the membrane for 1 h at room temperature with 2.5% ECL Prime™ blocking agent (GE Healthcare, Chicago, USA) dissolved in TBS. Membranes were incubated at 4°C overnight with primary antibodies (see **Supplementary Table 4** for the complete list of used antibodies) diluted in 2.5% ECL Prime™ blocking agent solution before applying three washing steps with TBS-T. Then, membranes were incubated with the appropriate secondary

antibodies diluted in 2.5% ECL Prime™ blocking agent solution for 1 h at room temperature. Following another three washing steps with TBS-T, chemiluminescent detection was performed by first incubating the membrane with Pierce® ECL Western Blotting Substrate (Thermo Fisher Scientific, Waltham, USA) and subsequent detection of the signal in auto-rapid mode in a ChemiDoc™ MP Imaging System (Bio-Rad, Hercules, USA). Colorimetric images were taken for determining the molecular weight of the signals. Calculation of optical densitometry was performed with ImageJ software.

Colony Forming Assay Following Radiochemotherapy

For radiochemotherapy treatment, cells were seeded into a 6-well plate at a density of 4×10^5 cells per well and treated with cisplatin (TEVA GmbH, Ulm, Germany) for 24 h at concentrations of 1.52×10^{-6} M that corresponded to the IC_5 value of KO #2 (**Supplementary Figure 11**). Twenty-four hours after start of the treatment, cells were trypsinized and used for radiobiological colony forming assay. Clonogenic survival was determined by seeding of 500 (ionizing radiation—IR only) or 750 (IR + cisplatin) cells in technical triplicates into 6-well plates containing 2 ml of complete growth medium. Cells were cultivated overnight and then irradiated with doses of 0, 2, 4, 6, and 8 Gy (Yxlon Y.TU 320; 200 kV X-rays, dose rate 1.3 Gy/min at 20 mA, filtered with 0.5 mm Cu). Irradiated cells were returned to the incubator for allowing recovery and growth for 6 days. Colonies were fixed by the addition of 600 µl of 37% formaldehyde solution (Merck, Darmstadt, Germany) directly to the culture medium and incubation at room temperature for 30 min. Following removal of this solution and a washing step with normal tap water, 1 ml of a 0.05% crystal violet solution (Sigma-Aldrich, St. Louis, USA) was added to each well for 30 min at room temperature for staining colonies. Crystal violet was removed, and wells were washed twice with normal tap water and dried overnight before manually counting colonies using a stereomicroscope (Zeiss, Oberkochen, Germany). Cell survival data were entered into the SPSS program for calculation of α and β values, curve fitting to the linear quadratic model, and determination of statistical significance.

Analysis of the TCGA Patient Cohort Data

From the TCGA patient cohort data set, Pearson coefficient was determined using SUMO software and significance was calculated by two-tailed, unpaired Student's *t* test. For evaluation of combined NRP2/GLI2 signature expression, the data for each of these genes were normalized to median across the entire dataset and log2 transformed. Further, the mean of two genes was calculated for each patient and the subset with known survival data was extracted from complete cohort. Finally, the up- and down-regulated groups for Kaplan–Meier analysis were defined as the mean of NRP2/GLI2 expression was positive or negative value accordingly.

Statistical Analysis

The cell survival curves were analyzed using the Statistical Package for the Social Sciences (SPSS) v23 software as described previously (51) by linear–quadratic formula $S(D)/S(0) = \exp-(\alpha D + \beta D2)$ using stratified linear regression. A $p < 0.05$ was considered statistically significant. Correlation of gene expression levels was evaluated by SUMO software using Pearson correlation coefficient. IC_{50} and IC_5 values (50 and 5% inhibitory concentration) were determined by non-linear regression using GraphPad Prism software (San Diego, USA).

DATA AVAILABILITY STATEMENT

All datasets generated for this study are included in the article/**Supplementary Material**.

AUTHOR CONTRIBUTIONS

AS performed most experiments and wrote and edited the manuscript. IG performed revision experiments and edited the manuscript. RB helped to teach CRISPR/Cas9 technology and designed the guide RNAs. SFu and KE provided cell lines and cDNA of cell lines and edited the manuscript. SFo and KD edited the manuscript. TM generated and validated the knockout clones from cell line RT112. TM, AD and MM supervised and guided AS, edited the manuscript, and aided in scientific questions including experimental design. AD helped perform radiochemotherapy and colony forming assay.

FUNDING

Work in AD lab was partially supported by grants from Deutsche Forschungsgemeinschaft (DFG) (273676790, 401326337, and 416001651), from Wilhelm Sander-Stiftung (2017.106.1), BMBF (Grant-No. 03Z1NN11), and DLR Project Management Agency (01DK17047). This work was in part supported by German Academic Exchange Service (DAAD) and the Federation of European Biochemical Societies (FEBS) for IG. Work in MM lab was partially supported by a grant from Deutsche Forschungsgemeinschaft (DFG) (273676790). The professorship of MM was also funded by the Rudolf Becker Foundation of Translational Prostate Cancer Research. MM was a member of the German BRIDGE consortium. This work was in part supported by the graduate academy of Technische Universität Dresden for AS.

ACKNOWLEDGMENTS

The authors kindly want to thank Vasyl Lukiyanchuk for analysis of TCGA datasets and for help with analysis of PCR array data and SPSS statistical analysis. We thank Jakob Püschel for help with radiobiological clonogenic analysis. We also thank Dorothee Pfitzmann for technical advice and providing cisplatin. The authors thank all members of AD and MM lab for useful discussions.

SUPPLEMENTARY MATERIAL

The Supplementary Material for this article can be found online at: https://www.frontiersin.org/articles/10.3389/fonc.2019.01461/full#Supplementary-material

REFERENCES

1. Cumberbatch MGK, Jubber I, Black PC, Esperto F, Figueroa JD, Kamat AM, et al. Epidemiology of bladder cancer: a systematic review and contemporary update of risk factors in 2018. *Eur Urol.* (2018) 74:784–95. doi: 10.1016/j.eururo.2018.09.001
2. Spiess PE, Agarwal N, Bangs R, Boorjian SA, Buyyounouski MK, Clark PE, et al. Bladder cancer, version 5.2017, NCCN clinical practice guidelines in oncology. *J Natl Compr Canc Netw.* (2017) 15:1240–67. doi: 10.6004/jnccn.2017.0156
3. Maase von der H, Sengelov L, Roberts JT, Ricci S, Dogliotti L, Oliver T, et al. Long-term survival results of a randomized trial comparing gemcitabine plus cisplatin, with methotrexate, vinblastine, doxorubicin, plus cisplatin in patients with bladder cancer. *J Clin Oncol.* (2005) 23:4602–8. doi: 10.1200/JCO.2005.07.757
4. Riou O, Chauvet B, Lagrange J-L, Martin P, Llacer Moscardo C, Charissoux M, et al. [Radiotherapy of bladder cancer]. *Cancer Radiother.* (2016) 20(Suppl):S196–9. doi: 10.1016/j.canrad.2016.07.010
5. Raby SEM, Choudhury A. Radiotherapy for high-grade T1 bladder cancer. *Eur Urol Focus.* (2018) 4:506–8. doi: 10.1016/j.euf.2018.07.017
6. James ND, Hussain SA, Hall E, Jenkins P, Tremlett J, Rawlings C, et al. Radiotherapy with or without chemotherapy in muscle-invasive bladder cancer. *N Engl J Med.* (2012) 366:1477–88. doi: 10.1056/NEJMoa1106106
7. Keck B, Wach S, Taubert H, Zeiler S, Ott OJ, Kunath F, et al. Neuropilin-2 and its ligand VEGF-C predict treatment response after transurethral resection and radiochemotherapy in bladder cancer patients. *Int J Cancer.* (2014) 136:443–51. doi: 10.1002/ijc.28987
8. Cao Y, Hoeppner LH, Bach S, Guangqi E, Guo Y, Wang E, et al. Neuropilin-2 Promotes Extravasation and Metastasis by Interacting with Endothelial 5 Integrin. *Cancer Res.* (2013) 73:4579–90. doi: 10.1158/0008-5472.CAN-13-0529
9. Boro A, Arlt MJ, Lengnick H, Robl B, Husmann M, Bertz J, et al. Prognostic value and *in vitro* biological relevance of Neuropilin 1 and Neuropilin 2 in osteosarcoma. *Am J Transl Res.* (2015) 7:640–53.
10. Samuel S, Gaur P, Fan F, Xia L, Gray MJ, Dallas NA, et al. Neuropilin-2 mediated β-catenin signaling and survival in human gastro-intestinal cancer cell lines. *PLoS ONE.* (2011) 6:e23208. doi: 10.1371/journal.pone.0023208
11. Rizzolio S, Tamagnone L. Multifaceted role of neuropilins in cancer. *Curr Med Chem.* (2011) 18:3563–75. doi: 10.2174/092986711796642544
12. Yasuoka H, Kodama R, Tsujimoto M, Yoshidome K, Akamatsu H, Nakahara M, et al. Neuropilin-2 expression in breast cancer: correlation with lymph node metastasis, poor prognosis, and regulation of CXCR4 expression. *BMC Cancer.* (2009) 9:237–7. doi: 10.1186/1471-2407-9-220
13. Dallas NA, Gray MJ, Xia L, Fan F, van Buren G, Gaur P, et al. Neuropilin-2-mediated tumor growth and angiogenesis in pancreatic adenocarcinoma. *Clin Cancer Res.* (2008) 14:8052–60. doi: 10.1158/1078-0432.CCR-08-1520
14. Cannonier SA, Gonzales CB, Ely K, Guelcher SA, Sterling JA. Hedgehog and TGFβ signaling converge on Gli2 to control bony invasion and bone destruction in oral squamous cell carcinoma. *Oncotarget.* (2016) 7:76062–75. doi: 10.18632/oncotarget.12584
15. Sasaki H, Nishizaki Y, Hui C, Nakafuku M, Kondoh H. Regulation of Gli2 and Gli3 activities by an amino-terminal repression domain: implication of Gli2 and Gli3 as primary mediators of Shh signaling. *Development.* (1999) 126:3915–24.
16. Javelaud D, Alexaki VI, Dennler S, Mohammad KS, Guise TA, Mauviel A. TGF-/SMAD/GLI2 signaling axis in cancer progression and metastasis. *Cancer Res.* (2011) 71:5606–10. doi: 10.1158/0008-5472.CAN-11-1194
17. Javelaud D, Pierrat M-J, Mauviel A. Crosstalk between TGF-β and hedgehog signaling in cancer. *FEBS Lett.* (2012) 586:2016–25. doi: 10.1016/j.febslet.2012.05.011
18. Hillman RT, Feng BY, Ni J, Woo WM, Milenkovic L, Hayden Gephart MG, et al. Neuropilins are positive regulators of Hedgehog signal transduction. *Genes Dev.* (2011) 25:2333–46. doi: 10.1101/gad.173054.111
19. Smith BN, Bhowmick NA. Role of EMT in metastasis and therapy resistance. *J Clin Med.* (2016) 5:17. doi: 10.3390/jcm5020017
20. Cheng GZ, Chan J, Wang Q, Zhang W, Sun CD, Wang L-H. Twist transcriptionally up-regulates AKT2 in breast cancer cells leading to increased migration, invasion, and resistance to paclitaxel. *Cancer Res.* (2007) 67:1979–87. doi: 10.1158/0008-5472.CAN-06-1479
21. Arumugam T, Ramachandran V, Fournier KF, Wang H, Marquis L, Abbruzzese JL, et al. Epithelial to mesenchymal transition contributes to drug resistance in pancreatic cancer. *Cancer Res.* (2009) 69:5820–8. doi: 10.1158/0008-5472.CAN-08-2819
22. McConkey DJ, Choi W, Marquis L, Martin F, Williams MB, Shah J, et al. Role of epithelial-to-mesenchymal transition (EMT) in drug sensitivity and metastasis in bladder cancer. *Cancer Metastasis Rev.* (2009) 28:335–44. doi: 10.1007/s10555-009-9194-7
23. Grandclement C, Pallandre JR, Valmary Degano S, Viel E, Bouard A, Balland J, et al. Neuropilin-2 expression promotes TGF-β1-mediated epithelial to mesenchymal transition in colorectal cancer cells. *PLoS ONE.* (2011) 6:e20444–14. doi: 10.1371/journal.pone.0020444
24. Fang D, Kitamura H. Cancer stem cells and epithelial-mesenchymal transition in urothelial carcinoma: possible pathways and potential therapeutic approaches. *Int J Urol.* (2017) 25:7–17. doi: 10.1111/iju.13404
25. Ramchandani D, Weber GF. Interactions between osteopontin and vascular endothelial growth factor: implications for cancer. *Biochim Biophys Acta.* (2015) 1855:202–22. doi: 10.1016/j.bbcan.2015.02.003
26. Wong JPC, Wei R, Lyu P, Tong OLH, Zhang SD, Wen Q, et al. Clinical and *in vitro* analysis of Osteopontin as a prognostic indicator and unveil its potential downstream targets in bladder cancer. *Int J Biol Sci.* (2017) 13:1373–86. doi: 10.7150/ijbs.21457
27. Coppola D, Szabo M, Boulware D, Muraca P, Alsarraj M, Chambers AF, et al. Correlation of osteopontin protein expression and pathological stage across a wide variety of tumor histologies. *Clin Cancer Res.* (2004) 10:184–90. doi: 10.1158/1078-0432.CCR-1405-2
28. Zhao H, Chen Q, Alam A, Cui J, Suen KC, Soo AP, et al. The role of osteopontin in the progression of solid organ tumour. *Cell Death Dis.* (2018) 9:356–15. doi: 10.1038/s41419-018-0391-6
29. Dennler S, Andre J, Alexaki I, Li A, Magnaldo T, Dijke ten P, et al. Induction of sonic hedgehog mediators by transforming growth factor-: Smad3-dependent activation of Gli2 and Gli1 Expression *in vitro* and *in vivo*. *Cancer Res.* (2007) 67:6981–6. doi: 10.1158/0008-5472.CAN-07-0491
30. Dennler S, André J, Verrecchia F, Mauviel A. Cloning of the human GLI2 Promoter: transcriptional activation by transforming growth factor-beta via SMAD3/beta-catenin cooperation. *J Biol Chem.* (2009) 284:31523–31. doi: 10.1074/jbc.M109.059964
31. Gemmill RM, Nasarre P, Nair-Menon J, Cappuzzo F, Landi L, D'Incecco A, et al. The neuropilin 2 isoform NRP2b uniquely supports TGFβ-mediated progression in lung cancer. *Sci Signal.* (2017) 10:eaag0528-7. doi: 10.1126/scisignal.aag0528
32. Hussein S, Mosaad H, Rashed HE, Ahmed S, Ragab A, Ismail EI. Molecular factors regulating E-cadherin expression in urothelial bladder cancer and their correlations with the clinicopathological features. *Mol Biol Rep.* (2017) 44:365–77. doi: 10.1007/s11033-017-4118-z
33. Lascombe I, Clairotte A, Fauconnet S, Bernardini S, Wallerand H, Kantelip B, et al. N-cadherin as a novel prognostic marker of progression in superficial urothelial tumors. *Clin Cancer Res.* (2006) 12:2780–7. doi: 10.1158/1078-0432.CCR-05-2387
34. Jäger T, Becker M, Eisenhardt A, Tilki D, Tötsch M, Schmid KW, et al. The prognostic value of cadherin switch in bladder cancer. *Oncol Rep.* (2010) 23:1125–32. doi: 10.3892/or_00000741
35. Luo Y, Zhu Y-T, Ma L-L, Pang S-Y, Wei L-J, Lei C-Y, et al. Characteristics of bladder transitional cell carcinoma with E-cadherin and N-cadherin double-negative expression. *Oncol Lett.* (2016) 12:530–6. doi: 10.3892/ol.2016.4671
36. Khorrami MH, Hadi M, Gharaati MR, Izadpanahi MH, Javid A, Zargham M. E-cadherin expression as a prognostic factor in transitional cell carcinoma of the bladder after transurethral resection. *Urol J.* (2012) 9:581–5.
37. Abufaraj M, Haitel A, Moschini M, Gust K, Foerster B, Özsoy M, et al. Prognostic role of N-cadherin expression in patients with invasive bladder cancer. *Clin Genitourin Cancer.* (2017) 16:e73-8. doi: 10.1016/j.urolonc.2017.01.012
38. Fung TM, Ng KY, Tong M, Chen J-N, Chai S, Chan K-T, et al. Neuropilin-2 promotes tumourigenicity and metastasis in oesophageal squamous cell carcinoma through ERK-MAPK-ETV4-MMP-E-cadherin deregulation. *J Pathol.* (2016) 239:309–19. doi: 10.1002/path.4728

39. Besharat ZM, Sabato C, Po A, Gianno F, Abballe L, Napolitano M, et al. Low expression of miR-466f-3p sustains epithelial to mesenchymal transition in sonic hedgehog medulloblastoma stem cells through Vegfa-Nrp2 signaling pathway. *Front Pharmacol.* (2018) 9:1281. doi: 10.3389/fphar.2018.01281
40. Evanno E, Godet J, Piccirilli N, Guilhot J, Milin S, Gombert JM, et al. Tri-methylation of H3K79 is decreased in TGF-β1-induced epithelial-to-mesenchymal transition in lung cancer. *Clin Epigenet.* (2017) 9:80. doi: 10.1186/s13148-017-0380-0
41. Nasarre P, Gemmill RM, Potiron VA, Roche J, Lu X, Barón AE, et al. Neuropilin-2 Is upregulated in lung cancer cells during TGF-β1-induced epithelial-mesenchymal transition. *Cancer Res.* (2013) 73:7111–21. doi: 10.1158/0008-5472.CAN-13-1755
42. Smit DJ, Gardiner BB, Sturm RA. Osteonectin downregulates E-cadherin, induces osteopontin and focal adhesion kinase activity stimulating an invasive melanoma phenotype. *Int J Cancer.* (2007) 121:2653–60. doi: 10.1002/ijc.23039
43. Nie J, Sage EH. SPARC inhibits adipogenesis by its enhancement of beta-catenin signaling. *J Biol Chem.* (2009) 284:1279–90. doi: 10.1074/jbc.M808285200
44. Alachkar H, Santhanam R, Maharry K, Metzeler KH, Huang X, Kohlschmidt J, et al. SPARC promotes leukemic cell growth and predicts acute myeloid leukemia outcome. *J Clin Invest.* (2014) 124:1512–24. doi: 10.1172/JCI70921
45. Orsulic S, Huber O, Aberle H, Arnold S, Kemler R. E-cadherin binding prevents beta-catenin nuclear localization and beta-catenin/LEF-1-mediated transactivation. *J Cell Sci.* (1999) 112(Pt 8):1237–45.
46. Rangaswami H, Bulbule A, Kundu GC. Osteopontin: role in cell signaling and cancer progression. *Trends Cell Biol.* (2006) 16:79–87. doi: 10.1016/j.tcb.2005.12.005
47. Shevde LA, Samant RS. Role of osteopontin in the pathophysiology of cancer. *Matrix Biol.* (2014) 37:131–41. doi: 10.1016/j.matbio.2014.03.001
48. Park M-G, Oh M-M, Yoon J-H, Park J-Y, Park H-S, Moon D-G, et al. The value of plasma osteopontin levels as a predictive factor of disease stage and recurrence in patients with bladder urothelial carcinoma: a prospective study. *Kaohsiung J Med Sci.* (2012) 28:526–30. doi: 10.1016/j.kjms.2012.04.014
49. Sanchez-Carbayo M, Socci ND, Lozano JJ, Li W, Charytonowicz E, Belbin TJ, et al. Gene Discovery in bladder cancer progression using cDNA microarrays. *AJPA.* (2010) 163:505–16. doi: 10.1016/S0002-9440(10)63679-6
50. Ran FA, Hsu PD, Wright J, Agarwala V, Scott DA, Zhang F. Genome engineering using the CRISPR-Cas9 system. *Nat Protoc.* (2013) 8:2281–08. doi: 10.1038/nprot.2013.143
51. Franken NAP, Rodermond HM, Stap J, Haveman J, van Bree C. Clonogenic assay of cells *in vitro*. *Nat Protoc.* (2006) 1:2315–9. doi: 10.1038/nprot.2006.339

Conflict of Interest: The authors declare that the research was conducted in the absence of any commercial or financial relationships that could be construed as a potential conflict of interest.

Copyright © 2020 Schulz, Gorodetska, Behrendt, Fuessel, Erdmann, Foerster, Datta, Mayr, Dubrovska and Muders. This is an open-access article distributed under the terms of the Creative Commons Attribution License (CC BY). The use, distribution or reproduction in other forums is permitted, provided the original author(s) and the copyright owner(s) are credited and that the original publication in this journal is cited, in accordance with accepted academic practice. No use, distribution or reproduction is permitted which does not comply with these terms.

frontiers in Oncology

REVIEW
published: 20 February 2020
doi: 10.3389/fonc.2020.00164

The Role of Cancer Stem Cells in Radiation Resistance

Christoph Reinhold Arnold[1]*, *Julian Mangesius*[1], *Ira-Ida Skvortsova*[1,2] and *Ute Ganswindt*[1]

[1] Department of Therapeutic Radiology and Oncology, Medical University of Innsbruck, Innsbruck, Austria, [2] EXTRO-Lab, Tyrolean Cancer Research Institute, Innsbruck, Austria

Cancer stem cells (CSC) are a distinct subpopulation within a tumor. They are able to self-renew and differentiate and possess a high capability to repair DNA damage, exhibit low levels of reactive oxygen species (ROS), and proliferate slowly. These features render CSC resistant to various therapies, including radiation therapy (RT). Eradication of all CSC is a requirement for an effective antineoplastic treatment and is therefore of utmost importance for the patient. This makes CSC the prime targets for any therapeutic approach. Albeit clinical data is still scarce, experimental data and first clinical trials give hope that CSC-targeted treatment has the potential to improve antineoplastic therapies, especially for tumors that are known to be treatment resistant, such as glioblastoma. In this review, we will discuss CSC in the context of RT, describe known mechanisms of resistance, examine the possibilities of CSC as biomarkers, and discuss possible new treatment approaches.

Keywords: cancer stem cells, radiation resistance, radiation therapy, DNA damage repair, reactive oxygen species, stem cell niche, quiescence

OPEN ACCESS

Edited by:
Marco Durante,
Helmholtz-Gemeinschaft Deutscher Forschungszentren (HZ), Germany

Reviewed by:
Emanuele Scifoni,
National Institute of Nuclear Physics (INFN), Italy
Claere Von Neubeck,
University of Duisburg-Essen, Germany

***Correspondence:**
Christoph Reinhold Arnold
christoph.arnold@i-med.ac.at

Specialty section:
This article was submitted to Radiation Oncology, a section of the journal Frontiers in Oncology

Received: *01 September 2019*
Accepted: *30 January 2020*
Published: *20 February 2020*

Citation:
Arnold CR, Mangesius J, Skvortsova I-I and Ganswindt U (2020) The Role of Cancer Stem Cells in Radiation Resistance. Front. Oncol. 10:164. doi: 10.3389/fonc.2020.00164

INTRODUCTION

Radiation therapy (RT) is one of the mainstays of cancer treatment. Roughly one half to two-third of all oncologic patients receive some form of RT in the course of their disease (1–5), either in a curative setting for primary treatment with or without other treatment modalities (i.e., surgery or chemotherapy, CHT) or in a palliative setting for the irradiation of symptomatic metastases. Importantly, the number of patients requiring RT is expected to increase in the foreseeable future (6). In short, RT exerts its effect by inducing DNA damage, either directly or indirectly via the production of water-derived radicals and reactive oxygen species (ROS) (7–9), which then interact with macromolecules including DNA, lipids and proteins. As a consequence, DNA damage response (DDR) is initiated and leads to the activation of the DNA damage repair machinery as well as the induction of checkpoint kinase pathways, which delay cell cycle progression in order to facilitate DNA repair (10–13). In case the DNA is damaged beyond repair, DDR signaling induces apoptosis, senescence or mitotic catastrophe, all of which imply the loss of reproductive capacity of a cell (14–16). Consequently, if successful, RT hinders cancer cells from further proliferation. In theory, every (cancerous) cell can be killed with RT given a high enough dose. However, the surrounding healthy tissue limits the applicable dose (17). RT is usually a balancing act between giving enough dose to achieve local tumor control and only as much dose as the surrounding tissue can tolerate. Despite a very high local tumor control rate, a non-negligible rate of therapy failure still constitutes one of the major limitations in radiation oncology (18, 19). Insufficient response to irradiation (i.e., radiation resistance) contributes to residual cancer mass, which is the key driver of locoregional or distant recurrence, both of which are negatively influencing the patient's prognosis as local recurrence often is associated with metastatic spread, which is almost always fatal.

In recent years evidence has accumulated showing that multiple genetically diverse clones co-exist within various kinds of tumors (20–24). Not all cells within a tumor are equally sensitive to RT. Understanding the diverse radiosensitivity of different tumor cell subpopulations is very important. It challenges the common practice of employing macroscopic bulk tumor responses (as measured with medical imaging) as the primary endpoint for determining the effectiveness of an anti-neoplastic treatment. While this is certainly a very practical approach, it is only then true if the bulk tumor response represents the response of all cells within the tumor, including the most resistant subpopulation within the tumor. This is most likely not the case for most tumors because not all subpopulations are equally affected by the treatment. The stem cell model of cancer development may explain genetic, functional, and phenotypical differences, such as increased therapy resistance, within a tumor, even within the same tumor clone. Cancer stem cells (CSC), albeit difficult to identify, are believed to contribute to resistance to various oncological therapies, including RT (25–34), making them a primary target for anti-cancer therapy. Hence, a proper understanding of differential sensitivity of cancer cells, especially CSC, to irradiation is vital in order to develop new or improve existing anti-cancer therapies. Most research on CSC has been done in breast cancer and glioma (35, 36). However, as CSC differ between entities results cannot be transferred to other tumors, at least not without caution.

CANCER STEM CELLS

Today, there are basically two largely accepted models for the origin of cancer: the standard (hierarchical) CSC model and the clonal evolution model. In the latter, genetic mutations accumulate with time and theoretically any cell can have tumorigenic potential (37). The CSC model describes a hierarchical organization of tumors with tumorigenic CSC at the apex which divide asymmetrically to form new CSC as well as differentiated non-tumorigenic progenies (34). Adding to the complexity of the CSC theory, is the fact that differentiation may be bidirectional. In this way, differentiated non-tumorigenic tumor cells may, instructed by niche signals, re-differentiate into CSC to replace lost stem cells. Even though data supporting the CSC hypothesis with its hierarchical organization of tumors is more solid, it is feasible that both, the CSC hypothesis and the clonal evolution model are not necessarily mutually exclusive.

The generation of CSC is not conclusively clarified, and several hypotheses exist (38). CSC may originate from normal stem cells, where random mutations during DNA replication may lead to them becoming malignant (39). Additionally, aberrant stromal signaling and pro-inflammatory conditions can lead to the malignant degeneration of normal stem cell (40). Alternatively, as stated earlier, CSC can be derived from differentiated cells. This can occur via genomic instability of tumor cells, horizontal genetic transfer, or microenvironmental signals. Genetic instability describes the acquisition of additional genetic mutations that provide any given differentiated tumor cell with stem cell traits so that it becomes a CSC (41). It is, however, unclear, whether stem cell traits shift from one cell to another in a stochastic manner during tumor evolution. In horizontal gene transfer, a normal stem cell may phagocyte fragmented DNA from tumor cells leading to their reprogramming and CSC formation (42). Microenvironmental signals include pro-inflammatory cytokines such as interleukin-6 (IL-6), which has been shown to facilitate dedifferentiation of non-CSC into CSC, or nuclear factor-kB (NF-kB), which maintains CSC numbers (43).

The frequency of CSC within a tumor is difficult to estimate and largely depends on the type of malignancy. In solid tumors, reported CSC rates are in the range from below 1% of all tumor cells to more than 80% (44–48). Similarly, the frequency of CSC in hematologic malignancies also displays a broad spectrum and ranges from <1% in acute myeloid leukemia (AML) up to over 80% in acute lymphoblastic leukemia (ALL) (49, 50). It has been shown in glioblastoma that CSC seem to reside predominantly in niches that are hypoxic, low in nutrients and have a low pH (51).

CSC are a distinct subpopulation within the heterogenous tumor mass and share several properties with normal stem cells (SC), the most important being the ability to self-renew (i.e., the potential of unlimited cell division) and the ability to give rise to more differentiated, mature cancer cells (34). Like in healthy tissue, stem cells initiate, promote, and maintain tumor development and growth (and re-growth after treatment) (52–55). It has been shown in glioma and breast cancer that the number of CSC in a tumor at the time of treatment is inversely correlated with clinical outcome (56, 57). Furthermore, repopulation of CSC after fractionated RT is one of the most important factors that determine local tumor control (58, 59). Therefore, inactivation of all CSC within a tumor is the prerequisite for a curative cancer treatment (60).

One major challenge regarding CSC is their correct identification as there is not one specific CSC marker, not least because of the high intra- and inter-tumor heterogeneity as well as tumor plasticity and the associated changes in genotype and phenotype. However, there are some cell surface marker that seem robust enough to use them as indicators for CSC. Two of these biomarkers are CD44 (found on CSC in cancers of the colon, esophagus, stomach, pancreas, breast, brain, lung, ovaries, prostate, liver, and the head and neck region) and CD133 (found in cancers of the colon, esophagus, stomach, pancreas, brain, lung, ovaries, prostate, liver, skin, and the head and neck region) (38, 61). Naturally, there are more surface molecules and usually combinations of these markers are used to identify and isolate CSC depending on the type of tumor that is investigated. It is important to emphasize that CSC differ between tumor entities, both phenotypically and functionally, and results from one type of cancer should not be translated to other types.

RADIOCURABILITY AND RADIATION THERAPY RESISTANCE

Following RT-induced DNA damage the balance of pro- and anti-apoptotic pathways skews toward cell death induction. However, in CSC pro-survival pathways seem to be more pronounced

and protect these cells from cell death, rendering CSC radiation resistant (27). Radiation resistance of CSC may either be primary, i.e., due to the constitutive upregulation of certain molecules and pathways (see below). Alternatively, radiation resistance of CSC may be acquired. Following RT, as is the case with any other antineoplastic therapy, intratumoral heterogeneity can theoretically promote clonal evolution through Darwinian selection and lead to the development of adaptive responses with the result of more resistant, aggressive, and invasive tumors (62). CSC clones with genomic alterations that protect them against RT are selected for and continue to sustain the tumor (63). Indeed, it is known that RT preferentially kills non-CSC, thereby enriching the tumor for CSC (64). In addition, RT has been shown to induce the reprogramming of non-CSC in breast cancer as well as squamous cell carcinoma of the head and neck (HNSCC) leads to the acquisition of functional CSC traits in order to compensate for cell loss in the stem cell compartment in response to cellular injury as is the case after RT (65, 66). Finally, RT leads to the recruitment of CSC in breast cancer from a quiescent state into the cell cycle (67, 68). In this way, RT contributes to the acquired or adaptive radioresistance via selective repopulation from the surviving CSC.

The number of CSC within a tumor predicts the radiation dose needed to eradicate the tumor. Therefore, in tumors with a higher proportion of CSC a given dose of irradiation leads to a lower probability of local control as compared to tumors with fewer CSC (69–71). From a clinical point of view, this implies a dose-volume dependency, as radiocurability of tumors inversely correlates with tumor volume (72) and with intrinsic radiosensitivity *in vitro* (73). Furthermore, the probability of successful irradiation also correlates with the number, density, and intrinsic radiosensitivity of CSC (60, 71) and the absolute number of CSC increases with tumor volume (70–72, 74). Importantly, survival of one single CSC after RT can lead to tumor relapse. Hence, eradication of the entire CSC population is of utmost importance for the patient. Nonetheless, one must keep in mind that CSC differ between tumor types and there is no general radiation resistance of CSC, as many patients can be cured with current concepts of conventional RT.

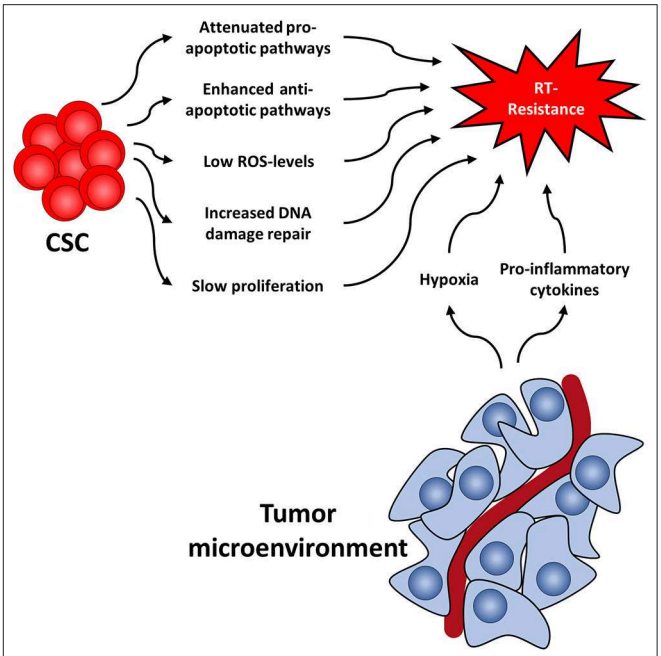

FIGURE 1 | Cancer stem cell-related factors as well as the tumor microenvironment both contribute to radioresistance and reveal new therapeutic approaches.

CELLULAR FACTORS FOR CSC RADIORESISTANCE

Several cellular features render CSC radioresistant. In the following, we will discuss the best-studied cellular factors, which include low levels of ROS, increased DNA damage repair capacity, or quiescence (**Figure 1**). These are common characteristics of healthy SC and CSC alike, presumably to protect their DNA from stress-induced damages.

ROS are involved in various physiological processes, such as proliferation, differentiation, metabolism, apoptosis, angiogenesis, wound healing, or motility (75, 76). Intracellular ROS levels are tightly and continuously regulated by ROS scavengers, which include superoxide dismutase, superoxide reductase, catalase, glutathione peroxidase, glutathione reductase, or apurinic/apyrimidinic endonuclease/redox effector factor (Ape1/Ref-1, also known as APEX1) (77). There is a multitude of publications showing that ROS scavengers are upregulated and highly efficient in CSC of various tumors (78–83) leading to low levels of ROS and protecting CSC from RT-induced cell death, as ROS is essential for the effect of RT (84). This protective effect of upregulated ROS scavengers even outweighs the effect of oxygen, a known potent radiosensitizer (85). Along this line, it has been shown that CSC produce less ROS upon radiation compared to non-CSC (86).

Secondly, DNA damage repair capacity following RT, especially regarding DNA double strand breaks (DSB), has been shown to be higher in CSC as compared to their non-tumorigenic counterparts (25, 87–90). This has been shown in CSC of several tumors, including glioma, nasopharyngeal carcinoma, prostate, lung, and breast cancer, and is mainly attributed to the activation of checkpoint-pathways in response to RT (90–98). The resulting delayed cell cycle progression allows for repair of the DNA damage. Interestingly, CSC have been shown to repair DNA damage preferably via homologous recombination (HR) instead of non-homologous end-joining (NHEJ), the latter being less accurate and more error-prone than HR (25, 99–101). A comprehensive review on DNA damage repair in CSC has recently been published (102).

Third, it has been shown in various studies that CSC proliferate more slowly than further differentiated cancer cells (78, 103, 104). This is of importance as RT is known to be more effective in killing rapidly proliferating tumor cells as compared to slowly dividing (i.e., quiescent or dormant) cells and quiescence is associated with relative radiation resistance (105, 106). This way, non-proliferating cells survive therapeutic

irradiations and remain quiescent for a various amount of time, which can range from weeks (78, 104) to even decades (107, 108). Once they continue to proliferate, these cells can cause a recurrence.

TUMOR MICROENVIRONMENT

Similar to healthy stem cells, CSC reside in specific niches that provide microenvironmental factors such as autocrine signaling and signals coming from stromal fibroblasts (cancer associated fibroblasts, CAF), immune cells, endothelial cells, and extracellular matrix components (109, 110). The exact composition of the niche is not well-defined for most tumors, as are the exact supporting signals. It is known, however, that the niche supplies CSC with oxygen and nutrients, supports stem cell functions, protects from insults such as radiation, and regulates responsiveness to a therapy (111). For instance, in breast cancer it has been shown that deregulation of the stem cell niche by increased expression of bone morphogenetic protein 2 (BMP2) can initiated and promote malignant stem cell transformation (112). Furthermore, at least in glioblastoma tumor samples, there are different types of niches, such as hypoxic peri-arteriolar niches, peri-vascular niches, peri-hypoxic niches, peri-immune niches, and extracellular niches (113). Whether other types of cancer have different types of niches, and what therapeutic implications this finding might have, still needs to be elucidated.

Like the tumor itself, the tumor microenvironment also responds to RT (114) (**Figure 1**). For instance, it has been shown that CAFs acquire a pro-malignant phenotype after RT of in colorectal cancer samples (115–117). Furthermore, CAFs induce autophagy following irradiation of lung cancer and melanoma cell lines leading to enhanced cancer cell recovery and tumor re-growth (118).

Additionally, RT induces pro-inflammatory cytokines in the tumor microenvironment (119, 120), including platelet-derived growth factor (PDGF), interleukin 1β (IL1β), tumor necrosis factor α (TNFα), transforming growth factor β (TGFβ), C-X-C motif chemokine 12 (CXCL12), and matrix metalloproteinases (MMP), and interleukin-6 (IL6). This leads to the upregulation of ROS scavengers in CSC (7) and activation of downstream STAT3 signaling, a cascade known to promote self-renewal in embryonic stem cells neu (121). Furthermore, this promotes survival of tumor cells, facilitates tumor regrowth and leads to the development of highly invasive CSC phenotypes (122, 123).

Another mechanism by which the niche protects CSC is hypoxia. Oxygen is a potent radiosensitizer and is needed for radiation-induced ROS production and in further consequence for cell death. Lack of oxygen is known to increase radiation resistance (124–126) and has been associated with early relapse after RT. Consequently, increasing tumor oxygenation improves the response to RT (127–129). In addition to the absolute lack of oxygen and the resulting low ROS levels, CSC in hypoxic niches upregulate ROS scanvengers (7, 130, 131), thereby further lowering ROS levels compared to normoxic CSC. This in turn leads to the activation of the hypoxia-inducible factor (HIF) signaling route (132–134). Interestingly, HIF1α and the respective regulated cytokines have also been shown to be increased following RT (135). HIF are important master regulators of transcription of hypoxia response elements, which activates pro-survival pathways such as the Notch, wingless and INT-1 (WNT) and Hedgehog pathway (136–138). These pathways have been shown to be important for CSC maintenance and can lead to radioresistance and accelerated repopulation of CSC during or after treatment, as has been shown in glioma, breast cancer, and prostate cancer (97, 139–142).

CSC AS BIOMARKER

There is accumulating evidence that CSC could be used as biomarkers to predict treatment response and estimate the likelihood of tumor relapse in cancer patients. It has been shown in various tumors, including urothelial cancer (143–145), gastric cancer (146–150), pancreatic cancer (151, 152), HNSCC (153–155), glioma (156–159), thyroid carcinoma (160, 161), hepatocellular carcinoma (162, 163), breast cancer (164), and lung cancer (165). However, it has been shown in ovarian cancer that the prognostic value of CD44 may depend on its isoform, with the transmembrane form indicating a better prognosis, while the presence of the soluble extracellular domain was associated with a worse prognosis (166). In a recent meta-analysis, overall CD44 expression in ovarian cancer was associated with a high TNM stage and a poor 5 year overall survival (167). Along this line, low expression of CD44 was shown to be an independent factor of poor prognosis in ovarian mucinous carcinoma (168). Interestingly, in breast cancer, it has been shown that CD44 was associated with longer disease-free-survival (DFS) in estrogen-receptor (ER) positive women, while CD44 positive tumors were associated with poor outcome in ER-negative patients (169). In a recent meta-analysis, Han and colleagues tried to generalize the prognostic significance of CD44 and its variant isoforms in advanced cancer patients. In this analysis of 15 articles with more than 1,200 patients, CD44 was slightly linked to a worse overall survival, but there was no correlation between CD44 expression and DFS, recurrence-free survival (RFS), or progression-free survival (PFS) (170).

Two studies from the German Cancer Consortium Radiation Oncology Group (DKTK-ROG) have shown that CSC marker expression is a potential biomarker for favorable prognosis in patients with locally advanced HNSCC, both after primary chemoradiotherapy (171) as well as following post-operative chemoradiotherapy (172). In a recent validation study from the same group, the addition of CD44 could further improve the prognostic performance of models using tumor volume, p16 status, and N stage (173).

Activity of the 26S proteasome, a protease complex with regulatory functions in cell cycle, DNA repair, and cell survival, is another CSC marker (131, 174–177). In this regard, low 26S proteasome activity correlated with high self-renewal capacity and high tumorigenicity in HNSCC cell lines (178). A high 26S proteasome activity

correlated with a longer survival and higher local control rates in patients who underwent chemoradiotherapy for HNSCC (95).

Another potential biomarker, especially for glioma, might be the stem cell marker CD133. In a recent meta-analysis including 21 articles with more than 1,550 patients, CD133 expression correlated with higher grade of gliomas and worse prognosis in glioma patients (179). Interestingly, in a recent *in vitro* analysis in glioma cell lines, CD133 expression could be downregulated by vincristine, a common chemotherapeutic drug (180). In a study by Wu and colleagues, CD133 promotor methylation was a significant prognostic factor for adverse PFS and overall survival, while there was no correlation between CD133 protein expression and survival (181). Additionally, there are other publications that showed no association of CD133 protein expression with survival (182, 183).

NOVEL TREATMENT APPROACHES

Increased understanding of CSC has led to new ideas for improving cancer therapy. It certainly seems feasible to combine conventional anti-neoplastic therapy (e.g., RT or CHT) to target the tumor bulk with CSC specific treatment in order to improve outcome as compared to monotherapies (184, 185). Inactivation of even only limited numbers of CSC might significantly improve local tumor control probability (70). However, the assumed plasticity of the CSC and non-CSC compartments, especially the possible shift of stem cell traits, increases the complexity of treatment responses of tumors. In an ideal situation where the CSC population is strictly static, drugs that specifically target CSC would lead to a massively improved treatment outcome, possibly even without the need of additional treatment modalities (e.g., RT or CHT). However, CSC plasticity render a CSC-targeting monotherapy virtually impossible, since after treatment, non-CSC may gain CSC traits and repopulate the tumor. Additionally, regarding the current CSC marker and their uncertainty in robustly identifying CSC, and to sufficiently distinguish them from healthy SC, a strictly CSC-based therapy seems to be still a long way off.

One conceivable possibility to eliminate CSC with RT more efficiently is to increase the applied dose. This is usually not feasible for the whole tumor due to dose constraints of the surrounding healthy tissue. Therefore, visualization of CSC could allow for larger doses of radiation in CSC rich regions while still respecting the dose constraints. Indeed, there are first studies in mice, where CD133+ glioblastoma cells could be detected non-invasively by PET and near-infrared fluorescence molecular tomography using antibody-labeled tracer (186). Subsequently, the same group showed that near-infrared photoimmunotherapy using phototoxic antibody conjugates was efficient not only in rendering CD133+ glioblastoma cells visible but also in inducing cell death (187).

Another means by which RT can be utilized to eliminate CSC more efficiently is the use of types of irradiation other than commonly used photon beams (188, 189). Particle beams of protons and carbon ions are being increasingly used due to their advantageous depth-dose curve and their higher cell-killing efficiency compared with photons (190). Preclinical studies deliver promising results when using proton irradiation. For instance, in CSC-like cells from two human NSCLC cell lines, irradiation with protons was more efficient than photon treatment in reducing cell viability. clonogenic survival, cell migration, and invasiveness, while increasing apoptosis and ROS levels (191). Furthermore, proton irradiation has been shown to be more cytotoxic, induce higher and longer cell cycle arrest, reduce cell adhesion and migration ability, and reduce the overall population of CSC in NSCLC cell lines compared to photon irradiation (192). Finally, in glioma stem cells from glioblastoma patients, similar results have been achieved (193). In this study, particle irradiation with protons and carbon ions has been shown to be more effective in cell killing compared to photons, likely because of the different quality of the induced DNA damage. Indeed, compared to photons, proton beam irradiation has been shown to increase ROS levels, induce more single and double strand DNA breaks, less DNA damage repair (as measured by H2AX phosphorylation), and decreased cell cycle recovery which led to increased apoptosis (194). Interestingly, primary human glioma stem cells that were resistant to photon treatment could be rendered sensitive with carbon ion irradiation via impaired capacity to repair carbon ion induced DNA double strand breaks (195). Importantly, this study also showed an individual heterogeneity in the amount and radiosensitivity of glioma stem cells from different patients, further complicating a one size fits all treatment. In the recent years, immune checkpoint inhibitors have greatly improved treatment outcomes for many cancers. In this regard, it has been shown that proton irradiation increased sensitivity of CSC from different cell lines, such as breast or prostate cancer, to cytotoxic T-cell killing (196). These findings offer a rationale for the combined use of proton irradiation with immunotherapy. Another important aspect of particle irradiation is the reduced dependence from tissue oxygenation. While photon irradiation is always strongly affected by the presence of oxygen in the induction and maintenance of DNA damage, high LET particle beams can be much less hindered by hypoxic conditions, which are often found in solid tumors. For example, Tinganelli et al. (197) showed the survival of mammalian cells exposed to different types of particle radiation in various oxygen concentrations, leading to a hypoxia-adapted irradiation plan. Hence, it seems feasible and promising to use particle irradiation in order to counteract tumor hypoxia. Taken together, these results suggest a potential advantage of particle beam irradiations in CSC eradication, eventually in combination with conventional photon irradiation: photon beam irradiation to the whole tumor and a boost of particle beams to hypoxic areas within the tumor. Alternatively, one can ideally use a properly optimized plan of carbon or oxygen beam, or, considering the potential of the most advanced particle centers, a multiple-ion irradiation (198). Another new strategy in combating glioblastoma is the interference with metabolic pathways. It has been shown that dichloroacetate (DCA), an orphan drug, has been shown to switch the metabolism in freshly isolated glioma stem cells from mitochondrial oxidative phosphorylation to cytoplasmic glycolysis, which in turn increased mitochondrial ROS and

induced apoptosis (199). In the same study, glioblastoma patients treated with the standard of care (i.e., radiation therapy and temozolomide) received oral DCA for up to 15 months. The drug was well-tolerated, and some patients showed prolonged radiologic stabilization and decelerated tumor progression. Additionally, DCA, in combination with PENAO [4-(N-(S-penicillaminylacetyl)amino) phenylarsonous acid] has been shown to increase radiosensitivity of glioma cells by inducing a cell cycle arrest, elevating ROS production, depolarizing mitochondrial membrane potential, increasing DNA damage, and inducing apoptosis (200).

Early experiments with CSC-directed antibodies have shown promising results. Gurtner et al. (201) used antibodies directed against CD44 that were loaded with highly cytotoxic drugs. In this experimental setting, these antibodies, combined with irradiation, led to an improved local tumor control. Considering the high expression of ROS scavengers in CSC, it may be reasonable to target these ROS scavengers. Pharmacological depletion of ROS scavengers (e.g., by treatment with buthionine sulfoximine (BSO), has been shown to reduce radiation resistance as well as clonogenic properties of CSC in breast cancer and HNSCC (202, 203). Additionally, the use of antioxidants during RT, which reduce ROS levels, might prove nonsensical, as high ROS levels are needed, especially in CSC, in order to facilitate RT-induced cell death.

Checkpoint pathways can be inhibited pharmacologically to prevent delayed cell cycle progression and hamper DNA damage repair in CSC as has been shown in glioma and prostate cancer (98, 204). Additionally, direct inhibition of DNA damage repair signaling has been shown to reduce radiation resistance in breast cancer CSC (92). Chemical inhibition of Notch signaling, a developmental pathway that is known to be essential for tissue homeostasis (205) has been shown to increase radiosensitivity in glioma CSC (206). However, most clinical studies regarding these signaling pathways focus on chemotherapy (207). There is preclinical data in mice with glioblastoma multiforme that were treated with RT and temozolomide combined with a Notch inhibitor. In this study, Notch inhibition had an anti-glioma stem cell effect which provided a survival benefit (208). Regarding clinical data, there is an ongoing trial testing a Notch inhibitor combined with whole-brain RT or stereotactic cranial RT [NCT01217411], but so far there are no results of this study available.

Overcoming tumor hypoxia is another method to improve cancer therapy. Nitroimidazole derivates can mimic the effect of oxygen and can produce reactive species in hypoxic cells. There have already been clinical trials with a clinically relevant sensitization and low toxicity (209, 210). Nitric oxide (NO) is also able to mimic oxygen and thereby to increase radiosensitivity in hypoxic tissue. In a first clinical trial, the NO donor glyceryl-trinitrate (GTN) has been shown to reduce hypoxia-induced progression of prostate cancer (211). Taken together, targeting the hypoxic niche of CSC might eventually improve treatment outcome following RT. An important task in this regard will be the correct identification of CSC for a given tumor, since CSC can differ between tumors both functionally/metabolically as well as phenotypically. Additionally, CSC share many properties and surface molecules with normal stem cells, making a clear distinction difficult and increasing the risk of unwanted side effects. Finally, it seems conceivable that drugs that interfere with spontaneous as well as RT-induced reprogramming of non-CSC into CSC could also be of value for cancer treatment. However, it needs to be investigated if these mechanisms are the same in normal steam cells and CSC before such drugs can be developed.

Another interesting approach to amplify the effect of radiation therapy, particularly on CSC, is the use of nanostructures that, after being endocytosed by cancer cells and following irradiation, release secondary electrons and large amounts of ROS (212). This could be especially effective in CSC, where ROS levels are generally lower. In this study, a significant tumor growth suppression and overall improvement in survival rate has been demonstrated in an *in vitro* and *in vivo* model of triple negative breast cancer.

CONCLUSION

There is growing evidence of a radiation resistance tumor subpopulation with increased DNA damage repair, increased survival signaling, and decreased ROS, that is furthermore protected by its environment. With refined understanding of these cells and their role in development and progression of cancer come new possibilities to improve cancer therapy. Targeting CSC, based on phenotype or function, seems promising. Nonetheless, we are just at the beginning and clinical data is still scarce. Major issues concern their correct identification and reliable distinction from healthy cells and the plasticity of the CSC department. It will be exciting to see which position CSC-specific therapies will occupy within the row of current anti-neoplastic therapies.

AUTHOR CONTRIBUTIONS

CA and JM performed the literature research. CA wrote the manuscript. I-IS and UG supervised the project.

REFERENCES

1. Delaney G, Jacob S, Featherstone C, Barton M. The role of radiotherapy in cancer treatment: estimating optimal utilization from a review of evidence-based clinical guidelines. *Cancer*. (2005) 104:1129–37. doi: 10.1002/cncr.21324
2. Tyldesley S, Delaney G, Foroudi F, Barbera L, Kerba M, Mackillop W. Estimating the need for radiotherapy for patients with prostate, breast, and lung cancers: verification of model estimates of need with radiotherapy utilization data from British Columbia. *Int J Radiat Oncol Biol Phys*. (2011) 79:1507–15. doi: 10.1016/j.ijrobp.2009.12.070
3. Zhang-Salomons J, Mackillop WJ. Estimating the lifetime utilization rate of radiotherapy in cancer patients: the multicohort current utilization table (MCUT) method. *Comp Methods Programs Biomed*. (2008) 92:99–108. doi: 10.1016/j.cmpb.2008.06.011

4. Rodriguez A, Borras JM, Lopez-Torrecilla J, Algara M, Palacios-Eito A, Gomez-Caamano A, et al. Demand for radiotherapy in Spain. *Clin Transl Oncol*. (2017) 19:204–10. doi: 10.1007/s12094-016-1525-x
5. Chierchini S, Ingrosso G, Saldi S, Stracci F, Aristei C. Physician And patient barriers to radiotherapy service access: treatment referral implications. *Cancer Manag Res*. (2019) 11:8829–33. doi: 10.2147/CMAR.S168941
6. Borras JM, Lievens Y, Barton M, Corral J, Ferlay J, Bray F, et al. How many new cancer patients in Europe will require radiotherapy by 2025? An ESTRO-HERO analysis. *Radiother Oncol*. (2016) 119:5–11. doi: 10.1016/j.radonc.2016.02.016
7. Holley AK, Miao L, St Clair DK, St Clair WH. Redox-modulated phenomena and radiation therapy: the central role of superoxide dismutases. *Antioxid Redox Signal*. (2014) 20:1567–89. doi: 10.1089/ars.2012.5000
8. Mladenov E, Magin S, Soni A, Iliakis G. DNA double-strand break repair as determinant of cellular radiosensitivity to killing and target in radiation therapy. *Front Oncol*. (2013) 3:113. doi: 10.3389/fonc.2013.00113
9. Srinivas US, Tan BWQ, Vellayappan BA, Jeyasekharan AD. ROS and the DNA damage response in cancer. *Redox Biol*. (2019) 25:101084. doi: 10.1016/j.redox.2018.101084
10. Morgan MA, Lawrence TS. Molecular pathways: overcoming radiation resistance by targeting DNA damage response pathways. *Clin Cancer Res*. (2015) 21:2898–904. doi: 10.1158/1078-0432.CCR-13-3229
11. Nikitaki Z, Michalopoulos I, Georgakilas AG. Molecular inhibitors of DNA repair: searching for the ultimate tumor killing weapon. *Future Med Chem*. (2015) 7:1543–58. doi: 10.4155/fmc.15.95
12. Turgeon MO, Perry NJS, Poulogiannis G. DNA damage, repair, and cancer metabolism. *Front Oncol*. (2018) 8:15. doi: 10.3389/fonc.2018.00015
13. Chatterjee N, Walker GC. Mechanisms of DNA damage, repair, and mutagenesis. *Environ Mol Mutagen*. (2017) 58:235–63. doi: 10.1002/em.22087
14. Roos WP, Thomas AD, Kaina B. DNA damage and the balance between survival and death in cancer biology. *Nat Rev Cancer*. (2016) 16:20–33. doi: 10.1038/nrc.2015.2
15. Wang L, Han S, Zhu J, Wang X, Li Y, Wang Z, et al. Proton versus photon radiation-induced cell death in head and neck cancer cells. *Head Neck*. (2019) 41:46–55. doi: 10.1002/hed.25357
16. Philchenkov A. Radiation-Induced cell death: signaling and pharmacological modulation. *Crit Rev Oncog*. (2018) 23:13–37. doi: 10.1615/CritRevOncog.2018026148
17. Hanna GG, Murray L, Patel R, Jain S, Aitken KL, Franks KN, et al. UK consensus on normal tissue dose constraints for stereotactic radiotherapy. *Clin Oncol*. (2018) 30:5–14. doi: 10.1016/j.clon.2017.09.007
18. Begg AC, Stewart FA, Vens C. Strategies to improve radiotherapy with targeted drugs. *Nat Rev Cancer*. (2011) 11:239–53. doi: 10.1038/nrc3007
19. Ogawa K, Yoshioka Y, Isohashi F, Seo Y, Yoshida K, Yamazaki H. Radiotherapy targeting cancer stem cells: current views and future perspectives. *Anticancer Res*. (2013) 33:747–54.
20. Gerlinger M, Rowan AJ, Horswell S, Math M, Larkin J, Endesfelder D, et al. Intratumor heterogeneity and branched evolution revealed by multiregion sequencing. *N Engl J Med*. (2012) 366:883–92. doi: 10.1056/NEJMoa1113205
21. Sottoriva A, Spiteri I, Piccirillo SG, Touloumis A, Collins VP, Marioni JC, et al. Intratumor heterogeneity in human glioblastoma reflects cancer evolutionary dynamics. *Proc Natl Acad Sci USA*. (2013) 110:4009–14. doi: 10.1073/pnas.1219747110
22. Andor N, Graham TA, Jansen M, Xia LC, Aktipis CA, Petritsch C, et al. Pan-cancer analysis of the extent and consequences of intratumor heterogeneity. *Nat Med*. (2016) 22:105–13. doi: 10.1038/nm.3984
23. Prasetyanti PR, Medema JP. Intra-tumor heterogeneity from a cancer stem cell perspective. *Mol Cancer*. (2017) 16:41. doi: 10.1186/s12943-017-0600-4
24. Meacham CE, Morrison SJ. Tumour heterogeneity and cancer cell plasticity. *Nature*. (2013) 501:328–37. doi: 10.1038/nature12624
25. Rycaj K, Tang DG. Cancer stem cells and radioresistance. *Int J Radiat Biol*. (2014) 90:615–21. doi: 10.3109/09553002.2014.892227
26. Adorno-Cruz V, Kibria G, Liu X, Doherty M, Junk DJ, Guan D, et al. Cancer stem cells: targeting the roots of cancer, seeds of metastasis, and sources of therapy resistance. *Cancer Res*. (2015) 75:924–9. doi: 10.1158/0008-5472.CAN-14-3225
27. Peitzsch C, Kurth I, Kunz-Schughart L, Baumann M, Dubrovska A. Discovery of the cancer stem cell related determinants of radioresistance. *Radiother Oncol*. (2013) 108:378–87. doi: 10.1016/j.radonc.2013.06.003
28. Chang JC. Cancer stem cells: role in tumor growth, recurrence, metastasis, and treatment resistance. *Medicine*. (2016) 95(1 Suppl. 1):S20–5. doi: 10.1097/MD.0000000000004766
29. Steinbichler TB, Dudas J, Skvortsov S, Ganswindt U, Riechelmann H, Skvortsova II. Therapy resistance mediated by cancer stem cells. *Semin Cancer Biol*. (2018) 53:156–67. doi: 10.1016/j.semcancer.2018.11.006
30. Phi LTH, Sari IN, Yang YG, Lee SH, Jun N, Kim KS, et al. Cancer stem cells (CSCs) in drug resistance and their therapeutic implications in cancer treatment. *Stem Cells Int*. (2018) 2018:5416923. doi: 10.1155/2018/5416923
31. Lytle NK, Barber AG, Reya T. Stem cell fate in cancer growth, progression and therapy resistance. *Nat Rev Cancer*. (2018) 18:669–80. doi: 10.1038/s41568-018-0056-x
32. Prieto-Vila M, Takahashi RU, Usuba W, Kohama I, Ochiya T. Drug resistance driven by cancer stem cells and their niche. *Int J Mol Sci*. (2017) 18:2574. doi: 10.3390/ijms18122574
33. Doherty MR, Smigiel JM, Junk DJ, Jackson MW. Cancer stem cell plasticity drives therapeutic resistance. *Cancers*. (2016) 8:8. doi: 10.3390/cancers8010008
34. Batlle E, Clevers H. Cancer stem cells revisited. *Nat Med*. (2017) 23:1124–34. doi: 10.1038/nm.4409
35. Bradshaw A, Wickremsekera A, Tan ST, Peng L, Davis PF, Itinteang T. Cancer stem cell hierarchy in glioblastoma multiforme. *Front Surg*. (2016) 3:21. doi: 10.3389/fsurg.2016.00021
36. Bai X, Ni J, Beretov J, Graham P, Li Y. Cancer stem cell in breast cancer therapeutic resistance. *Cancer Treat Rev*. (2018) 69:152–63. doi: 10.1016/j.ctrv.2018.07.004
37. Rich JN. Cancer stem cells: understanding tumor hierarchy and heterogeneity. *Medicine*. (2016) 95(1 Suppl 1):S2–7. doi: 10.1097/MD.0000000000004764
38. Atashzar MR, Baharlou R, Karami J, Abdollahi H, Rezaei R, Pourramezan F, et al. Cancer stem cells: a review from origin to therapeutic implications. *J Cell Physiol*. (2020) 235:790–803. doi: 10.1002/jcp.29044
39. Tomasetti C, Vogelstein B. Cancer etiology. Variation in cancer risk among tissues can be explained by the number of stem cell divisions. *Science*. (2015) 347:78–81. doi: 10.1126/science.1260825
40. White AC, Lowry WE. Refining the role for adult stem cells as cancer cells of origin. *Trends Cell Biol*. (2015) 25:11–20. doi: 10.1016/j.tcb.2014.08.008
41. Beck B, Blanpain C. Unravelling cancer stem cell potential. *Nat Rev Cancer*. (2013) 13:727–38. doi: 10.1038/nrc3597
42. Bjerkvig R, Tysnes BB, Aboody KS, Najbauer J, Terzis AJ. Opinion: the origin of the cancer stem cell: current controversies and new insights. *Nat Rev Cancer*. (2005) 5:899–904. doi: 10.1038/nrc1740
43. Lau EY, Ho NP, Lee TK. Cancer stem cells and their microenvironment: biology and therapeutic implications. *Stem Cells Int*. (2017) 2017:3714190. doi: 10.1155/2017/3714190
44. Joshua B, Kaplan MJ, Doweck I, Pai R, Weissman IL, Prince ME, et al. Frequency of cells expressing CD44, a head and neck cancer stem cell marker: correlation with tumor aggressiveness. *Head Neck*. (2012) 34:42–9. doi: 10.1002/hed.21699
45. O'Brien CA, Pollett A, Gallinger S, Dick JE. A human colon cancer cell capable of initiating tumour growth in immunodeficient mice. *Nature*. (2007) 445:106–10. doi: 10.1038/nature05372
46. Singh SK, Hawkins C, Clarke ID, Squire JA, Bayani J, Hide T, et al. Identification of human brain tumour initiating cells. *Nature*. (2004) 432:396–401. doi: 10.1038/nature03128
47. Quintana E, Shackleton M, Sabel MS, Fullen DR, Johnson TM, Morrison SJ. Efficient tumour formation by single human melanoma cells. *Nature*. (2008) 456:593–8. doi: 10.1038/nature07567
48. Al-Hajj M, Wicha MS, Benito-Hernandez A, Morrison SJ, Clarke MF. Prospective identification of tumorigenic breast cancer cells. *Proc Natl Acad Sci USA*. (2003) 100:3983–8. doi: 10.1073/pnas.0530291100
49. Lapidot T, Sirard C, Vormoor J, Murdoch B, Hoang T, Caceres-Cortes J, et al. A cell initiating human acute myeloid leukaemia after transplantation into SCID mice. *Nature*. (1994) 367:645–8. doi: 10.1038/367645a0

50. Kong Y, Yoshida S, Saito Y, Doi T, Nagatoshi Y, Fukata M, et al. CD34+CD38+CD19+ as well as CD34+CD38-CD19+ cells are leukemia-initiating cells with self-renewal capacity in human B-precursor ALL. *Leukemia*. (2008) 22:1207–13. doi: 10.1038/leu.2008.83
51. Mondal S, Bhattacharya K, Mandal C. Nutritional stress reprograms dedifferention in glioblastoma multiforme driven by PTEN/Wnt/Hedgehog axis: a stochastic model of cancer stem cells. *Cell Death Discov*. (2018) 4:110. doi: 10.1038/s41420-018-0126-6
52. Chen J, Li Y, Yu TS, McKay RM, Burns DK, Kernie SG, et al. A restricted cell population propagates glioblastoma growth after chemotherapy. *Nature*. (2012) 488:522–6. doi: 10.1038/nature11287
53. Driessens G, Beck B, Caauwe A, Simons BD, Blanpain C. Defining the mode of tumour growth by clonal analysis. *Nature*. (2012) 488:527–30. doi: 10.1038/nature11344
54. Schepers AG, Snippert HJ, Stange DE, van den Born M, van Es JH, van de Wetering M, et al. Lineage tracing reveals Lgr5+ stem cell activity in mouse intestinal adenomas. *Science*. (2012) 337:730–5. doi: 10.1126/science.1224676
55. Kreso A, Dick JE. Evolution of the cancer stem cell model. *Cell Stem Cell*. (2014) 14:275–91. doi: 10.1016/j.stem.2014.02.006
56. Vlashi E, Lagadec C, Vergnes L, Matsutani T, Masui K, Poulou M, et al. Metabolic state of glioma stem cells and nontumorigenic cells. *Proc Natl Acad Sci USA*. (2011) 108:16062–7. doi: 10.1073/pnas.1106704108
57. Ginestier C, Hur MH, Charafe-Jauffret E, Monville F, Dutcher J, Brown M, et al. ALDH1 is a marker of normal and malignant human mammary stem cells and a predictor of poor clinical outcome. *Cell Stem Cell*. (2007) 1:555–67. doi: 10.1016/j.stem.2007.08.014
58. Baumann M, Dorr W, Petersen C, Krause M. Repopulation during fractionated radiotherapy: much has been learned, even more is open. *Int J Radiat Biol*. (2003) 79:465–7. doi: 10.1080/0955300031000160259
59. Hessel F, Krause M, Petersen C, Horcsoki M, Klinger T, Zips D, et al. Repopulation of moderately well-differentiated and keratinizing GL human squamous cell carcinomas growing in nude mice. *Int J Radiat Oncol Biol Phys*. (2004) 58:510–8. doi: 10.1016/j.ijrobp.2003.09.065
60. Butof R, Dubrovska A, Baumann M. Clinical perspectives of cancer stem cell research in radiation oncology. *Radiother Oncol*. (2013) 108:388–96. doi: 10.1016/j.radonc.2013.06.002
61. Abbaszadegan MR, Bagheri V, Razavi MS, Momtazi AA, Sahebkar A, Gholamin M. Isolation, identification, and characterization of cancer stem cells: a review. *J Cell Physiol*. (2017) 232:2008–18. doi: 10.1002/jcp.25759
62. Kreso A, O'Brien CA, van Galen P, Gan OI, Notta F, Brown AM, et al. Variable clonal repopulation dynamics influence chemotherapy response in colorectal cancer. *Science*. (2013) 339:543–8. doi: 10.1126/science.1227670
63. Diehn M, Cho RW, Clarke MF. Therapeutic implications of the cancer stem cell hypothesis. *Semin Radiat Oncol*. (2009) 19:78–86. doi: 10.1016/j.semradonc.2008.11.002
64. Martins-Neves SR, Cleton-Jansen AM, Gomes CMF. Therapy-induced enrichment of cancer stem-like cells in solid human tumors: where do we stand? *Pharmacol Res*. (2018) 137:193–204. doi: 10.1016/j.phrs.2018.10.011
65. Lagadec C, Vlashi E, Della Donna L, Dekmezian C, Pajonk F. Radiation-induced reprogramming of breast cancer cells. *Stem Cells*. (2012) 30:833–44. doi: 10.1002/stem.1058
66. Gao X, Sishc BJ, Nelson CB, Hahnfeldt P, Bailey SM, Hlatky L. Radiation-Induced reprogramming of pre-senescent mammary epithelial cells enriches putative CD44(+)/CD24(-/low) stem cell phenotype. *Front Oncol*. (2016) 6:138. doi: 10.3389/fonc.2016.00138
67. Vlashi E, Kim K, Lagadec C, Donna LD, McDonald JT, Eghbali M, et al. *In vivo* imaging, tracking, and targeting of cancer stem cells. *J Natl Cancer Inst*. (2009) 101:350–9. doi: 10.1093/jnci/djn509
68. Lagadec C, Vlashi E, Della Donna L, Meng Y, Dekmezian C, Kim K, et al. Survival and self-renewing capacity of breast cancer initiating cells during fractionated radiation treatment. *Breast Cancer Res*. (2010) 12:R13. doi: 10.1186/bcr2479
69. Baumann M, Krause M, Thames H, Trott K, Zips D. Cancer stem cells and radiotherapy. *Int J Radiat Biol*. (2009) 85:391–402. doi: 10.1080/09553000902836404
70. Baumann M, Krause M, Hill R. Exploring the role of cancer stem cells in radioresistance. *Nat Rev Cancer*. (2008) 8:545–54. doi: 10.1038/nrc2419
71. Yaromina A, Krause M, Thames H, Rosner A, Krause M, Hessel F, et al. Pre-treatment number of clonogenic cells and their radiosensitivity are major determinants of local tumour control after fractionated irradiation. *Radiother Oncol*. (2007) 83:304–10. doi: 10.1016/j.radonc.2007.04.020
72. Dubben HH, Thames HD, Beck-Bornholdt HP. Tumor volume: a basic and specific response predictor in radiotherapy. *Radiother Oncol*. (1998) 47:167–74. doi: 10.1016/S0167-8140(97)00215-6
73. Gerweck LE, Zaidi ST, Zietman A. Multivariate determinants of radiocurability. I: prediction of single fraction tumor control doses. *Int J Radiat Oncol Biol Phys*. (1994) 29:57–66. doi: 10.1016/0360-3016(94)90226-7
74. Baumann M, Dubois W, Suit HD. Response of human squamous cell carcinoma xenografts of different sizes to irradiation: relationship of clonogenic cells, cellular radiation sensitivity *in vivo*, and tumor rescuing units. *Radiat Res*. (1990) 123:325–30. doi: 10.2307/3577740
75. Di Meo S, Reed TT, Venditti P, Victor VM. Role of ROS and RNS sources in physiological and pathological conditions. *Oxid Med Cell Longev*. (2016) 2016:1245049. doi: 10.1155/2016/1245049
76. Zhang J, Wang X, Vikash V, Ye Q, Wu D, Liu Y, et al. ROS and ROS-mediated cellular signaling. *Oxid Med Cell Longev*. (2016) 2016:4350965. doi: 10.1155/2016/4350965
77. Skvortsova I, Debbage P, Kumar V, Skvortsov S. Radiation resistance: cancer stem cells (CSCs) and their enigmatic pro-survival signaling. *Semin Cancer Biol*. (2015) 35:39–44. doi: 10.1016/j.semcancer.2015.09.009
78. Skvortsov S, Jimenez CR, Knol JC, Eichberger P, Schiestl B, Debbage P, et al. Radioresistant head and neck squamous cell carcinoma cells: intracellular signaling, putative biomarkers for tumor recurrences and possible therapeutic targets. *Radiother Oncol*. (2011) 101:177–82. doi: 10.1016/j.radonc.2011.05.067
79. Skvortsov S, Debbage P, Skvortsova I. Proteomics of cancer stem cells. *Int J Radiat Biol*. (2014) 90:653–8. doi: 10.3109/09553002.2013.873559
80. Zhang Y, Martin SG. Redox proteins and radiotherapy. *Clin Oncol*. (2014) 26:289–300. doi: 10.1016/j.clon.2014.02.003
81. Chang CW, Chen YS, Chou SH, Han CL, Chen YJ, Yang CC, et al. Distinct subpopulations of head and neck cancer cells with different levels of intracellular reactive oxygen species exhibit diverse stemness, proliferation, and chemosensitivity. *Cancer Res*. (2014) 74:6291–305. doi: 10.1158/0008-5472.CAN-14-0626
82. Diehn M, Cho RW, Lobo NA, Kalisky T, Dorie MJ, Kulp AN, et al. Association of reactive oxygen species levels and radioresistance in cancer stem cells. *Nature*. (2009) 458:780–3. doi: 10.1038/nature07733
83. Yang M, Liu P, Huang P. Cancer stem cells, metabolism, and therapeutic significance. *Tumour Biol*. (2016) 37:5735–42. doi: 10.1007/s13277-016-4945-x
84. Szumiel I. Ionizing radiation-induced oxidative stress, epigenetic changes and genomic instability: the pivotal role of mitochondria. *Int J Radiat Biol*. (2015) 91:1–12. doi: 10.3109/09553002.2014.934929
85. Lagadec C, Dekmezian C, Bauche L, Pajonk F. Oxygen levels do not determine radiation survival of breast cancer stem cells. *PLoS ONE*. (2012) 7:e34545. doi: 10.1371/journal.pone.0034545
86. Phillips TM, McBride WH, Pajonk F. The response of CD24(-/low)/CD44+ breast cancer-initiating cells to radiation. *J Natl Cancer Inst*. (2006) 98:1777–85. doi: 10.1093/jnci/djj495
87. Al-Assar O, Mantoni T, Lunardi S, Kingham G, Helleday T, Brunner TB. Breast cancer stem-like cells show dominant homologous recombination due to a larger S-G2 fraction. *Cancer Biol Ther*. (2011) 11:1028–35. doi: 10.4161/cbt.11.12.15699
88. Abdullah LN, Chow EK. Mechanisms of chemoresistance in cancer stem cells. *Clin Transl Med*. (2013) 2:3. doi: 10.1186/2001-1326-2-3
89. Yang ZX, Sun YH, He JG, Cao H, Jiang GQ. Increased activity of CHK enhances the radioresistance of MCF-7 breast cancer stem cells. *Oncol Lett*. (2015) 10:3443–9. doi: 10.3892/ol.2015.3777
90. Zhang P, Wei Y, Wang L, Debeb BG, Yuan Y, Zhang J, et al. ATM-mediated stabilization of ZEB1 promotes DNA damage response and radioresistance through CHK1. *Nat Cell Biol*. (2014) 16:864–75. doi: 10.1038/ncb3013
91. Desai A, Webb B, Gerson SL. CD133+ cells contribute to radioresistance via altered regulation of DNA repair genes in human lung cancer cells. *Radiother Oncol*. (2014) 110:538–45. doi: 10.1016/j.radonc.2013.10.040

92. Yin H, Glass J. The phenotypic radiation resistance of CD44+/CD24(-or low) breast cancer cells is mediated through the enhanced activation of ATM signaling. *PLoS ONE*. (2011) 6:e24080. doi: 10.1371/journal.pone.0024080
93. Wang WJ, Wu SP, Liu JB, Shi YS, Huang X, Zhang QB, et al. MYC regulation of CHK1 and CHK2 promotes radioresistance in a stem cell-like population of nasopharyngeal carcinoma cells. *Cancer Res*. (2013) 73:1219–31. doi: 10.1158/0008-5472.CAN-12-1408
94. Ropolo M, Daga A, Griffero F, Foresta M, Casartelli G, Zunino A, et al. Comparative analysis of DNA repair in stem and nonstem glioma cell cultures. *Mol Cancer Res*. (2009) 7:383–92. doi: 10.1158/1541-7786.MCR-08-0409
95. Ahmed SU, Carruthers R, Gilmour L, Yildirim S, Watts C, Chalmers AJ. Selective inhibition of parallel DNA damage response pathways optimizes radiosensitization of glioblastoma stem-like cells. *Cancer Res*. (2015) 75:4416–28. doi: 10.1158/0008-5472.CAN-14-3790
96. Carruthers R, Ahmed SU, Strathdee K, Gomez-Roman N, Amoah-Buahin E, Watts C, et al. Abrogation of radioresistance in glioblastoma stem-like cells by inhibition of ATM kinase. *Mol Oncol*. (2015) 9:192–203. doi: 10.1016/j.molonc.2014.08.003
97. Cojoc M, Peitzsch C, Kurth I, Trautmann F, Kunz-Schughart LA, Telegeev GD, et al. Aldehyde dehydrogenase is regulated by β-Catenin/TCF and promotes radioresistance in prostate cancer progenitor cells. *Cancer Res*. (2015) 75:1482–94. doi: 10.1158/0008-5472.CAN-14-1924
98. Wang X, Ma Z, Xiao Z, Liu H, Dou Z, Feng X, et al. Chk1 knockdown confers radiosensitization in prostate cancer stem cells. *Oncol Rep*. (2012) 28:2247–54. doi: 10.3892/or.2012.2068
99. Mladenov E, Magin S, Soni A, Iliakis G. DNA double-strand-break repair in higher eukaryotes and its role in genomic instability and cancer: cell cycle and proliferation-dependent regulation. *Semin Cancer Biol*. (2016) 37–38:51–64. doi: 10.1016/j.semcancer.2016.03.003
100. Her J, Bunting SF. How cells ensure correct repair of DNA double-strand breaks. *J Biol Chem*. (2018) 293:10502–11. doi: 10.1074/jbc.TM118.000371
101. Mao Z, Bozzella M, Seluanov A, Gorbunova V. Comparison of nonhomologous end joining and homologous recombination in human cells. *DNA Repair*. (2008) 7:1765–71. doi: 10.1016/j.dnarep.2008.06.018
102. Skvortsov S, Debbage P, Lukas P, Skvortsova I. Crosstalk between DNA repair and cancer stem cell (CSC) associated intracellular pathways. *Semin Cancer Biol*. (2015) 31:36–42. doi: 10.1016/j.semcancer.2014.06.002
103. Moore N, Lyle S. Quiescent, slow-cycling stem cell populations in cancer: a review of the evidence and discussion of significance. *J Oncol*. (2011) 2011:396076. doi: 10.1155/2011/396076
104. Skvortsova I, Skvortsov S, Stasyk T, Raju U, Popper BA, Schiestl B, et al. Intracellular signaling pathways regulating radioresistance of human prostate carcinoma cells. *Proteomics*. (2008) 8:4521–33. doi: 10.1002/pmic.200800113
105. Pece S, Tosoni D, Confalonieri S, Mazzarol G, Vecchi M, Ronzoni S, et al. Biological and molecular heterogeneity of breast cancers correlates with their cancer stem cell content. *Cell*. (2010) 140:62–73. doi: 10.1016/j.cell.2009.12.007
106. Touil Y, Igoudjil W, Corvaisier M, Dessein AF, Vandomme J, Monte D, et al. Colon cancer cells escape 5FU chemotherapy-induced cell death by entering stemness and quiescence associated with the c-Yes/YAP axis. *Clin Cancer Res*. (2014) 20:837–46. doi: 10.1158/1078-0432.CCR-13-1854
107. Kleffel S, Schatton T. Tumor dormancy and cancer stem cells: two sides of the same coin? *Adv Exp Med Biol*. (2013) 734:145–79. doi: 10.1007/978-1-4614-1445-2_8
108. Li J, Jiang E, Wang X, Shangguan AJ, Zhang L, Yu Z. Dormant cells: the original cause of tumor recurrence and metastasis. *Cell Biochem Biophys*. (2015) 72:317–20. doi: 10.1007/s12013-014-0477-4
109. Lyssiotis CA, Kimmelman AC. Metabolic Interactions in the Tumor Microenvironment. *Trends Cell Biol*. (2017) 27:863–75. doi: 10.1016/j.tcb.2017.06.003
110. Roper J, Yilmaz OH. Metabolic teamwork in the stem cell niche. *Cell Metab*. (2017) 25:993–4. doi: 10.1016/j.cmet.2017.04.019
111. Borovski T, De Sousa EMF, Vermeulen L, Medema JP. Cancer stem cell niche: the place to be. *Cancer Res*. (2011) 71:634–9. doi: 10.1158/0008-5472.CAN-10-3220
112. Chapellier M, Maguer-Satta V. BMP2, a key to uncover luminal breast cancer origin linked to pollutant effects on epithelial stem cells niche. *Mol Cell Oncol*. (2016) 3:e1026527. doi: 10.1080/23723556.2015.1026527
113. Aderetti DA, Hira VVV, Molenaar RJ, van Noorden CJF. The hypoxic peri-arteriolar glioma stem cell niche, an integrated concept of five types of niches in human glioblastoma. *Biochim Biophys Acta Rev Cancer*. (2018) 1869:346–54. doi: 10.1016/j.bbcan.2018.04.008
114. Ishii G. Crosstalk between cancer associated fibroblasts and cancer cells in the tumor microenvironment after radiotherapy. *EBioMedicine*. (2017) 17:7–8. doi: 10.1016/j.ebiom.2017.03.004
115. Tommelein J, De Vlieghere E, Verset L, Melsens E, Leenders J, Descamps B, et al. Radiotherapy-activated cancer-associated fibroblasts promote tumor progression through paracrine IGF1R activation. *Cancer Res*. (2018) 78:659–70. doi: 10.1158/0008-5472.CAN-17-0524
116. Papadopoulou A, Kletsas D. Human lung fibroblasts prematurely senescent after exposure to ionizing radiation enhance the growth of malignant lung epithelial cells *in vitro* and *in vivo*. *Int J Oncol*. (2011) 39:989–99. doi: 10.3892/ijo.2011.1132
117. Hawsawi NM, Ghebeh H, Hendrayani SF, Tulbah A, Al-Eid M, Al-Tweigeri T, et al. Breast carcinoma-associated fibroblasts and their counterparts display neoplastic-specific changes. *Cancer Res*. (2008) 68:2717–25. doi: 10.1158/0008-5472.CAN-08-0192
118. Wang Y, Gan G, Wang B, Wu J, Cao Y, Zhu D, et al. Cancer-associated fibroblasts promote irradiated cancer cell recovery through autophagy. *EBioMedicine*. (2017) 17:45–56. doi: 10.1016/j.ebiom.2017.02.019
119. Jarosz-Biej M, Smolarczyk R, Cichon T, Kulach N. Tumor microenvironment as a "game changer" in cancer radiotherapy. *Int J Mol Sci*. (2019) 20(13). doi: 10.3390/ijms20133212
120. Jiang W, Chan CK, Weissman IL, Kim BYS, Hahn SM. Immune priming of the tumor microenvironment by radiation. *Trends Cancer*. (2016) 2:638–45. doi: 10.1016/j.trecan.2016.09.007
121. Matsui WH. Cancer stem cell signaling pathways. *Medicine*. (2016) 95(1 Suppl. 1):S8–19. doi: 10.1097/MD.0000000000004765
122. Kuonen F, Secondini C, Ruegg C. Molecular pathways: emerging pathways mediating growth, invasion, and metastasis of tumors progressing in an irradiated microenvironment. *Clin Cancer Res*. (2012) 18:5196–202. doi: 10.1158/1078-0432.CCR-11-1758
123. Sofia Vala I, Martins LR, Imaizumi N, Nunes RJ, Rino J, Kuonen F, et al. Low doses of ionizing radiation promote tumor growth and metastasis by enhancing angiogenesis. *PLoS ONE*. (2010) 5:e11222. doi: 10.1371/journal.pone.0011222
124. Elming PB, Sorensen BS, Oei AL, Franken NAP, Crezee J, Overgaard J, et al. Hyperthermia: the optimal treatment to overcome radiation resistant hypoxia. *Cancers*. (2019) 11:60. doi: 10.3390/cancers11010060
125. Baumann R, Depping R, Delaperriere M, Dunst J. Targeting hypoxia to overcome radiation resistance in head & neck cancers: real challenge or clinical fairytale? *Expert Rev Anticancer Ther*. (2016) 16:751–8. doi: 10.1080/14737140.2016.1192467
126. Epel B, Maggio MC, Barth ED, Miller RC, Pelizzari CA, Krzykawska-Serda M, et al. Oxygen-Guided radiation therapy. *Int J Radiat Oncol Biol Phys*. (2019) 103:977–84. doi: 10.1016/j.ijrobp.2018.10.041
127. Gallez B, Neveu MA, Danhier P, Jordan BF. Manipulation of tumor oxygenation and radiosensitivity through modification of cell respiration. A critical review of approaches and imaging biomarkers for therapeutic guidance. *Biochim Biophys Acta Bioenerg*. (2017) 1858:700–11. doi: 10.1016/j.bbabio.2017.01.002
128. Horsman MR, Overgaard J. The impact of hypoxia and its modification of the outcome of radiotherapy. *J Radiat Res*. (2016) 57(Suppl. 1):i90-i8. doi: 10.1093/jrr/rrw007
129. Eisenbrey JR, Shraim R, Liu JB, Li J, Stanczak M, Oeffinger B, et al. Sensitization of hypoxic tumors to radiation therapy using ultrasound-sensitive oxygen microbubbles. *Int J Radiat Oncol Biol Phys*. (2018) 101:88–96. doi: 10.1016/j.ijrobp.2018.01.042
130. Schulz A, Meyer F, Dubrovska A, Borgmann K. Cancer stem cells and radioresistance: DNA repair and beyond. *Cancers*. (2019) 11:862. doi: 10.3390/cancers11060862
131. Krause M, Dubrovska A, Linge A, Baumann M. Cancer stem cells: radioresistance, prediction of radiotherapy outcome and specific targets for

combined treatments. *Adv Drug Deliv Rev*. (2017) 109:63–73. doi: 10.1016/j.addr.2016.02.002
132. Schoning JP, Monteiro M, Gu W. Drug resistance and cancer stem cells: the shared but distinct roles of hypoxia-inducible factors HIF1α and HIF2α. *Clin Exp Pharmacol Physiol*. (2017) 44:153–61. doi: 10.1111/1440-1681.12693
133. Balamurugan K. HIF-1 at the crossroads of hypoxia, inflammation, and cancer. *Int J Cancer*. (2016) 138:1058–66. doi: 10.1002/ijc.29519
134. Peitzsch C, Perrin R, Hill RP, Dubrovska A, Kurth I. Hypoxia as a biomarker for radioresistant cancer stem cells. *Int J Radiat Biol*. (2014) 90:636–52. doi: 10.3109/09553002.2014.916841
135. Kim W, Kim MS, Kim HJ, Lee E, Jeong JH, Park I, et al. Role of HIF-1α in response of tumors to a combination of hyperthermia and radiation *in vivo*. *Int J Hyperthermia*. (2018) 34:276–83. doi: 10.1080/02656736.2017.1335440
136. Nwabo Kamdje AH, Takam Kamga P, Tagne Simo R, Vecchio L, Seke Etet PF, Muller JM, et al. Developmental pathways associated with cancer metastasis: Notch, Wnt, and Hedgehog. *Cancer Biol Med*. (2017) 14:109–20. doi: 10.20892/j.issn.2095-3941.2016.0032
137. Chatterjee S, Sil PC. Targeting the crosstalks of Wnt pathway with Hedgehog and Notch for cancer therapy. *Pharmacol Res*. (2019) 142:251–61. doi: 10.1016/j.phrs.2019.02.027
138. Qiang L, Wu T, Zhang HW, Lu N, Hu R, Wang YJ, et al. HIF-1α is critical for hypoxia-mediated maintenance of glioblastoma stem cells by activating Notch signaling pathway. *Cell Death Differ*. (2012) 19:284–94. doi: 10.1038/cdd.2011.95
139. Wang J, Wakeman TP, Lathia JD, Hjelmeland AB, Wang XF, White RR, et al. Notch promotes radioresistance of glioma stem cells. *Stem Cells*. (2010) 28:17–28. doi: 10.1002/stem.261
140. Duru N, Fan M, Candas D, Menaa C, Liu HC, Nantajit D, et al. HER2-associated radioresistance of breast cancer stem cells isolated from HER2-negative breast cancer cells. *Clin Cancer Res*. (2012) 18:6634–47. doi: 10.1158/1078-0432.CCR-12-1436
141. Woodward WA, Chen MS, Behbod F, Alfaro MP, Buchholz TA, Rosen JM. WNT/β-catenin mediates radiation resistance of mouse mammary progenitor cells. *Proc Natl Acad Sci USA*. (2007) 104:618–23. doi: 10.1073/pnas.0606599104
142. Oren O, Smith BD. Eliminating cancer stem cells by targeting embryonic signaling pathways. *Stem Cell Rev Rep*. (2017) 13:17–23. doi: 10.1007/s12015-016-9691-3
143. Wu CT, Lin WY, Chang YH, Chen WC, Chen MF. Impact of CD44 expression on radiation response for bladder cancer. *J Cancer*. (2017) 8:1137–44. doi: 10.7150/jca.18297
144. Hagiwara M, Kikuchi E, Kosaka T, Mikami S, Saya H, Oya M. Variant isoforms of CD44 expression in upper tract urothelial cancer as a predictive marker for recurrence and mortality. *Urol Oncol*. (2016) 34:337.e19–26. doi: 10.1016/j.urolonc.2016.03.015
145. Yikilmaz TN, Dirim A, Ayva ES, Ozdemir H, Ozkardes H. Clinical use of tumor markers for the detection and prognosis of bladder carcinoma: a comparison of CD44, Cytokeratin 20 and Survivin. *Urol J*. (2016) 13:2677–83. doi: 10.22037/uj.v13i3.3294
146. Szczepanik A, Sierzega M, Drabik G, Pituch-Noworolska A, Kolodziejczyk P, Zembala M. CD44(+) cytokeratin-positive tumor cells in blood and bone marrow are associated with poor prognosis of patients with gastric cancer. *Gastric Cancer*. (2019) 22:264–72. doi: 10.1007/s10120-018-0858-2
147. Watanabe T, Okumura T, Hirano K, Yamaguchi T, Sekine S, Nagata T, et al. Circulating tumor cells expressing cancer stem cell marker CD44 as a diagnostic biomarker in patients with gastric cancer. *Oncol Lett*. (2017) 13:281–8. doi: 10.3892/ol.2016.5432
148. Kodama H, Murata S, Ishida M, Yamamoto H, Yamaguchi T, Kaida S, et al. Prognostic impact of CD44-positive cancer stem-like cells at the invasive front of gastric cancer. *Br J Cancer*. (2017) 116:186–94. doi: 10.1038/bjc.2016.401
149. Fang M, Wu J, Lai X, Ai H, Tao Y, Zhu B, et al. CD44 and CD44v6 are correlated with gastric cancer progression and poor patient prognosis: evidence from 42 Studies. *Cell Physiol Biochem*. (2016) 40:567–78. doi: 10.1159/000452570
150. Bitaraf SM, Mahmoudian RA, Abbaszadegan M, Mohseni Meybodi A, Taghehchian N, Mansouri A, et al. Association of Two CD44 Polymorphisms with clinical outcomes of gastric cancer patients. *Asian Pac J Cancer Prev*. (2018) 19:1313–8. doi: 10.22034/APJCP.2018.19.5.1313
151. Hsu CP, Lee LY, Hsu JT, Hsu YP, Wu YT, Wang SY, et al. CD44 Predicts early recurrence in pancreatic cancer patients undergoing radical surgery. *In Vivo*. (2018) 32:1533–40. doi: 10.21873/invivo.11411
152. Poruk KE, Blackford AL, Weiss MJ, Cameron JL, He J, Goggins M, et al. Circulating tumor cells expressing markers of tumor-initiating cells predict poor survival and cancer recurrence in patients with pancreatic ductal adenocarcinoma. *Clin Cancer Res*. (2017) 23:2681–90. doi: 10.1158/1078-0432.CCR-16-1467
153. Ludwig N, Szczepanski MJ, Gluszko A, Szafarowski T, Azambuja JH, Dolg L, et al. CD44(+) tumor cells promote early angiogenesis in head and neck squamous cell carcinoma. *Cancer Lett*. (2019) 467:85–95. doi: 10.1016/j.canlet.2019.10.010
154. Rodrigues M, Xavier FCA, Andrade NP, Lopes C, Miguita Luiz L, Sedassari BT, et al. Prognostic implications of CD44, NANOG, OCT4, and BMI1 expression in tongue squamous cell carcinoma. *Head Neck*. (2018) 40:1759–73. doi: 10.1002/hed.25158
155. Lee JR, Roh JL, Lee SM, Park Y, Cho KJ, Choi SH, et al. Overexpression of cysteine-glutamate transporter and CD44 for prediction of recurrence and survival in patients with oral cavity squamous cell carcinoma. *Head Neck*. (2018) 40:2340–6. doi: 10.1002/hed.25331
156. Hou C, Ishi Y, Motegi H, Okamoto M, Ou Y, Chen J, et al. Overexpression of CD44 is associated with a poor prognosis in grade II/III gliomas. *J Neurooncol*. (2019) 145:201–10. doi: 10.1007/s11060-019-03288-8
157. Nishikawa M, Inoue A, Ohnishi T, Kohno S, Ohue S, Matsumoto S, et al. Significance of glioma stem-like cells in the tumor periphery that express high levels of CD44 in tumor invasion, early progression, and poor prognosis in glioblastoma. *Stem Cells Int*. (2018) 2018:5387041. doi: 10.1155/2018/5387041
158. Liu WH, Lin JC, Chou YC, Li MH, Tsai JT. CD44-associated radioresistance of glioblastoma in irradiated brain areas with optimal tumor coverage. *Cancer Med*. (2020) 9:350–60. doi: 10.1002/cam4.2714
159. Mooney KL, Choy W, Sidhu S, Pelargos P, Bui TT, Voth B, et al. The role of CD44 in glioblastoma multiforme. *J Clin Neurosci*. (2016) 34:1–5. doi: 10.1016/j.jocn.2016.05.012
160. Bi Y, Meng Y, Wu H, Cui Q, Luo Y, Xue X. Expression of the potential cancer stem cell markers CD133 and CD44 in medullary thyroid carcinoma: a ten-year follow-up and prognostic analysis. *J Surg Oncol*. (2016) 113:144–51. doi: 10.1002/jso.24124
161. Han SA, Jang JH, Won KY, Lim SJ, Song JY. Prognostic value of putative cancer stem cell markers (CD24, CD44, CD133, and ALDH1) in human papillary thyroid carcinoma. *Pathol Res Pract*. (2017) 213:956–63. doi: 10.1016/j.prp.2017.05.002
162. Luo Y, Tan Y. Prognostic value of CD44 expression in patients with hepatocellular carcinoma: meta-analysis. *Cancer Cell Int*. (2016) 16:47. doi: 10.1186/s12935-016-0325-2
163. Zhao Q, Zhou H, Liu Q, Cao Y, Wang G, Hu A, et al. Prognostic value of the expression of cancer stem cell-related markers CD133 and CD44 in hepatocellular carcinoma: from patients to patient-derived tumor xenograft models. *Oncotarget*. (2016) 7:47431–43. doi: 10.18632/oncotarget.10164
164. Xu H, Tian Y, Yuan X, Liu Y, Wu H, Liu Q, et al. Enrichment of CD44 in basal-type breast cancer correlates with EMT, cancer stem cell gene profile, and prognosis. *Onco Targets Ther*. (2016) 9:431–44. doi: 10.2147/OTT.S97192
165. Hu B, Ma Y, Yang Y, Zhang L, Han H, Chen J. CD44 promotes cell proliferation in non-small cell lung cancer. *Oncol Lett*. (2018) 15:5627–33. doi: 10.3892/ol.2018.8051
166. Sosulski A, Horn H, Zhang L, Coletti C, Vathipadiekal V, Castro CM, et al. CD44 Splice Variant v8–10 as a marker of serous ovarian cancer prognosis. *PLoS ONE*. (2016) 11:e0156595. doi: 10.1371/journal.pone.0156595
167. Lin J, Ding D. The prognostic role of the cancer stem cell marker CD44 in ovarian cancer: a meta-analysis. *Cancer Cell Int*. (2017) 17:8. doi: 10.1186/s12935-016-0376-4
168. Matuura H, Miyamoto M, Takano M, Soyama H, Aoyama T, Yoshikawa T, et al. Low Expression of CD44 is an independent factor of poor prognosis in ovarian mucinous carcinoma. *Anticancer Res*. (2018) 38:717–22. doi: 10.21873/anticanres.12277

169. Horimoto Y, Arakawa A, Sasahara N, Tanabe M, Sai S, Himuro T, et al. Combination of cancer stem cell markers CD44 and CD24 is superior to ALDH1 as a prognostic indicator in breast cancer patients with distant metastases. *PLoS ONE*. (2016) 11:e0165253. doi: 10.1371/journal.pone.0165253
170. Han S, Huang T, Li W, Wang X, Wu X, Liu S, et al. Prognostic value of CD44 and its isoforms in advanced cancer: a systematic meta-analysis with trial sequential analysis. *Front Oncol*. (2019) 9:39. doi: 10.3389/fonc.2019.00039
171. Linge A, Lohaus F, Lock S, Nowak A, Gudziol V, Valentini C, et al. HPV status, cancer stem cell marker expression, hypoxia gene signatures and tumour volume identify good prognosis subgroups in patients with HNSCC after primary radiochemotherapy: a multicentre retrospective study of the German Cancer Consortium Radiation Oncology Group (DKTK-ROG). *Radiother Oncol*. (2016) 121:364–73. doi: 10.1016/j.radonc.2016.11.008
172. Linge A, Lock S, Gudziol V, Nowak A, Lohaus F, von Neubeck C, et al. Low cancer stem cell marker expression and low hypoxia identify good prognosis subgroups in HPV(-) HNSCC after postoperative radiochemotherapy: a multicenter study of the DKTK-ROG. *Clin Cancer Res*. (2016) 22:2639–49. doi: 10.1158/1078-0432.CCR-15-1990
173. Linge A, Schmidt S, Lohaus F, Krenn C, Bandurska-Luque A, Platzek I, et al. Independent validation of tumour volume, cancer stem cell markers and hypoxia-associated gene expressions for HNSCC after primary radiochemotherapy. *Clin Transl Radiat Oncol*. (2019) 16:40–7. doi: 10.1016/j.ctro.2019.03.002
174. Dong BW, Qin GM, Luo Y, Mao JS. Metabolic enzymes: key modulators of functionality in cancer stem-like cells. *Oncotarget*. (2017) 8:14251–67. doi: 10.18632/oncotarget.14041
175. Voutsadakis IA. Proteasome expression and activity in cancer and cancer stem cells. *Tumour Biol*. (2017) 39:1010428317692248. doi: 10.1177/1010428317692248
176. Banno A, Garcia DA, van Baarsel ED, Metz PJ, Fisch K, Widjaja CE, et al. Downregulation of 26S proteasome catalytic activity promotes epithelial-mesenchymal transition. *Oncotarget*. (2016) 7:21527–41. doi: 10.18632/oncotarget.7596
177. Lenos KJ, Vermeulen L. Cancer stem cells don't waste their time cleaning-low proteasome activity, a marker for cancer stem cell function. *Ann Transl Med*. (2016) 4:519. doi: 10.21037/atm.2016.11.81
178. Lagadec C, Vlashi E, Bhuta S, Lai C, Mischel P, Werner M, et al. Tumor cells with low proteasome subunit expression predict overall survival in head and neck cancer patients. *BMC Cancer*. (2014) 14:152. doi: 10.1186/1471-2407-14-152
179. Han M, Guo L, Zhang Y, Huang B, Chen A, Chen W, et al. Clinicopathological and Prognostic Significance of CD133 in glioma patients: a meta-analysis. *Mol Neurobiol*. (2016) 53:720–7. doi: 10.1007/s12035-014-9018-9
180. Li B, McCrudden CM, Yuen HF, Xi X, Lyu P, Chan KW, et al. CD133 in brain tumor: the prognostic factor. *Oncotarget*. (2017) 8:11144–59. doi: 10.18632/oncotarget.14406
181. Wu X, Wu F, Xu D, Zhang T. Prognostic significance of stem cell marker CD133 determined by promoter methylation but not by immunohistochemical expression in malignant gliomas. *J Neurooncol*. (2016) 127:221–32. doi: 10.1007/s11060-015-2039-z
182. Kim KJ, Lee KH, Kim HS, Moon KS, Jung TY, Jung S, et al. The presence of stem cell marker-expressing cells is not prognostically significant in glioblastomas. *Neuropathology*. (2011) 31:494–502. doi: 10.1111/j.1440-1789.2010.01194.x
183. Melguizo C, Prados J, Gonzalez B, Ortiz R, Concha A, Alvarez PJ, et al. MGMT promoter methylation status and MGMT and CD133 immunohistochemical expression as prognostic markers in glioblastoma patients treated with temozolomide plus radiotherapy. *J Transl Med*. (2012) 10:250. doi: 10.1186/1479-5876-10-250
184. Linkous AG, Yazlovitskaya EM. Novel radiosensitizing anticancer therapeutics. *Anticancer Res*. (2012) 32:2487–99.
185. Shigdar S, Lin J, Li Y, Yang CJ, Wei M, Zhus Y, et al. Cancer stem cell targeting: the next generation of cancer therapy and molecular imaging. *Ther Deliv*. (2012) 3:227–44. doi: 10.4155/tde.11.148
186. Gaedicke S, Braun F, Prasad S, Machein M, Firat E, Hettich M, et al. Noninvasive positron emission tomography and fluorescence imaging of CD133+ tumor stem cells. *Proc Natl Acad Sci USA*. (2014) 111:E692–701. doi: 10.1073/pnas.1314189111
187. Jing H, Weidensteiner C, Reichardt W, Gaedicke S, Zhu X, Grosu AL, et al. Imaging and selective elimination of glioblastoma stem cells with theranostic near-infrared-labeled CD133-specific antibodies. *Theranostics*. (2016) 6:862–74. doi: 10.7150/thno.12890
188. Dini V, Belli M, Tabocchini MA. Targeting cancer stem cells: protons versus photons. *Br J Radiol*. (2019) 2019:20190225. doi: 10.1259/bjr.20190225
189. Vitti ET, Parsons JL. The Radiobiological effects of proton beam therapy: impact on DNA damage and repair. *Cancers*. (2019) 11:946. doi: 10.3390/cancers11070946
190. Durante M, Loeffler JS. Charged particles in radiation oncology. *Nat Rev Clin Oncol*. (2010) 7:37–43. doi: 10.1038/nrclinonc.2009.183
191. Zhang X, Lin SH, Fang B, Gillin M, Mohan R, Chang JY. Therapy-resistant cancer stem cells have differing sensitivity to photon versus proton beam radiation. *J Thorac Oncol*. (2013) 8:1484–91. doi: 10.1097/JTO.0b013e3182a5fdcb
192. Narang H, Kumar A, Bhat N, Pandey BN, Ghosh A. Effect of proton and gamma irradiation on human lung carcinoma cells: gene expression, cell cycle, cell death, epithelial-mesenchymal transition and cancer-stem cell trait as biological end points. *Mutat Res*. (2015) 780:35–46. doi: 10.1016/j.mrfmmm.2015.07.006
193. Pecchia I, Dini V, Ricci-Vitiani L, Biffoni M, Balduzzi M, Fratini E, et al. Glioblastoma stem cells: radiobiological response to ionising radiations of different qualities. *Radiat Prot Dosimetry*. (2015) 166:374–8. doi: 10.1093/rpd/ncv299
194. Alan Mitteer R, Wang Y, Shah J, Gordon S, Fager M, Butter PP, et al. Proton beam radiation induces DNA damage and cell apoptosis in glioma stem cells through reactive oxygen species. *Sci Rep*. (2015) 5:13961. doi: 10.1038/srep13961
195. Chiblak S, Tang Z, Campos B, Gal Z, Unterberg A, Debus J, et al. Radiosensitivity of patient-derived glioma stem cell 3-dimensional cultures to photon, proton, and carbon irradiation. *Int J Radiat Oncol Biol Phys*. (2016) 95:112–9. doi: 10.1016/j.ijrobp.2015.06.015
196. Gameiro SR, Malamas AS, Bernstein MB, Tsang KY, Vassantachart A, Sahoo N, et al. Tumor cells surviving exposure to proton or photon radiation share a common immunogenic modulation signature, rendering them more sensitive to T cell-mediated killing. *Int J Radiat Oncol Biol Phys*. (2016) 95:120–30. doi: 10.1016/j.ijrobp.2016.02.022
197. Tinganelli W, Durante M, Hirayama R, Kramer M, Maier A, Kraft-Weyrather W, et al. Kill-painting of hypoxic tumours in charged particle therapy. *Sci Rep*. (2015) 5:17016. doi: 10.1038/srep17016
198. Sokol O, Kramer M, Hild S, Durante M, Scifoni E. Kill painting of hypoxic tumors with multiple ion beams. *Phys Med Biol*. (2019) 64:045008. doi: 10.1088/1361-6560/aafe40
199. Michelakis ED, Sutendra G, Dromparis P, Webster L, Haromy A, Niven E, et al. Metabolic modulation of glioblastoma with dichloroacetate. *Sci Transl Med*. (2010) 2:31ra4. doi: 10.1126/scitranslmed.3000677
200. Shen H, Decollogne S, Dilda PJ, Hau E, Chung SA, Luk PP, et al. Dual-targeting of aberrant glucose metabolism in glioblastoma. *J Exp Clin Cancer Res*. (2015) 34:14. doi: 10.1186/s13046-015-0130-0
201. Gurtner K, Hessel F, Eicheler W, Dorfler A, Zips D, Heider KH, et al. Combined treatment of the immunoconjugate bivatuzumab mertansine and fractionated irradiation improves local tumour control *in vivo*. *Radiother Oncol*. (2012) 102:444–9. doi: 10.1016/j.radonc.2011.10.013
202. Boivin A, Hanot M, Malesys C, Maalouf M, Rousson R, Rodriguez-Lafrasse C, et al. Transient alteration of cellular redox buffering before irradiation triggers apoptosis in head and neck carcinoma stem and non-stem cells. *PLoS ONE*. (2011) 6:e14558. doi: 10.1371/journal.pone.0014558
203. Rodman SN, Spence JM, Ronnfeldt TJ, Zhu Y, Solst SR, O'Neill RA, et al. Enhancement of radiation response in breast cancer stem cells by inhibition of thioredoxin- and glutathione-dependent metabolism. *Radiat Res*. (2016) 186:385–95. doi: 10.1667/RR14463.1
204. Bao S, Wu Q, McLendon RE, Hao Y, Shi Q, Hjelmeland AB, et al. Glioma stem cells promote radioresistance by preferential activation of the DNA damage response. *Nature*. (2006) 444:756–60. doi: 10.1038/nature05236

205. Karamboulas C, Ailles L. Developmental signaling pathways in cancer stem cells of solid tumors. *Biochim Biophys Acta*. (2013) 1830:2481–95. doi: 10.1016/j.bbagen.2012.11.008
206. Shen Y, Chen H, Zhang J, Chen Y, Wang M, Ma J, et al. Increased notch signaling enhances radioresistance of malignant stromal cells induced by glioma stem/ progenitor cells. *PLoS ONE*. (2015) 10:e0142594. doi: 10.1371/journal.pone.0142594
207. Cojoc M, Mabert K, Muders MH, Dubrovska A. A role for cancer stem cells in therapy resistance: cellular and molecular mechanisms. *Semin Cancer Biol*. (2015) 31:16–27. doi: 10.1016/j.semcancer.2014.06.004
208. Yahyanejad S, King H, Iglesias VS, Granton PV, Barbeau LM, van Hoof SJ, et al. NOTCH blockade combined with radiation therapy and temozolomide prolongs survival of orthotopic glioblastoma. *Oncotarget*. (2016) 7:41251–64. doi: 10.18632/oncotarget.9275
209. Wardman P. Chemical radiosensitizers for use in radiotherapy. *Clin Oncol*. (2007) 19:397–417. doi: 10.1016/j.clon.2007.03.010
210. Overgaard J. Hypoxic radiosensitization: adored and ignored. *J Clin Oncol*. (2007) 25:4066–74. doi: 10.1200/JCO.2007.12.7878
211. Siemens DR, Heaton JP, Adams MA, Kawakami J, Graham CH. Phase II study of nitric oxide donor for men with increasing prostate-specific antigen level after surgery or radiotherapy for prostate cancer. *Urology*. (2009) 74:878–83. doi: 10.1016/j.urology.2009.03.004
212. Cheng K, Sano M, Jenkins CH, Zhang G, Vernekohl D, Zhao W, et al. Synergistically enhancing the therapeutic effect of radiation therapy with radiation activatable and reactive oxygen species-releasing nanostructures. *ACS Nano*. (2018) 12:4946–58. doi: 10.1021/acsnano.8b02038

Conflict of Interest: The authors declare that the research was conducted in the absence of any commercial or financial relationships that could be construed as a potential conflict of interest.

Copyright © 2020 Arnold, Mangesius, Skvortsova and Ganswindt. This is an open-access article distributed under the terms of the Creative Commons Attribution License (CC BY). The use, distribution or reproduction in other forums is permitted, provided the original author(s) and the copyright owner(s) are credited and that the original publication in this journal is cited, in accordance with accepted academic practice. No use, distribution or reproduction is permitted which does not comply with these terms.

frontiers in Oncology

REVIEW
published: 17 March 2020
doi: 10.3389/fonc.2020.00319

Novel Therapeutic Strategies for Ovarian Cancer Stem Cells

Nastassja Terraneo[1], *Francis Jacob*[2], *Anna Dubrovska*[3,4,5,6] *and Jürgen Grünberg*[1]*

[1] Center for Radiopharmaceutical Sciences ETH-PSI-USZ, Paul Scherrer Institute, Villigen, Switzerland, [2] Ovarian Cancer Research, Department of Biomedicine, University Hospital Basel and University of Basel, Basel, Switzerland, [3] OncoRay-National Center for Radiation Research in Oncology, Faculty of Medicine and University Hospital Carl Gustav Carus, Technische Universität Dresden, Dresden, Germany, [4] German Cancer Consortium (DKTK), Partner Site Dresden, Dresden, Germany, [5] German Cancer Research Center (DKFZ), Heidelberg, Germany, [6] Helmholtz-Zentrum Dresden-Rossendorf, Institute of Radiooncology-OncoRay, Dresden, Germany

Ovarian cancer (OC) is one of the most lethal gynecologic malignancies. Due to the lack of specific symptoms and screening methods, this disease is usually diagnosed only at an advanced and metastatic stage. The gold-standard treatment for OC patients consists of debulking surgery followed by taxane combined with platinum-based chemotherapy. Most patients show complete clinical remission after first-line therapy, but the majority of them ultimately relapse, developing radio- and chemoresistant tumors. It is now proposed that the cause of recurrence and reduced therapy efficacy is the presence of small populations of cancer stem cells (CSCs). These cells are usually resistant against conventional cancer therapies and for this reason, effective targeted therapies for the complete eradication of CSCs are urgently needed. In this review article, we highlight the mechanisms of CSC therapy resistance, epithelial-to-mesenchymal transition, stemness, and novel therapeutic strategies for ovarian CSCs.

Keywords: ovarian cancer, cancer stem cells, epithelial-to-mesenchymal transition, L1CAM, radioimmunotherapy, Auger electron and alpha particle emitters, therapeutic strategies

OPEN ACCESS

Edited by:
Paul N. Span, Radboud University Nijmegen Medical Centre, Netherlands

Reviewed by:
Yoshihiko Hirohashi, Sapporo Medical University, Japan
Janneke Hoogstad-van Evert, Radboud University Nijmegen Medical Centre, Netherlands

***Correspondence:**
Jürgen Grünberg
juergen.gruenberg@psi.ch

Specialty section:
This article was submitted to Radiation Oncology, a section of the journal Frontiers in Oncology

Received: *30 September 2019*
Accepted: *21 February 2020*
Published: *17 March 2020*

Citation:
Terraneo N, Jacob F, Dubrovska A and Grünberg J (2020) Novel Therapeutic Strategies for Ovarian Cancer Stem Cells. Front. Oncol. 10:319. doi: 10.3389/fonc.2020.00319

INTRODUCTION

Ovarian Cancer

Ovarian cancer (OC), which is a generic term for several different malignant tumors, is one of the most frequent cancer types in females (1). OC is the leading cause of cancer death among gynecological malignancies, and according to estimates, in 2019 ∼22,530 new cases of OC will be diagnosed and 13,980 OC-related deaths will occur in the U.S. (2). About 75% of all ovarian tumors and 90–95% of ovarian malignancies are epithelial ovarian cancer (EOC) (3) of different origin (4). The 5-year survival rate of OC varies from 30 to 92%, depending on the dissemination of the disease at the time of diagnosis (5). This type of cancer usually shows non-specific symptoms during the early development (e.g., abdominal distension and pain, loss of appetite, or increased urinary frequency) and currently there are still no reliable early screening strategies available (6). The most common sign of advanced disease is abdominal swelling due to ascitic fluids accumulation (7). OC is consisting of different histological subtypes with distinctive molecular genetic features, clinical presentations, and prognostic outcomes. In 2014, the new WHO criteria recognized five principal epithelial OC histotypes: high-grade serous (HGSC), low-grade serous (LGSC), endometrioid, clear cell, and mucinous carcinoma (8). Among them, HGSC is the most common histologic subtype of OC, with a poor 5-year survival rate of 35–40% and accounting for 70–80% of OC deaths (5, 9). Because of the lack of diagnostic methods, ∼75% of patients show the metastatic spread in the

peritoneal cavity and adjacent organs at diagnosis, which corresponds to FIGO stages (International Federation of Gynecology and Obstetrics stages) III and IV (10). The FIGO OC staging system was first published in 1973 and revised in 2014 (11, 12). Stage I EOC (disease is confined to one or both ovaries) is usually associated with good survival rates and surgery alone is sufficient as a therapeutic approach; unfortunately, it is quite rare since most of the patients are diagnosed only at stages III and IV (13). At stage II, tumor includes either one or both ovaries with pelvic dissemination and spread into the uterus and/or fallopian tubes. This group makes up <10% and it is considered curable, usually with chemotherapy (12). Stage III EOC tumor implicates one or both ovaries with spread to the peritoneum, lymph nodes and/or other sites outside the pelvis. The majority of OC are HGSCs and patients are diagnosed at stage III (14). Stage IV is characterized by distant metastases affecting the liver, spleen and lymph nodes and/or to other organs or tissues outside the peritoneal cavity such as the lungs and bones.

Ovarian Cancer Treatments

Current first-line treatment regimen for OC patients comprises complete debulking surgery. The reductive tumor procedure includes hysterectomy, omentectomy, and other affected tissues possible to remove. The goal of surgery is to reduce tumor burden and minimize residual disease, which is inversely proportional to survival (15). Indeed, residual lesions smaller than 2 cm have been associated with better survival than bigger ones (16). At the same time, debulking surgery allows to precisely establish the histologic subtype of the disease and, therefore, it is very important for diagnosis. Even though surgery is the basis for OC treatment, it is rarely curative alone for patients with advanced disease and it needs to be combined with chemotherapy.

In late 1990s, two phase III clinical trials combined cisplatin (CDDP) with paclitaxel (PTX) as adjuvant treatment for advanced stage OC (17). Ever since, the combination of taxane and platinum derivatives, like CDDP and carboplatin (CBT), has been used as a standard therapeutic approach for OC patients, leading to response rate, and complete clinical remission of 60–80% (18). Nevertheless, the majority of these patients will ultimately relapse with a median progression-free survival of 18 months (19). Usually, response rates to second-line chemotherapy are proportional to treatment-free interval (20). Different combinations of chemotherapeutics have been tested to overcome chemoresistance following first-line paclitaxel-platinum treatment, but clinical responses are short-lived and led to only minor survival improvements for patients with chemoresistant tumors (21). So far, radiation therapy (RT) has played a minor role in ovarian cancer. Abdominopelvic RT was associated with serious side effects and poor therapeutic efficacy for most of the patients (22, 23). Acute toxicity was most commonly due to cramps, diarrhea, nausea, vomiting and more severe myelosuppression, whereas long-term toxicity was associated with bowel obstruction (23, 24). The poor therapeutic effect was due to the limitation of dosage that causes toxicity to radiosensitive organs such as blood building system or kidney. Maybe new approaches in radiotherapy could lead to wider use of RT in OC [reviewed in Fields et al. (25) and Iorio et al. (26)]. Likewise, the use of radiolabeled antibodies for the management of advanced ovarian cancer after cytoreductive surgery and chemotherapy is limited and of no success so far. Antibodies directed to CA-125 (mAb OC-125) and MUC1 (mAb HMFG1) antigens labeled with iodine-131 or yttrium-90, respectively showed little or no therapeutic benefit in ovarian cancer patients (27, 28). Different reasons for the treatment failure were discussed. The dose of radiation may have been too low because of insufficient binding of the antibody or the lack of antigen expression in residual micrometastases. Furthermore, yttrium-90 is not the ideal isotope for irradiation of small tumor nodules. No pharmacokinetics was performed, and it is possible that there was limited systemic exposure to the intact radioimmunoconjugate. In addition, the anti-MUC1 antibody HMFG1 is not actively internalized into target tumor cells. In contrast to RT, radioimmunotherapy (RIT) is a targeted therapy were the antibody brings the radiation to the tumor site also to disseminated metastases. Non-specific irradiation of healthy tissue is normally low due to the clearing of the mAb from the blood. The dose-limiting organ is the bone marrow [reviewed in Larson et al. (29)]. New promising RIT approaches for the treatment of OC will be discussed during this report.

The better understanding of tumor biology and chemoresistance over the past years supported the development of molecular targeted therapies, improving survival and increasing the quality of life in OC patients. Many different inhibitors, such as tyrosine kinase inhibitors (30) and monoclonal antibodies (mAbs) targeting multiple crucial cancer pathways, including angiogenesis, cell survival, cell growth, metastasis formation and DNA repair, are currently tested in clinical trials (31). The most promising investigational agents include vascular endothelial growth factor (VEGF)-specific inhibitors and poly (ADP-ribose) polymerase inhibitors (PARPi). Bevacizumab (Avastin®, Genentech, Inc.), a recombinant humanized mAb against VEGF, blocks angiogenesis, enhancing the efficacy of standard therapy. In 2004, Bevacizumab has been clinically approved in the U.S. as the first angiogenesis inhibitor for colon cancer (32). In 2018, based on phase III GOG-0218 clinical study (NCT00262847), the FDA approved its use in combination with CBT and PTX, followed by single-agent bevacizumab for the treatment of patients with advanced (stage III or IV) ovarian epithelial, primary peritoneal or fallopian tube cancer after initial surgery (33). PARP enzymes are involved in different cellular functions, including DNA single-strand break (SSB) repair through base-excision repair by PARP1 (34). The first PARPi approved in the clinic was Olaparib (AZD2281, Ku-0059436 trade name Lynparza), an orally administered drug (35). In 2014, based on phase III SOLO-2 (NCT01874353) and phase II Study 19 (NCT00753545) clinical trials, Olaparib obtained an accelerated FDA approval as maintenance treatment for patients with a recurrent ovarian epithelial, fallopian tube or primary peritoneal cancer, who are in complete or partial response to platinum-based chemotherapy (35–38). In the same year, based on phase II Study 19 and phase II Study 42 (NCT01078662), the EMA authorized Olaparib as maintenance treatment for patients with platinum-sensitive, relapsed BRCA-mutated (germline or somatic) HGSC, who responded to the last platinum-based

chemotherapy (38, 39). Other types of tumorigenic pathway inhibitors targeting PI3K/AKT, mTOR, Src, and FRα are still in the early phase of development (38). To date, no effective cure for OC has been found. Considering the heterogeneous nature of OC and the lack of a common deregulated pathway in most patients, individualized therapy seems to be essential to improve survival.

TUMOR HETEROGENEITY

Two main models have been used to explain histological and molecular heterogeneity, a common feature of most solid tumors: the clonal evolution (CE) or stochastic model and the cancer stem cell (CSC) or hierarchical model. In recent times a third model, called the plasticity model, linking CE, and CSC models has been postulated (**Figure 1**).

The Clonal Evolution or Stochastic Model

In the 1970s, with the discovery that mutations in oncogenes and tumor suppressor genes trigger most human cancers, Nowell introduced the clonal evolution (CE) concept (40). The CE model assumes that every tumor cell is biologically equivalent and potentially able to drive tumor progression (41). The majority of cancer cells have only restricted proliferative potential and tumor progression is driven by the acquisition of gene mutations and epigenetic alterations in the original clone (42, 43). The progress from early to invasive carcinoma implicates the stepwise acquisition of random mutations in specific cancer genes, leading to uncontrolled proliferation and high tumor heterogeneity (44).

The Cancer Stem Cell or Hierarchical Model

In the early 1990s, with the introduction of new technologies such as fluorescence-activated cell sorting (FACS) and mouse xenografts assays for hematopoietic stem cells, Dick and colleagues found that tumor engraftment in acute myelogenous leukemia (AML) could only be initiated by $CD34^{+}$/CD38- cell population (45). In 2003, Clarke et al. applied for the first time the same experimental approach to solid breast cancer (46). Using xenograft assay, they showed that as few as 100 $CD44^{+}/CD24^{-}$/low breast cancer cells were sufficient to induce tumors, in contrast to thousands of cells expressing different markers (46). Moreover, this tumorigenic population has been passaged several times and these cells were always able to induce tumors recapitulating the original tumor composition, forming both $CD44^{+}/CD24^{-}$/low tumorigenic and non-tumorigenic cells. Afterwards, similar studies on other solid tumors, such as brain, breast, prostate and colon cancer, were published (47, 48). Most studies on CSCs have been performed in a similar way. Generally, small populations of cells defined by a specific marker or marker panel and expressed in a heterogeneous way in a particular type of tumor, are isolated from cell lines or primary tumors. When transplanted into immunodeficient mice, these cells can induce tumor growth over weeks or months and to reproduce the heterogeneity of the initial tumor (49). A frequency of CSCs present in a given tumor population can be analyzed in limiting dilution assay (LDA) by transplanting increasing dilutions of single tumor cell suspensions. LDA analysis *in vivo* is the gold standard to determine the CSC frequency in a given tumor cell population (50, 51). In addition to LDA, subsequent transplantation assays provide an important information about

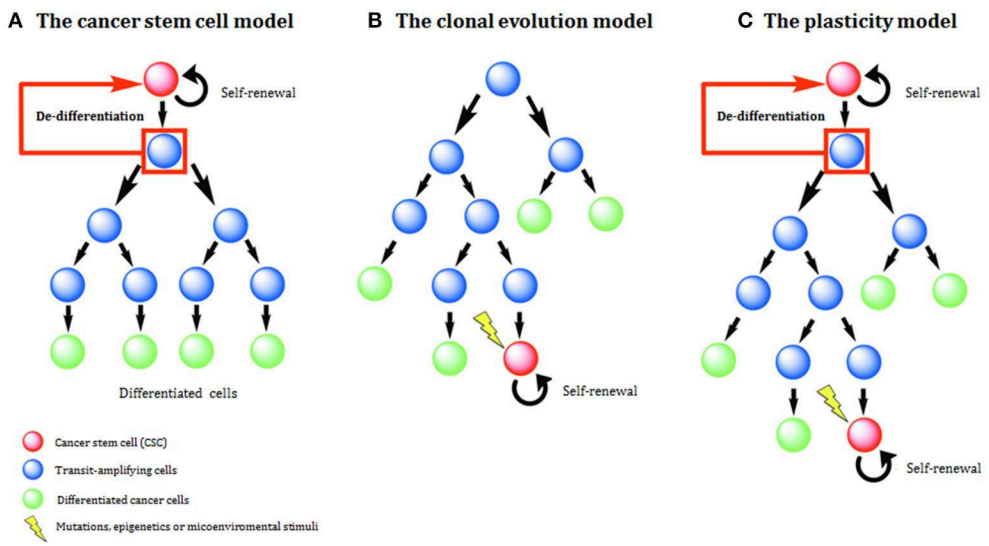

FIGURE 1 | Models of tumor development and heterogeneity. **(A)** The cancer stem cell (CSC) model of tumor development. Genetic or epigenetic mutations activate stem-like programs in a single cell, generating a CSC. This CSC is able to indefinite self-renewal and/or differentiation and all derived tumor cells have a hierarchical inheritance pattern. **(B)** The clonal evolution (CE) model of tumor development. Due to the acquisition of epigenetic and genetic mutations through time, any cell might have tumorigenic potential. Tumor heterogeneity is due to the propagation of cells carrying genetic mutations. **(C)** The plasticity model highlights the plastic state of cancer stemness. Based on the model, differentiated non-tumorigenic cancer cells can potentially revert back to CSCs.

the long-term self-renewal and tumor regeneration capacity of the tentative CSC populations (52). An emerging gene engineering technologies including applications of CRISPR-*Cas9* system for target genome editing substantially simplified generation of knockin or knockout cell and mice models. The genetically modified patient-derived organoid and mice models where a given cell population can be traced *in vivo* is an important tool to identify tumor cell of origin (53, 54). Nevertheless, because of technical issues, many theoretical and experimental details about the CSC model have remained unexplored and the frequency of CSCs in solid tumors is highly variable. Technical issues include inconstant purity of tumor cell isolation, the necessity of more solid and reliable markers and the challenges related to xenotransplant assays that offer a different environment than the original tumor niche (55).

The CSC model suggests that the origin and the progression of many cancers are driven by small subpopulations of cells with stem-like properties; however, this model does not address the question of whether tumors arise from normal stem cells. Instead, it suggests that, regardless of the cell-of-origin, many cancers are hierarchically organized in the same manner as normal tissues and CSCs share similar molecular properties to normal stem cells. In accord with this model, tumors have a hierarchical structure, with tumorigenic CSCs at the top that generate both intermediate progenitors (also called transit-amplifying cells) and terminally differentiated cells. Considering that the same CSC populations can originate from different cancer subtypes, the frequency of CSCs can highly vary among tumor types and also within the same tumor, leading to tumor heterogeneity (56). CSCs, like non-neoplastic stem cells, have extensive proliferative potential and generate the differentiated progeny that form most of the tumor mass and it is highly sensitive to cancer therapies. Additionally, these cells can remain quiescent for prolonged periods of time, which renders them unresponsive toward radiation and chemical insults, including cytotoxic drugs designed to target fast-proliferating tumor cells (57). Interestingly, recent studies have highlighted some common features (58, 59) but also many differences in stem cell programs operating in CSCs and non-neoplastic stem cells (60).

The Plasticity Model

It is now evident that one model does not exclude the other and both might contribute to cancer development, depending on tumor type and stage (61).

In recent years, an alternative model based on cellular plasticity, which links the CE and the CSC models, has emerged (61–63). The plasticity model proposes that cancer cells in different types of tumors including OC can switch between stem cell-like and differentiated states so that some differentiated non-tumorigenic cancer cells can de-differentiate to become CSCs (64). Therefore, CSC-like phenotype is flexible and dynamic, instead of being a fixed property of tumor cells. Signaling within the tumor microenvironment (tumor niche), including oxygenation, cell-to-cell contact and secreted factors, could induce differentiated tumor cells to re-acquire stem cell-like properties (62). Additionally, radio- and chemotherapy treatments have been shown to enrich CSC subpopulations in residual tumors because of selective pressure on drug-resistant cells (65–67) and due to tumor cell plasticity (64). Even though the CSC state has high plasticity, it is of high clinical importance as a potential marker for clinical outcome and target for anti-cancer treatment (68, 69).

OVARIAN CANCER STEM CELLS

Regardless of the high response rate to standard therapy, most OC patients develop recurrent chemoresistant disease (70). Recurrence is believed to be caused by the presence of residual tumor-propagating cells that cannot be completely eradicated by surgical and/or pharmacological regimens (9). Accumulating evidence suggests that among these residual cancer cells some have the key stem cell-like properties such as self-renewal and differentiation (71, 72). This small population of cells appears to form and to sustain the tumor bulk population, being responsible for disease recurrence after the first-line treatment (73). In some studies, these cells have been isolated by flow cytometry and were discovered to be enriched in a side population (SP) able to efflux the Hoechst33342 dye by cell transporters using the same mechanism with which normal cells efflux toxic drugs (74, 75). Further investigations revealed that these cells have several characteristics in common with normal tissue stem cells. In 2005, Bapat et al. were one of the first groups that characterized the presence of ovarian CSCs from patient ascites, showing tumorigenic properties of these cells (71). In addition to self-renewal and the ability to give rise to more differentiated progeny, CSCs are highly tumorigenic and display increased resistance against conventional cancer therapies (76–78). As of today, there are still considerable controversies on the OC CSCs due to the heterogeneity of CSC phenotypes, plasticity of CSC states as well as limitations of the current research methodology for CSC characterization. Nevertheless, reliable markers of OC CSCs have been successfully validated by xenograft transplantations of the serial tumor cell dilutions (limiting dilution assay) along with serial tumor transplantation and lineage-tracing assays (79–82). These analyses are currently "gold standard" assays to measure key CSC properties such as self-renewal and multipotency (52). In support of these preclinical findings, clinical significance of CSCs was recently confirmed by a number of studies demonstrated the association of CSC markers with clinicopathological parameters and clinical outcomes of OC patients (69).

Ovarian Cancer Stem Cell Markers

The proportion of CSCs can vary depending on tumor type and in the context of OC, CSC frequency shows high interpatient variability (83). Considering CSCs resistance against conventional cancer treatments, the development of more efficient tumor therapies requires effective identification and functional characterization of these cell populations. The expression of several individuals or combined cell surface markers has been associated with CSCs (**Table 1**). The multiplicity of CSC markers, along with their plasticity, might pose a challenge to detect successful CSC-targeting therapeutic strategies. For this reason, it is important to select

TABLE 1 | List of some putative CSC markers.

CSC marker	Protein function	References
CD133	Pentaspan transmembrane glycoprotein—membrane organization	(52–61)
ALDH	Detoxifying enzyme–drug resistance	(62–70)
CD44	Cell adhesion molecule—receptor for hyaluronic acid	(47, 73–77)
CD24	Mucin-like cell adhesion molecule	(78–80, 84)
CD326	Epithelial cell adhesion molecule (EpCAM)	(38, 81–83, 85)

reliable molecular markers that could be used to develop new therapies.

One of the best-characterized CSC surface markers is the transmembrane glycoprotein CD133 (also known as AC133 and Prominin-1), initially identified as hematopoietic stem cell marker supporting stem cell maintenance and expansion (85, 86). CD133 localizes to plasma membrane protrusions and microvilli, indicating its role in membrane organization (86). Several recent studies revealed the role of CD133 as a positive regulator of Wnt, PI3K and EGFR signaling pathways (87, 88). However, the exact physiological function of CD133 in normal and cancer cells is still elusive. CD133 was first characterized as CSC marker in glioblastoma (89) and later it was found to be widely expressed in tumor-initiating cells of different tumors (e.g., ovarian, liver, lung, pancreatic and prostate cancer) (90). Several groups have identified the expression of CD133 in OC cells, which is connected with tumor initiation, self-renewal and chemoresistance (91, 92). Some published studies indicated the phenotypic heterogeneity and plasticity of CD133 expression (80). This finding might explain why some data did not support the link between CD133 and ovarian CSCs, showing inconsistent expression and no increased spherogenic or tumorigenic properties of CD133+ in comparison to the CD133− counterpart (93, 94). Inconsistent CD133 detection because of different immunoreactivity of primary anti-CD133 antibody clones might also account for discrepancies in the identification of CSCs (95).

The human genome encodes 19 aldehyde dehydrogenase (ALDH) enzymes implicated in detoxification of endogenous and exogenous aldehydes via NAD(P)+-dependent oxidation (96, 97). Upon chemotherapy and irradiation, these enzymes catalyze the oxidation of aldehydes (oxygen, carbon, and hydrogen) to carboxylic acids to prevent DNA damage. ALDH modulates the expression of drug transporters to efflux chemotherapeutic agents, contributing to cell-acquired drug resistance against conventional cancer therapies (98). Additionally, the ALDH protein family catalyzes the oxidation of retinoic acid, which regulates the differentiation of normal stem cells and CSCs (99). The ALDH1 subgroup is highly expressed in normal and CSCs. Among ALDH1 isozymes, ALDH1A1 is more widely expressed in CSCs of different cancer types than ALDH1A2 and ALDH1A3 (100). The study of the ALDH1 expression in 24 types of normal and six types of epithelial tumor tissues revealed that increased expression of ALDH1 was significantly associated with poor outcomes for 439 patients with serous OC (68). Furthermore, ALDH expression in combination with CD133 correlates with poor patient prognosis and characterizes an ovarian CSC population (76, 101). However, recent research suggested that ALDH is a better marker to identify ovarian CSCs than CD133, as ALDH correlates with tumorigenicity and spheroid formation (102). It is now well-known that only cancer progenitor cells have the ability to proliferate under non-differentiating and non-adherent conditions, forming 3D tumor spheres (103). These spheres are enriched by cells displaying stem cell-like properties, including the upregulation of some stem cell-specific genes, high ALDH activity, self-renewal ability along with high proliferative and differentiation properties (102, 104, 105). Consequently, sphere-forming cells display aggressive growth, migration, invasion, clonogenic survival, anchorage-independent growth, and reduced drug responsiveness *in vitro* (105).

CD44 cell transmembrane glycoprotein has been associated with several signal transduction pathways, including NANOG and EGFR-Ras-ERK (106). The main CD44 ligand is hyaluronic acid, a component of the extracellular matrix, which is positively associated with OC migration and metastatic spread (107, 108). CD44 is expressed in both normal and ovarian CSCs and it is associated with sphere-forming ability, self-renewal, chemoresistance, tumorigenicity, proliferation and invasiveness (109). Additionally, high expression of CD44 correlates with epithelial-to-mesenchymal transition (110) and with stem cell-like properties, contributing to tumor invasion, metastasis, disease recurrence and chemoresistance (111). The co-expression of CD44 with the c-Kit receptor CD117 was shown to define an ovarian subpopulation with tumor-initiating capacity (72). C-kit regulates survival, proliferation and chemoresistance of ovarian CSCs through PI3K/AKT and Wnt/β-catenin-ATP-binding cassette G2 signaling (112).

CD24 is a glycosylphosphatidylinositol-anchored membrane glycoprotein recognized as a positive or negative marker for CSCs in numerous cancer types. The low expression of CD24 combined with high CD44 (CD44+/CD24−/low) is used to identify breast CSCs (46). On the contrary, several data indicated CD24 as a positive marker for ovarian CSCs. A population of CD24+ cells isolated from OC samples and cell lines was shown to display high expression of stemness-related genes, high tumor initiation and fast tumor growth along with increased sphere-forming ability (113, 114). Besides, Davidson and colleagues demonstrated that tumor cells collected from OC peritoneal fluids exhibited higher levels of CD24 than solid tumors, suggesting an enrichment of CSCs (115).

Epithelial cell adhesion molecule (EpCAM), also called CD326, is a transmembrane glycoprotein overexpressed in many carcinomas (116). Several studies described a controversial role of EpCAM in carcinogenesis. Being an adhesion molecule, EpCAM regulates homophilic adhesion interactions, which might inhibit metastatic invasion (116). However, depending on the microenvironment, EpCAM is also able to suppress E-cadherin adhesions, supporting metastasis formation. EpCAM has been recognized as an additional marker for CSCs in different tumor types (55). High expression of EpCAM in OC is associated with tumor recurrence, chemoresistance and poor patient

prognosis (117). Cells co-expressing CD24, CD44, and EpCAM showed stem cell-like characteristics, high tumorigenicity *in vivo* as well as enhanced migration, invasion and colony-formation *in vitro* and this population could be enriched by chemotherapy (50, 118).

There are also several stem cell-associated genes that play a role in the maintenance and development of ovarian CSCs. *LIN28*, *OCT4*, *SOX2*, and *NANOG* transcription factors (TFs) regulate and maintain pluripotency in embryonic stem cells (119). The co-expression of *LIN28* and *OCT4* identifies a population of ovarian CSCs and correlates with advanced tumor grade (120). *NANOG* is closely associated with HGSC, high chemoresistance and poor overall patient survival (121). *SOX2* is required to maintain ovarian CSCs and its expression correlates with chemoresistance and poor prognosis (122).

Mechanisms of Cancer Stem Cell Therapy Resistance

Conventional therapies are often not sufficient to eliminate CSC populations because of intrinsic resistance mechanisms and epigenetic plasticity of the cells (123, 124). This means in many cases, tumor relapse is caused by the incomplete elimination of all CSCs, since a single CSC seems to be sufficient to regrow a tumor [**Figure 2**; (125)].

Several molecular mechanisms, such as enhancement of DNA repair and DNA damage response (DDR), increased drug efflux, efficient scavenging of reactive oxygen species (ROS) and signals from the microenvironment, support the resistance of CSCs toward conventional cancer therapies [**Figure 3**; (126)].

Increased DNA Pepaire Capacity

Radiation and many chemotherapeutic drugs (e.g., DNA crosslinkers, DNA synthesis, and topoisomerase inhibitors) induce DNA damage, which, if not repaired, can lead to cell death (127). Among different types of DNA damages caused by radiation and chemotherapy, DSBs are the most lethal lesions if not repaired (128). DSBs are usually repaired by error-free homologous recombination (HR) or error-prone non-homologous end joining (NHEJ) mechanisms (129). In response to radiation, DNA repair is initiated and controlled by the DNA damage response (DDR). For the purpose of stalling cell cycle progression and give time to the cells to repair DNA damage, DDR triggers the activation of checkpoint kinase signaling pathways such as ataxia telangiectasia mutated (ATM)-checkpoint kinase 2 (Chk2) and ATM-Rad3-related (ATR)-checkpoint kinase (Chk1) (130, 131). CSC populations of glioblastoma, prostate, lung, breast cancer and many others, have been shown to possess high DNA repair capacity, mainly due to increased activation of ATR-Chk1 and ATM-Chk2 pathways (130). Recent reports demonstrated increased HR-dependent DNA repair proficiency of CSCs in OC that makes them more resistant to PARP inhibition (132). Different populations of OC CSCs have a high resistance to the platinum agents due to the altered regulation of cell cycle checkpoint, upregulation of the Fanconi Anemia DNA repair proteins (*FANCD2*, *FANCJ*) (133), *MLH1,* and *BRCA1* (134) and increased expression of DNA polymerase eta (135).

ROS Scavenging

Radiation-induced damages include the formation of ROS, which are chemically reactive free radicals produced by oxygen metabolism. ROS are involved in many physiological signaling pathways regulating metabolism, cell proliferation, migration, angiogenesis and wound healing (136). However, in high amounts, ROS can produce oxidative DNA damage, alter proteins and cell membrane lipid bilayer, leading to cell arrest and cell death (137). The cells control ROS levels through ROS scavenging molecules (e.g., glutathione peroxidase, superoxide dismutase, and catalase), which balance the production and the elimination of these products (137). CSCs isolated from different tumors exhibit more efficient ROS scavenging systems and a lower level of ROS production compared to non-CSC

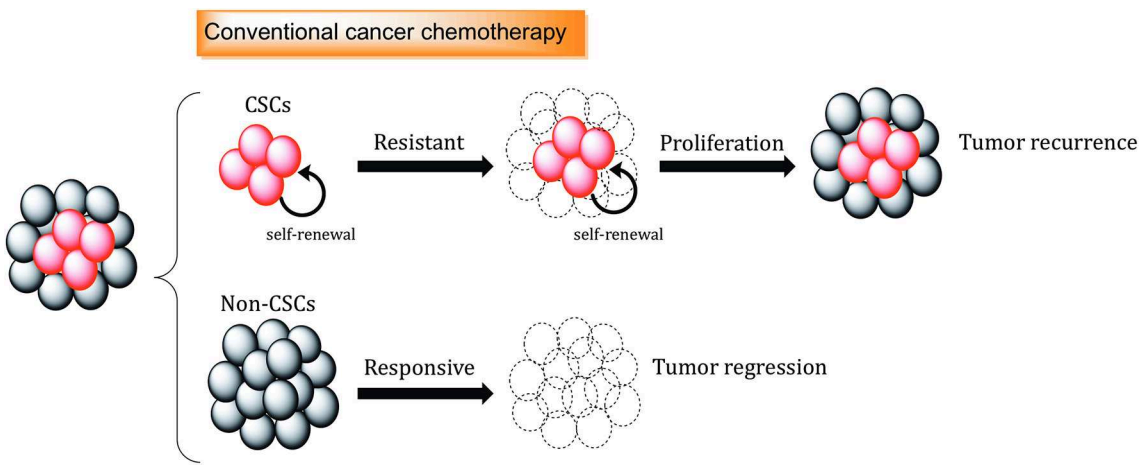

FIGURE 2 | The role of cancer stem cells in drug resistance. Standard chemotherapeutics are not able to kill cancer stem cells (CSCs), which can promote tumor regrowth and eventually result in disease relapse. Different mechanisms, including increased.

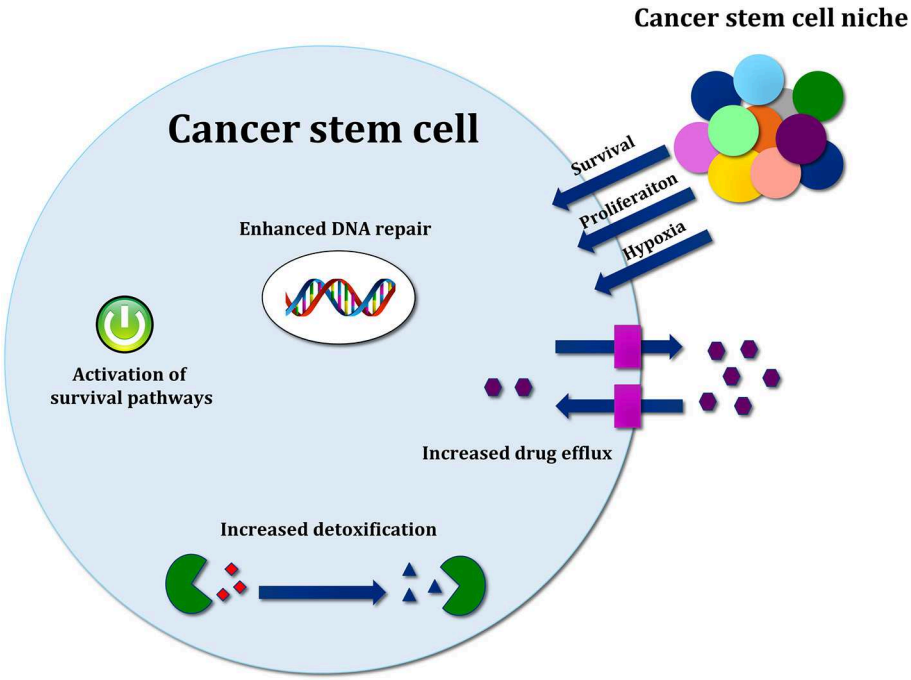

FIGURE 3 | Mechanisms of cancer stem cell resistance toward conventional therapy. Therapy resistance mechanisms include drug efflux by ABC transporters, increased detoxification by ALDH activity, efficient ROS scavenging, and activation of developmental pathways mediating survival. Signals released by cancer stem cell (CSC) niche are also important to support survival, proliferation and therapy resistance.

populations (138, 139). ALDH positive population in OC has an upregulation of NRF2 (Nuclear factor erythroid 2-like) signaling driving the cytoprotective response to the oxidative stress (140).

Enhanced Drug Efflux by ABC Transporters

Another important mechanism for CSC drug resistance is the high expression of ATP-binding cassette (ABC) transporters. The human genome encodes 49 *ABC* genes and these proteins are essential to maintain homeostasis and to protect the cells against environmental insults in many normal tissues (e.g., liver, intestine, blood-brain barrier, placenta, kidney, and normal stem cells) (141). Three ABC transporter proteins, P-glycoprotein (P-gp, MDR1, ABCB1), multidrug resistance protein 1 (MRP1, ABCC1), and breast cancer resistance protein (BCRP, ABCG2), have been shown to play a role in multidrug resistance of various types of cancers like OC, breast, lung, colon and others (142). Due to broad substrate spectrum specificity, their expression provides tumor resistance toward the major classes of chemotherapeutic drugs (126). CSC populations of different tumors, including breast cancer, lung cancer, retinoblastoma, neuroblastoma, and glioblastoma, have been demonstrated to overexpress ABC transporters, which correlates with high drug resistance (143).

Aldehyde Dehydrogenase Activity and Activation of Developmental Pathways

Supplementary intrinsic mechanisms underlying CSC therapy resistance are mediated by high ALDH activity and activation of developmental pathways essential for embryonic development and tissue homeostasis like the canonical Wnt/β-catenin, Notch and Hedgehog pathways (126). Notch signaling contributes to survival and platinum resistance of ovarian CSCs and it has been determined that Notch 3 expression is associated with poor prognosis for OC patients (144). Hedgehog signaling is aberrantly activated in OC and this pathway affects cell growth, motility, invasion, and tumorigenesis (145). Wnt/β-catenin is involved in stem cell proliferation and differentiation. CSCs of many tumors were found to overexpress β-catenin, which promotes stemness (146). In OC, genetic mutations in the Wnt pathway are rare, but recent data demonstrated that the activation of Wnt signaling could be regulated by the tumor microenvironment, contributing to ovarian tumorigenesis (147).

Cancer Stem Cell Niche and Their Microenvironment

Growing bodies of evidence showed that microenvironmental stimuli coming from the specific niche in which CSCs reside could influence and regulate treatment responsiveness (**Figure 4**). Additionally, autocrine signaling and stimuli coming from stromal fibroblasts, immune cells and extracellular matrix (ECM) as well as oxygen, nutrient supply and tissue pH, might affect CSC properties and metastatic dissemination (136).

Matrix metalloproteinases (MMPs) are extracellular proteases able to degrade and cleave ECM molecules, remodeling CSC niche and releasing growth factors and cytokines, thus, being suggested to regulate signaling pathways that control proliferation, differentiation and tumor invasion (148).

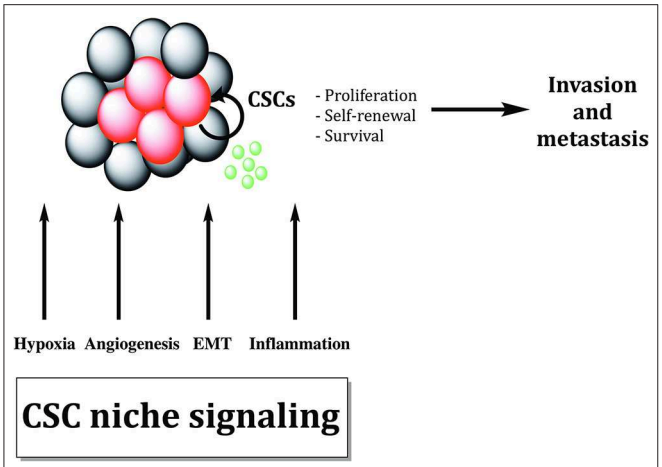

FIGURE 4 | Cancer stem cells are sustained by biological processes within the cancer stem cell niche. Different biological processes like EMT, hypoxia, inflammation, and angiogenesis maintain cancer stem cells (CSCs). Cytokines and growth factors produced by tumor cells and tumor-associated cells increase proliferation and survival of CSCs, promoting tumor invasion and metastasis formation.

Tumor and stroma-derived growth factors and cytokine regulating stemness and resistance comprise interleukin-6 (IL-6), interleukin-8 (IL-8), chemokine (C-X-C motif) ligand 12 (CXCL12), chemokine (C-X-C motif) receptor type 4 (CXCR4), chemokine (C-C motif) ligand 2 (CCL2), platelet-derived growth factor (PDGF), transforming growth factor-beta 1 (TGF-β1), tumor necrosis factor-alpha (TNFα), epidermal growth factor (EGF), VEGF and fibroblast growth factor (FGF) (62, 126). IL-6, which is secreted by tumor-associated stroma has been shown to play an important role in the enrichment of OC stem cells after treatment with platinum agents (149). Dual expression of CXCR4 and CD133 has been used to identify an OC population with stem cell-like properties that regulate tumor development and chemoresistance (92). The formation of new vessels, also known as angiogenesis, supports tumor growth and it is tightly regulated by angiogenic activators including VEGF, FGF, PDGF, and EGF (150). Bao et al. determined that glioblastoma CD133+ CSCs highly express VEGFA, which contributes to the angiogenic process by interacting with the microenvironment (151). A recent study revealed that VEGFA stimulates OC stem cells by activation of the epigenetic mechanisms inducing loss of miR128-2 and upregulation of Bmi1 (152).

The association between inflammation and cancer development has been suggested for numerous types of tumors (153). The accumulation of proliferating tumor cells mimics a chronic inflammation and the activated stroma cells produce a number of cytokines, angiogenic factors and chemokines, which in turn recruit more immune cells including monocytes and macrophages. The most common inflammatory molecules released in the microenvironment by tumor-associated macrophages (TAMs) are the EMT-inducers TGF-β1 and TNFα (154). EMT confers stem cell-like phenotype to cancer cells, enhancing motility and drug resistance.

In addition, tissue oxygenation influence CSC properties, maintaining cells in a quiescent (hypoxia) or activated (normoxia) state. For example, hypoxia is a major stimulant of CXCL12, which is secreted by tumor stroma fibroblasts and is involved in the early stage of malignant transformation of OC (139). Hypoxia makes CSCs more resistant to various environmental insults and it is the major stimulant of angiogenesis. Hypoxia-inducible factor (HIF) target genes, such as *GLUT-1*, *VEGF*, *OCT4* and Notch, are crucial regulating proliferation, tumorigenicity and self-renewal in different cancers (155). HIF induces stem cell properties in OC cells (156) and promotes OC stem cells adaptive stress response (157) and resistance to therapy (158). Hypoxia has been demonstrated to promote the acquisition of stem cell-like state through the increased expression of CSC markers like CD133 and CD44, along with CSC-related genes such as *SOX2* (155). Moreover, hypoxia is also tightly associated with chemo- and radioresistance. Low oxygen conditions maintain CSCs in a quiescent state with a low proliferation rate and since most conventional cytotoxic drugs target proliferating cells, CSCs cannot be destroyed. It is also recognized that the local concentration of oxygen improves radiotherapy efficacy since DNA lesions caused by ROS react with oxygen-generating stable DNA peroxides (159). Tumor oxygenation and oxygen therapeutics have been utilized as radiosensitizers to improve patients' response to radiotherapy (160).

Epithelial-To-Mesenchymal Transition and Stemness

In recent years, high plasticity of CSCs and stemness have been increasingly linked to EMT. EMT is an essential cellular process usually involved in embryogenesis, wound healing and tumorigenesis. During tumor progression, neoplastic cells switch from an epithelial-like state to gain mesenchymal properties. Therefore, EMT allows cancer cells to become migratory and invasive, acquiring multiple properties associated with high-grade malignancies (161). EMT is suggested to be a reversible process where mesenchymal-like cells might transition back into an epithelial state, a process called mesenchymal-to-epithelial transition (MET). A number of TFs, referred as EMT-TFs, are associated with EMT and can be classified into three main protein families: Snail (Snail and Slug), ZEB (ZEB1 and ZEB2), and basic helix-loop-helix (TWIST1, TWIST2, and TCF3) families (162). These TFs coordinate changes in gene expression resulting in suppression of genes associated with the epithelial state, like E-cadherin, and in upregulation of genes correlated with the mesenchymal state, including N-cadherin and vimentin (162). The activation of some of these TFs, including Slug, ZEB1, ZEB2, TWIST1, and Snail1, has been linked to the expression of stem cell-related genes and self-renewal in various tumor types (163). The EMT process is controlled by a variety of cytokines and growth factors and among them TGF-β signaling plays a fundamental role. TGF-β signaling regulates ovarian CSCs through the modulation of tissue transglutaminase 2 (TGM2), which promotes EMT, metastasis and stem cell-like phenotype (164, 165). Hypoxia, through the expression

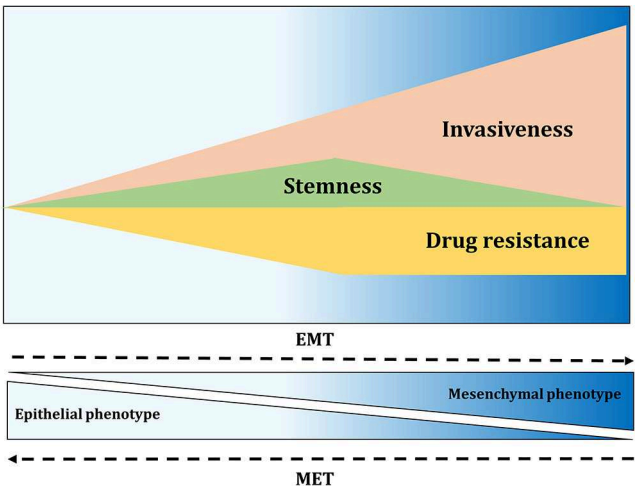

FIGURE 5 | EMT contributes to invasiveness, stemness, and drug resistance. Activation of EMT results in migration and fast tissue invasion. Furthermore, EMT activation affects tumor-initiating properties of cancer cells, with the greatest properties found at the intermediate level of EMT. Drug resistance of cancer cells also seems to be highest in cells with intermediate EMT phenotype.

of HIF-1α and HIF-2α, regulates CSC-associated genes and induces EMT via the TGF-β signaling pathway, which in turn contributes to stemness (166). Cancer cells with an intermediate EMT phenotype display stem cell-like properties accompanied by enhanced resistance to several anti-cancer drugs [**Figure 5**; (124)]. In 2011, Strauss and colleagues identified a minor population of OC cells in a transitory epithelial/mesenchymal hybrid stage (i.e., partial or intermediate EMT), which means that these cells expressed at the same time epithelial and mesenchymal markers, respectively linked to adhesion and migration (167). The observation that these cells drive tumor growth *in vivo* and have the capacity of self-renewal provided a link between stemness and phenotypic plasticity. Many other studies have highlighted a connection between partial EMT, drug resistance and tumor-initiating ability, showing that this phenotype enables the formation of highly metastatic circulating-tumor cells clusters (168). Therefore, EMT gives a hint about the plasticity model, showing that plasticity enhances invasion potential and tumor-initiating properties of cells that arrive at the metastatic site (169). Stemness is therefore not a fixed and inherent property but instead, CSCs and non-CSCs can bidirectionally interconvert between these two states (168).

NOVEL THERAPEUTIC STRATEGIES FOR OVARIAN CANCER

High-throughput approaches have identified numerous potential therapeutic targets to treat cancer cells specifically. The current focus of anti-cancer drug discovery is the development of molecular targeted therapies rather than conventional cytotoxic drugs. A major challenge remains to find agents and strategies that select and eliminate the source of tumor recurrence after therapy, along with bulk tumor cells. It became increasingly evident that CSCs are crucial for disease recurrence and chemoresistance, thus targeting these cells seems a promising way to reach complete tumor eradication.

TABLE 2 | Emerging therapies targeting ovarian cancer stem cell-associated pathways.

Drug	Target	Identifier	Phase	Condition	Combination
Metformin	Anti-diabetic drug	NCT02122185	II	Advanced OC	Yes
Sonidegib	Hedgehog inhibitor	NCT01954355	I	Advanced OC	Yes
Vismodegib	Hedgehog inhibitor	NCT00739661	II	OC in second or third complete remission	No
Ipafricept	Wnt inhibitor	NCT02092363	I	Recurrent platinum-sensitive OC	Yes
Defactinib	FAK inhibitor	NCT01778803	I	Advanced OC	Yes

Clinical trial information accessed via https://clinicaltrials.gov with National Clinical Trial Number (NCT Number).

Inhibition of Cancer Stem Cell-Associated Pathways

Novel therapies have been employed to target CSC-specific markers or pathways critical for regulation and maintenance of stem cell-like properties (**Table 2**).

Metformin hydrochloride is clinically used as an anti-diabetic drug for type 2 diabetes. Recent studies have reported its ability to enhance chemotherapy efficacy in different cancer types by targeting CSCs. Metformin showed a synergic effect with standard chemotherapeutic agents, reducing tumor relapse rate (170). Shank and colleagues elucidated a potential mechanism behind this effect, demonstrating that the treatment with metformin reduced $ALDH^+$ ovarian CSCs, proliferation and angiogenesis *in vitro* and *in vivo*. This effect was additive in combination with CDDP (171). The outcomes of combinational treatment with metformin and chemotherapy in patients with stage III and IV OC are currently investigated in phase II clinical trial (NCT02122185) (172). Treatment of OC cell lines with the FDA approved PARPi olaparib and rucaparib enriched cells with highly efficient DNA repair mechanisms. These cells expressed the CSC markers CD133 and CD117 (132). This might explain why patients who received PARPi treatment develop resistance in spite of a good initial therapy response. Several developmental pathways, including Notch, Wnt and Hedgehog, are crucial for self-renewal and regulation of CSCs (173). The inhibition of these pathways in combination with traditional chemotherapy has been proposed as a promising therapeutic strategy for recurrent diseases.

Sonidegib is an FDA approved Hedgehog inhibitor for basal cell carcinoma. Sonidegib was tested in phase I clinical trial in combination with PTX (NCT01954355) as a treatment for patients with advanced OC, demonstrating anti-tumoral activity. Based on this study, a recommended dose for phase II trial has been identified (174). The second Hedgehog

inhibitor, Vismodegib, was used in phase II clinical trial as maintenance therapy for patients diagnosed with OC in second or third complete remission (NCT00739661) (175). However, no significant survival benefit was observed (5.8 months for placebo vs. 7.5 months for the treatment group), implying that the blockage of the Hedgehog pathway alone is probably not enough to destroy recurrent disease (175). The Wnt inhibitor Ipafricept reduces CSC frequency, promotes cell differentiation in patient-derived OC xenografts and in phase I clinical trial in association with carboplatin and PTX for recurrent platinum-sensitive OC (NCT02092363), 82% of patients achieved a partial or complete response (176). Focal adhesion kinase (FAK) is a cytoplasmic protein overexpressed in CSCs of different tumors and it maintains interaction with stromal cells to activate intracellular signaling cascades (62). Defactinib, an oral inhibitor of FAK, exhibited modest activity in phase I clinical trial in combination with PTX for advanced OC (NCT01778803), suggesting that targeting the CSC niche might offer a suitable therapy strategy (177).

New Radioimmunotherapy Approaches

At the Center for Radiopharmaceutical Sciences of the Paul Scherrer Institute we developed the anti-L1 cell adhesion molecule (L1CAM) chimeric monoclonal antibody chCE7 for radioimmunotherapeutic (RIT) approaches to cancer. The L1CAM is a 200–220 kDa type I membrane glycoprotein of the immunoglobulin superfamily, containing six immunoglobulin-like domains and five fibronectin type III repeats followed by a transmembrane region and a highly conserved cytoplasmic tail (178–180). Firstly, L1CAM was identified as a protein of the nervous system and during brain development it was shown to play an important role in morphogenic events like neurite outgrowth, fasciculation, adhesion and neuronal cell migration (181). L1CAM is expressed in human peripheral nerve bundles and human kidneys, while it is absent in other human tissues comprising heart, lung, colon, liver, thymus or testis (181, 182). Low levels of L1CAM are also detectable in hematopoietic cells (181). L1CAM is overexpressed in various types of human cancers, including ovarian and endometrial carcinoma, colon cancer, melanoma and glioblastoma, and it usually correlates with advanced tumor stage and poor prognosis (179, 180). L1CAM expression in cancer supports motility and invasion, promoting aggressive tumor growth and metastasis formation (180). Additionally, L1CAM in combination with CD133 characterized a new ovarian CSC population (82). This protein exhibits static and motility-promoting functions, eliciting different signaling pathways depending on the binding partners; L1CAM homophilic interactions support static cell-cell binding while binding of L1CAM to integrin induces motility and invasiveness (180).

Indeed, the restricted expression of L1CAM allowed the use of anti-L1CAM mAbs for OC targeted therapies (183). Previous work revealed that chCE7 binds near the RGD sequence in the sixth Ig-like domain of human L1CAM, preventing its binding with integrin (184). RIT using copper-67 and the radiolanthanides lutetium-177 (^{177}Lu) and terbium-161 (^{161}Tb) was demonstrated to increase the efficiency of antibody-based L1CAM therapy in preclinical OC models (183, 185, 186). The antigen-antibody complex usually internalizes by endocytosis and the coupled metallic radionuclides are trapped in the cell (187). Therapeutic results for RIT in solid tumors (as adjuvant therapy after primary surgery and/or chemotherapy) have been modest during recent years and the main obstacles include low radiosensitivity, poor lymphatic drainage, limited diffusion of the antibody through tumor mass, poor vascularization and lack of homogeneous targeting (188). To overcome these limitations, several new strategies, including bioengineering development of different antibody formats to improve tumor penetration, pre-targeting approaches, the use of alpha particle or Auger electron emitters, as well as dose fractionation, have been developed over the past years (188). Furthermore, RIT has been combined with other chemotherapeutics, including DNA-damaging agents (e.g., CDDP), microtubules-stabilizing agents (e.g., PTX) and protein kinase inhibitors (PKIs) providing cellular radiosensitization effects (189, 190). PTX enhances anti-L1CAM RIT effectiveness, blocking cancer cells in the radiosensitive G2/M cell cycle phase. Our group could recently demonstrate that *in vivo* combination therapy with ^{177}Lu-DOTA-chCE7 [^{177}Lu was coupled to the mAb via the chelator 1,4,7,10-tetraazacyclododecane-N-N'-N"-N"'-tetraacetic acid (DOTA)] and PTX significantly extended overall survival of ovarian tumor-bearing mice (55 days RIT+PTX vs. 18 days PTX and 29 days RIT) (189).

Different properties of alpha-particles and Auger electrons, including short path length and high density of released energy in tissue, make them appropriate for targeted therapies against small volume diseases like metastases (<1 cm diameter) and for eradicating radioresistant CSCs (191).

The low-linear energy transfer (LET) refers to the energy released over the track length of the radiation in biological tissues. At equal absorbed dose, high-LET particles result in relatively high deposition of energy in tumor cells, which renders these forms of radiation more cytotoxic than low-LET radiations (**Figure 6**).

Most beta-particles emit low-LET radiations of 0.1–1 keV/μm, while alpha-particles have high-LET values of 50–230 keV/μm and Auger electrons intermediate-LET of 4 to 26 keV/μm (192). Low-LET of beta-particle emitters is due to intermediate energy (0.5–2.3 MeV) and long-range in biological tissues (0.5–12 mm), producing easily reparable sparse DNA lesions (193). Additionally, beta-particles kill tumor cells surrounding target cells independently from antigen expression, by the so-called "cross-fire" effect. Because of heterogeneous antigen expression among tumor cells, cross-fire irradiation is suitable when not all tumor cells can be specifically targeted by radiolabeled antibodies. However, the long path of these particles can also induce bone marrow toxicity. In contrast, alpha-particles have high energy (5–9 MeV) and intermediate path length (50–100 μm), which restricts their effect to 5–10 cell diameters (193). Auger electrons have low energy (0.001–1 KeV) and subcellular nanometer range (<1 μm) (193). These characteristics minimize the non-specific irradiation of non-targeted surrounding healthy tissues. Most importantly, it makes it possible to locally deliver high-absorbed doses and lethally damage tumor cells, inducing densely localized DNA DSBs. Besides DNA damage,

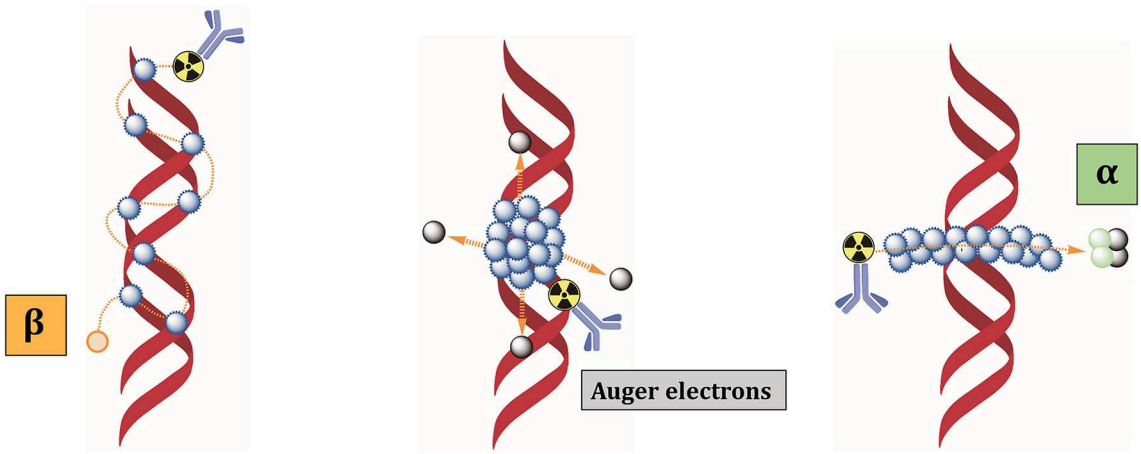

FIGURE 6 | Cellular damages induced by different LET radiations. **(A)** Low-LET radiations produced by beta-particles induce individual DNA lesions that can be easily repaired by the DNA repair machinery. **(B)** Auger electrons are released as a cascade close to cell membrane or DNA, producing clusters of lethal DNA lesions. **(C)** Alpha radiations have high-LET and produce multiple damages along a linear track that are difficult to repair. Blue dots: ionizations/excitations.

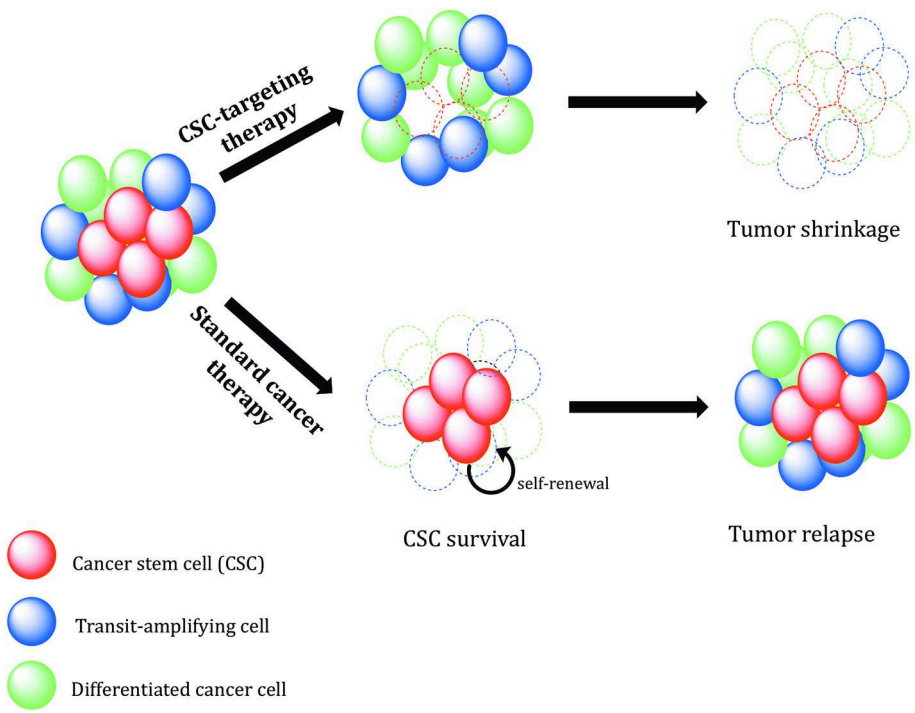

FIGURE 7 | Therapeutic relevance of cancer stem cells. Conventional cancer therapies mostly kill the tumor bulk population, while therapy-resistant cancer stem cells (CSCs) survive and continue to proliferate, leading to tumor recurrence. CSC-specific therapies need to be designed in order to precisely eradicate CSCs. Without self-renewing CSCs to drive tumor progression, the tumor shrinks, and regresses.

these short-range electrons damage the cell membrane and elicit radiation-induced bystander effect (194). For this reason, alpha-particle and Auger electron-emitting nuclides are very attractive for RIT against therapy-resistant CSCs. Our group could recently demonstrate that L1CAM, combined with CD133, defines a new ovarian CSC population and L1CAM is responsible

for the radioresistance of these cells (82). This cell population showed high spherogenic and clonogenic capabilities and highly expressed some CSC- and EMT-related genes. Additionally, these cells demonstrated high tumorigenicity, fast-tumor growth and self-renewal when transplanted in nude mice. CRISPR-*Cas9* deletion of L1CAM demonstrated that L1CAM expression correlates with EMT phenotype. Since L1CAM is not expressed in normal stem cells and it is present in the bulk population of cancer cells, anti-L1CAM RIT using Auger electrons and alpha-particle emitters would be a promising new option for ovarian CSCs therapy. In this context, we could clearly demonstrate in a comparative anti-L1CAM RIT study using ^{177}Lu- and^{161}Tb-labeled mAb chCE7 that ^{161}Tb was better by 82.6% compared to ^{177}Lu under equitoxic conditions in a preclinical OC xenograft model (186). ^{161}Tb emits 16 times more Auger and conversion electrons per decay (3–50 keV) than ^{177}Lu. Both radiolanthanides have similar ß–energy of 134 keV (^{177}Lu; mean) or 154 keV (^{161}Tb; mean). Data were taken from "National Nuclear Data Centre Brookhaven National Laboratory."

Some RIT approaches for OC using alpha-particle emitters showed their great potential to treat microresidual diseases in preclinical models (194, 195). In 2017, Kasten et al. used the mAb 376.96, which recognizes the B7-H3 epitope expressed on ovarian CSCs and on the bulk population, radiolabeled with lead-212 (^{212}Pb) to treat tumor-bearing mice. Mice treated with ^{212}Pb-376.96, alone or combined with carboplatin, showed two to three times longer survival than control groups (195). Recent outcomes from a phase I clinical study indicated minimal toxicity of intraperitoneal (i.p) administration of ^{212}Pb-TCMC-trastuzumab in patients with advanced OC (196).

CONCLUSIONS

The CSC heterogeneity and plasticity of CSC state is currently the largest obstacle to move CSC research toward clinical translation. Nevertheless, although the cancer stemness is now considered as a dynamic state rather than an entity, CSC-related biomarkers might be a powerful tool for prediction of patients' clinical outcomes, and targeting of CSC OC population might prove beneficial for the treatment of this deadly disease. Common knowledge about ovarian CSCs has made remarkable progress over the last years; still, there are many limitations and challenges related to disease complexity and current experimental techniques. Future studies are expected to employ clinically relevant models such as patient-derived xenografts, orthotopic mice models, and organoid cultures. Genetically engineered mice models provide opportunity to trace and validate potential CSC populations in the context of a fully functional immune system and tumor stroma. The inherent heterogeneity of OC provides therapeutic challenges and it is further complicated by the acquired heterogeneity driven by microenvironmental and therapeutic pressure. Clinical trials should consider the high heterogeneity regarding CSC markers to select the proper patient cohort. CSC frequency and content should be monitored during clinical trials to assess therapy response. Considering the possibility of bulk tumor cell reprogramming, an optimal therapeutic regimen should combine therapeutic drugs showing wide cytotoxic effects on non-CSCs in combination and/or followed by a therapy targeting resistant CSCs (**Figure 7**) (197). To reach this goal, research needs to focus on the identification of new and reliable signaling pathways that influence CSC maintenance, differentiation, drug resistance, DNA damage repair, and their plasticity. In addition, it would be helpful to identify new CSC cell surface markers that are not expressed in normal stem cells but are also present in the bulk population of tumor cells, like L1CAM in ovarian CSCs. In recent years, there has been a veritable renaissance of radiotherapeutic approaches and new promising radioisotopes were introduced in pre- and clinical trials. Especially alpha- and Auger-emitters allow the sterilization of radioresistant cells such as cancer stem cells due to their high-LET.

AUTHOR CONTRIBUTIONS

NT and JG designed the manuscript. NT wrote the first draft and illustrated the manuscript. NT, JG, FJ, and AD edited and reviewed the manuscript.

FUNDING

This work was supported by the Swiss Cancer Research Foundation (KFS 3585-02-2015) to JG.

ACKNOWLEDGMENTS

We would like to thank Prof. Dr. Roger Schibli, Prof. Dr. med. Viola Heinzelmann-Schwarz, and Dr. Martin Béhé for their support and useful scientific discussions.

REFERENCES

1. Ring KL, Pakish J, Jazaeri AA. Immune checkpoint inhibitors in the treatment of gynecologic malignancies. *Cancer J.* (2016) 22:101–7. doi: 10.1097/PPO.0000000000000179
2. Siegel RL, Miller KD, Jemal A. Cancer statistics, 2019. *CA Cancer J Clin.* (2019) 69:7–34. doi: 10.3322/caac.21551
3. Zhang XY, Zhang PY. Recent perspectives of epithelial ovarian carcinoma. *Oncol Lett.* (2016) 12:3055–58. doi: 10.3892/ol.2016.5107
4. Klotz DM, Wimberger P. Cells of origin of ovarian cancer: ovarian surface epithelium or fallopian tube? *Arch Gynecol Obstet.* (2017) 296:1055–62. doi: 10.1007/s00404-017-4529-z
5. Torre LA, Trabert B, DeSantis CE, Miller KD, Samimi G, Runowicz CD, et al. Ovarian cancer statistics, 2018. *CA Cancer J Clin.* (2018) 68:284–96. doi: 10.3322/caac.21456
6. Hamilton W, Peters TJ, Bankhead C, Sharp D. Risk of ovarian cancer in women with symptoms in primary care: population based case-control study. *BMJ.* (2009) 339:b2998. doi: 10.1136/bmj.b2998
7. Goff BA, Mandel LS, Melancon CH, Muntz HG. Frequency of symptoms of ovarian cancer in women presenting to primary care clinics. *JAMA.* (2004) 291:2705–12. doi: 10.1001/jama.291.22.2705
8. Lu Z, Chen J. [Introduction of WHO classification of tumours of female reproductive organs, fourth edition]. *Zhonghua Bing Li Xue Za Zhi.* (2014) 43:649–50. doi: 10.3760/cma.j.issn.0529-5807.2014.10.001

9. Bowtell DD, Bohm S, Ahmed AA, Aspuria PJ, Bast RC Jr, Beral V, et al. Rethinking ovarian cancer II: reducing mortality from high-grade serous ovarian cancer. *Nat Rev Cancer.* (2015) 15:668–79. doi: 10.1038/nrc4019
10. Jelovac D, Armstrong DK. Recent progress in the diagnosis and treatment of ovarian cancer. *CA Cancer J Clin.* (2011) 61:183–203. doi: 10.3322/caac.20113
11. Mutch DG, Prat J. 2014 FIGO staging for ovarian, fallopian tube and peritoneal cancer. *Gynecol Oncol.* (2014) 133:401–4. doi: 10.1016/j.ygyno.2014.04.013
12. Prat J, FIGO Committee on Gynecologic Oncology. Staging classification for cancer of the ovary, fallopian tube, and peritoneum: abridged republication of guidelines from the international federation of gynecology and obstetrics (figo). *Obstet Gynecol.* (2015) 126:171–4. doi: 10.1097/AOG.0000000000000917
13. Kurta ML, Edwards RP, Moysich KB, McDonough K, Bertolet M, Weissfeld JL, et al. Prognosis and conditional disease-free survival among patients with ovarian cancer. *J Clin Oncol.* (2014) 32:4102–12. doi: 10.1200/JCO.2014.55.1713
14. Heintz AP, Odicino F, Maisonneuve P, Quinn MA, Benedet JL, Creasman WT, et al. Carcinoma of the ovary. *FIGO*. 26th annual report on the results of treatment in gynecological cancer. *Int J Gynaecol Obstet.* (2006) 95:S161–92. doi: 10.1016/S0020-7292(06)60033-7
15. Elattar A, Bryant A, Winter-Roach BA, Hatem M, Naik R. Optimal primary surgical treatment for advanced epithelial ovarian cancer. *Cochrane Database Syst Rev.* (2011) 8:CD007565. doi: 10.1002/14651858.CD007565.pub2
16. Mutch DG. Surgical management of ovarian cancer. *Semin Oncol.* (2002) 29:3–8. doi: 10.1053/sonc.2002.31589
17. Piccart MJ, Bertelsen K, James K, Cassidy J, Mangioni C, Simonsen E, et al. Randomized intergroup trial of cisplatin-paclitaxel versus cisplatin-cyclophosphamide in women with advanced epithelial ovarian cancer: three-year results. *J Natl Cancer Inst.* (2000) 92:699–708. doi: 10.1093/jnci/92.9.699
18. Kigawa J. New strategy for overcoming resistance to chemotherapy of ovarian cancer. *Yonago Acta Med.* (2013) 56:43—50.
19. Kim A, Ueda Y, Naka T, Enomoto T. Therapeutic strategies in epithelial ovarian cancer. *J Exp Clin Cancer Res.* (2012) 31:14. doi: 10.1186/1756-9966-31-14
20. Gore ME, Fryatt I, Wiltshaw E, Dawson T. Treatment of relapsed carcinoma of the ovary with cisplatin or carboplatin following initial treatment with these compounds. *Gynecol Oncol.* (1990) 36:207–11. doi: 10.1016/0090-8258(90)90174-J
21. Agarwal R, Kaye SB. Ovarian cancer: strategies for overcoming resistance to chemotherapy. *Nat Rev Cancer.* (2003) 3:502–16. doi: 10.1038/nrc1123
22. Thomas GM, Dembo AJ. Integrating radiation therapy into the management of ovarian cancer. *Cancer.* (1993) 71(4 Suppl):1710–8. doi: 10.1002/cncr.2820710441
23. Haie C, Pejovic-Lenfant MH, George M, Michel G, Gerbaulet A, Prade M, et al. Whole abdominal irradiation following chemotherapy in patients with minimal residual disease after second look surgery in ovarian carcinoma. *Int J Radiat Oncol Biol Phys.* (1989) 17:15–9. doi: 10.1016/0360-3016(89)90364-7
24. Whelan TJ, Dembo AJ, Bush RS, Sturgeon JF, Fine S, Pringle JF, et al. Complications of whole abdominal and pelvic radiotherapy following chemotherapy for advanced ovarian cancer. *Int J Radiat Oncol Biol Phys.* (1992) 22:853–8. doi: 10.1016/0360-3016(92)90779-H
25. Fields EC, McGuire WP, Lin L, Temkin SM. Radiation treatment in women with ovarian cancer: past, present, and future. *Front Oncol.* (2017) 7:177. doi: 10.3389/fonc.2017.00177
26. Iorio GC, Martini S, Arcadipane F, Ricardi U, Franco P. The role of radiotherapy in epithelial ovarian cancer: a literature overview. *Med Oncol.* (2019) 36:64. doi: 10.1007/s12032-019-1287-8
27. Mahe MA, Fumoleau P, Fabbro M, Guastalla JP, Faurous P, Chauvot P, et al. A phase II study of intraperitoneal radioimmunotherapy with iodine-131-labeled monoclonal antibody OC-125 in patients with residual ovarian carcinoma. *Clin Cancer Res.* (1999) 5(10 Suppl):3249s—53s.
28. Verheijen RH, Massuger LF, Benigno BB, Epenetos AA, Lopes A, Soper JT, et al. Phase III trial of intraperitoneal therapy with yttrium-90-labeled HMFG1 murine monoclonal antibody in patients with epithelial ovarian cancer after a surgically defined complete remission. *J Clin Oncol.* (2006) 24:571–8. doi: 10.1200/JCO.2005.02.5973
29. Larson SM, Carrasquillo JA, N-Cheung KV, Press OW. Radioimmunotherapy of human tumours. *Nat Rev Cancer.* (2015) 15:347–60. doi: 10.1038/nrc3925
30. Batchelor TT, Gerstner ER, Emblem KE, Duda DG, Kalpathy-Cramer J, Snuderl M, et al. Improved tumor oxygenation and survival in glioblastoma patients who show increased blood perfusion after cediranib and chemoradiation. *Proc Natl Acad Sci USA.* (2013) 110:19059–64. doi: 10.1073/pnas.1318022110
31. Hanahan D, Weinberg RA. The hallmarks of cancer. *Cell.* (2000) 100:57–70. doi: 10.1016/S0092-8674(00)81683-9
32. Yang B, Wang JJ. Industry news: avastin approved for metastatic colorectal cancer. *Discov Med.* (2004) 4:79–80.
33. Burger RA, Enserro D, Tewari KS, Brady MF, Bookman MA, Fleming GF, et al. Final overall survival (OS) analysis of an international randomized trial evaluating bevacizumab (BEV) in the primary treatment of advanced ovarian cancer: a NRG oncology/Gynecologic Oncology Group (GOG) study. *J Oncol.* (2018) 36:5517. doi: 10.1200/JCO.2018.36.15_suppl.5517
34. Dantzer F, de La Rubia G, Menissier-De Murcia J, Hostomsky Z, de Murcia G, and Schreiber V. Base excision repair is impaired in mammalian cells lacking Poly(ADP-ribose) polymerase-1. *Biochemistry.* (2000) 39:7559–69. doi: 10.1021/bi0003442
35. Kim G, Ison G, McKee AE, Zhang H, Tang S, Gwise T, et al. FDA approval summary: olaparib monotherapy in patients with deleterious germline brca-mutated advanced ovarian cancer treated with three or more lines of chemotherapy. *Clin Cancer Res.* (2015) 21:4257–61. doi: 10.1158/1078-0432.CCR-15-0887
36. Pujade-Lauraine E, Ledermann JA, Selle F, Gebski V, Penson RT, Oza AM, et al. investigators, Olaparib tablets as maintenance therapy in patients with platinum-sensitive, relapsed ovarian cancer and a BRCA1/2 mutation (SOLO2/ENGOT-Ov21): a double-blind, randomised, placebo-controlled, phase 3 trial. *Lancet Oncol.* (2017) 18:1274–84. doi: 10.1016/S1470-2045(17)30469-2
37. Matulonis UA, Harter P, Gourley C, Friedlander M, Vergote I, Rustin G, et al. Olaparib maintenance therapy in patients with platinum-sensitive, relapsed serous ovarian cancer and a BRCA mutation: overall survival adjusted for postprogression poly(adenosine diphosphate ribose) polymerase inhibitor therapy. *Cancer.* (2016) 122:1844–52. doi: 10.1002/cncr.29995
38. Cortez AJ, Tudrej P, Kujawa KA, Lisowska KM. Advances in ovarian cancer therapy. *Cancer Chemother Pharmacol.* (2018) 81:17–38. doi: 10.1007/s00280-017-3501-8
39. Domchek SM, Aghajanian C, Shapira-Frommer R, Schmutzler RK, Audeh MW, Friedlander M, et al. Efficacy and safety of olaparib monotherapy in germline BRCA1/2 mutation carriers with advanced ovarian cancer and three or more lines of prior therapy. *Gynecol Oncol.* (2016) 140:199–203. doi: 10.1016/j.ygyno.2015.12.020
40. Nowell PC. The clonal evolution of tumor cell populations. *Science.* (1976) 194:23–8. doi: 10.1126/science.959840
41. Dick JE, Looking ahead in cancer stem cell research. *Nat Biotechnol.* (2009) 27:44–6. doi: 10.1038/nbt0109-44
42. Abelson S, Collord G, Ng SWK, Weissbrod O, Mendelson Cohen N, Niemeyer E, et al. Prediction of acute myeloid leukaemia risk in healthy individuals. *Nature.* (2018) 559:400–4. doi: 10.1038/s41586-018-0317-6
43. Turajlic S, Xu H, Litchfield K, Rowan A, Horswell S, Chambers T, et al. Deterministic evolutionary trajectories influence primary tumor growth: tracerx renal. *Cell.* (2018) 173:595–610.e11. doi: 10.1016/j.cell.2018.03.043
44. Hardin H, Zhang R, Helein H, Buehler D, Guo Z, Lloyd RV. The evolving concept of cancer stem-like cells in thyroid cancer and other solid tumors. *Lab Invest.* (2017) 97:1142–51. doi: 10.1038/labinvest.2017.41
45. Bonnet D, Dick JE. Human acute myeloid leukemia is organized as a hierarchy that originates from a primitive hematopoietic cell. *Nat Med.* (1997) 3:730–7. doi: 10.1038/nm0797-730
46. Al-Hajj M, Wicha MS, Benito-Hernandez A, Morrison SJ, Clarke MF. Prospective identification of tumorigenic breast cancer cells. *Proc Natl Acad Sci USA.* (2003) 100:3983–8. doi: 10.1073/pnas.0530291100
47. Ebben JD, Treisman DM, Zorniak M, Kutty RG, Clark PA, Kuo JS. The cancer stem cell paradigm: a new understanding of tumor development and treatment. *Expert Opin Ther Targets.* (2010) 14:621–32. doi: 10.1517/14712598.2010.485186

48. Yang T, Rycaj K, Liu ZM, Tang DG. Cancer stem cells: constantly evolving and functionally heterogeneous therapeutic targets. *Cancer Res.* (2014) 74:2922–7. doi: 10.1158/0008-5472.CAN-14-0266
49. Cabrera MC, Hollingsworth RE, Hurt EM. Cancer stem cell plasticity and tumor hierarchy. *World J Stem Cells.* (2015) 7:27–36. doi: 10.4252/wjsc.v7.i1.27
50. Wei X, Dombkowski D, Meirelles K, Pieretti-Vanmarcke R, Szotek PP, Chang HL, et al. Mullerian inhibiting substance preferentially inhibits stem/progenitors in human ovarian cancer cell lines compared with chemotherapeutics. *Proc Natl Acad Sci USA.* (2010) 107:18874–9. doi: 10.1073/pnas.1012667107
51. Srivastava AK, Banerjee A, Cui T, Han C, Cai S, Liu L, et al. Inhibition of mir-328-3p impairs cancer stem cell function and prevents metastasis in ovarian cancer. *Cancer Res.* (2019) 79:2314–26. doi: 10.1158/0008-5472.CAN-18-3668
52. Rycaj K, Tang DG. Cell-of-origin of cancer versus cancer stem cells: assays and interpretations. *Cancer Res.* (2015) 75:4003–11. doi: 10.1158/0008-5472.CAN-15-0798
53. Cortina C, Turon G, Stork D, Hernando-Momblona X, Sevillano M, Aguilera M, et al. Stephan-otto attolini, sancho e, and batlle E. A genome editing approach to study cancer stem cells in human tumors. *EMBO Mol Med.* (2017) 9:869–79. doi: 10.15252/emmm.201707550
54. Driessens G, Beck B, Caauwe A, Simons BD, Blanpain C. Defining the mode of tumour growth by clonal analysis. *Nature.* (2012) 488:527–30. doi: 10.1038/nature11344
55. Visvader JE, Lindeman GJ. Cancer stem cells in solid tumours: accumulating evidence and unresolved questions. *Nat Rev Cancer.* (2008) 8:755–68. doi: 10.1038/nrc2499
56. Michor F, Polyak K. The origins and implications of intratumor heterogeneity. *Cancer Prev Res.* (2010) 3:1361–4. doi: 10.1158/1940-6207.CAPR-10-0234
57. Kuhlmann JD, Hein L, Kurth I, Wimberger P, Dubrovska A. Targeting Cancer Stem Cells: Promises and Challenges. *Anticancer Agents Med Chem.* (2016) 16:38–58. doi: 10.2174/1871520615666150716104152
58. LE. Iv Santaliz-Ruiz Xie X, Old M, Teknos TN, Pan Q. Emerging role of nanog in tumorigenesis and cancer stem cells. *Int J Cancer.* (2014) 135:2741–8. doi: 10.1002/ijc.28690
59. Strainiene E, Binkis M, Urnikyte S, Stankevicius V, Sasnauskiene A, Kundrotas G, et al. Microenvironment dependent gene expression signatures in reprogrammed human colon normal and cancer cell lines. *BMC Cancer.* (2018) 18:222. doi: 10.1186/s12885-018-4145-8
60. Ye X, Tam WL, Shibue T, Kaygusuz Y, Reinhardt F, Ng Eaton E, et al. Distinct EMT programs control normal mammary stem cells and tumour-initiating cells. *Nature.* (2015) 525:256–60. doi: 10.1038/nature14897
61. Rich JN. Cancer stem cells: understanding tumor hierarchy and heterogeneity. *Medicine.* (2016) 95:S2–7. doi: 10.1097/MD.0000000000004764
62. Plaks V, Kong N, Werb Z. The cancer stem cell niche: how essential is the niche in regulating stemness of tumor cells? *Cell Stem Cell.* (2015) 16:225–38. doi: 10.1016/j.stem.2015.02.015
63. Antoniou A, Hebrant A, Dom G, Dumont JE, Maenhaut C. Cancer stem cells, a fuzzy evolving concept: a cell population or a cell property? *Cell Cycle.* (2013) 12:3743–8. doi: 10.4161/cc.27305
64. Cui T, Srivastava AK, Han C, Wu D, Wani N, Liu L, et al. DDB2 represses ovarian cancer cell dedifferentiation by suppressing ALDH1A1. *Cell Death Dis.* (2018) 9:561. doi: 10.1038/s41419-018-0585-y
65. Chen X, Liao R, Li D, Sun J. Induced cancer stem cells generated by radiochemotherapy and their therapeutic implications. *Oncotarget.* (2017) 8:17301–12. doi: 10.18632/oncotarget.14230
66. Abubaker K, Latifi A, Luwor R, Nazaretian S, Zhu H, Quinn MA, et al. Short-term single treatment of chemotherapy results in the enrichment of ovarian cancer stem cell-like cells leading to an increased tumor burden. *Mol Cancer.* (2013) 12:24. doi: 10.1186/1476-4598-12-24
67. Ward Rashidi MR, Mehta P, Bregenzer M, Raghavan S, Fleck EM, Horst EN, et al. Engineered 3d model of cancer stem cell enrichment and chemoresistance. *Neoplasia.* (2019) 21:822–36. doi: 10.1016/j.neo.2019.06.005
68. Deng S, Yang X, Lassus H, Liang S, Kaur S, Ye Q, et al. Distinct expression levels and patterns of stem cell marker, aldehyde dehydrogenase isoform 1 (ALDH1), in human epithelial cancers. *PLoS ONE.* (2010) 5:e10277. doi: 10.1371/journal.pone.0010277
69. Tao Y, Li H, Huang R, Mo D, Zeng T, Fang M, et al. Clinicopathological and Prognostic Significance of Cancer Stem Cell Markers in Ovarian Cancer Patients: Evidence from 52 Studies. *Cell Physiol Biochem.* (2018) 46:1716–26. doi: 10.1159/000489586
70. Vaughan S, Coward JI, Bast RC, Berchuck A, Berek JS, Brenton JD, et al. Rethinking ovarian cancer: recommendations for improving outcomes. *Nat Rev Cancer.* (2011) 11:719–25. doi: 10.1038/nrc3144
71. Bapat SA, Mali AM, Koppikar CB, Kurrey NK. Stem and progenitor-like cells contribute to the aggressive behavior of human epithelial ovarian cancer. *Cancer Res.* (2005) 65:3025–9. doi: 10.1158/0008-5472.CAN-04-3931
72. Zhang S, Balch C, Chan MW, Lai HC, Matei D, Schilder JM, et al. Identification and characterization of ovarian cancer-initiating cells from primary human tumors. *Cancer Res.* (2008) 68:4311–20. doi: 10.1158/0008-5472.CAN-08-0364
73. Reya T, Morrison SJ, Clarke MF, Weissman IL. Stem cells, cancer, and cancer stem cells. *Nature.* (2001) 414:105–11. doi: 10.1038/35102167
74. Dou J, Jiang C, Wang J, Zhang X, Zhao F, Hu W, et al. Using ABCG2-molecule-expressing side population cells to identify cancer stem-like cells in a human ovarian cell line. *Cell Biol Int.* (2011) 35:227–34. doi: 10.1042/CBI20100347
75. Hu L, McArthur C, Jaffe RB. Ovarian cancer stem-like side-population cells are tumourigenic and chemoresistant. *Br J Cancer.* (2010) 102:1276–83. doi: 10.1038/sj.bjc.6605626
76. Silva IA, Bai S, McLean K, Yang K, Griffith K, Thomas D, et al. Aldehyde dehydrogenase in combination with CD133 defines angiogenic ovarian cancer stem cells that portend poor patient survival. *Cancer Res.* (2011) 71:3991–4001. doi: 10.1158/0008-5472.CAN-10-3175
77. Clevers H, The cancer stem cell: premises, promises and challenges. *Nat Medicine.* (2011) 17:313–9. doi: 10.1038/nm.2304
78. Pieterse Z, Amaya-Padilla MA, Singomat T, Binju M, Madjid BD, Yu Y, et al. Ovarian cancer stem cells and their role in drug resistance. *Int J Biochem Cell Biol.* (2019) 106:117–26. doi: 10.1016/j.biocel.2018.11.012
79. Janzen DM, Tiourin E, Salehi JA, Paik DY, Lu J, Pellegrini M, et al. Erratum: Corrigendum: An apoptosis-enhancing drug overcomes platinum resistance in a tumour-initiating subpopulation of ovarian cancer. *Nat Commun.* (2016) 7:10703. doi: 10.1038/ncomms10703
80. Stewart JM, Shaw PA, Gedye C, Bernardini MQ, Neel BG, Ailles LE. Phenotypic heterogeneity and instability of human ovarian tumor-initiating cells. *Proc Natl Acad Sci USA.* (2011) 108:6468–73. doi: 10.1073/pnas.1005529108
81. Choi YJ, Ingram PN, Yang K, Coffman L, Iyengar M, Bai S, et al. Identifying an ovarian cancer cell hierarchy regulated by bone morphogenetic protein 2. *Proc Natl Acad Sci USA.* (2015) 112:E6882–8. doi: 10.1073/pnas.1507899112
82. Terraneo N, Jacob F, Peitzsch C, Dubrovska A, Krudewig C, Huang YL, et al. L1 cell adhesion molecule confers radioresistance to ovarian cancer and defines a new cancer stem cell population. *Cancers.* (2020) 12:217. doi: 10.3390/cancers12010217
83. Meacham CE, Morrison SJ. Tumour heterogeneity and cancer cell plasticity. *Nature.* (2013) 501:328–37. doi: 10.1038/nature12624
84. Yap TA, Sandhu SK, Carden CP JS. de Bono: Poly(ADP-ribose) polymerase (PARP) inhibitors: exploiting a synthetic lethal strategy in the clinic. *CA Cancer J Clin.* (2011) 61:31–49. doi: 10.3322/caac.20095
85. Yin AH, Miraglia S, Zanjani ED, Almeida-Porada G, Ogawa M, Leary AG, et al. AC133, a novel marker for human hematopoietic stem and progenitor cells. *Blood.* (1997) 90:5002–12. doi: 10.1182/blood.V90.12.5002
86. Glumac PM, LeBeau AM. The role of CD133 in cancer: a concise review. *Clin Transl Med.* (2018) 7:18. doi: 10.1186/s40169-018-0198-1
87. Brossa A, Papadimitriou E, Collino F, Incarnato D, Oliviero S, Camussi G, et al. Role of CD133 molecule in wnt response and renal repair. *Stem Cells Transl Med.* (2018) 7:283–94. doi: 10.1002/sctm.17-0158
88. Jang JW, Song Y, Kim SH, Kim JS, Kim KM, Choi EK, et al. CD133 confers cancer stem-like cell properties by stabilizing EGFR-AKT

signaling in hepatocellular carcinoma. *Cancer Lett.* (2017) 389:1–10. doi: 10.1016/j.canlet.2016.12.023
89. Singh SK, Clarke ID, Terasaki M, Bonn VE, Hawkins C, Squire J, et al. Identification of a cancer stem cell in human brain tumors. *Cancer Res.* (2003) 63:5821–8.
90. Grosse-Gehling P, Fargeas CA, Dittfeld C, Garbe Y, Alison MR, Corbeil D LA. Kunz-Schughart: CD133 as a biomarker for putative cancer stem cells in solid tumours: limitations, problems and challenges. *J Pathol.* (2013) 229:355–78. doi: 10.1002/path.4086
91. Curley MD, Therrien VA, Cummings CL, Sergent PA, Koulouris CR, Friel AM, et al. CD133 expression defines a tumor initiating cell population in primary human ovarian cancer. *Stem Cells.* (2009) 27:2875–83. doi: 10.1002/stem.236
92. Cioffi M, D'Alterio C, Camerlingo R, Tirino V, Consales C, Riccio A, et al. Identification of a distinct population of CD133(+)CXCR4(+) cancer stem cells in ovarian cancer. *Sci Rep.* (2015) 5:10357. doi: 10.1038/srep10357
93. Sharrow AC, Perkins B, Collector MI, Yu W, Simons BW, Jones RJ. Characterization of aldehyde dehydrogenase 1 high ovarian cancer cells: Towards targeted stem cell therapy. *Gynecol Oncol.* (2016) 142:341–8. doi: 10.1016/j.ygyno.2016.03.022
94. Kusumbe AP, Mali AM, Bapat SA. CD133-expressing stem cells associated with ovarian metastases establish an endothelial hierarchy and contribute to tumor vasculature. *Stem Cells.* (2009) 27:498–508. doi: 10.1634/stemcells.2008-0868
95. Hermansen SK, Christensen KG, Jensen SS, Kristensen BW. Inconsistent immunohistochemical expression patterns of four different CD133 antibody clones in glioblastoma. *J Histochem Cytochem.* (2011) 59:391–407. doi: 10.1369/0022155411400867
96. Jackson B, Brocker C, Thompson DC, Black W, Vasiliou K, Nebert DW, et al. Update on the aldehyde dehydrogenase gene (ALDH) superfamily. *Hum Genomics.* (2011) 5:283–303. doi: 10.1186/1479-7364-5-4-283
97. Xu X, Chai S, Wang P, Zhang C, Yang Y, Yang Y, et al. Aldehyde dehydrogenases and cancer stem cells. *Cancer Lett.* (2015) 369:50–7. doi: 10.1016/j.canlet.2015.08.018
98. Januchowski R, Wojtowicz K, Sterzyska K, Sosiska P, Andrzejewska M, Zawierucha P, et al. Inhibition of ALDH1A1 activity decreases expression of drug transporters and reduces chemotherapy resistance in ovarian cancer cell lines. *Int J Biochem Cell Biol.* (2016) 78:248–59. doi: 10.1016/j.biocel.2016.07.017
99. Ma I, Allan AL. The role of human aldehyde dehydrogenase in normal and cancer stem cells. *Stem Cell Rev.* (2011) 7:292–306. doi: 10.1007/s12015-010-9208-4
100. Tomita H, Tanaka K, Tanaka T, Hara A. Aldehyde dehydrogenase 1A1 in stem cells and cancer. *Oncotarget.* (2016) 7:11018–32. doi: 10.18632/oncotarget.6920
101. Kryczek I, Liu S, Roh M, Vatan L, Szeliga W, Wei S, et al. Expression of aldehyde dehydrogenase and CD133 defines ovarian cancer stem cells. *Int J Cancer.* (2012) 130:29–39. doi: 10.1002/ijc.25967
102. Ishiguro T, Sato A, Ohata H, Ikarashi Y, Takahashi RU, Ochiya T, et al. Establishment and characterization of an *in vitro* model of ovarian cancer stem-like cells with an enhanced proliferative capacity. *Cancer Res.* (2016) 76:150–60. doi: 10.1158/0008-5472.CAN-15-0361
103. Dontu G, Abdallah WM, Foley JM, Jackson KW, Clarke MF, Kawamura MJ, et al. *In vitro* propagation and transcriptional profiling of human mammary stem/progenitor cells. *Genes Dev.* (2003) 17:1253–70. doi: 10.1101/gad.1061803
104. Yang L, Lai D. Ovarian cancer stem cells enrichment. *Methods Mol Biol.* (2013) 1049:337–45. doi: 10.1007/978-1-62703-547-7_25
105. Liao J, Qian F, Tchabo N, Mhawech-Fauceglia P, Beck A, Qian Z, et al. Ovarian cancer spheroid cells with stem cell-like properties contribute to tumor generation, metastasis and chemotherapy resistance through hypoxia-resistant metabolism. *PLoS ONE.* (2014) 9:e84941. doi: 10.1371/journal.pone.0084941
106. Wang L, Xu T, Cui M. Are ovarian cancer stem cells the target for innovative immunotherapy? *Onco Targets Ther.* (2018) 11:2615–26. doi: 10.2147/OTT.S155458
107. Bourguignon LY, Zhu H, Zhou B, Diedrich F, Singleton PA, Hung MC. Hyaluronan promotes CD44v3-Vav2 interaction with Grb2-p185(HER2) and induces Rac1 and Ras signaling during ovarian tumor cell migration and growth. *J Biol Chem.* (2001) 276:48679–92. doi: 10.1074/jbc.M106759200
108. Carpenter PM, Dao AV. The role of hyaluronan in mesothelium-induced motility of ovarian carcinoma cells. *Anticancer Res.* (2003) 23:3985–90.
109. Sacks JD, Barbolina MV. Expression and function of CD44 in epithelial ovarian carcinoma. *Biomolecules.* (2015) 5:3051–66. doi: 10.3390/biom5043051
110. Dosch JS, Ziemke EK, Shettigar A, Rehemtulla A JS. Sebolt-Leopold: Cancer stem cell marker phenotypes are reversible and functionally homogeneous in a preclinical model of pancreatic cancer. *Cancer Res.* (2015) 75:4582–92. doi: 10.1158/0008-5472.CAN-14-2793
111. Xu H, Tian Y, Yuan X, Wu H, Liu Q, Pestell RG, et al. The role of CD44 in epithelial-mesenchymal transition and cancer development. *Onco Targets Ther.* (2015) 8:3783–92. doi: 10.2147/OTT.S95470
112. Chau WK, Ip CK, Mak AS, Lai HC, Wong AS. c-Kit mediates chemoresistance and tumor-initiating capacity of ovarian cancer cells through activation of Wnt/beta-catenin-ATP-binding cassette G2 signaling. *Oncogene.* (2013) 32:2767–81. doi: 10.1038/onc.2012.290
113. Burgos-Ojeda D, Wu R, McLean K, Chen YC, Talpaz M, Yoon E, et al. $CD24^+$ ovarian cancer cells are enriched for cancer-initiating cells and dependent on jak2 signaling for growth and metastasis. *Mol Cancer Ther.* (2015) 14:1717–27. doi: 10.1158/1535-7163.MCT-14-0607
114. Gao MQ, Choi YP, Kang S, Youn JH, Cho NH. $CD24^+$ cells from hierarchically organized ovarian cancer are enriched in cancer stem cells. *Oncogene.* (2010) 29:2672–80. doi: 10.1038/onc.2010.35
115. Davidson B. CD24 is highly useful in differentiating high-grade serous carcinoma from benign and malignant mesothelial cells. *Hum Pathol.* (2016) 58:123–7. doi: 10.1016/j.humpath.2016.08.005
116. van der Gun BT, Melchers LJ, Ruiters MH, de Leij LF, McLaughlin PM, Rots MG. EpCAM in carcinogenesis: the good, the bad or the ugly. *Carcinogenesis.* (2010) 31:1913–21. doi: 10.1093/carcin/bgq187
117. Tayama S, Motohara T, Narantuya D, Li C, Fujimoto K, Sakaguchi I, et al. The impact of EpCAM expression on response to chemotherapy and clinical outcomes in patients with epithelial ovarian cancer. *Oncotarget.* (2017) 8:44312–25. doi: 10.18632/oncotarget.17871
118. Meirelles K, Benedict LA, Dombkowski D, Pepin D, Preffer FI, Teixeira J, et al. Human ovarian cancer stem/progenitor cells are stimulated by doxorubicin but inhibited by Mullerian inhibiting substance. *Proc Natl Acad Sci USA.* (2012) 109:2358–63. doi: 10.1073/pnas.1120733109
119. Yu J, Vodyanik MA, Smuga-Otto K, Antosiewicz-Bourget J, Frane JL, Tian S, et al. Induced pluripotent stem cell lines derived from human somatic cells. *Science.* (2007) 318:1917–20. doi: 10.1126/science.1151526
120. Peng S, Maihle NJ, Huang Y. Pluripotency factors Lin28 and Oct4 identify a sub-population of stem cell-like cells in ovarian cancer. *Oncogene.* (2010) 29:2153–9. doi: 10.1038/onc.2009.500
121. Siu MK, Wong ES, Kong DS, Chan HY, Jiang L, Wong OG, et al. Stem cell transcription factor NANOG controls cell migration and invasion via dysregulation of E-cadherin and FoxJ1 and contributes to adverse clinical outcome in ovarian cancers. *Oncogene.* (2013) 32:3500–9. doi: 10.1038/onc.2012.363
122. Wen Y, Hou Y, Huang Z, Cai J, Wang Z. SOX2 is required to maintain cancer stem cells in ovarian cancer. *Cancer Sci.* (2017) 108:719–31. doi: 10.1111/cas.13186
123. Kreso A, John Dick E. Evolution of the cancer stem cell model. *Cell Stem Cell.* (2014) 14:275–91. doi: 10.1016/j.stem.2014.02.006
124. Shibue T, Weinberg RA. EMT, CSCs, and drug resistance: the mechanistic link and clinical implications. *Nat Rev Clin Oncol.* (2017) 14:611–29. doi: 10.1038/nrclinonc.2017.44
125. Li SS, Ma J, Wong AST. Chemoresistance in ovarian cancer: exploiting cancer stem cell metabolism. *J Gynecol Oncol.* (2018) 29:e32. doi: 10.3802/jgo.2018.29.e32
126. Cojoc M, Mabert K, Muders MH, Dubrovska A. A role for cancer stem cells in therapy resistance: cellular and molecular mechanisms. *Semin Cancer Biol.* (2015) 31:16–27. doi: 10.1016/j.semcancer.2014.06.004
127. Cheung-Ong K, Giaever G, Nislow C. DNA-damaging agents in cancer chemotherapy: serendipity and chemical biology. *Chem Biol.* (2013) 20:648–59. doi: 10.1016/j.chembiol.2013.04.007

128. Mladenov E, Magin S, Soni A, Iliakis G. DNA double-strand break repair as determinant of cellular radiosensitivity to killing and target in radiation therapy. *Front Oncol.* (2013) 3:113. doi: 10.3389/fonc.2013.00113
129. Ranjha L, Howard SM, Cejka P. Main steps in DNA double-strand break repair: an introduction to homologous recombination and related processes. *Chromosoma.* (2018) 127:187–214. doi: 10.1007/s00412-017-0658-1
130. Krause M, Dubrovska A, Linge A, Baumann M. Cancer stem cells: Radioresistance, prediction of radiotherapy outcome and specific targets for combined treatments. *Adv Drug Deliv Rev.* (2017) 109:63–73. doi: 10.1016/j.addr.2016.02.002
131. Morgan MA, Lawrence TS. Molecular Pathways: Overcoming Radiation Resistance by Targeting DNA Damage Response Pathways. *Clin Cancer Res.* (2015) 21:2898–904. doi: 10.1158/1078-0432.CCR-13-3229
132. Bellio C, DiGloria C, Foster R, James K, Konstantinopoulos PA, Growdon WB, et al. PARP inhibition induces enrichment of DNA repair-proficient CD133 and CD117 positive ovarian cancer stem cells. *Mol Cancer Res.* (2019) 17:431–45. doi: 10.1158/1541-7786.MCR-18-0594
133. Meng E, Mitra A, Tripathi K, Finan MA, Scalici J, McClellan S L. et al. ALDH1A1 maintains ovarian cancer stem cell-like properties by altered regulation of cell cycle checkpoint and DNA repair network signaling. *PLoS ONE.* (2014) 9:e107142. doi: 10.1371/journal.pone.0107142
134. Saygin C, Wiechert A, Rao VS, Alluri R, Connor E, Thiagarajan PS, et al. CD55 regulates self-renewal and cisplatin resistance in endometrioid tumors. *J Exp Med.* (2017) 214:2715–32. doi: 10.1084/jem.20170438
135. Srivastava AK, Han C, Zhao R, Cui T, Dai Y, Mao C, et al. Enhanced expression of DNA polymerase eta contributes to cisplatin resistance of ovarian cancer stem cells. *Proc Natl Acad Sci USA.* (2015) 112:4411–6. doi: 10.1073/pnas.1421365112
136. Sena LA, Chandel NS. Physiological roles of mitochondrial reactive oxygen species. *Mol Cell.* (2012) 48:158–67. doi: 10.1016/j.molcel.2012.09.025
137. Kumari S, Badana AK, G MM, S G, and Malla R. Reactive oxygen species: a key constituent in cancer survival. *Biomark Insights.* (2018) 13:1177271918755391. doi: 10.1177/1177271918755391
138. Diehn M, Cho RW, Lobo NA, Kalisky T, Dorie MJ, Kulp AN, et al. Association of reactive oxygen species levels and radioresistance in cancer stem cells. *Nature.* (2009) 458:780–3. doi: 10.1038/nature07733
139. Bensimon J, Biard D, Paget V, Goislard M, Morel-Altmeyer S, Konge J, et al. Forced extinction of CD24 stem-like breast cancer marker alone promotes radiation resistance through the control of oxidative stress. *Mol Carcinog.* (2016) 55:245–54. doi: 10.1002/mc.22273
140. Kim D, Choi BH, Ryoo IG, Kwak MK. High NRF2 level mediates cancer stem cell-like properties of aldehyde dehydrogenase (ALDH)-high ovarian cancer cells: inhibitory role of all-trans retinoic acid in ALDH/NRF2 signaling. *Cell Death Dis.* (2018) 9:896. doi: 10.1038/s41419-018-0903-4
141. Vasiliou V, Vasiliou K, Nebert DW. Human ATP-binding cassette (ABC) transporter family. *Hum Genomics.* (2009) 3:281–90. doi: 10.1186/1479-7364-3-3-281
142. Sun YL, Patel A, Kumar P, Chen ZS. Role of ABC transporters in cancer chemotherapy. *Chin J Cancer.* (2012) 31:51–7. doi: 10.5732/cjc.011.10466
143. Phi LTH, Sari IN, Yang YG, Lee SH, Jun N, Kim KS, et al. Cancer Stem Cells (CSCs) in drug resistance and their therapeutic implications in cancer treatment. *Stem Cells Int.* (2018) 2018:5416923. doi: 10.1155/2018/5416923
144. McAuliffe SM, Morgan SL, Wyant GA, Tran LT, Muto KW, Chen YS, et al. Targeting Notch, a key pathway for ovarian cancer stem cells, sensitizes tumors to platinum therapy. *Proc Natl Acad Sci USA.* (2012) 109:E2939–48. doi: 10.1073/pnas.1206400109
145. Kwon MJ, Shin YK. Regulation of ovarian cancer stem cells or tumor-initiating cells. *Int J Mol Sci.* (2013) 14:6624–48. doi: 10.3390/ijms14046624
146. Borah A, Raveendran S, Rochani A, Maekawa T, Kumar DS. Targeting self-renewal pathways in cancer stem cells: clinical implications for cancer therapy. *Oncogenesis.* (2015) 4:e177. doi: 10.1038/oncsis.2015.35
147. Barbolina MV, Burkhalter RJ, Stack MS. Diverse mechanisms for activation of Wnt signalling in the ovarian tumour microenvironment. *Biochem J.* (2011) 437:1–12. doi: 10.1042/BJ20110112
148. Kessenbrock K, Wang CY, Werb Z. Matrix metalloproteinases in stem cell regulation and cancer. *Matrix Biol.* (2015) 44–46:184–90. doi: 10.1016/j.matbio.2015.01.022
149. Wang Y, Zong X, Mitra S, Mitra AK, Matei D, Nephew KP. IL-6 mediates platinum-induced enrichment of ovarian cancer stem cells. *JCI Insight.* (2018) 3:122360. doi: 10.1172/jci.insight.122360
150. Cabarcas SM, Mathews LA, Farrar WL. The cancer stem cell niche–there goes the neighborhood? *Int J Cancer.* (2011) 129:2315–7. doi: 10.1002/ijc.26312
151. Bao S, Wu Q, Sathornsumetee S, Hao Y, Li Z, Hjelmeland AB, et al. Stem cell-like glioma cells promote tumor angiogenesis through vascular endothelial growth factor. *Cancer Res.* (2006) 66:7843–8. doi: 10.1158/0008-5472.CAN-06-1010
152. Jang K, Kim M, Gilbert CA, Simpkins F, Ince TA, Slingerland JM. VEGFA activates an epigenetic pathway upregulating ovarian cancer-initiating cells. *EMBO Mol Med.* (2017) 9:304–18. doi: 10.15252/emmm.201606840
153. Mantovani A. The inflammation - cancer connection. *FEBS J.* (2018) 285:638–40. doi: 10.1111/febs.14395
154. Prieto-Vila M, Takahashi RU, Usuba W, Kohama I, Ochiya T. Drug resistance driven by cancer stem cells and their niche. *Int J Mol Sci.* (2017) 18:2574. doi: 10.3390/ijms18122574
155. Heddleston JM, Li Z, Lathia JD, Bao S, Hjelmeland AB, Rich JN. Hypoxia inducible factors in cancer stem cells. *Br J Cancer.* (2010) 102:789–95. doi: 10.1038/sj.bjc.6605551
156. Qin J, Liu Y, Lu Y, Liu M, Li M, Li J, et al. Hypoxia-inducible factor 1 alpha promotes cancer stem cells-like properties in human ovarian cancer cells by upregulating SIRT1 expression. *Sci Rep.* (2017) 7:10592. doi: 10.1038/s41598-017-09244-8
157. Kitajima S, Lee KL, Hikasa H, Sun W, Huang RY, Yang H, et al. Hypoxia-inducible factor-1alpha promotes cell survival during ammonia stress response in ovarian cancer stem-like cells. *Oncotarget.* (2017) 8:114481–94. doi: 10.18632/oncotarget.23010
158. He M, Wu H, Jiang Q, Liu Y, Han L, Yan Y, et al. Hypoxia-inducible factor-2α directly promotes BCRP expression and mediates the resistance of ovarian cancer stem cells to adriamycin. *Mol Oncol.* (2019) 13:403–21. doi: 10.1002/1878-0261.12419
159. Sonveaux P. ROS and radiotherapy: more we care. *Oncotarget.* (2017) 8:35482–83. doi: 10.18632/oncotarget.16613
160. Graham K, Unger E. Overcoming tumor hypoxia as a barrier to radiotherapy, chemotherapy and immunotherapy in cancer treatment. *Int J Nanomed.* (2018) 13:6049–58. doi: 10.2147/IJN.S140462
161. Dongre A, Weinberg RA. New insights into the mechanisms of epithelial-mesenchymal transition and implications for cancer. *Nat Rev Mol Cell Biol.* (2019) 20:69–84. doi: 10.1038/s41580-018-0080-4
162. De Craene B, Berx G. Regulatory networks defining EMT during cancer initiation and progression. *Nat Rev Cancer.* (2013) 13:97–110. doi: 10.1038/nrc3447
163. Liao TT, Yang MH. Revisiting epithelial-mesenchymal transition in cancer metastasis: the connection between epithelial plasticity and stemness. *Mol Oncol.* (2017) 11:792–804. doi: 10.1002/1878-0261.12096
164. Cao L, Shao M, Schilder J, Guise T, Mohammad KS, Matei D. Tissue transglutaminase links TGF-beta, epithelial to mesenchymal transition and a stem cell phenotype in ovarian cancer. *Oncogene.* (2012) 31:2521–34. doi: 10.1038/onc.2011.429
165. Rafehi S, Ramos Valdes Y, Bertrand M, McGee J, Prefontaine M, Sugimoto A, et al. TGFbeta signaling regulates epithelial-mesenchymal plasticity in ovarian cancer ascites-derived spheroids. *Endocr Relat Cancer.* (2016) 23:147–59. doi: 10.1530/ERC-15-0383
166. Yeo CD, Kang N, Choi SY, Kim BN, Park CK, Kim JW, et al. The role of hypoxia on the acquisition of epithelial-mesenchymal transition and cancer stemness: a possible link to epigenetic regulation. *Korean J Intern Med.* (2017) 32:589–99. doi: 10.3904/kjim.2016.302
167. Strauss R, Li ZY, Liu Y, Beyer I, Persson J, Sova P, et al. Analysis of epithelial and mesenchymal markers in ovarian cancer reveals phenotypic heterogeneity and plasticity. *PLoS ONE.* (2011) 6:e16186. doi: 10.1371/annotation/8c637352-3614-406c-89dc-e78d10fa069c
168. Jolly MK, Boareto M, Huang B, Jia D, Lu M, Ben-Jacob E, et al. Implications of the hybrid epithelial/mesenchymal phenotype in metastasis. *Front Oncol.* (2015) 5:155. doi: 10.3389/fonc.2015.00155
169. Latifi A, Abubaker K, Castrechini N, Ward AC, Liongue C, Dobill F, et al. Cisplatin treatment of primary and metastatic epithelial ovarian carcinomas

generates residual cells with mesenchymal stem cell-like profile. *J Cell Biochem.* (2011) 112:2850–64. doi: 10.1002/jcb.23199
170. Iliopoulos D, Hirsch HA, Struhl K. Metformin decreases the dose of chemotherapy for prolonging tumor remission in mouse xenografts involving multiple cancer cell types. *Cancer Res.* (2011) 71:3196–201. doi: 10.1158/0008-5472.CAN-10-3471
171. Shank JJ, Yang K, Ghannam J, Cabrera L, Johnston CJ, Reynolds RK, et al. Metformin targets ovarian cancer stem cells in vitro and in vivo. *Gynecol Oncol.* (2012) 127:390–7. doi: 10.1016/j.ygyno.2012.07.115
172. Buckanovich RJ, Brown J, Shank J, Griffith KA, Reynolds RK, Johnston C, et al. A phase II clinical trial of metformin as a cancer stem cell targeting agent in stage IIc/III/IV ovarian, fallopian tube, and primary peritoneal cancer. *J Clin Oncol.* (2017) 35:5556. doi: 10.1200/JCO.2017.35.15_suppl.5556
173. Al-Alem LF, Pandya UM, Baker AT, Bellio C, Zarrella BD, Clark J, et al. Ovarian cancer stem cells: what progress have we made? *Int J Biochem Cell Biol.* (2019) 107:92–103. doi: 10.1016/j.biocel.2018.12.010
174. Stathis A, Hess D, von Moos R, Homicsko K, Griguolo G, Joerger M, et al. Swiss group for clinical cancer: phase i trial of the oral smoothened inhibitor sonidegib in combination with paclitaxel in patients with advanced solid tumors. *Invest New Drugs.* (2017) 35:766–72. doi: 10.1007/s10637-017-0454-z
175. Kaye SB, Fehrenbacher L, Holloway R, Amit A, Karlan B, Slomovitz B, et al. A phase II, randomized, placebo-controlled study of vismodegib as maintenance therapy in patients with ovarian cancer in second or third complete remission. *Clin Cancer Res.* (2012) 18:6509–18. doi: 10.1158/1078-0432.CCR-12-1796
176. O'Cearbhaill RE, McMeekin DS, Mantia-Smaldone G, Gunderson C, Sabbatini P, Cattaruzza F, et al. Phase 1b of WNT inhibitor ipafricept (IPA, decoy receptor for WNT ligands) with carboplatin (C) and paclitaxel (P) in recurrent platinum-sensitive ovarian cancer (OC). *J Clin Oncol.* (2016) 34(15 Suppl):2515. doi: 10.1200/JCO.2016.34.15_suppl.2515
177. Patel MR, Infante JR, Moore KN, Keegan M, Poli A, Padval M, et al. Phase 1/1b study of the FAK inhibitor defactinib (VS-6063) in combination with weekly paclitaxel for advanced ovarian cancer. *J Clin Oncol.* (2014) 32:5521. doi: 10.1200/jco.2014.32.15_suppl.5521
178. Debiec H, Christensen EI, Ronco PM. The cell adhesion molecule L1 is developmentally regulated in the renal epithelium and is involved in kidney branching morphogenesis. *J Cell Biol.* (1998) 143:2067–79. doi: 10.1083/jcb.143.7.2067
179. Altevogt P, Doberstein K, Fogel M. L1CAM in human cancer. *Int J Cancer.* (2016) 138:1565–76. doi: 10.1002/ijc.29658
180. Kiefel H, Bondong S, Hazin J, Ridinger J, Schirmer U, Riedle S, et al. L1CAM: a major driver for tumor cell invasion and motility. *Cell Adh Migr.* (2012) 6:374–84. doi: 10.4161/cam.20832
181. Huszar M, Moldenhauer G, Gschwend V, Ben-Arie A, Altevogt P, Fogel M. Expression profile analysis in multiple human tumors identifies L1 (CD171) as a molecular marker for differential diagnosis and targeted therapy. *Hum Pathol.* (2006) 37:1000–8. doi: 10.1016/j.humpath.2006.03.014
182. Meli ML, Carrel F, Waibel R, Amstutz H, Crompton N, Jaussi R, et al. Novak-Hofer: Anti-neuroblastoma antibody chCE7 binds to an isoform of L1-CAM present in renal carcinoma cells. *Int J Cancer.* (1999) 83:401. doi: 10.1002/(sici)1097-0215(19991029)83:3<401::aid-ijc17>3.0.co;2-a
183. Knogler K, Grünberg J, Zimmermann K, Cohrs S, Honer M, Ametamey S, et al. Novak-Hofer: copper-67 radioimmunotherapy and growth inhibition by anti-L1-cell adhesion molecule monoclonal antibodies in a therapy model of ovarian cancer metastasis. *Clin Cancer Res.* (2007) 13:603–11. doi: 10.1158/1078-0432.CCR-06-1486
184. Friedli A, Fischer E, Novak-Hofer I, Cohrs S, Ballmer-Hofer K, Schubiger PA, et al. The soluble form of the cancer-associated L1 cell adhesion molecule is a pro-angiogenic factor. *Int J Biochem Cell Biol.* (2009) 41:1572–80. doi: 10.1016/j.biocel.2009.01.006
185. Fischer E, Grünberg J, Cohrs S, Hohn A, Waldner-Knogler K, Jeger S, et al. L1-CAM-targeted antibody therapy and (177)Lu-radioimmunotherapy of disseminated ovarian cancer. *Int J Cancer.* (2012) 130:2715–21. doi: 10.1002/ijc.26321
186. Grünberg J, Lindenblatt D, Dorrer H, Cohrs S, Zhernosekov K, Koster U, et al. Anti-L1CAM radioimmunotherapy is more effective with the radiolanthanide terbium-161 compared to lutetium-177 in an ovarian cancer model. *Eur J Nucl Med Mol Imaging.* (2014) 41:1907–15. doi: 10.1007/s00259-014-2798-3
187. Novak-Hofer I, Amstutz HP, Morgenthaler JJ, Schubiger PA. Internalization and degradation of monoclonal antibody chCE7 by human neuroblastoma cells. *Int J Cancer.* (1994) 57:427–32. doi: 10.1002/ijc.2910570322
188. Bartholoma MD. Radioimmunotherapy of solid tumors: approaches on the verge of clinical application. *J Labelled Comp Radiopharm.* (2018) 61:715–26. doi: 10.1002/jlcr.3619
189. Lindenblatt D, Fischer E, Cohrs S, Schibli R, Grünberg J. Paclitaxel improved anti-L1CAM lutetium-177 radioimmunotherapy in an ovarian cancer xenograft model. *EJNMMI Res.* (2014) 4:54. doi: 10.1186/s13550-014-0054-2
190. Lindenblatt D, Terraneo N, Pellegrini G, Cohrs S, Spycher PR, Vukovic D, et al. Combination of lutetium-177 labelled anti-L1CAM antibody chCE7 with the clinically relevant protein kinase inhibitor MK1775: a novel combination against human ovarian carcinoma. *BMC Cancer.* (2018) 18:922. doi: 10.1186/s12885-018-4836-1
191. Ghaffari H, Beik J, Talebi A, Mahdavi SR, Abdollahi H. New physical approaches to treat cancer stem cells: a review. *Clin Transl Oncol.* (2018) 20:1502–21. doi: 10.1007/s12094-018-1896-2
192. Aghevlian S, Boyle AJ, Reilly RM. Radioimmunotherapy of cancer with high linear energy transfer (LET) radiation delivered by radionuclides emitting alpha-particles or Auger electrons. *Adv Drug Deliv Rev.* (2017) 109:102–18. doi: 10.1016/j.addr.2015.12.003
193. Pouget JP, Navarro-Teulon I, Bardies M, Chouin N, Cartron G, Pelegrin A, et al. Clinical radioimmunotherapy–the role of radiobiology. *Nat Rev Clin Oncol.* (2011) 8:720–34. doi: 10.1038/nrclinonc.2011.160
194. Cornelissen B, Vallis KA. Targeting the nucleus: an overview of Auger-electron radionuclide therapy. *Curr Drug Discov Technol.* (2010) 7:263–79. doi: 10.2174/157016310793360657
195. Kasten BB, Arend RC, Katre AA, Kim H, Fan J, Ferrone S, et al. B7-H3-targeted (212)Pb radioimmunotherapy of ovarian cancer in preclinical models. *Nucl Med Biol.* (2017) 47:23–30. doi: 10.1016/j.nucmedbio.2017.01.003
196. Meredith RF, Torgue JJ, Rozgaja TA, Banaga EP, Bunch PW, Alvarez RD, et al. Safety and outcome measures of first-in-human intraperitoneal alpha radioimmunotherapy with 212Pb-TCMC-Trastuzumab. *Am J Clin Oncol.* (2018) 41:716–21. doi: 10.1097/COC.0000000000000353
197. Mittal S, Mifflin R, Powell DW. Cancer stem cells: the other face of Janus. *Am J Med Sci.* (2009) 338:107–12. doi: 10.1097/MAJ.0b013e3181ad5865

Conflict of Interest: The authors declare that the research was conducted in the absence of any commercial or financial relationships that could be construed as a potential conflict of interest.

Copyright © 2020 Terraneo, Jacob, Dubrovska and Grünberg. This is an open-access article distributed under the terms of the Creative Commons Attribution License (CC BY). The use, distribution or reproduction in other forums is permitted, provided the original author(s) and the copyright owner(s) are credited and that the original publication in this journal is cited, in accordance with accepted academic practice. No use, distribution or reproduction is permitted which does not comply with these terms.

Advantages of publishing in Frontiers

OPEN ACCESS
Articles are free to read for greatest visibility and readership

FAST PUBLICATION
Around 90 days from submission to decision

HIGH QUALITY PEER-REVIEW
Rigorous, collaborative, and constructive peer-review

TRANSPARENT PEER-REVIEW
Editors and reviewers acknowledged by name on published articles

Frontiers
Avenue du Tribunal-Fédéral 34
1005 Lausanne | Switzerland

Visit us: www.frontiersin.org
Contact us: info@frontiersin.org | +41 21 510 17 00

REPRODUCIBILITY OF RESEARCH
Support open data and methods to enhance research reproducibility

DIGITAL PUBLISHING
Articles designed for optimal readership across devices

FOLLOW US
@frontiersin

IMPACT METRICS
Advanced article metrics track visibility across digital media

EXTENSIVE PROMOTION
Marketing and promotion of impactful research

LOOP RESEARCH NETWORK
Our network increases your article's readership